US Army Corps
of Engineers
Construction Engineering
Research Laboratories

USACERL Technical Report 98/47
February 1998

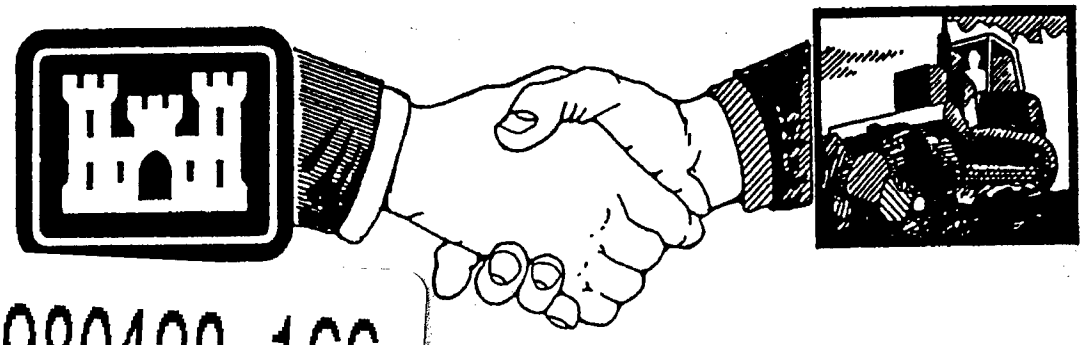
CONSTRUCTION PRODUCTIVITY ADVANCEMENT RESEARCH (CPAR) PROGRAM

Fiber-Reinforced Polymer Composite Materials Systems to Enhance Reinforced Concrete Structures

by
Orange S. Marshall, Jr., John P. Busel, Pamalee A. Brady, Douglas S. Barno, Peter Bong, M. Arockiasamy, Alexander M. Vaysburd, Srinivasa L. Iyer, Marco Arduini, Antonio Nanni, and Piyush K. Dutta

Approved for public release; distribution is unlimited.

DTIC QUALITY INSPECTED 3



19980428 166

A Corps/Industry Partnership To Advance
Construction Productivity and Reduce Costs

The contents of this report are not to be used for advertising, publication, or promotional purposes. Citation of trade names does not constitute an official endorsement or approval of the use of such commercial products. The findings of this report are not to be construed as an official Department of the Army position, unless so designated by other authorized documents.

DESTROY THIS REPORT WHEN IT IS NO LONGER NEEDED

DO NOT RETURN IT TO THE ORIGINATOR

USER EVALUATION OF REPORT

REFERENCE: USACERL Technical Report 98/47, *Fiber-Reinforced Polymer Composite Materials Systems to Enhance Reinforced Concrete Structures*

Please take a few minutes to answer the questions below, tear out this sheet, and return it to USACERL. As user of this report, your customer comments will provide USACERL with information essential for improving future reports.

1. Does this report satisfy a need? (Comment on purpose, related project, or other area of interest for which report will be used.)

_____

_____

_____

2. How, specifically, is the report being used? (Information source, design data or procedure, management procedure, source of ideas, etc.)

_____

_____

3. Has the information in this report led to any quantitative savings as far as manhours/contract dollars saved, operating costs avoided, efficiencies achieved, etc.? If so, please elaborate.

_____

_____

4. What is your evaluation of this report in the following areas?

   a. Presentation: _____

   b. Completeness: _____

   c. Easy to Understand: _____

   d. Easy to Implement: _____

   e. Adequate Reference Material: _____

   f. Relates to Area of Interest: _____

   g. Did the report meet your expectations? _____

   h. Does the report raise unanswered questions? _____

i. General Comments. (Indicate what you think should be changed to make this report and future reports of this type more responsive to your needs, more usable, improve readability, etc.)

_____

_____

_____

_____

_____

_____

5. If you would like to be contacted by the personnel who prepared this report to raise specific questions or discuss the topic, please fill in the following information.

Name: _____

Telephone Number: _____

Organization Address: _____

_____

_____

6. Please mail the completed form to:

Department of the Army
CONSTRUCTION ENGINEERING RESEARCH LABORATORIES
ATTN: CECER-TR-I
P.O. Box 9005
Champaign, IL 61826-9005

REPORT DOCUMENTATION PAGE

Form Approved
OMB No. 0704-0188

Public reporting burden for this collection of information is estimated to average 1 hour per response, including the time for reviewing instructions, searching existing data sources, gathering and maintaining the data needed, and completing and reviewing the collection of information. Send comments regarding this burden estimate or any other aspect of this collection of information, including suggestions for reducing this burden, to Washington Headquarters Services, Directorate for information Operations and Reports, 1215 Jefferson Davis Highway, Suite 1204, Arlington, VA 22202-4302, and to the Office of Management and Budget, Paperwork Reduction Project (0704-0188), Washington, DC 20503.

1. AGENCY USE ONLY *(Leave Blank)*	2. REPORT DATE	3. REPORT TYPE AND DATES COVERED
	February 1998	Final

4. TITLE AND SUBTITLE
Fiber-Reinforced Polymer Composite Materials Systems to Enhance Reinforced Concrete Structures

5. FUNDING NUMBERS
CPAR
LW4

6. AUTHOR(S)
Orange S. Marshall Jr., John P. Busel, Pamalee A. Brady, Douglas S. Barno, Peter Bong, M. Arockiasamy, Alexander M. Vaysburd, S

7. PERFORMING ORGANIZATION NAME(S) AND ADDRESS(ES)
U.S. Army Construction Engineering Research Laboratories (USACERL)
P.O. Box 9005
Champaign, IL 61826-9005

8. PERFORMING ORGANIZATION REPORT NUMBER
TR 98/47

9. SPONSORING / MONITORING AGENCY NAME(S) AND ADDRESS(ES)
Headquarters, U.S. Army Corps of Engineers
ATTN: CEMP-ET
20 Massachusetts Ave. NW
Washington, DC 20314-1000

10. SPONSORING / MONITORING AGENCY REPORT NUMBER

11. SUPPLEMENTARY NOTES
Copies are available from the National Technical Information Service, 5285 Port Royal Road, Springfield, VA 22161.

12a. DISTRIBUTION / AVAILABILITY STATEMENT
Approved for public release; distribution is unlimited.

12b. DISTRIBUTION CODE

13. ABSTRACT (Maximum 200 words)

The use of fiber-reinforced polymer (FRP) composites was investigated for purposes of enhancing, protecting, repairing, or upgrading reinforced concrete structures. Design methods and repair applications were addressed, as were durability issues and in-field test methods for performance verification.

Investigations included shear rehabilitation techniques for concrete beams, in-field test methods to determine the bond strength of FRP composites, and low-temperature evaluation of FRP performance. Field demonstrations included evaluation of carbon fiber-reinforced polymer tendons for post-tensioning of double-tee beams and wall repair at a sewage treatment facility. Also, a feasibility study and laboratory tests were performed to evaluate glass fiber-reinforced polymer cables as tie-back tension members, and a test fixture was designed and fabricated to evaluate post-stressing tendon drape angle performance. Design examples were developed for shear upgrade of concrete beams, post-tensioning of double-tee beams, and tie-back rod arrangements. Finally, a model was developed to predict failure mechanisms for reinforced concrete beams with FRP sheets or plates bonded to the bottom tensile face.

14. SUBJECT TERMS
CPAR
civil engineering
fiber-reinforced concrete
composite materials

15. NUMBER OF PAGES
390

16. PRICE CODE

17. SECURITY CLASSIFICATION OF REPORT	18. SECURITY CLASSIFICATION OF THIS PAGE	19. SECURITY CLASSIFICATION OF ABSTRACT	20. LIMITATION OF ABSTRACT
Unclassified	Unclassified	Unclassified	SAR

Foreword

This study was conducted for Headquarters, U.S. Army Corps of Engineers under the Construction Productivity Advancement Research (CPAR) program; Work Unit LW4, "Development and Demonstration of Advanced Composite Materials Systems to Enhance/Protect or Repair/Upgrade Reinforced Concrete Civil Engineering Structures." The technical monitors were M.K. Lee (CECW-EG), D. Chen (CEMP-ET), and C. Harris (CEMP-CE).

The work was performed by the Materials Science and Technology Division (FL-M) of the Facilities Technology Laboratory (FL), U.S. Army Construction Engineering Research Laboratories (USACERL). The CPAR Industry Partner was the Composites Institute (CI) of the Society of Plastics Industries (SPI), Catherine A. Randazzo, Executive Director. The USACERL Principal Investigator was Orange S. Marshall Jr., and the CI Principal Investigator is John P. Busel. The USACERL Associate Investigators are Pamalee A. Brady and Richard G. Lampo. Peter Bong is a USACERL student contractor assisting in the study. CPT Curtis L. Decker assisted in the experimental testing. James Gambill and William Gordon performed the instrumentation design and application and conducted the laboratory testing at USACERL. Douglas S. Barno is Consulting Director, Market Development, CI. Dr. M. Arockiasamy is a professor and director of the Center for Infrastructure and Constructed Facilities at Florida Atlantic University. Alexander M. Vaysburd is Director, Research and Development, at Structural Preservations Systems, Inc. Dr. Srinivasa L. Iyer is professor of Civil Engineering at South Dakota School of Mines and Technology. Dr. Piyush K. Dutta is a Principal Investigator at the U.S. Army Cold Regions Research and Engineering Laboratory. Dr. Marco Arduini is Technical Officer at the University of Bologna, Italy, and Dr. Antonio Nanni is the V&M Jones Professor of Civil Engineering at the University of Missouri, Rolla. Dr. Ilker R. Adiguzel is Acting Chief, CECER-FL-M, and L. Michael Golish is Acting Chief, CECER-FL.

COL James A. Walter is the Commander of USACERL and Dr. Michael J. O'Connor is Director.

Contents

SF 298 iii

Foreword iv

List of Figures and Tables vii

1 Introduction 1

Background 1
Objective 2
Approach 3
Units of Weight and Measure 6

2 FRP Composites as Construction Materials 7

Definition of Composites 7
Barriers to Using Composites in Construction 9
Current Materials Systems 10
Survey of Existing Concrete Repair Technologies 12

3 Technical Needs For FRP Repair Of Reinforced Concrete Structures 15

Applications Needed 15
Addressing End-User Concerns 15
Performance Considerations 16
Need for Specifications 19
Fireproofing 19

4 Design Methods and Repair Applications 21

Shear Rehabilitation of Beams Using FRP Overlays 21
Strengthening Damaged Reinforced Concrete Beams Using CFRP Tendons 30
Computer Modeling of Repair/Upgrade of Reinforced Concrete Beams 33
Feasibility Study of Using FRP Tendons/Rods for Tie-back Applications 35

5 Test Methods for Performance Verification 39

Established FRP Composite Inspection Techniques 39
Field Inspection Technique for Bond Strength 39
FRP Tendon/Rod Drape Angle Test Fixture 42

6 FRP Bond Durability 44
Effects of Severe Environments 44
Thermal Effects on FRP Bond 45

7 Conclusions, Recommendations, and Commercialization 53
Conclusions 53
Recommendations 57
Commercialization and Technology Transfer 58

References 63

Glossary 68

Appendix A: FRP Repair of Reinforced Concrete Beams With Insufficient Shear Capacity A1

Appendix B: Strengthening Damaged Reinforced Concrete Beams Using CFRP Tendons B1

Appendix C: Parametric Study of Beams With Externally Bonded FRP Reinforcement C1

Appendix D: Feasibility Study on Using GFRP for Tie-Back Arrangements D1

Appendix E: Low-Temperature Evaluation of FRP Composites Bonded to Concrete E1

Appendix F: Evaluation of In-Field Test Methods to Determine Bond Strength of CFRP Repair Systems for Reinforced Concrete F1

Appendix G: Tendon Drape Angle Test Fixture Specification G1

Appendix H: Specifications for Clark-Schwebel Tech-Fab Structural Grids H1

Distribution

List of Figures and Tables

Figures

All figures are located at the end of respective appendices

Tables

Table 2.1. General system descriptions of alternative FRP composite concrete repair materials. 8
Table 2.2. Technical barriers to new FRP composite technology deployment. 9
Table 2.3. Institutional barriers to new FRP composite technology deployment. 10
Table 2.4. Types of FRP composite materials systems for concrete repair. 11
Table 2.5. Comparison of FRP material systems. 12
Table 3.1. FRP composite opportunity matrix for externally reinforced concrete structures. 15
Table 3.2. Outline of proposed ACI guideline document. 20
Table 4.1. Composite material properties. 23
Table 4.2. Principal experimental test results for hybrid joists. 26
Table 5.1. Established nondestructive evaluation techniques for composites. 39

1 Introduction

Background

Many of the nation's bridges and other civil engineering structures are deteriorating due to problems with reinforced concrete. This problem includes the U.S. Army Corps of Engineers (USACE) infrastructure, much of which has long exceeded its design life and is seriously deteriorating. Factors contributing to this deterioration include the effects of the environment (harsh climate, application of de-icing salts, seismic activity, etc.), the increase in the amount and weight of truck traffic, and the general under-design of older structures that are needed to satisfy today's demands.

Many critical structures are located in areas of potential seismic activity. Earthquakes over the past decade in southern California have demonstrated the need for civil engineering structures with greater seismic resistance; reinforced concrete structures throughout the affected area were extensively damaged or destroyed.

Affordable solutions to extend the useful life of existing structures, or to protect them against earthquake damage, are needed. Developing practical and commercially viable methods for the *in situ* protection, repair, or upgrade of civil engineering structures is of high priority. One promising way to address this need is to use advanced composite materials systems and application techniques that would permit *in situ* repair or seismic upgrade while providing long-term protection from deterioration.

Many benefits may be expected to arise from the use of externally applied composites to enhance reinforced concrete beams, columns, and structural decks. These include high strength-to-weight ratio, resistance to corrosion, relative ease of application, minimal disruption of traffic during application, minimal maintenance, and greater durability compared to traditional construction materials. By developing advanced composite materials systems to enhance and protect existing reinforced concrete structures, or repair and upgrade undamaged existing structures, billions of dollars may be saved while ensuring uninterrupted operations and human safety. Such systems also could

be exported or licensed internationally, thereby promoting expanded markets for the U.S. construction materials industry.

Investigation and demonstration of such beneficial composites-based systems for reinforced concrete applications were authorized under the USACE Construction Productivity Advancement Research (CPAR) program. The lead CPAR USACE Laboratory was the U.S. Army Construction Engineering Research Laboratories (USACERL), Champaign, IL. Other participating laboratories were the U.S. Naval Facilities Engineering Services Center (NFESC), Port Hueneme, CA; the U.S. Army Cold Regions Research Laboratory, Hanover, NH; and the U.S. Army Waterways Experiment Station, Vicksburg, MS. The Industry CPAR Partner was the Composites Institute, New York, NY. Other participating organizations (i.e., "Partner Participants") were the American Concrete Institute (ACI), Detroit, MI; the American Society of Civil Engineers (ASCE), Washington, DC; the California Department of Transportation (CALTRANS); and the Federal Highway Administration (FHWA), McLean, VA.

Properly designed and manufactured advanced composite upgrade/repair systems can and should be compatible with current construction industry practices. Although it is likely that many advanced composite upgrade/repair systems will require new combinations of existing materials and new fabrication processes, this investigation was executed using modifications of current composite-fabricating processes to produce the required shapes and materials combinations. Application and installation techniques will generally be variations on accepted industry practice, so the chance of success is high and the potential payback from success of this project is exceptional.

Objective

The objective of this work was to develop, test, demonstrate, and commercialize advanced composite materials systems for in-place strengthening, repair, or upgrade of concrete civil engineering structures including bridge columns, beams, and decking. Systems developed in this CPAR will enhance structural protection against seismic damage as well as rehabilitate or upgrade deteriorated civil engineering structures.

Approach

This project was conducted according to the CPAR-CRDA work plan shown below.

Phase I

Task A: Identify Structural System Requirements for Concrete Columns, Beams, and Decking

A1. Define mechanical and operational environment requirements, e.g., thermal, chemical, and periodic conditions including projected seismic loading conditions (USACERL, CI).

A2. Define physical performance requirements (USACERL, CI).

A3. Define installation and jobsite requirements (USACERL, CI).

A4. Establish cost targets for materials, labor, and installed systems (USACERL, CI).

Task B: Survey and Document Related Existing Systems Technologies

B1. Survey existing repair/upgrade technologies and experiences (all material types) in the U.S., Western Europe and Japan (USACERL, CI).

B2. Characterize and compare to identified requirements and needs from Task A (USACERL, CI).

B3. Determine performance/design/cost deficiencies of existing systems (USACERL, CI).

Task C: Develop Preliminary Designs for a Family of Innovative Advanced Composite Materials Systems for Repair/Upgrade of Concrete Civil Engineering Structurals

C1. Assess design enhancement potential for most promising existing systems (USACERL, CI).

C2. Develop preliminary designs (and new forms of materials if required) to meet the identified mechanical, physical, operating, and installation requirements from Task A (USACERL, CI).

C3. Model new or enhanced designs using computerized techniques (USACERL, CI).

Phase II

Task D: Fabrication Specimens for Laboratory Testing

D1. Fabricate laboratory test specimens (CI).

D2. Obtain selected commercial systems for comparisons (CI).

Task E: Develop and Conduct Laboratory Testing of Model Systems

E1. Assess mechanical properties against relevant environmental conditions e.g., temperature, humidity (USACERL, CI).

E2. Assess results relative to optimized designs and manufacturing processes (CI).

E3. Review designs with peer group of expert practitioners to validate the design assumptions and suitability for workplace conditions (CI).

E4. Conduct coupon and scale-modeled tests (USACERL, CI).

Task F: Conduct Full-Scale Testing on Selected Systems

F1. Select systems for full-scale testing (USACERL, CI).

F2. Conduct tests and analyze results (USACERL, CI).

Phase III

Task G: Select Most Promising Systems

G1. Analyze all results to date and, in cooperation with peer review group, select systems for further development (USACERL, CI).

Task H: Enhance/Optimize Designs, Materials, Manufacturing and Installation Processes

H1. Enhance designs for performance improvement (USACERL, CI).

H2. Optimize materials for cost and performance (CI).

H3. Investigate manufacturing methods optimization (CI).

H4. Optimize installation techniques (USACERL, CI).

Task I: Design and Construct Full-Scale Demonstration Test Facilities at Selected Sites

I1. Site and facilities selection (USACERL, CI).

I2. Design, fabrication, and construction (USACERL, CI).

I3. Instrumentation systems for performance monitoring. Link to current "Smart Composites" CRDA between USACERL and CI (USACERL, CI).

Phase IV

Task J: Commercialization/Technology Transfer Plans

J1. Development of material system specifications and design and construction standards (USACERL, CI).

J2. Recommend/leverage the adoption of specifications and standards as well as design guidance within the civil engineering community, e.g., Corps of Engineers, FHWA, and other Federal agencies, e.g., ASCE, ASTM, AASHTO, etc. (USACERL, CI).

J3. Promote widespread national commercialization of optimized advanced composites materials systems for repair/upgrade of concrete civil engineering structures (CI).

J4. In association with ACI, ASCE, and AASHTO, organize and conduct a series of national workshops/seminars to promote the commercial use of optimized advanced composites materials systems for the repair/upgrade of concrete civil engineering structures (CI).

Task K: Final Report (USACERL, CI).

Units of Weight and Measure

U.S. standard units of measure are used throughout this report. The table below may be used to convert these units into Standard International (SI) units.

SI Conversion Factors

To convert from these units	To these units	Multiply by
in	mm	25.4
in^2	mm^2	645.16
in^3	mm^3	16387
in^4	mm^4	416231.4
ksi	kPa	6894.76
Msi	MPa	6894.76
kips	kN	4.45
ft	m	0.3048
ft^2	m^2	0.0929
psi	Pa	6894.76
psf	kg/m^2	4.882
°F	°C	5/9 (°F - 32)
lb	gm	453.59
lbf	N	4.45

2 FRP Composites as Construction Materials

Definition of Composites

The generic definition of composites is a combination of two or more materials (constituents) differing in form or composition on a macroscale, yet the constituents retain their identities (i.e., they do not dissolve or merge into each other) and act in concert to perform a particular function. For the purposes of this report the term "FRP," or fiber-reinforced polymer, is used to identify any form of composite material. The definition of an FRP composite used in structural/civil applications is "A matrix of polymeric material that is reinforced by fibers or other reinforcing material" (Composites Institute 1995a). This includes thermosets, thermoplastics, or elastomers that are reinforced by fibers or other material with a significant aspect ratio of length to width. Other terminology for composites include fiber-reinforced plastic, glass fiber reinforced plastic (GFRP), carbon fiber-reinforced plastic (CFRP), reinforced plastics (RP), and others. Classical composites comprise a polymer matrix (polyester, vinylester, epoxy, phenolic, thermoplastic, etc.) which is reinforced with fibers (glass, carbon, aramid, etc.), in much the same way as concrete is reinforced with steel. The fabrication of composites is just as important as the materials. Depending on the application, performance requirements, size, production volume, production rate, cost, and others, composites can be produced by over ten different methods.

Composites have been used for more than 50 years. Composite materials have demonstrated to be instrumental in high-performance applications where traditional materials have failed, especially in aggressive environments. Currently, FRP composites are tracked in eight different market segments. They are transportation, construction, marine, business equipment, corrosion-resistant equipment, electrical, consumer, and aircraft/aerospace. Composites are used mostly in transportation, followed by construction. According to the Composites Institute, 1997 shipments of composites reached 3.2 billion pounds. Composites account for approximately 5% of the annual output of the U.S. plastics industry (Composites Institute 1995a). The use of FRP composites in specific infrastructure applications has been shown to be technically superior, however, commercial deliveries in this market are low compared to the current markets, and are therefore not tracked. The Composites Institute Market

Development Alliance believes that the infrastructure market is potentially huge and is dependent on the proper selection of materials for the right applications.

Composite materials offer many advantages over conventional materials. Properly designed and fabricated composite products provide one or more of the following benefits (Composites Institute 1995b):

- high strength
- oriented strength
- light weight
- high strength-to-weight ratio
- corrosion resistance
- parts consolidation
- design flexibility
- low maintenance
- dimensional stability
- high dielectric strength
- low tooling cost
- recyclability
- ability to incorporate post-consumer and post-industrial materials.

To deliver these benefits, FRP composites can be produced in a variety of forms. The considerations an engineer may encounter are shown in Table 2.1.

Table 2.1. General system descriptions of alternative FRP composite concrete repair materials.

Consideration Item	Alternatives
Fiber reinforcement constituents	Glass, carbon, aramid
Polymer constituents	Polyester, vinyl ester, epoxy
Forms	Woven or stitched fabric, unidirectional sheet, tow or yarn, prepreg, preform, laminate plate, rod/cable, or hybrid fibers/reinforcements
Application methods	Hand lay-up, filament winding, vacuum assisted-resin transfer molding, any compaction process
Matrix binder or adhesive	Polyester, vinyl ester, epoxy, polyurethane
Curing process	Ambient temperature cure, elevated temperature cure
Protective finish/Coating	Filler & Additives: UV, fire, moisture, chemical, etc.

Effective application of composites technology will promote the development of:

- stronger, more efficient structures that incorporate traditional materials
- tailored composite properties that complement traditional materials
- new combinations of materials whose total performance exceeds the limits of performance of either material by itself
- composites that take full advantage of the properties of each constituent material
- greater construction site productivity
- the ability to repair existing civil engineering structures *in-situ* or upgrade to enhance performance (ACI 440, April 1995).

Barriers to Using Composites in Construction

FRP structural composite technology holds great promise for the U.S. civil engineering infrastructure and construction industry, but several barriers must first be overcome. These barriers fall into two categories: technical and institutional. Technical barriers are engineering, scientific, manufacturing, or operational problems that prevent the acceptance of new technologies into existing markets. Economic necessity requires FRP structural composite products to (1) be cost-competitive or less expensive on a first-cost (installed) basis, (2) provide significant life-cycle cost advantages, and (3) be constructed (at least for the first several product generations) using current standard industry practices. Specific technical barriers are summarized in Table 2.2.

Table 2.2. Technical barriers to new FRP composite technology deployment.

Technical Barrier	Primary Influence Factor
Lack of end-use performance standards	ASCE, ACI, CoE, etc.
Characterization of mechanical and physical properties	ACI, CI
Design calculations via credible third-party	ACI, CI
Cost (first cost, life-cycle, etc.)	CI
Constructability (adhesive vs. mechanical bonding, etc.)	CI, CoE
Durability (properties retention, fire performance, etc.)	ACI, CI
Test methods (long term and accelerated)	ASCE, ACI, CI

Institutional barriers relate to the conservative nature of the construction industry, the fear of liability, and the lack of 50 years of in-place structural performance data. Also, there is little interaction between the composites industry and the construction industry. Specifically, there are few communication channels or technology transfer mechanisms in place among the

composites industry, civil engineers, and specifiers. Institutional barriers are summarized in Table 2.3.

Table 2.3. Institutional barriers to new FRP composite technology deployment.

	Primary Influence Factors			
Barrier/Critical Issue	**USACERL**	**Lab Participants**	**CI**	**Partner Participants**
Low U.S. civil engineering R&D investment	X	X		ACI, ASCE, CERF, CONREF
Little or no "industrial" R&D			X	ACI, ASCE, CERF, CONREF
Fragmented and decentralized civil engineering industry influence factors	X	X		ACI, ASCE, CERF, CONREF
Liability and litigation				ACI, ASCE, CERF, CONREF
Codes and specifications (complex, decentralized, duplicating & overlapping)	X	X		ACI, ASCE, CERF, CONREF
Lack of practitioner education	X	X	X	ACI, ASCE, CONREF
Contract Delivery System (public sector)	X	X		
Industry-specific issues • Multiple pre-competitive technologies • Reluctance to share proprietary technologies • Limited U.S. based technologies			X X X	
Difficulty in securing demonstration sites	X	X		ACI, ASCE, CERF, CONREF
Involvement/support from other CoE labs	X	X		

Current Materials Systems

Currently, there are composite material systems that are used in both demonstration and commercial jobs to repair, upgrade, or strengthen reinforced concrete structures. These systems are summarized in Table 2.4.

The selection of the proper FRP composite materials for a specific application may vary depending on job site conditions, material performance, and cost. These systems are summarized in Table 2.5.

Table 2.4. Types of FRP composite materials systems for concrete repair.*

Type of System	Material Supplier/Product Name	Basic Materials
Hand Wet Layup of Unidirectional Tape, Sheets or Fabric	Tonen Corporation/Forca Tow Sheet™ (MBrace Composite Strengthening System - joint effort with Master Builders Inc. and Structural Preservation Systems Inc.	carbon/epoxy
	Mitsubishi Chemical America/Replark™	carbon/epoxy
	Toray Industries Inc. -Mitsui Construction/FITS™ -Sho-Bond Corporation	carbon/epoxy, aramid/epoxy
Hand Layup of Wet Fabric	Fyfe Co. L.L.C. (formerly Hexcel Fyfe L.L.C.)/Tyfo®S Fibrwrap™	E-glass/epoxy carbon/epoxy hybrid fiber/epoxy
Adhesive Bonding of Prefabricated Shells	CMI, Inc./Snap-Tite™ Composite Column Reinforcement System	E-glass/iso-polyester, vacuum molded, urethane adhesive
	Hardcore DuPont L.L.C./Hard Shell™	E-glass/epoxy vinly ester, vacuum-RTM molded, epoxy adhesive
Adhesive Bonding of Precured Sheet Laminate	Sika Corporation/CarboDur™	carbon/epoxy, pultruded laminate, epoxy adhesive
Winding of Prepreg Tow	XXsys Technologies, Inc.(Robo-Wrapper machine)	carbon/epoxy
Wet Winding of Tow	Mitsubishi-Obayashi/Carbon Fiber Retrofitting System (CRS)	carbon/epoxy
In-situ Resin Infusion	Hardcore DuPont L.L.C.	E-glass/vinyl ester
Cables/Tendons/Rods	Mitsubishi Chemical America/Leadline™	carbon/epoxy
	NEPTCO	carbon/epoxy glass/epoxy

* Systems listed in the table were available before the completion of this CPAR project. This study was successful in providing the impetus for developing at least one new FRP composite concrete repair system – Structural Grids, patent pending by Clark-Schwebel Tech-Fab Co., Anderson, SC. The system is described in Chapter 7 under "Technology Transfer and Commercialization."

Table 2.5. Comparison of FRP material systems.

Technique	Characteristics	Issue/Concerns
Wet Layup	Use of a wet bath or impregnator Manual or semi-automated process Ambient cure Flexible Ease of use in restricted areas	Quality control of mix Complete wet-out Nonuniform resin distribution Fiber wrinkling during application Control of cure Environmental issues
Automated Wet Winding	Use of dry tow impregnated in a wet bath Use of continuous fiber Fiber tension assists consolidation Ambient cure	Quality control of mix Complete wet-out Nonuniform resin distribution Control of cure Environmental issues
Automated Prepreg Winding	Automated winding of prepreg tow Control of incoming material Use of continuous fiber Elevated temperature cure Control of application of tow	Prepregging cost and shelf life Space limitations
Adhesive Bonding of Shells	Use of prefabricated sections Adhesive bonding in the field Rapid procedure Ease of fabrication	Lack of fiber continuity Shear lag effect Durability of the adhesive Limited to columns
Adhesive Bonding of Precured Sheet Laminates	Pultruded laminate	Durability of adhesive Compaction of laminate Uniform bondline
In-Situ Resin Infusion	Placement of dry fabric followed by infusion under vacuum Fills cracks in substrate during application Good for nonuniform geometries	Proper wet-out Excessive resin use finished appearance Difficulty in applying vacuum
Tendons/Rods/Cables	Factory manufactured products Easy installation	Dependable anchorage Overall durability

Survey of Existing Concrete Repair Technologies

The concrete repair industry has developed many methods to repair deteriorated concrete surfaces. The repair method chosen is dependent on many factors such as structural loading of concrete member, amount of steel reinforcement, cause of deterioration, site conditions, and cost. Traditional methods vary from using a polymer patching material to full replacement of a concrete member.

Steel plates have been used extensively for more than 20 years in Belgium, France, Japan, Poland, South Africa, Switzerland, United Kingdom, and the United States. In the case of beams, steel plates are attached to the tension face

or to the lateral face of girders to enhance its flexural or shear capacity. The plates are either bolted or bonded in place. Disadvantages of using steel plates include handling large heavy plates, positioning the plates in the proper location, drilling bolt holes where there may be a lack of work space, and most of all, corrosion of the steel plate at the bond line.

The repair of columns or piles has used either bolted or welded steel jacketing. This method demands an extensive site preparation for installation of the jacket. The disadvantages of this method are similar to the application of steel plates to beams.

Post-tensioning is considered one of the most effective methods, and it has a long and widespread history of application. Axially or eccentrically placed tendons are externally post-tensioned to counteract tensile and flexural stresses. Post-tensioning has become an acceptable and relatively common strengthening method because of its practical advantages. Post-tensioning may provide minimal traffic interruption, scaffolding, and site preparation, both tendons and anchorages may be prefabricated, and the application requires relatively accurate fabrication and construction with the ability of monitoring the performance.

Traditional methods, while good, have certain disadvantages that provide unique opportunities for FRP composites. In the past ten years, FRP has been used in many demonstration projects around the world to repair, upgrade/strengthen, and retrofit reinforced concrete members. Many types of FRP products were used to repair beams, columns, slabs, chimneys, and walls. FRP products used were made from either (1) continuous carbon, aramid, or glass fibers impregnated with a polymer (resin), (2) prefabricated preformed geometries such as rods, cables, or plates, or (3) applied in-situ by hand layup using dry fabrics or unidirectional sheets saturated with epoxy resin.

The primary use of the FRP sheet or precured laminate materials was to act in unison with the existing concrete structures by providing increased flexural and shear strength. This was accomplished by transferring a portion of the load into the composite through either a layer of resin or adhesive. The failure mode is an important consideration when using composite materials for retrofit. The most critical failure modes include debonding or sudden peel off of the FRP laminates. It was concluded that the preparation of the substrate as well as the selection and application of adhesive needs careful attention to ensure that classical and noncatastrophic failures predominate.

The literature review found that adhesive bonding of FRP to concrete is expected to be the primary mode of repair/retrofit. Adhesives for the construction industry are classified as solvent free, such as epoxy, polyester, acrylic, and water borne polyvinyl acetate. Selection of adhesives for a specific application depends on the type and magnitude of loads, surface conditions and the anticipated environmental and thermal conditions. The proper application method, including surface preparation and curing conditions, is critical to the development of good bond strength.

In the United States, the use of composite materials for structural retrofit is in the research and demonstration stage. However, in many European countries and particularly in Japan, FRP materials are being used extensively in practical applications. In recent years, FRP composites have been used in many practical applications in the United States as it pertains to seismic upgrades. CALTRANS and the University of California San Diego has led an effort of research and testing to apply composites in many seismic applications, particularly columns.

Japan has used carbon FRP to strengthen beams, columns, slabs, and chimneys. Carbon unidirectional sheets applied in-situ, and carbon tow applied by automation using filament winding are predominate. However, in the mid-1980s, carbon sheets bonded to the tensile side of beams were extensively investigated by Urs Meir at EMPA (Swiss Federal Laboratory). In the United States, glass/epoxy fabric was used for seismic upgrade of columns, beams, and slabs in such applications as bridge piers, slabs, and columns in parking garages, and walls.

Field demonstrations of FRP materials were first conducted in the late 1980s. Various types of structures were repaired, such as reinforced concrete beams and slabs on bridges in Switzerland and columns or chimneys in Japan.

3 Technical Needs For FRP Repair Of Reinforced Concrete Structures

Applications Needed

FRP composite materials have many applications in the repair or upgrade of reinforced concrete structures. Applications where composites have been demonstrated are summarized in Table 3.1. The current project focused on applications for which widespread adoption is feasible. The California Department of Transportation (CALTRANS) has demonstrated leadership and expertise in the design, testing, and analysis of column elements within California. The engineer has not defined a need to use FRP composites for seismic upgrade of beams and slabs. Therefore, the CPAR project focused on other applications, such as repair and strengthening of beams, slabs, and decks.

Table 3.1. FRP composite opportunity matrix for externally reinforced concrete structures.

Reinforcement Service Need	Columns	Beams	Decking
Repair	X	X	X
Strengthening (upgraded service)	X	X	X
Seismic	Other groups	N/A	N/A

Addressing End-User Concerns

The structural engineering profession has the responsibility for ensuring the safety, serviceability, and feasibility of the constructed facility. While some engineers are involved in research and development activities, most are engaged in the design of structures. This includes hundreds of different types of structures, including bridges, buildings, industrial plants, dams, water treatment facilities, power stations, reactors, tunnels, pipelines, and transmission towers. The structural systems for these facilities range greatly.

The protection of life and property requires that safety be the principal focus of the engineer. The engineer must fully understand the environment and use of

the structure and the behavior of the materials of construction. This knowledge is then used to predict structural behavior. An important part of the process is judgment to make allowances for uncertainty involved in the prediction of load effects and structural response.

Serviceability of the structure requires that all aspects of performance be acceptable for the intended use. Deflection and cracking must be limited so that they are virtually invisible to the layperson. Vibration and noise should be controlled. Serviceability requirements constitute an almost limitless list and must be carefully tailored to the needs of the particular structure. The key to meeting a structure's serviceability requirements is a full understanding of the structure's behavior throughout all of its loading and environmental phases. This understanding, in turn, requires a thorough understanding of the materials comprising the structure and its members. Typically, engineers work with a known definition of material properties versus defining material requirements to meet a specific need. This conventional engineering approach cannot capitalize on the many special capabilities of composite materials.

To address the informational needs of prospective users of composites for civil engineering applications, the following approach was taken:

1. Articulate user needs by answering key questions: What does not work using existing (traditional) technologies? What are the disadvantages in past composite/concrete repair applications? What are the needs/recommendations identified from past research on composite applications to civil engineering?
2. Identify codes and engineering protocols for designing with composites. This includes defining the mechanical behavior of FRP systems and determining what processes are appropriate for designing with composites. Additional identification of construction needs is required.
3. Select demonstration programs to address identified user needs. This requires a multifaceted approach by research, government, and commercial sectors of the industry.

Activities toward this end are discussed in the following sections.

Performance Considerations

To assure a reasonable quality for FRP materials systems and minimize the likelihood of repair problems and failures in the newly developing repair and upgrade industry using FRP materials systems, the CPAR team developed minimum performance targets for those systems. If, as a minimum, a repair or

upgrade system does not meet these targets, it is likely that it will not function as well as it is intended for repairing or upgrading concrete structures. In addition, these targets help define minimum criteria for new system developers and for construction specifications.

The following text defines the minimum acceptable performance considerations for an FRP composite concrete repair/upgrade system. The performance considerations are organized into three categories: general requirements, mechanical property requirements, and installation/fabrication requirements.

General Requirements

For all reinforced concrete structurals and structures:

1. Under normal service conditions (e.g., exposure to road salts, alkalines, acids, UV, sea water, fresh water, petroleum products, and environmental thermal cycles) the mechanical properties as defined below shall not degrade more than 40% over the design life of the repair/upgrade.
2. The repair/upgrade system shall have less than 5% increase in weight due to water absorption as determined by ASTM D 570 or equivalent.
3. The repair/upgrade system shall resist adhesion of graffiti materials.
4. The repair/upgrade system shall not exhibit resin cracking over temperature fluctuations from – 20 °F to 140 °F.
5. Damage to the repair/upgrade system due to impact and vandalism shall be repairable to its original mechanical properties.
6. The failure mode of the repaired/upgraded component will be ductile in nature. The system must exhibit cohesive failure and not adhesive failure. The system/component will not fail by buckling.
7. The repair/upgrade system will not degrade anodically.
8. The repair/upgrade system shall have an adhesive strength greater than the cohesive strength of the substrate to which it adheres. The adhesive strength shall not degrade more than 20% over the design life of the repair/upgrade.

For beams, slabs, and decks

Working load deflections of a repair/upgrade will not exceed those of the original element.

For walls

1. Repair/upgrade system will be able to accommodate openings without impairing system strength, stability, and stiffness.

2. In-plane shear resistance will be equal to the original wall or meet upgrade requirements with the appropriate load and resistance factors.
3. The system will limit in-plane horizontal displacement to 1/150 of the height under appropriately factored loads.

For the interior of habitable structures

The repair/upgrade system shall have a fire resistance rating of not less than 2 hr as defined in National Fire Protection Association standards 251, Standard Methods of Fire Tests of Building Construction and Materials, standard 88A, Standards for Parking Structures and ASTM E119 (Methods for Fire Tests of Building Materials). In addition, the system shall successfully pass standard tests for class I flame spread (ASTM E84, Surface Burning Characteristics of Building Materials) and/or equivalents.

Mechanical Property Requirements

1. The repair/upgrade system shall have a Coefficient of Thermal Expansion less than 15 x 10^{-6} in/in/°F (8.33 x 10^{-6} mm/mm/°C) as determined by ASTM D 696 or equivalent.
2. Long term exposure to UV shall not degrade the matrix and expose reinforcing fibers for the design life of the system.
3. Long term stress relaxation of prestressed repair/upgrade elements will be limited to 15%.

Installation/Fabrication Requirements

1. Voids in the system shall not exceed 0.75 in^2 (484 mm^2) per yd^2 (m^2) or 2% of the matrix volume, whichever is less as determined by ASTM D 2734 or equivalent.
2. The repair/upgrade system shall have a fiber content of not less than 35% as determined by ASTM D 3171 or equivalent.
3. The degree of cure for the system shall be sufficient to meet the performance requirements and mechanical properties above.
4. Installation of the system shall not require worker air supply for worker safety. Under normal installation and service conditions it shall have no negative impact or pose a hazard to the environment.
5. No refrigeration of composite materials will be needed on site. All materials must be handled in all weather conditions from 40 °F to 100 °F (4 °C to 38 °C).
6. NDE test methods or in-situ instrumentation in conjunction with production control panels will be utilized to assure quality control.

7. Jobsite materials handling and waste disposal shall comply with OSHA and EPA regulations. The maximum practical recycle of waste materials will be incorporated.

Need for Specifications

As part of the in-kind support of this work from the American Concrete Institute (ACI), Committee 440F is currently working on a guidance document entitled "Guidelines for Selection, Design, and Installation of Fiber Reinforced Polymer (FRP) Systems for Externally Strengthening Concrete Structures." The purpose of this guideline is twofold: (1) to provide information that the engineer may use to select one or more commercially available FRP systems and (2) to develop a structural design to improve the structural performance of a reinforced concrete structure using externally bonded FRP reinforcement. An outline of the guideline's subject matter is shown in Table 3.2. The document is planned for publication in 1998.

In addition to the ACI 440F document, ASTM created several new committees that are focused to create standard test methods for concrete repair material systems. Committee ASTM D20.18.01 was created to develop test methods for reinforcement for concrete. A working subcommittee was tasked with developing test methods to evaluate the performance of tendons used for post-tensioning, as well as bond strength for externally applied laminates. The objective of the bond strength test methods was to provide an in-field testing method to determine the quality of the FRP materials used for concrete repair. This document is currently in writing by the committee. No timetable has been established for the release of this test method.

Fireproofing

The effects of extreme high temperature, such as a building on fire, are usually only a concern if the repair or upgrade is on the interior of an occupied structure. While it is often an initial concern, fireproofing is rarely a critical issue since most FRP composite repair and upgrade applications supplement existing steel reinforcing in the structure and are not normally used to completely support the structure. This is why steel plate bonding has been an acceptable repair procedure for many years. Each FRP composite material system supplier specifies its own fire protection system based on the application. Fire protection systems may be in the form of spray-applied resin matrix coatings that have fire inhibitor additives. Another form that may be acceptable

for building applications is fiber insulation boards intended for protecting the FRP composite materials. The fire protection system should be certified for the specific system and application by a code-writing body such as Underwriters Laboratories®.

Table 3.2. Outline of proposed ACI guideline document.

CHAPTER	TOPIC
1.0	Introduction Scope - Background - Economics and Cost of Alternatives
2.0	General Requirements - Assessment of Existing Structure - Structural Design of Needed Strengthening - Durability and Modes of Deterioration - Acceptance of Proprietary Systems - Drawings and Specifications
3.0	Properties of Materials - Resins - Fibers - Composite Product Forms
4.0	Assessment and Evaluation of Existing Structures - Condition of Overall Structure and Its Members - Condition of Concrete
5.0	General Design Considerations
6.0	Structural Design of Repairs - FRP Composite Design - Design Philosophy - Changing Modes of Structural Behavior - Temporary Shoring Needs for Construction - Differences in E-Modulus of Substrate and FRP Laminates - Flexure - Tension - Shear - Fatigue - Ply Layup Design - Detailing Laps and Splices - Selection of Protective Coating
7.0	Shipping, Storage, and Handling
8.0	Preparation of Concrete Surfaces
9.0	Installation Procedures
10.0	Quality Control and Quality Assurance
11.0	Glossary

4 Design Methods and Repair Applications

Shear Rehabilitation of Beams Using FRP Overlays

Overview

In a previous CPAR study (Saleh et al. 1997), prefabricated reinforced concrete hybrid joists were tested in four-point bending to assess their flexural strength. During tests, two joists failed at between 3.5 and 4 in. of midspan deflection whereas similar joists from the same study achieved midspan deflections of more than 10 in. Crack patterns indicated a shear failure caused by insufficient shear reinforcement. Two remaining joists (the same type that failed prematurely) were made available for the current study to evaluate the effectiveness of FRP composites in improving shear capacity of deficient beams. A detailed description of the study is presented in Appendix A.

FRP Significance

Previous studies of rectangular beams have shown that FRP wraps of the full cross section improve the load capacity of the section. The challenge of applying an FRP wrap to a beam with an integral slab and the benefits of such an upgrade have not been assessed. The technology has potential application to highway bridges constructed in accordance with ACI codes of the 1950s and 1960s where these bridges may have less shear capacity than flexural capacity or require added load capacity. A proven repair method for this application may provide a cost-effective solution for military installations and Corps of Engineers civil works facilities as well as state departments of transportation.

An innovative method of beam shear repair involves the use of FRP externally bonded to the faces of the member where shear capacity is deficient. Several schemes are available: FRP plates bonded to the sides, strips of FRP material bonded to the sides, or a jacket or wrap placed along the shear span. FRP addresses the traditional material weaknesses of steel. FRP is not susceptible to corrosion and is relatively conducive to field prepping and hand lay-up. There have been several studies investigating the use of externally bonded FRP sheets (Al-Sulaimani et al. 1994; Chajes et al. 1995; and Norris et al. 1997) to improve strength and stiffness of R/C beams. However, most studies have dealt with

improving flexural strength. Only a few studies specifically addressed shear. Following is a discussion of test results of full scale prestressed high-strength concrete joists which had insufficient shear reinforcement and were strengthened in shear with FRP.

Experimental Program

Two concrete joists repaired or upgraded with FRP were tested under four-point bending. The results of these tests were compared with those of two control specimens. One control specimen was properly reinforced, HJ-7, and one, HJ-6, had insufficient shear reinforcement. Of the two joists tested in this program, HJ4, was loaded to a point where shear cracks developed. The joist was unloaded and an FRP system applied. The same FRP system was applied to another joist, HJ-3, prior to any loading. Following curing of the FRP system, the joists were instrumented and tested to evaluate their improved shear performance. There was no attempt to increase the flexural capacity of the joists beyond that provided by internal steel reinforcing.

Test Specimens

The hybrid joist design used in the experiments is intended to combine the benefits of prestressed concrete double tees and open-web steel joists. It was envisioned for use in office construction. A length of 32 ft and a tributary width of 4 ft were chosen for the initial design. Loads of 50 pounds per square foot (psf) office live load and 20 psf superimposed dead load were assumed. All loads were assumed to be uniformly applied along the joist length. This resulted in a superimposed total uniform service load of 70 psf and an ultimate load of 113 psf.

The overall configuration of the joist is shown in Figure A.1. Six prestressing tendons were used, two straight and four draped. The cast-in-place concrete flanges of HJ-3 and HJ-4 had a thickness of 4 in. and width of 6 ft. The flanges of control joists HJ-6 and HJ-7 were 4 ft wide. The concrete mix used in the hybrid joist specimen webs was a high-performance concrete (HPC) with a design strength of 12,000 psi at 28 days. Ready-mixed concrete was used in the slabs of all specimens. The mix was specified to be 5000 psi. The tendons used were manufactured by the American Spring Wire Corporation (26300 Miles Rd., Cleveland, OH 44146). These tendons were 1/2 in. diameter, 270 ksi, low relaxation. Shear reinforcement in the webs consisted of bar reinforcement, Grade 60. A welded wire fabric mesh, Grade 75, was used as reinforcement for the cast-in-place slab. Detailed descriptions of each joist design are provided in Saleh, Brady, Einea, Tadros, and Decker (1997).

Performance criteria were specified for the two joists to be repaired. It was required that their shear capacity be increased 15 kips over a length 3 ft-10 in. from each end and 10 kips over the following 4 ft. HJ-3 and HJ-4 were wrapped on three sides with Fyfe Company's TYFO S Fibrwrap™ along the outer 8 ft of each end. Standard structural engineering practice for shear designs was used to determine the jacket thickness. Calculations were based on controlling shear crack widths to maintain aggregate interlock and proper shear transfer through the concrete. The FRP was specified as TYFO S Fibrwrap™ System and manufactured by the Fyfe Co. It consisted of two layers of SEH-51 fabric saturated with TYFO S epoxy. Table 4.1 lists the composite properties. The allowable jacket strain, ε_{aj} = 0.004, represents 20% of the ultimate composite strain. The calculations resulted in the requirement for two layers of SEH-51, with the main fiber strength vertical, over the extreme 4 ft. The next 4 ft required only one layer per the calculations however Fyfe Co. recommended the use of a minimum of two layers (Gee 1996). No additional anchorage system was used due to the potential interference with the prestressing tendons of the existing joist.

Table 4.1. Composite material properties.

Property	Value	Test Method
Tensile Strength at 0° (ksi)	65	ASTM D3039
Tensile Strength at 90° (ksi)	6.0	ASTM D3039
Elastic Modulus (ksi)	3,250	
Ultimate Strain	0.02	ASTM D3039
Coefficient of Thermal Expansion	4.3×10^{-6}	

Prior to application of the composite overlay the joist surfaces were prepared. Paint on the outer 8 ft of the webs was removed; beam corners were rounded to a minimum radius of 1.5 in., and smoothing of the concrete faces where CFRP was to be applied was done using an electric grinder. Once completed, creases in the web left by concrete form lining were filled with a rapid strength repair mortar. After the mortar was cured, the surface of the beams was again ground and then cleaned. Cracks in the concrete of HJ-4 created during pre-loading were not filled as they were less than 1/16 in. wide. The two part epoxy TYFO™ S Tack Coat was mixed and troweled onto the surface of the beams where the repair/upgrade was to be applied. While the tack coat began setting up, the reinforcing fabric was cut to the proper length and infused with the TYFO™ S two part epoxy. The fabric was then laid up around the end of the joist from just beneath the slab, around the web and up to the slab/web intersection again The material was placed vertically (main fibers vertical) in bands of 4 ft (1.2m).

Adjacent bands were placed with a butt splice. In regions of taper, the bands were applied as four pieces, two per side ensuring that main fibers remained vertical on joist faces. The material was carried under the joist where permitted. Figure A.3 shows a repaired joist.

Because of lack of Cab-O-Sil™ in the tack coat, the system applicators had great difficulty getting the FRP system to adhere properly to the concrete prior to curing. The cure time was also slow because of high atmospheric humidity. Upon cure it was noted that the FRP had slipped down on both HJ-3 and HJ-4. A gap, uncovered by FRP, existed beneath the bottom of the slab on the web. In most locations the gap was not significant; however, on the North end of HJ-3 the gap was observed to be 1.25 in., Figure A.9. After curing, voids between the composite and the joist were filled with epoxy.

Test Instrumentation and Setup

Test specimens HJ-3, HJ-4, HJ-6, and HJ-7 were instrumented with displacement potentiometers, strain gages and linear variable displacement transducers. Internal strain gages were located so as to measure strains in both prestressing tendons and reinforcement. Strain gages were placed on the external FRP surface at the locations of the most dramatic shear cracks, other previous shear failure areas, and at the FRP lap joints to monitor strain in the composite. Gages were symmetrically placed at each end of the joists. Displacements were measured by potentiometers at the center of the joist, beneath one web post and a distance 25% of the span length from a support along the inclined portion of the joist. All recorded potentiometer displacements were absolute, measured with respect to the laboratory floor. Displacement measurements were also taken manually on the west and east faces of the slab at each joist end, and along the east slab face at the center and beneath each actuator.

The test setup on the USACERL Structural Load Floor is shown in Figure A.17 Each specimen was tested as a simply supported beam under two symmetrical point loads with a clear span of 31 ft and a shear span of 11 ft - 3 in. Vertical loads were applied by 50-kip hydraulic actuators suspended from a load frame. The actuators were centered directly over the web posts of the specimens and were operated under stroke control. Specimens were loaded at a constant rate to a specified stroke limit. The actuators were maintained at this stroke while the joist was inspected for cracks; these were marked. Measured readings of deflections were taken at selected locations and the deflection data were checked. The test was continued until the specimen failed or the deflection limit of the test set-up was reached. Data were recorded throughout the test.

Of the two repaired specimens, HJ-4 was damaged to a predetermined level defined subsequent to testing the control beams, which were unrepaired. The beam was then unloaded and repaired. Loading of HJ-4 continued until the bottom of the joist was ¼ inch from the load floor. The joist was then unloaded. HJ-3 was not loaded prior to upgrading it with FRP. It was loaded in the same manner as HJ-4. HJ-3 was tested to failure.

Experimental Results

The measured load and deflection, strains in FRP, and crack development and failure of each specimen are discussed. Results of the two repaired beams are compared with two control beams.

The experimental load versus midspan deflection curves for joists HJ-3, HJ-4, HJ-6, and HJ-7 are shown in Figure A.18. Table 4.2 summarizes principal test results, including cracking load, location of first crack, failure load, equivalent uniform superimposed (SI) load at failure for the test configuration, and type of failure. The FRP repaired joist, HJ-4 resisted a peak load of 56.6 kips, approximately 690 percent of the SI service load or 422 percent of the SI ultimate load. The upgraded joist HJ-3 failed at a load of 52.6 kips, 393 percent of the ultimate SI design load. The two control joists, HJ-6 and HJ-7, failed at 48.7 kips, and 65.0 kips respectively. HJ-6 failed at well below the anticipated capacity but still 363 percent of the ultimate superimposed service (SI) design load. The premature failure was attributed to insufficient shear reinforcement. All joists were able to achieve their peak load repeatedly for several loading/unloading cycles.

Initial stiffness (below 0.2 ksf) of all specimens is similar. After this point the stiffnesses of HJ-3 and HJ-4 were less than for either control joist. HJ-3 displayed more flexible response than the damaged or repaired joist HJ-4. It also deflected much more than HJ-6. HJ-4, while able to deflect significantly, was not able to match the performance of HJ-7. The limited deflection capacity of HJ-6 emphasizes the effects of insufficient shear reinforcement.

Figures A.32 and A.33 show load versus strain in the FRP material for HJ-3 and HJ-4 respectively. Strain gages along the beam web show elongation of transverse FRP with increasing load. In HJ-4, FRP strains do not begin to increase appreciably until the actuator load is approximately 12 kips, indicating the widening of shear cracks in the concrete beneath the FRP and the developing shear resistance in the FRP. Strain in gages ES4 and ES5, closest to the allowable strain of .004 but much less than the ultimate strain of .02. The

Table 4.2. Principal experimental test results for hybrid joists.

Joist no.	Experimental cracking load* (kips)	First Crack Location	Applied Failure load* (kips)	Total Failure Load (kips)	Equivalent Uniform Load (ksf)	Type of failure
HJ-3		midspan, bottom chord	52.0	53.0	0.62	Shear
HJ-4		midspan, bottom chord	56.6	56.6**	0.67	no failure
HJ-6	11.7	midspan, bottom chord	48.0	49.0	0.57	Shear
HJ-7	31.5	midspan bottom chord	64.0	65.0	0.76	Flexure

* Sum of two actuators.

** No failure occurred.

limited capacity of HJ-3 is shown by the much lower strain values of gages ES4 and ES5 than for HJ-4.

None of the joists experienced any cracking when the prestressing tendons were released. Cracks were marked on each of the joists throughout testing. In HJ-6, limited cracking occurred in the bottom chord early in the test series. As actuator stroke was increased, cracking in the shear spans became evident; cracks in the bottom chord did not develop further. An inclined crack developed near the support and progressed upward along the web/slab interface (Figure A.34). With further stroke application this crack extended further into the slab and failure ultimately occurred in this North end of the joist (Figure A.35).

Figure A.36 shows crack development for HJ-7. Initial flexural cracks formed along the bottom chord at midspan. Cracks were regularly spaced, and they became more numerous and closely spaced as the displacement was increased. Near the end of testing, when the load was not increasing but the specimen was able to deflect significantly more, inclined cracks developed in the shear spans of the members. No actual failure was observed in specimen HJ-7. The joist continued to deflect after reaching an ultimate load capacity.

Cracking in HJ-3 initiated as for HJ-7 with flexural cracks in the web bottom chord. At an applied stroke of approximately 5 in. a crack began to develop along the edge of the FRP at the intersection between the joist web and slab, Figure A.37(b). A gap of more than 1 in. of exposed concrete existed at where the FRP had slipped down from the web/slab interface. The horizontal crack

began near the point where the FRP lapped. As the horizontal crack progressed toward the North end of the joist, cracks also developed in the bottom of the slab perpendicular to the joist span. This cracking was associated with popping sounds as if the FRP were debonding from the joist. A maximum deflection of approximately 9 in. was achieved before complete collapse of the joist occurred by peeling of the top slab from the web at the construction joint at a distance of approximately 56.75 in. from the North end, Figure A.38(a). The FRP separated from the joist by buckling over the web depth at a distance approximately 41 in. from the joist's North end. Two other vertical splits were evident in the FRP at approximately 6 in. and 25.5 in. from the North end. Investigation of the failure revealed the concrete in the area of the FRP repair had completely broken up. The total length of crumbled concrete was approximately 50 in. Examination of the TYFO™ S Fibrwrap System showed it to be adhered to the perimeter concrete even at failure. Failure was in the concrete. This was precipitated by the weakness created by the gap in the FRP repair at the top of the web.

Initial testing of HJ-4 without FRP repair produced crack patterns similar to those for HJ-6, Figure A.39. After repair, testing began again. Existing cracks in the web bottom chord between struts increased in size and additional cracks developed near the edge of the FRP repair area, Figures A.40 (a) and (b). The test was stopped when there was no further vertical space between the web bottom chord and the floor for the joist to deflect. The joist did not fail. At the test conclusion, the FRP repair showed no signs of damage. The beam exhibited ductile response throughout the test.

Design Procedure

Based on standard structural engineering design principals and the experimental test results a simple procedure was developed to design FRP composite system repairs for reinforced concrete joists deficient in shear capacity. This design procedure is a step by step process wherein load demands are assessed for an existing member cross-section, a repair is designed based on specified engineering properties of the FRP composite system to achieve the required capacity, and stresses and deflections for the repaired joist are checked. Figure A.30 shows the flowchart for the joist design procedure.

Design criteria are based on *Building Code Requirements for Reinforced Concrete*, ACI 318-95 (1995). Load and strength reduction factors as specified by the code are used. Flexural strength is calculated using strain compatibility. Additionally, the International Conference of Building Officials has developed a draft document on the subject of "Acceptance Criteria for Concrete and Reinforced and Unreinforced Masonry Strengthening Using Fiber-reinforced

Composite Systems" (ICBO 1997). This document provides good guidance for the establishment of minimum requirements for evaluating FRP systems for strengthening concrete elements.

The design procedure assumes the joist is uniformly loaded at all stages with a simple span and roller supports. If the beam has been damaged, a conservative assumption of the concrete shear capacity of $V_c = 0$ is recommended. The degree of upgrade/repair required is represented by the difference between the load demand and the existing section capacity. The ratio of shear capacity to shear demand should exceed that of the flexural capacity to flexural demand. Shear enhancement is provided by fiber-reinforced composite materials with fibers oriented essentially perpendicular to the member's axis. Fiber orientation is critical when determining FRP properties. Important properties to define for design are:

f_{sj} , allowable FRP tensile stress

f_{uj} , ultimate FRP tensile stress

σ_j , allowable bond stress

E_j , FRP modulus of elasticity

ε_{aj} , allowable FRP strain

ε_{uj} , ultimate FRP strain.

The optimal jacket configuration should therefore be assumed whenever possible. This configuration is to wrap the entire section in the FRP. If this is not possible the use of anchors should be considered so that bond is not the primary means of force transfer.

Bond, flexural, and shear stresses should be checked for the upgraded/repaired joist configuration. An estimate of the load deflection relationship should be checked using structural analysis methods. The member should be designed to fail by ductile flexural failure mode. For the strengthening of existing reinforced concrete beams with FRP it is recommended that the repair/upgrade be designed such that ultimate failure occurs by yielding of the steel reinforcing bars before a compressive failure of the concrete. The final shear capacity of the upgraded/repaired beam should be approximately 1.5 to 2.0 times the flexural capacity. Deflections limits should be evaluated relative to ACI code requirements. Detailing considerations should also be defined.

Results and Summary

The results of tests performed in this study indicate that significant increase in shear strength can be achieved by the application of FRP to concrete beams deficient in shear capacity. When the FRP jacket is properly applied over the shear span of the member, the failure mode of a member may be altered from that of a brittle shear failure to a ductile flexural failure. However, the repaired joist was not able to achieve the strength and stiffness levels of a properly reinforced specimen.

The effectiveness of an FRP upgrade or repair requires careful preparation of the concrete surface, selection of a tough epoxy, and placement of the fabric. A gap between the web and slab that was not covered by the FRP initiated failure in a joist upgraded with FRP. While the joist deflected significantly more than a control beam that failed in shear, the mode of failure was similarly sudden and brittle. This joist's overall stiffness was not as great as for the two control joists. Bond between the FRP and concrete was shown to be very good.

Connectivity between the joist web and slab were also shown to be very important as all test joists tended to separate along this interface after testing was completed. Both joists that failed in shear failed along this interface. Insufficient shear reinforcement may also affect the quality of tendon anchorage, concrete confinement, and anchorage of the web to the cast-in-place slab. Proper application of FRP can assist in providing the latter two of these requirements but will not aid in anchoring prestressing tendons.

When designed or repaired with adequate shear reinforcement, the behavior of the test joists was exceptional. Failure loads for the control joist and the repaired joist were very high compared with design service and ultimate loads. Failure was also very ductile for these members, with deflection capacity extending well beyond the point at which the ultimate load was reached.

Additional analytical and experimental studies should be undertaken to establish the benefits of supplemental anchorage for improving the bond of the FRP to the reinforced concrete structural member. Construction methods for ensuring proper placement and curing of the FRP in the repair process should be refined. In addition, the effects of environmental factors, e.g., temperature and moisture on the epoxy joint, as well as the performance of upgraded beams under fatigue loading should be examined. The design procedure outlined in this report should be incorporated into an Engineering Technical Letter for distribution to all Corps of Engineers district offices.

Strengthening Damaged Reinforced Concrete Beams Using CFRP Tendons

Overview

Deterioration of the infrastructure presents a significant challenge to the construction industry to ensure safety and integrity of existing structural systems. Concrete repair and rehabilitation with innovative techniques have received considerable attention during the recent years. The objective of any repair should be to produce a durable system to serve the intended purpose at a relatively low cost, with only limited and predictable change over time, and without deterioration and distress throughout its intended life cycle.

External post-tensioning and the addition of epoxy-bonded steel plates to the tension flange are widely and effectively used to strengthen beams/girders and floor systems in existing reinforced concrete structures. The method of retrofitting reinforced concrete members with steel plate bonding has certain problems, namely, the difficulty in handling the heavy steel plates and a risk of corrosion at the steel/adhesive interface. These problems led to a promising development in strengthening deteriorated reinforced concrete beams/girders with external post-tensioning using Fiber Reinforced Plastics (FRP) laminates/ strand rods which offer an excellent alternative due to its superior corrosion resistance and high strength to weight ratio.

A demonstration was conducted using carbon FRP (CFRP) tendons at the Tropicana Condominium, 4001 South Ocean Drive, Lantana, FL. The 5-story condominium, constructed in the 1950s, used both precast, reinforced concrete single- and double-tee beams that formed the floors and ceilings of each floor. The beams had no prestressing and were constructed as a joist system. The first floor beams were deteriorated considerably as evidenced by concrete spalling, cracking, and either partial or complete exposure of bundled rebars. It is suspected that the damage to the beams was largely due to the damp marine environment since the condominium is located approximately one quarter mile away from the Atlantic ocean and exposed to standing water in the building's crawl space. The beams were originally designed using three #7 bars (bundled) at the center and two #7 bars (bundled) at the ends. The beams have a span of 24 ft 3 in. clear between grade beams/girders. To restore the intended service life of the beams, an external post-tensioning of CFRP tendon and anchorage system was used and system's performance monitored. The results were documented and the strengthening process and procedures are discussed in Appendix B.

Objective

The objective of this field demonstration was to study the effectiveness of using CFRP tendons to restore the intended service life of damaged reinforced concrete beams. This was accomplished by installing adequate instrumentation in existing corroded reinforced concrete double-tee beams repaired with external post-tensioning using LEADLINE™ tendons with anchorages, and acquiring short- and long-term measurements during and after post-tensioning.

Significance of FRP

The use of unbonded, post-tensioned FRP reinforcement for strengthening is of significant relevance for structural members requiring repair. This repair technique termed "supplementary prestress" has been used with conventional steel tendons in the longitudinal direction, but also in the vertical and inclined directions for large beams. Additional benefits for using longitudinal tendons are stiffening of the system, closing of the flexural cracks, and a mild increase in shear capacity.

The benefits of using FRP tendons in this situation included corrosion resistance and high tensile stress that are constant through the length of the tendon. The challenge for using FRP tendons is to provide an easy to install and reliable system with noncorrosive anchors that are capable of long term performance without prestress losses in the tendon-anchor system.

Discussion

The tendons used for this field demonstration were LEADLINE™ tendons provided by Mitsubishi Chemical Corporation. LEADLINE™, made by the pultrusion process, provides FRP rods with linearly oriented carbon fibers that have higher strength and better properties than twisted carbon fiber cables of the same diameter. Structural Preservation Systems, Inc. (SPS) did the repair/ strengthening work. This product was selected for this job because it has a higher tensile strength and elastic modulus compared to typical steel tendons, corrosion resistance, low creep and stress relaxation losses, and lightweight (1/5 the unit weight of steel).

The field instrumentation consisted of load cells, electrical resistance strain gages, digimatic micrometer points, and a deflectometer. Hydraulic jacks were used to prestress the LEADLINE™ tendons at load increments of approximately 3,000 lb up to a maximum of 12,000 lb. The four LEADLINE™ tendons were tensioned in succession one at a time. For each applied prestressing force

increment, the force, anchorage slip, strains in the tendons, concrete and anchorages, and deflection at midspan were monitored using Data Acquisition System, strain indicator, digimatic micrometer and deflectometer.

Results and Summary

Based on the studies on the performance of the existing corroded reinforced concrete double-tee beams strengthened with external post tensioning using LEADLINE™ tendons with anchorages, the following conclusions can be drawn:

1. The field measurements over a period of over one year demonstrate the successful application of the LEADLINETM tendon for strengthening and repairing of the existing corroded reinforced concrete beams in harsh marine and coastal environments.
2. Conventional strengthening design method for either reinforced concrete or prestressed concrete is applicable to the strengthening design of the corroded reinforced concrete beam with LEADLINETM tendon. The number of LEADLINETM tendons and the prestress level in the tendon were determined based on the strength limit state and the ultimate strength of the tendons.
3. The initial loss of the prestressing force in the LEADLINETM tendon due to the curvature frictional effects and elastic shortening of the concrete resulting from sequential stressing of the tendons can vary from 9 to 14%.
4. The relative slip in the anchorages is almost negligible during the process of post tensioning of the double-tee beams. The prestress loss in LEADLINETM tendon due to the slip in the anchorage during the 1 year period of observation was found to be very small, which demonstrates the efficient performance of the grout system used in the anchorage.
5. The loss in prestress in the LEADLINETM tendons due to creep effects of concrete in the existing reinforced concrete double-tee beams under study is insignificant.
6. The loss in prestress due to relaxation of the LEADLINETM tendons was approximately 5% in the first 7 days which compares to the published value of 2 to 3% for carbon FRP rod. However, the prestress loss due to relaxation increased to 10 to 12% of the initial jacking force after 100 days and then remained constant thereafter.
7. Careful attention and care need be exercised considering the physical field constraints on the preparation of the anchorage system, prestressing of the tendons and setting of the anchorage on to the existing structure so as to minimize the loss of prestress in the LEADLINETM tendons.

Computer Modeling of Repair/Upgrade of Reinforced Concrete Beams

Overview

A method to repair existing reinforced concrete flexural members is to externally bond FRP reinforcement to the soffit in need of repair. The upgrade of existing reinforced concrete beams and slabs with FRP materials bonded to their soffit may be needed for a variety of different reasons: reduce the vertical deflection at service *(stiffening criterion)*, improve the maximum load capacity *(strengthening criterion)*, or limit the width and the distribution of cracks in concrete *(durability criterion)*. Since the designer has generally no control over the existing structural element in need of repair, the geometry and properties of existing steel reinforcement or the concrete which cannot be modified, he can only select the area of the FRP reinforcement and its stiffness to satisfy stiffening and strengthening requirements.

Independently of the repair strategy selected, it is essential to understand the consequences of the design choice in terms of crack propagation and failure mechanism. In fact, it has been observed in the literature that different failure mechanisms, from ductile to very brittle, occur as externally bonded FRP reinforcement is added to a flexural member (Saadatmanesh and Ehsani 1994; Chajes et al. 1994; Arduini, D'Ambrisi, and Di Tommaso 1994; Arduini, Di Tommaso, and Nanni 1995). Those failures may be FRP tensile rupture, concrete crushing, debonding between FRP and concrete, or shear-tension failure resulting from a combination of shear and normal tensile stress in the concrete in the plane of the longitudinal steel bars.

The first two failure mechanisms occur after large deflection of the member and are synonyms of better structural performance. The third and fourth failure mechanisms are brittle and occur at values of the applied load lower than expected with conventional design models whereby the stiffening/strengthening resources of the FRP plate are of little advantage.

Appendix C presents an analytical study of reinforced concrete beams of representative geometries and materials, repaired with FRP plates of various thickness and mechanical properties. The model allows for the nonlinear behavior of the reinforced concrete member due to the diffusion of flexural cracks. This is essential for a correct interpretation of experimental results.

FRP Significance

The study intends to identify in a rational fashion, the parameters that affect performance of flexural members repaired with externally bonded FRP reinforcement. These parameters must include preexisting materials and geometry as well as repair materials. The study of the inter-relationship among these parameters leads to the understanding of the limiting factors and the possible modes of failure. This analytical study and the eventual experimental verification are necessary for the development of sound design guidelines. It is noted that the results reported in Appendix C are not absolutely general but relate to selected reinforced concrete beam geometries and materials.

Test Methodology Discussion Summary

A model was developed for simply supported rectangular reinforced concrete beams with FRP bonded to the tensile face. Three typical reinforced concrete beam cross sections were considered with height-to-width ratios of 0.5, 1 and 4. Two compressive strength levels (20 and 30 MPa), and two shear span to reinforcement depth ratios (4.5 and 7) were considered. All other parameters related to material and geometry of the beams were maintained constant.

Reinforced concrete beams were cast and tested in four-point bending to verify the model and failure mechanisms which the model indicates. Additionally, if the designer selects to use prefabricated FRP plates for the repair or upgrade, effects of adhesive mechanical properties were examined.

Results and Summary

In summary, FRP repair of existing reinforced concrete flexural members may be structurally necessary for two reasons: stiffening or strengthening. Depending on the criterion and the conditions (i.e., materials and geometries) of the existing member, the repair method may be more or less effective.

If a designer is only concerned with stiffening, the repaired element is not required to carry any additional service load. In general, stiffening is always attainable. For the same FRP thickness, the higher the FRP stiffness, the better the results. The failure mode of the repaired system may become brittle, depending on several parameters, which include existing member conditions as well as repair parameters (e.g., p/l ratio).

If a designer is concerned with strengthening an existing structural member and improving its load carrying capacity at service of a given amount, the success of

the repair and the selection of the FRP stiffness, thickness, and bonded length have to be based on the limitations imposed by:

- shear strength of the existing member
- mode of failure of the repaired system
- deflection at new service load.

In general, the bonded length of FRP should be as long as possible to have a better use of the FRP strength resources and to activate failures such as concrete crushing or FRP rupture. The adhesive for prefabricated FRP plates should have high ultimate elongation.

The results of the analysis are shown in terms of repaired-to-unrepaired strength and deflection ratios. They indicate that brittle failure mechanisms can develop at loads much lower than expected when considering only flexural performance controlled by concrete crushing and FRP tensile rupture. The analytical model used for the parametrization accounts for brittle failure mechanisms induced by debonding of the FRP reinforcement or shear-tension failure in concrete in the plane of the main longitudinal steel reinforcing bars. Even when considering the limitation of the reinforced concrete member due to its unmodifiable shear resistance, it is shown that the application of FRP reinforcement can considerably increase load resistance capacity and limit deflection at service.

Feasibility Study of Using FRP Tendons/Rods for Tie-back Applications

Overview

Abutments of bridges and dams behave as retaining walls to resist the lateral pressure from the earth backfill. Some abutments tend to move or rotate due to the vibration of the backfill, movement of traffic above the fill, or hydrostatic pressure in combination with backfill pressure. These effects on the abutment result in lateral movement of the wall or rotation of the wall with reference to the base. The conventional method of rehabilitating these walls is by using some type of tie-back arrangement. This involves installing a tension member to hold the walls from further movement and some type of anchorage for the tension member into the soil in the backfill area. Traditionally, steel cables or bars are used for the tension member and a concrete dead man is used to anchor them. Since movement of the wall may continue at a lower rate, soil conditions and the distance between the wall and the dead man become very important in controlling the stresses in the tension members. Depending on the backfill soil

condition, generally twice the height of the wall is required for the length of the tension member.

There are two problems with using steel cables as the tension members to hold the walls. First, the steel is buried in soil (backfill) and, with the presence of moisture, is subject to corrosion over time. The second problem is the development of high stresses in high modulus steel (29 Msi) due to the movement of the wall. These two problems require an alternate high strength material that is noncorrosive and has a low modulus. Glass Fiber Reinforced Plastic (GFRP) is a solution to these problems. A ½ in. diameter GFRP cable has a tensile strength of 195 ksi, a modulus of nearly 7.2 Msi and will not corrode in moist soil. A feasibility study for the use of GFRP for tie-back arrangements is documented in Appendix D.

Objective

This study focuses on the feasibility of using GFRP cables for a tie-back arrangement instead of steel cables where corrosion and wall movement are very critical. Using the south abutment of Leech Lake Dam in Minnesota as an application example, a design was developed for similar sites.

Significance of Using FRP

The significance of using FRP for this type of application depends on the comparative performance of FRP with conventional materials in design, economy, and standards. Rehabilitation of abutment walls against lateral movement is a well defined engineering problem.

Design

Design of tie-back arrangements requires a tension member with high tensile strength and the ability to stretch to accommodate movement of the wall in a high moisture content back fill. GFRP cables have a high tensile strength with no deterioration in soil with high moisture content. Therefore GFRP cable is a good substitute for steel in a tie-back arrangement. Design procedures using GFRP cables are similar to conventional methods using steel cables. The total soil pressure is calculated for a particular case to determine the number of GFRP cables required to hold the wall. The design strength of the GFRP is the only thing different from steel bars. A design example shown in the appendix illustrates the method of design.

Economy

Either DYWIDAG steel bars (DYWIDAG, Munich, Germany) or GFRP cables can do the job. With 150 ksi strength steel, the DYWIDAG bars require a 5/8 in. diameter while GFRP cable needs a ½ in. nominal diameter. The current cost of DYWIDAG bar is $1.50 per foot while the cost of the GFRP cable used for this study is $1.10 per foot. In addition, the steel rods will corrode and require more length for the tie-back arrangement since the modulus is nearly four times that of the GFRP cables. This length difference translates into a shorter excavation requirement and associated savings in construction costs using GFRP. GFRP cables are also economical compared to the cost of Carbon or Aramid FRP cables that are much higher in cost. The GFRP material is the best choice for this application.

Codes and Specifications

No codes or specifications are available for the use of conventional materials, such as steel, for this type of application. Therefore, the lack of specifications will not affect the use of the GFRP cables for tie-back arrangements. The GFRP cables should be supplied from a reliable source, however, with required mechanical properties.

Laboratory Tests and a Typical Design Example

One of the advantages in using GFRP cables over steel is its low modulus and its mode of failure with the movement of a wall in the field. This was demonstrated in the laboratory by tensioning the steel and GFRP cables in stages to simulate the movement of the wall. A 5/8 in. diameter DYWIDAG bar and two GFRP cables were held between two fixed rigid bulk heads. The details of the test setup are shown in Appendix D. The two cables and the steel bar were pulled or tensioned with an external jack at a rate of approximately 1/2 in. per day to simulate the movement of a wall. Strain gages were used to monitor the strain in the cables and rod. On the fourth day, the steel rod started yielding while the GFRP continued the linear stress strain at this stage. Stretching of the GFRP cables and steel bar was continued until they failed. The test results are shown in Appendix D.

The materials behaved as expected in this test with steel yielding at 2-5/8 in. elongation at a very early stage, the 6th day, while the GFRP failed on the 11th day with nearly 5 in. extension on an 18 ft length. Tension tests were conducted on the GFRP cable to determine the Ultimate strength, Modulus, and Ultimate strain. They were found to be 195 Ksi, 7.2 Msi, and 2.7% (27,400 micro-in)

respectively. Details of these test results are shown in Appendix D. Therefore, the GFRP cable can withstand more movement of the wall without failure (in relation to the yielding) while steel will continue to extend without taking additional load, and fail. The limits of design depend upon the criteria established for the project.

In general, the steel yielding is considered as failure. Here, GFRP has a definite advantage over steel for resisting wall movement. The GFRP modulus is nearly one fourth that of steel and the failure mode was very slow with enough warning of failure of the structure. A complete design example for a 15 ft high abutment with steel and GFRP cables is shown in Appendix D.

Results and Summary

Advantages to using the GFRP cables instead of steel bars or cables are as follows:

1. The length of the tie-back cables can be reduced to a minimum required from the soil properties and height of the wall (in this case only twice the height of the wall). This will reduce the overall cost of earth work needed for the project in addition to savings in cable lengths.
2. No corrosion of the tie-back cables.
3. The lower modulus of GFRP cables reduces high stress development in the cables in the event of movement of the wall, resulting in less likelihood of failure.
4. The cost of GFRP cable is less or equal to the cost of DYWIDAG bar.
5. Adjustment of tension in the cables, something not possible in the steel cables, is possible with GFRP cables.

5 Test Methods for Performance Verification

Established FRP Composite Inspection Techniques

Composites have many inspection techniques that are proven in other markets. Table 5.1 summarizes these techniques.

Table 5.1. Established nondestructive evaluation techniques for composites.

Test Method	Voids	Delamination	Other Damage	Cost
Visual Inspection	Good	Good	Good	none
Tap Test	Good	Good	n/a	none
Thermal Infrared Imaging (Thermography)	Good	Good	Limited	Moderate
Acoustic Emission - Ultrasonic Through Transmission - Ultrasonic Pulse Echo - Ultrsonic Resonance		Fair	Fair	Moderate
Laser Holography		Good, Limited	n/a	High
X-Ray Imaging	Fair	Good	n/a	High
Neutron Radiography	Poor	n/a	n/a	High

These techniques may be good for traditional composites parts, but in some cases, some of these techniques may not be applicable to infrastructure applications. Other methods available to composites are (1) piezoelectric sensors or (2) fiber optics. Evaluations of both methods are under investigation by leading academic institutions and the U.S. Army Corps of Engineers. New methods under consideration employ the use of embedded tags that are cured in the composite that would measure continuous performance, loading history, incipient failure, or simply the degree of cure.

Field Inspection Technique for Bond Strength

Overview

In 1994, Structural Preservations Systems, Inc. (SPS), and Gannett Flemming performed a supplemental strengthening of reinforced concrete tank walls at the waste water treatment plant in Hollidaysburg, PA. A carbon fiber composite

system was applied on an experimental basis to a 140 square foot surface inside the East wall to strengthen an inadequately reinforced section and a 2 foot wide sheet centered over vertical cracks from the bottom to the top of the North wall was applied to control crack growth. Following 2-1/2 years in service, SPS conducted durability performance tests on the FRP system.

In spite of many advantages of the FRP materials, very limited experience of the material and the structural implications of the use of these materials for repair and strengthening of concrete structures exist. The use of FRP for repairs is still hampered by the lack of standards, and the lack of training documents to educate engineers, contractors, and laborers. Standard test methods are needed for the fibers, epoxy, and combined FRP composite system including the FRP bonded to the substrate. To make innovation possible by the use of these new materials, reliable data on their properties must be available.

Despite the fact that the use of FRP for repair and strengthening of concrete structures is growing all over the world, standard bond testing procedures have still not been devised. Consequently, many projects have been carried out without any reliable monitoring of their quality. Recently some attempts have been made to overcome this problem. SPS tested several unconventional in-situ tensile bond testing techniques which have been developed to meet the demand for improved field evaluation and quality control. Appendix F describes the test program.

FRP Significance

There is considerable pressure to develop and use reliable in-situ bond strength test methods. Unfortunately, development of such methods has not kept pace with the materials development, primarily because of the lack of appropriate field data needed for its development. The development of and adherence to reliable QC/QA test methods are avenues to wider use of composite materials for repair and strengthening of concrete structures.

Test Methodology

The transfer of force from the concrete substrate into the carbon fiber laminate occurs by shear stress. Therefore, it is important to be able to evaluate this property of the composite system for design and quality control. The mere magnitude of bond strength obtained in tension should not be compared with that of the shear, due to the fact that the stress mechanisms that cause failure are different in both methods. However, the comparison between the shear and

the tensile bond strength can be very useful for the prediction of the real performance of a strengthening system in practice.

Although a variety of different test methods were analyzed, two test methods were selected by the authors for use in site testing the pull-off tensile bond test and the torsion shear bond test. In the modified ACI 503 pull-off test, a 1/8-in. partial depth core was cut to below the interface between the concrete and the CFRP and a steel 2-in. diameter steel disk was applied with epoxy. Once the epoxy was cured, a tensile force was applied to the probe using a pull-off apparatus, and the tensile bond strength was calculated for the specimen. Since the use of a core drill is not always easy in on-site quality assurance, especially where access is difficult, a pull-off test utilizing a 2-in. square steel plate was also performed. The plate was adhered to the CFRP surface and CFRP laminate was cut along the perimeter of the plate using a small grinder. The pull-off strength was determined as with the partial core testing.

An *in situ* shear test was evaluated. Test probes 1 in. and 2 in. in diameter were adhered to the CFRP using an epoxy adhesive. Torsion was applied using a calibrated torque wrench with a series of hinges to eliminate any possible bonding moment due to the eccentricity. The torque was gradually increased manually until failure. The maximum value at failure and the failure mode were recorded.

Test results of the tensile and shear bond strengths using different testing systems are presented in Table 1 of Appendix F. The results of the pull-off tests in Zone #1 when square probes were used demonstrate a close numerical correlation with the test results with circular probes.

Results and Summary

The following conclusions can be drawn from this study:

- The pull-off test using square plates and torsion shear bond test demonstrate that both are practical test methods that can be performed in the field. But both methods need more development and precision.
- No numerical correlation of pull-off tensile strength and torsion shear strength was possible.
- The look at the described test methods shows an urgent need for further research and adaptation of the standard test methods, materials and procedures to on-site demands including surface preparation of FRP, surface preparation of steel probes, quality of the epoxy glue, curing conditions, and duration.

- Further extensive tests ought to be carried out to confirm the above correlation.

FRP Tendon/Rod Drape Angle Test Fixture

Overview

FRP prestressing tendons must occasionally be bent around turning points. This condition occurs when prestressing I-girders, T-beams, and similar precast members and when post-tensioning beams and girders. Recently, FRP tendons and rods have been used successfully in these applications. It is a common industry practice to drape prestressing and post stressing tendons around turning points to create king- or queen-post strengthening systems. An examination of some typical beams and repair systems suggests that the total turning angle varies from 0 degrees to 15 degrees.

FRP Significance

No standard test methods exist for evaluating the performance of FRP rods or tendons for these types of applications. This research is important in order to develop a standard test fixture for use in ASTM standards to evaluate performance of FRP tendons and rods when draped around turning points up to 20 degrees.

Objective

The CPAR team worked with ASTM Committee D-20.18 on FRP reinforcing to address the drape angle design limitation and develop a consistent test procedure for new and emerging FRP tendon and rod manufacturers to evaluate the tensile capacities of their products at drape angles up to 20 degrees.

FRP Tendon Test Fixture Design

Typical designs call for the stressing of FRP tendons to be a maximum of 50% of their ultimate strength for glass and 60% for carbon. The actual tendon strength will be reduced by bending around a turning point. To evaluate the magnitude of strength reductions from bending, a test fixture was designed and fabricated.

Some of the considerations that were taken into account in the design include the ultimate strength of the straight tendons to be tested, the length needed

between anchors and bending pin to assure that end or pin effects do not overlap, forces on the pin and anchorage connections, pin diameters, and the test machine configuration.

The tendon mounting fixture consisted of two steel mounting plates with a steel pin to serve as the turning point, and a steel anchor point for the end of the tendon. The pin and anchor points were installed between the two plates. The test assembly was then mounted in a loading frame with a hydraulic actuator suspended above it (Figure F.6). The test fixture was designed to test 0.31 in. diameter FRP tendons around 2 in., 4 in., and 6 in. diameter pins at angles of 0, 5, 10, 15, and 20 degrees.

Results and Summary

A test fixture was designed and constructed for testing the ultimate tensile strength of FRP tendons at drape angles varying from 0 to 20 degrees around king- or queen-post diameters from 2 to 6 in. The design and specifications will be submitted to ASTM D20.18 for incorporation into draft test specifications for FRP tendons.

6 FRP Bond Durability

Effects of Severe Environments

Overview

Reinforced concrete structures are often required to resist loads over a long time under potentially corrosive environments. Composites appear to exhibit excellent resistance to the aggressive environments that normally cause corrosion of typical steel reinforcement.

When a concrete structure is strengthened with an externally bonded FRP, the most critical aspect of its behavior is that the composite action in the system must be preserved during the designed service life of the structure. This behavior is governed primarily by the ability of the bond to transfer stresses, and this in turn, depends on the bond between two entirely different components of the system: existing concrete substrate, and FRP strength and durability. In 1994, a supplemental strengthening of reinforced concrete basin walls was performed at the Hollidaysburg Sewage Treatment Plant in Pennsylvania. Carbon fiber sheets were applied on two walls to control potential overstress and existing cracking of the under-reinforced concrete walls.

The overall objective of the testing program performed by Structural Preservation Systems, Inc., and Gannet Fleming, Inc., was to perform durability testing of the CFRP strengthening system in severe environment. More specifically, the objective was to study the bond behavior between the concrete and CFRP under different environmental exposures. Appendix F is a description of the study.

FRP Significance

Deficiencies and weaknesses in the bond when exposed to long term severe environment can be detrimental to overall performance of the composite system. There is limited information concerning the durability of the described strengthening systems in severe environments. More data is necessary before confidence and reliability can be assured.

Test Methodology

After more than 2.5 years in service, a durability testing program was performed on the waste water treatment facility strengthening repair. Included in the test program were visual examination and natural exposure bond testing in three zones: (1) dry, exposed to ultraviolet (UV) rays and frost action; (2) splash, exposed to freezing and thawing action in water saturated condition, wetting and drying, UV, and chemical attack by waste water elements; and (3) submerged, exposed to chemical attack by waste water elements.

Test results of the tensile and shear bond strengths using different testing systems are presented in Table 1 of Appendix F. In direct tension the predominant failure mode was a combination of partial failure in the concrete and between the concrete and CFRP. The average tensile stress at failure was 329 psi which is more than adequate tensile bond between parent concrete and CFRP. In shear tests the predominant mode of failure was in the bond between the steel probe and CFRP. The average shear stress at failure was 1,492 psi, which exceeds more than three times the required value of 370 psi. The overall averages were calculated by averaging all the readings irrespective of the mode of failures.

Results and Summary

The bond between the existing concrete and CFRP strengthening system in severe environment demonstrates good performance after 2.5 years in service.

Thermal Effects on FRP Bond

The objective of this CPAR project was to develop, test, demonstrate, and commercialize advanced composite materials systems for in-place repairing, strengthening, or upgrading concrete structures including columns, beams, and decks. Because of polymeric composite's inherent characteristics of inducing thermal stresses under severe temperature fluctuations, CRREL's research under this project was to study and analyze if the cold climatic conditions would impair the performance of these "composite-repaired" concrete structures.

Overview

To improve structural performance, bonding of steel plates to concrete with epoxy resin is a common practice in the rehabilitation of bridges and buildings. In cold regions, because of de-icing salt and other corrosion agents, the bond at

the glued steel-concrete interface deteriorates rendering the structure vulnerable to loss of strength and possible collapse. This CPAR project has addressed the use of unidirectional FRP sheets of carbon (CFRP) and glass (GFRP) bonded together with a polymer matrix (epoxy, polyester, vinyl ester) to form a composite material as a substitute for steel. The advantages claimed by this system are: immunity to corrosion, a low volume to weight ratio, and elimination of joints in the reinforcing plates. Although this new construction technology has gained a foothold in the construction industry (Meier 1987) for about a decade, no major effort has previously been directed toward the study of the potential degradation of the FRP itself, and its bond to concrete under the severe climatic conditions of the cold regions.

Degradation of fiber reinforced plastic composites in severe cold is well known (Lord and Dutta 1987). Extreme changes in temperature of composite materials result in several important effects. Most materials expand and contract as temperature rises and falls. In fiber-reinforced polymer matrix composites, the coefficient of thermal expansion of the matrix is usually an order of magnitude greater than that of the fibers. A decrease in temperature, due either to cooling during the fabrication process or to low-temperature operating conditions, causes the matrix to shrink. Contraction of the matrix is resisted by relatively stiff fibers through fiber-matrix interface bonding, setting up residual stresses within the material microstructure. The magnitude of the residual stresses is proportional to the difference in curing and operating temperatures of the composite material. Where large temperature differentials exist, for example, in the Arctic and the Antarctic regions of the world, sufficiently large stresses may induce microcracking in the material. These microcracks in turn, can reduce the stiffness of the composite, increase permeability and water ingression through fiber/matrix interface, and thus finally contribute to the degradation processes.

Another very important effect of lower temperatures is embrittlement and the accompanying change in matrix strength and stiffness. Most resin matrix materials become stiffer and stronger as they are cooled. These changes can influence the modes of failure. At low temperatures the compressive strength increases and the material fails more violently than at warmer temperatures (Dutta 1994). The energy absorption before failure at low temperature is higher than at room temperature. This particular aspect of high energy release at failure should be taken into consideration in designing with composites.

In cold regions, the freeze-thaw cycling effects on a composite's durability are also important considerations. If a composite contains a significant percentage of interconnected voids that are filled with water, the freeze-thaw effect on the strength, within the normal range of temperature (+30 °C to -20 °C), could be

significant. Commercially available good quality glass fiber composites usually contain about 0.4% voids which do not allow appreciable frozen moisture to cause any serious damage. However, low temperature thermal cycling induced stresses can result in the formation of microcracks in the resin matrix or in the resin-fiber interface. Under prolonged thermal cycling they can grow in density and can result in stiffness degradation and degradation of other matrix dominated properties.

Test Program

The ultimate capacity of the externally bonded FRP-reinforced beam without any internal reinforcement is limited by the strength of the FRP bond to the concrete, or the tensile strength of the FRP, whichever is lower. When internal steel or other reinforcement is present, the external FRP reinforcement simply shares the tensile load with this internal reinforcement. Six series of tests relevant to low temperature performance and durability of composite repaired concrete systems were performed at CRREL. The tests include the following and are briefly described below:

1. review of the state-of-the-art composites durability under severe cold climatic conditions
2. influence of low-temperature on load capacity of beams repaired with a new composite bonding technique
3. low-temperature fatigue-load effect on bond strength and failure load
4. low-temperature thermal cycling effect on composite bond to concrete
5. influence of low temperature on the strength development along bond length
6. develop a new test technique for bond strength study by tension loading.

Appendix E is a complete description of the testing series.

Low-temperature load capacity of a newly developed system

Four large beams of 7 in. x 9 in. x 88 in. were fabricated with two #4 rebars on the tension side and two #3 rebars on the compression side. The objective was to investigate the influence of the thickness (ply) on load, deflection, and strain at room temperature for a low level load, and at low temperature (-30 °C) for load-to-failure.

On the tension side two of the beams were bonded with stitched unidirectional carbon fabric of one-ply thickness, and two others were bonded with five-ply thickness using the Ohio Department of Transportation (ODOT) developed adhesive bonding process. The beams were instrumented with multiple strain

gages including locations at interfaces and at the midspan locations on the top and bottom side. Prior to testing the beams were subjected to 6 freeze-thaw cycles between room temperature and -50 °C.

For the low-load, baseline, room-temperature testing, the test beam was installed in the four-point 100,000 lb_f capacity flexural test machine in the CRREL High Strength Advanced Material (HISAM) testing cold room. The cold room was first warmed up to approximately 20 °C. The beam was also ensured to reach the same temperature by monitoring imbedded thermocouples. The test beam was loaded to 10,000 lb_f and then unloaded. Load, deflection, and strains were measured using a Megadac data logger sampling each parameter every second. After completion of testing at room temperature the temperature of the room was lowered to -30 °C. Each beam was then loaded to failure again measuring the load, deflection, and strain in the process. It was observed that, for the single-layup bond, the failure load averaged at 26,000 lb_f and, for the five-layup bond, the failure load averaged 31,300 lb_f, a mere 20% increase in strength with use of five times more CFRP material.

Low-temperature fatigue test

Six concrete beams of 6 in. x 6 in. x 84 in. were cast with two #3 bars in compression and two #4 bars in tension as longitudinal reinforcement. Shear reinforcements were provided with #2 stirrups at 4 in. spacing in the end regions and at 6 in. spacing throughout midsection. The cement : sand : aggregate mix was 1 : 2.5 : 2.5, with a water cement ratio of 0.55. The average compressive strength of this concrete as determined from cylinder tests was 3,975 psi. Two adhesive types were tested: Sikadur-30 and Hysol EA 9330. Sika Corporation supplied the unidirectional carbon laminates for bonding. The beams were precracked under four point flexure to 65% of their ultimate load to simulate damage in the beams. The bottom tension faces were prepared by sand blasting, roughening, and cleaning, before applying the adhesive and laminate. The laminate's bond surface was also thoroughly cleaned with acetone and a rag. The two-part adhesive liquid was mixed thoroughly with an electric hand mixer. The prepared adhesive was then applied to the concrete surface with a serrated spatula to produce a uniform 0.2 in. thick layer. The adhesive was also applied to the laminate surface to 0.2 in. thickness. Once the laminate was placed on the beam, a roller was used to press the laminate into the adhesive forcing out excess adhesive at the side. The Hysol adhesive is not as viscous as the Sikadur 30, and thus was difficult to control thickness. The Hysol thickness was about 0.1 in. Steel weight pressure was applied to the beam for 2 days and following that the beams were cured for additional 5 days.

Strain gages were attached to both tension and compression sides of the beam prior to casting. Surface concrete strain gages were attached after application of the laminate. After mounting the beam in the CRREL four-point portable bending test fixture, all strain gages, including the test fixture load cell, were connected through an external bridge and amplifier system to the Megadac data logger. The mid-span deflection was measured with a micrometer dial gauge manually for check. One beam of the Sikadur-30 system and another of the Hysol 9330 system were subjected to 1,000,000 cycles of fatigue loading at 4 cycles per second, with a maximum load of 5500 lb_f and minimum load of 2000 lb_f. Periodically static tests were performed and deflection, strain, and crack propagation recorded. After room temperature tests, the mobile flexural testing machine was moved into a cold room set at a temperature of –20 °C. After stabilizing the temperature the remaining two of the Sikadur and Hysol adhesive bonded beams were subjected to 1,000,000 cycles each as before. After the fatigue loading the beams were loaded to the four point bending test until failure.

Low-temperature thermal cycling tests

Ten concrete beams of 3 in. x 3 in. x 12 in. were cast unreinforced with mix ratio of cement: sand: gravel as 1 : 2.2 : 3, and water cement ratio of 0.52. The beams were cured in lime for 14 days. Carbon composite laminates were then bonded to the tension surface, five with Sikadur and five with Hysol adhesive systems. Two specimens were kept for control and the remaining eight were thermally cycled for 200 cycles between +20 °C and -30 °C. Following thermal cycling the beams were tested at room temperature in a four point bending fixture. No significant degradation of the thermally cycled specimens was observed.

Low-temperature bond strength test in flexure

The purpose of this test was to investigate at low temperature the failure modes of the bonded CFRP strips in three-point flexural loading, and the influence of using prime coat for bonding of the CFRP. Fourteen 3 in. x 4 in. x 15 in. concrete beams were fabricated; six beams were bonded after prime coating (PC) the surface before applying adhesive, and in the remaining eight beams, adhesive was applied without prime coating (WPC). Six of these beam specimens were reserved for thermal cycling testing, and the remaining three from the PC group and five from the WPC group were tested under three-point bending. One specimen of WPC group was tested at room temperature, which failed at approximately 2955 lb_f with 0.04 in deflection. Two specimens of the PC group and five specimens of the WPC group were tested at low temperature (-30 °C),

which gave an average failure loads of 3225 lb_f and 3418 lb_f, indicating that the prime coat reduced the bond strength.

New testing technique for thermal effects on bond strength

In beam applications the bonded FRP on the tension side fails primarily under interfacial shear stress. It is important to know if the low temperature makes the concrete-composite glue bond line brittle and weak. A suitable testing system, in which the mixed-mode failures are mostly eliminated, is thus desirable. It is also desirable to know to what distance from the crack edge, and at what rate the shear strength, over the bonded area, is developed. A new test method, called the 'split-block test method' is under development in cooperation with the Ohio DOT. In this method, two prismatic blocks of concrete with central holes are bonded with FRP composite strips. The blocks are then pulled apart by applying tension load through two bolts, each one aligned through the central hole of each block. Initial tests of this system proved to be successful.

Two groups of split block concrete specimens were manufactured for this test. Group A had a 3 in. bond length, and group B a 6 in. bond length. The Ohio DOT proprietary adhesive/CFRP composite system was applied on 9 specimens of group A and 4 specimens of group B. Again, in applying the adhesive, 4 specimens in group A were prime coated (PC) and 5 were not (WPC). In group B, 2 were PC and 2 were WPC.

Both room-temperature and low-temperature (-35 °C) tests were performed in the MTS machine applying tension loads to the bolts and measuring load and displacement simultaneously. At room temperature group A, WPC specimen failed at 2750 lb_f, and at low temperature at 2908 lb_f, showing the effect of increased failure load at low temperature. No room-temperature test was done for group B WPC specimens. At low temperature, group A PC specimens failed at an average load of 2353 lb_f, and group B PC specimens at 2787 lb_f, showing approximately 18% increase in failure load an for additional three inch bond length increase (i.e., 100% bond length increase) on each block. At low temperature, group A WPC specimens failed at an average load of 2949 lb_f, and group B WPC specimens at 3394 lb_f, again, showing a 15% increase in failure load. Strain gages were mounted along the strips and their data are being analyzed.

Results and Summary

The tests show that, on a short-term basis, there is no adverse influence of low temperature on the composite bond performance with concrete. In most cases

the load capacities increased over those at room temperature. Specific conclusions are summarized below.

Load capacity tests

For the thin one-ply bond in the four point bending load capacity tests, the mode of failure was tensile accompanied by debonding, as opposed to the shear bonding of the five-ply composite.

Within about 30% load capacity there was no significant difference in the load deflection characteristics (stiffness) between the room temperature and low temperature (-30 °C).

The low temperature failure loads were in general higher than the room temperature loads.

Fatigue tests

The failure loads of the full size beams following 1,000,000 cycle fatigue loading at room and low temperatures were not significantly different, but the deflection and strain at low temperatures were lower indicating higher stiffness.

Thermal cycling

The data from the small size specimens which were tested in 4-point bending after 200 thermal cycle showed no significant degradation of the thermally cycled specimens.

Bond strength test

At low temperature the bond strength improved. The influence of prime coating was negative for both room and low temperature.

Bond strength development tensile test

This special test also showed that low temperature increased the bond strength and prime coating reduced the strength. More strength is developed over a longer bond length. The length over which bond strength develops is an important parameter which can be studied by this test.

FRP fabrics or plates are a potentially viable replacement for steel/epoxy bond material for external reinforcement and repairing of concrete. However, their

reliability under the mechanical and environmental load, creep, and durability have remained open to questions.

7 Conclusions, Recommendations, and Commercialization

Conclusions

FRP composite materials that are used as external reinforcement to repair reinforced concrete civil engineering structures are commercially available in many forms. Criteria for selecting composite materials and forms depend on the application and engineer requirements.

Composites offer many potential performance and life-cycle cost benefits over conventional concrete repair techniques, such as light weight, high strength, corrosion resistance, dimensional stability, and design flexibility. However, technical and institutional barriers have thus far prevented widespread application in the U.S. construction industry. The major hurdle is assuring designers and engineers, through durability testing and demonstrations, that FRP composite systems are serviceable and economical. The key to exploiting the beneficial properties of composites on a large scale is to demonstrate the effectiveness of currently available materials.

This CPAR work focused on commercially available FRP composite systems with emphasis on (1) development of construction guidelines through ACI Committee 440F, (2) laboratory and field evaluation of durability issues, and (3) demonstrations of the technology. Questions pertaining to the durability of composites, and their reliability under mechanical and environmental loads, were addressed. This CPAR work is expected to help lower barriers to the widespread application of FRP composite systems for the repair and enhancement of reinforced concrete structures. As currently available systems gain acceptance by designers and engineers, it is expected that the industry will be spurred into developing new generations of composites-based construction materials.

From the tests and demonstrations conducted here, the following conclusions are drawn:

In the South Florida Condo field demonstration, externally post-tensioned carbon fiber reinforced polymer (CFRP) tendons and special anchorages were successfully demonstrated to strengthen the existing corroded reinforced concrete double-tee beams. CFRP tendons demonstrated corrosion resistance in a harsh marine coastal environment. Measurements made over more than a year indicate that the performance of the beams strengthened with the CFRP tendons satisfied the engineering requirements. Conventional strengthening design methods for either reinforced concrete or prestressed concrete can be applied to the strengthening of corroded reinforced concrete beams using CFRP tendons. The number of CFRP tendons required and the prestress level in the tendons are based on the strength limit state and the ultimate strength of the tendons.

Careful attention must be exercised to minimize the loss of prestress during preparation of the anchorage system, prestressing of the tendons, and installation of the anchorage to an existing structure to minimize the loss of prestress in the tendons. Loss of prestressing force observed in the CFRP tendons was accounted for mainly by two factors:

- curvature frictional effects and elastic shortening of the concrete due to sequential stressing of the tendons, varying from about 9 to 14%
- tendon relaxation, which was measured at about 5% of the initial jacking force during the first 7 days, rose to a maximum of 10 to 12% after 100 days.

The prestress loss due to slip in the anchorage of the CFRP tendons during the period of observation was found to be insignificant, demonstrating the efficient performance of the grout system used in the anchorage. Losses in prestress due to creep effects of the concrete in the existing reinforced concrete double-tee beams also were insignificant.

In applications where GFRP cables are used in tie-back arrangements, significant advantages over steel bars or cables are possible. The length of the tie-back cables can be reduced to a minimum based on the soil properties and height of the wall — in the current study, only twice the height of the wall. The shorter cable length will reduce the overall cost of earthwork for a project and will lower costs on cable. Furthermore, because GFRP cables are corrosion-resistant in wet or damp soils, they have a significantly longer life expectancy than steel. Also, because GFRP cables have a lower modulus of elasticity than steel post-tensioning bars, wall movements will not produce such high stresses on the cables, which in turn reduces the likelihood of failure. GFRP tendons and cables are less than or equal to the cost of equivalent DYWIDAG steel post-tensioning bars. In addition, the properties of GFRP cables enables tension

adjustment (if needed) over the service life of a structure — something not possible with steel cables.

Beam-strengthening tests conducted at USACERL showed that significant increase in shear strength is achieved by the application of FRP to concrete beams that are deficient in shear capacity. When the FRP wrap is properly applied over the shear span of the member, the failure mode of that member may be altered from a brittle shear failure to a ductile flexural failure. However, in this test, the repaired beam was not able to achieve the strength and stiffness levels of a specimen properly reinforced with steel.

The effectiveness of an FRP repair or upgrade of a concrete beam requires careful preparation of the surface; proper selection of a tough, flexible polymer resin; and proper placement of the fabric. The bond between the FRP and concrete was shown to be very good, but a gap between the web and slab that was not covered by the FRP during beam repair led to a failure in the upgraded beam. While this beam deflected significantly more than a control beam that failed in shear, the mode of failure was similarly sudden and brittle. This beam's overall stiffness was not as great as that of either control beam.

Connectivity between the beam web and slab was also shown to be very important, as all test beams tended to separate along this interface after testing was completed. Both beams that failed in shear failed along this interface. Insufficient shear reinforcement may also affect the quality of tendon anchorage, concrete confinement, and anchorage of the web to the cast-in-place slab. Proper application of FRP will assist in providing concrete confinement and anchorage of the web to the cast-in-place slab, but will not aid in anchoring the prestressing tendons.

When designed or repaired with adequate shear reinforcement, the behavior of the test beams was exceptional. Failure loads for the control beam and the repaired beam were very high compared with design service and ultimate loads. Failure was also very ductile for these members, with deflection capacity extending well beyond the point at which the ultimate load was reached.

In reinforced concrete applications, existing flexural members may be structurally upgraded using FRP either for stiffening or strengthening. Depending on the criteria and the conditions of the existing member (i.e., materials and geometry), the repair method may be more or less effective.

In general, if a designer is only concerned with stiffening and the repaired element is not required to carry any additional service load, stiffening is always

attainable. For a given thickness of FRP material, the higher the stiffness of the FRP material, the better the results. The failure mode of the repaired system may become brittle, however, depending on several parameters, which include existing member conditions as well as repair parameters (e.g., p/l ratio). If a designer is concerned with strengthening an existing structural member and improving its load-carrying capacity at service of a given amount, several factors must be considered. The success of the repair and the selection of the FRP stiffness, thickness, and bonded length have to be based on the limitations imposed by (1) shear strength of the existing member, (2) mode of failure of the repaired system, and (3) deflection at the new service load. Also, the bonded length of FRP should be as long as possible to make better use of the FRP strength resources and to activate failures such as concrete crushing or FRP rupture. The adhesive used to bond the FRP to the concrete substrate should have high ultimate elongation.

The results of the analysis in terms of repaired-to-unrepaired strength and deflection ratios indicate that brittle failure mechanisms can develop at loads much lower than expected when considering only flexural performance controlled by concrete crushing and FRP tensile rupture. The analytical model accounts for brittle failure mechanisms induced by debonding of the FRP reinforcement or shear-tension failure in concrete in the plane of the main longitudinal steel reinforcing bars. Even when considering the limitation of the reinforced concrete member due to its unmodified shear resistance, it is shown that the application of FRP reinforcement can considerably increase load resistance capacity and limit deflection at service.

Currently there are no generally accepted testing procedures used to identify the quality of field installed FRP composites. Proposed in-field pull-off testing using square plates and the torsion shear bond test demonstrate that both test methods are practical and can be performed in the field by engineers. However, both methods need more development and precision. No numerical correlation of pull-off tensile strength and torsion shear strength was possible. There is an urgent need for further development and adaptation of standard test methods, materials, and procedures to mimic on-site conditions including surface preparation of FRP, surface preparation of steel probes, quality of the resin or adhesive, curing conditions, and duration of cure.

Field inspection of a CFRP strengthening system exposed to severe environments for more than 30 months showed that the bond between the existing concrete and FRP performed as designed. In laboratory freeze-thaw testing, results showed that, on a short-term basis, low temperature has no adverse impact on the bonding of composite to concrete. In almost all cases the load

capacities increased over those at room temperature. In one load capacity test (thin one-ply bond in four-point bending), the mode of failure was tensile accompanied by debonding, as opposed to the shear debonding of the five-ply composite. Within about 30% load capacity there was no significant difference in the load deflection characteristics (stiffness) between room temperature and low temperature (-30 °C). The low temperature failure loads were generally higher than the room temperature loads.

No significant difference with the failure loads was observed using full-size beams following million-cycle fatigue loading both at room temperature and low temperature, but the deflection and strain at low temperatures were lower, indicating higher stiffness. The data from the small specimens tested in 4-point bending after 200 thermal cycles showed no significant degradation of the thermally cycled specimens. At low temperature the bond strength improved. The influence of a primer coating was negative at both room temperature and low temperature. Low temperature increased the bond strength and the primer coating reduced the strength. More strength is developed over a longer bond length. The length over which bond strength develops is an important parameter that can be studied through this test.

As a result of the post-tensioning demonstration of CFRP tendons, a test fixture was designed and constructed for testing the ultimate tensile strength of FRP tendons at drape angles varying from 0 degrees to 20 degrees around king- or queen-post diameters from 2 in. to 6 in. This type of fixture is needed for proposed ASTM test methods on FRP reinforcing for concrete.

Recommendations

It is recommended that further analytical and experimental studies be conducted to establish the benefits of supplemental anchorage for improving the bond of the FRP to reinforced concrete structural members. Methods for ensuring proper surface preparation and proper installation of the FRP in the repair process should be refined. In addition, the effects of environmental factors (e.g., temperature and moisture) on the epoxy interface and performance of upgraded beams under fatigue loading should be examined. It also is recommended that the design procedure outlined in this report be incorporated into an Engineering Technical Letter.

Further tests are needed to establish ASTM test methods for determining the in-field quality of FRP installations. Standard pull-off tensile strength and torsion shear strength tests are needed to assist field engineers during

inspections. These procedures will allow engineers to specify FRP materials for repair in the absence of comprehensive durability studies.

It is recommended that the design specifications for the drape angle test fixture should be submitted to ASTM Committee D20.18 for incorporation into draft test specifications for FRP tendons.

Commercialization and Technology Transfer

Technology Transfer Plan

The Composites Institute's Market Development Alliance (MDA) has developed a pre-commercialization model which provides crosscutting mechanisms to accelerate the steps required to demonstrate and commercialize new FRP composite products. This plan outlines a recommended process to expedite technology transfer for using FRP composites to repair or strengthen reinforced concrete structures.

This plan assumes the need for repair/upgrade of concrete structures is only in the U.S. It is recognized that a much larger international opportunity exists for these new products. However, the tech transfer activities for international commercialization are beyond the scope of this plan.

One of the technology transfer goals is to establish some form of industry organization (e.g., FRP Composites Concrete Repair Council) to carry out portions of the technology transfer plan. Based on the above assumptions, the MDA Technology Transfer plan comprises the following steps.

1. Establish a Concrete Repair Council

The Composites Institute Market Development Alliance plans to initiate the formation of a Concrete Repair Council, similar to CI's existing councils, by inviting all interested FRP composites concrete repair material suppliers to join together under the Composites Institute. In the interim, the CI MDA will represent the FRP concrete repair material suppliers to the customer while the council is forming.

The council can serve many functions. First, it could be the voice of the industry by providing the engineer a source of information on FRP composites. Second, it could interface with other key trade, technical, and professional organizations

(TTPOs) in this market area; and third, the council could prepare technical and promotional materials covering the following information:

- General background on FRP composites
- An illustrated history of the FRP composites used in concrete repair applications and CPAR project achievements
- Handbook of industry construction practices for concrete repair systems such as recommendations on handling, storage, installation, connections, maintenance, repair, and technical support
- Manufacturers literature and technical information
- Summary of "expert" resources (consultants, universities, TTPOs, etc.)

2. Establish a Technology Transfer Advisory Board

The purpose of the Technology Transfer Advisory Board is to bring the "reality" of the marketplace into the development process at a stage which is early enough to influence significant technical decisions. The Technology Transfer Advisory Board may include architects, designers, structural engineers, contractors, owner/operators of concrete facilities, key TTPOs, code bodies, and regulatory organizations that have a "stake" in the application of this technology. The Advisory Board's role is to continually provide the FRP concrete repair material suppliers with the following critical information:

- Characterize traditional materials and construction practices (strengths, weaknesses, needs, and industry influence factors)
- Identify performance-based specifications for various applications
- Identify installed cost targets
- Provide direction in the development of standards and other regulatory approvals
- Recommend and coordinate continuing demonstration projects
- Serve as a "reality check" for project decisions
- Provide liaison to key industry influence factors
- Act as technology advocates within their respective communities

3. Develop Industry-Level Construction Documents and Preliminary Standards

A critical technology transfer step is the development of construction documentation (means and methods), preliminary specifications and standards that represent recommended industry practice and leads to approval of the developed products. By and large, the U.S. concrete construction community has no widely recognized approval mechanism to accomplish this. ACI has

oversight through Committee 440-F, but is not expected to complete the proposed provisional standard before completion of the CPAR project.

One possibility is to approach the Civil Engineering Research Foundation's new Civil Engineering Innovative Technology Evaluation Center (CE-ITEC) to design an evaluation and testing plan for the Concrete Repair Council. Expected feedback from the CE-ITEC process will identify areas for product improvement and required modifications to practice that provides an iterative loop back into the research and/or development phase. This will be outside of the timing and scope of the current CPAR project. Assuming that the evaluation process validates the product, the next step is widespread, but focused demonstrations to the prospective market.

4. Continuing Demonstrations

The MDA will continue to support field demonstration projects to encourage acceptance of FRP technology in this market. Demonstrations conducted on a regional or local basis could include key industry influence. Generally speaking, the number of field demonstrations of the technology will be directly proportional to the size and fragmentation of the target market. Regional demonstrations can be organized in conjunction with the Advisory Board and participating trade, technical, or professional organizations. It is recommended that the U.S. Army Corps of Engineers identify specific demonstrations sufficient to satisfy their particular needs.

5. Continuing Promotion and Publicity

An important aspect of the technology transfer plan is to create focused promotional literature for the engineer and publicize case histories in current construction journals or magazines. Examples of this activity include articles in ENR, Roads & Bridges, ASCE publications, etc. Whenever possible, demonstration sites will be used as promotional vehicles for chapters of local TTPOs by providing tours to such organizations.

6. Education and Training

To introduce the technology to the engineer, an education and training package is planned to be developed. These materials can be created in association with the key trade and professional organizations of the concrete construction industry. Education packages can be widely publicized through the industry media. Educational materials are currently being developed in ACI 440E and will include slide presentations and handout materials. A possible alternative is

for the Composites Institute to develop a web site to introduce the technology and be made available through CE-Net when that service is operational in early 1998.

Individual companies have developed or are developing design guidelines and procedures for their specific systems. The design guidelines being developed by ACI Committee 440F will be generic for the use of FRP composites for concrete repair.

Coordination of focused workshops is another key aspect of education. The Composites Institute for example can provide an education workshop or focused sessions at its annual ICE (International Composites Exposition) conference. Other workshops can be planned at traditional construction conferences such as ACI, ICRI, or ASCE. Live product demonstrations could take place at key TTPO venues including ACI, ASCE, ICRI, PCI, and ICE. Plans include presenting technical papers at every major industry event that discusses the achievements of this CPAR project.

To introduce the technology to the Corps of Engineers, a module on concrete repair using FRP composites can be added to existing Corps of Engineer training courses and conferences such as the Corrosion Course held at USACERL every year and the World Wide DEH Conference. If funding is available, an engineering technical letter as well as other guidance for the use of FRP for repair of reinforced concrete structures can be developed and disseminated throughout the Corps. Specialized workshops can also be developed directed toward Corps personnel for training and education in the technology. A training course to introduce composites to civil engineers is planned for 6 to 12 months after the official release of the ACI 440F design guideline document. Such a course would be offered in two parts: Part I, "Introduction to Composites," and Part II, "Basic Design Guidelines for Concrete Repair Using FRP Composites." The length of the course is yet to be determined. It would be offered at the Corps district engineer level.

7. Continuing Commercial Proliferation

The above steps are the essential elements of a full-scale commercial launch. Additional activities include exhibits at industry trade shows, demonstrations at national, regional, and local levels. The technology transfer plan seeks to integrate FRP composites development into the mainstream of the existing industry structure using the resources and contacts of the U.S. concrete construction community.

Commercialization

This CPAR project was successful in providing the impetus for developing at least one new FRP composite concrete repair system: Structural Grids, patent pending by Clark-Schwebel Tech-Fab Co., Anderson, SC. The system combines the adhesive bonding of precured sheet laminates and hand lay-up. The system was developed for exterior application to concrete and masonry structures, but the manufacturer initially sees more commercial potential in other markets (e.g., pavement underlayments). Clark-Schwebel made this system commercially available in January 1998. Appendix H provides technical specifications for the Structural Grids system.

References

Al-Sulaimani, G.J., A. Sharif, I.A. Basunbul, M.H. Baluch, B.N. Ghaleb, "Shear Repair for Reinforced Concrete by Fiberglass Plate Bonding," *ACI Structural Journal*, vol 91, no.3, July-August 1994, pp 458-464.

American Concrete Institute (ACI). (1995). "Building code requirements for reinforced concrete and commentary." ACI 318-95, Detroit, Michigan.

American Concrete Institute, Committee 440 (Fiber Reinforced Plastic Reinforcement), "State-of-the-Art Report on Composite Reinforced Concrete", Detroit, MI, April 1995, 126 pp.

American Society of Civil Engineers, "Infrastructure - A Good Investment", New York, NY, 1993.

ACI Committee 318, "Building Code Requirements for Reinforced Concrete," ACI 318-89, American Concrete Institute, Detroit, MI, 1992, pp. 338.

ACI-ASCE Committee 326, (1962), Shear and Diagonal Tension, Pt 2, J. ACI, vol. 59, no. 2, pp. 277-333.

Arduini M., A. D'Ambrisi, A. Di Tommaso, "Shear failure of concrete beams reinforced with FRP plates", *Proceedings of New Materials and Methods for Repair ASCE*, San Diego, Nov. 13-16, 1994, pp 415-423.

Arduini M, A. Di Tommaso, A. Nanni, "Brittle Failure in FRP Plate and Sheet Bonded Beams," *ACI Structural Journal*, 1995 (submitted).

Arduini M., A. Di Leo, "Composite behavior of partially plated beams in the linear elastic range" ACI Spring Convention, Washington DC, March 15 -20, 1992, 10 pp.

Arockiasamy, M., (1997), Damage process of CFRP composites and the concrete interface under fatigue loading at low temperatures, CRREL Technical Note (Unpublished).

Bader, M.G., "Tensile strength of uniaxial composites," *Science and Engineering of Composite Materials*, vol 1, 1988, pp 1-11

Baumert, M.E., M.F. Green, and M.A. Erki, "Low temperature behavior of concrete beams strengthened with FRP sheets," *Proceedings of the 1996 CSCE Annual Conference*, Canadian Society of Civil Engineering, Montreal, Quebec (1996a),.

Baumert, M.E., M.F. Green, and M.A. Erki, "A Review of Low Temperature Response of Reinforced Concrete Beams Strengthened with FRP sheets. Advanced Composite Materials in Bridges and Structures," *Proceedings of the Second International Conference on Advanced Composite*

Materials in Bridges and Structures, Montreal, August 11-14, M.M.El-Badry, Ed., Published by the Canadian Society for Civil Engineering, pp. 565-572 (1996b).

Berwanger, C., and A. F. Sarkar, "Effect of temperature and age on thermal expansion and modulus of elasticity of concrete. Behavior of Concrete under Temperature Extremes," ACI SP-39, (1973) pp 1-22.

Bogetti, T.A., J.W. Gillespie.Jr., and R.L. McCollough, "Influence of processing on the development of residual stresses in thick section thermoset composites. in Thick Section Composites Technology," (eds. E. S.Wright and B.M.Halpin, Jr.), *Sagamore Army Materials Research Conference Proceedings, Oct. 23-26, 1989*, Plymouth, MA, (1992) pp 121-138.

Browne, R.D., and P.B. Bamforth, "The use of concrete for cryogenic storage: a summary of research, past and present," First International Conference on Cryogenic Concrete, 25-27 March, New Castle, London, The Concrete Society, 1981, pp. 135-166.

Civil Engineering Research Foundation, "Materials for Tomorrow's Infrastructure: A Ten-Year Plan for Deploying High-Performance Construction Materials and Systems", Washington, D.C., December 1994, 198 pp.

The Composites Institute of the Society of the Plastics Industry, Inc., "Annual Statistical Report of U.S. Composites Industry Shipments", New York, NY, January 1995a.

The Composites Institute of the Society of the Plastics Industry, Inc., "Introduction to Composites" 3rd Edition, New York, NY, January 1995b.

The Composites Institute of the Society of the Plastics Industry, Inc., "Annual Statistical Midyear Report", New York, NY, September 1997, 6 pages.

Chajes, M.J., W.W. Finch, T.F. Januszka, T.A. Thomson, "Bond and Force Transfer of Composite Material Plates Bonded to Concrete," *ACI Structural Journal*, vol.93, no.2, March-April 1996, pp 208-217.

Chajes, M.J., T.F. Januszka, D.R. Mertz, T.A. Thomson, W.W. Finch, "Shear Strengthening of Reinforced Concrete Beams Using Externally Applied Composite Fabrics," *ACI Structural Journal*, vol.92, no.3, May-June 1995, pp 295-303.

Chajes, M.J., T.A. Thomson, B. Tarantino, "Reinforcement of Concrete Structures Using Externally Bonded Composite Materials," *Non-Metallic Reinforcement for Concrete Structures (Proceedings)*, 1995, E&FN Spon, London, pp 501-508.

Chajes M.J., T.A. Thomson, T.F. Januszka, W. Finch, "Flexural strengthening of concrete beams using externally bonded composite materials", *Construction and Building Materials*, vol 8, no. 3, 1994, pp 1212-1225.

Dutta, P.K., "Low-temperature compressive strength of glass-fiber-reinforced polymer composites," *Journal of Offshore Mechanics and Arctic Engineering*, vol.116, 1994, pp 167-172.

Dutta, P.K., " Tensile strength of unidirectional fiber Composites at low temperatures," *Proceedings of the Sixth Japan-U.S. Conference on Composite Materials*, June 22-24, Orlando, Florida, Technomic Publishing, 1992, pp 782-792.

Dutta, P.K., "Structural fiber composite materials for cold regions," *ASCE Journal of Cold Regions Engineering,* vol 2, no 3, September 1988, pp 124-134.

Dutta, P.K., J. Kalafut, and D. Farrell, "Performance of Laminated Composites in Cold," *Proceedings of the Army Science Conference*, vol 2, 25-27 October 1988, Fort Monroe, Hampton, VA, Office of the Assistant Secretary of the Army (RD&A), pp 269-281.

Dutta, P.K.,() "Fiber composite materials in an arctic environment," *Structural Materials, Proceedings of ASCE Specialty Conference- Seventh Annual Structures Congress*, May 1-5, 1989, San Francisco, California, pp 216-225.

Dutta, P.K., and R.G. Lampo, "Behavior of fiber reinforced plastics as construction materials in extreme environments," *Proceedings of Third Offshore and Polar Engineering Conference*, Singapore, 6-11 June 1993. pp 339-344.

Dutta, P.K., and D. Hui, "Low temperature and freeze-thaw durability of thick composites, Composites: Part B: Engineering," *Elsevier Science Limited*, vol. 27B, no. 3/4, 1996, pp 371-379.

Emmons, Peter H., "Concrete Repair and Maintenance Illustrated", R.S. Means Company, Inc., Kingston, MA, 1994.

Engineered Materials Handbook, Vol. 1, "Composites," ASM International, Metals Park, OH, 1987, p 36.

Federal Highway Administration, "National Bridge Inventory (Chapter 3), in Highway Bridge Replacement and Rehabilitation Program, Eleventh Report of the Secretary of Transportation to the United States Congress", Washington, D.C., April 1993.

Frostig, Y. et al. "High-order theory for sandwich-Beam behavior with transversely flexible core", ASCE Engineering Mechanics Div., vol. 118, no. 5, May 1992, pp 1026-1043.

Gee, Duane J., Memorandum of 21 June 1996.

Hoa, S.V., M. Xie, and X.R. Xiao, "Repair of steel reinforced concrete with carbon/epoxy composites, Advanced Composite Materials in Bridges and Structures," *Proceedings of the Second International Conference on Advanced Composite Materials in Bridges and Structures*, Montreal, August 11-14, 1996, M.M.El-Badry, Ed., Canadian Society for Civil Engineering, pp 573-580.

Hoshijima, T., H. Yagi, T. Tanaka and T. Ando, "Properties of CFRP for Concrete Structures," First International Conference on Composites in Infrastructure, ICCI '96, Tuscon, AZ, January 1996, pp 227-241.

International Conference of Building Officials Evaluation Service, Inc., "Acceptance Criteria for Concrete and Reinforced and Unreinforced Masonry Strengthening Using Fiber-reinforced Composite Systems," AC125, April 1997.

Jones, R.M., "Mechanics of Composite Materials," (Hemisphere Publishing Corporation, 1975) pp 193-198.

Kaiser, H., Bewehren von stahlbeton mit kohlenstoffaserverstarkten epoxidharzen. (Strengthening of reinforced concrete with epoxy-bonded carbon-fiber plastics), Ph D Thesis, Diss ETH Nr. 8918, Zurich (1989).

Lord, H.W., P.K. and Dutta, "On the design of polymeric composite structures for cold regions applications," *Journal of Reinforced Plastics and Composites*, vol. 7, 1988, pp 434-458.

Madhukar, M.S., and P.K. Dutta, *Effect of matrix stiffness on wavy fiber behavior in single-carbon-fiber-epoxy composites.* Special Report 94-10, 1994, (U.S. Army Cold Regions Research and Engineering Laboratory, Hanover, NH).

Madhukar, M.S., and L.T. Drzal, "Fiber-matrix adhesion and its effect on composite mechanical properties: II. Longitudinal (0°) and transverse (90°) tensile and flexural behavior of graphite/epoxy composites," *Journal of Composite Materials*, vol 25, 1991, pp 958-991.

Meier, U. "Bridge repair with high performance composite materials." Material und Technik, vol 4, 1987, pp 125-128 (in German).

Model Code 90, CEB-FIP Committee, Lausanne, 1993.

Morton, S., (1997). Personal communication, Ohio Department of Transportation.

Naderi, M., "Internal Research Report," (Civil Engineering Department, The Queen's University of Belfast, 1985).

Neville, A.M., Properties of Concrete.3rd ed. (John Wiley and Sons, 1991).

Nilson, A.H., and G. Winter, Design of Concrete Structures (McGraw Hill Inc., 1991) p 135.

Norris, T., H. Saadatmanesh, and M.R. Ehsani, "Shear and Flexural Strengthening of R/C Beams with Carbon Fiber Sheets," *ASCE Journal of Structural Engineering*, vol 123, no. 7, July 1997.

Rostasy, F.S., U. Schneider, and G. Weidermann, "Behavior of mortar and concrete at very low temperatures," *Cement and Concrete Research*, vol 9, 1979, pp 365-376.

Rosen, S.L., Fundamental Principles of Polymeric Materials (John Wiley and Sons, 1993) pp 9-31.

Saadatmanesh H., M. Ehsani, "RC beams strengthened with GFRP plates" Part I and Part II, *Journal of Structural Engineering*, ASCE, vol. II 7, no. 11, Nov. 1994, pp 3434-3455.

Saadatmanesh, H. and M. Ehsani, "Fiber Composite Plates Can Strengthen Beams," *Concrete International*, vol 12, no.3, March 1990, pp 65-71.

Tsai, S.W., and H.T. Hahn, Introduction to Composite Materials (Technomic Publishing Company, 1980) pp 244-246.

Wang, A.S.D., "On fracture mechanics of matrix cracking in composite laminates," *Proceedings of Intn'l. Symposium on Composite Materials and Structures*, 1986, Beijing, pp 576-584.

Yamane, S., H. Kasami, and T. Okuno, "Properties of concrete at very low temperatures," *International Symposium on Concrete and Concrete Structures*, 1978, ACI SP 55, pp 207-221.

Glossary

Term	Definition
AASHTO	American Association of State Highway and Transportation Officials
ACI	American Concrete Institute
ASCE	American Society of Civil Engineers
ASTM	American Society of Testing and Materials
C	centigrade
CE-ITEC	Civil Engineering Innovative Technology Evaluation Center
CERF	Civil Engineering Research Foundation
CFRP	Carbon Fiber Reinforced Polymer (Plastic)
CI	Composites Institute
ConREF	Concrete Research & Education (ACI)
CPAR	Construction Productivity Advancement Research
CRREL	Cold Regions Research and Engineering Laboratory
design Life	The planned life of a structure at the time it was engineered and constructed.
Ductility	That property of a material by virtue of which it may undergo large permanent deformation without rupture. The ability of a material to deform plastically before fracturing.
economic life	The time span from date of first functional use until the maintenance and repair costs are no longer justified based upon the replacement cost or utility of the structure.
EMPA	Swiss Federal Laboratory
ENR	Engineering and News Record
EPA	Environmental Protection Agency
F	Fahrenheit
FHWA	Federal Highway Administration
FRP	Fiber Reinforced Polymer
FRP composite	A fiber-reinforced polymer comprised of a matrix of polymeric material reinforced by fibers or other reinforcement with a discernible aspect ratio of length to thickness. A combination of two or more materials (reinforcing elements, fillers, and composite
Ft	feet
GDP	Gross Domestic Product
GFRP	Glass Fiber Reinforced Polymer (Plastic)
Gm	Grams
Gpa	Gigapascal
HPC	High Performance Concrete
ICBO	International Conference of Building Officials
in.	Inch
ICRI	International Concrete Repair Institute

k-ft	Thousand Feet
Kg	Kilogram
Kips	Kilopound (1000 lb)
KN	Kilonewton
ksf	Thousand Pounds per Square Foot
ksi	Thousand Pounds per Square Inch
lbf	Pounds Force
m	Meter
MDA	Market Development Alliance
mm	Millimeter
MPa	Megapascal
Msi	Million Pounds per Square Inch
N	Newton
NDE	Nondestructive Evaluation
ODOT	Ohio Department of Transportation
OSHA	Occupational Safety & Health Administration
Pa	Pascal
PCI	Prestressed Concrete Institute
preservation	The process of maintaining a structure in its present condition and arresting further deterioration.
protection	The process of maintaining a structure in its present condition by minimizing the potential for deterioration or damage in the future.
psf	Pounds per Square Foot
psi	Pounds per Square Inch
QA	Quality Assurance
QC	Quality Control
R&D	Research and Development
RC	Reinforced Concrete
rehabilitation	The process of repairing or modifying a structure to a desired useful condition.
repair	To replace or correct deteriorated, damaged, or faulty materials, components, or elements of a concrete structure.
repair systems	The materials and techniques used for repair.
restoration	The process of re-establishing the materials, form, and appearance of a structure to those of a particular era of the structure.
retrofit	To make modifications to a structure to add new enhancements to it.
RP	Reinforced Plastic
SI	Super Imposed
strengthen/upgrade	The process of restoring the capacity of weakened components or elements to their original capacity or increasing the strength of components or elements of a concrete structure.
TM	Trade Mark
TPO	Trade and Professional Organization
TRB	Transportation Research Board (FHWA)
TTPO	Trade-Technical-and-Professional Organization
traditional methods	Accepted concrete and steel repair/upgrade methods

TRIP	The Road Information Program
USACERL	U.S. Army Construction Engineering Research Laboratories
UV	Ultraviolet

Appendix A: FRP Repair of Reinforced Concrete Beams with Insufficient Shear Capacity

Introduction

Previous studies of rectangular beams have shown that FRP wraps of the full cross section improve the capacity of the section. The challenge of applying an FRP wrap to a beam with slab and the benefits of such an upgrade have not been assessed. The technology has potential application to highway bridges constructed in accordance with American Concrete Institute (ACI) codes of the 1950s and 1960s where these bridges may have less shear capacity than flexural capacity or require added load capacity. A proven repair method for this application may provide a cost-effective solution for military installations and Corps of Engineers civil works facilities as well as state departments of transportation.

Shear repair of reinforced concrete beams using externally bonded materials is not a new concept. For many years, sheets of steel were applied to the tensile face of damaged beams. The steel was effective in increasing both the shear and flexural capacities of the member. However, there are two major disadvantages with this method. First, bonding the steel to the beam is quite difficult in the field due to its bulk. Second, the plate is obviously susceptible to corrosion resulting in loss of adhesive bond.

An innovative method of beam shear repair involves the use of FRP externally bonded to the faces of the member where shear capacity is deficient. Several schemes are available: FRP plates bonded to the sides, strips of FRP material bonded to the sides, or a jacket or wrap placed along the shear span. FRP addresses the traditional material weaknesses of steel. FRP is non-susceptible to corrosion and is relatively conducive to field prepping and hand lay-up. There have been several studies investigating the use of externally bonded FRP sheets to improve strength and stiffness of R/C beams. However, most studies have

dealt with improving flexural strength. Only a few studies specifically addressed shear.

Al-Sulaimani et al. (1994) tested simply supported R/C beams with fiberglass in all three configurations (plates, strips, and wrap) under four-point loading. The specimens were 6 in. x 6 in. in cross section and 49.2 in. in length. Compression and tension reinforcement as well as web stirrups were present. These beams were pre-damaged before retrofit and were designed to fail in shear (the stirrups served mostly to confine the flexural reinforcement). They determined that fiberglass plates and strips bonded to the sides of the beams produced a modest (25 to 30%) increase in shear capacity. This repair technique, however, did not provide enough of an improvement to prevent a shear mode of failure. Also, the fiberglass plates and strips peeled off. Beams fitted with a fiberglass wrap nearly doubled the beams' shear capacity. This increase was sufficient to produce a flexural mode of failure.

Chajes et al. (May 1995) investigated R/C beams with aramid, glass, and graphite wraps loaded in four-point bending. These specimens were structural tees in cross section having a 7.5 in. depth, 5.5 in. wide flange, 2.5 in. thick web and 48 in. length. These beams were completely lacking in shear reinforcement but contained enough flexural reinforcement (only tension steel) such that a shear failure would occur. While all beams experienced an increase in ultimate capacity they still failed in shear. The glass and graphite wraps were torn along the diagonal crack. The aramid wrap allowed the failed beams to carry some load. It is important to note that the purpose of their experimentation was not to force flexural failure. Based on the amount of reinforcing steel placed, shear failure was bound to occur, and the effectiveness of the system to increase shear capacity was determined. As a result, the FRP wrap was shown to be effective for shear repair. Chajes et al. (1995) published another paper where the beams were designed to fail in flexure. The only shear reinforcement would be provided by the FRP wrap. In this experiment, the beams developed sufficient shear capacity and failed in flexure.

Based on these results, it is known that composite wraps are potentially very effective in shear rehabilitation. Both research groups stated the need for full scale testing. This paper discusses the test results of full scale prestressed high-strength concrete joists which had insufficient shear reinforcement and were strengthened in shear with FRP.

Fiber-Reinforced Composites

A composite is a combination of two or more materials (reinforcing elements, fillers, and matrix binder) with different form or composition which, when combined into a material system, exhibit properties which are a combination of its individual components. The system constituents retain their distinct identities, meaning they do not dissolve or merge completely into each other, but act in concert to provide an overall function. The matrix can be a ceramic, metal, or polymer. Fillers may be mineral or metallic powders. Reinforcing can be particles, fibers, rods, or bars. For example, reinforced concrete is a composite consisting of steel reinforcement, sand and gravel fillers, and a portland cement matrix.

Fiber reinforced composites or fiber reinforced polymers (FRP) consist primarily of a typical reinforcement of glass, carbon or aramid fibers, and a polymer matrix. Fillers to modify the physical, mechanical, thermal, electrical, and other properties or to lower the cost or density, may or may not be included. The polymer matrix may be a thermoplastic, a thermoset, or an elastomer. A thermoplastic polymer, polyethylene, polyvinyl chloride, or polystyrene for example, is one which becomes pliable or plastic when heated and then becomes hard again when cooled. A thermoset polymer changes into a crosslinked, substantially infusible material when cured by heat or chemical reaction. Epoxy, polyester, and polyurethane are examples of thermosets. An elastomer is a rubber-like polymer which recovers its original shape and size after removal of a deforming force.

The key component of an FRP is the fibrous reinforcement; it is the primary load bearing component. The matrix serves as the mechanism by which loads are transferred within the member from one fiber to another. Each type of fiber has certain advantages and disadvantages; reinforcement is selected on the basis of its physical, mechanical, and thermal properties.

Modern glass fibers were first developed in the 1930s for military purposes. Soon after, its primary commercial use was for the reinforcement of plastics. E-glass is the standard because of its electrical and mechanical properties. This fiber has a tensile strength nearly double that of steel and has modified versions that resist strong acids. An interesting characteristic of glass fibers is that they are elastic - elongating until failure without yielding. After the load is released the fiber returns to its original length.

Carbon fibers are the most widely used variety of reinforcement having a very wide range of physical properties. Their strength can vary from that of steel to

about four times that. What separates carbon fiber reinforced polymer (CFRP) from the rest is its low weight. Its performance based on stiffness to density is very high. It also has very good fatigue and damping characteristics. Manufactured carbon fibers can vary from the weakest of all fibers to among the strongest. Likewise, their price also varies from inexpensive for the weaker fibers to expensive for the strongest fibers. The most commonly produced versions of CFRP are the intermediate strength fibers. They have tensile strengths stronger than glass and somewhat weaker than aramids.

Like carbon, aramid fibers are lightweight, have high tensile strengths, and good damping and wear resistance. They also have excellent fiber toughness. A popular version of the aramid fiber is marketed under the trademark Kevlar. However, its drawbacks are low resistance to acid attack and high cost.

As the manufacture of FRP composites improve and their mechanical properties are better understood, they are being used in a wider variety of applications. Because of the ultra-conservative nature of the civil engineering community and the relatively short history of FRP composites use, fiber-reinforced composites are just beginning to be considered as a civil engineering material alternative to steel and reinforced concrete. Although many factors, including material form, will significantly influence any design, some general differences between metals and composites may make the latter appear to be the more attractive choice. Differences between composites and metals are as follows:

- Unidirectional aramid and carbon fiber reinforced epoxies provide a specific tensile strength (ratio of material strength to density) that is approximately four to six times greater than that of steel or aluminum
- Unidirectional carbon fiber reinforced epoxies provide a specific modulus (ratio of material stiffness to density) that is approximately 3½ to 5 times greater than that of steel or aluminum. Aramid falls between carbon and glass fiber reinforced epoxies
- Comparing efficiently designed structural elements, the fatigue endurance limit for aramid and carbon fiber reinforced epoxies may approach 60% of the ultimate tensile strength. For aluminum and steel, this value is considerably lower
- Because of the properties listed above, aramid, carbon, and hybrid fiber reinforced plastics can provide structures that are 25 to 45% lighter than aluminum structures designed to the same functional requirements. Impact energy values for aramid-epoxy composites are significantly higher than those for carbon fibers and aerospace aluminum alloys
- Fiber-reinforced polymers can be designed with excellent structural damping features to provide lower vibration transmission than metals

- Fibrous composites are more versatile than metals and can be tailored to meet performance needs and complex design requirements. Design requirements sometimes cannot be satisfied by metal alloys within the critical weight limitations
- The properties mentioned above can be balanced with cost by hybridization (mixing different fibers in a given composite to attain an optimum combination of properties)
- Corrosion and other attributes of fibrous composites will contribute to reduced lifecycle cost
- Composite parts can eliminate joints/fasteners, providing part simplification and integrated design

FRP Composites consist primarily of fiber reinforcement and a polymer. Fibers that are typically used for civil and structural engineering applications are E-glass, carbon, and aramid; polymers are either polyester, vinyl ester, or epoxy. A major reason these polymers are used is because they cure by chemical reaction at ambient temperature. FRP composites may take several forms. The fibers can be in a woven or stitched fabric, or unidirectional sheet, tow or yarn. The composite may be a prepreg (fabric with uncured polymer infusion at the factory), preform (extruded, cast, or shaped at the factory), laminate plate, rod/cable, or a hybrid of these. Various methods exist for applying composites to a structural member. They include hand lay-up, filament winding, vacuum resin transfer molding, and any compaction process. When preforms or laminate plates are used for repair or upgrade, matrix binders or adhesives made of polyester, vinyl ester, epoxy, or polyurethane are used to bond them to the structural members. Depending upon the composite specifications, additives, fillers, or coatings may also be incorporated in the composite to provide UV and/or fire resistance and special moisture or chemical resistance.

Experimental Program

Test Specimens

The hybrid joist design used in the experiments is intended to combine the benefits of prestressed concrete double tees and open-web steel joists but overcome their shortcomings. The hybrid joist was envisioned for use in office construction. A length of 32 ft and a tributary width of 8 ft were chosen for the initial design. Loads of 50 psf office live load and 20 psf superimposed dead load were assumed. All loads were assumed to be uniformly applied along the joist length. This resulted in a superimposed total uniform service load of 70 psf and an ultimate load of 113 psf.

The overall configuration of the joist is shown in Figure A.1.* The joist webs had a constant thickness of 6 in. Joist web ends were 10 in. deep; the depth of all other joist web elements was 6 in. Overall depth of the web was 24 in. Three openings were located along the joist length. Prestressing tendons were located in the top and bottom chords of the web. The prestressing tendon profile is shown in Figure A.2. Six tendons were used, two straight and four draped. Figure A.3 summarizes the web reinforcement of each of the beams. The cast-in-place concrete flanges of HJ-3 and HJ-4 had a thickness of 4 in. and width of 6 ft. The flanges of joists HJ-6 and HJ-7 were 4 ft wide. The slab was reinforced with welded wire fabric (WWF), 4 X 4-W4.0 X W4.0, placed at a height of 2 in. Detailed descriptions of each joist design are provided in Saleh, Brady, Einea, Tadros, and Decker (1997).

Four prestressed high-strength concrete tee-beams with integral web openings were tested. Two joists were used as control specimens. One control joist had insufficient shear reinforcement; one joist was properly reinforced, designated HJ-6 and HJ-7 respectively. The other two joists were repaired, HJ-4, or upgraded, HJ-3, with FRP to improve their shear performance. Joist designations are shown in Table A.1.**

Performance criteria were specified for the two joists to be repaired. It was required that their shear capacity be increased 15 kips over a length 3 ft-10 in. from each end and 10 kips over the following 4 ft. The two repaired beams were wrapped on three sides with Fyfe's TYFO S Fibrwrap™ along the outer 8 ft of each end of HJ-3 and HJ-4, Figure A.4. The FRP repair design was based on the following material properties:

f_{aj} = 12 ksi (conservative estimate of allowable jacket stress)

f_{uj} = 65 ksi (ultimate jacket stress, minimum)

E_j = 3250 ksi (modulus of elasticity of jacket)

ε_{aj} = 0.004 (allowable jacket strain)

ε_{uj} = 0.02 (ultimate jacket strain)

* All figures are found at the end of this Appendix.
** All tables are found at the end of this Appendix.

u_{aj} = 400 psi (allowable bond stress)

t_j = 0.051 in. (jacket thickness per layer)

Standard structural engineering practice for shear designs was used to determine the jacket thickness. Calculations were based on controlling shear crack widths to maintain aggregate interlock and proper shear transfer through the concrete. The allowable jacket strain, εaj = 0.004, represents 20% of the ultimate composite strain. The calculations resulted in the requirement for two layers of SEH-51, with the main fiber strength vertical, over the extreme 4 ft. The next 4 ft required only one layer per the calculations, however, the Fyfe Co. recommended the use of a minimum of two layers (Gee 1996).

No additional anchorage system was used due to the potential interference with the prestressing tendons of the existing joist.

Materials

1. Concrete. The concrete mix used in the hybrid joist specimen webs was a high-performance concrete (HPC). It provided special performance requirements including ease of placement and consolidation without compromising strength, superior long-term mechanical properties, early high strength, volume stability, and long life in severe environments. The HPC concrete strength used was designed to have a strength of 12,000 psi at 28 days. Figure A.5 shows the time versus strength curves for the concrete used in the webs. Ready-mixed concrete was used in the slabs of all specimens. The mix was specified to be 5,000 psi and consisted of Type I cement with a maximum aggregate size of 1.0 in. limestone. The mix corresponded to dry weight proportions of 1.0:3.0:2.6 (cement : fine aggregate : coarse aggregate). On the day of testing all cylinders were also tested. Compression tests were conducted in accordance with ANSI/ASTM C39-86.

2. Steel. The tendons used were manufactured by the American Spring Wire Corporation (26300 Miles Rd., Cleveland, OH 44146). These tendons were 1/2 in. diameter, 270 ksi, low relaxation. The stress-strain curve for these tendons is shown in Figure A.6. The shear reinforcement in the webs consisted of bar reinforcement, Grade 60. A welded wire fabric mesh, Grade 75, was used as reinforcement for the cast-in-place slab.

3. FRP. The FRP was specified as TYFO™ S Fibrwrap System and manufactured by Fyfe Co. L.L.C. of San Diego, CA. The TYFO™ S epoxy is a two-component, solvent-free, moisture insensitive epoxy matrix material. It is a

high elongation material which gives optimum properties as a matrix for the TYFO™ fiber system. The epoxy has no offensive odor and maintains its properties up to 140 °F. Table A.2 lists the epoxy properties. The TYFO™ fiber system is a plain weave, predominately warp unidirectional fabric comprised of a warp (0 degree orientation) of E-glass roving and a weft (90 degree orientation) of aramid, E-glass, and Thermoplastic Adhesive. The ratio of warp fiber to weft fiber is 17.5 to 1 by weight. Table A.3 lists the yarn properties and Table A.4 the fabric properties. Two layers of the TYFO™ S Fibrwrap System were used. Table A.5 lists the composite laminate specifications and Table A.6 the composite properties. The system has been tested and develops an allowable shear stress of greater than 350 psi without anchors.

Fabrication

The webs of the joists were prestressed and cast horizontally, i.e., on their sides as shown in Figure A.7. Hold-down devices were used at the draping points to position the tendons and resist the prestressing forces. The concrete mix was placed in the forms and vibrated to ensure consolidation of the concrete. The specimens were covered with wet burlap that was kept moist for the first 3 days. The specimens cured at room temperature for 7 days. Cylinders measuring 4 in. diameter by 8 in. tall were cast and cured with the joists under the same conditions. The concrete strength was monitored by compression testing of cylinders to assess when the required release strength was achieved. When the strength reached 7000 psi the tendons were released by alternately torch cutting a tendon on each face at the joist ends. Casting and release dates for each specimen are shown in Table A.7. The webs were then turned vertically and stored in the lab. The webs were then positioned vertically upright and level. The slab forms were then constructed around them. After concrete placement, the forms and test cylinders were covered with wet burlap followed by plastic sheets. The burlap was maintained moist for 4 days following casting. After 7 days the forms were stripped. Figure A.8 shows the final shape of the joists.

Prior to application of the composite overlay the joist surfaces were prepared. This involved removing the paint on the outer 8 ft of the webs, rounding the corners at the bottom of the beam web to a minimum radius of 1.5 in., and removing trowel marks and smoothing out rough areas using an electric grinder. Once completed, creases in the web left by the concrete form lining were filled with a rapid strength repair mortar. After the mortar was cured, the surface of the beams was again ground and then cleaned using methyl ethyl ketone to remove any excess dust. Cracks in the concrete of HJ-4 created during pre-loading were ignored since they were less than 1/16 in. wide. The two part

epoxy TYFO™ S Tack Coat was mixed and troweled onto the surface of the beams where the repair/upgrade was to be applied.

While the tack coat began setting up, the reinforcing fabric was cut to the proper length using scissors and infused with the TYFO™ S two part epoxy. This was done by laying the fabric out flat and evenly spreading the resin on the fabric by hand to saturate the fabric. The fabric was then laid up around the end of the joist from just beneath the slab, around the web and up to the slab/web intersection again, Figure A.9. The material was placed vertically (main fibers vertical) in bands of 52 in. (1.2m) on the sides of the joist. Adjacent bands were placed with a 4 in. butt splice. In regions of taper, the bands were applied as four pieces, two per side ensuring that main fibers remained vertical on joist faces. The material was carried under the joist and excess cut off.

Because of lack of Cab-O-Sil™ in the tack coat, the system applicators had great difficulty getting the FRP system to adhere properly to the concrete prior to curing. The cure time was also slow because of high humidity. Upon cure it was noted that the FRP had slipped down on both HJ-3 and HJ-4. A gap, uncovered by FRP, existed beneath the bottom of the slab on the web. In most locations the gap was not significant; however, on the North end of HJ-3 the gap was observed to be 1.25 in., Figure A.10. After curing, voids between the composite and the joist were filled with epoxy, Figure A.11.

Instrumentation and Data Recording

Test specimens HJ-3, HJ-4, HJ-6, and HJ-7 were instrumented with displacement potentiometers, strain gages, and linear variable displacement transducers. Tables A.8 and A.9 summarize the instrumentation plans for HJ-3 and HJ-4. Figure A.13 shows the layout of internal strain gages for HJ-3 and HJ-4. Internal strain gages were located so as to measure strains in both prestressing tendons and reinforcement. Once the composite was cured, strain gages were placed on the external surface at the locations of the most dramatic shear cracks, other previous shear failure areas, and at the FRP lap joints to monitor strain in the composite. Gages were symmetrically placed at each end of the joists. Figure A.13 shows the location of these gages for HJ-3 and Figure A.14 shows the gage locations for HJ-4. LVDT locations were the same for all joists (Figure A.15). Displacements were measured by potentiometers at the center of the joist, beneath one web post and a distance 25% of the span length from a support along the inclined portion of the joist, Figure A.16. All recorded potentiometer displacements were absolute, measured with respect to the laboratory floor. Displacement measurements were also taken manually on the

west and east faces of the slab at each joist end, and along the east slab face at the center and beneath each actuator.

Figure A.17 is a functional block diagram of the instrumentation, data acquisition, and test control systems used at USACERL. All of the transducer output signals were connected to a Hewlett Packard[1] Model 3052A data logging system. The system was controlled by computer through an instrument controller interface bus. The record channels were scanned at a predetermined sampling rate, and the data were recorded in ASCII text files on the computer.

The loading system consisted of two CGS/Lawerence Model 307-50 electro-hydraulic actuators (controlled by closed-loop servo controllers) and a function generator. The actuators were operated in a displacement-control mode. In this mode, the function generator supplies a slowly changing command signal to the controllers. The controllers send a drive signal to each of the actuators, which causes the actuators to move until the displacement measured by LVDTs located inside each actuator is equal to the command signal. The actuators also include load transducers that measure the applied load.

Test Procedure

The test setup on the USACERL Structural Load Floor is shown in Figure A.18. Each specimen was tested as a simply supported beam under two symmetrical point loads with a clear span of m (31 ft) and a shear span of m (11 ft - 3 in.). Vertical loads were applied by 50-kip hydraulic actuators suspended from a load frame. The actuators were centered directly over the web posts of the specimens. In testing at USACERL the stroke of each actuator was calibrated to zero after making contact with the specimen; a small pre-load was associated with this positioning. Specimens were loaded at a constant rate to a specified stroke limit. The actuators were maintained at this stroke while the joist was inspected for cracks; these were marked. Measured readings of deflections were taken at selected locations and the deflection data were checked. Stroke was then further applied to the specimen until the stroke limit of the actuators was reached. The full stroke (i.e., full load) was then removed from the specimen. Steel plates were added between the actuator and the beam. The actuators were then moved into contact with the specimen again; this was associated with a

[1] Hewlett Packard Co., 5301 Stevens Creek Blvd., Santa Clara, CA 95052-8059.

small pre-load. The test was continued in the same manner until the specimen failed. Data were recorded during loading and unloading cycles.

Of the two repaired specimens, HJ-4 was damaged to a predetermined level defined subsequent to testing the control beams, which were unrepaired. The beam was then unloaded and repaired. HJ-3 was not loaded prior to upgrading it with FRP. After repair, the beams were loaded at a constant rate of 0.2 in./min. in increments of 1 in. At each displacement increment, measured readings of deflections were taken at selected locations and deflection data were checked. Loading of HJ-4 continued until the bottom of the joist was ¼ in. from the load floor. The joist was then unloaded. HJ-3 was loaded in the same manner as HJ-4. The joist was tested to failure.

Experimental Results

The measured load and deflection, strains in concrete, steel rebar and FRP, and crack development and failure of each specimen are discussed. Results of the two repaired beams are compared with two control beams.

Load and Deflection

Table A.11 summarizes principal test results, including cracking load, location of first crack, failure load, equivalent uniform superimposed (SI) load at failure for the test configuration, and type of failure. All load values in the table represent the sum of the two actuator loads. The experimental cracking load was determined at the time the first crack was observed. Joist HJ-4 was loaded to a peak of 55.2 kips. After the FRP repair, HJ-4 was reloaded to a peak of 56.6 kips, approximately 690% of the SI service load or 422% of the SI ultimate load. The upgraded joist HJ-3 was then tested, and failed at a load of 52.6 kips, 393% of the ultimate SI design load. The two control joists, HJ-6 and HJ-7, failed at 48.7 kips and 65.0 kips respectively. HJ-6 failed at well below the anticipated capacity but still 363% of the ultimate SI service design load. The premature failure was attributed to insufficient shear reinforcement.

Deflection parameters, including camber at tendon release and experimental deflections due to the applied loads are summarized in Table A.12. For the 31 ft clear span and 6 ft tributary width, the experimental deflections at the load equivalent to live load (LL), 3.5 kips, and the load equivalent to SI dead load (DL) + LL, 4.1 kips, are much lower than the ACI 318-95 limitations of L/360 (1.0 in.), and L/240 (1.55 in.), respectively, for specimens HJ-3 and HJ-4. Similarly HJ-6, and HJ-7 with 4 ft tributary widths deflected much less than

the ACI limitations under loads of 2.3 kips and 4.0 kips for (LL) and (SIDL + LL), respectively. HJ-4 with the FRP repair permitted a midspan displacement of more than 11.3 in. without failing. The test was stopped as there was a lack of space to further deflect the joist. HJ-3 was able to deflect 7.7 in. before failure was initiated.

The experimental load versus midspan deflection curves for joists HJ-3, HJ-4, HJ-6, and HJ-7 are shown in Figure A.19. Initial stiffness (below .2 psf) of all specimens is similar. After this point the stiffnesses of HJ-3 and HJ-4 were less than for either control joist. HJ-3 displayed more flexible response than the damaged or repaired joist HJ-4. HJ-4 was not able to achieve the performance of the control beam HJ-7 which had sufficient shear reinforcement. All joists were able to achieve their peak load repeatedly for several loading/unloading cycles. HJ-4 achieved the peak load for 5 cycles before the test was stopped. Its stiffness did not change significantly from cycle to cycle, Figure A.20.

Deflection profiles along the joist length were approximated using potentiometer data as well as manual measurements from the joists' top flanges. A deflection profile is shown for HJ-3 with respect to load increments of a single actuator in Figure A.21. Figure A.22 shows deflection profiles for HJ-4 prior to repair and after the joist was repaired with FRP. HJ-3 deflected more than either the original or repaired HJ-4 for comparable load levels up to 25 kips. It also deflected much more than HJ-6. Similar plots for the other tested joists are shown in Figure A.23 and A.24. HJ-4, while able to deflect significantly was not able to match the performance of HJ-7. The shapes of HJ-3 and HJ-4 are much like that of the control joist, HJ-7. The shapes reflect the constant moment between load points and the marked stiffness variation along the specimen length. The increased curvature with increasing load also reflects progressively greater cracking in the center section of the joists. The deflected shape of HJ-6 emphasizes the effects of insufficient shear reinforcement in the joist's inability to benefit from the prestressing and optimized shape.

Strains

Three types of strain readings were used in testing the family of hybrid joists: internal strain of reinforcement and external strain on FRP surfaces — both measured by strain gages — and displacement measured over a specified gage length on concrete surfaces by LVDTs. For the latter measurements cracks may have developed within the gage length, and the strain (displacement/displacement) may be greater than the maximum concrete strain range of 0.003 – 0.004 for compression or 0.0001 – 0.0002 for tension.

Strain distribution over section depth is shown in Figures A.25 and A.26 for three critical sections of HJ-3 and HJ-4 with FRP repairs. The distribution was approximated from concrete strain measurements near the top of the section and prestressing strand strains above and below the openings. Similar plots are shown in Figures A.27 and A.28 for HJ-6 and HJ-7, respectively. Strain along prestressing tendon length is shown in Figures A.29 and A.30 for HJ-3 and HJ-4 respectively. Figures A.31 and A.32 show strand strain measurements for HJ-6 through HJ-7.

Strains at the end and midspan of HJ-3 are similar in magnitude to those of HJ-6. It is apparent from Figure A.25 that the full prestressing capacity could not be developed in these joists. This is further shown in Figure A.29 where results of internal strain measurements along the strands for both top and bottom strands of repaired joist HJ-3 are presented. Strains in tendons were greatest in the shear span of this joist. In the constant moment region, strains are much less for both top and bottom tendons. From the strut section strain distribution, we can see that the neutral axis lies at a depth approximately 5 in. from the top of slab in HJ-3. From Figures A.29 and A.31 it is apparent that failure occurred before the full prestressing capacity could be developed in these joists.

Comparing Figures A.26, A.25, and A.28, strain distribution in the repaired joist HJ-4 is quite different from that of either HJ-3 or HJ-7. The neutral axis indicated by the midspan strain is located at the member midheight. Peak strains in top and bottom prestressing strands of HJ-4 were greater than those in HJ-7, Figure A.30 versus Figure A.32. However, strain distribution over bottom tendon length is much more uniform in HJ-7 providing greater ultimate flexural capacity of this section. HJ-4 did not approach the load capacity of HJ-7.

To assess the stress in the strands, the strains shown must be added to the strain due to prestressing and related to the elastic modulus of the material. The strand was fully tensioned, so the effective strain due to the prestress is approximately 6705 micro strain [$(f_{se}/E_s) = 0.75\ (270) / (30{,}000)\ (10^6) = 6750$ micro strain]. All strains were below the ultimate strand strain of 35,000 micro strain. Again, the lack of strain developed in the strand indicates the poor performance of HJ-6. During testing it was observed that the bottom chord of HJ-7 appeared to arch upward between the struts; this may be related to the larger strains shown at the struts than the midspan for some load levels.

Figures A.33 and A.34 show load versus strain in the FRP material for HJ-3 and HJ-4 respectively. Strain gages along the beam web show elongation of transverse FRP with increasing load. In HJ-4 FRP strains do not begin to

increase appreciably until the actuator load is approximately 12 kips indicating the widening of shear cracks in the concrete beneath the FRP and the developing shear resistance in the FRP. Strain in gages ES4 and ES5, closest to the beam center, reached a peak value greater than .005 in./in. This is above the allowable strain of .004 but much less than the ultimate strain of .02. The limited capacity of HJ-3 is shown by the much lower strain values of gages ES4 and ES5 than for HJ-4.

Cracking and Failure Mechanism

None of the joists cracked when the prestressing tendons were released. During handling, specimen HJ-7 developed a crack across the slab through its depth near the south strut. Cracks were marked on each of the joists throughout testing. Cracking and failure mechanisms resulting from testing of HJ-6 and HJ-7 were compared with those of the two hybrid joists upgraded or repaired with FRP. Early in the test series, limited cracking occurred in the bottom chord of HJ-6. As actuator stroke was increased, cracking in the shear spans became evident but the cracks in the bottom chord did not develop further. In HJ-6 an inclined crack developed near the support and progressed upward along the web/slab interface (Figure A.35). This crack progressed into the slab and failure ultimately occurred in this North end of the joist (Figure A.36).

Figure A.37 shows crack development for HJ-7. Initial flexural cracks formed along the bottom chord at midspan. Cracks were regularly spaced, and they became more numerous and closely spaced as the displacement was increased. Near the end of testing, when the load was not increasing but the specimen was able to deflect significantly more, inclined cracks developed in the shear spans of the members. No actual failure was observed in specimen HJ-7. The joist continued to deflect after reaching an ultimate load capacity.

Cracking in HJ-3 initiated as for HJ-7 with flexural cracks in the web bottom chord. At an applied stroke of approximately 5 in. a crack began to develop along the edge of the FRP at the intersection between the joist web and slab, Figure A.38(b). A gap of more than 1 in. of exposed concrete existed where the FRP had slipped down from the web/slab interface. The horizontal crack began near the point where the FRP lapped. As the horizontal crack progressed toward the North end of the joist, cracks also developed in the bottom of the slab perpendicular to the joist span as well, Figure A.38(a). These were associated with popping sounds as if the FRP were debonding from the joist. A vertical crack in the FRP was observed at a distance approximately 6 in. from the North end of the joist. This occurred at a stroke of approximately 7.5 in. A maximum deflection of approximately 9 in. was achieved before complete collapse of the

joist occurred by fracture of the top slab at a distance of approximately 56.75 in. from the North end. The FRP separated from the joist by buckling over the web depth at a distance approximately 41 in. from the joist North end. A third vertical break in the FRP was observed at 25.5 in. from the end, Figure A.39 (a). These cracks in the FRP were accompanied by peeling of the top slab from the web at the construction joint, Figure A.39 (b). Investigation of the failure revealed the concrete in the area of the FRP repair had completely broken up. The total length of crumbled concrete was approximately 50 in. Examination of the TYFO™ S Fibrwrap System showed it to be adhered to the perimeter concrete even at failure. Failure was in the concrete. This was precipitated by the weakness created by the gap in the FRP repair at the top of the web.

Initial testing of HJ-4 without FRP repair produced crack patterns similar to those for HJ-6, Figure A.40. After repair testing began again, existing cracks between struts increased in size and additional cracks were observed to develop near the edge of the FRP repair area, Figure A.41 (a) and (b). The test had to be stopped when there was no further vertical space between the web bottom chord and the floor for the joist to deflect. The joist did not fail. At the test conclusion, the FRP repair showed no signs of damage. The beam exhibited ductile response throughout the test.

Experimental Test Conclusions

HJ-4, while being damaged prior to application of the FRP repair, was able to deflect as much as HJ-7. However HJ-4 with FRP repair was not able to achieve the strength and stiffness levels of a properly reinforced specimen, HJ-7. The shear mode failure of HJ-3 was initiated by a gap on the joist web where the FRP had slipped during curing. Its performance was not improved over HJ-6.

Design Procedure for Hybrid Joists

Overview

Based on standard structural engineering design principals and the experimental test results, a simple procedure was developed to design FRP composite system repairs for reinforced concrete joists deficient in shear capacity. This design procedure is a step-by-step process wherein load demands are assessed for an existing member cross-section, a repair is designed based on specified engineering properties of the FRP composite system to achieve the required capacity, and stresses and deflections for the repaired joist are checked. Figure A.31 shows the flowchart for the joist design procedure.

Design Criteria and Assumptions

Design criteria are based on *Building Code Requirements for Reinforced Concrete*, ACI 318-95 (1995). Load and strength reduction factors as specified by the code are used. Flexural strength is calculated using strain compatibility.

The International Conference of Building Officials has developed a draft document on the subject of "Acceptance Criteria for Concrete and Reinforced and Unreinforced Masonry Strengthening Using Fiber-reinforced Composite Systems" (ICBO 1997). This document provides good guidance for the establishment of minimum requirements for evaluating FRP systems for strengthening concrete elements.

The joist is assumed to be uniformly loaded at all stages with a simple span and roller supports.

Design Procedure

Define Loading

As stated above, uniform loading of the beam is assumed. Service loading is defined as the unfactored load. This will generally be a combination of the beam self-weight, superimposed dead load, and live load. Ultimate load is typically defined as shown below:

$$\text{Ultimate Load} = 1.4\,DL + 1.7\,LL$$

where: DL is the sum of the self-weight and superimposed dead load and

LL is the live load

Calculate the service load for each loading stage. Calculate the ultimate loads acting on the joist. Again, it must be noted that the CPAR test results do not support the use of this type of hybrid joist where concentrated loads will be applied.

Define Capacity of Existing Beam Section

Flexural and shear capacity of the section should be computed without use of reduction factors based on the existing properties.

Flexural capacity is based on strain compatibility and equilibrium. A maximum concrete compressive strain of .003 is being assumed. The ultimate moment capacity, M_u is computed as:

$$M_u = A_s f_y \left(d - \frac{a}{2} \right)$$

where: $a = \dfrac{A_x f_y}{0.85 f_c' b}$

and a = depth of equivalent rectangular stress block, in.

A_s = the area of flexural reinforcement, in.^{2}

f_y = yield stress of reinforcement, ksi

d = distance from extreme compression fiber to extreme tension steel, in.

f_c' = compressive strength of concrete, ksi

b = section width, in.

Shear capacity is a function of the concrete shear strength and shear reinforcement:

$$V_n = V_c + V_x \qquad \text{(ACI, 1995 Equation 11-2)}$$

where V_c is nominal shear strength provided by concrete computed as:

$$V_c = 2\sqrt{f_c'}\, b_w d \qquad \text{(ACI, 1995 Equation 11-3)}$$

for members subjected to shear and flexure only. If the beam has been damaged a conservative assumption of the concrete shear capacity is $V_c = 0$.

V_s is nominal shear strength provided by shear reinforcement and computed as:

$$V_s = \frac{A_v f_y d}{s} \qquad \text{(ACI,1995 Equation 11-15)}$$

where A_v is the area of shear reinforcement within a distance.

Determine Load Requirement for Upgrade/Repair

The degree of upgrade/repair required is represented by the difference between the load demand and the existing section capacity. The ratio of shear capacity to shear demand should exceed that of the flexural capacity to flexural demand. This is to ensure that a shear failure mode, which can occur without warning and may be catastrophic, does not occur. Rather a ductile mode of failure with obvious signs of distress, as would occur in a flexural failure, is desirable. The final shear capacity of the upgraded/repaired beam should be approximately 1.5 to 2.0 times the flexural capacity. The upgrade/repair demand will be represented as V_{req} - required additional shear capacity.

Determine FRP properties

Shear enhancement is provided by fiber-reinforced composite materials with fibers oriented essentially perpendicular to the member's axis. Fiber orientation is critical when determining FRP properties. Important properties to define for design are:

f_{sj} , allowable FRP tensile stress

f_{uj} , ultimate FRP tensile stress

σ_j , allowable bond stress

E_j , FRP modulus of elasticity

ε_{aj} , allowable FRP strain

ε_{uj}, ultimate FRP strain

ICBO limits allowable composite material stress, f_{aj} , to be 0.004 E_j and less than 0.75 f_{uj}.

Determine configuration and calculate thickness of FRP

Research directed toward determining effective configurations of FRP shear repairs for beams by Al-Sulaimani et al. (1994) showed that the use of strips or wings on the beam faces provided comparable increases in shear capacity. However, the mode of failure for these sections tested was still in shear. Shear

repair by a jacket on three sides performed better than repair by strips or wings. The wings of the jacket were well anchored at the bottom of the beam so that no premature peeling failure occurred. Additionally the continuity provided by the geometry of the jacket minimized the effect of stress concentrations in the plates. The beams repaired with FRP jacket exhibited a higher capacity than those of the strip or wing upgrade and ultimately failed in flexure.

A jacket configuration should, therefore, be assumed whenever possible. It is optimal to wrap the entire section in the FRP. If this is not possible the use of anchors should be considered so that bond is not the primary mechanism of force transfer.

Assuming a layer thickness of t_j.

$$V_{req} = 2t_j f_{aj} H \sin\theta$$

where H is the depth of the FRP and θ is the angle of the fibers relative to the member axis. This equation assumes a shear crack inclination of 45 degrees. ICBO recommends the following equation:

$$V_{req} = 2.86 t_j f_{aj} H \sin^2\theta$$

Check Stresses

Bond, flexural, and shear stresses should be checked for the upgraded/repaired joist configuration.

Check stresses due to service loads.

Check stresses at ultimate loading using ACI 318-95 approximate equations or the strain compatibility method:

$$V_u = V_c + V_s + V_p$$

where: V_u, V_c and V_s are defined above and V_p is computed as

$$V_P = 2F_P = 2\left[\sigma_{uj}\left(\frac{dH}{2}\right)\right] \text{ (Al-Sulaimani et al. 1994)}$$

This equation assumes a full U-jacket is used, that shear distribution is uniform over the depth of jacket, with the absence of stress concentrations; therefore, the ultimate stress of the material may be achieved.

Check bond shear stress. ICBO guidance requires that where the performance of the composite material depends on bond, the bond strength of fiber-reinforced composite material to concrete [u_j] shall not be less than the characteristic flexural tension capacity f_t' of the concrete. Under ultimate flexural strength conditions, bond stress between fiber-reinforced composite material and concrete shall not exceed:

$$u_j = \frac{d\left(t_f f_j\right)}{dx} \leq 0.75 f_t'$$

where x is the direction parallel to the fiber. This value should be evaluated at sections where the rate of change in fiber net force, $t_f f_j$, is a maximum. This will normally correspond to locations of maximum shear force.

Check Deflections

An estimate of the load deflection relationship should be checked using structural analysis methods. Deflection limits should be evaluated relative to ACI code requirements.

Determine failure mode

The member should be designed to fail by ductile flexural failure mode. For the strengthening of existing reinforced concrete beams with FRP it is recommended that the repair/upgrade be designed such that ultimate failure occurs by yielding of the steel reinforcing bars before a compressive failure of the concrete. Yielding of the steel bars should not occur before reaching the permitted service loads.

Detailing

For rectangular sections where shear enhancement provided by transverse fiber-reinforced composite material, section corners must be rounded to a radius not less than ¾ in. (20mm) before placement of the composite material.

Design Example

Assumptions

The concrete weight is 150 pcf.

Concrete compressive strength is 4 ksi,

Steel reinforcement yield stress is 60 ksi.

Shear reinforcement consists of #3 U-stirrups at 6 in. o.c. over the length of the beam.

FRP properties

Beam is originally designed to carry 4 k/ft uniform load. Check shear capacity.

$$V_u = \frac{4 \times 25}{2} = 50 \text{ kips}$$

Shear at critical section (at distance d from end) by similar triangles:

$$V_u \text{ at } d = \frac{50 \times (12.5 - 1.5)}{12.5} = 44 \text{ kips}$$

$$V_u < \phi V_n$$

where: $\phi V_n = \phi V_c + \phi V_s$

$$V_c = 2\sqrt{f'c}\, b_w d = 2\sqrt{4000}\,(12)(18) = 27.3 \text{ kips}$$

$$V_s = \frac{A_v F_y d}{s} = \frac{(0.22)(60)(18)}{6} = 39.6 \text{ kips}$$

$\phi V_n = (0.85)(27.3+39.6) = 56.7$ kips > 44 kips **OK**

$$\text{Minimum: } A_v = 50\frac{b_w s}{F_y} = \frac{(50)(12)(6)}{60000} = 0.06 \text{ in}^2$$

A_v (provided = 0.22 in^2) > A_v (required = 0.06 in^2) **OK**

Now, suppose uniform load increases to 6.5 k/ft.

V_u at critical section = 71.5 kips

Shear deficiency = 71.5 - 56.7 = 14.8 kips (say 15 kips)

We need FRP wrap from end to point along beam where shear is less than 56.7 kips.

$$x = \frac{(56.7)(11)}{71.5} = 8.72 \text{ feet (say 9 feet)}$$

Requires FRP wrap from end to 9 feet

Using Fibrwrap™ Jacket and TYFO TC epoxy adhesive

$$V_{req} < 2t_j f_{sj} d\cot 45°$$

where: t_j = 0.051 inches (jacket thickness)

f_{sj} = 12 ksi (allowable jacket stress)

and assuming 45° crack inclination

$$\text{number of jackets} = \frac{15}{2(12)(18)(1)(0.051)} = 0.68 \text{ (1 layer required)}$$

$$\text{check bond stress:} \quad u = \frac{15}{(18)(9 \times 12)} = 8 \text{ psi} < 400 \text{ psi allowable } \mathbf{OK}$$

Compute material required assuming a U-shaped jacket wrap.

Surface area = 2ends(8"+8"+5")(48") = 2496sq.in x 2 layers ---> 34.7 sq.ft

Surface area = 2ends(24"+24"+5")(48") = 14384sq.in x 2 layers ---> 200 sq.ft

Summary

The results of tests performed in this study indicate that significant increase in shear strength can be achieved by the application of FRP to concrete beams deficient in shear capacity. When an FRP jacket is properly applied over the

shear span of the member the failure mode of a member may be altered from that of a brittle shear failure to a ductile flexural failure mode. However, the repaired joist was not able to achieve the strength and stiffness levels of a properly reinforced specimen.

The effectiveness of an FRP upgrade or repair requires careful preparation of concrete surface, selection of a tough epoxy, and placement of the fabric. A gap between the web and slab that was not covered by the FRP proved to initiate failure in a joist upgraded with FRP. While the joist deflected significantly more than a control beam that failed in shear the mode of failure was similarly sudden and brittle. This joist's overall stiffness was not as great as for the two control joists. Bond between the FRP and concrete was shown to be very good.

Connectivity between the joist web and slab were also shown to be very important as all test joists tended to separate along this interface after testing was completed. Both joists that failed in shear failed along this interface. Insufficient shear reinforcement may also affect the quality of tendon anchorage, concrete confinement, and anchorage of the web to the cast-in-place slab. Proper application of FRP can assist in providing the latter two of these requirements but will not aid in anchoring prestressing tendons.

When designed or repaired with adequate shear reinforcement, the behavior of the test joists was exceptional. Failure loads for specimens HJ-4 and HJ-7 were very high compared with design service and ultimate loads. Failure was also very ductile for these members, with deflection capacity extending well beyond the point at which the ultimate load was reached. The hybrid joist behaved very much like a traditional prestressed precast concrete beam except that the hybrid system had the capability to carry 30% more load than the conventional prestressed double tee before first cracks appeared.

Additional analytical and experimental studies should be undertaken to establish the benefits of supplemental anchorage for improving the bond of the FRP to the reinforced concrete structural member. Construction methods for ensuring proper placement and curing of the FRP in the repair process should be refined. In addition, the effects of environmental factors, e.g., temperature and moisture on the epoxy joint, as well as the performance of upgraded beams under fatigue loading should be examined.

References

American Concrete Institute (ACI). (1995). "Building code requirements for reinforced concrete and commentary." ACI 318-95, Detroit, Michigan.

Al-Sulaimani, G.J., A. Sharif, I.A., Basunbul, M.H. Baluch, and B.N. Ghaleb, "Shear Repair for Reinforced Concrete by Fiberglass Plate Bonding," *ACI Structural Journal*, vol 91, no. 3, (July-August 1994), pp 458-464.

Chajes, M.J., W.W. Finch, T.F. Januszka, and T.A. Thomson, "Bond and Force Transfer of Composite Material Plates Bonded to Concrete," *ACI Structural Journal*, vol 93, no. 2, (March-April 1996), pp 208-217.

Chajes, M.J., T.F. Januszka, D.R. Mertz, T.A. Thomson, and W.W. Finch, "Shear Strengthening of Reinforced Concrete Beams Using Externally Applied Composite Fabrics," *ACI Structural Journal*, vol 92, no. 3, (May-June 1995), pp 295-303.

Chajes, M.J., T.A. Thomson, and B. Tarantino, "Reinforcement of Concrete Structures Using Externally Bonded Composite Materials," *Non-Metallic Reinforcement for Concrete Structures (Proceedings)*, (1995), E&FN Spon, London, pp 501-508.

Engineered Materials Handbook, Volume 1, "Composites," ASM International, Metals Park, OH, (1987), p 36.

Gee, Duane J., Memorandum of 21 June 1996.

International Conference of Building Officials Evaluation Service, Inc., "Acceptance Criteria for Concrete and Reinforced and Unreinforced Masonry Strengthening Using Fiber-reinforced Composite Systems," AC125, (April 1997).

Norris, T., H. Saadatmanesh, and M.R. Ehsani, "Shear and Flexural Strengthening of R/C Beams with Carbon Fiber Sheets," *ASCE Journal of Structural Engineering*, vol 123, no. 7, (July 1997).

Saadatmanesh, H. and M.R. Ehsani, "Fiber Composite Plates Can Strengthen Beams," *Concrete International*, vol 12, no. 3, (March 1990), pp 65-71.

List of Appendix A Figures and Tables

Figures

Figure A1. Joist configuration. 27
Figure A2. Joist prestressing tendon profile....27
Figure A3. HJ-3 and HJ-4 web reinforcement. 28
Figure A4. FRP joist repair. 28
Figure A5. High performance concrete strength versus time. 29
Figure A6. Prestressing tendon stress versus strain. 29
Figure A7. Prestressing and casting of hybrid joists. 30
Figure A8. Completed hybrid joist construction. 30
Figure A9. FRP application. 31
Figure A10. Gap in FRP upgrade of HJ-3. 31
Figure A11. Epoxy injection of voids. 32
Figure A12. Internal strain gage layout for HJ-3, HJ-4, HJ-6 and HJ-7. 32
Figure A13. External strain gage layout on HJ-3. 33
Figure A14. External strain gage layout on HJ-4. 33
Figure A15. LVDT locations on test specimens. 34
Figure A16. Potentiometer locations on test specimens....34
Figure A17. Block diagram of data recording system. 35
Figure A18. Test set up. 35
Figure A19. Load versus deflection for HJ-3, HJ-4, HJ-6 and HJ-7....36
Figure A20. Load versus deflection cycles for HJ-4. 37
Figure A21. Deflected shape for HJ-3. 37
Figure A22. Deflected shape for HJ-4....38
Figure A23. Deflected Shape of HJ-6. 39
Figure A24. Deflected shape for HJ-7. 39
Figure A25. Strain distribution for HJ-3....40
Figure A26. Strain distribution for HJ-4....41
Figure A27. Strain distribution for HJ-6....42
Figure A28. Strain distribution for HJ-7....43
Figure A29. Strain distribution along strand length of HJ-3. 44
Figure A30. Strain distribution along strand length of HJ-4. 45

Figure A31. Strain distribution along strand length of HJ-6. 46
Figure A32. Strain distribution along strand length of HJ-7. 47
Figure A33. HJ-3 Upgrade FRP Strains....48
Figure A34. HJ-4 Repair FRP Strains....49
Figure A35. Crack patterns for HJ-6....50
Figure A36. Failure of HJ-6....50
Figure A37. Crack patterns for HJ-7....51
Figure A38. Crack patterns for HJ-3....52
Figure A39. Failure of HJ-3....53
Figure A40. Crack Patterns of HJ-4 prior to FRP repair. 54
Figure A41. Crack patterns for HJ-4....55
Figure A42. Shear Repair Design Procedure Flow Chart....56
Figure A43. Simply Supported Beam....56
Figure A44. Shear Diagram. 57
Figure A45. FRP Wrap Repair. 57

Tables

Table A1. Hybrid Joists Tested....58
Table A2. Epoxy Material Properties....58
Table A3. Yarn Properties 58
Table A4. Fabric Properties....58
Table A5. Composite Laminate Specification....59
Table A6. Composite Material Properties....59
Table A7. Casting and release dates for each hybrid joist web. 59
Table A8. Instrumentation for HJ-3 upgraded with FRP....60
Table A9. Instrumentation for HJ-4 without FRP Repair 62
Table A10. Instrumentation for HJ-4 with FRP Repair 64
Table A11. Principal experimental test results for hybrid joists. 66
Table A12. Camber and deflection for hybrid joists (in.). 66

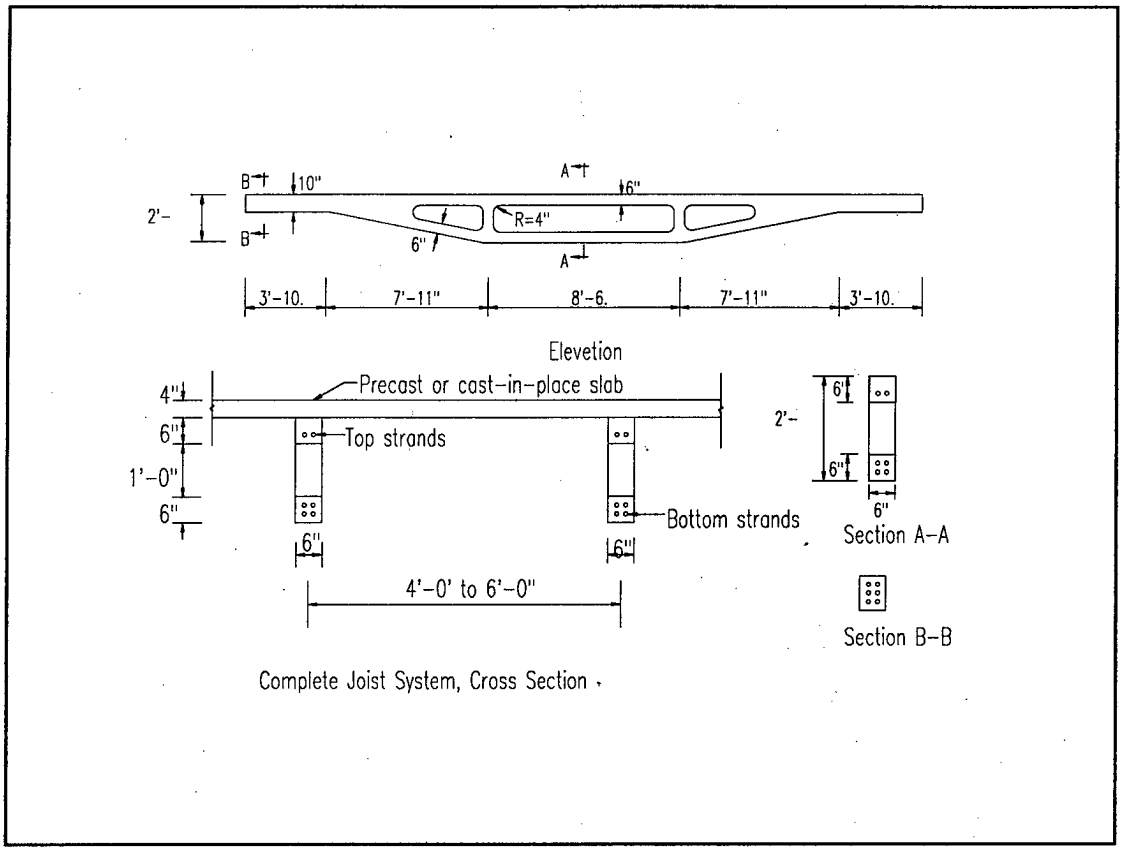


Figure A1. Joist configuration.

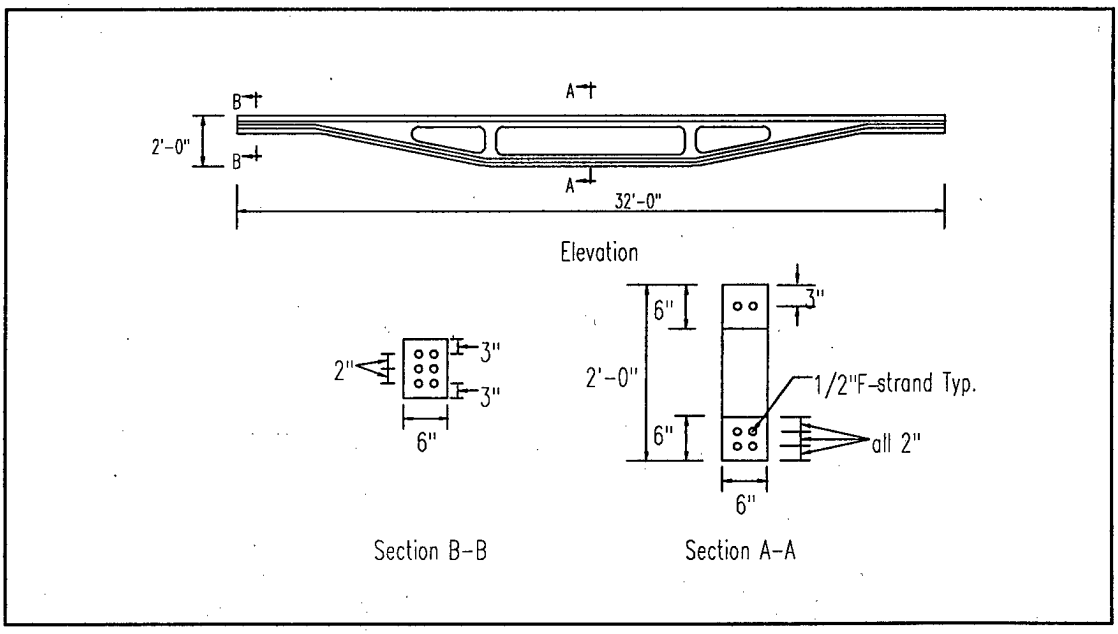


Figure A2. Joist prestressing tendon profile.

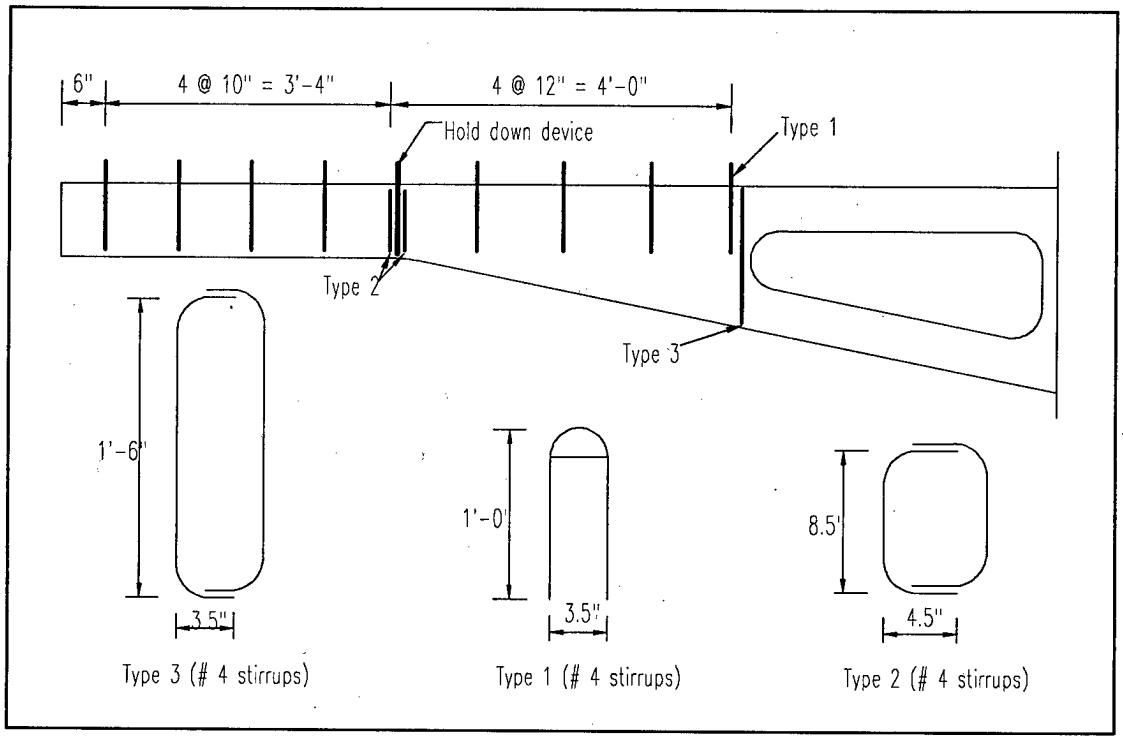


Figure A3. HJ-3 and HJ-4 web reinforcement.

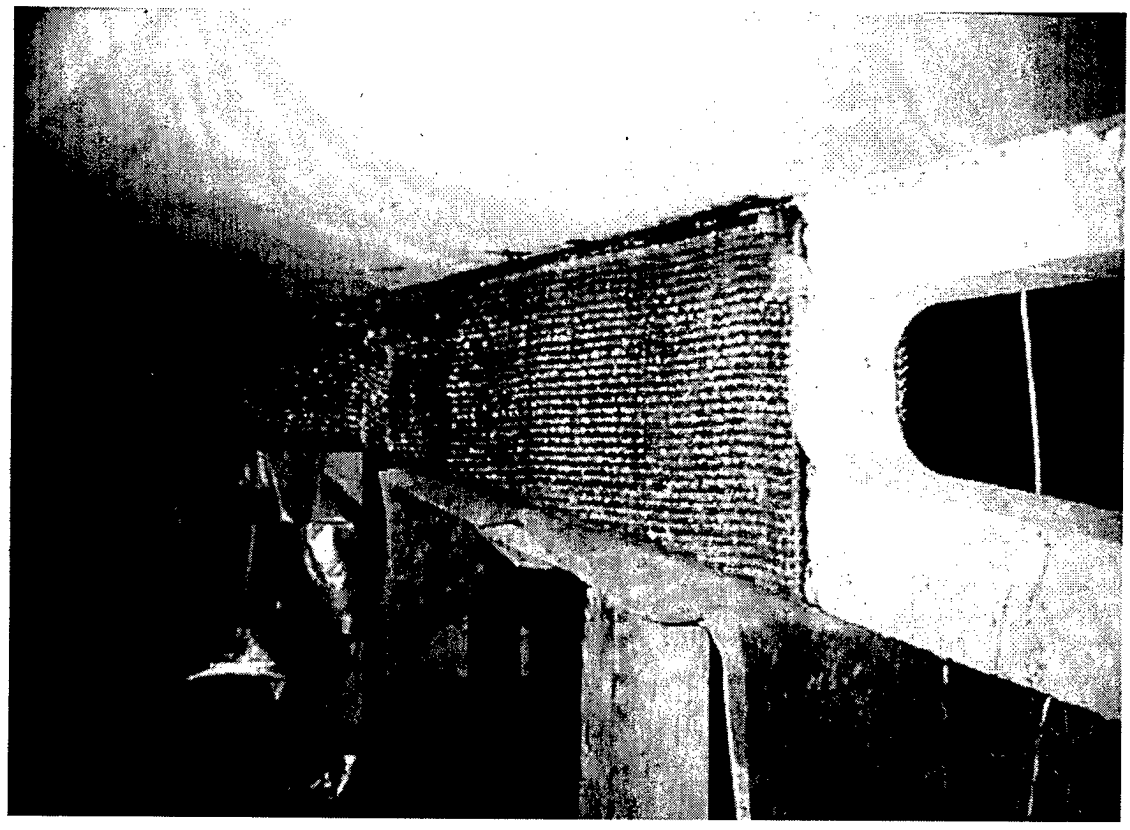


Figure A4. FRP joist repair.

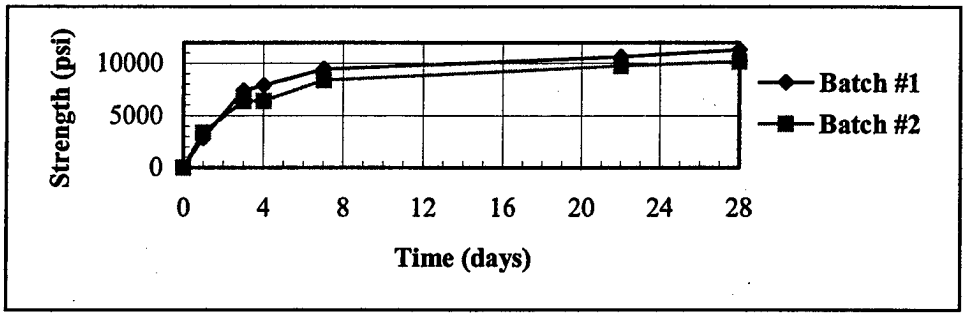


Figure A5. High performance concrete strength versus time.

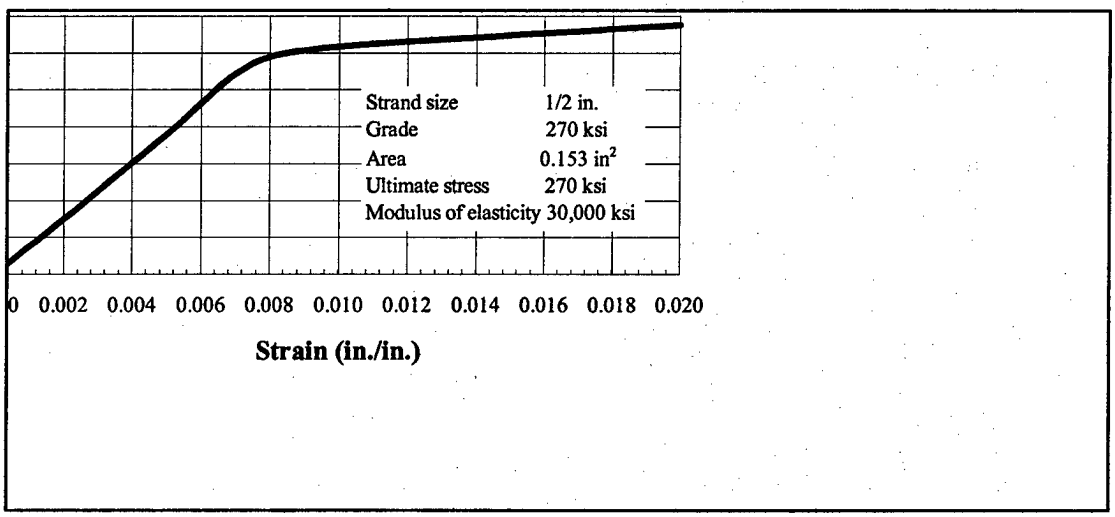


Figure A6. Prestressing tendon stress versus strain.

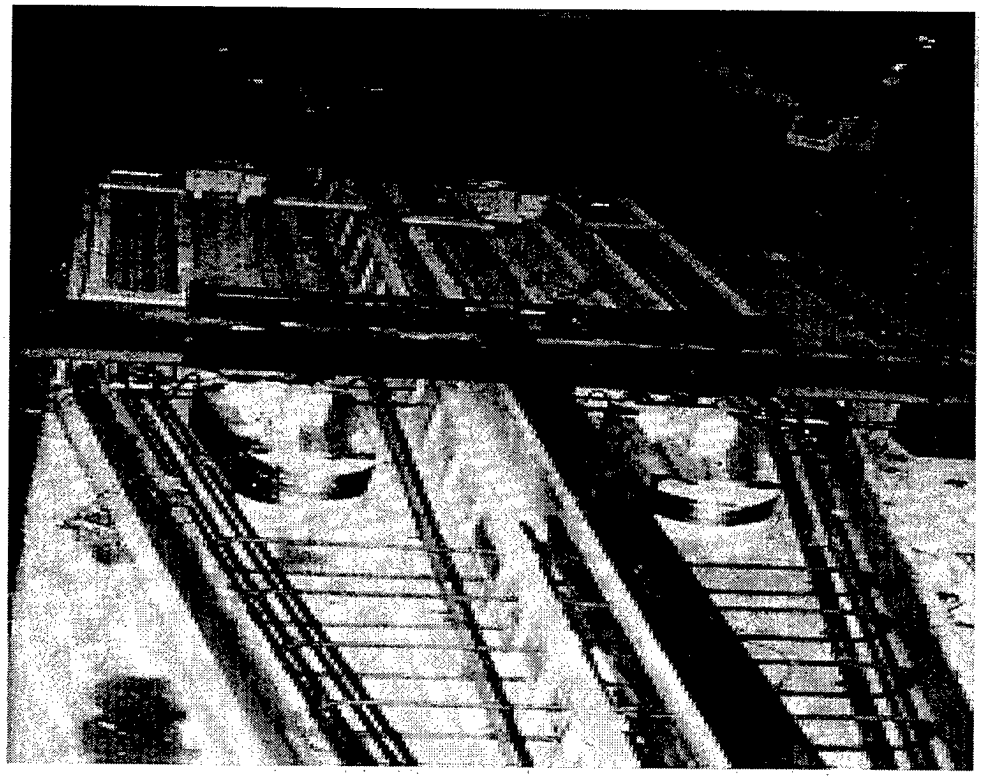


Figure A7. Prestressing and casting of hybrid joists.

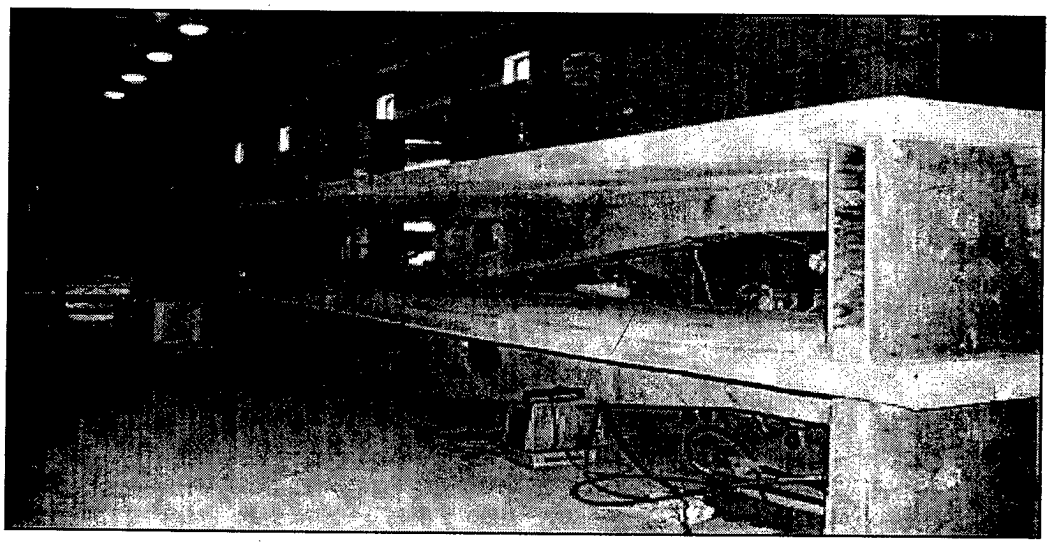


Figure A8. Completed hybrid joist construction.



Figure A9. FRP application.

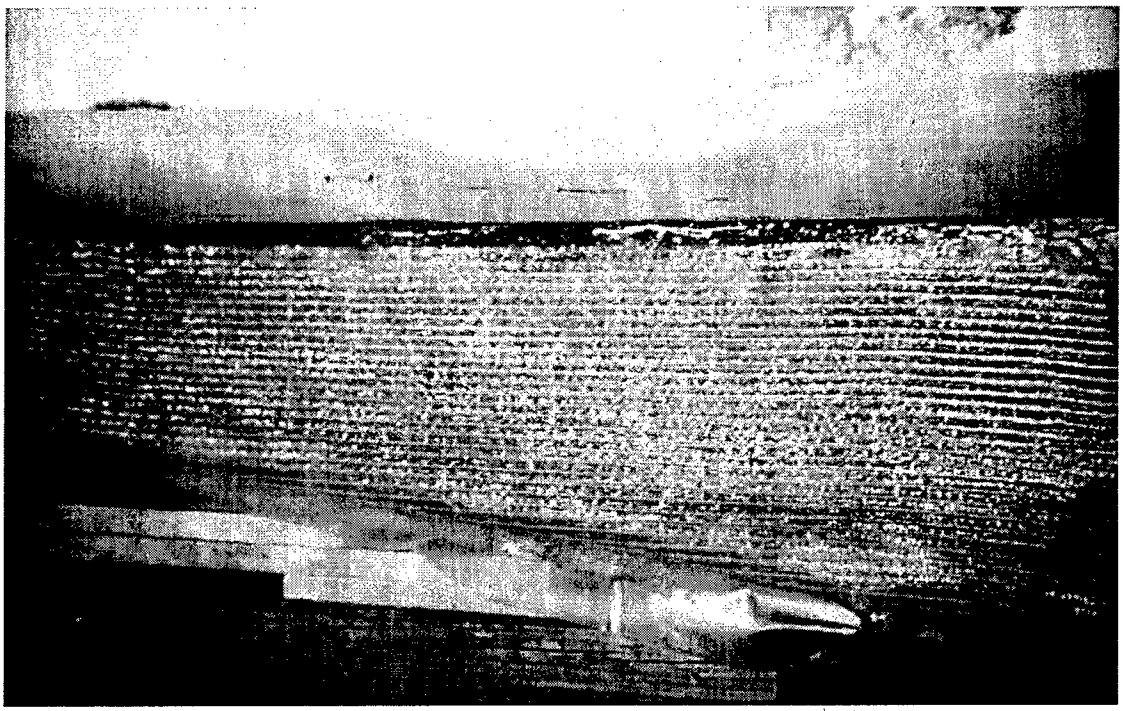


Figure A10. Gap in FRP upgrade of HJ-3.

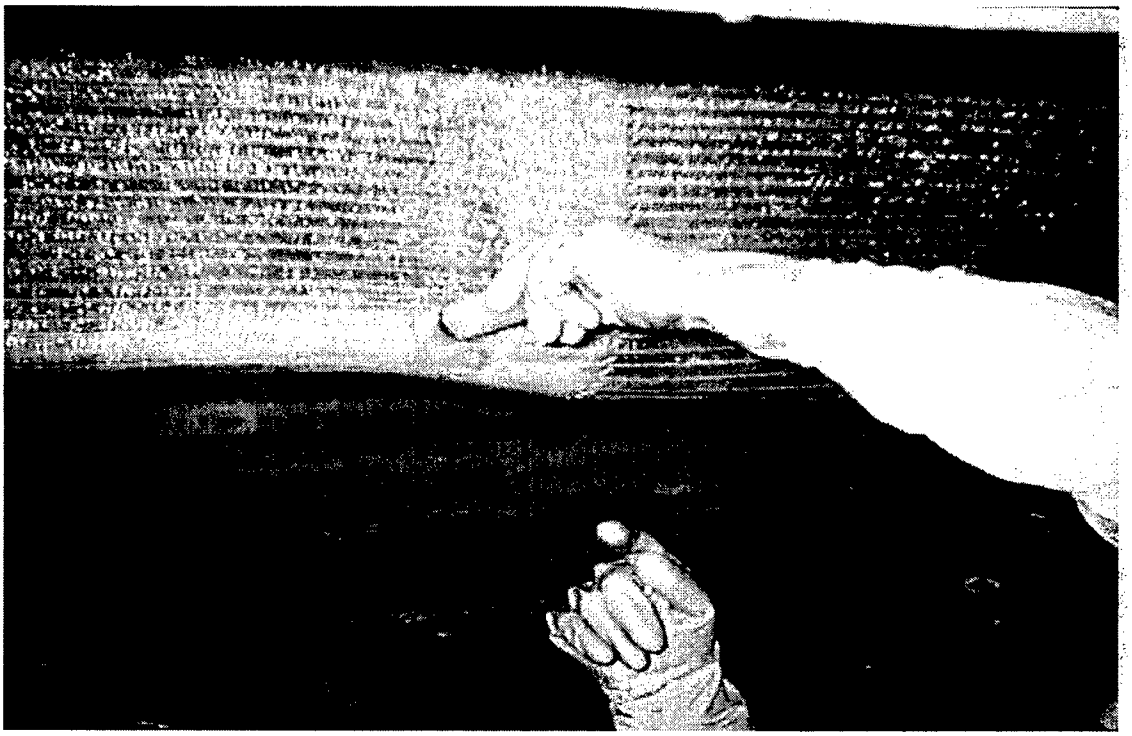


Figure A11. Epoxy injection of voids.

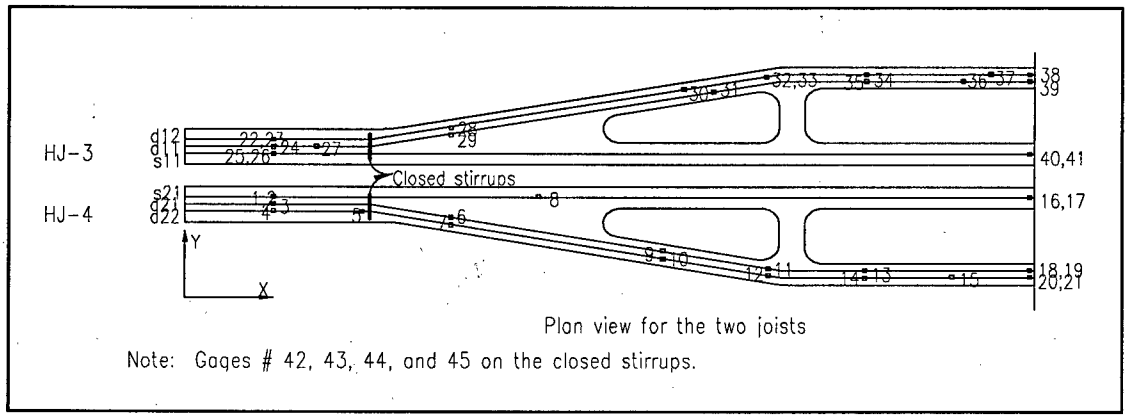


Figure A12. Internal strain gage layout for HJ-3, HJ-4, HJ-6 and HJ-7.

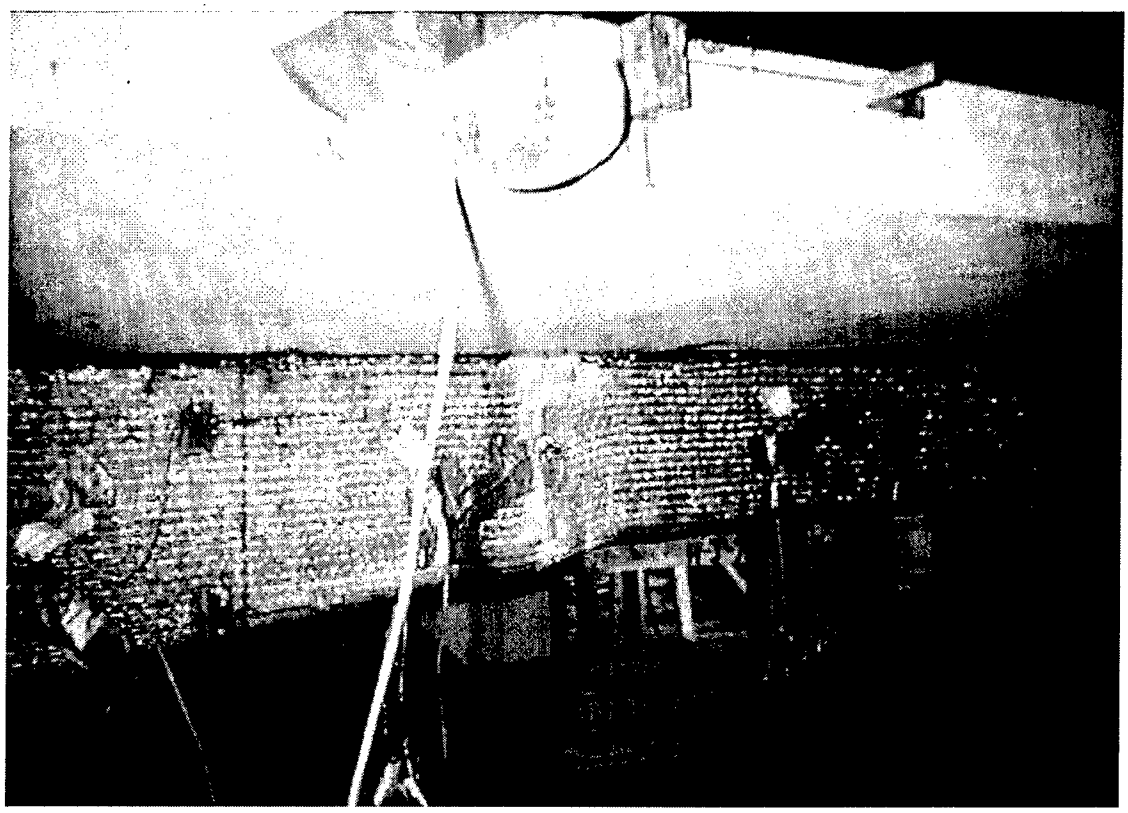


Figure A13. External strain gage layout on HJ-3.

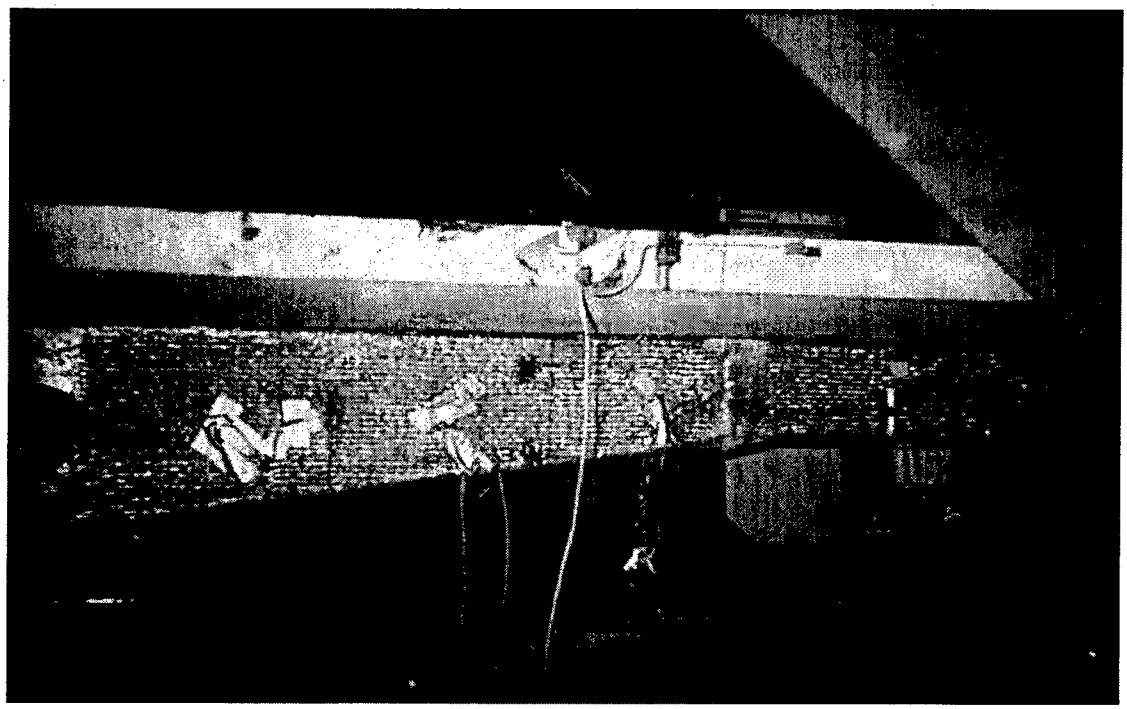


Figure A14. External strain gage layout on HJ-4.

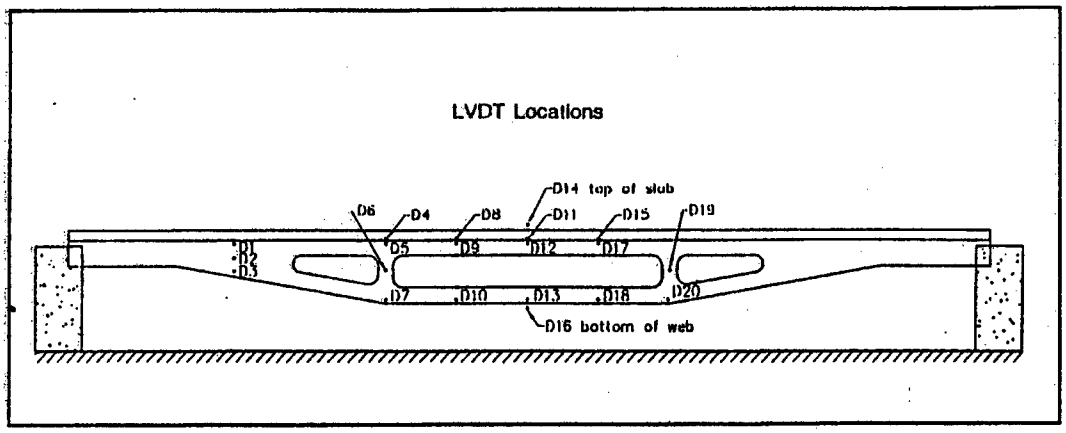


Figure A15. LVDT locations on test specimens.

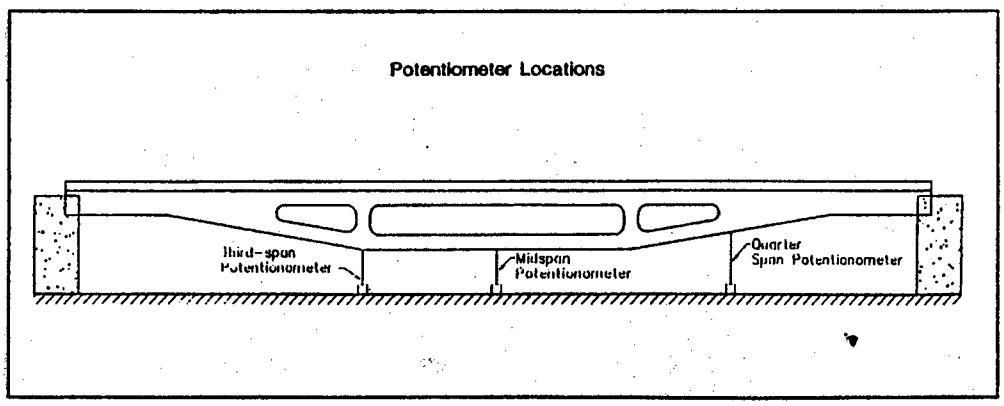


Figure A16. Potentiometer locations on test specimens.

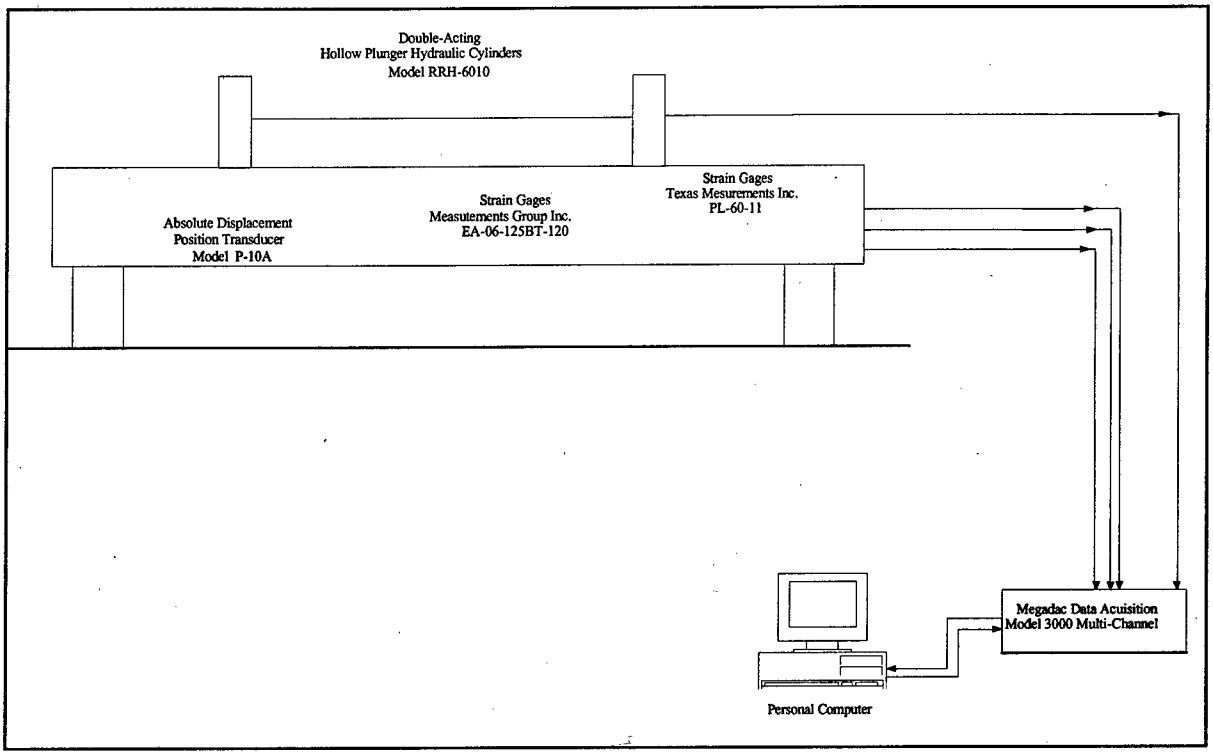


Figure A17. Block diagram of data recording system.

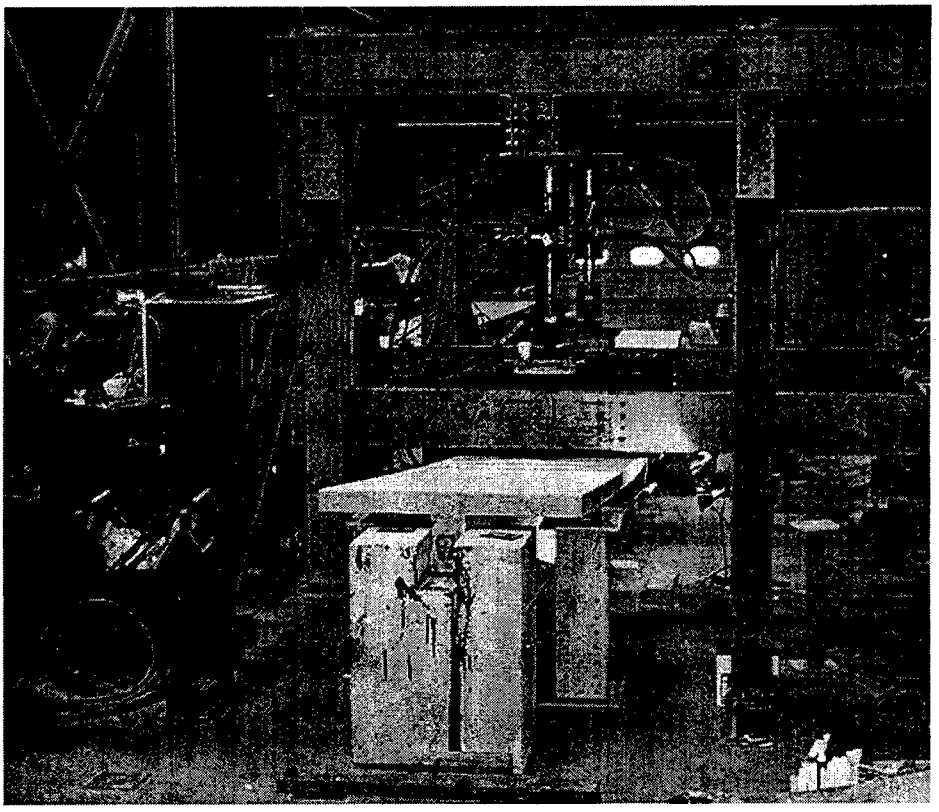


Figure A18. Test setup.

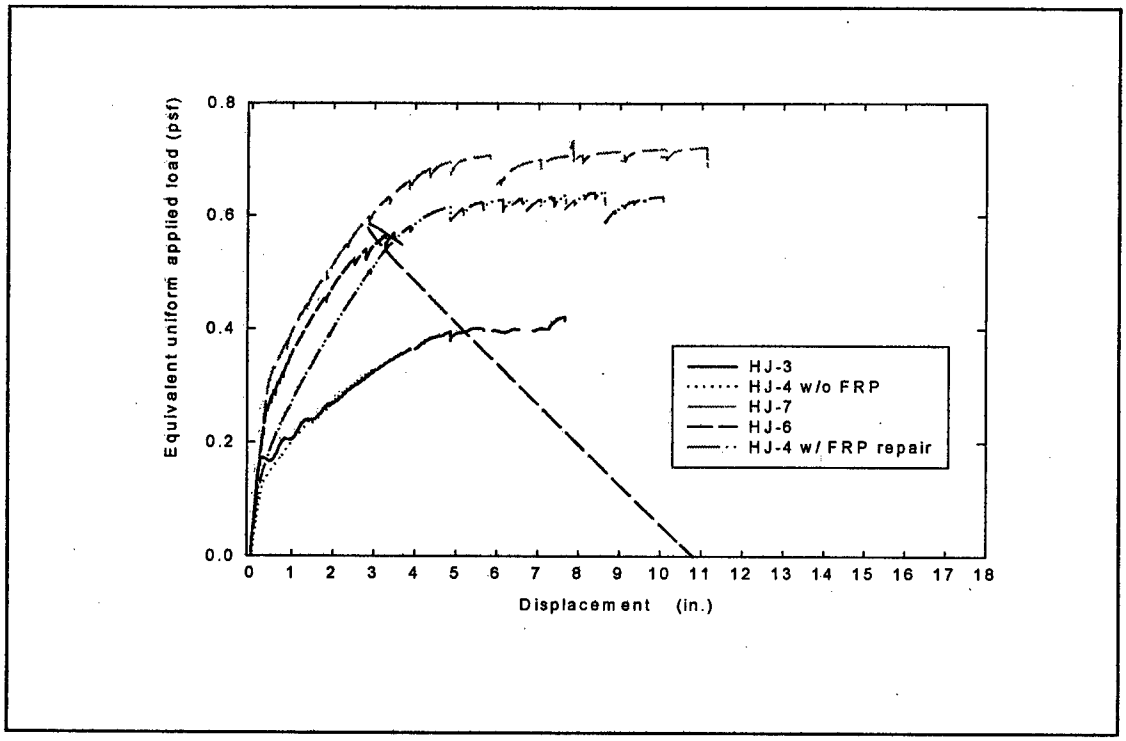


Figure A19. Load versus deflection for HJ-3, HJ-4, HJ-6 and HJ-7.

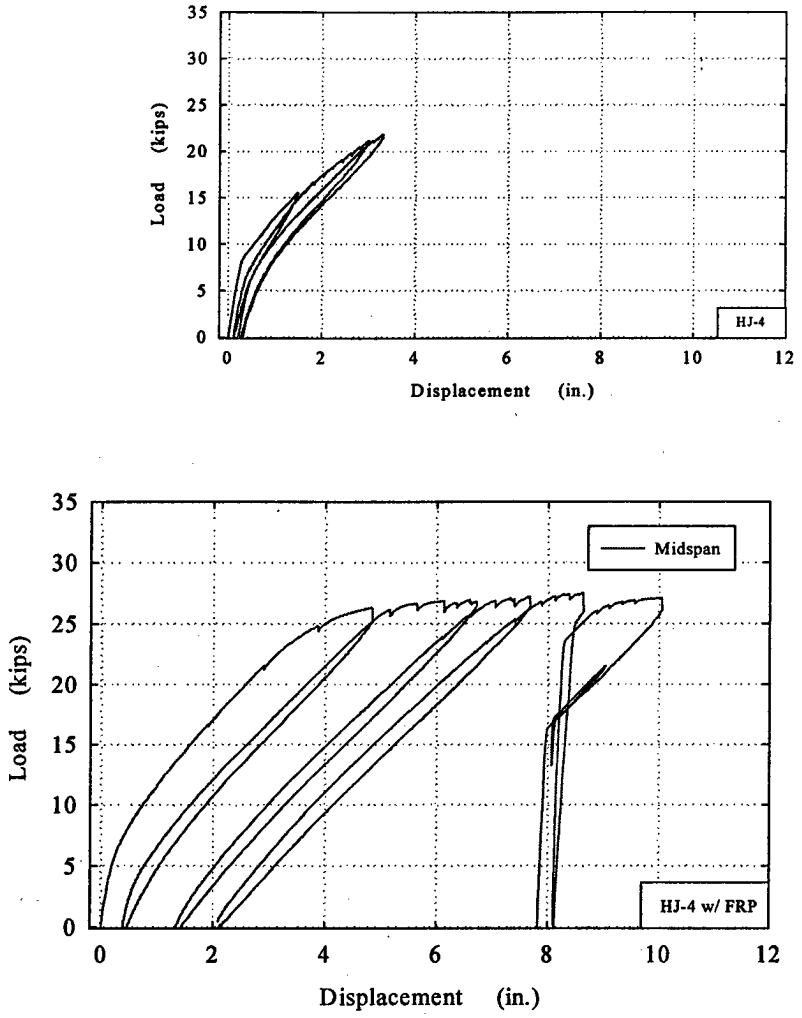


Figure A20. Load versus deflection cycles for HJ-4.

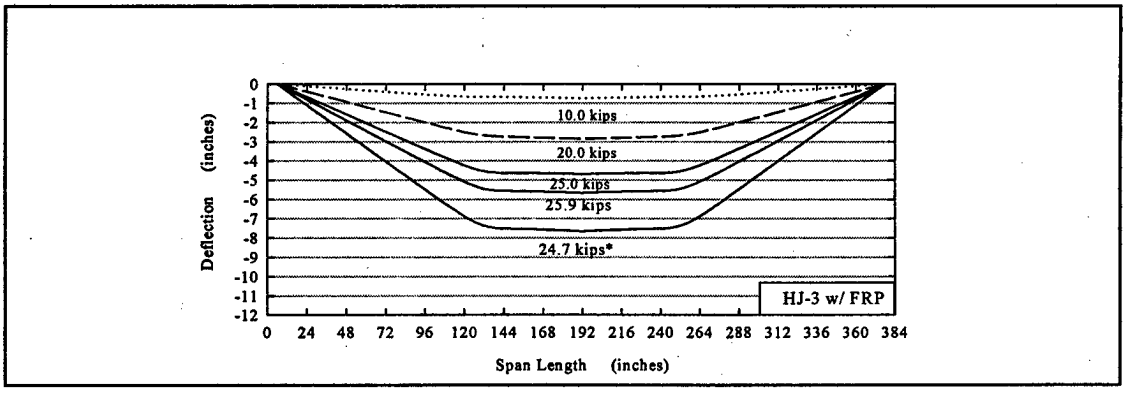
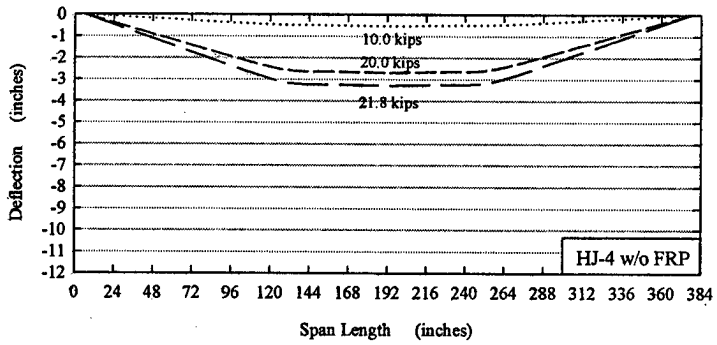
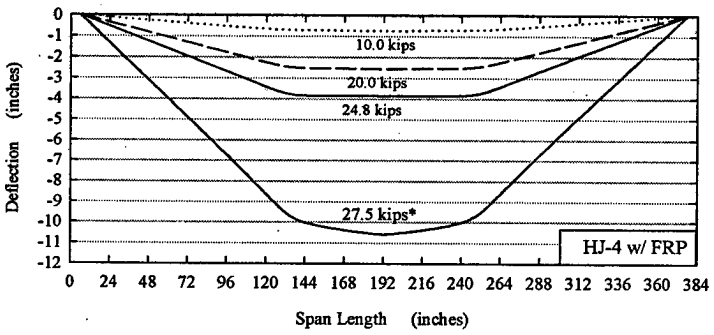


Figure A21. Deflected shape for HJ-3.



a. HJ-4 prior to repair



b. HJ-4 after repaired with FRP

Figure A22. Deflected shape for HJ-4.

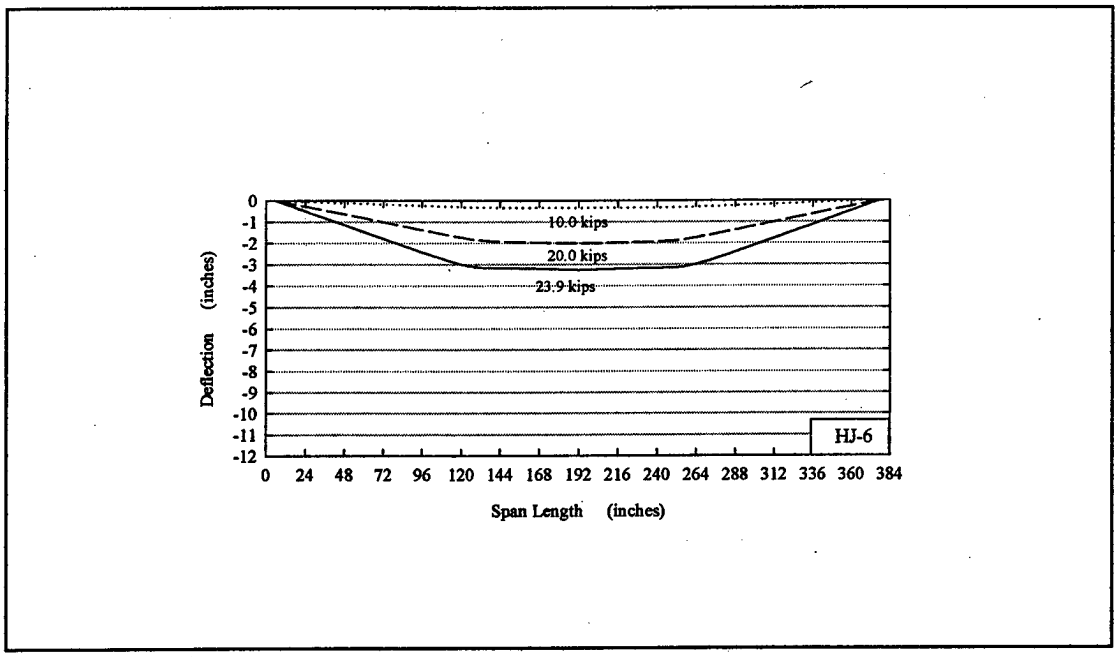


Figure A23. Deflected Shape of HJ-6.

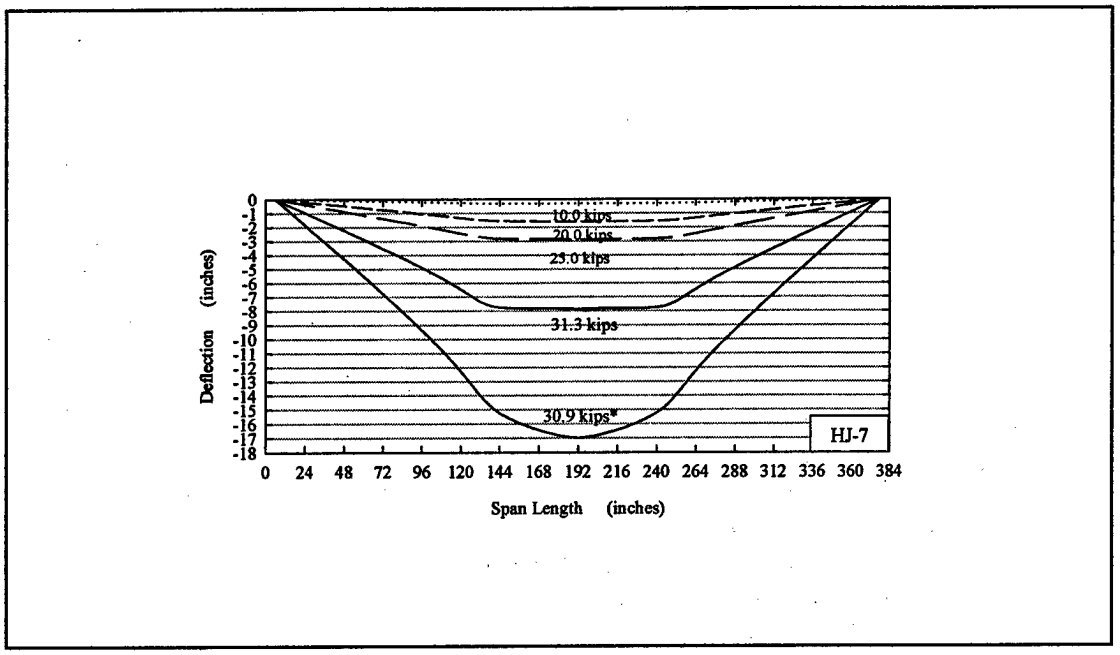


Figure A24. Deflected shape for HJ-7.

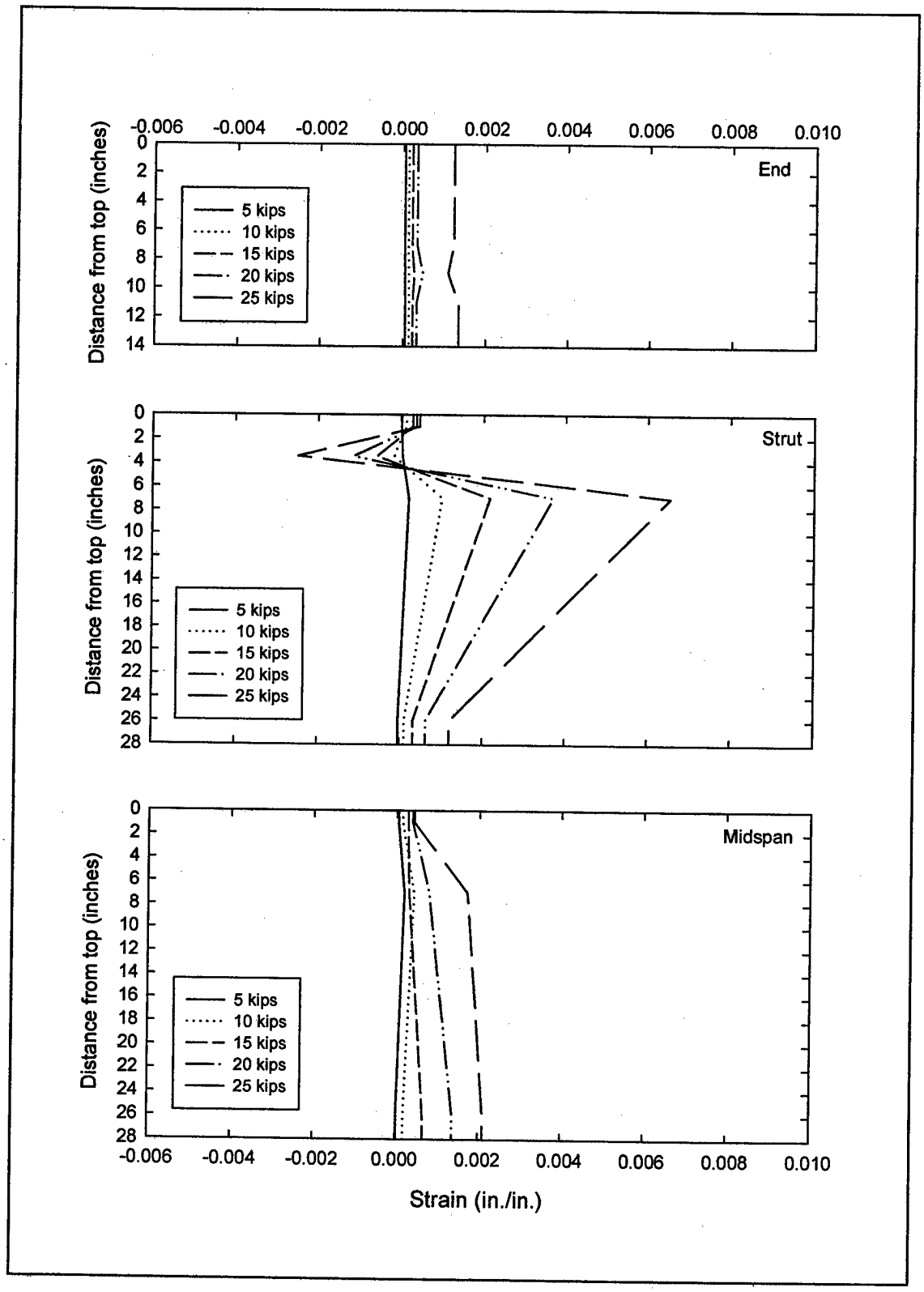


Figure A25. Strain distribution for HJ-3.

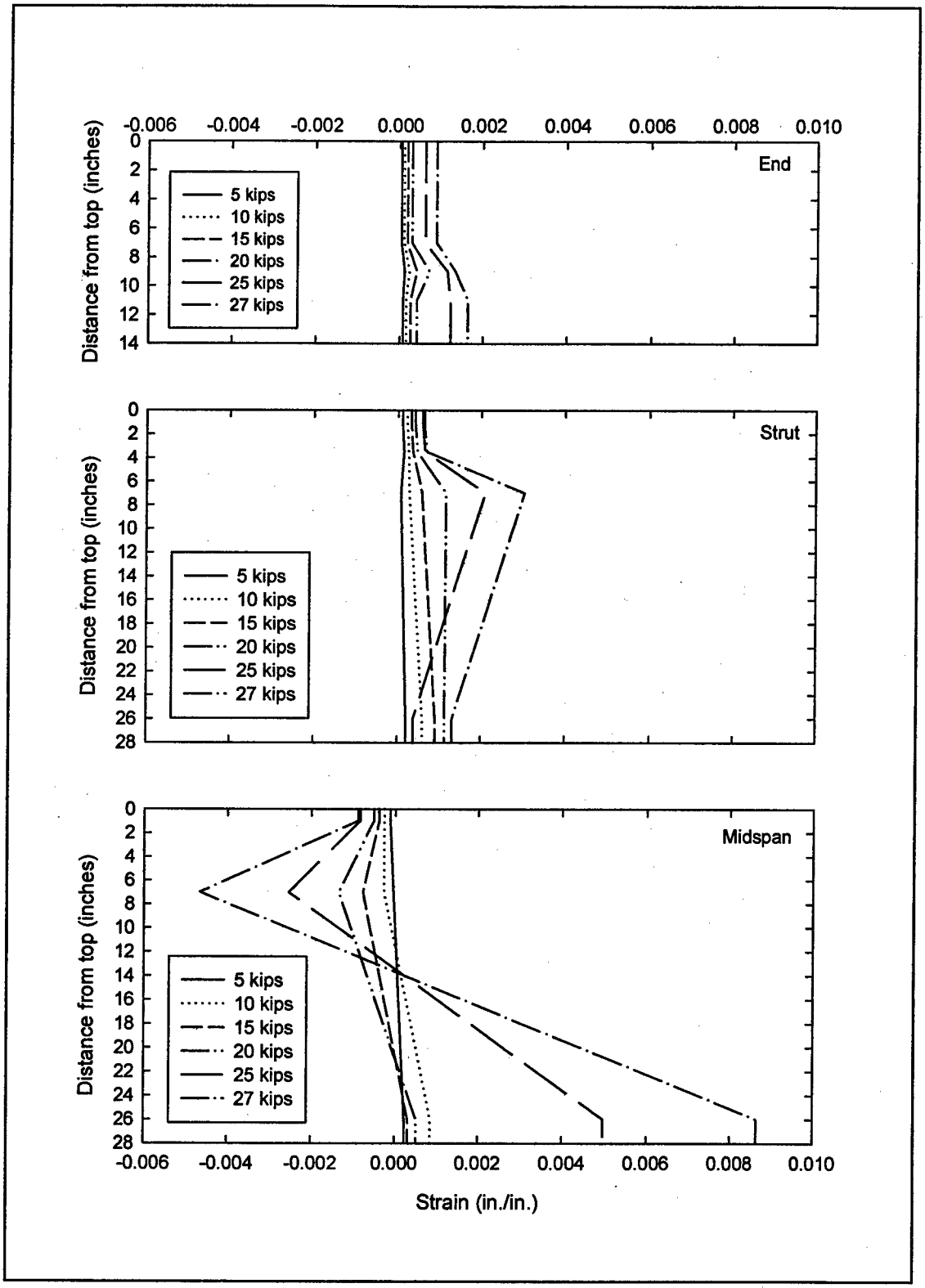


Figure A26. Strain distribution for HJ-4.

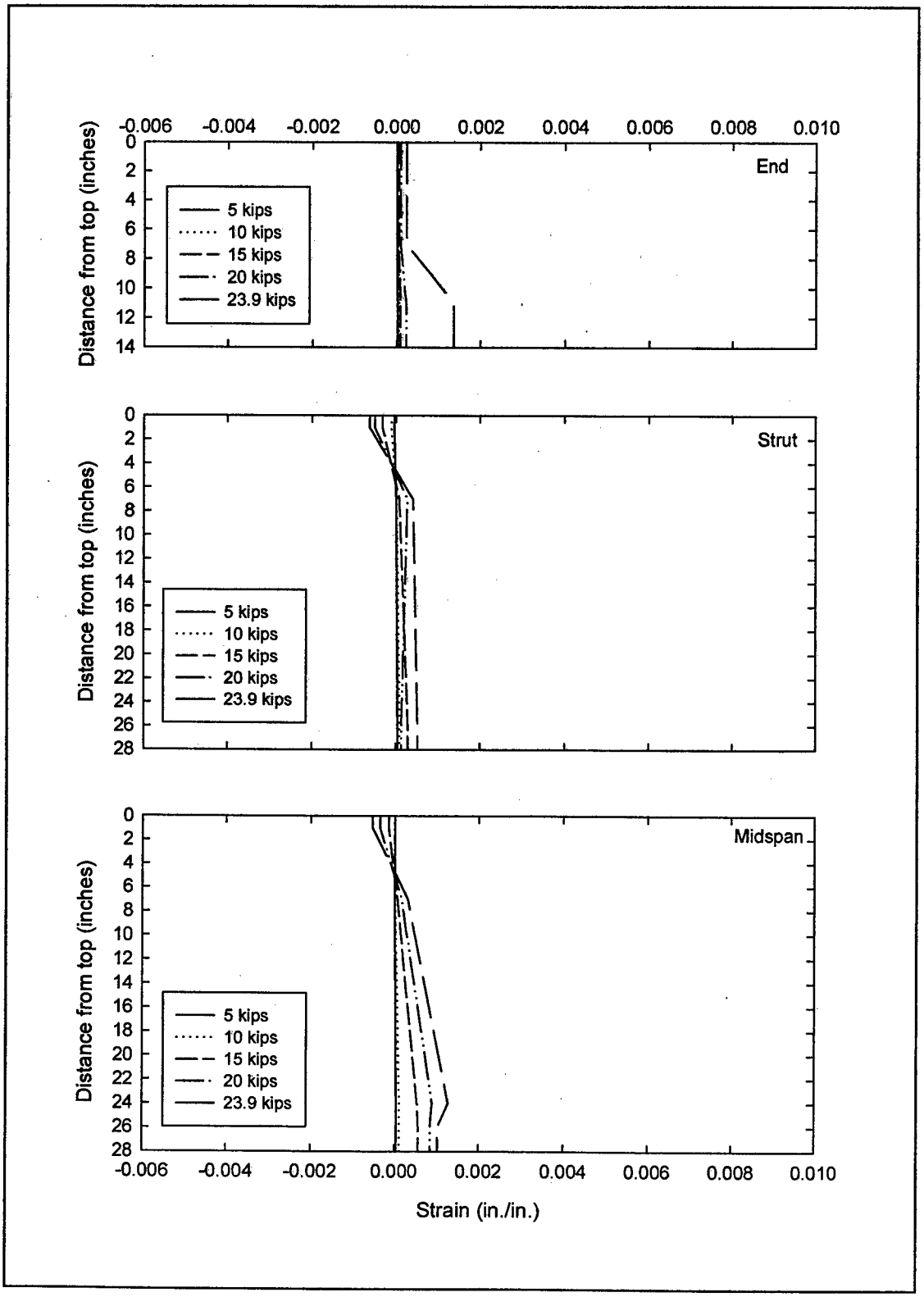


Figure A27. Strain distribution for HJ-6.

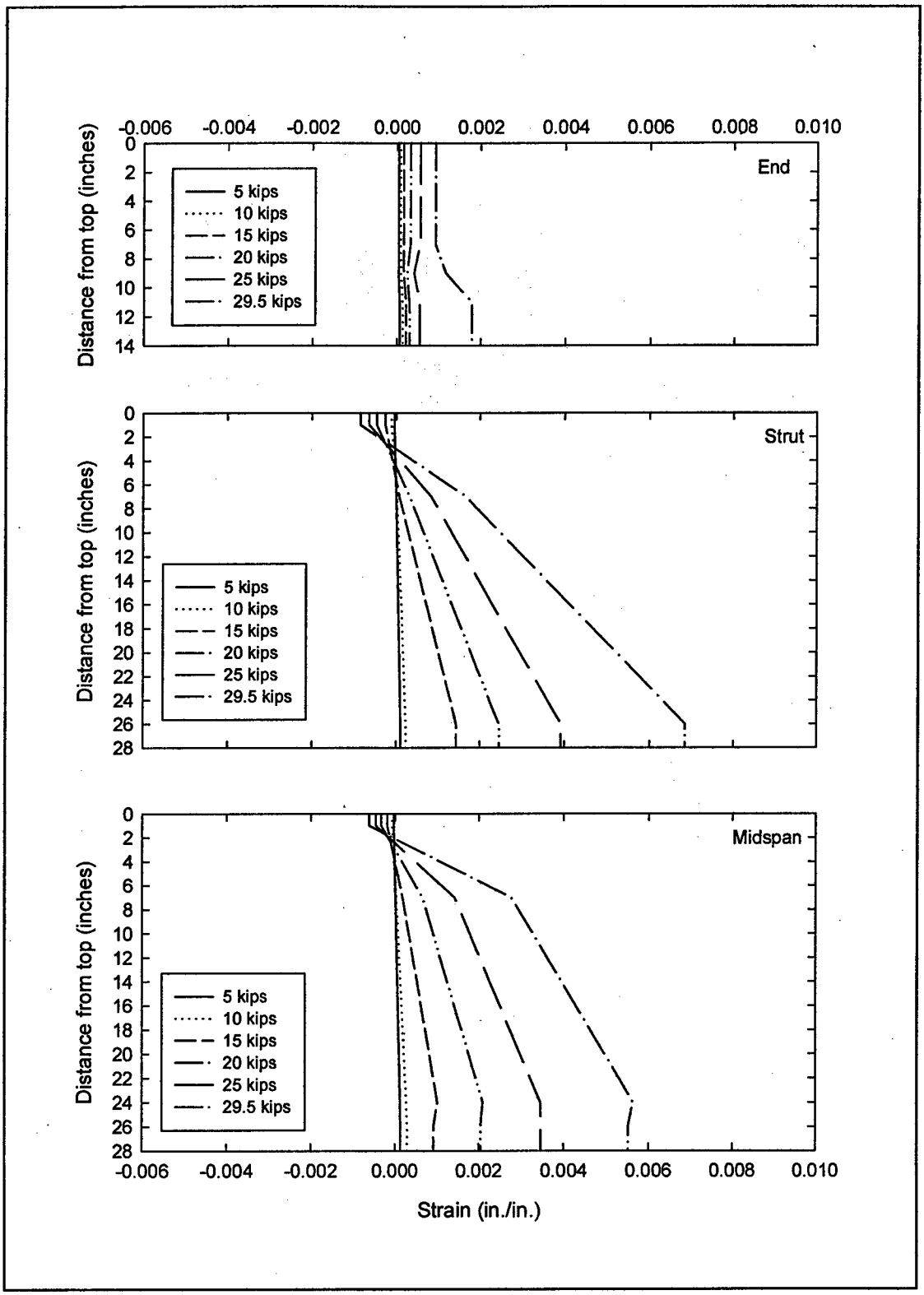


Figure A28. Strain distribution for HJ-7.

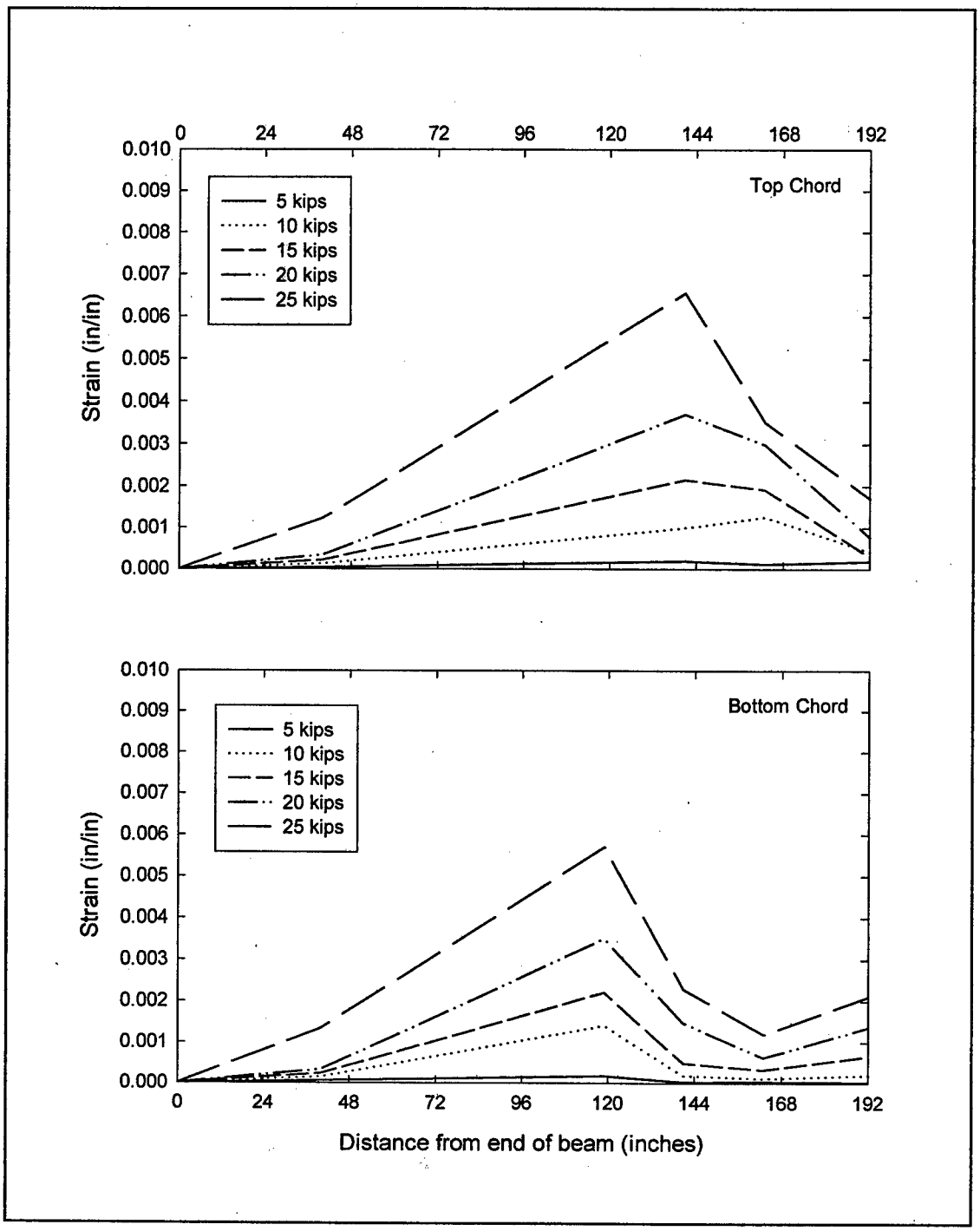


Figure A29. Strain distribution along strand length of HJ-3.

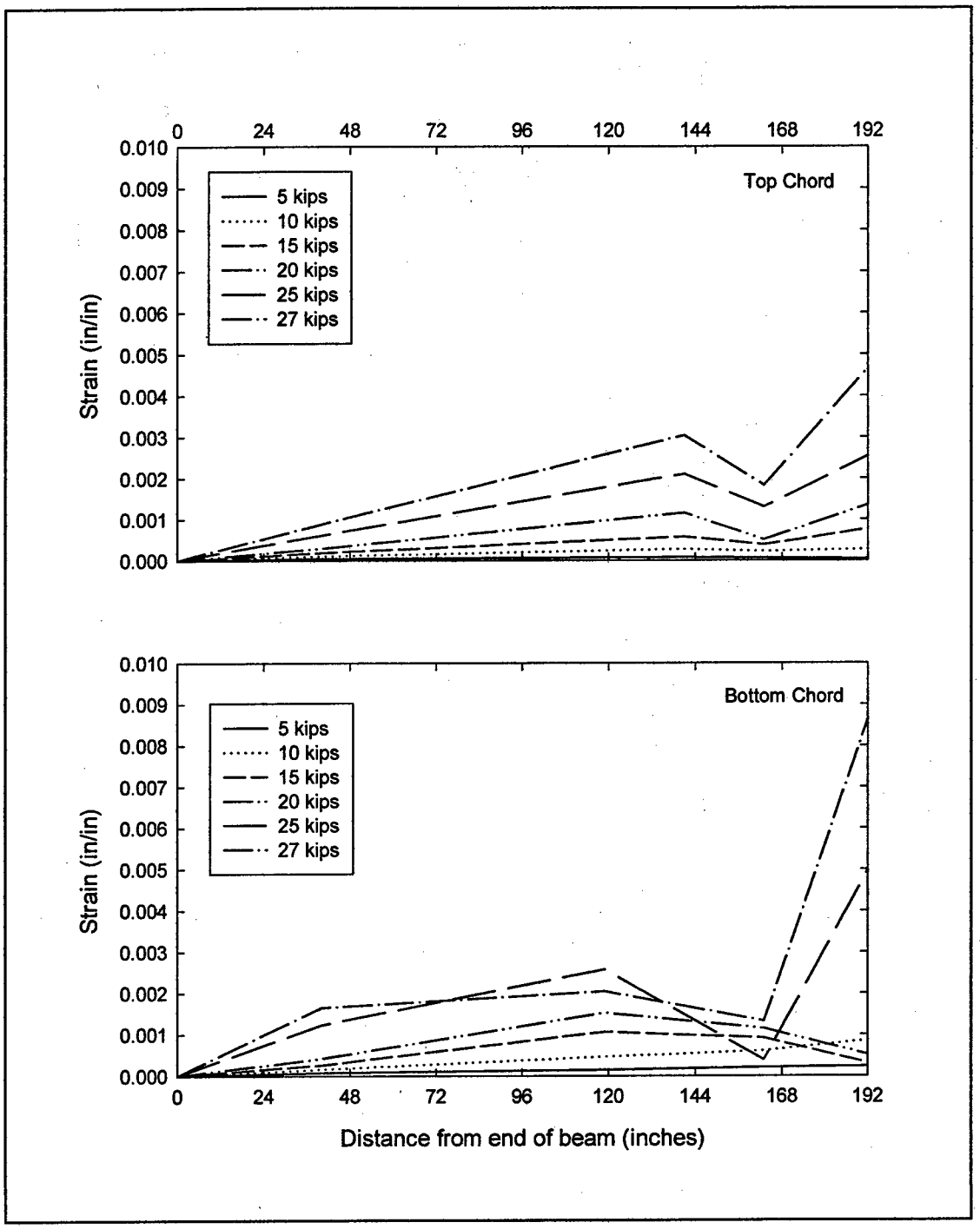


Figure A30. Strain distribution along strand length of HJ-4.

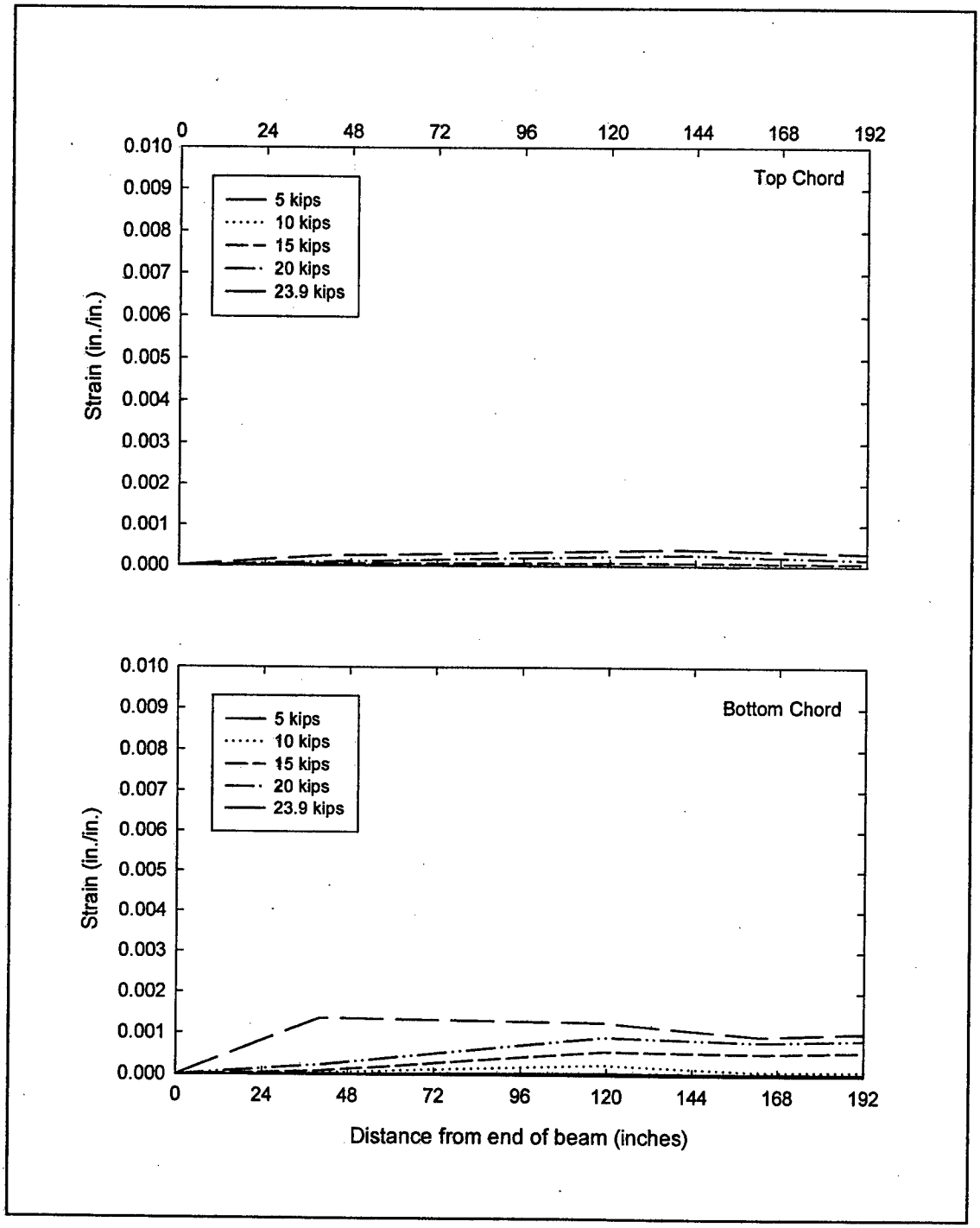


Figure A31. Strain distribution along strand length of HJ-6.

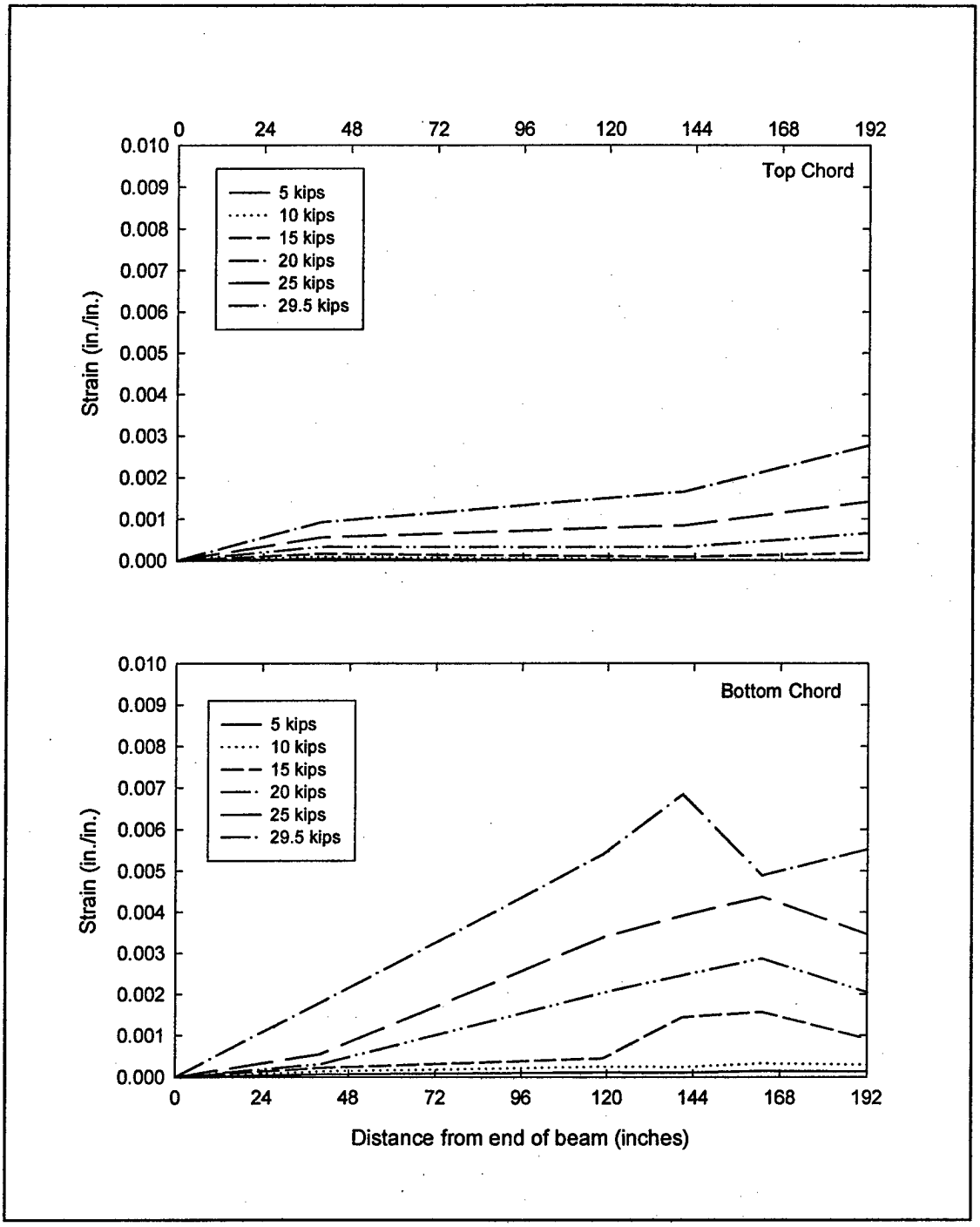


Figure A32. Strain distribution along strand length of HJ-7.

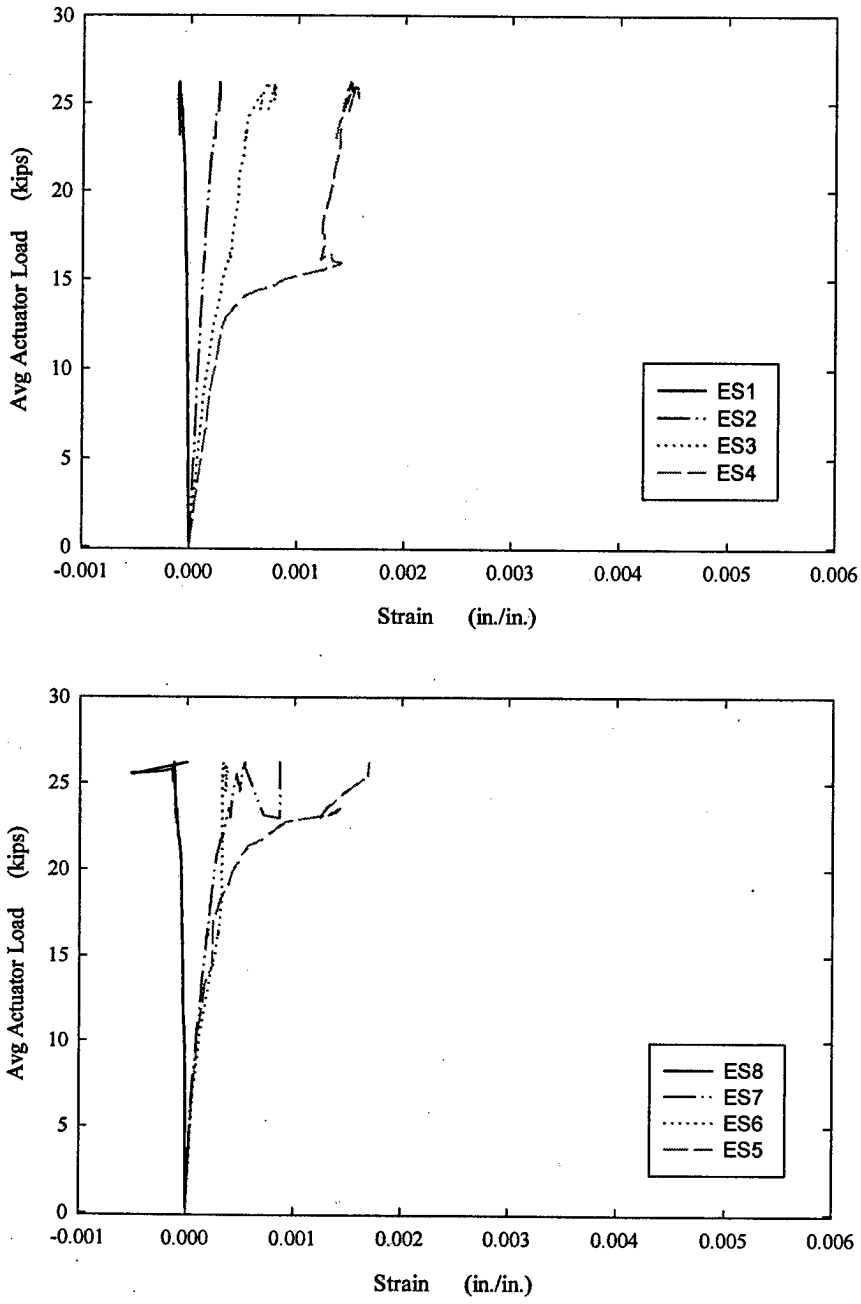


Figure A33. HJ-3 Upgrade FRP Strains.

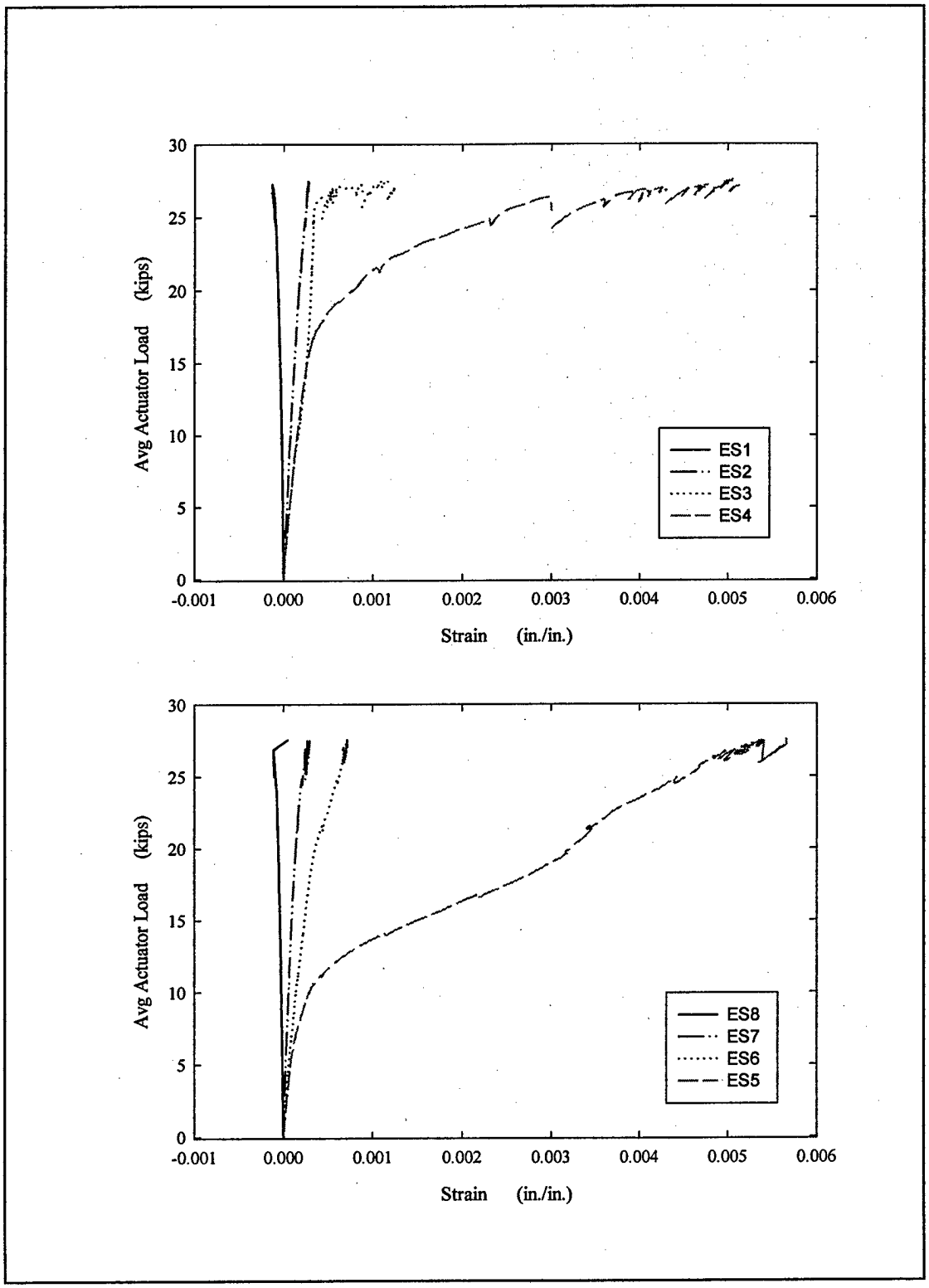


Figure A34. HJ-4 Repair FRP Strains.

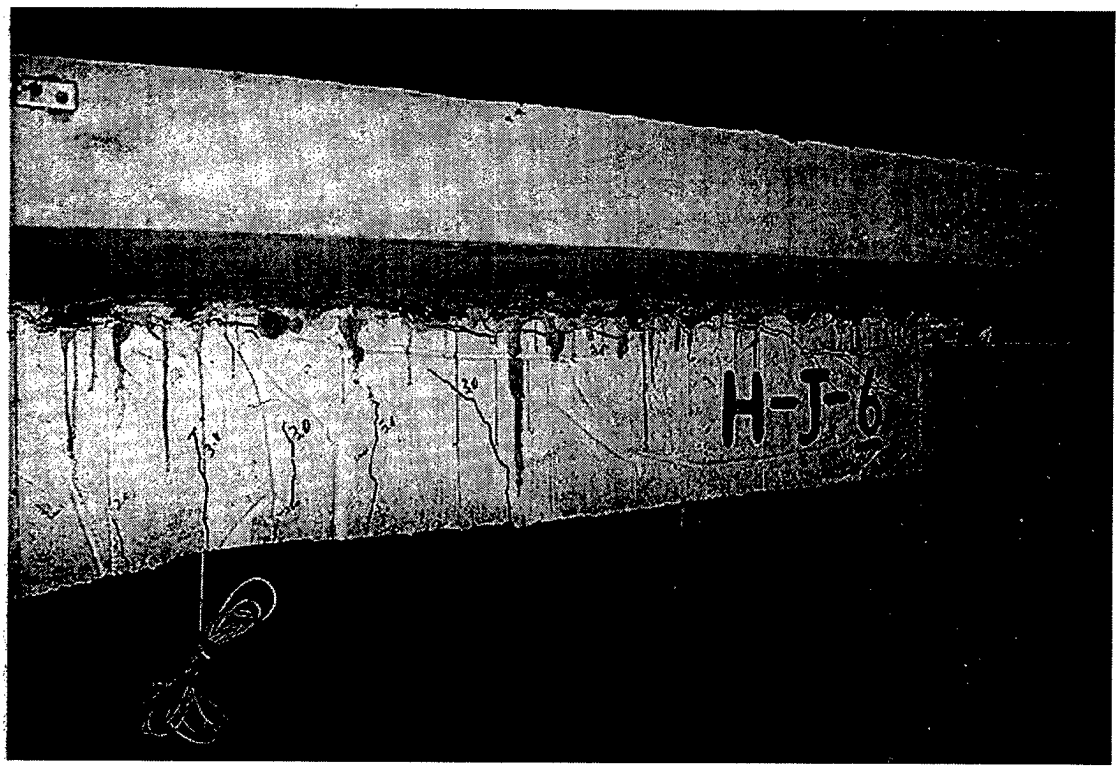


Figure A35. Crack patterns for HJ-6.

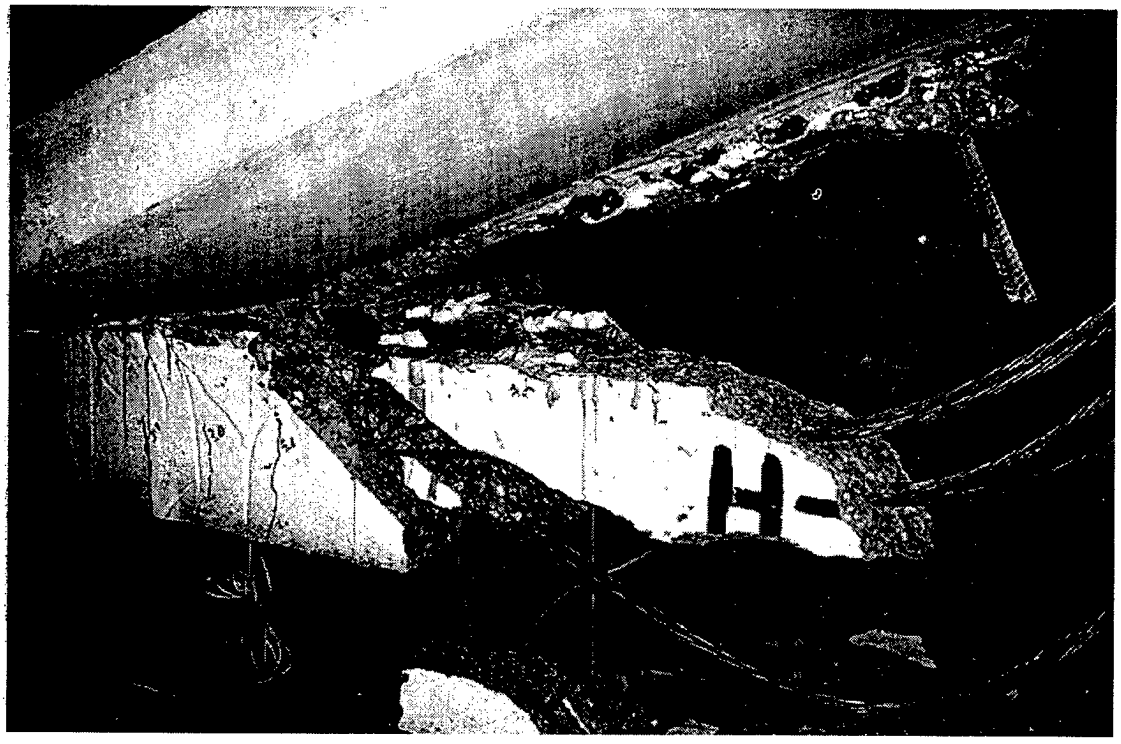


Figure A36. Failure of HJ-6.

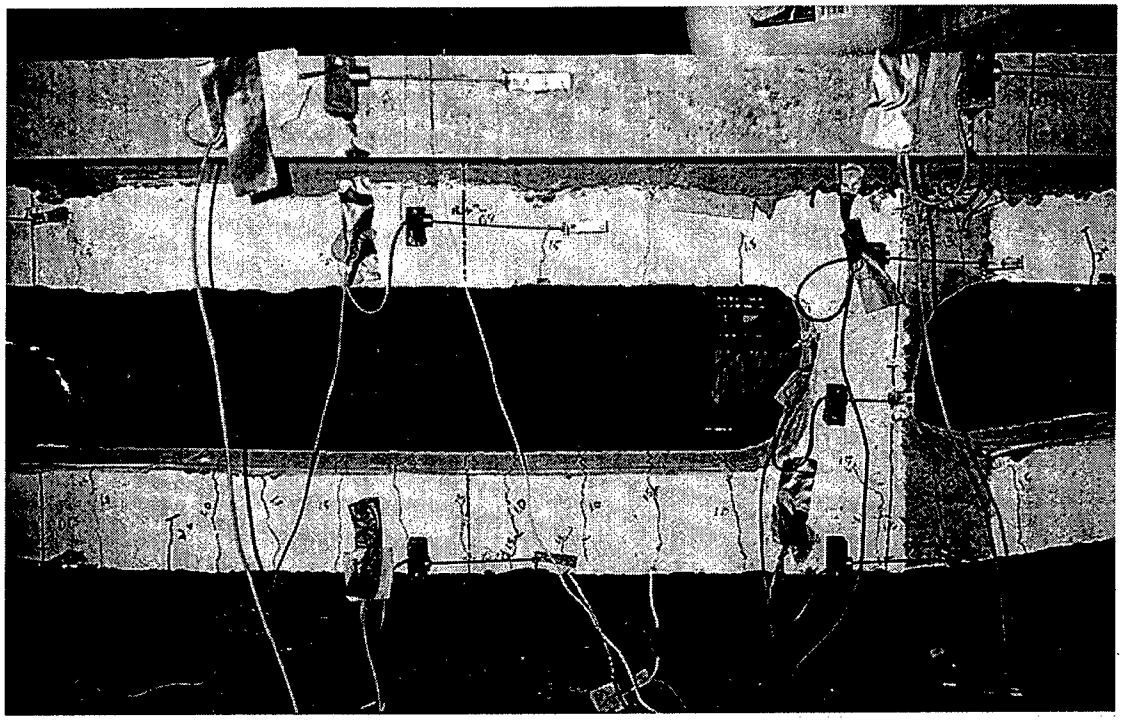


Figure A37. Crack patterns for HJ-7.



a. Cracks at slab/web interface and in slab at North end of HJ-3.

b. Detail of crack at frp edge at slab/web interface of HJ-3.

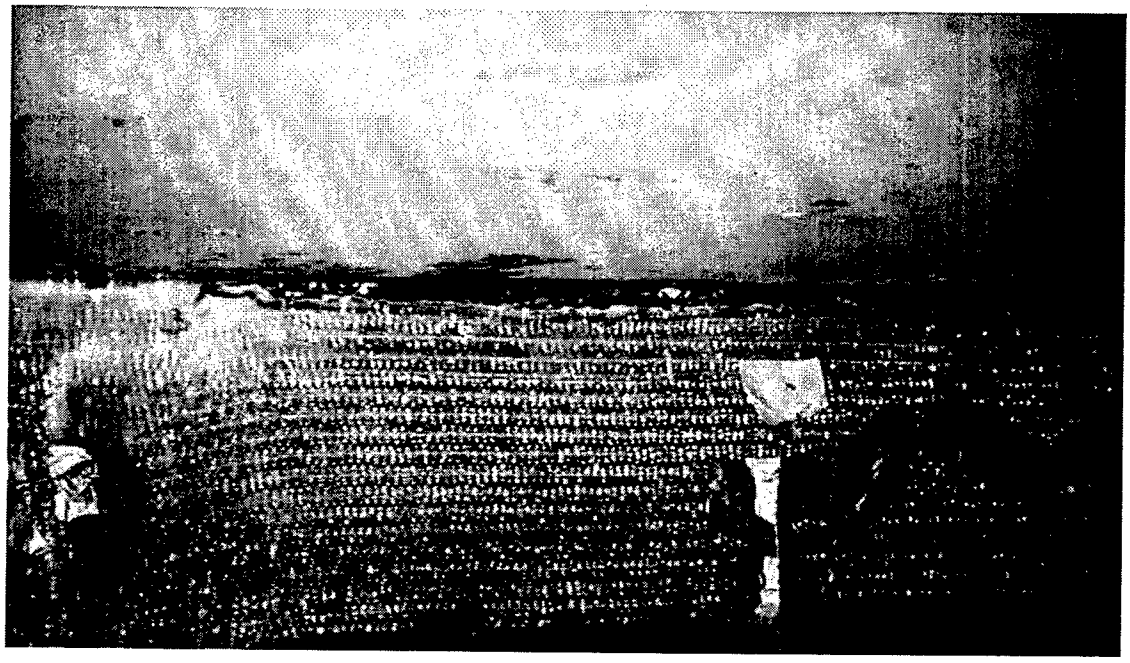
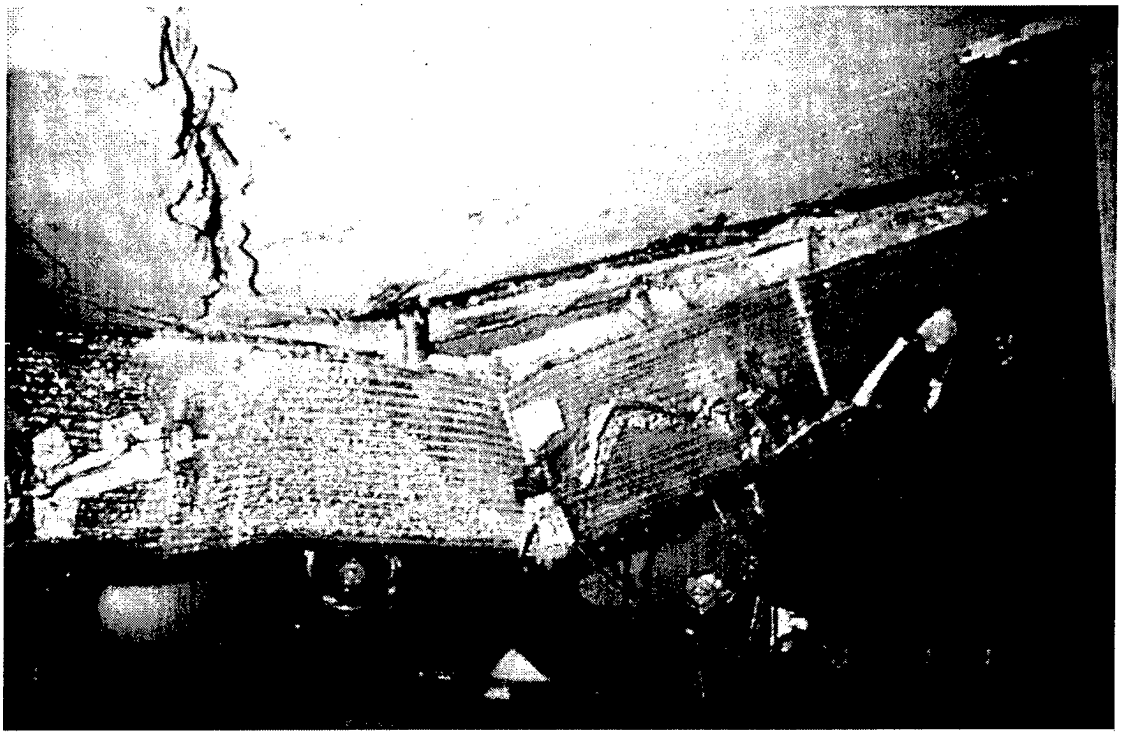


Figure A38. Crack patterns for HJ-3.



a. Failure at North end of HJ-3

b. Detail of crack and separation at slab/web interface at failure of HJ-3.

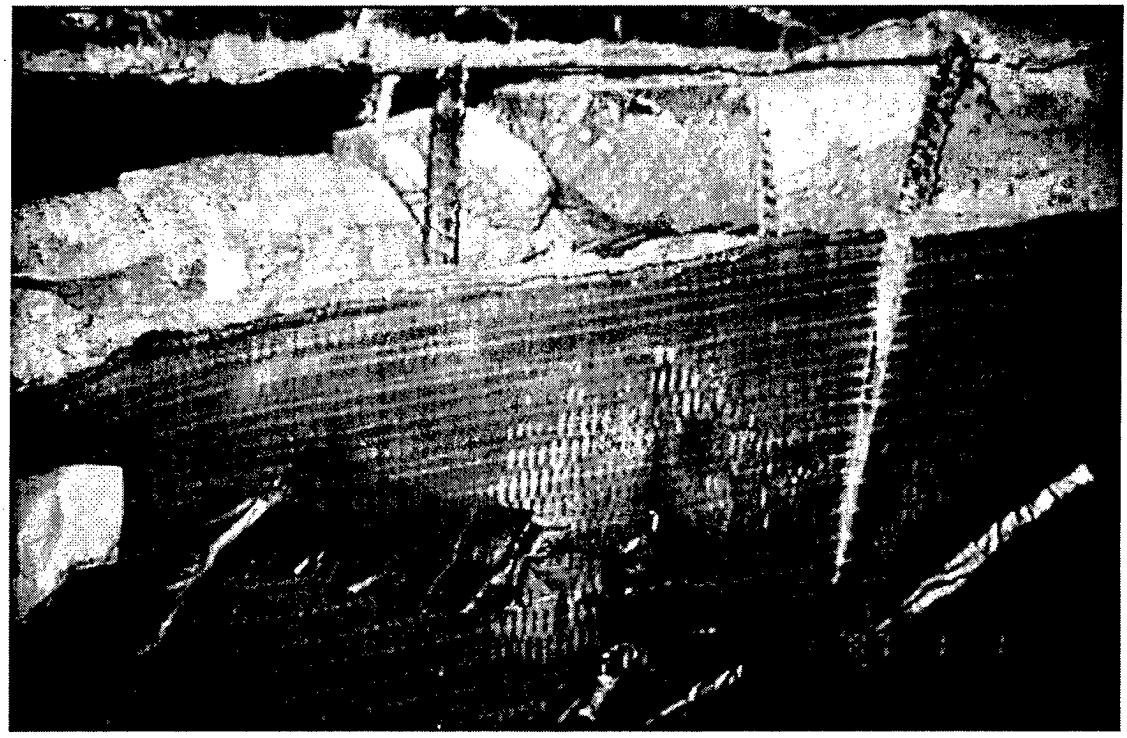


Figure A39. Failure of HJ-3.

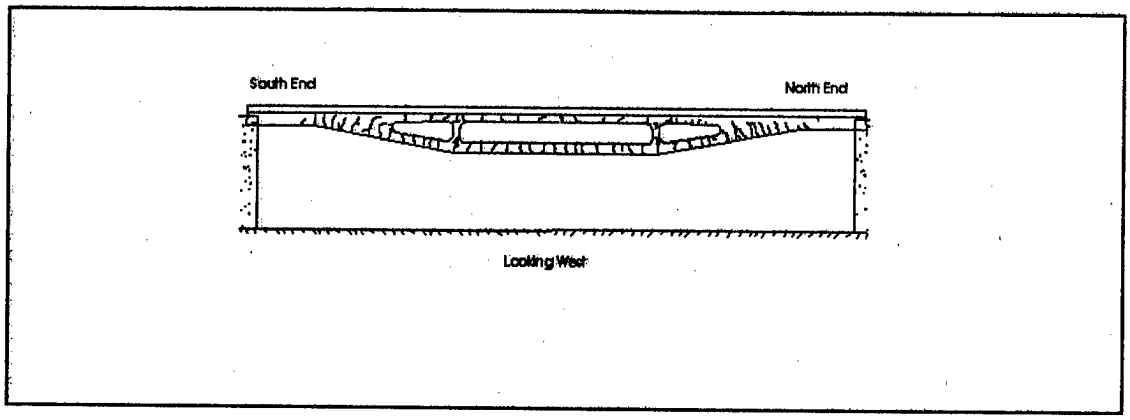
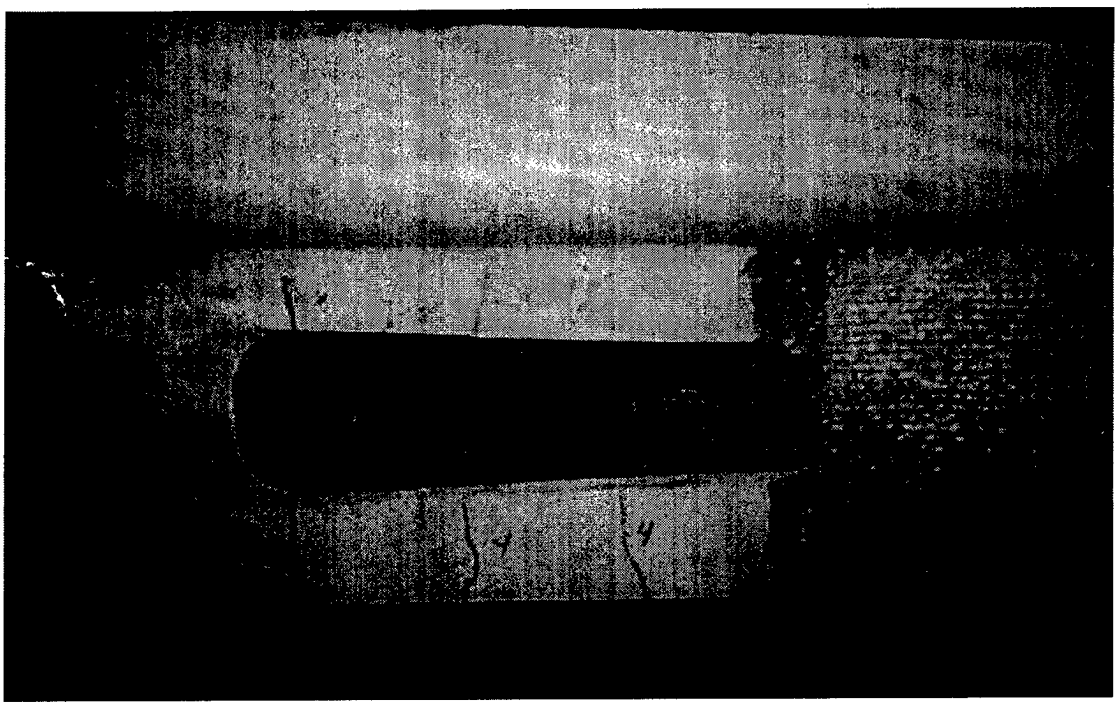


Figure A40. Crack Patterns of HJ-4 prior to FRP repair.



a. Cracks at North end of joist

b. Cracks at South end of joist

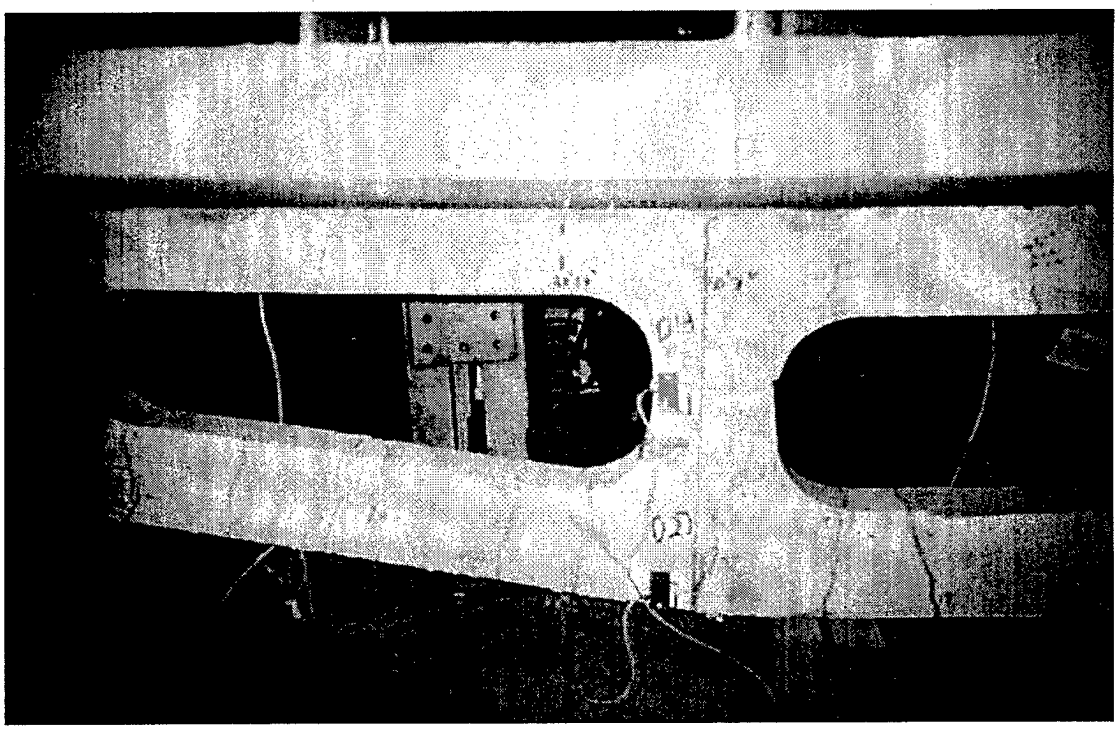


Figure A41. Crack patterns for HJ-4.

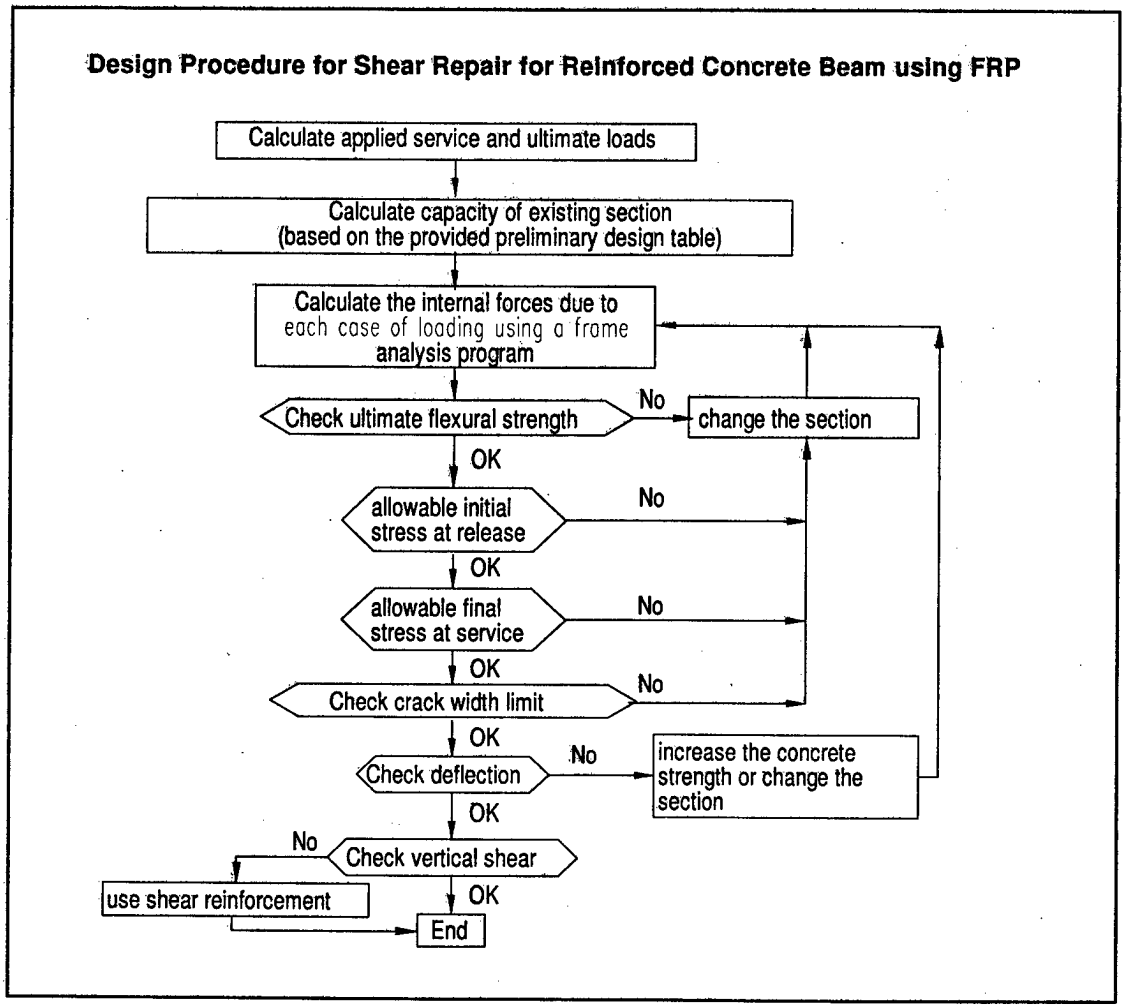


Figure A42. Shear Repair Design Procedure Flow Chart.

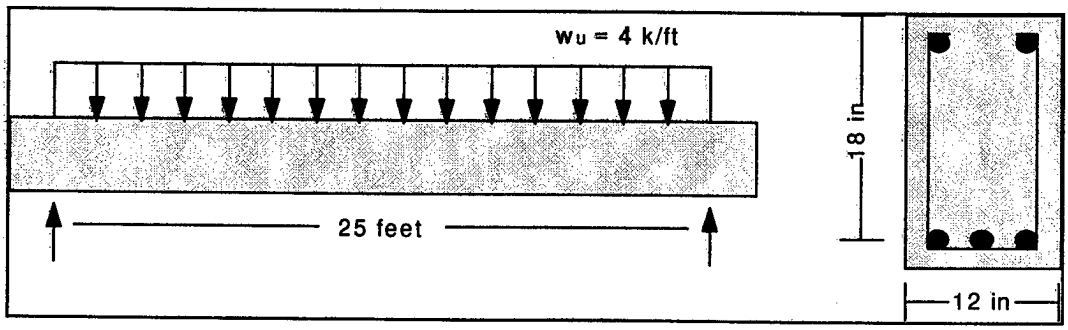


Figure A43. Simply Supported Beam.

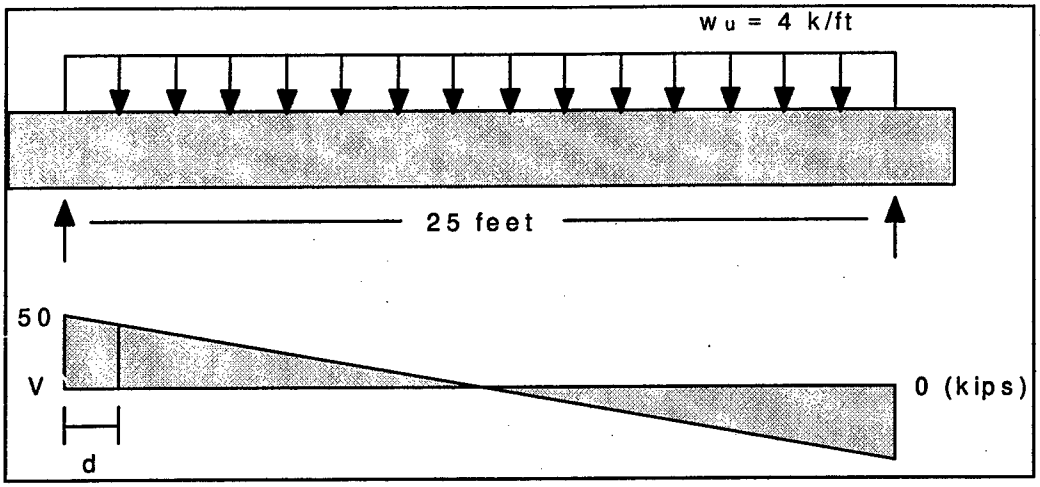


Figure A44. Shear Diagram.

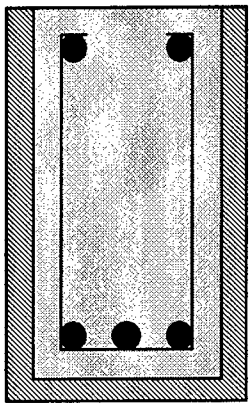


Figure A45. FRP Wrap Repair.

Table A1. Hybrid Joists Tested

Joist Designation	Configuration	Web Shear Reinforcement	Slab Width (ft)
HJ-3	Upgraded with FRP	Figure 4.6	6
HJ-4	Tested, then repaired with FRP	Figure 4.6	6
HJ-6	Insufficient shear reinforcement	Figure 4.8	4
HJ-7	Proper shear reinforcement	Figure 4.8	4

Table A2. Epoxy Material Properties

Property	Average	Minimum	Test Method
-Tg @ 45% RH	120°F	100°F	
-Tg @ 95% RH	110°F	95°F	
-Tg 140OF Postcure (24 Hours)	180°F	140°F	
Tensile Strength	10,100 psi	9,500 psi	ASTM D 638 Type 1
Tensile Modulus	461,000 psi	425000 psi	ASTM D 638 Type 1
Elongation Percent	5.00%	3.50%	ASTM D 638 Type 1
Flexural Strength	11,500 psi	10,500 psi	ASTM D 790
Flexural Modulus	400,000 psi	375,000 psi	ASTM D 790

Curing Schedule 72 hours post cure at 140°F

Table A3. Yarn Properties

Property	E-glass	Polyaramid	Test Method
Yield/Denier	1200 and 250 ypp	2160 denier	
Density (g/cc)	2.54	1.44	ASTM D 792
Tensile Strength (psi)	440,000	400,000	SIM 13*
Tensile Modulus (psi)	10,500,000	17,000,000	STM 13
Elongation (%)	4.2	2.5	STM 13

* Seguin Test Method - Hexel Manufacturing facility standard methods based on appropriate Standardized testing procedure

Table A4. Fabric Properties

Property	Average Value	Minimum Value	Test Method
Areal Weight (oz/sq. yd.)	27.2	24.4	STM 18
Tensile Strength dry 1" strip (Break Load lb.)	1800	1600	STM 27
Air Permeability (cu. ft./min.)	22	20	STM 26

Table A5. Composite Laminate Specification

Property	Value	ASTM Method
Ultimate Tensile Strength min. (primary fiber direction)*	65,000 psi	D 3039
Elongation at break, min.	2.00%	D 3039
Tensile Modulus	3.0×10^6 psi	
Ultimate Tensile Strength min. (90 degrees to primary fiber direction)	4,800 psi	D 3039

* Tensile retained 7 days @ 100% RH, 1,000 hours ozone, 1,000 hours alkali, 1,000 hours salt water, and 1,000 hours at 140°F
Cured for 48 hours at 140°F Using Hexcel Sample Preparation

Table A6. Composite Material Properties

Property	Value	Test Method
Tensile Strength at 0° (ksi)	65	ASTM D3039
Tensile Strength at 90° (ksi)	6.0	ASTM D3039
Elastic Modulus (ksi)	3,250	
Ultimate Strain	0.02	ASTM D3039
Coefficient of Thermal Expansion	4.3×10^{-6}	

Table A7. Casting and release dates for each hybrid joist web.

Specimen	Casting Date	Release Date
HJ-3	1/29/96	2/5/96
HJ-4	1/29/96	2/5/96
HJ-6	2/12/96	2/16/96
HJ-7	6/20/96	6/24/96

Table A8. Instrumentation for HJ-3 upgraded with FRP

Hybrid Joist Test			HJ-3		Date:	August 12, 1996	
USA Construction Engineering Research Laboratories						Champaign, IL	
Instrument	CERL Name/ Cable #	CIR Name	Conversion Factor (per volt)	Location (X - Dir.) (in.)	Location (Y - Dir.) (in.)	Gage Length (in.)	Comments
Cell_N		N / A	5.000 kips	141.000	N / A	N / A	Concentrated Load - 50 Kip Actuator
Stroke_N		N / A	0.300 inches	141.000	N / A	N / A	
Cell_S		N / A	5.000 kips	250.000	N / A	N / A	Concentrated Load - 50 Kip Actuator
Stroke_S		N / A	0.300 inches	250.000	N / A	N / A	
POT_N	P1	N / A	1.994 inches	141.000	N / A	N / A	Third span Deflection - Potentiometer
POT_Mid	P2	N / A	1.996 inches	192.000	N / A	N / A	Midspan Deflection - Potentiometer
POT_S	P3	N / A	2.000 inches	278.000	N / A	N / A	Quarter span Deflection - Potentiometer
Int_1	IS1 / 3	s19	0.00150 in/in	40.000	N / A	N / A	Placed by the CIR
Int_2	IS2 / 2	s20	0.00150 in/in	40.000	N / A	N / A	Placed by the CIR
Int_3	IS3 / 1	s21	0.00150 in/in	40.000	N / A	N / A	Placed by the CIR
Int_4	IS4 / 12	s28	0.00150 in/in	141.000	N / A	N / A	Placed by the CIR
Int_5	IS5 / 11	s26	0.00150 in/in	119.000	N / A	N / A	Placed by the CIR
Int_6	IS6 / 10	s30	0.00150 in/in	141.000	N / A	N / A	Placed by the CIR
Int_7	IS7 / 15	s31	0.00150 in/in	163.000	N / A	N / A	Placed by the CIR
Int_8	IS8 / 14	s27	0.00150 in/in	119.000	N / A	N / A	Placed by the CIR
Int_9	IS9 / 13	s33	0.00150 in/in	163.000	N / A	N / A	Placed by the CIR
Int_10	IS10 / 18	s34	0.00150 in/in	192.000	N / A	N / A	Placed by the CIR
Int_11	IS11 / 17	s35	0.00150 in/in	192.000	N / A	N / A	Placed by the CIR
Int_12	IS12 / 16	s36	0.00150 in/in	192.000	N / A	N / A	Placed by the CIR
LVDT_1	D1	N / A	0.00500 in.	75.500	1.000	7.205	Measured from the Top of the Slab
LVDT_2	D2	N / A	0.00500 in.	74.000	3.000	6.417	Measured from the Bottom Face of the Slab
LVDT_3	D3	N / A	0.00500 in.	73.000	12.250	4.134	Measured from the Bottom Face of the Slab
LVDT_4	D4	N / A	0.00500 in.	145.000	1.000	6.220	Measured from the Top of the Slab
LVDT_5	D5	N / A	0.00500 in.	143.000	3.500	7.480	Measured from the Bottom Face of the Slab
LVDT_6	D6	N / A	0.00500 in.	142.500	11.000	2.677	Measured from the Bottom Face of the Slab
LVDT_7	D7	N / A	0.00500 in.	142.000	22.750	2.756	Measured from the Bottom Face of the Slab
LVDT_8	D8	N / A	0.00500 in.	170.500	1.000	7.520	Measured from the Top of the Slab
LVDT_9	D9	N / A	0.00500 in.	N / A	N / A	N / A	Not used for this test, Sensor moved to D7
LVDT_10	D10	N / A	0.00500 in.	169.250	22.750	5.630	Measured from the Bottom Face of the Slab
LVDT_11	D11	N / A	0.00500 in.	193.500	1.000	5.276	Measured from the Top of the Slab
LVDT_12	D12	N / A	0.00500 in.	194.000	3.000	5.433	Measured from the Bottom Face of the Slab
LVDT_13	D13	N / A	0.00500 in.	194.000	22.500	5.039	Measured from the Bottom Face of the Slab
LVDT_14	D14	N / A	0.00500 in.	193.500	N / A	5.197	Placed on top of Slab
LVDT_15	D15	N / A	0.00500 in.	243.000	N / A	2.677	Not used for this test
LVDT_16	D16	N / A	0.00500 in.	194.000	N / A	6.850	Placed on bottom side of Web
LVDT_17	D17	N / A	- 0.00500 in.	222.000	2.250	2.677	Measured from the Bottom Face of the Slab
LVDT_18	D18	N / A	0.00500 in.	222.000	22.500	4.803	Measured from the Bottom Face of the Slab
LVDT_19	D19	N / A	- 0.00500 in.	242.000	10.000	3.268	Measured from the Bottom Face of the Slab
LVDT_20	D20	N / A	0.00500 in.	242.000	22.000	2.480	Measured from the Bottom Face of the Slab

Hybrid Joist Test			HJ-3		Date:	August 12, 1996	
USA Construction Engineering Research Laboratories						Champaign, IL	
Instrument	**CERL** Name/ Cable #	**CIR** Name	**Conversion** Factor (per volt)	**Location** (X - Dir.) (in.)	**Location** (Y - Dir.) (in.)	**Gage** Length (in.)	Comments
Ext. Str._1	ES1	N / A	0.00150 in/in				
Ext. Str._2	ES2	N / A	0.00150 in/in				
Ext. Str._3	ES3	N / A	0.00150 in/in	See Attached Figure for External			
Ext. Str._4	ES4	N / A	0.00150 in/in	Strain Gage Locations			
Ext. Str._5	ES5	N / A	0.00150 in/in				
Ext. Str._6	ES6	N / A	0.00150 in/in				
Ext. Str._7	ES7	N / A	0.00150 in/in				
Ext. Str._8	ES8	N / A	0.00150 in/in				

*** +X direction is defined as running north to south with north being 0. Measurements taken to the north face of the LVDT blocks.

*** +Y direction is defined as running up to down with 0 being the bottom face of the slab, except where noted that measurement was taken from the top of the slab. Measurement was taken to the middle of the circular opening in the block.

IMPORTANT NOTE: Sensor for D7 was not working. Sensor from D9 was placed in location of D7.

Table A9. Instrumentation for HJ-4 without FRP Repair

Hybrid Joist Test			HJ-4		Date: June 3, 1996		
USA Construction Engineering Research Laboratories					(First Test without FRP)		
Instrument	CERL Name/ Cable #	CIR Name	Conversion Factor (per volt)	Location (X - Dir.) (in.)	Location (Y - Dir.) (in.)	Gage Length (in.)	Comments
Cell_N		N / A	5.000 kips	141.000	N / A	N / A	Concentrated Load - 50 Kip Actuator
Stroke_N		N / A	0.300 inches	141.000	N / A	N / A	
Cell_S		N / A	5.000 kips	250.000	N / A	N / A	Concentrated Load - 50 Kip Actuator
Stroke_S		N / A	0.300 inches	250.000	N / A	N / A	
POT_N	P1	N / A	1.994 inches	141.000	N / A	N / A	Third span Deflection - Potentiometer
POT_Mid	P2	N / A	1.996 inches	192.000	N / A	N / A	Midspan Deflection - Potentiometer
POT_S	P3	N / A	2.000 inches	278.000	N / A	N / A	Quarter span Deflection - Potentiometer
Int_1	IS1 / 19	s19	0.00150 in/in	40.000	N / A	N / A	Placed by the CIR
Int_2	IS2 / 16	s20	0.00150 in/in	40.000	N / A	N / A	Placed by the CIR
Int_3	IS3 / 21	s21	0.00150 in/in	40.000	N / A	N / A	Placed by the CIR
Int_4	IS4 / 28	s28	0.00150 in/in	141.000	N / A	N / A	Placed by the CIR
Int_5	IS5 / 26	s26	0.00150 in/in	119.000	N / A	N / A	Placed by the CIR
Int_6	IS6 / 30	s30	0.00150 in/in	141.000	N / A	N / A	Placed by the CIR
Int_7	IS7 / 31	s31	0.00150 in/in	163.000	N / A	N / A	Placed by the CIR
Int_8	IS8 / 27	s27	0.00150 in/in	119.000	N / A	N / A	Placed by the CIR
Int_9	IS9 / 33	s33	0.00150 in/in	163.000	N / A	N / A	Placed by the CIR
Int_10	IS10 / 34	s34	0.00150 in/in	192.000	N / A	N / A	Placed by the CIR
Int_11	IS11 / 35	s35	0.00150 in/in	192.000	N / A	N / A	Placed by the CIR
Int_12	IS12 / 36	s36	0.00150 in/in	192.000	N / A	N / A	Placed by the CIR
LVDT_1	D1	N / A	0.00494 in.	72.750	1.000	7.205	Measured from the Top of the Slab
LVDT_2	D2	N / A	0.00497 in.	71.375	3.000	6.063	Measured from the Bottom Face of the Slab
LVDT_3	D3	N / A	0.00495 in.	69.125	12.250	2.913	Measured from the Bottom Face of the Slab
LVDT_4	D4	N / A	0.00497 in.	145.125	1.000	5.748	Measured from the Top of the Slab
LVDT_5	D5	N / A	0.00496 in.	143.375	3.500	5.197	Measured from the Bottom Face of the Slab
LVDT_6	D6	N / A	0.00496 in.	143.375	11.000	2.559	Measured from the Bottom Face of the Slab
LVDT_7	D7	N / A	0.00496 in.	142.375	22.750	5.236	Measured from the Bottom Face of the Slab
LVDT_8	D8	N / A	0.00495 in.	168.125	1.000	5.236	Measured from the Top of the Slab
LVDT_9	D9	N / A	0.00496 in.	167.375	3.000	2.441	Measured from the Bottom Face of the Slab
LVDT_10	D10	N / A	0.00499 in.	168.375	22.750	2.441	Measured from the Bottom Face of the Slab
LVDT_11	D11	N / A	0.00489 in.	195.000	1.000	6.417	Measured from the Top of the Slab
LVDT_12	D12	N / A	0.00496 in.	193.875	3.000	7.283	Measured from the Bottom Face of the Slab
LVDT_13	D13	N / A	0.00496 in.	195.500	22.500	5.197	Measured from the Bottom Face of the Slab

Hybrid Joist Test HJ-4 Date: June 3, 1996

USA Construction Engineering Research Laboratories (First Test without FRP)

Instrument	CERL Name/ Cable #	CIR Name	Conversion Factor (per volt)	Location (X - Dir.) (in.)	Location (Y - Dir.) (in.)	Gage Length (in.)	Comments
LVDT_14	D14	N / A	0.00491 in.	194.750	N / A	6.260	Placed on top of Slab
LVDT_15	D15	N / A	0.00496 in.	N / A	N / A	N / A	Not used for this test, Sensor moved to D13
LVDT_16	D16	N / A	0.00500 in.	195.250	N / A	6.299	Placed on bottom side of Web
LVDT_17	D17	N / A	-0.00503 in.	220.000	2.250	7.638	Measured from the Bottom Face of the Slab
LVDT_18	D18	N / A	0.00487 inches	220.375	22.500	4.055	Measured from the Bottom Face of the Slab
LVDT_19	D19	N / A	-0.00501 in.	244.000	10.000	2.362	Measured from the Bottom Face of the Slab
LVDT_20	D20	N / A	0.00500 in.	244.125	22.000	2.717	Measured from the Bottom Face of the Slab

*** +X direction is defined as running north to south with north being 0. Measurements taken to the north face of the LVDT blocks.

*** +Y direction is defined as running up to down with 0 being the bottom face of the slab, except where noted that measurement was taken from the top of the slab. Measurement was taken to the middle of the circular opening in the block.

IMPORTANT NOTES: Sensor for D15 was moved into the D13 position. D15 position was not used.

Table A10. Instrumentation for HJ-4 with FRP Repair

Hybrid Joist Test HJ-4 (2nd Test with FRP)
USA Construction Engineering Research Laboratories
Champaign, IL

Date: August 2 1996

Instrument	CERL Name / Cable #	CIR Name	Conversion Factor (per volt)	Location (X - Dir.) (in.)	Location (Y - Dir.) (in.)	Gage Length (in.)	Comments
Cell_N		N / A	5.000 kips	141.000	N / A	N / A	Concentrated Load - 50 Kip Actuator
Stroke_N		N / A	0.300 inches	141.000	N / A	N / A	
Cell_S		N / A	5.000 kips	250.000	N / A	N / A	Concentrated Load - 50 Kip Actuator
Stroke_S		N / A	0.300 inches	250.000	N / A	N / A	
POT_N	P1	N / A	2.000 inches	141.000	N / A	N / A	Third span Deflection - Potentiometer
POT_Mid	P2	N / A	2.000 inches	192.000	N / A	N / A	Midspan Deflection - Potentiometer
POT_S	P3	N / A	2.000 inches	278.000	N / A	N / A	Quarter span Deflection - Potentiometer
Int_1	IS1 / 19	s19	0.00150 in/in	40.000	N / A	N / A	Placed by the CIR
Int_2	IS2 / 16	s20	0.00150 in/in	40.000	N / A	N / A	Placed by the CIR
Int_3	IS3 / 21	s21	0.00150 in/in	40.000	N / A	N / A	Placed by the CIR
Int_4	IS4 / 28	s28	0.00150 in/in	141.000	N / A	N / A	Placed by the CIR
Int_5	IS5 / 26	s26	0.00150 in/in	119.000	N / A	N / A	Placed by the CIR
Int_6	IS6 / 30	s30	0.00150 in/in	141.000	N / A	N / A	Placed by the CIR
Int_7	IS7 / 31	s31	0.00150 in/in	163.000	N / A	N / A	Placed by the CIR
Int_8	IS8 / 27	s27	0.00150 in/in	119.000	N / A	N / A	Placed by the CIR
Int_9	IS9 / 33	s33	0.00150 in/in	163.000	N / A	N / A	Placed by the CIR
Int_10	IS10 / 34	s34	0.00150 in/in	192.000	N / A	N / A	Placed by the CIR
Int_11	IS11 / 35	s35	0.00150 in/in	192.000	N / A	N / A	Placed by the CIR
Int_12	IS12 / 36	s36	0.00150 in/in	192.000	N / A	N / A	Placed by the CIR
LVDT_1	D1	N / A	0.00500 inches	72.750	1.000	7.205	Measured from the Top of the Slab
LVDT_2	D2	N / A	0.00500 inches	69.000	3.000	6.000	Measured from the Bottom Face of the Slab
LVDT_3	D3	N / A	0.00500 inches	68.500	12.000	3.125	Measured from the Bottom Face of the Slab
LVDT_4	D4	N / A	0.00500 inches	145.125	1.000	5.748	Measured from the Top of the Slab
LVDT_5	D5	N / A	0.00500 inches	143.375	3.500	5.197	Measured from the Bottom Face of the Slab
LVDT_6	D6	N / A	0.00500	143.375	11.000	2.559	Measured from the Bottom

Hybrid Joist Test HJ-4 (2nd Test with FRP)
USA Construction Engineering Research Laboratories
Champaign, IL

Date: August 2 1996

Instrument	CERL Name / Cable #	CIR Name	Conversion Factor (per volt)	Location (X - Dir.) (in.)	Location (Y - Dir.) (in.)	Gage Length (in.)	Comments
			inches				Face of the Slab
LVDT_7	D7	N / A	0.00500 inches	142.375	22.750	5.236	Measured from the Bottom Face of the Slab
LVDT_8	D8	N / A	0.00500 inches	168.125	1.000	5.236	Measured from the Top of the Slab
LVDT_9	D9	N / A	N / A	N / A	N / A	N / A	Not used for this test, Sensor moved to D5
LVDT_10	D10	N / A	0.00500 inches	168.375	22.750	2.441	Measured from the Bottom Face of the Slab
LVDT_11	D11	N / A	0.00500 inches	195.000	1.000	6.417	Measured from the Top of the Slab
LVDT_12	D12	N / A	0.00500 inches	193.875	3.000	7.283	Measured from the Bottom Face of the Slab
LVDT_13	D13	N / A	0.00500 inches	195.500	22.500	5.197	Measured from the Bottom Face of the Slab
LVDT_14	D14	N / A	0.00500 inches	194.750	N / A	6.260	Placed on top of Slab
LVDT_15	D15	N / A	N / A	N / A	N / A	N / A	Not used for this test, Sensor moved to D13
LVDT_16	D16	N / A	0.00500 inches	195.250	N / A	6.299	Placed on bottom side of Web
LVDT_17	D17	N / A	- 0.00500 in.	220.000	2.250	7.638	Measured from the Bottom Face of the Slab
LVDT_18	D18	N / A	0.00500 inches	220.375	22.500	4.055	Measured from the Bottom Face of the Slab
LVDT_19	D19	N / A	- 0.00500 in.	244.000	10.000	2.362	Measured from the Bottom Face of the Slab
LVDT_20	D20	N / A	0.00500 inches	244.125	22.000	2.717	Measured from the Bottom Face of the Slab
Ext. Str._1	ES1	N / A	0.00150 in / in				
Ext. Str._2	ES2	N / A	0.00150 in / in				
Ext. Str._3	ES3	N / A	0.00150 in / in				See Attached Figure for External Strain Gage Locations
Ext. Str._4	ES4	N / A	0.00150 in / in				
Ext. Str._5	ES5	N / A	0.00150 in / in				
Ext. Str._6	ES6	N / A	0.00150 in / in				
Ext. Str._7	ES7	N / A	0.00150 in / in				

Hybrid Joist Test HJ-4 (2nd Test with FRP)
USA Construction Engineering Research Laboratories
Champaign, IL

Date: August 2 1996

Instrument	CERL Name / Cable #	CIR Name	Conversion Factor (per volt)	Location (X - Dir.) (in.)	Location (Y - Dir.) (in.)	Gage Length (in.)	Comments
Ext. Str._8	ES8	N / A	0.00150 in / in				

*** +X direction is defined as running north to south with north being 0. Measurements taken to the north face of the LVDT blocks.

*** +Y direction is defined as running up to down with 0 being the bottom face of the slab, except where noted that measurement was taken from the top of the slab. Measurement was taken to the middle of the circular opening in the block.

IMPORTANT NOTES:
Sensor for D15 was moved into the D13 position. D15 position was not used.
Sensor for D9 was moved into the D5 position. D9 position was not used.

Table A11. Principal experimental test results for hybrid joists.

Joist designation	Experimental cracking load* (kips)	First Crack Location	Applied Failure load* (kips)	Total Failure Load (kips)	Equivalent Uniform Load (ksf)	Type of failure
HJ-3		midspan, bottom chord	52.0	53.0	0.62	shear
HJ-4		midspan, bottom chord	56.6	56.6**	0.67	no failure
HJ-6	11.7	midspan, bottom chord	48.0	49.0	0.57	shear
HJ-7	31.5	midspan bottom chord	64.0	65.0	0.76	flexure

* Sum of two actuators.
**No failure occurred.

Table A12. Camber and deflection for hybrid joists (in.).

Joist designation	Camber at release	LL Deflection	SIDL + LL Deflection	Deflection at peak load	Deflection at failure
HJ-3	0.40	.09	.14	5.66	12.58
HJ-4 without FRP	0.45	.10	.16	7.66	7.67*
HJ-4 with FRP repair	NA	.10	.16	8.62	10.06*
HJ-6	0.45	0.03	0.16	3.52	3.52
HJ-7	0.38	0.02	0.14	16.6	16.6

* Deflection at end of test; no failure occurred.

Appendix B: Strengthening Damaged Reinforced Concrete Beams Using CFRP Tendons

Overview

Several types of fiber-reinforced polymer (FRP) reinforcing and prestressing systems have been developed for the concrete construction and repair industry. These repair systems include FRP reinforcing bars, prestressing systems, and sheet-type products that are adhesively bonded to walls, floors, beams and columns. Steel bar and prestressing systems have long been used to externally strengthen structures and adhesively bonded steel plates have been widely used in Europe for over 15 years. FRP products can improve structural performance and are more durable in aggressive environments as compared to steel.

In this part of the CPAR study a field demonstration of carbon FRP (CFRP) tendons used in the repair and strengthening of precast reinforced concrete beams in South Florida condominium was monitored. Specifically, this field demonstration provided the opportunity to investigate the short- and long-term behavior of a CFRP prestressing system used to retrofit/ strengthen deteriorated reinforced concrete single and double-tee beams. Corrosion in the tensile zone steel reinforcing bars damaged the beams. In this demonstration, the repair/ strengthening work was completed by Structural Preservation Systems, Inc. (SPS). The product investigated in this demonstration was LEADLINE ™ CFRP tendons provided by Mitsubishi Chemical Corporation (MCC). The design of the repair and strengthening work was under the auspices of the condominium owners hired engineering company, Chalaire & Associates.

The repair concept, proposed by SPS and authorized by Chalaire & Associates, is a 'first in the world' use for this type of FRP repair. The prestressing concept developed by Penn State University is unique because it combines the use of CFRP prestressing rods and a new expansive cement grouted ground anchor-type anchorage for externally post-tensioning reinforced concrete beams. Use of

the LEADLINE™ CFRP prestressing system was justified for this project because of its structural properties, durability, and corrosion resistance.

The results of this investigation can provide the basis and assurance for using FRP prestressing systems for retrofit strengthening of civil engineering structures. The methodology used in this field evaluation study can also serve as a guideline for the future field observations of other FRP products.

The objective of this investigation was to determine whether CFRP tendons are viable as a concrete repair technique. Instrumentation was installed in the existing corroded reinforced concrete double-tee beams strengthened with external post-tensioning LEADLINE™ tendons with anchorages to acquire short- and long-term measurements during and after post-tensioning. The results were documented to evaluate the strengthening process and procedures used by Structural Preservation (SPS).

Location And Conditions At Condominium

A demonstration was conducted using CFRP tendons at Tropicana Condominium, 4001 South Ocean Drive, Lantana, FL, just south of Palm Beach. The condominium, constructed in 1950s, is approximately one-quarter mile from the Atlantic Ocean. All floors of the condominium were constructed with precast reinforced concrete single and double-tee beams. For all above grade floors, the double-tee beams extend beyond the building walls to form the floor of balconies. The ground level double-tee beams are supported on reinforced concrete grade beams with a two foot high air space between the bottom of the stems and the earth that is open to outside air flow.

The problem with the condominium structure is that all exposed concrete portions of the double-tee beams have absorbed salt from the ocean air and has subsequently caused severe corrosion of the tensile steel reinforcing bars in the bottom of the double-tee beam stems. Associated cracking and spalling of the concrete cover over the reinforcing bars reduced the load carrying capacity of the beams.

The reinforced concrete double-tee beams in the first floor have deteriorated considerably with concrete spalling, cracking and either partial or complete exposure of bundled steel rebars due to the damp marine environment. The beams were designed with 3 #7 bars (bundled) at the center and 2 #7 bars

(bundled) at the ends. The beams have a clear span of 24 ft - 3 in. between grade beams / girders.

Field Instrumentation

The actual setup of the instrumentation at the site is shown in Figure B1.* Load cells LC1 and LC2 are positioned at the southern ends of the LEADLINE tendons 1 and 4 (Fig. B2). The anchorages A1, A2, A3 and A4 also at the southern ends are instrumented with electrical resistance strain gages in the axial and circumferential directions (Fig. B3). The electrical resistance strain gages are installed at both the northern and southern quarter span points in the LEADLINE tendons 1 and 4 and at the southern quarter span points in LEADLINE tendons 2 and 3. Figure B4 shows an electrical resistance strain gage installed on a typical LEADLINE tendon. Electrical resistance strain gages are also set up at the exterior concrete web surfaces of the double-tee beam at the midspan. Stud points spaced over a gage length of 6 in. for digimatic micrometer measurements are mounted at both the northern and southern quarter span points in the LEADLINE tendons 1 and 4. Stud points spaced at 6 in. gage length over a typical LEADLINE tendon are shown in Figure B5. A Digimatic micrometer is used to monitor the deformation over the gage length with time. Stud points are also attached at the regions extending over the end of the tendons and anchorages to measure the relative slip (Fig. B6). The deflection is measured with reference to a reference pointer firmly attached to the bottom of the flange between the webs of the double-tee beam at the midspan.

External Post Tensioning

A hydraulic jack was used to prestress the LEADLINE tendons at load increments of approximately 3,000 lbs. The maximum force at the jacking end was 12,000 lbs. and the four LEADLINE tendons were tensioned in succession one at a time. The sequence of post tensioning of the tendons was the following: LEADLINE 1, LEADLINE 4, LEADLINE 2 and LEADLINE 3. For each applied prestressing force increment, the force, anchorage slip, strains in the tendons,

* All figures are found at the end of this Appendix.

concrete and anchorages, and deflection at midspan were monitored using data acquisition system, strain indicator, Digimatic micrometer, and deflectometer.

Prestress Losses During Post Tensioning

Frictional Loss due to Curvature Effect

The LEADLINE tendon profile in the double-tee beam is shown in Figure B7. When the LEADLINE tendon is tensioned by the hydraulic jack, the prestressing force varies along the length of the tendon due to change in curvature and friction between the tendon and the metallic pipes. Curvature frictional loss results from the change of angle of the tendon profile. The curvature friction loss in the tendon can be computed from

$$\Delta f_{pF} = -f_1 \mu \alpha \quad \text{.....(1)}$$

where f_1 = stress in the tendon due to initial prestress,

μ= curvature friction coefficient,

α = angle change between any two points on the tendon in radians.

The computed curvature frictional loss in a typical LEADLINE tendon is shown in Figure B8.

Elastic Shortening of Concrete

Concrete shortens when a prestressing force is applied to the member. The stress in the LEADLINE tendons would not be affected by the elastic shortening of the concrete, if all the tendons were post-tensioned simultaneously. However, in the present case the four LEADLINE tendons were stressed one at a time for the strengthening of the reinforced concrete double-tee beam. The prestress force in the last tendon (LEADLINE tendon 3) will not be influenced by the elastic shortening, while the LEADLINE tendons 1, 4 and 2 experience a loss due to the stressing of the subsequent tendons. For n number of tendons sequentially tensioned, the elastic shortening loss for the post tensioned element is given by

$$\Delta f_{pES} = \frac{1}{n} \sum_{j=1}^{n} (\Delta f_{pES})_j \quad \text{.....(2)}$$

$$\Delta f_{pES} = \frac{1}{n}\sum_{j=1}^{n}(\Delta f_{pES})_j \quad \text{.....(2)}$$

where j denotes the number of jacking operations.

The concrete strains in the web of the double-tee beam due to the applied prestress are computed to be only 33 με at the fiber distance of 1.0 in. from the centroid and 96 με at the centroid. The recorded concrete strains were approximately in the same range of the computed values.

Initial Losses in Prestress

The prestressing forces at different loading stages in LEADLINE tendons 1 and 4 are given in Tables B1* and B2. The drop in the prestressing force in LEADLINE tendon 1 was relatively small after securing the nuts in position on the anchorage at the jacking end. However, the decrease in the prestress in LEADLINE tendon 4 was significant between the stages 4 and 5. This was due to the difficulty encountered in securing the nuts adequately due to the tight working space constraints imposed at the site.

The initial loss of the prestress force in the LEADLINE tendons taking into account the curvature frictional effects and elastic shortening of the concrete is shown in Table B3. The percentage of the initial loss varies approximately from 9-14%.

Long Term Effects And Performance

Variation in Environmental Parameters

The changes in daily temperatures and humidities in South Florida are significantly large over the periods of observation from April 1996 until June 1997. The recorded variations in the maximum and minimum temperatures and humidities in the morning and evening are shown in Figures B9 and B10.

* Tables are found at the end of this appendix.

Slip in the Anchorages

The relative slip of the LEADLINE tendons in the anchorage is almost negligible during the process of post tensioning of the double-tee beams. However, it is important to examine the slip of the tendons with respect to the anchorages as a function of time. The changes in length between the stud points in the regions of the anchorages and LEADLINE tendons were analyzed to determine the amount of slip over the period of time. Figure B11 shows the slip of the LEADLINE tendon 1 in the anchorage at the northern end while those of the LEADLINE tendon 4 at the northern and southern ends are given in Figures 12 and 13 respectively. The steep increase in slip during the period from 11th day to 31st day and a corresponding decrease in the slip from 31st day to 43rd day may not be realistic in tendon 4 (Fig. B13). Generally, it can be seen from Figures B11, B12 and B13 that the slip takes place over the initial period of the first 60 days from the day of prestressing and then tends to remain at a steady state. The corresponding prestress losses due to slip in LEADLINE tendons 1 and 4 are presented in Figures B14 and B15. The loss due to slip appears to increase steeply from 23rd day to 37th day and then decreases significantly from 37th day to 64th day in tendon 1 (Fig. B14). However, the prestress loss in LEADLINE tendon 1 due to slip appears to be steady after the 64th day at an approximate value of only about 60 lbs. and that in LEADLINE tendon 4 is also relatively small with a magnitude of about 70 lbs.

Relaxation in LEADLINE Tendons and Creep in Concrete

The strains in the LEADLINE tendons 1 and 4 were monitored by digimatic micrometer and electrical resistance strain gages. The variations in the strains based on the digimatic micrometer observations and the electrical resistance strain gages are shown in Figures B16 and B17. The recorded strains in the tendons indicate a trend to a steady state over the period of observation. The changes in magnitudes of the forces with respect to time in tendons 1 and 4 due to relaxation and slip in the anchorages are presented in Figures B18 and B19. The losses in prestress in the tendons 1 and 4 due to relaxation are shown in Figures B20 and B21 and the magnitude can be taken as 10-12% of the initial jacking force.

The prestressing force in the LEADLINE tendon may also be influenced by the creep effect on concrete. The creep coefficient at time t, for loading at age t_0 is given by,

$$\varphi(t,t_0) = \frac{(t-t_0)^{0.6}}{10+(t-t_0)^{0.6}}\varphi_u \quad \text{.....(3)}$$

$$\varphi_u = \varphi(t_\infty, t_0) \quad \text{.....(4)}$$

$$\varphi_u = 2.35\gamma_c \quad \text{.....(5)}$$

where φ_u is the ultimate creep, γ_c is a correction factor, the product of several parameters depending upon ambient relative humidity, average thickness of the member or its volume-to-surface ratio and the temperature. For a structural member similar to the existing double-tee beam under study, which is relatively old, the creep coefficient does not vary with respect to time and therefore, the creep effects are negligible.

Variations in Grout Pressures with Time

The initial variations in grout pressure buildup with time were monitored from the electrical resistance strain gages installed in the circumferential direction on an anchorage. The typical variations in circumferential strains due to grout pressures are shown in Figure B22. The grout pressures are calculated based on the measured circumferential strains and the thick cylinder theory. The maximum grout pressure developed in the anchorage is approximately 5000 psi. after 7 days.

The changes in the circumferential strains in the anchorages as a function of time are monitored at the site and shown in Figures B23 and B24. The circumferential strains during the initial period of the first 20 days are compressive. This could be due to the effect of relaxation on the circumferential strain during the initial period. Further additional relaxation in the tendon is also caused due to the upward forces from the tendons acting on the metallic pipes at midspan region due to prestressing of the adjoining double-tee beams. After the 20th day, the strains tend to increase corresponding to increases in the grout pressure. The maximum increase in grout pressures corresponding to the observed changes in strains is approximately 4000 psi.

The variations in the axial strains in the anchorages A1 and A4 at the southern end are shown in Figures B25 and B26. The changes in the axial strains are influenced by several parameters including the slip in the anchorage, grout pressure and the relaxation in the LEADLINE tendons. The maximum increase

in grout pressure computed based on the measured axial strains of anchorage is approximately 3000 psi.

The anchorages at the southern end are located close to an opening in the basement wall and hence exposed to moisture during the rainy days. The strain gages are protected adequately against moisture intrusion; however, they seem to have been affected by exposure to continuous moist environment and hence the data were affected due to malfunctioning of the strain gages after a period of the first 149 days.

Design Concepts And Analysis

Design Concepts

At the ultimate load level, the required nominal moment of resistance of the existing beam under design has to be at least greater than the factored moment M_u. The factored moment is computed based on a combination of factored live and dead loads. The ultimate load effect for the strengthened beam with external post tensioning can be taken as U = 1.4 D + 1.7 L, where D = dead load and L = the live load effects.

In the case of the existing reinforced concrete beam (Fig. B27), the center of gravity of the LEADLINE tendon can be determined knowing the given beam depth and the position of the LEADLINE tendon from the compression fiber. The total prestress force in the LEADLINE tendon can be calculated as

$$T = \frac{\left(M_u / \varphi\right)}{\left(d - \frac{a}{2}\right)} \qquad \text{.....(6)}$$

Knowing the total prestressing force and the design prestress based on a load factor and the ultimate strength for a given size LEADLINE tendon, the number of tendons is determined for the strengthening of the member by external post tensioning.

Illustrative Design Examples

T-Beam

Given Data

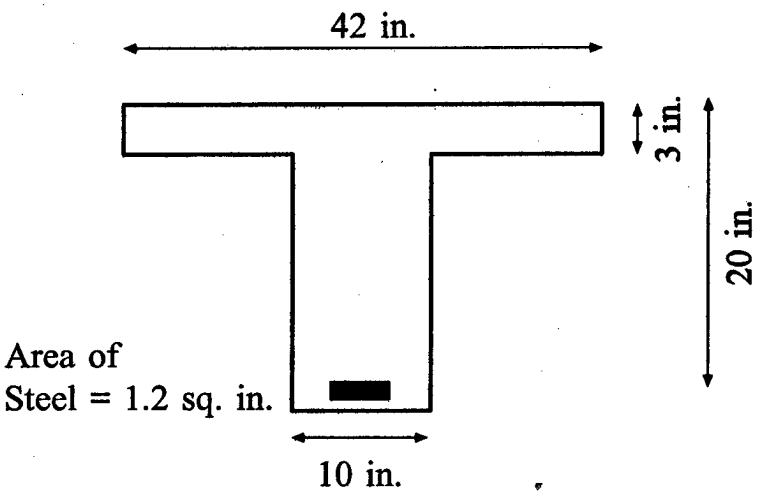
Compressive strength of the concrete $f'_c = 4000$ psi

Yield strength of steel $f_y = 40{,}000$ psi

Dead load $W_D = 310$ lb/ft

Live load $W_L = 100$ psf

Span $L = 22$ ft.



Nominal moment of resistance

Depth of equivalent rectangular stress block $a = \dfrac{A_s f_y}{0.85 f'_c b}$

$$= \frac{(1.2)(60{,}000)}{0.85(4000)(42)}$$

$$= 0.504 \text{ in.}$$

Depth of neutral axis $c = \frac{a}{\beta_1}$

$= \frac{0.504}{0.85}$

$= 0.60\text{in.} < h_f = 3.0\text{ in.}$

The neutral axis lies within the flange and hence T-beam section is treated as a rectangular section:

$\varphi M_n = \varphi A_s f_y (d-a/2)$

$= (0.9)(1.2)(40{,}000)(20-\frac{0.504}{2})$

$= 851{,}040$ in-lb

$= 70.92$ ft-kips

Selection of LEADLINE tendons

Centroid of the section from the top surface $\bar{y} = \frac{42\times3\times1.5+17\times10\times11.5}{(42\times3+10\times17)}$

$= 7.24$ in.

Depth of the centroid from the bottom surface $= 20 - 7.24$

$= 12.76$in.

Eccentricity e for prestressing tendons $= 12.76 + 6$

(assuming 6 in. dia. pipe for deviator) $= 18.76$ in.

Required prestressing force $P_e = \frac{70.92\times12}{18.76}$

$= 45.40$ kips

Use four 8mm dia. intended spiral LEADLINE tendons with an effective prestress of 11.35 kips in each tendon.

Area of concrete $A_c = 42 \times 3 + 17 \times 10$

$= 296 \text{ in}^2$

Moment of inertia of the section

$$I = \frac{42 \times 3^3}{12} + 42 \times 3 \times (7.24 - 1.5)^2 + \frac{10 \times 17^3}{12} + 10 \times 17 \times (11.5 - 7.24)^2$$

$= 11{,}425 \text{ in}^4$

Modulus of rupture $f_r = 7.5\sqrt{f'_c}$

$= 7.5\sqrt{4000}$

$= 474.3$ psi.

Allowable concrete extreme fiber stresses

In tension $f_{ti} = 6\sqrt{f'_c} = 0.380$ ksi

In compression $f_{ci} = -0.6\, f'_c = -2.4$ ksi

Assuming loss of prestress as 15 % of the initial prestress

$$P_i = \frac{45.4}{0.85}$$

$= 53.41$ kips

Radius of gyration, r

$$r^2 = \frac{I_g}{A_c}$$

$$= \frac{11425}{296}$$

$$= 38.60 \text{ in}^2$$

$$S^t = \frac{I_g}{y^t}$$

$$= \frac{11425}{7.24}$$

$$= 1578 \text{ in}^3$$

$$S_b = \frac{I_g}{y_b}$$

$$= \frac{11425}{12.76}$$

$$= 895 \text{ in}^3$$

Moment due to dead load $M_D = \frac{W_D L^2}{8}$

$$= \frac{310 \times 22^2}{8}$$

$$= 18.755 \text{ k-ft.}$$

Stress at the top concrete fiber, $f^t = -\frac{P_i}{A_c}\left(1 - \frac{ec_t}{r^2}\right) - \frac{M_D}{S^t}$

$$= -\frac{53.41}{296}\left(1 - \frac{(18.76)(7.24)}{(38.6)}\right) - \frac{18.755 \times 12}{1578}$$

$$= 0.302 \text{ ksi} < f_{ti} = 0.380 \text{ ksi.} \quad \therefore \text{O.K.}$$

Stress at the bottom concrete fiber, $f_b = -\frac{P_i}{A_c}\left(1 + \frac{ec_b}{r^2}\right) + \frac{M_D}{S_b}$

$$= -\frac{53.41}{296}\left(1+\frac{(18.76)(12.76)}{(38.6)}\right)+\frac{18.755\times 12}{895}$$

$= -1.02$ ksi $< f_{ci} = -2.4$ ksi. $\therefore$ O.K.

Allowable concrete stresses at service load

In tension $f_t = 6\sqrt{f'_c} = 0.380$ ksi

In compression $f_c = -0.45\, f'_c = -1.8$ ksi

Live load $W_L = 100(42/12) = 350$ lb/ ft.

Moment due to live load $M_L = \frac{W_L L^2}{8}$

$$= \frac{350\times 22^2}{8}$$

$= 21.175$ k-ft.

Total moment $M_T = M_D + M_L$

$= 18.755 + 21.175$

$= 39.93$ k-ft.

Stress at the top concrete fiber, $f^t = -\frac{P_e}{A_c}\left(1-\frac{ec_t}{r^2}\right)-\frac{M_T}{S^t}$

$$= -\frac{45.4}{296}\left(1-\frac{(18.76)(7.24)}{(38.6)}\right)-\frac{39.93\times 12}{1578}$$

$= 0.083$ ksi $< f_t = 0.380$ ksi. $\therefore$ O.K.

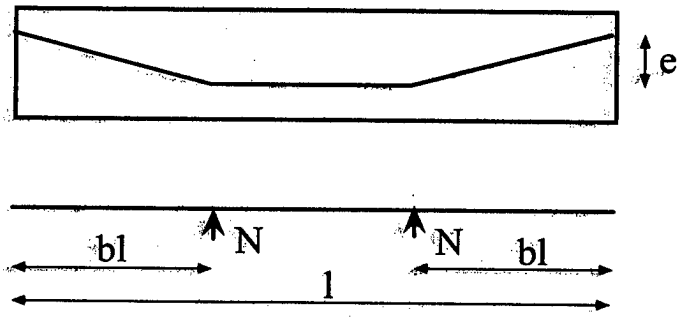
Stress at the bottom concrete fiber, $f_b = -\frac{P_e}{A_c}\left(1+\frac{ec_b}{r^2}\right)+\frac{M_L}{S_b}$

$$= -\frac{45.4}{296}\left(1+\frac{(18.76)(12.76)}{(38.6)}\right)+\frac{39.93\times 12}{895}$$

$$= -0.569 \text{ ksi} < f_c = -1.8 \text{ ksi.} \quad \therefore \text{O.K.}$$

The stresses in both top and bottom faces are below the modulus of rupture and the section is uncracked and hence the whole section participates in resisting the moment.

Check for deflection



Upward force $N = \frac{Pe}{bl}$

$$= \frac{45.4\times 18.76}{10.5\times 12}$$

$$= 6.76 \text{ kips.}$$

Upward deflection due to prestressing $= \frac{b(3-4b^2)Nl^3}{24EI}$

$$= \frac{0.477(3-4(0.477)^2)6.76(22\times 12)^3}{24(3605)(11425)}$$

$$= 0.125 \text{ in.} \uparrow$$

Deflection due to dead and live loads $= \frac{5W_T l^4}{384EI}$

$$= \frac{5(310+350)(22\times12)^4}{384(3605\times10^3)(11425)}$$

$$= 1.014 \text{ in.} \downarrow$$

Total deflection = 1.014-0.125

$$= 0.889 \text{ in.} \downarrow$$

Allowable deflection $= \frac{1}{240}$ (ACI 318: Table 9.5(b))

$$= \frac{22\times12}{240}$$

$$= 1.1 \text{ in.} > 0.889 \text{ in.} \quad \therefore \text{OK.}$$

Double-Tee Beam

Given Data

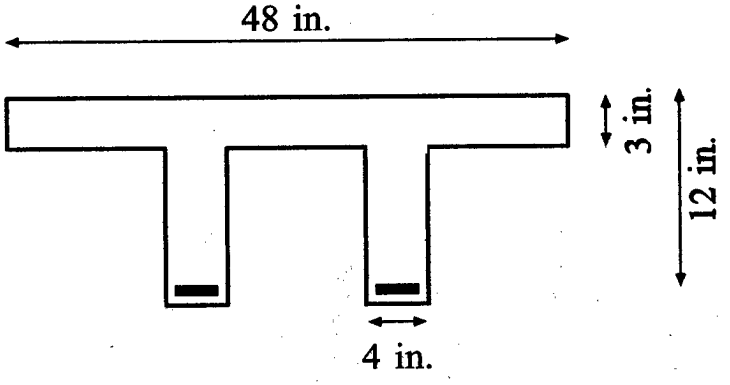
Compressive strength of the concrete $f'_c = 4000$ psi.

Yield strength of steel $f_y = 40{,}000$ psi.

Dead load $W_D = 250$ lb/ ft.

Live load $W_L = 120$ lb/ ft.

Span $L = 20$ ft.



Ultimate moment of resistance

Ultimate load $W_u = 1.4 \times 250 + 1.7 \times 120 = 554$ lb/ ft.

Ultimate moment $M_u = \frac{W_u L^2}{8}$

$= \frac{554 \times (20)^2}{8}$

$= 27.7$ k-ft.

Selection of LEADLINE tendons

Centroid of the section from the top surface $\bar{y} = \frac{48 \times 3 \times 1.5 + 2 \times 4 \times 12 \times 9}{(48 \times 3 + 2 \times 4 \times 12)}$

$= 3.75$ in.

Depth of the centroid from the bottom surface $= 15 - 3.75$

$= 11.25$ in.

Eccentricity e for prestressing tendons $= 11.25 + 6$

(assuming 6 in. dia. pipe for deviator) $= 17.25$ in.

Load applied for producing equivalent moment $P_e = \frac{27.7 \times 12}{17.25}$

$= 19.3$ kips

Use two 8mm dia. intended spiral LEADLINE tendons with an effective prestress of 9.65 kips in each tendon.

Area of concrete $A_c = 48 \times 3 + 2 \times 4 \times 12$

$= 240$ in^2

Moment of inertia of the section

$$I = \frac{48 \times 3^3}{12} + 48 \times 3 \times (3.75 - 1.5)^2 + 2 \times \frac{4 \times 12^3}{12} + 2 \times 4 \times 12 \times (9 - 3.75)^2$$

$$= 4027.5 \text{ in}^4$$

Modulus of rupture $f_r = 7.5\sqrt{f'_c}$

$$= 7.5\sqrt{4000}$$

$$= 474.3 \text{ psi.}$$

Allowable concrete extreme fiber stresses

In tension $f_{ti} = 6\sqrt{f'_c} = 0.380$ ksi

In compression $f_{ci} = -0.6\, f'_c = -2.4$ ksi

Assuming loss of prestress as 15 % of the initial prestress

$$P_i = \frac{23.32}{0.85}$$

$$= 27.44 \text{ kips}$$

$$r^2 = \frac{I_g}{A_c}$$

$$= \frac{4027.5}{240}$$

$$= 16.78 \text{ in}^2 00000000$$

$$S^t = \frac{I_g}{y^t}$$

$$= \frac{4027.5}{3.75}$$

$$= 1074 \text{ in}^3$$

$$S_b = \frac{I_g}{y_b}$$

$$= \frac{4027.5}{11.25}$$

$$= 358 \text{ in}^3$$

Moment due to dead load $M_D = \frac{W_D L^2}{8}$

$$= \frac{250 \times 20^2}{8}$$

$$= 12.5 \text{ k-ft.}$$

Stress at the top concrete fiber, $f^t = -\frac{P_i}{A_c}\left(1 - \frac{ec_t}{r^2}\right) - \frac{M_D}{S^t}$

$$= -\frac{22.7}{240}\left(1 - \frac{(17.25)(3.75)}{(16.78)}\right) - \frac{12.5 \times 12}{1074}$$

$$= 0.12 \text{ ksi} < f_{ti} = 0.380 \text{ ksi.} \quad \therefore \text{ O.K.}$$

Stress at the bottom concrete fiber, $f_b = -\frac{P_i}{A_c}\left(1 + \frac{ec_b}{r^2}\right) + \frac{M_D}{S_b}$

$$= -\frac{22.7}{240}\left(1+\frac{(17.25)(11.25)}{(16.78)}\right)+\frac{12.5\times 12}{358}$$

$= -0.77$ ksi $< f_{ci} = -2.4$ ksi. $\therefore$ O.K.

Allowable concrete stresses at service load

In tension $f_t = 6\sqrt{f'_c} = 0.380$ ksi

In compression $f_c = -0.45\, f'_c = -1.8$ ksi

Moment due to live load $M_L = \frac{W_L L^2}{8}$

$$= \frac{120\times 20^2}{8}$$

$= 6.00$ k-ft.

Total moment $M_T = M_D + M_L$

$= 12.5+6.0$

$= 18.5$ k-ft.

Stress at the top concrete fiber, $f^t = -\frac{P_e}{A_c}\left(1-\frac{ec_t}{r^2}\right)-\frac{M_T}{S^t}$

$$= -\frac{19.3}{240}\left(1-\frac{(17.25)(3.75)}{(16.78)}\right)-\frac{18.5\times 12}{1074}$$

$= 0.023$ ksi $< f_t = 0.380$ ksi. $\therefore$ O.K.

Stress at the bottom concrete fiber, $f_b = -\frac{P_e}{A_c}\left(1+\frac{ec_b}{r^2}\right)+\frac{M_L}{S_b}$

$$= -\frac{19.3}{240}\left(1+\frac{(17.25)(11.25)}{(16.78)}\right)+\frac{18.5\times 12}{358}$$

$= -0.39 \text{ ksi} < f_c = -1.8 \text{ ksi}. \therefore \text{O.K.}$

The stresses in both top and bottom faces are below the modulus of rupture and the section is uncracked and hence the whole section participates in resisting the moment.

Check for deflection

Upward force $N = \frac{Pe}{bl}$

$$= \frac{19.3 \times 14.25}{9.5 \times 12}$$

$= 2.92$ kips.

Upward deflection due to prestressing $= \frac{b(3-4b^2)Nl^3}{24EI}$

$$= \frac{0.475(3-4(0.475)^2)2.92(20 \times 12)^3}{24(3605)(4027.5)}$$

$= 0.115$ in. ↑

Deflection due to dead and live loads $= \frac{5W_T l^4}{384EI}$

$$= \frac{5(250+120)(20 \times 12)^4}{384(3605 \times 10^3)(4027.5)}$$

$= 1.1$ in. ↓

Total deflection $= 1.1\text{-}0.115$

$= 0.985$ in. ↓

Allowable deflection $= \frac{1}{240}$ (ACI 318: Table 9.5(b))

$$= \frac{22 \times 12}{240}$$

$$= 1.1 \text{ in.} > 0.985 \text{ in.} \quad \therefore \text{ OK.}$$

Conclusions And Recommendations

Based on the studies on the performance of the existing corroded reinforced concrete double-tee beams strengthened with external post tensioning using LEADLINE tendons with anchorages, the following conclusions can be summarized:

1. The field measurements over a period of over one year demonstrate the successful application of the LEADLINE tendon for strengthening and repairing of the existing corroded reinforced concrete beams in harsh marine and coastal environment.
2. Conventional strengthening design method for either reinforced concrete or prestressed concrete is applicable to the strengthening design of the corroded reinforced concrete beam with LEADLINE tendon. The number of LEADLINE tendons and the prestress level in the tendon are determined based on the required prestressing force at the strength limit state and the ultimate strength of the tendons.
3. The initial loss of the prestressing force in the LEADLINE tendon due to the curvature frictional effects and elastic shortening of the concrete resulting from sequential stressing of the tendons can vary from 9-14%.
4. The relative slip in the anchorages is almost negligible during the process of post tensioning of the double-tee beams. The prestress loss in the LEADLINE tendons due to the slip in the anchorage during the one year period of observation was found to be very small, which demonstrates the efficient performance of the grout system used in the anchorage.
5. The loss in prestress in the LEADLINE tendons due to creep effects of concrete in the existing reinforced concrete double-tee beams under study is insignificant.
6. The loss in prestress due to relaxation of the LEADLINE tendons is approximately 5% in the first seven days which compares to the published value of 2-3% for Carbon FRP rod (Hoshijima et al. 1996). However, the prestress loss due to relaxation increases to 10-12% of the initial jacking force after 100 days and then remains constant thereafter.
7. Careful attention and care need be exercised considering the physical field constraints on the preparation of the anchorage system, prestressing of the tendons and setting of the anchorage on to the existing structure so as to minimize the loss of prestress in the LEADLINE tendons.

Reference

T. Hoshijima, H. Yagi, T. Tanaka and T. Ando, " Properties of CFRP for Concrete Structures", First International Conference on Composites in Infrastructure, ICCI '96, Tucson, AZ, January , 1996, pp. 227-241.

List of Appendix B Figures and Tables

Figures

Figure B1a. Details of instrumentation set up (electrical resistance strain gages and load cells).....25
Figure B1b. Details of instrumentation set up (digimatic micrometer points and deflectometer).....26
Figure B2. Typical loadcell arrangement.....27
Figure B3. Strain gages attached over the anchorages.....27
Figure B4. Typical strain gage attachment over leadline at quarter span.....28
Figure B5. Micrometer stud points attached to leadline.....28
Figure B6. Micrometer stud points attached at anchorage.....29
Figure B7. Leadline tendon profile in the double-T beam.....30
Figure B8. Force distribution in tendon considering curvature friction.....31
Figure B9. Temperature with time.....32
Figure B10. Humidity with time.....33
Figure B11. Measured slip with time in NE Anchorage in tendon 1.....34
Figure B12. Measured slip with time in NW Anchorage in tendon 4.....35
Figure B13. Measured slip with time in SW Anchorage in tendon 4.....36
Figure B14. Prestress loss in tendon 1 due to Anchorage slip.....37
Figure B15. Prestress loss in tendon 4 due to Anchorage slip.....38
Figure B16. Measured strains with time (based on digimatic micrometer).....39
Figure B17. Measured strains with time (based on electrical resistance strain gages).....40
Figure B18. Measured prestress force in tendon 1 with time.....41
Figure B19. Measured prestress force in tendon 4 with time.....42
Figure B20. Prestress loss due to relaxation in tendon 1 with time.....43
Figure B21. Prestress loss due to relaxation in tendon 4 with time.....44
Figure B22. Initial circumferential strain with time.....45
Figure B23. Circumferential strain based on SG#1 with time.....46
Figure B24. Circumferential strain based on SG#11 with time.....47
Figure B25. Axial strain based on SG#0 with time.....48
Figure B26. Axial strain based on SG#10 with time.....49
Figure B27. Strain and stress distribution in a typical beam.....50

Tables

Table B1. Prestress at different loading stages in leadline tendon 1. 51
Table B2. Prestress at different loading stages in leadline tendon 4. 51
Table B3. Prestress forces in leadline tendons. 51

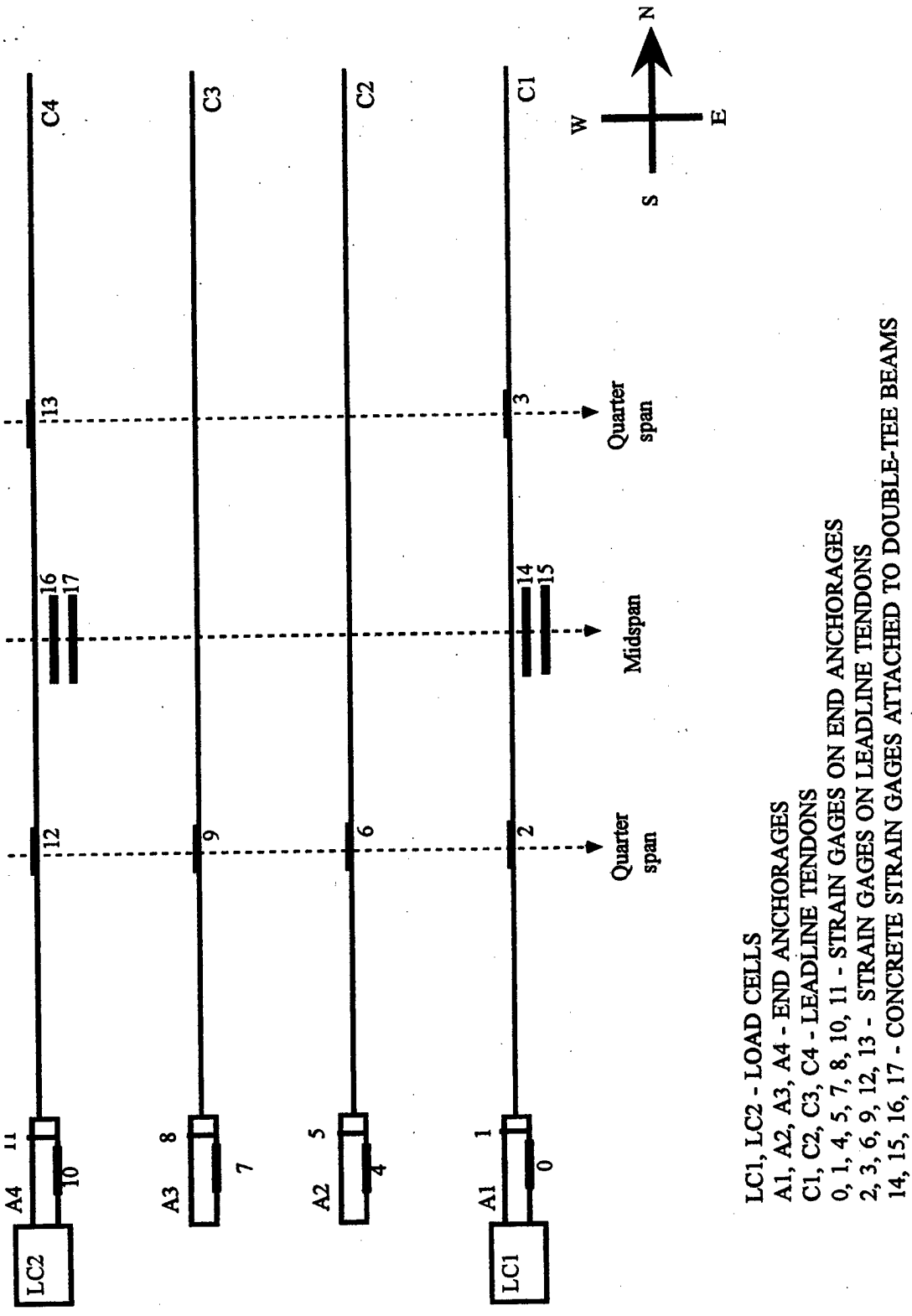


Figure B1a. Details of instrumentation set up (electrical resistance strain gages and load cells).

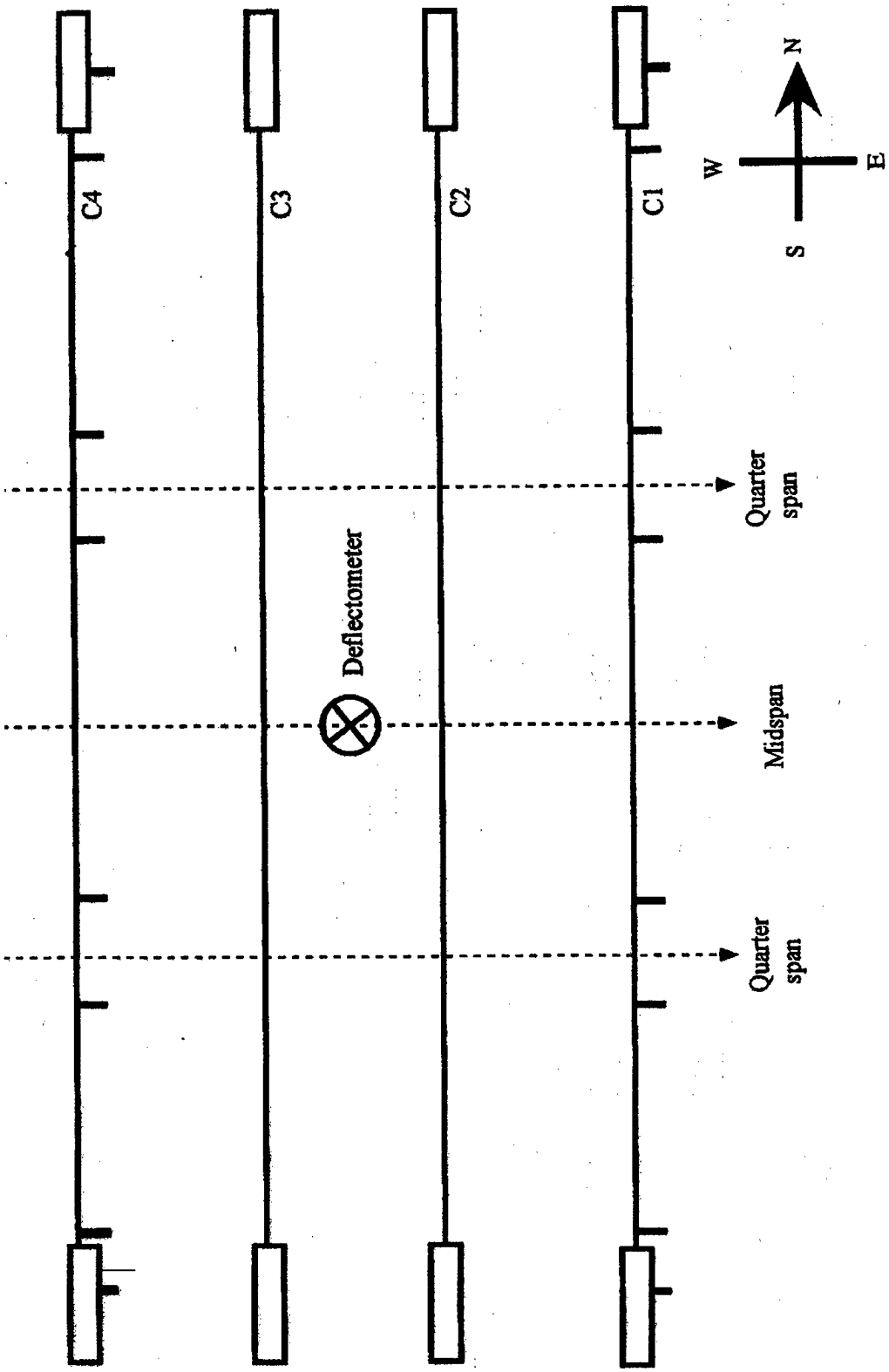


Figure B1b. Details of instrumentation set up (digimatic micrometer points and deflectometer).

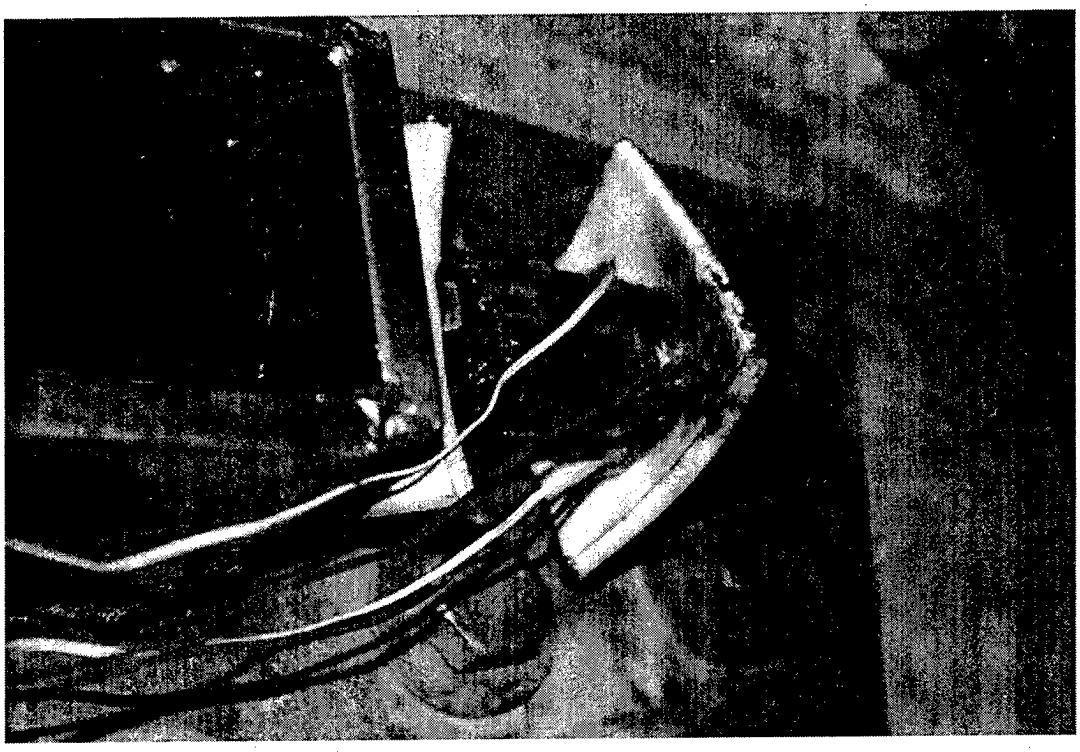


Figure B2. Typical loadcell arrangement.

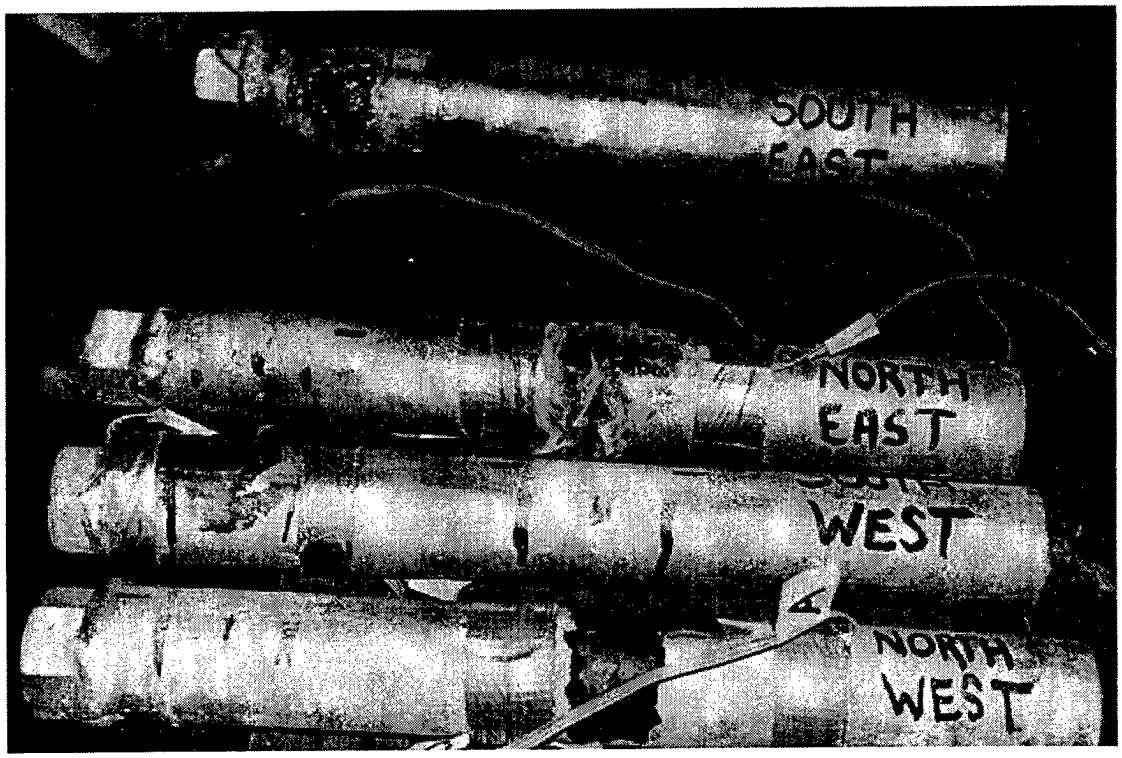


Figure B3. Strain gages attached over the anchorages.

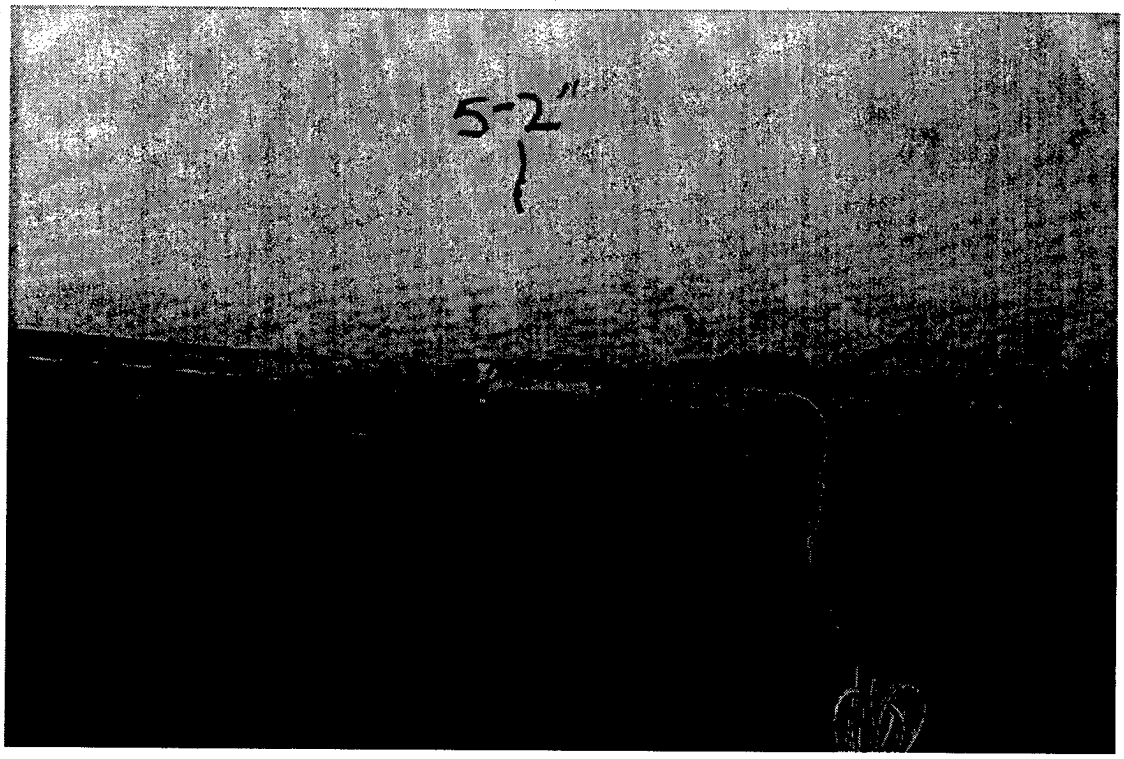


Figure B4. Typical strain gage attachment over leadline at quarter span.

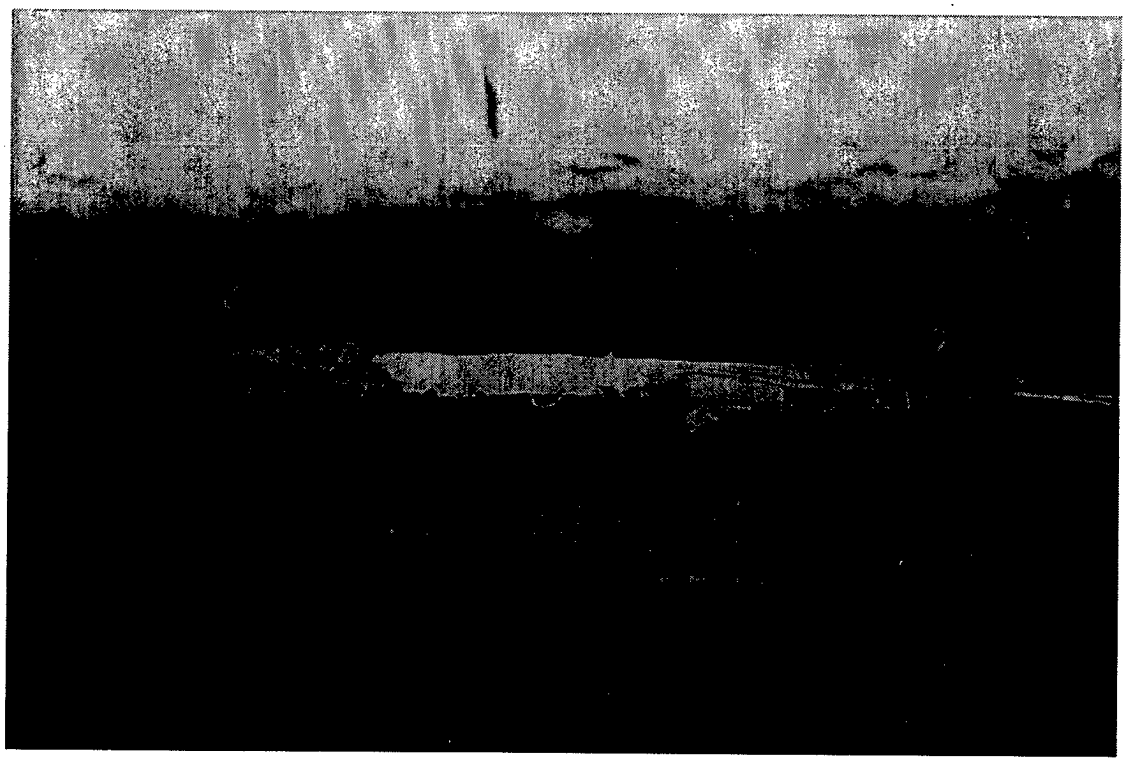


Figure B5. Micrometer stud points attached to leadline.

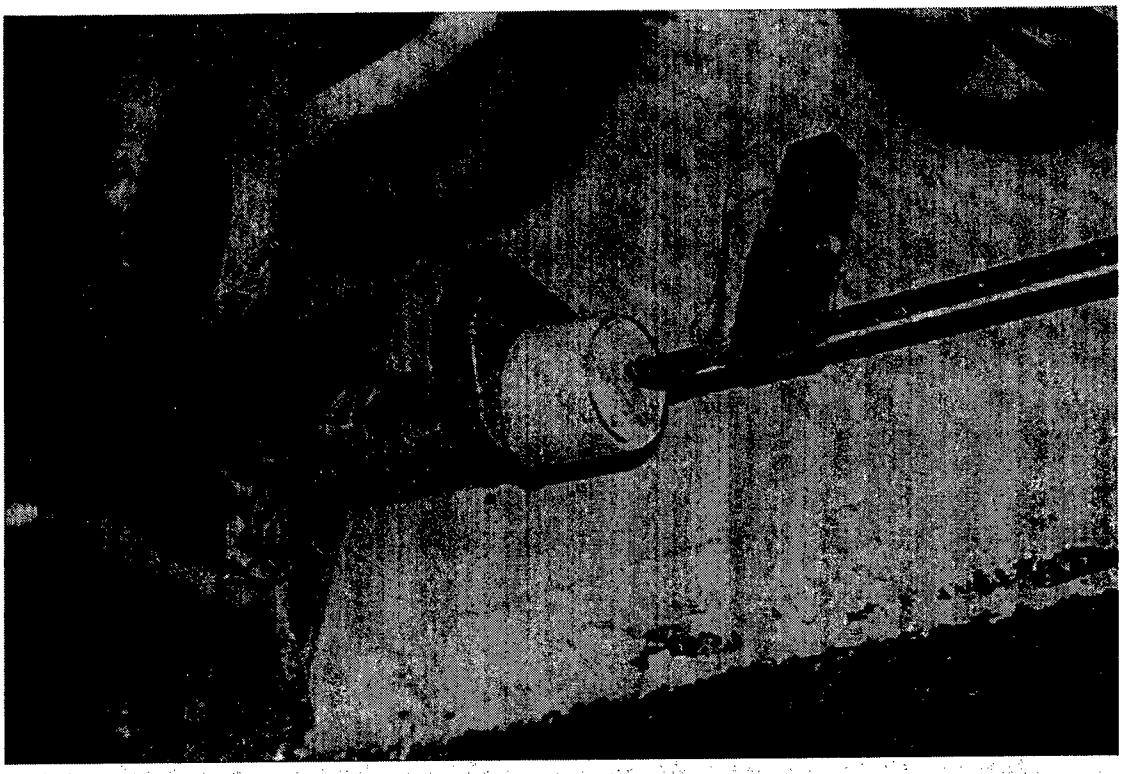


Figure B6. Micrometer stud points attached at anchorage.

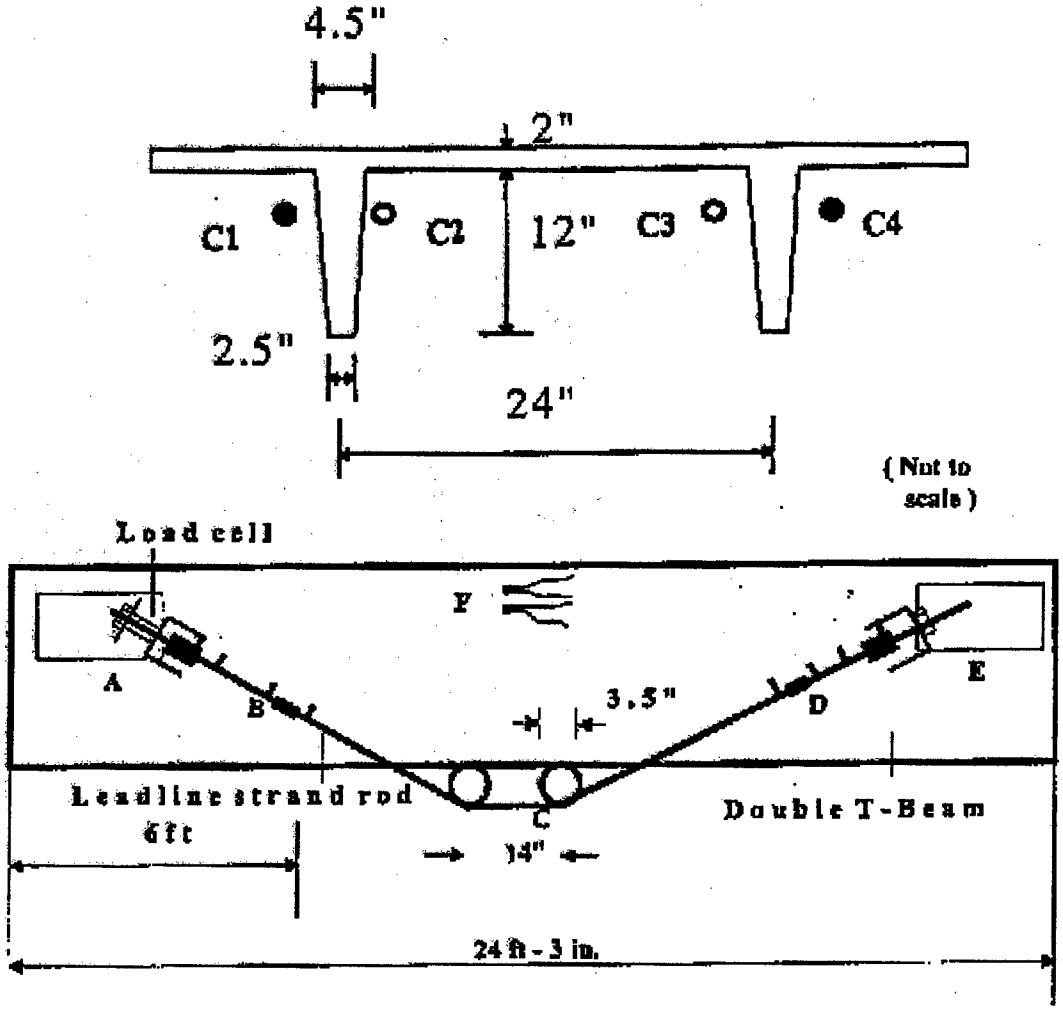


Figure B7. Leadline tendon profile in the double-T beam.

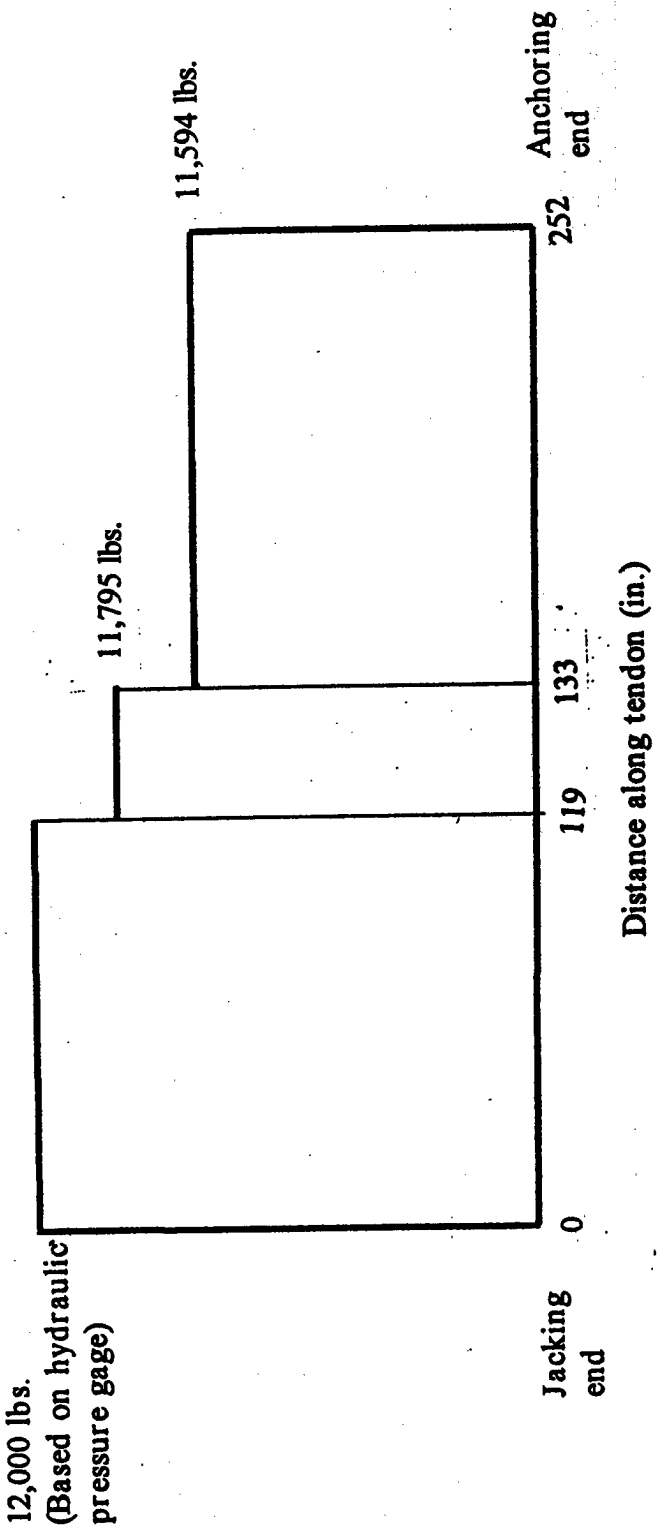


Figure B8. Force distribution in tendon considering curvature friction.

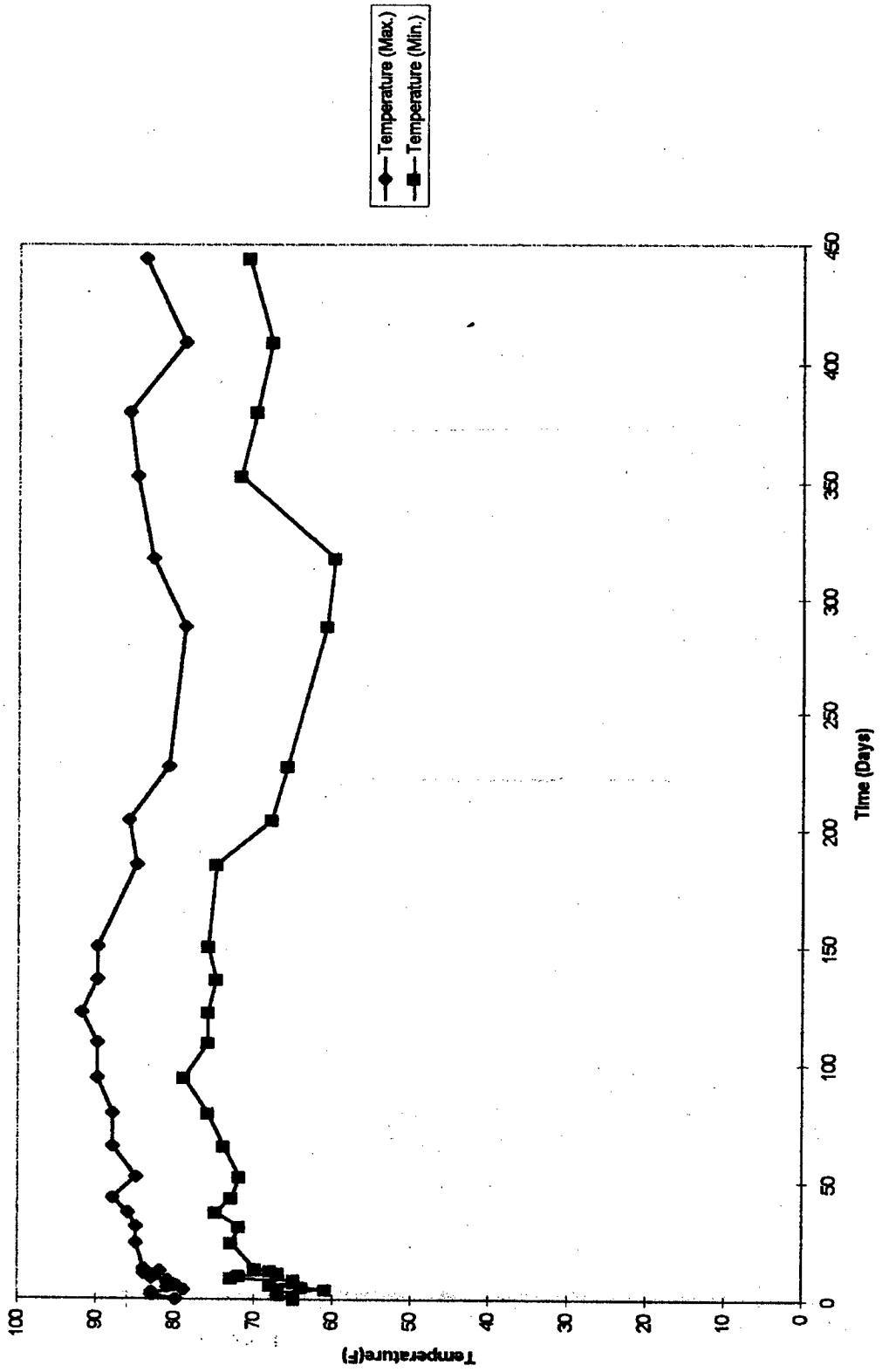


Figure B9. Temperature with time.

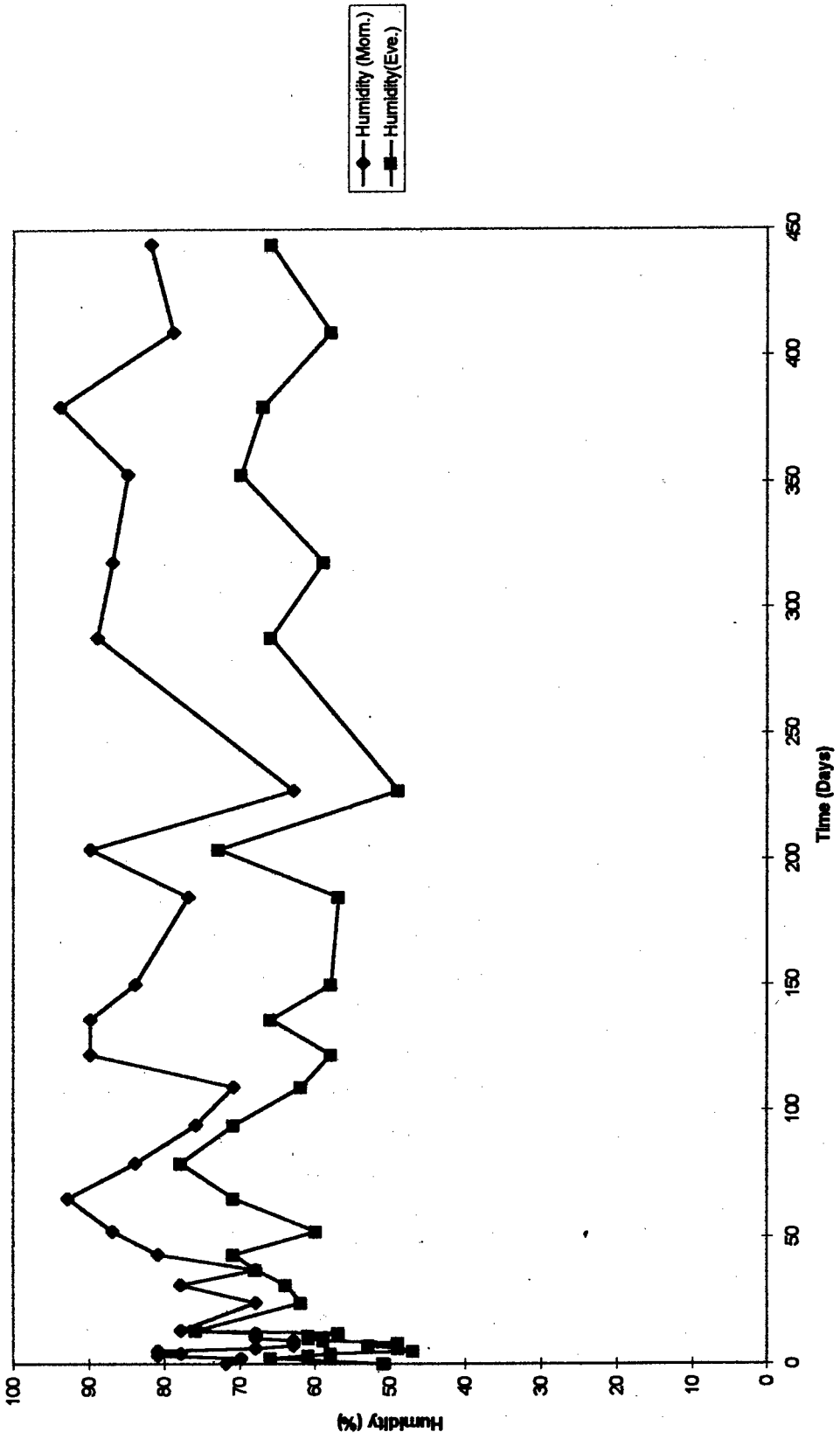


Figure B10. Humidity with time.

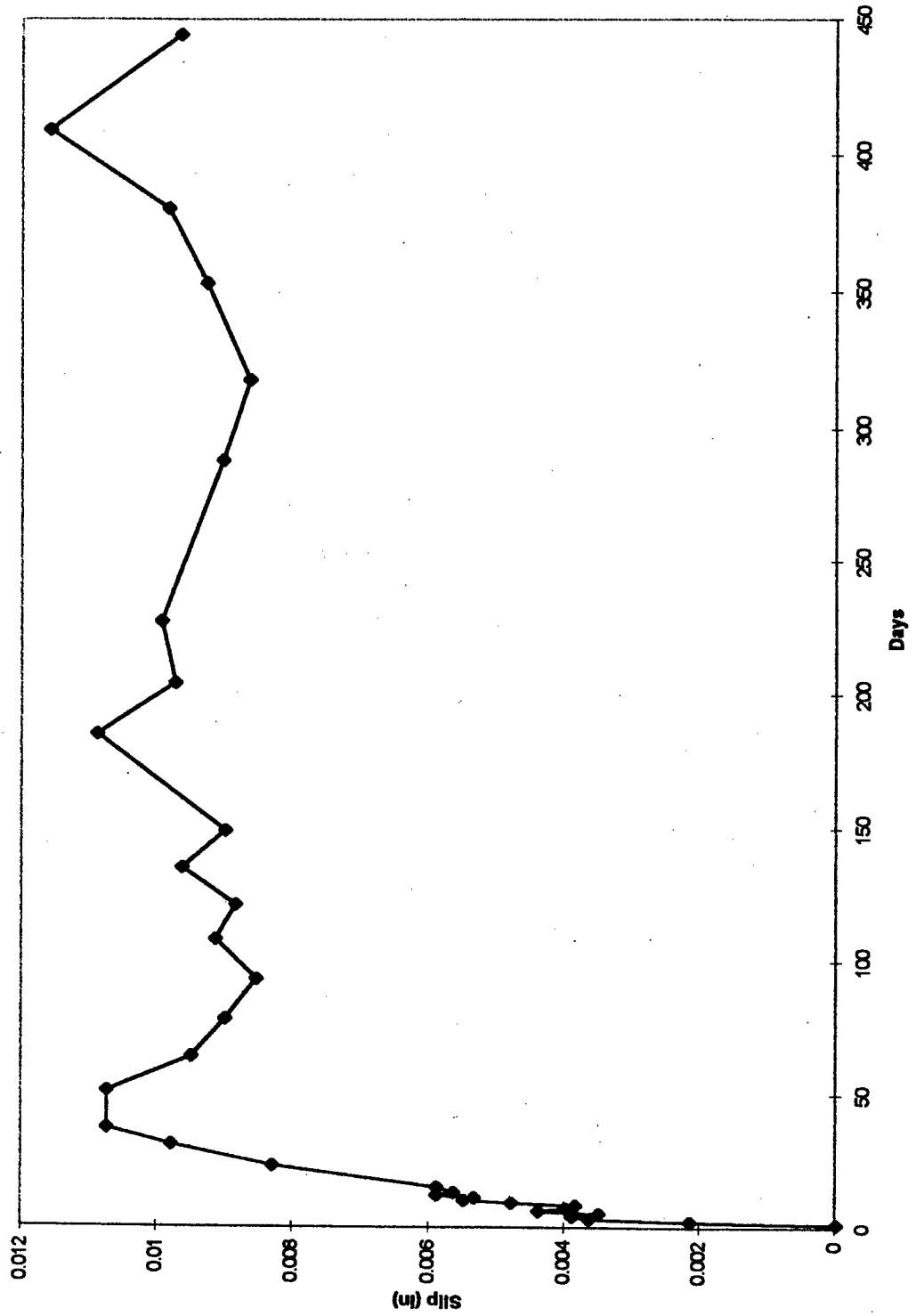


Figure B11. Measured slip with time in NE Anchorage in tendon 1.

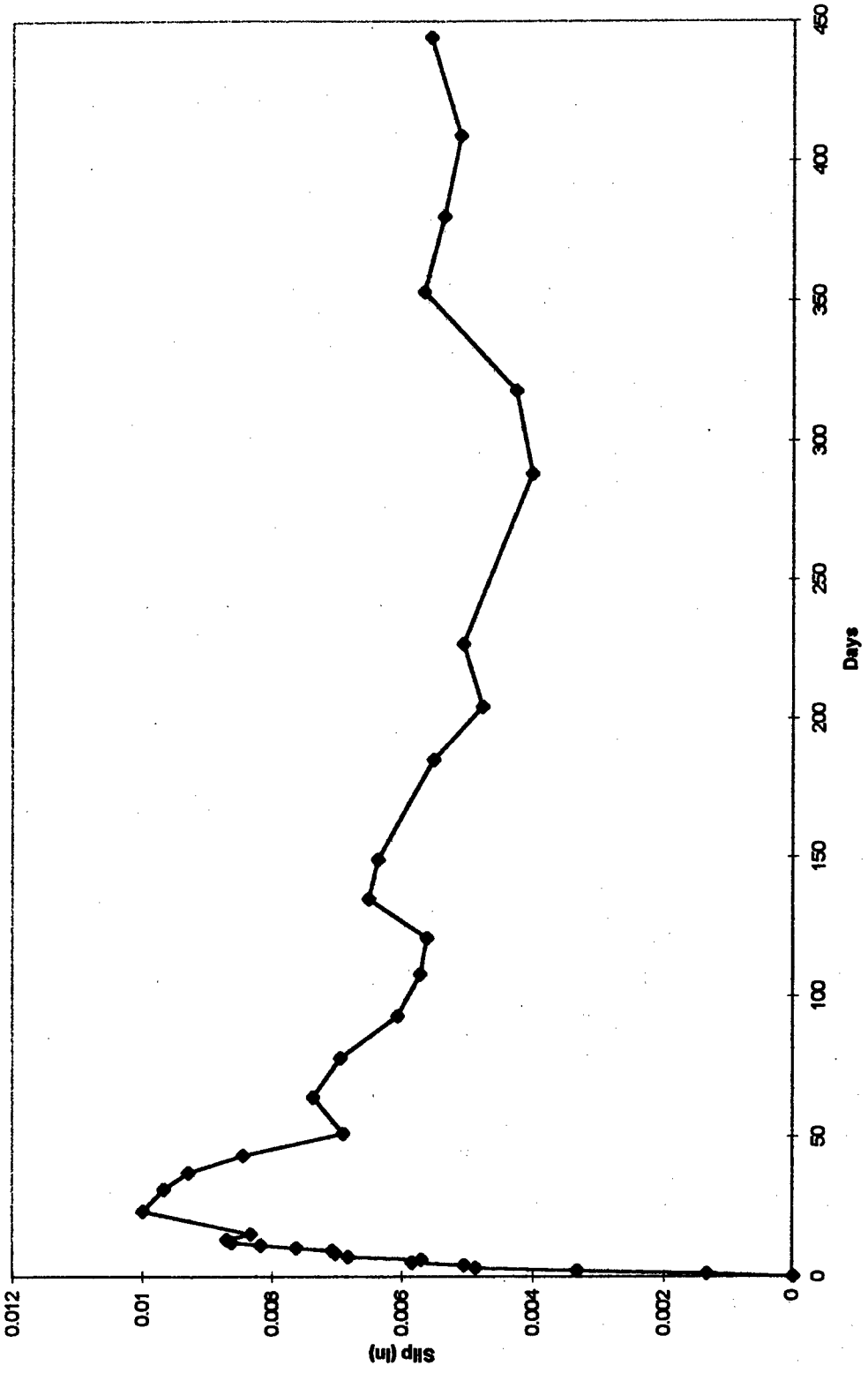


Figure B12. Measured slip with time in NW Anchorage in tendon 4.

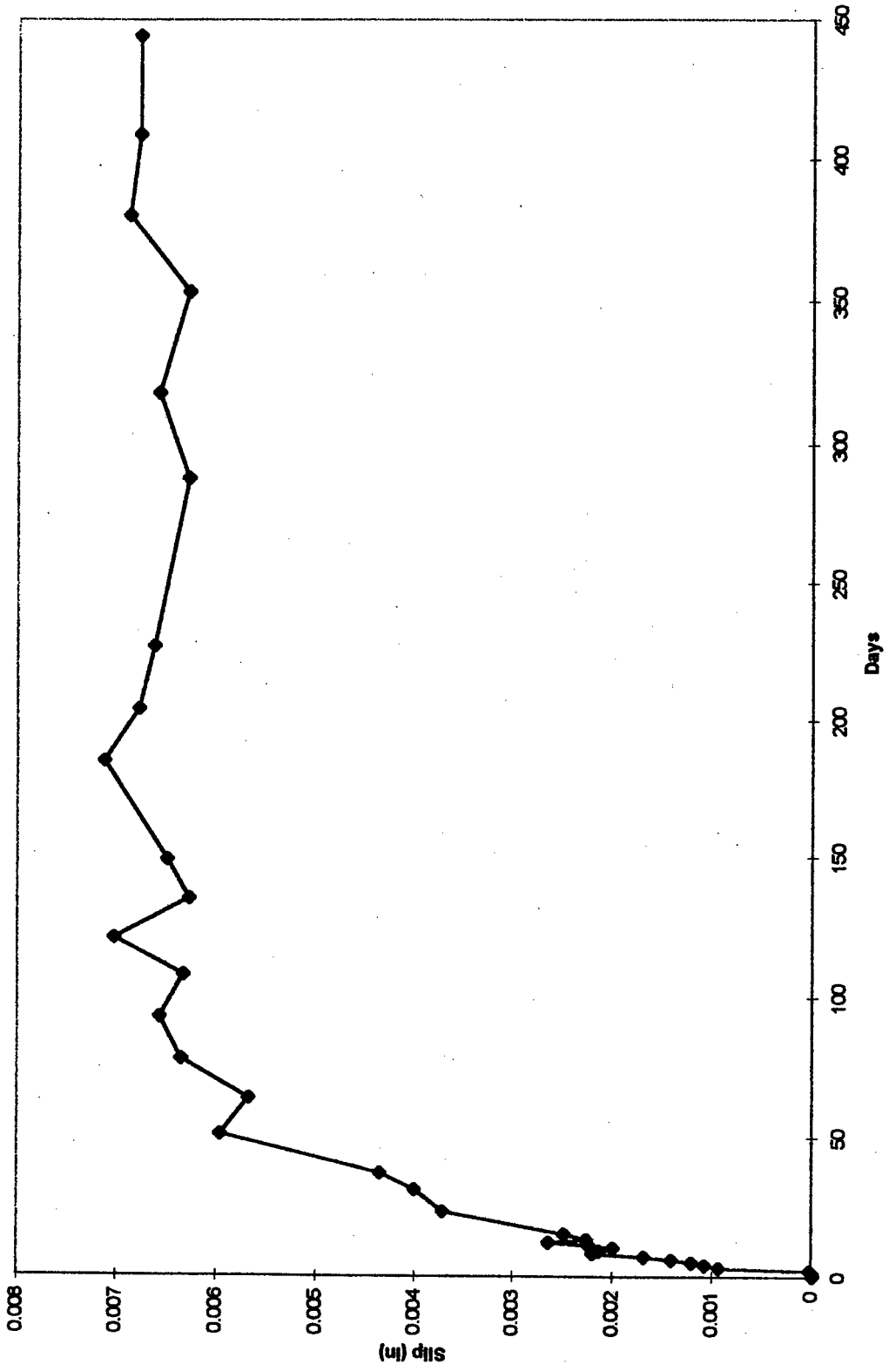


Figure B13. Measured slip with time in SW Anchorage in tendon 4.

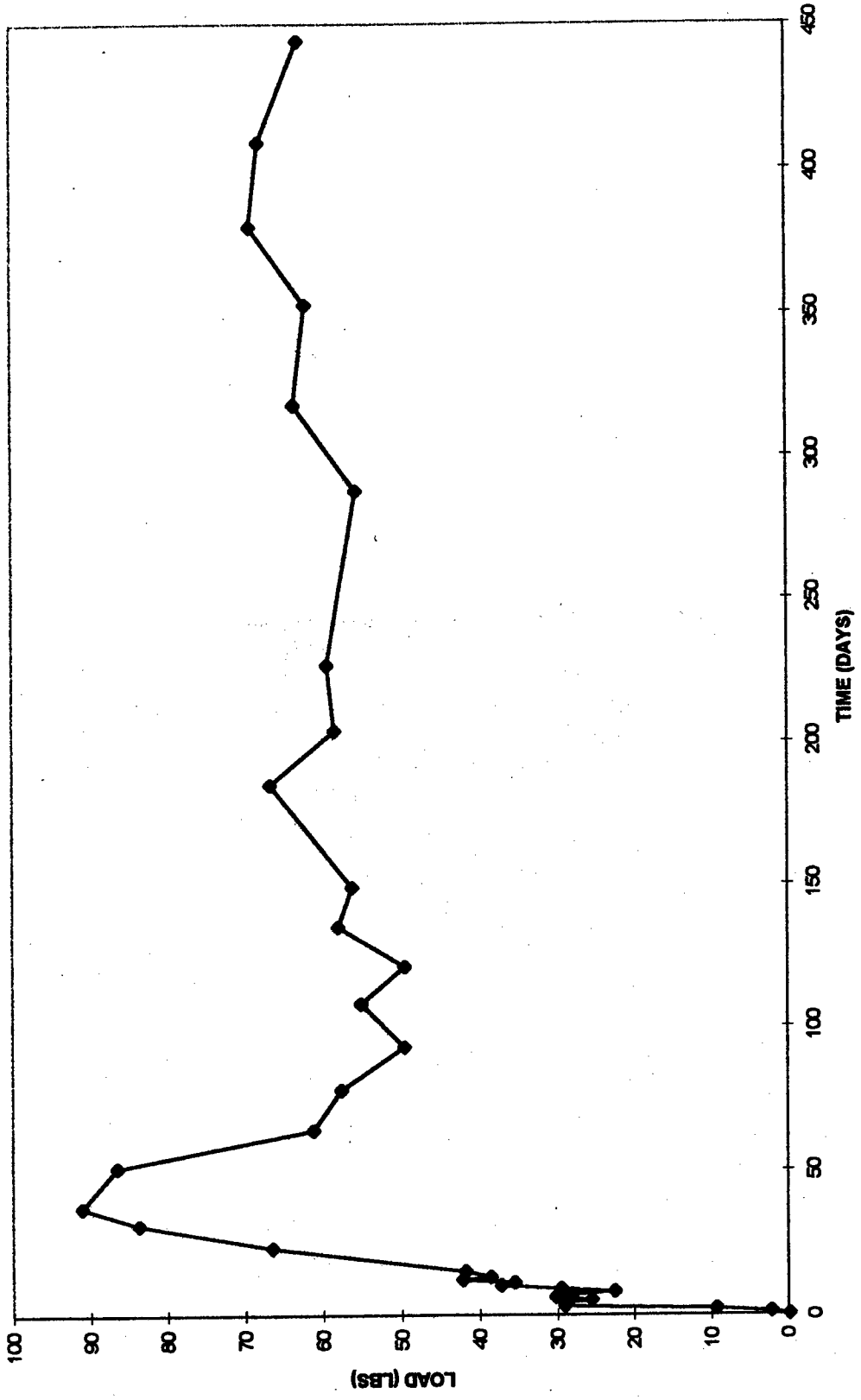


Figure B14. Prestress loss in tendon 1 due to Anchorage slip.

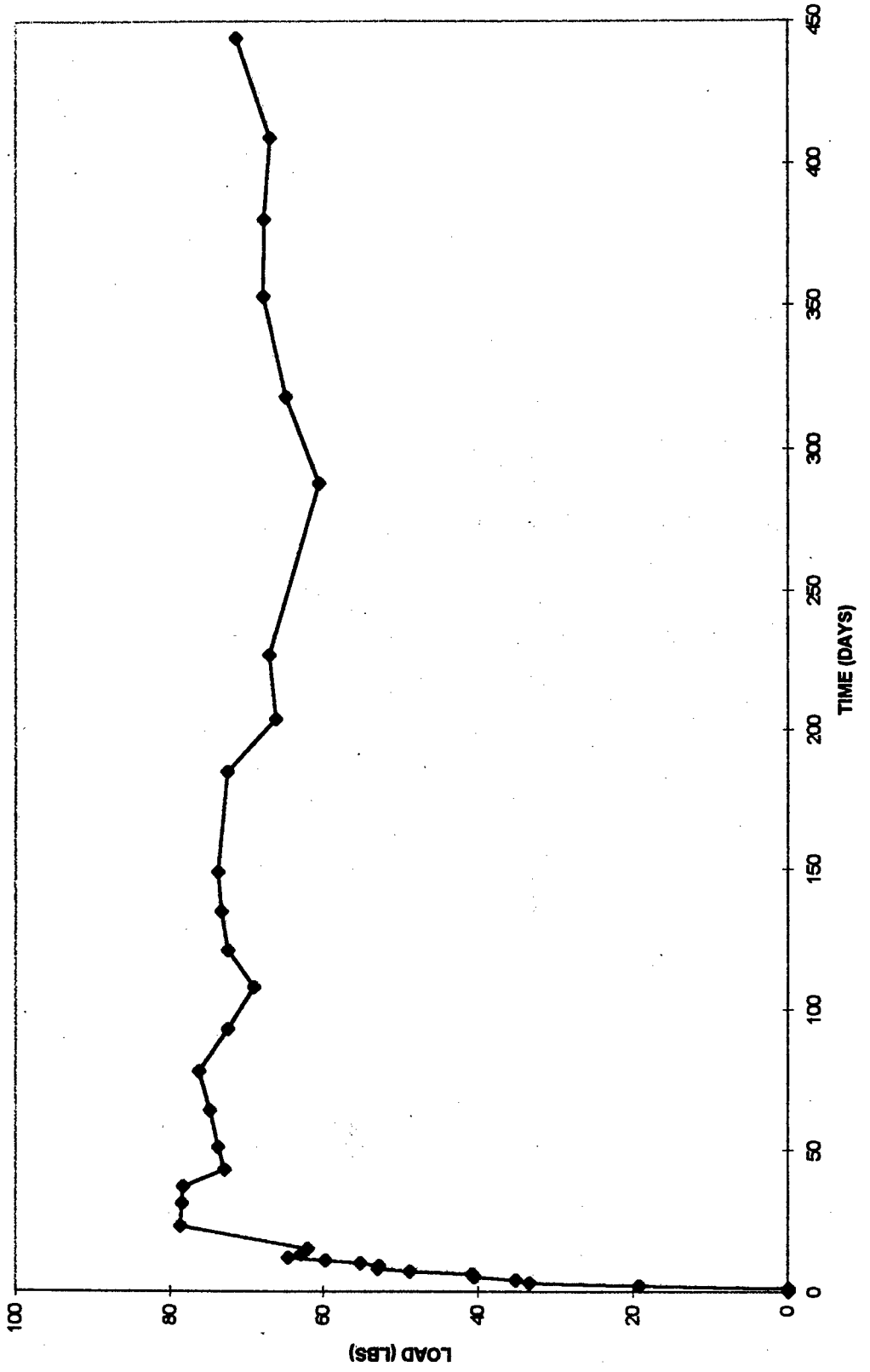


Figure B15. Prestress loss in tendon 4 due to Anchorage slip.

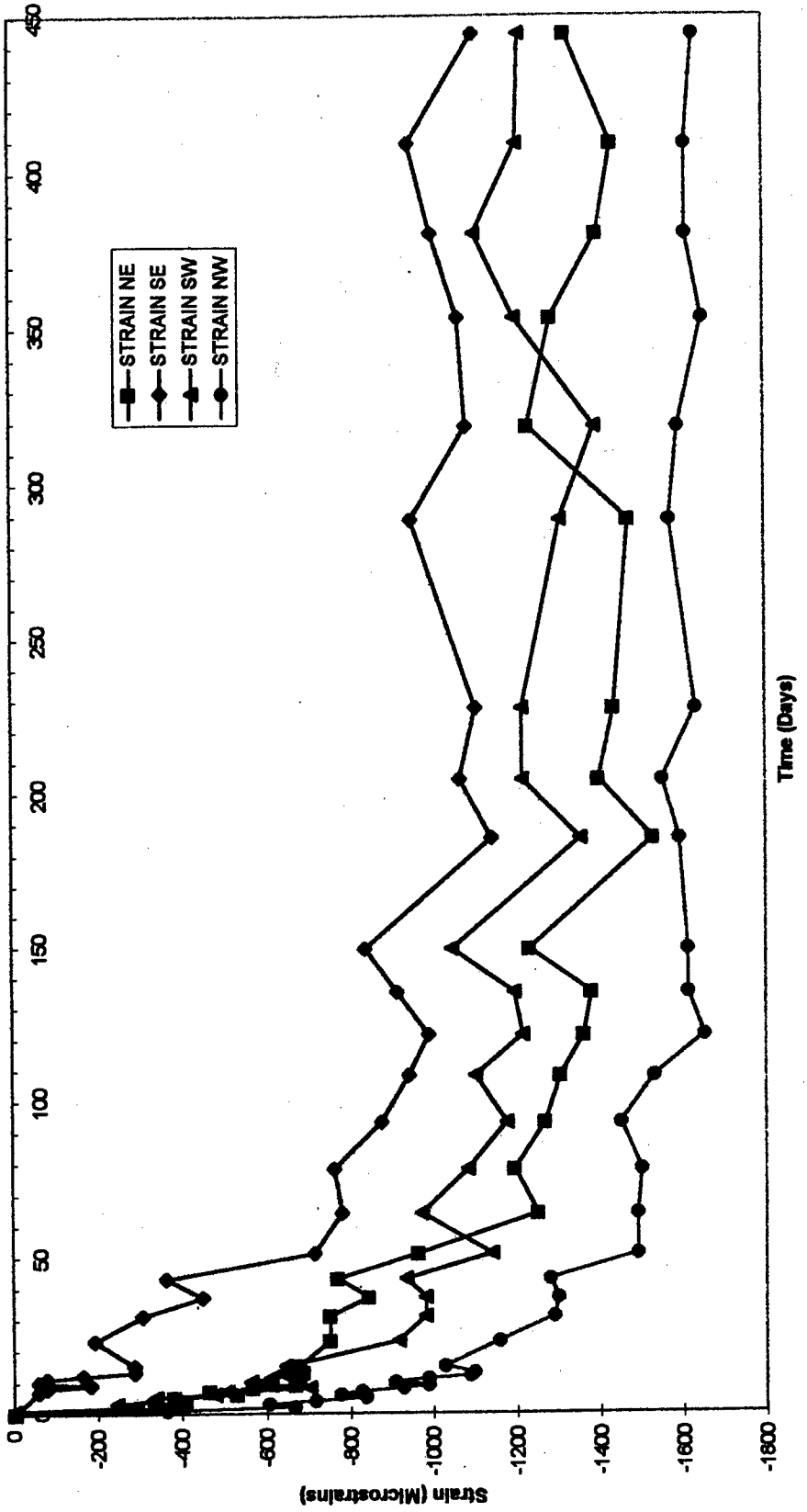


Figure B16. Measured strains with time (based on digimatic micrometer).

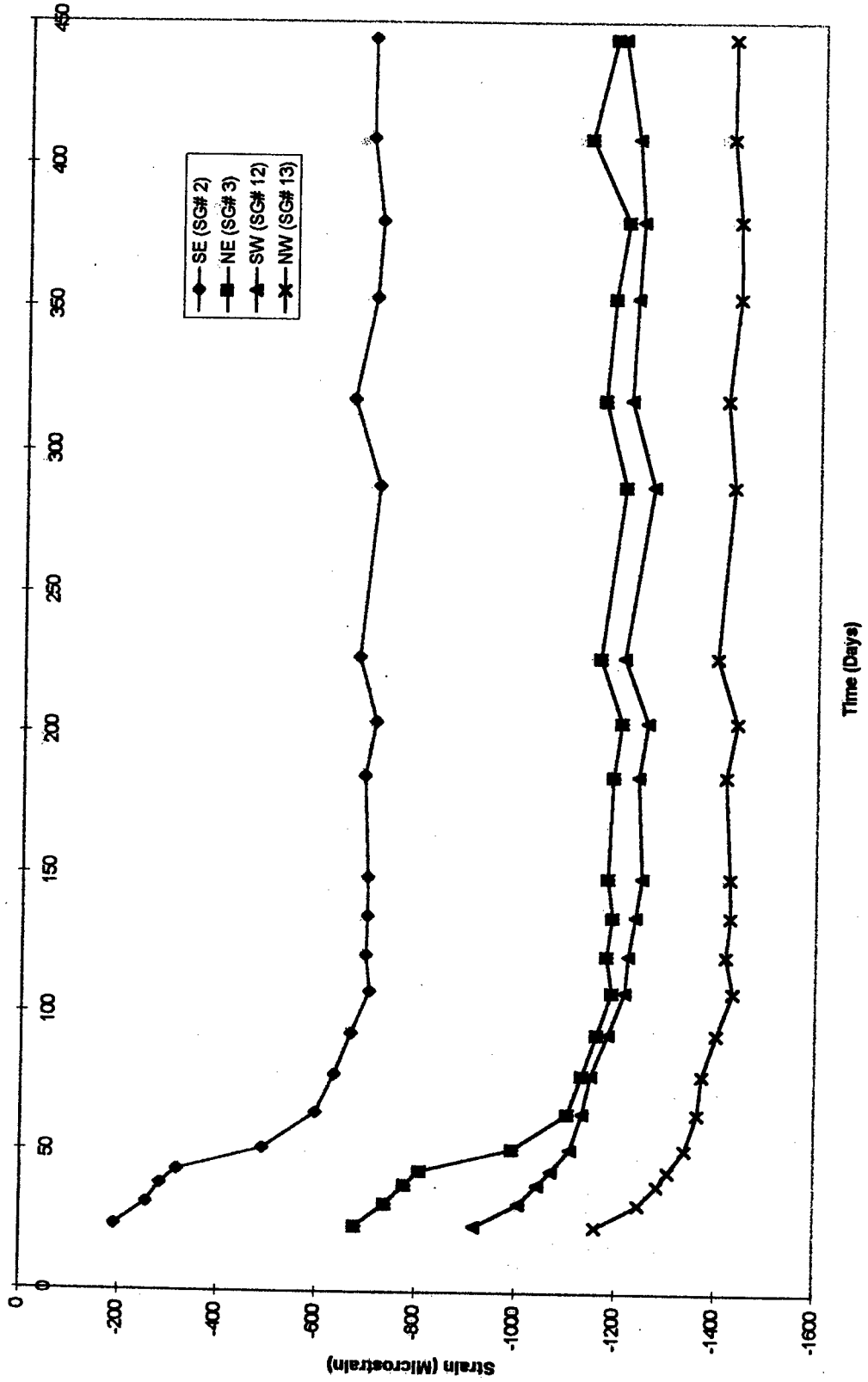


Figure B17. Measured strains with time (based on electrical resistance strain gages).

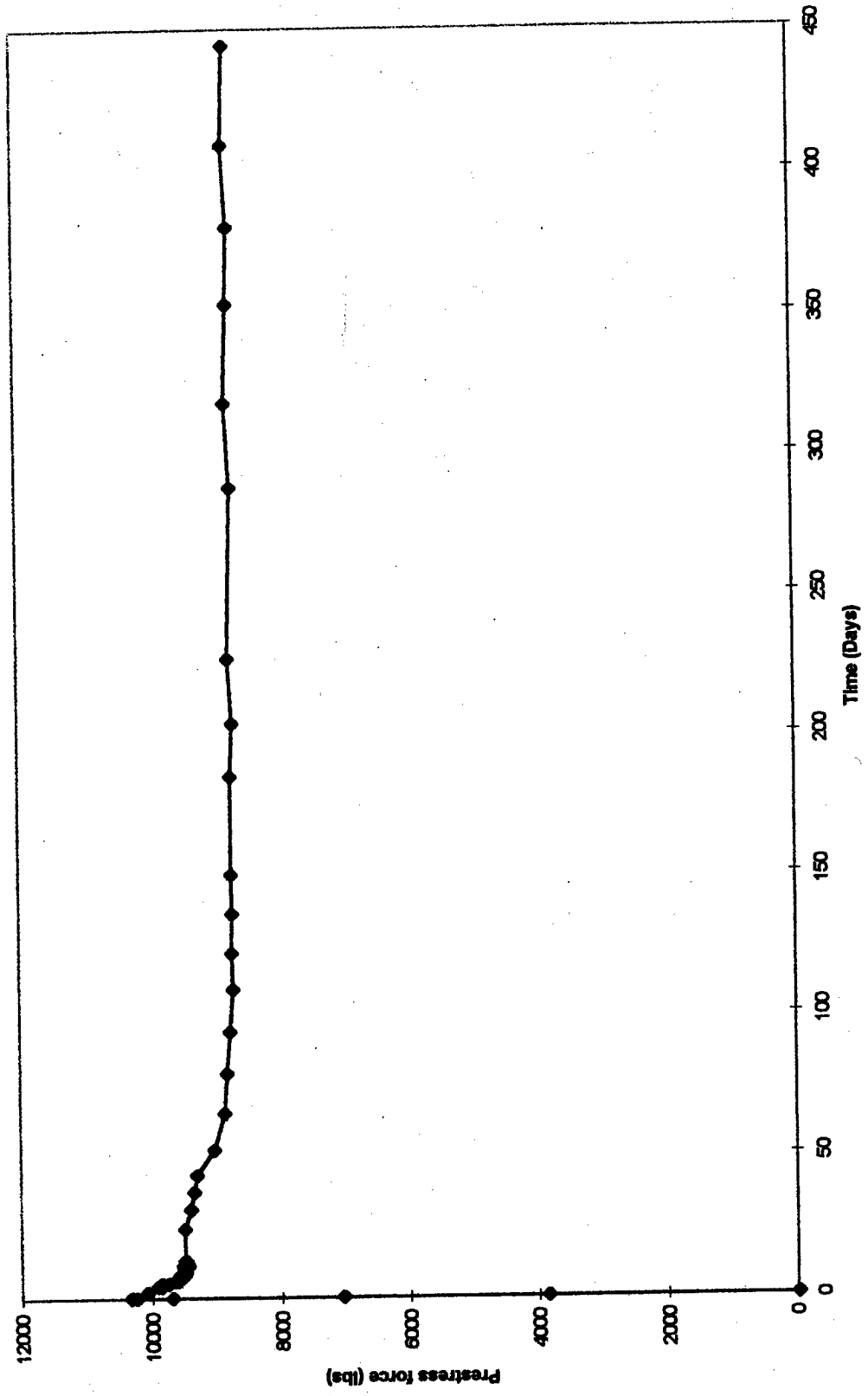


Figure B18. Measured prestress force in tendon 1 with time.

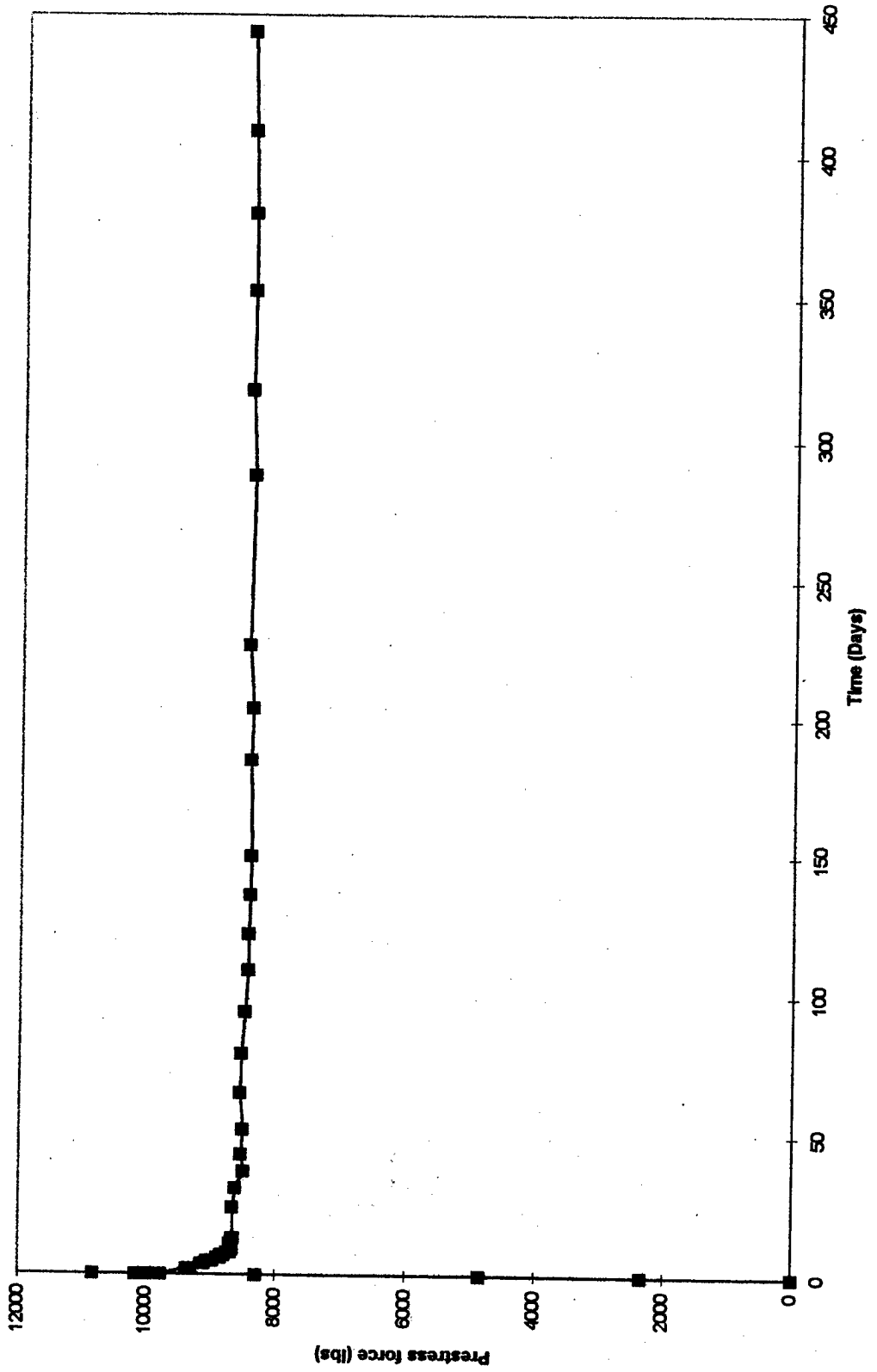


Figure B19. Measured prestress force in tendon 4 with time.

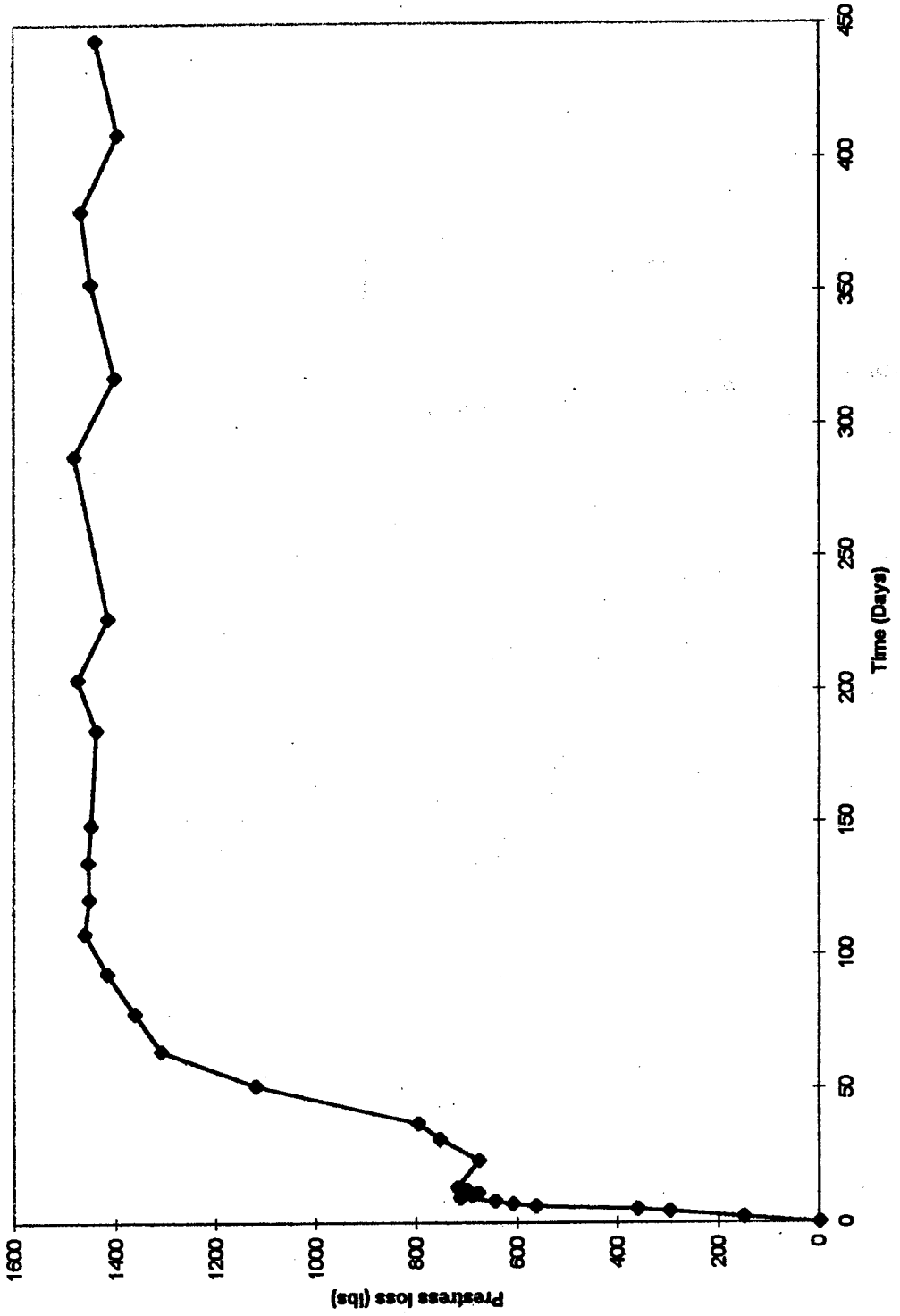


Figure B20. Prestress loss due to relaxation in tendon 1 with time.

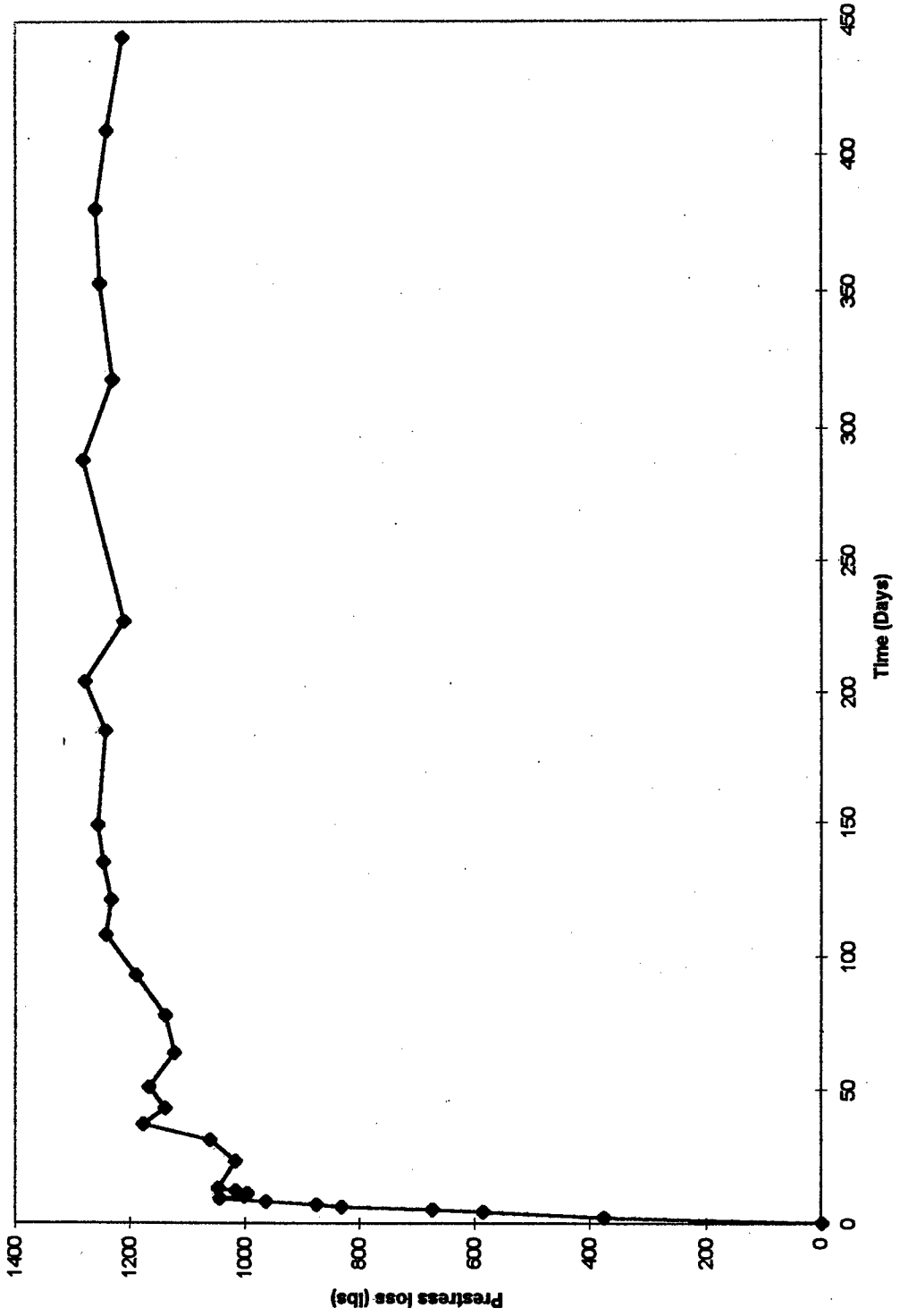


Figure B21. Prestress loss due to relaxation in tendon 4 with time.

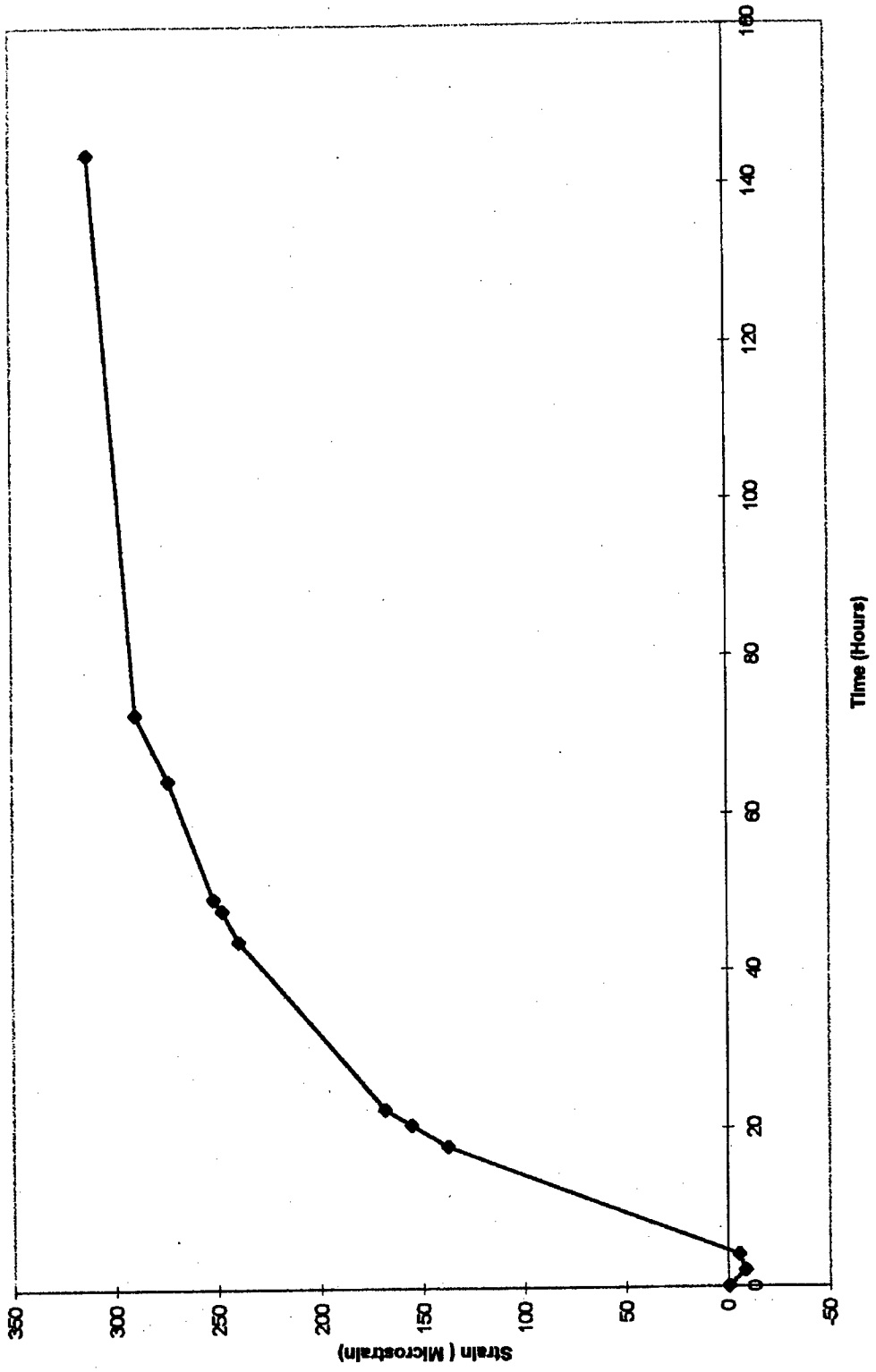


Figure B22. Initial circumferential strain with time.

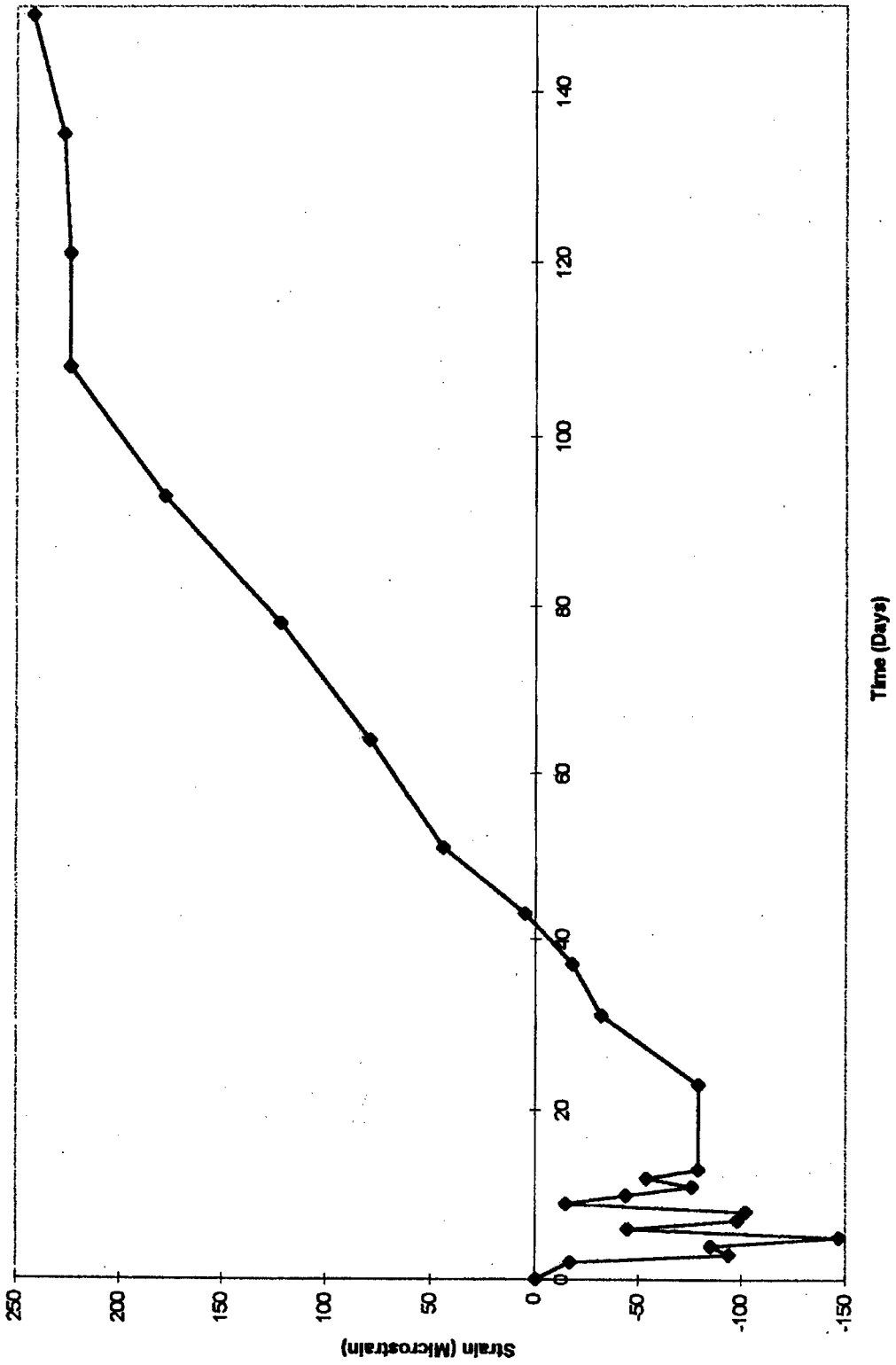


Figure B23. Circumferential strain based on SG#1 with time.

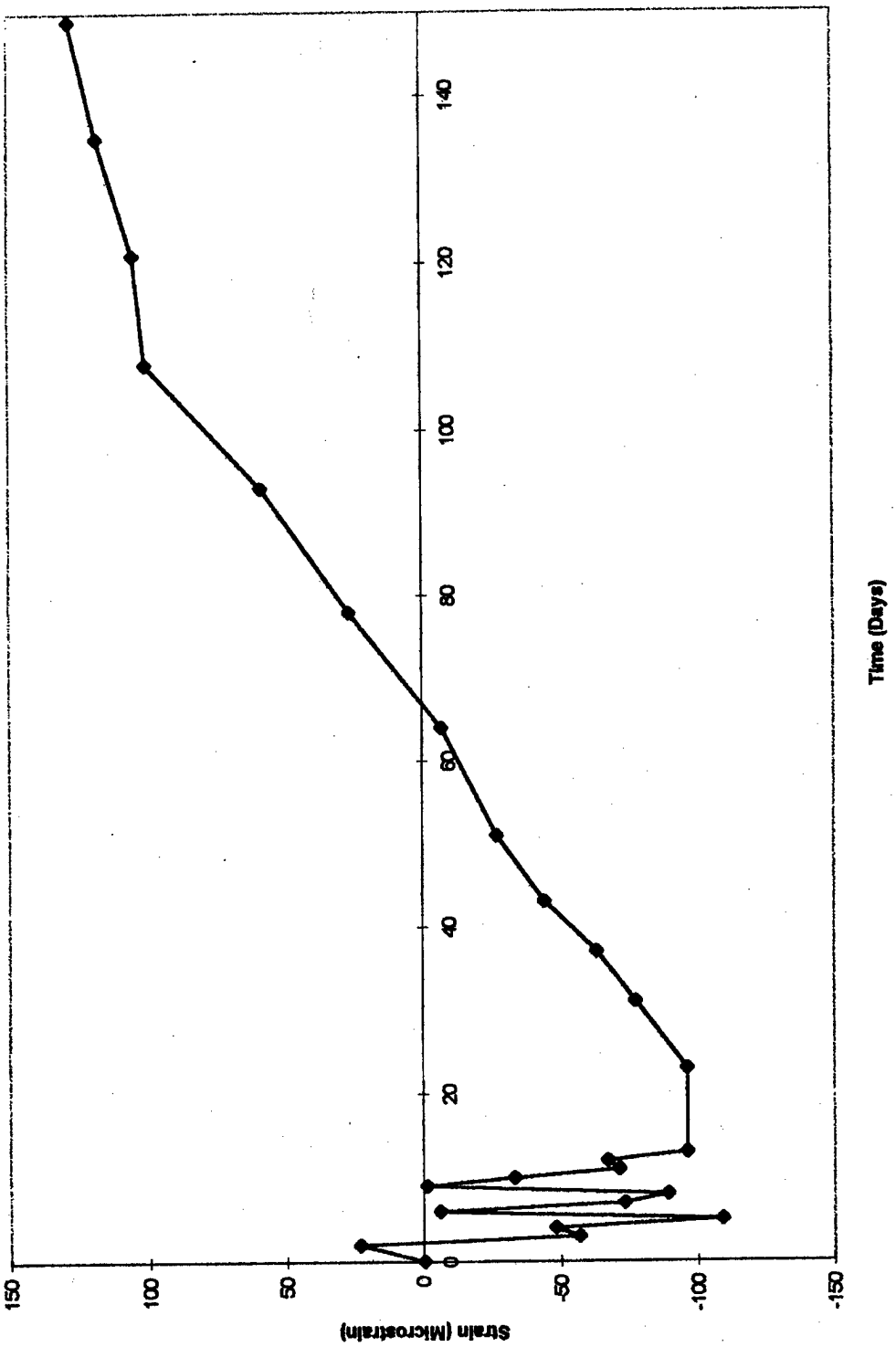


Figure B24. Circumferential strain based on SG#11 with time.

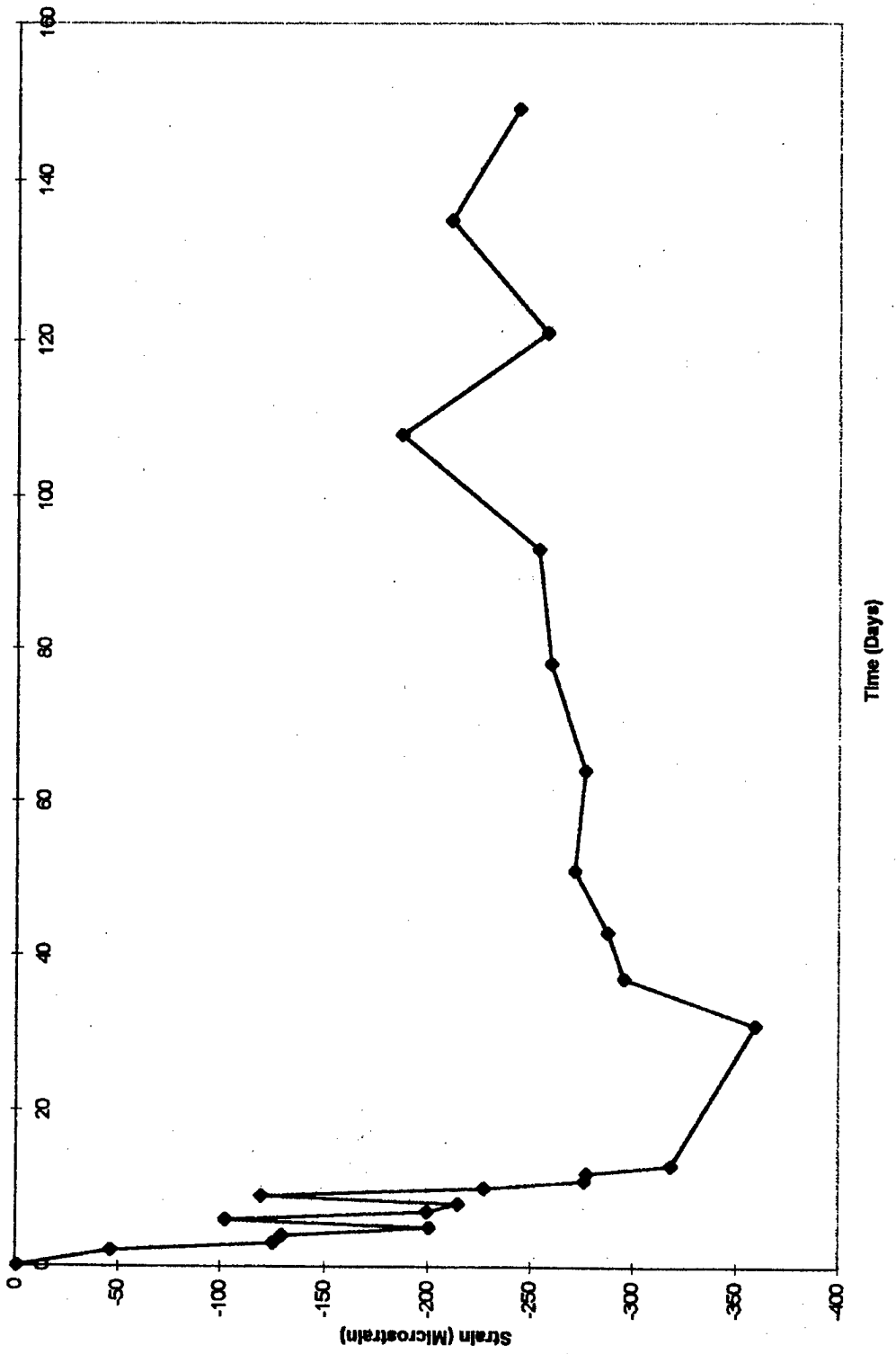


Figure B25. Axial strain based on SG#0 with time.

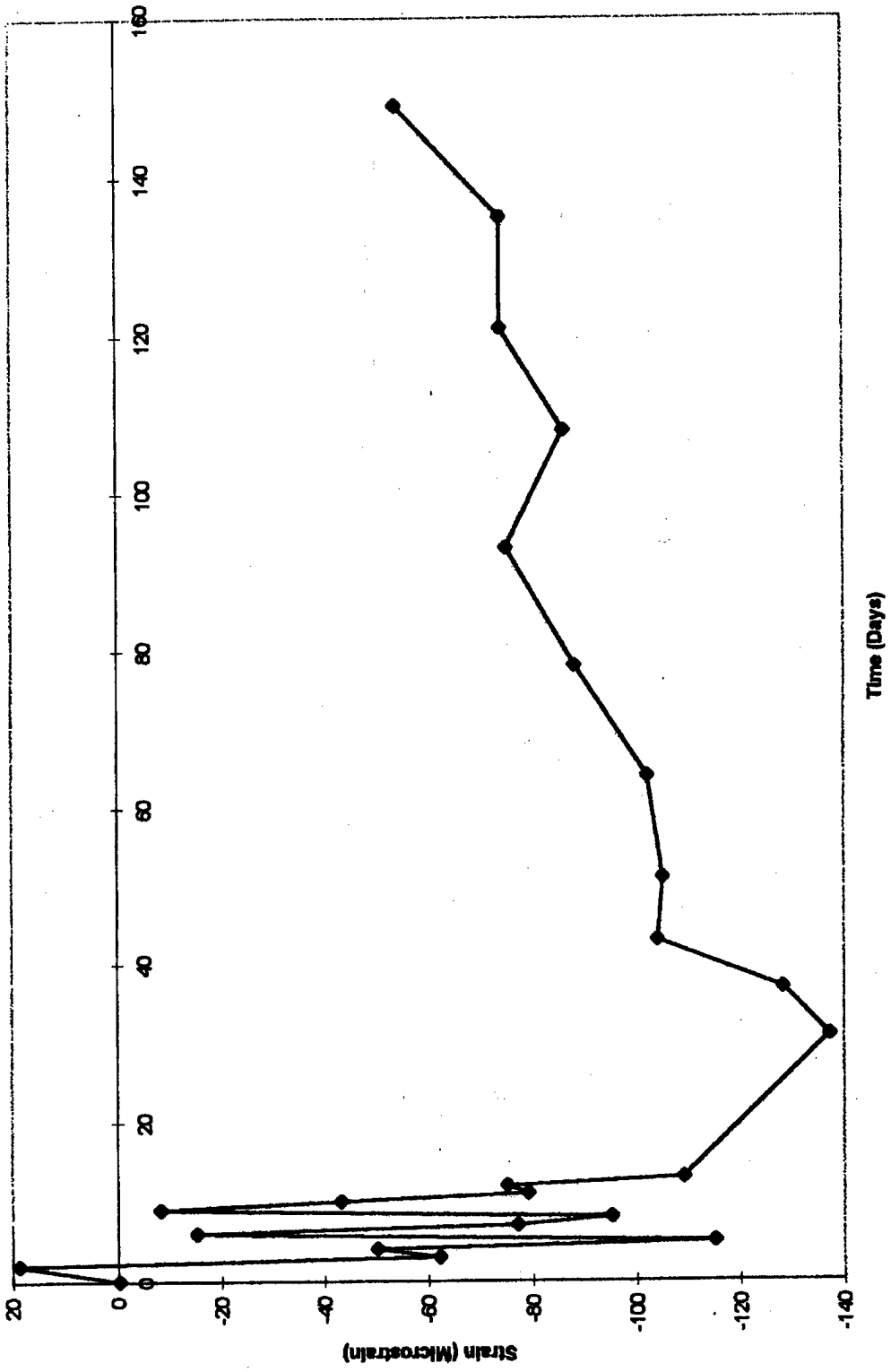


Figure B26. Axial strain based on SG#10 with time.

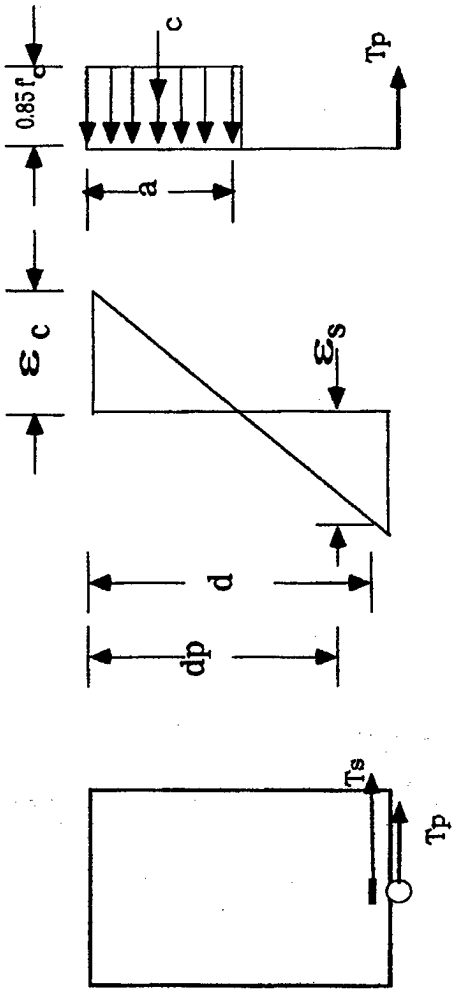


Figure B27. Strain and stress distribution in a typical beam.

Table B1. Prestress at different loading stages in leadline tendon 1.

Stages	Prestress force (lbs) (Measured at anchoring end)	Comments
1	3874	After first load increment
2	7058	After second load increment
3	9706	After third load increment
4	10343	After final load
5	10329	After anchoring of tendon 1 by securing the nuts

Table B2. Prestress at different loading stages in leadline tendon 4.

Stages	Prestress force (lbs) (Measured at anchoring end)	Comments
1	2357	After first load increment
2	4864	After second load increment
3	8309	After third load increment
4	10832	After final load
5	10166	After anchoring of tendon 4 by securing the nuts

Table B3. Prestress forces in leadline tendons.

	Jacking end (lbs)		Computed prestress losses (lbs)		Anchoring end (lbs)		Percent
Leadline tendon	Hydraulic pressure gage	Measured prestress	Elastic shortening	Curvature frictional effect	Computed prestress	Measured force	Loss based on force from gage pressure
1	12,000	12,582	449.5	406	11,144.5	10,343	13.8
4	12,000	11,958	449.5	406	11,144.5	10,832	9.7

Appendix C: Parametric Study of Beams With Externally Bonded FRP Reinforcement

Overview

The reinforcement of existing reinforced concrete beams and slabs with FRP materials bonded to their soffit may be needed for different reasons: to reduce the vertical deflection at service *(stiffening criterion)*, improve the maximum load capacity *(strengthening criterion)*, or limit the width and the distribution of cracks in concrete *(durability criterion)*. The durability criterion is not addressed in this paper. The designer has generally no control over the existing structural element in need of repair. Geometry and properties of existing steel reinforcement and concrete cannot be modified. To satisfy stiffening and strengthening requirements, the designer may select the area of the FRP reinforcement and its stiffness. For the choice of the adhesive, the designer usually relies on the selection made by the manufacturer of the FRP material system.

For the stiffening criterion, assuming that cross sections remain plane during deformation and perfect bond exists at the concrete-adhesive-FRP interfaces, it seems preferable to select the FRP reinforcement with the highest stiffness to reduce deflection under service conditions. For the strengthening criterion and under the same assumptions, it seems logical to increase the area of the FRP reinforcement as much as possible in order to increase load resistance capacity. Independently of the repair strategy, it is essential to understand the consequences of the design choice in terms of crack propagation and failure mechanism. In fact, it has been observed in the literature that different failure mechanisms, from ductile to very brittle, occur as externally bonded FRP reinforcement is added to a flexural member (Saadatmanesh and Ehsani 1994; Chajes et al 1994; Arduini, D'Ambrisi, and Di Tommaso 1994; Arduini, Di Tommaso, and Nanni 1995).

With reference to a simply supported, FRP-repaired, reinforced concrete beam loaded at 4-point, four possible failure mechanisms (Arduini, Di Tommaso, and Nanni 1995) have been summarized in the sketches of Figure C1* and are listed below:

- FRP tensile rupture (R) due to FRP excessive elongation in the zone of maximum moment
- Concrete crushing (C) due to excessive concrete compressive strain in the zone of maximum moment
- Debonding between FRP and concrete (D) due to failure at the concrete-adhesive interface. This failure mechanism can initiate at any flexural crack and propagates from there to the end of the FRP reinforcement
- Shear-tension failure (S) resulting from a combination of shear and normal tensile stress in the concrete in the plane of the longitudinal steel bars. This failure mechanism initiates at the ends of the FRP plate, results in the propagation of a horizontal crack, and causes separation of the concrete cover.

The first two failure mechanisms occur after large deflection of the member and are synonyms of better structural performance. In the case of FRP rupture, the main steel reinforcement is past yielding. Moreover, from an economical point of view, the rupture of the FRP plate seems to be desirable because it means that all the mechanical resources of FRP (an expensive material) are utilized.

The third and fourth failure mechanisms are brittle and occur at values of the applied load lower than expected with conventional design models. In both cases, the stiffening/ strengthening resources of the FRP plate are of little advantage. Anchoring the FRP plate ends, not applicable to slabs, may attain a higher ultimate load and an increase in ductility. However, the improvements are not very significant (Arduini, Di Tommaso, and Nanni 1995).

This paper presents an analytical study of reinforced concrete beams of representative geometries and materials, repaired with FRP plates of various thickness and mechanical properties. The validity of the model used for the study was verified previously (Arduini, Di Tommaso, and Nanni 1995). The model allows for the non-linear behavior of the reinforced concrete member due to the diffusion of flexural cracks. This is essential for a correct interpretation of

* All figures are found at the end of this appendix.

experimental results. In fact, the elastic solution to the problem of repaired reinforced concrete with FRP composites can not be effectively applied as explained below.

Researchers (Frostig et al. 1992; Arduini and Di Leo 1992) have shown that in the elastic state, at the interface of concrete and adhesive, shear and normal stress (τ and σ) can be calculated using equations in hyperbolic functions derived from seventh order (or higher) differential equations when applying boundary conditions that depend on beam load and support configuration. The resulting stress distribution shows significant stress concentration only at the very ends of the FRP reinforcement. Experiments have shown that, during the phase of flexural cracking in concrete, the distribution of τ and σ along the adhesive-concrete interface changes dramatically from that of the elastic phase. In the area around each crack, high stress concentration originates due to the presence of the FRP plate that opposes the opening of the flexural crack. Generally, this occurs early during the loading stage of the beam, since concrete has low tensile strength. Therefore, the brittle mechanism detected by the elastic solutions at the end of the plate is never activated nor does control the true failure mechanism. Only in particular situations such as with very thick FRP plates, the failure of the beam could occur before flexural cracking of the concrete and be successfully predicted by elastic analysis.

Research Significance

The paper intends to identify in a rational fashion the parameters that affect performance of flexural members repaired with externally bonded FRP reinforcement. These parameters must include preexisting materials and geometry as well as repair materials. The study of the inter-relationship among these parameters leads to the understanding of the limiting factors and the possible modes of failure. This analytical study and the eventual experimental verification are necessary for the development of sound design guidelines. It is noted that the results reported in the paper are not absolutely general but relate to selected reinforced concrete beam geometries and materials.

Model

With reference to Figure C2, a simply supported beam with a span equal to 2l is subdivided into n segments of length Dx. For each segment j, the external moments due to the applied load (4-point configuration) are computed and

equilibrium conditions are imposed for the three subsystems of the segment (i.e., concrete, adhesive, and FRP). Via equilibrium, the shear (τ) and normal (σ) stresses along the adhesive-concrete (τ_{a1}, σ_{a1}) and adhesive-FRP (τ_{a2}, σ_{a2}) interfaces for each segment of the beam are calculated (Arduini, Di Tommaso, and Nanni 1995). Failure can originate at the end of a segment where the combination of maximum τ_{a1} and σ_{a1} crosses the MohrCoulomb failure domain of the interface adhesive-concrete (failure types S or D). The other possible failure types occur when the maximum tensile strain of the plate is reached (failure type R) or when the maximum compressive strain in concrete is reached (failure type C).

The constitutive laws for the four constituent materials considered by the model are as follows. Compressive concrete is non-linear and is influenced by the confinement action due to closed stirrups (if provided) according to the CEB-FIP Model Code 90 (1993). Tensile concrete is elasto-softening. Steel is elasto-hardening. FRP and adhesive are perfectly elastic.

Some assumptions are made to simplify the problem:

- Plane cross sections remain in plane during loading
- The Mohr-Coulomb failure surface for the adhesive-concrete interface does not change in the presence flexural cracks. This means that no interaction exists between horizontal normal stress, shear, and vertical normal stress
- The interface between adhesive and FRP is considered much stronger than the corresponding concrete-adhesive interface
- The FRP plate and the adhesive layer are considered "thin" and only subjected axial force

In order to allow for the study of the effects of stiffness and thickness of the adhesive layer, the model considers the normal force in the adhesive (N_a) as part of the equilibrium equation expressions (see sketch in Figure C2). During the concrete crack propagation, local tensile failure in the adhesive may be recorded. Where this phenomenon occurs, the stress transfer for both σ_{a1} and τ_{a1}, applied to the adhesive-concrete interface of that segment, is neglected.

The shear stress distribution at the interface adhesive-concrete for each segment is considered triangular and the maximum value is calculated, for a generic j segment, from:

$$(t_{a,j})_{max} = (N_{j+1} + N_{a,j+1} - N_j - N_{a,j}) \frac{2}{b \times Dx} \qquad (1)$$

Where:

– N_j is the normal force in the FRP plate in the j segment

– N_{aj} is the normal force in the adhesive in the j segment

– b is the beam width

– Dx is the segment length

The normal stress distribution at the same interface is also triangular and its maximum value in a generic j segment of the beam is:

$$(\sigma_{a,j})_{max} = (N_{j+1} - N_j) \cdot \left(dv + t_a + \frac{t_p}{2} \right) + (N_{a,j=1} - N_{a,j}) \cdot \left(dv + \frac{t_a}{2} \right) \frac{6}{b \cdot Dx^2} \qquad (2)$$

Where:

– dv_j is the increment of vertical displacement of the j+ 1 segment with respect to i

– t_p is the FRP thickness

– t_a is the adhesive thickness

Since no shear reinforcement can be added to the existing member, its nominal shear capacity (V_n) is also calculated in order to determine whether or not it becomes the controlling factor after repair. V_n is computed according to ACI 318-89 (ACI 1992) and can be expressed as (in SI units):

$$V_n = \frac{\sqrt{f_{ck}}bd}{6} + \frac{A_s f_{yk} d}{s} \qquad (3)$$

where:

– f_{ck} is the characteristic compression strength of concrete

– f_{yk} is the characteristic tensile yielding of steel

– s is the stirrups spacing

- d is the effective depth of the steel reinforcement

- A_s is the stirrups area

Parametric Study

Materials And Geometries

The parameters that influence the behavior of an reinforced concrete beam repaired with FRP can be failure subdivided into two groups.

The first group consists of properties and geometries of the constituents of the existing reinforced concrete member including support conditions and loading configuration. In this paper three doubly reinforced rectangular cross-sections were considered with height-to-width (h/b) ratios of 0.5, 1, and 4. The first cross-section was intended to represent the case of a slab and did not include any shear reinforcement. For all beam types, a simply-supported configuration was adopted using 4-point loading, and shear span-to-reinforcement depth (a/d) ratios of 4.5 and 7. Two compressive concrete strengths were adopted (20 and 30 MPa). The longitudinal steel reinforcement ratio was taken as 0.5 ρ_{max}, with ρ_{max} equal to 75% of the balanced reinforcement ratio as for ACI 318-89. A minimum area of compressive reinforcement was taken into account. The shear reinforcement ratio $\rho_v = A_v/bs$ was assumed constant and equal to 0.003. Table C1* reports the characteristic mechanical properties of concrete and steel as used in the study adopting the subsequent simbology:

- E: elastic longitudinal Young modulus

- v: Poisson ratio

- f_{ck}: characteristic concrete compression strength

- f_{yk}: characteristic tensile yielding of steel

- f_{tk}: characteristic concrete tensile strength

* All tables are found at the end of this appendix.

- τ_u: concrete shear strength

- ε_{cu}: ultimate compression strain, according to Arduini and Di Leo (1992)

- ε_u: ultimate tensile strain

The mean strengths adopted in the model are 1. 1 8 higher and are reported with the same symbol without the subscript k.

The second group of parameters refers to the properties and geometries of the repair materials (FRP composite and adhesive). In this study, the thickness of the FRP (t_p) was varied in the range of 0 to 2 n-un. The bonded length of the FRP-to-shear span (p/a) ratio was varied between 0.60 and 0.95. Three FRP stiffness values with corresponding maximum strain at failure were considered. Table C2 reports the mechanical characteristics of the FRP materials. For reference to real products, it may be said that they vary from high-modulus carbon FRP to glass FRP. For the adhesive, two stiffness values with corresponding maximum strain at failure were adopted. The adhesive thickness was maintained equal to 1 mm for all cases. Mechanical properties of the adhesives are reported in Table C2.

Results For One Beam Type

If the scope of the design is the stiffening criterion, the expected outcome must be a reduction of the maximum deflection of the member under service loads. For this study, it was necessary to define the service load level as a fraction of the ultimate flexural capacity. The ratio between ultimate and service load was assumed to be 1.5, as it would result from a reasonable combination of dead and live loads, which have load factors of 1.4 and 1.7, respectively, according to ACI 318-89. The deflection at service load ($F_s = F_u/1.5$) was computed for beams with FRP repair (d_{sr}) and for identical beams without repair (d_s). The ratio d_{sr}/d_s is plotted as a function of the FRP plate thickness t_p in Figure C3. This diagram represents the case of beams with the following characteristics: h/b= 1; a/d = 4.5; f_{ck} = 30 MPa and the adhesive type is Al. Curves were obtained for p/a ratios varying between 0.6 and 0.95. Only the two limiting cases are shown in the figure, since the effect of this ratio is almost insignificant. Three families of curves can be observed depending on the FRP stiffness. As expected, the reduction of the deflection ratio at service is strongly influenced by FRP stiffness and thickness.

When one considers the strengthening criterion, the outcome of interest is the ratio between ultimate load of the FRP repaired beam (F_{ur}) and the ultimate load of the unrepaired beam (F_u). Figures C4a, C4b, and C4c are the summary of the F_{ur}/F_u ratio plotted as a function of the FRP plate thickness for the same beam material and geometry combinations used in Figure C3. Each portion of the figure represents a family of four curves obtained for a given FRP stiffness at the variation of the FRP bonded length-to-shear span (p/a) ratio. With reference to the family of curves obtained for the highest FRP stiffness (i.e., E1 in Figure C4a), it is observed that the ultimate strength ratio is strongly affected by the p/a ratio. For values of p/a less than 0.65, there is practically no benefit in repairing the beam for strength. Moreover, points on the diagram at FRP thickness values of 0.0, 0.1, 0.5, 1.0, and 2.0 mm are labeled with a letter that indicates the type of failure as previously discussed. When no FRP material is used (t_p = 0), concrete crushing is the dominant failure mode. When the thickness of FRP is 0.1 mm, the dominant failure mode is rupture of the FRP independently of the p/a ratio. When thickness of the FRP is 0.5 mm, rupture of the FRP is only obtained for the case of p/a equal to 0.95. In all other cases, shear-tension failure is the dominant mode. This failure type is brittle and therefore undesirable. In addition, the occurrence of shear-tension or debonding failure indicates that it is no longer possible to increase the flexural capacity of the member by increasing the FRP thickness. This is clearly shown in the diagram for the remaining parts of the four curves. A final observation is related to the horizontal line indicating the value of the ultimate load ratio as controlled by shear capacity. The line is horizontal because the repair method does not improve shear strength of the existing reinforced concrete member.

Considerations similar to the ones reported above can be repeated for the remaining two family curves obtained for E2 and E3 in Figures C4b and C4c. In general, the lower the FRP stiffness, the higher needs to be its thickness to obtain a given strength improvement.

When one considers the strengthening criterion, it is also mandatory to determine whether or not the deflection of the repaired member under the new (and higher) service load is acceptable. A possible way to address this issue is by considering the ratio between deflection at service of the repaired system under the new load (d_{nsr}) and the deflection at service of the unrepaired system under the old load (d_s). The cases of new and old loads were assumed to be equal to $F_{ur}/1.5$ and $F_u/1.5$, respectively. Figures C5a, C5b, and C5c are a summary of the variation of the d_{nsr}/d_s ratio as a function of the FRP thickness for the same cases given in Figures C4a, C4b, and C4c). The diagrams are constructed as previously described and the data labels correspond to the ones given in Figures

C4a, C4b, and C4c). The most important observation at this point is that, if the deflection for the repaired system under the new service load cannot exceed that of the unrepaired system under the old load, then only d_{nsr}/d_s values equal or less than 1.0 become acceptable.

In order to better understand the failure mechanisms of the repaired beams presented in the previous diagrams, Figures C6 and C7 present the distribution of selected stresses as a function of the position along the beam axis (expressed as distance from the support-to-half span ratio = x/l) under the ultimate load. These stresses are: maximum shear stress at the adhesive-concrete interface ($\tau_{a1,max}$), maximum tensile stress at the same interface ($\sigma_{a1,max}$), horizontal tensile stress at the bottom concrete fiber (σ_1), and longitudinal tensile stress in the FRP plate (σ_p). σ_1, becomes 0 if the tensile strength of concrete is overcome and this does represent a flexural crack propagation. The case presented in Figure C6 is that dominated by rupture of the FRP (i.e., E1, t_p = 0.5 mm, and p/a=0.95). The case presented in Figure C7 is that dominated by shear tension failure in the concrete (i.e., E1,tp = 2.0 mm, and p/a=0.85). In the first case (see Figure C6), rupture of the FRP occurs in the constant moment region (σ_p = 2000 MPa), and is reached when almost the entire beam has experienced flexural cracking (σ_1 is indicated as 0 value). The shear stress has maximum values at the end of the plate and near the constant moment region, but they are well below the ultimate value of 5.5 MPa. In the second case (see Figure C7), when the FRP thickness is high, the maximum shear stress is responsible for failure at the end of the FRP plate. In this case, only 60% of the beam has experienced flexural cracking, and the stress in the FRP plate is small (500 MPa).

The FRP debonding mechanism (the other brittle failure mode) can be activated at the FRP plate end or in any zone where a flexural concrete crack is generated. The latter case is mainly noted with long and high strength FRP plates.

Resins used for adhering FRP to concrete may have low modulus and high deformability as well as high modulus and low deformability. Two representative types are shown in Table C2. Even though the thickness of the adhesive layer was kept constant in this study, it is noted from Equation 2 that the normal vertical stress (σ_{a1}) is directly proportional to the adhesive thickness. Therefore, the thinner the adhesive layer, the lower the likelihood of concrete failure.

Table C3 presents a comparison of the results obtained with the reinforced concrete beam described above when A1 and A2 adhesives are used. The first three columns in the table show the FRP parameters. Columns 4 and 6 compare the failure mode for adhesives A1 and A2, respectively, and Columns 5 and 7,

compare the F_{ur}/F_u ratio. When A2 is used, the debonding failure mechanism prevails with a significant decrease of the ultimate load capacity. This failure mechanism is facilitated by the low ultimate strain of the adhesive. As the adhesive fails in uniaxial tension in a given zone, there is no shear and normal stress transfer between FRP and concrete. At the ends of this zone, a high shear and normal stress transfer is needed to balance the normal force in the unbonded FRP plate. This concentration of stress causes the concrete failure. With regard to the stiffening criterion, the results (not shown here) are similar for both adhesives because deflections are comparatively small under service load.

Results For Three Beam Types

In the second part of the parametrization analysis, the effects of different h/b and a/d ratios and strength of concrete are considered. The parameters maintained constant are $\rho = 0.5\ \rho_{max}$, p/a = 0.85, FRP type E2, and adhesive type A1. Figures C8a, C8b, and C8c present the evolution of the d_{sr}/d_s, F_{ur}/F_u and d_{nsr}/d_s ratios as a function of a parameter k defined as:

$$k = \frac{E_p A_p}{EI} \frac{h}{b} a^3$$

where:

- I is the gross moment of inertia ($bh^3/12$)

- Ep is the elastic modulus of FRP

- AP is the area of the cross section of FRP (t_p b)

In each figure three families of two curves are shown. Each family was obtained for a given h/b and a/d ratio. The two curves per family are function of the concrete compressive strength, 20 and 30 MPa, respectively.

Figure C8a seems to indicate that deep beams (h/b = 4) can hardly be stiffened. Sizable results can be obtained with slab-type sections (h/b = 0.5). The best results are obtained for a square-shaped section at a/d = 4.

Similarly, Figure C8b seems to indicate that strengthening is more suitable for slab-type sections and square-shaped sections. It is worth noting that more FRP reinforcement could be added in the slab-type section with 30 MPa concrete since the failure mode is not of the brittle type. The six horizontal lines represent the

F_{ur}/F_u ratio based on the shear strength of each beam type. Two lines are given for each beam as the compressive strength of concrete varies from 20 to 30 MPa. Three observations are made:

- The F_{ur}/F_u ratio of the 20 MPa concrete is higher than that corresponding to 30 MPa concrete. In fact, as f_{ck} increases, more flexural steel reinforcement is added to maintain $\rho = 0.5\ \rho_{max}$. Therefore, flexural capacity increases in a way directly proportional to f_{ck}, whereas the concrete contribution to shear capacity only increases proportionally to the square root of f_{ck}.
- The slab-type beam is without stirrups and therefore it has a relatively low shear strength. The efficiency of the FRP repair may be low in this type of application.
- For the deep beam, shear strength seems not to be a limiting factor.

The grouping of the three families of curves is not that evident in Figure C8c. For both the slab-type section and the deep section, deflection under new service load is higher than deflection under old service load. As for the previous case of Figures C5a, C5b, and C5c, the service load levels are computed by dividing the ultimate loads by a factor of 1.5. This diagram points out that service load for FRP strengthened beams may need to be reduced to less than $F_{ur}/1.5$ to prevent unacceptable deflections.

Results For A Beam Subjected To Uniformly Distributed Load

The case presented in Figures C9a and C9b is relative to a simply supported beam with a total span-to-height (2l/h) ratio of 6.7 and subjected to uniformly distributed load. The h/b ratio is equal to 3, l_p/l is equal 0.85, concrete has a strength of 30 MPa, ρ equals $0.5\ \rho_{max}$, ρ_v equals 0.003, and the adhesive is type A1.

For the stiffening criterion, Figure C9a shows the ratio between the mid-span deflection of the repaired beams (d_{sr}) and the mid-span deflection of the unrepaired beam (d_s) as a function of the FRP plate thickness (t_p), for three different FRP types. It is reminded that deflections are at the same service load level for repaired and unrepaired beams. A significant reduction of vertical displacement is only attainable with a very stiff FRP plate.

For the strengthening criterion, Figure C9b reports the ratio between ultimate linear load of the repaired beams (q_{ur}) and the ultimate linear load of the unrepaired one (q_u) as a function of the FRP thickness. The shear capacity due to concrete and stirrups is only 40% higher of the flexural unrepaired strength.

Therefore the extent of FRP repair is limited. FRP with low modulus and high thickness gives the best performance even in tenns of failure mechanism provided that shear strength near the supports does not become the controlling factor.

Conclusions

In summary, FRP repair of existing reinforced concrete flexural members may be structurally necessary for two reasons: stiffening or strengthening. Depending on the criterion and the conditions (i.e., materials and geometries) of the existing member, the repair method may be more or less effective.

If a designer is only concerned with stiffening, the repaired element is not required to carry any additional service load. In general, stiffening is always attainable. For the same FRP thickness, the higher the FRP stiffness, the better the results. The failure mode of the repaired system may become brittle, depending on several parameters, which include existing member conditions as well as repair parameters (e.g., p/l ratio). If a designer is concerned with strengthening an existing structural member and improving its load carrying capacity at service of a given amount, the success of the repair and the selection of the FRP stiffness, thickness, and bonded length has to be based on the limitations imposed by:

- shear strength of the existing member
- mode of failure of the repaired system
- deflection at new service load.

In general, the bonded length of FRP should be as long as possible to have a better use of the FRP strength resources and to activate failures such as concrete crushing or FRP rupture. The adhesive should have high ultimate elongation.

References

Saadatmanesh H., Ehsani M. "RC beams strengthened with GFRP plates" Part I and Part II, Journal of Structural Engineering, ASCE, vol. II 7, no. 11, Nov. 1994, pp. 3434-3455.

Chajes M.J., Thomson T.A., Januszka T.F., Finch W., "Flexural strengthening of concrete beams using externally bonded composite materials", Construction and Building Materials, 1994, Vol. 8, No. 3 pp. 1212-1225.

Arduini M., D'Ambrisi A., Di Tommaso A. "Shear failure of concrete beams reinforced with FRP plates", Proc., New Materials and Methods for Repair ASCE, S. Diego, Nov. 13-16, 1994, pp. 415-423.

Arduini M, Di Tommaso A., Nanni A., "Brittle Failure in FRP Plate and Sheet Bonded Beams," ACI Structural J., 1995. (submitted)

Frostig Y. et al. "High-order theory for sandwich-beam behavior with transversely flexible core", ASCE Engineering Mechanics Div., Vol. 118, No. 5, May 1992, pp. 1026-1043.

Arduini M., Di Leo A., "Composite behavior of partially plated beams in the linear elastic range" ACI Spring Convention Washington DC, March 15 -20, 1992, 10 pp.

Model Code 90, CEB-FIP Committee, Lausanne, 1993.

ACI Committee 318, "Building Code Requirements for Reinforced Concrete," ACI 318-89, American Concrete Institute, Detroit, MI, 1992, pp. 338.

List of Appendix C Figures and Tables

Figures

Figure C1. Typical failure mechanisms of reinforced concrete beams repaired with FRP composites.....16

Figure C2. Analytical discrete model.....16

Figure C3. Ratio between deflection d_{sr}, for the FRP reinforced beam and deflection for the reinforced concrete one d_s vs. FRP plate thickness t_p (identical service load, different type of FRP materials).....17

Figure C4a. Ratio between ultimate load of the FRP reinforced beam F_{ur} and the ultimate load of the reinforced concrete one F_u vs. FRP plate thickness t_p for the FRP type E I.....18

Figure C4b. Ratio between ultimate load of the FRP reinforced beam F_{ur} and the ultimate load of the reinforced concrete one F_u vs. FRP plate thickness t_p for the FRP type E2.....19

Figure C4c. Ratio between ultimate load of the FRP reinforced beam F_{ur} and the ultimate load of the reinforced concrete one F_u vs. FRP plate thickness t_p for the FRP type E3.....20

Figure C5a. Ratio between deflection at new service load of the FRP reinforced beam d_{nsr} and the deflection at the service load of the reinforced concrete beam d_s vs. FRP plate thickness t_p for the FRP type E1.....21

Figure C5b. Ratio between deflection at new service load of the FRP reinforced beam d_{nsr} and the deflection at the service load of the reinforced concrete beam d_s vs. FRP plate thickness t_p for the FRP type E2.....22

Figure C5c. Ratio between deflection at new service load of the FRP reinforced beam d_{nsr} and the deflection at the service load of the reinforced concrete beam d_s vs. FRP plate thickness t_p for the FRP type E3.....23

Figure C6. Distribution of selected stresses along the axis of FRP reinforced beam (FRP rupture).....24

Figure C7. Distribution of selected stresses along the axis of FRP reinforced beam (Shear/tensile failure).....25

Figure C8a. Ratio between deflection at service load for the FRP reinforced beam d_{sr} and deflection at service load for the reinforced concrete one d_s vs. parameter k.....26

Figure C8b. Ratio between ultimate load of the FRP reinforced beam F_{ur} and the ultimate load of the reinforced concrete beam F_u vs. parameter k.....27

Figure C8c. Ratio between deflection at new service load of the FRP reinforced beam d_{nsr} and the deflection at the service load of the reinforced concrete beam d_s vs. parameter k.....28

Figure C9a. Ratio between deflection at service load for the reinforced beam d_{sr} and deflection at service load for the reinforced concrete one d_s vs. FRP thickness t_p for reinforced concrete beams with distributed uniformly load. 29

Figure C9b. Ratio between ultimate linear load of the FRP reinforced beam q_{ur} and the ultimate linear load of the reinforced concrete beam q_u vs. FRP thickness t_p for reinforced concrete beams with distributed uniformly load....30

Tables

Table C1. Mechanical properties of concrete and steel. 31

Table C2. Mechanical properties of FRP and adhesive. 31

Table C3. Effect of adhesive....32

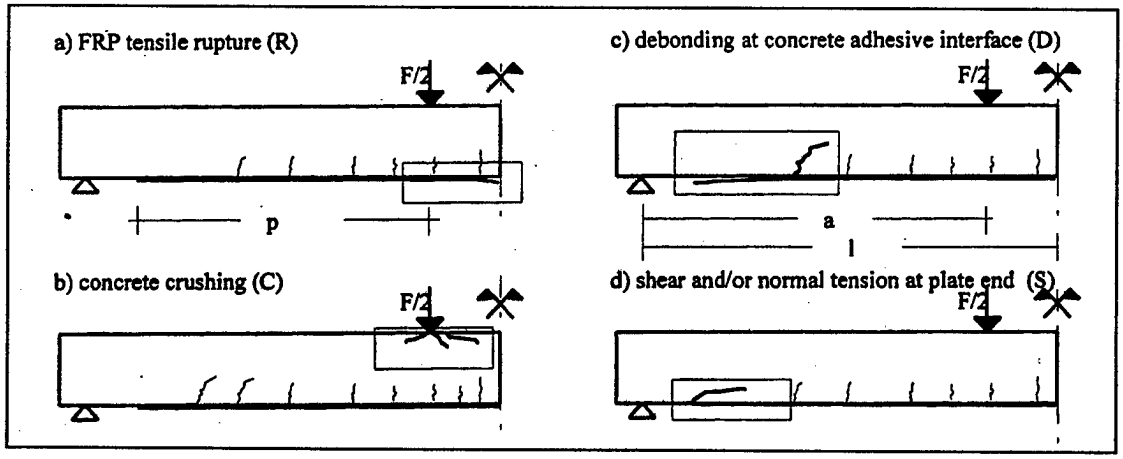


Figure C1. Typical failure mechanisms of reinforced concrete beams repaired with FRP composites.

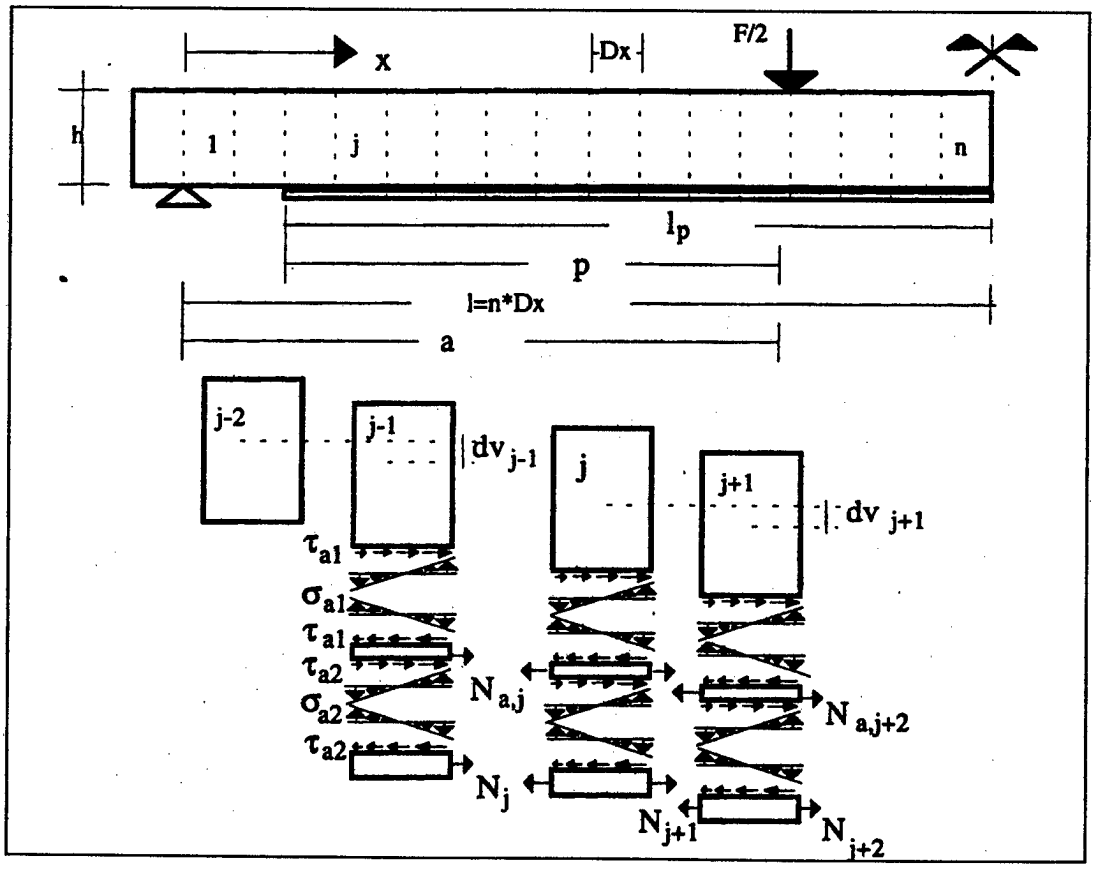


Figure C2. Analytical discrete model.

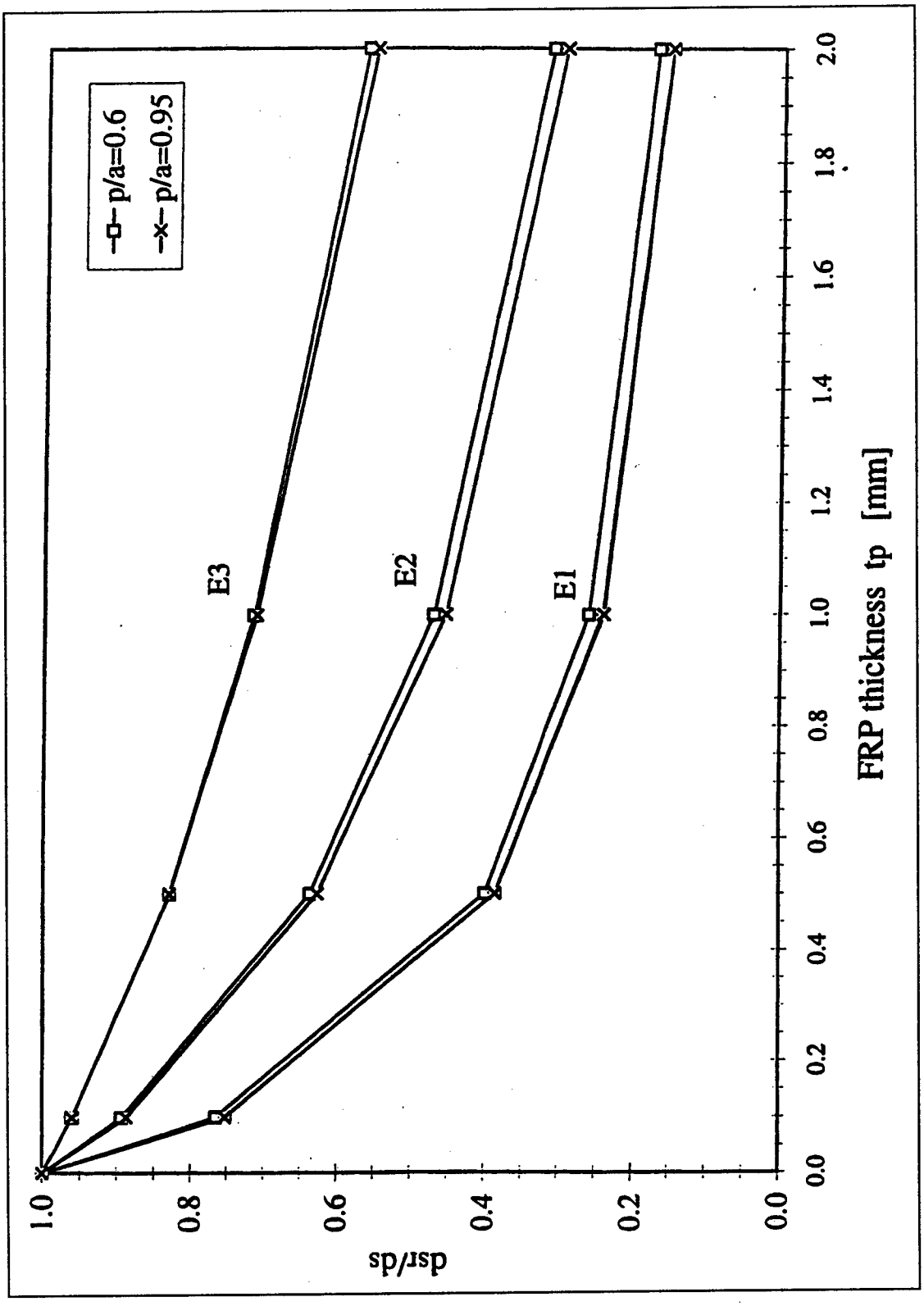


Figure C3. Ratio between deflection d_{sr}, for the FRP reinforced beam and deflection for the reinforced concrete one d_s vs. FRP plate thickness t_p (identical service load, different type of FRP materials).

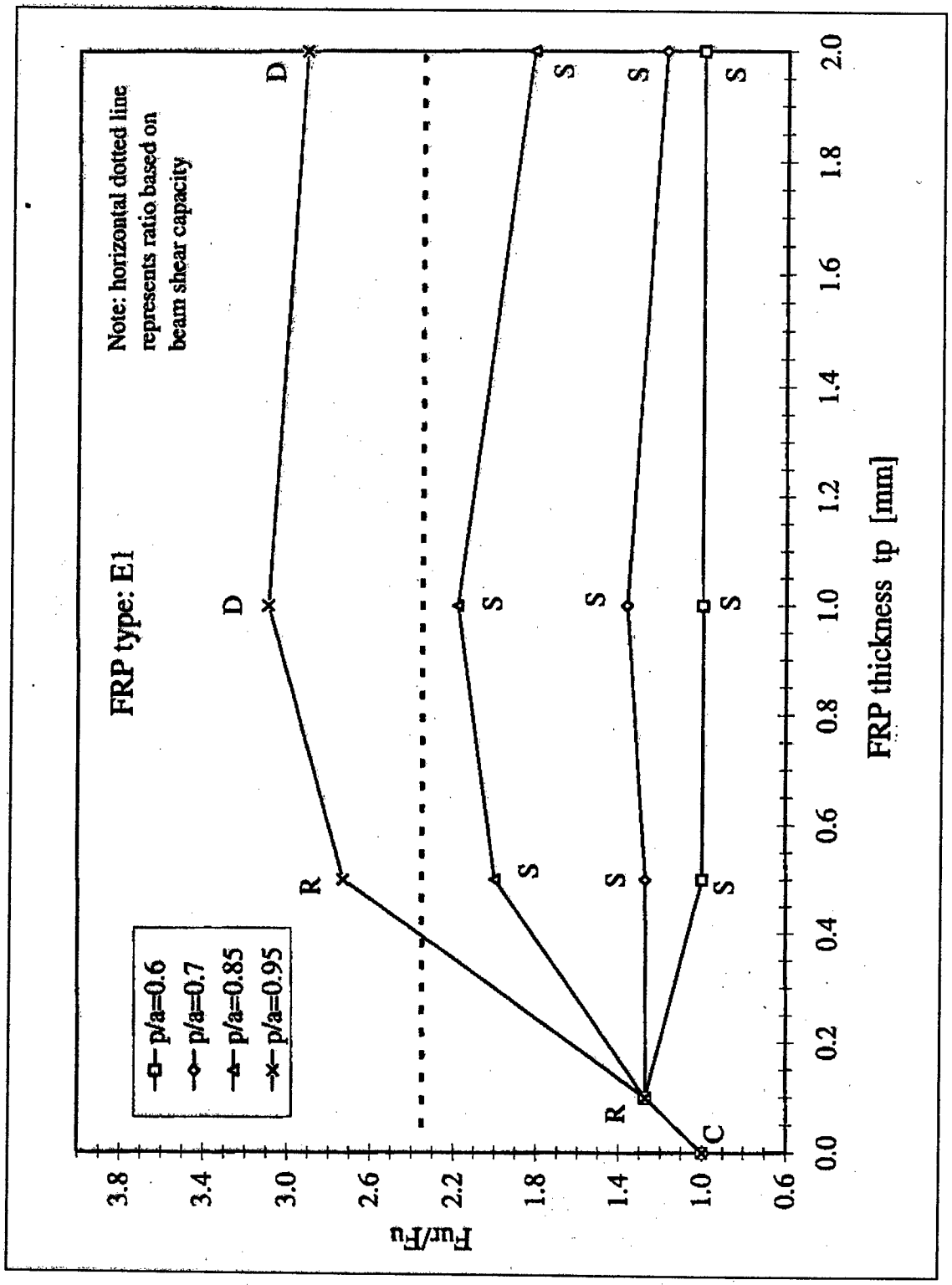


Figure C4a. Ratio between ultimate load of the FRP reinforced beam F_{ur} and the ultimate load of the reinforced concrete one F_u vs. FRP plate thickness t_p for the FRP type E I.

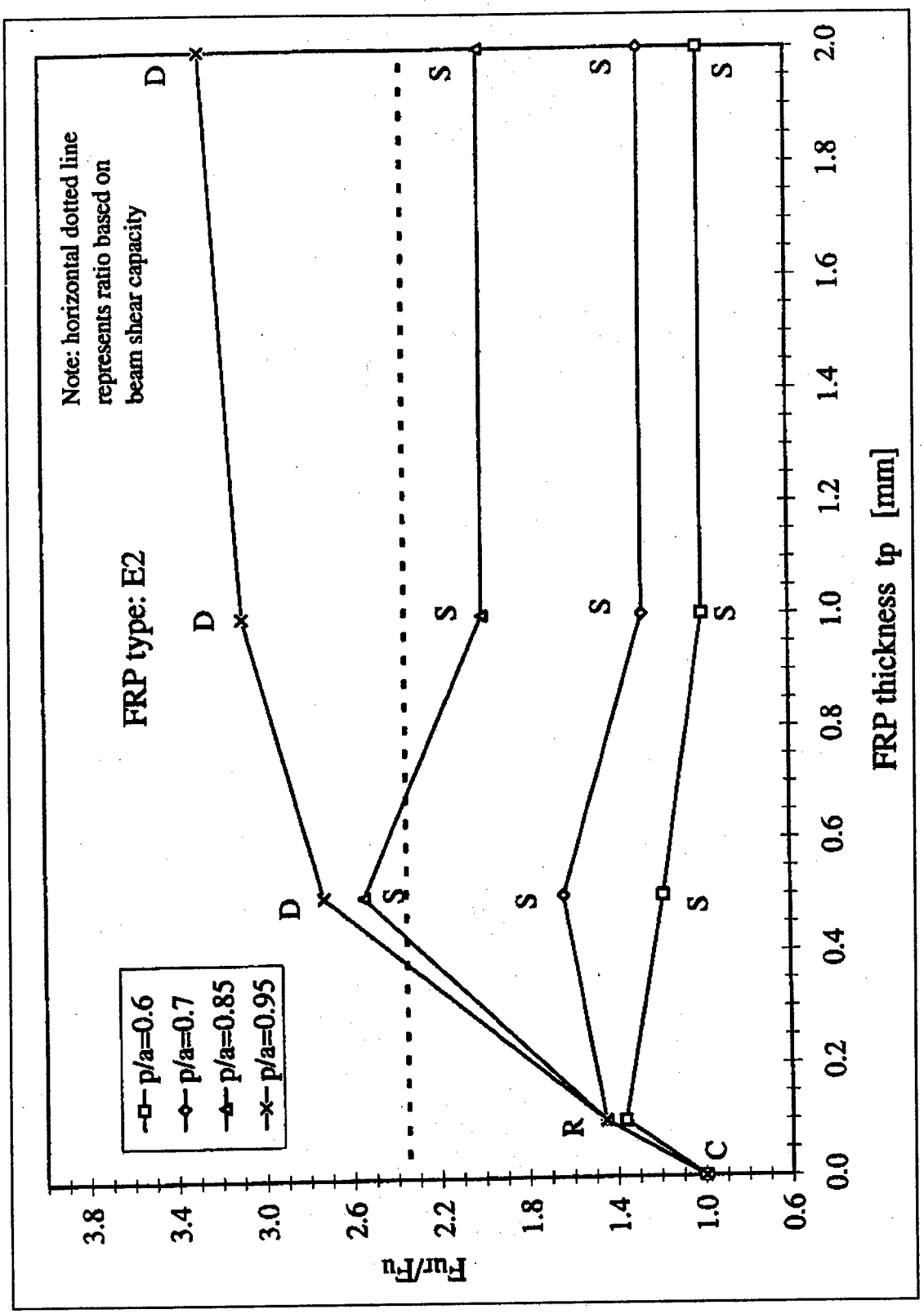


Figure C4b. Ratio between ultimate load of the FRP reinforced beam F_{ur} and the ultimate load of the reinforced concrete one F_u vs. FRP plate thickness t_p for the FRP type E2.

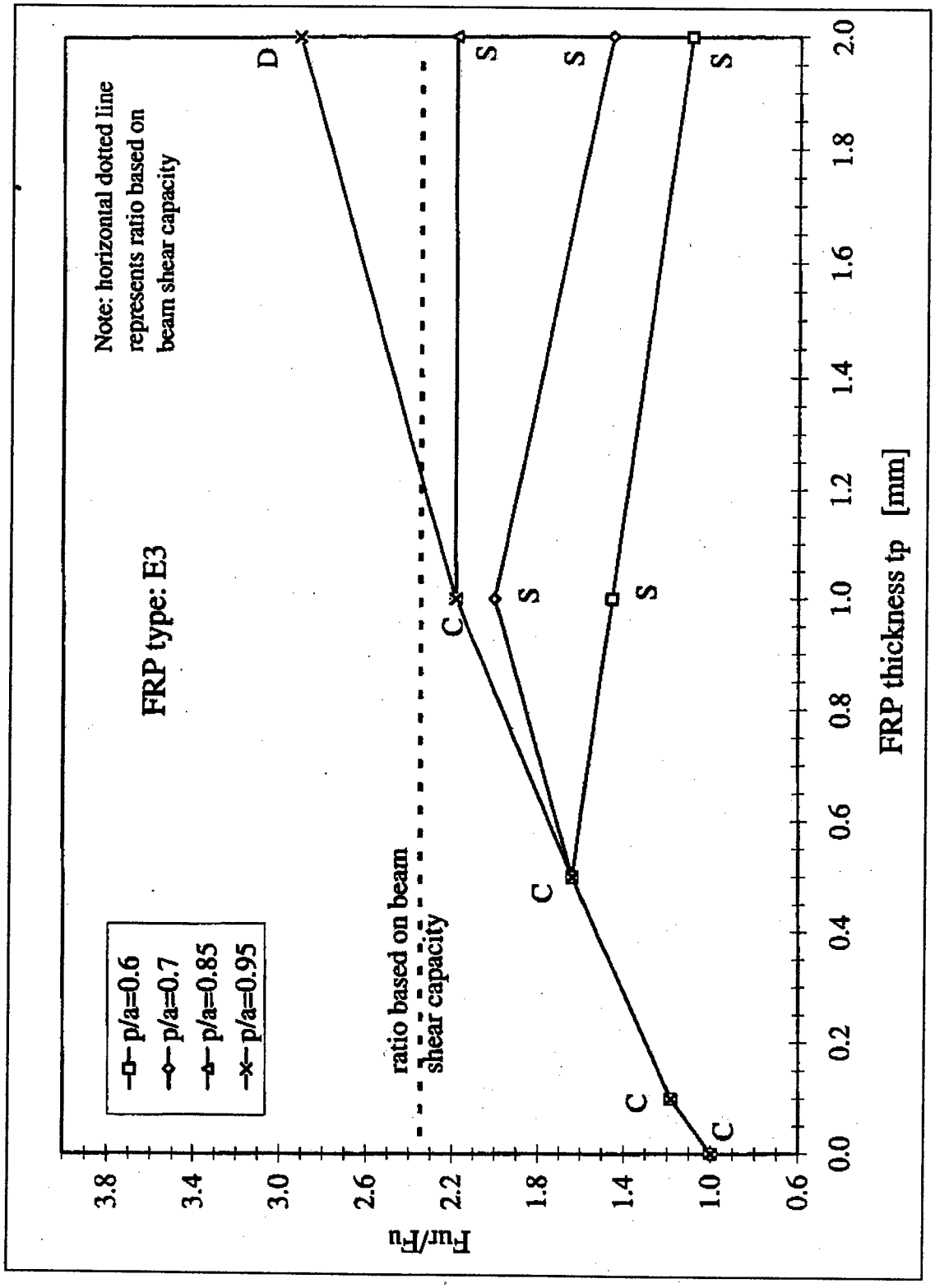


Figure C4c. Ratio between ultimate load of the FRP reinforced beam F_{ur} and the ultimate load of the reinforced concrete one F_u vs. FRP plate thickness t_p for the FRP type E3.

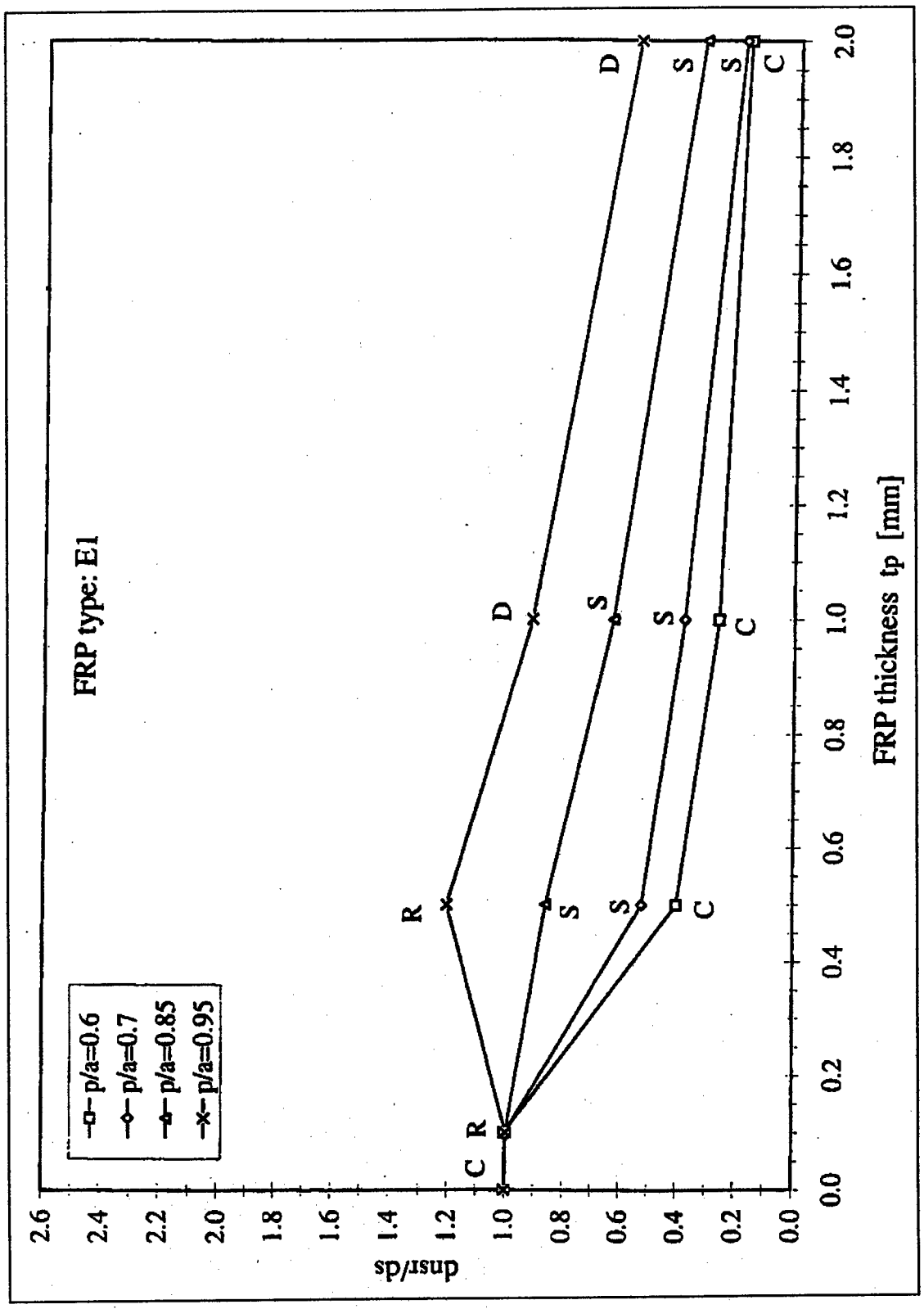


Figure C5a. Ratio between deflection at new service load of the FRP reinforced beam d_{nsr} and the deflection at the service load of the reinforced concrete beam d_s vs. FRP plate thickness t_p for the FRP type E1.

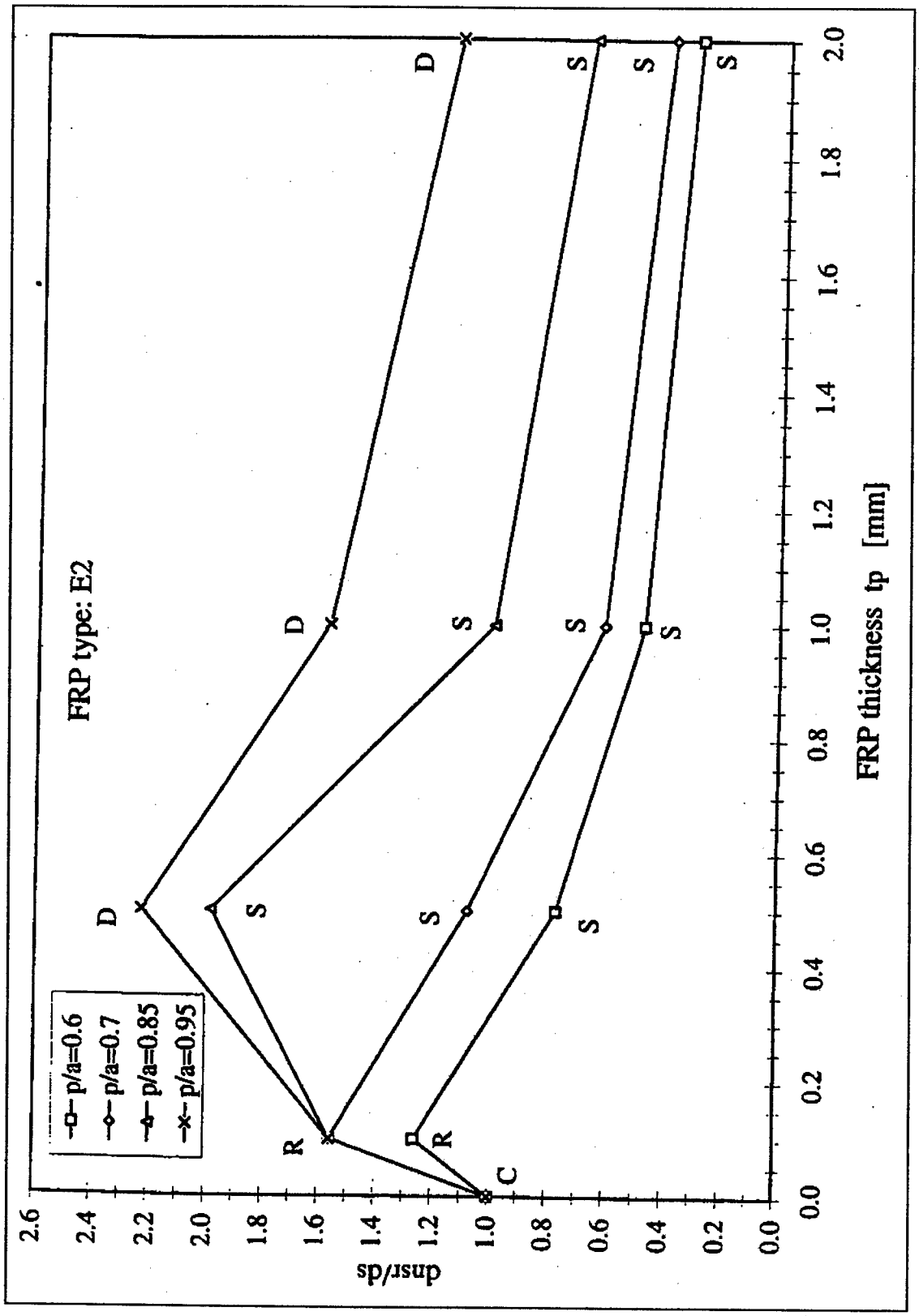


Figure C5b. Ratio between deflection at new service load of the FRP reinforced beam d_{nsr} and the deflection at the service load of the reinforced concrete beam d_s vs. FRP plate thickness t_p for the FRP type E2.

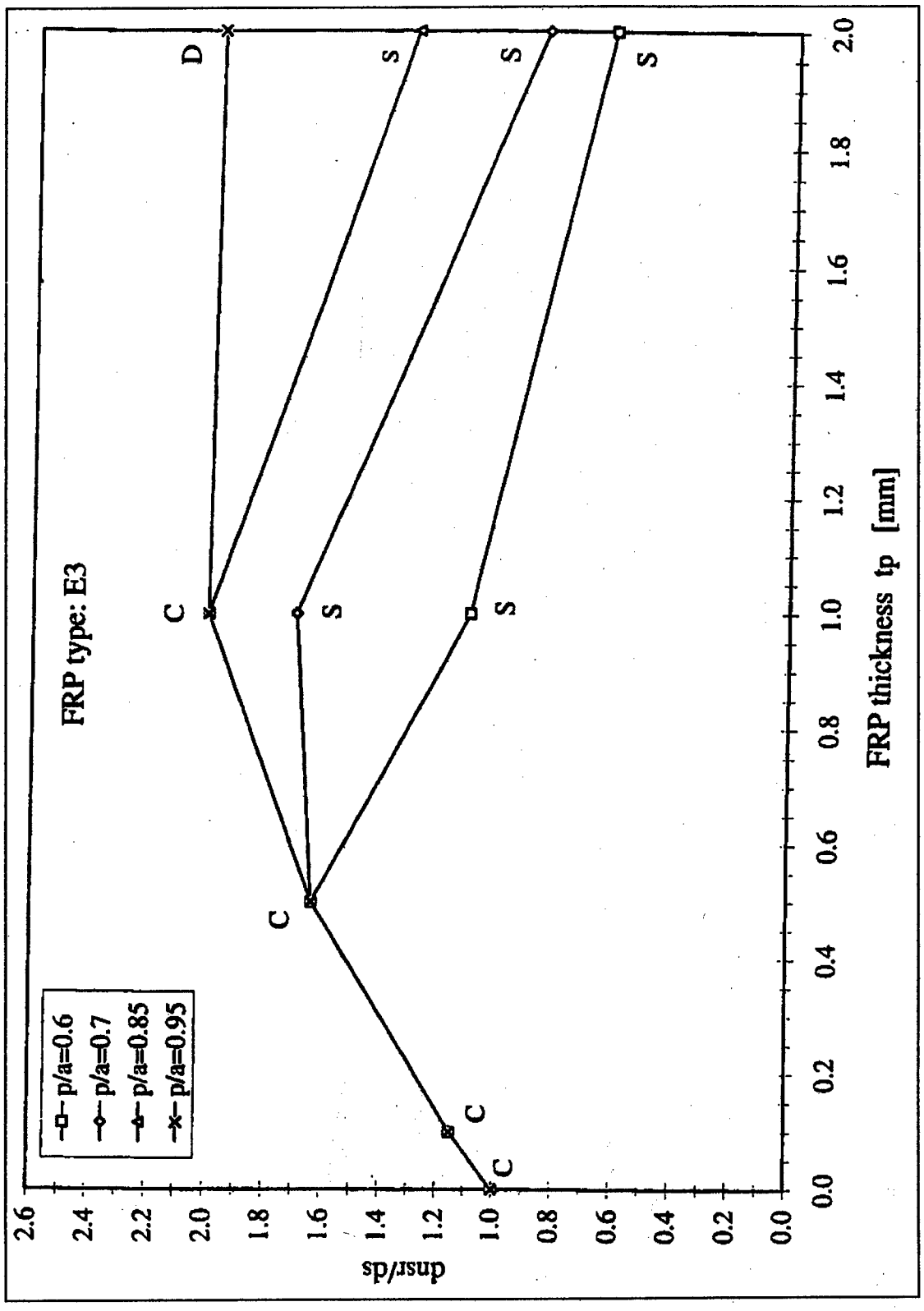


Figure C5c. Ratio between deflection at new service load of the FRP reinforced beam d_{nsr} and the deflection at the service load of the reinforced concrete beam d_s vs. FRP plate thickness t_p for the FRP type E3.

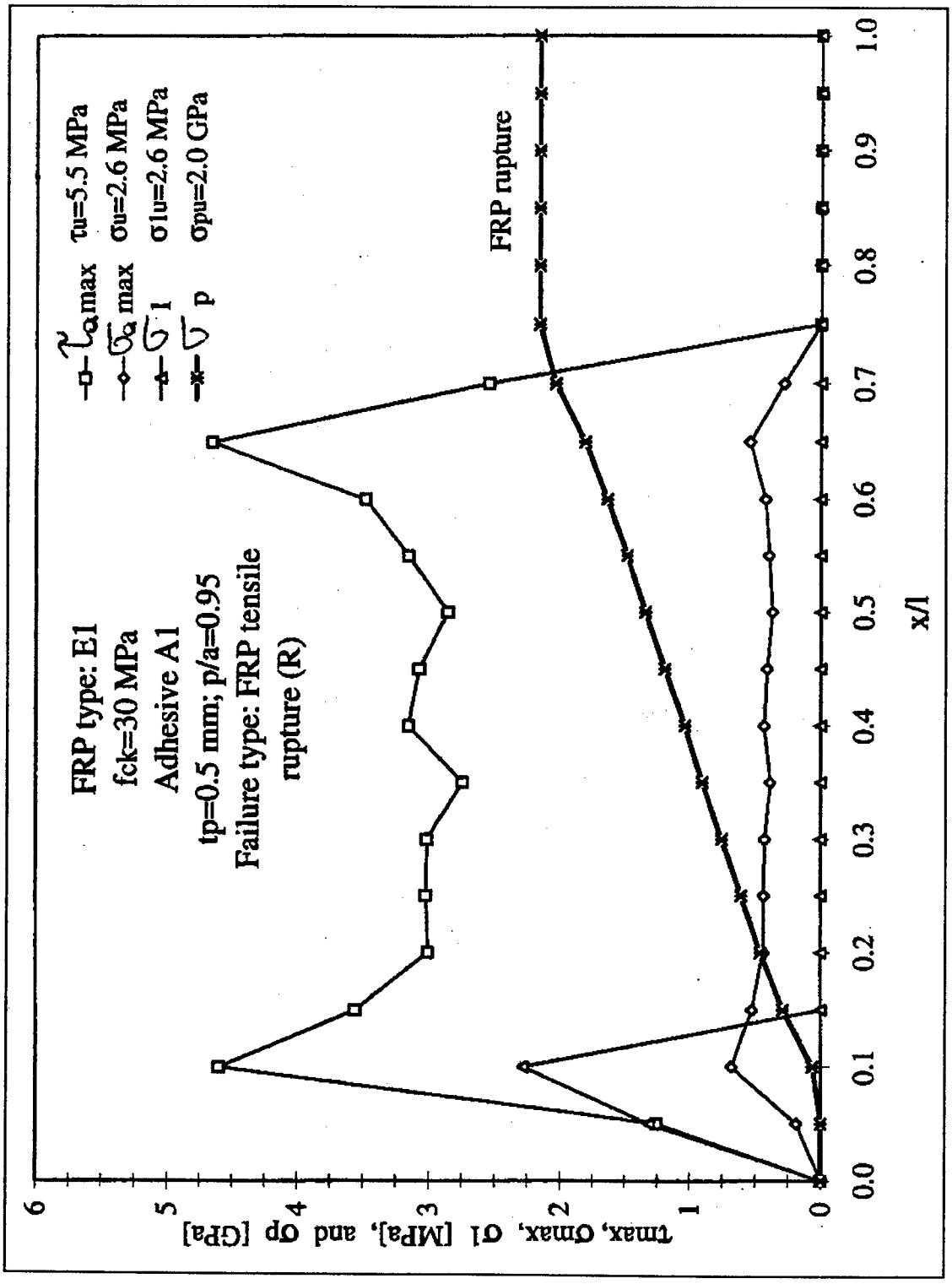


Figure C6. Distribution of selected stresses along the axis of FRP reinforced beam (FRP rupture).

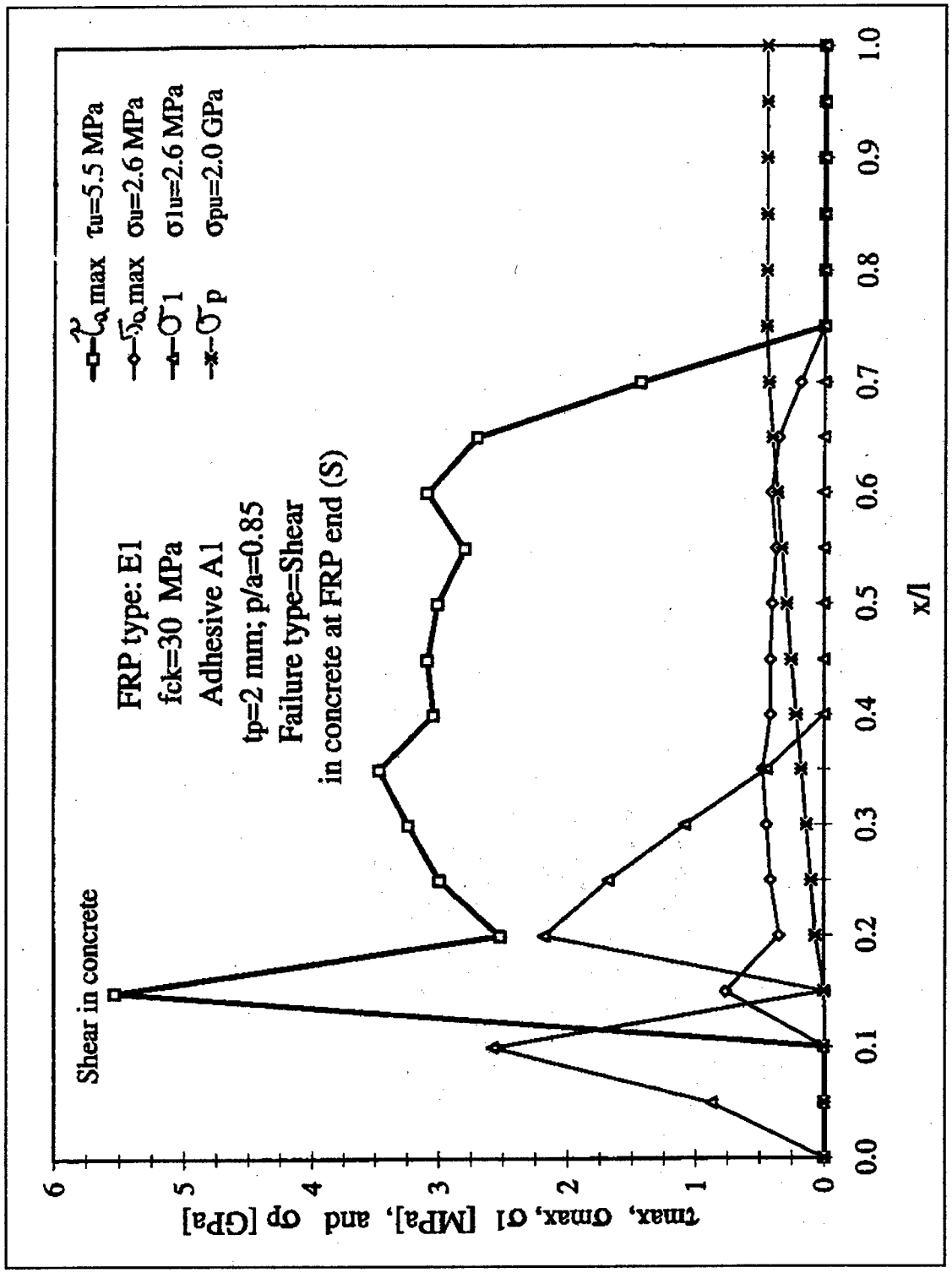


Figure C7. Distribution of selected stresses along the axis of FRP reinforced beam (Shear/tensile failure).

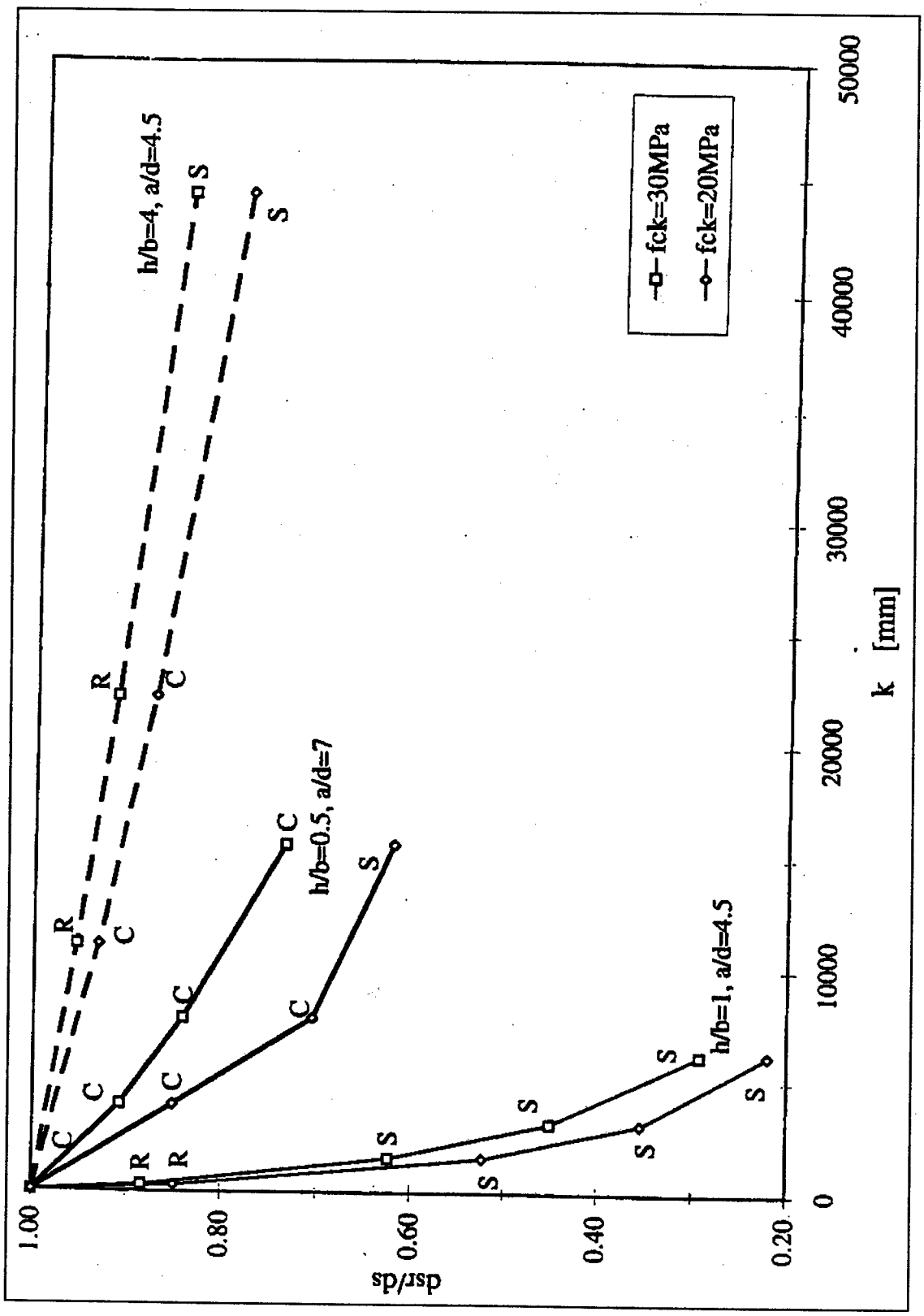


Figure C8a. Ratio between deflection at service load for the FRP reinforced beam d_{sr} and deflection at service load for the reinforced concrete one d_s vs. parameter k

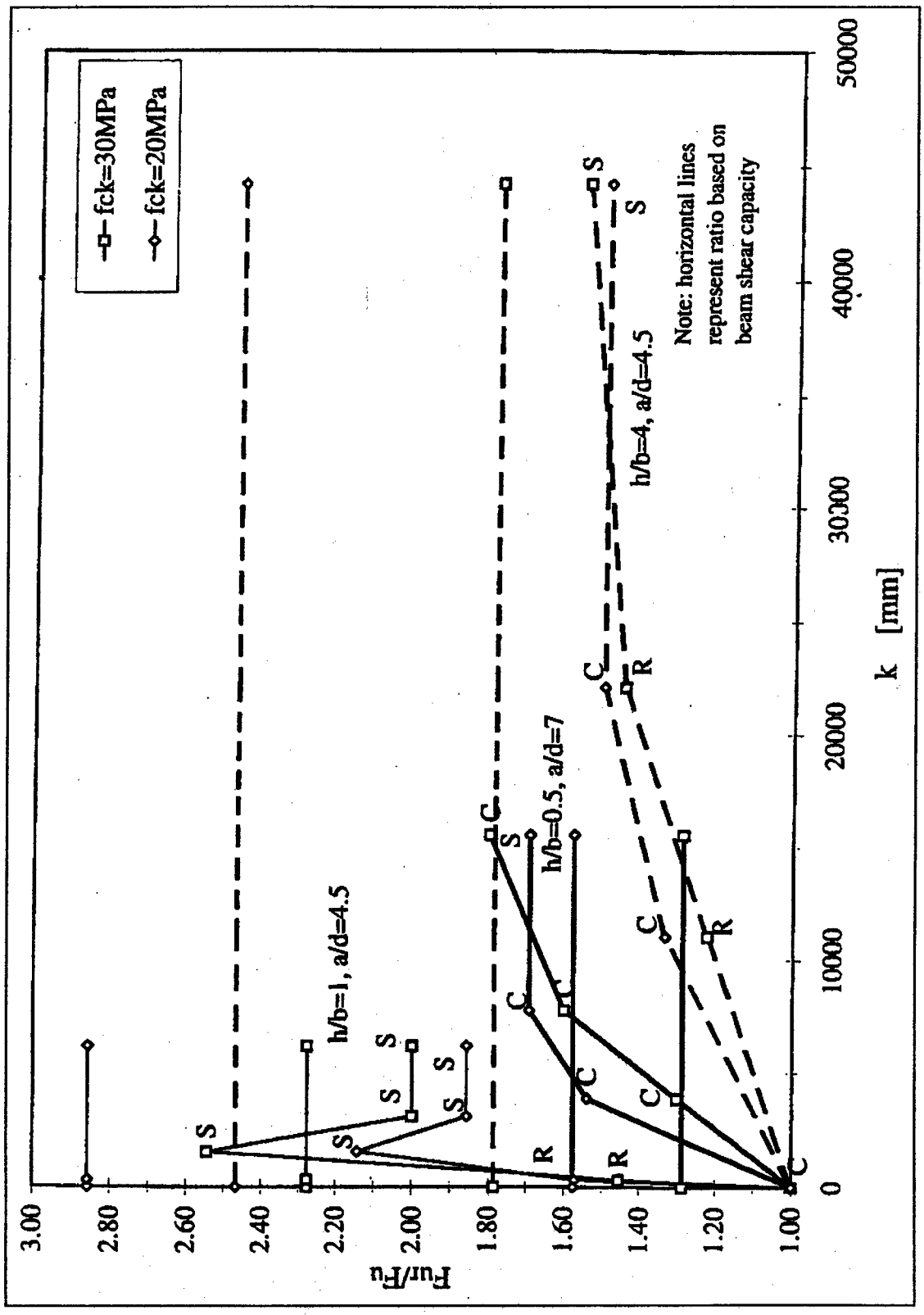


Figure C8b. Ratio between ultimate load of the FRP reinforced beam F_{ur} and the ultimate load of the reinforced concrete beam F_u vs. parameter k

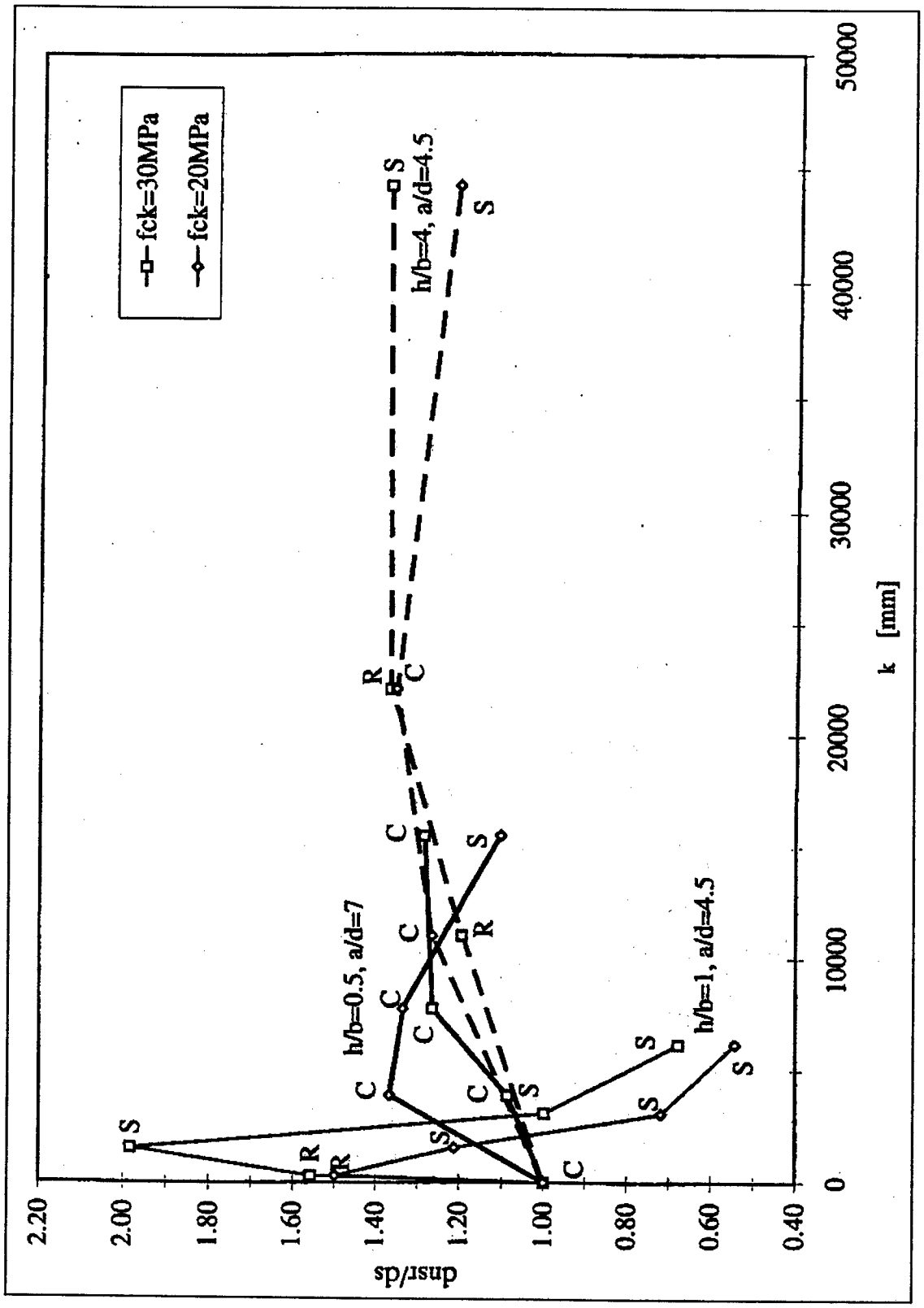


Figure C8c. Ratio between deflection at new service load of the FRP reinforced beam d_{nsr} and the deflection at the service load of the reinforced concrete beam d_s vs. parameter k

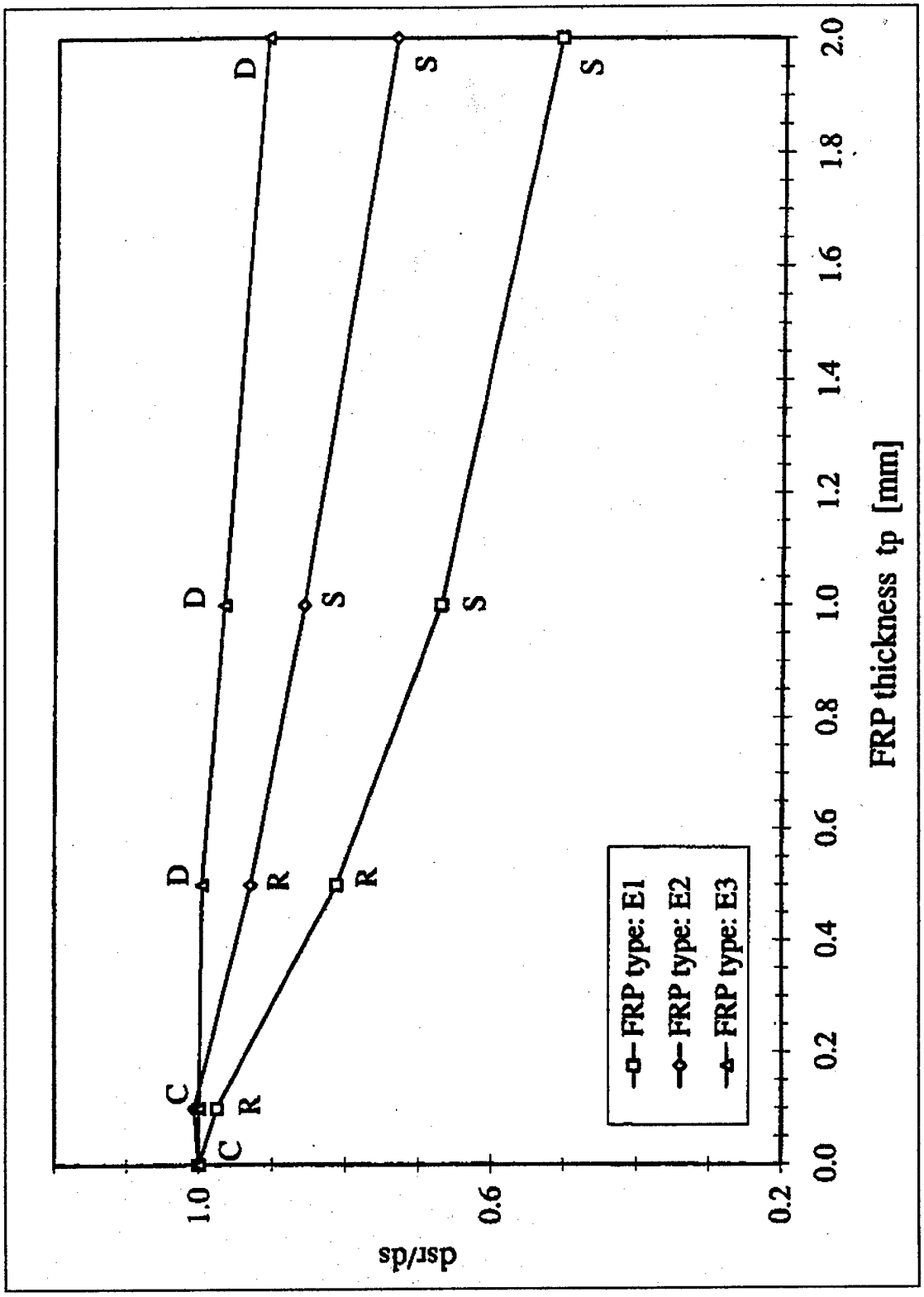


Figure C9a. Ratio between deflection at service load for the reinforced beam d_{sr} and deflection at service load for the reinforced concrete one d_s vs. FRP thickness t_p for reinforced concrete beams with distributed uniformly load.

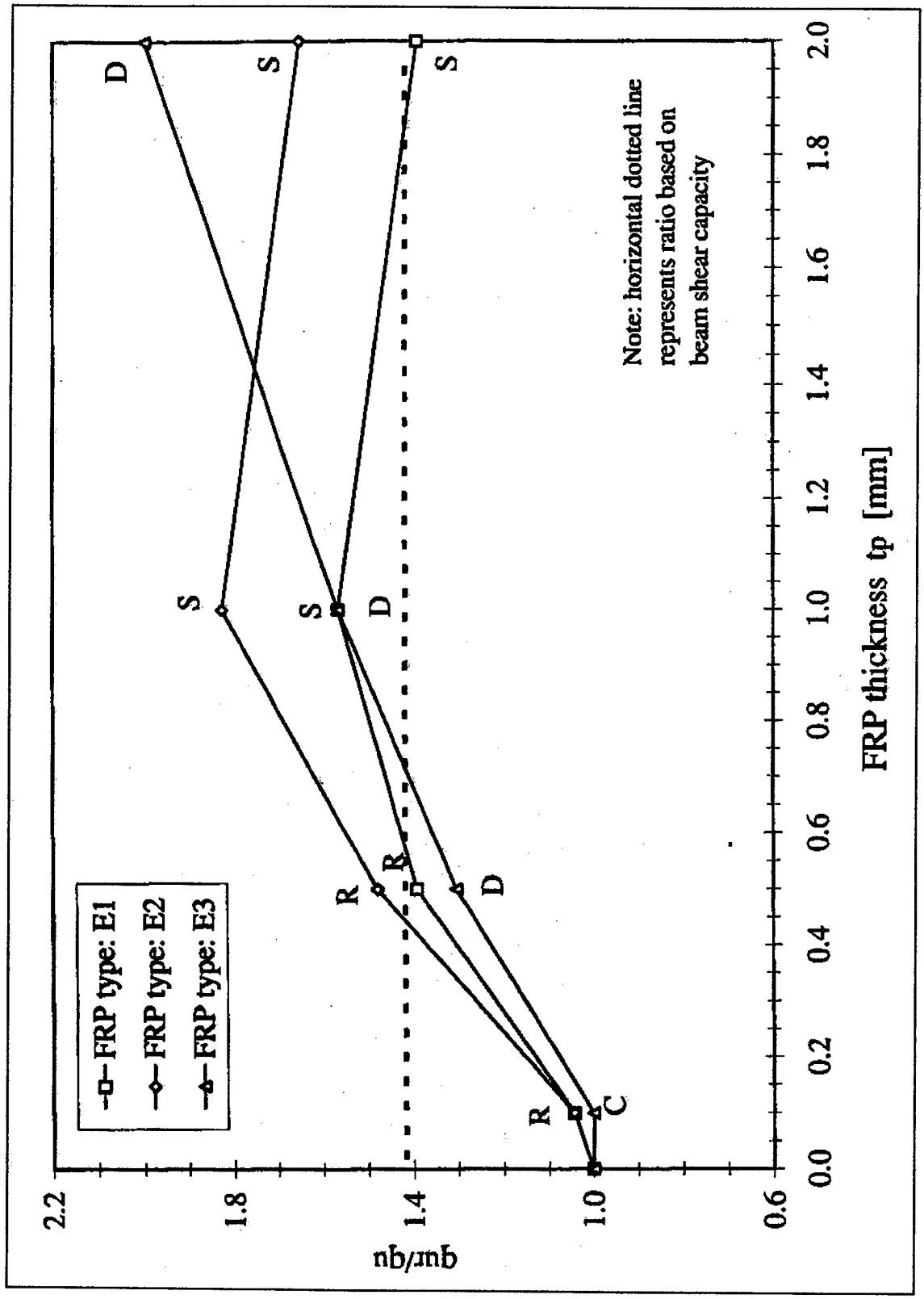


Figure C9b. Ratio between ultimate linear load of the FRP reinforced beam q_{ur} and the ultimate linear load of the reinforced concrete beam q_u vs. FRP thickness t_p for reinforced concrete beams with distributed uniformly load.

Table C1. Mechanical properties of concrete and steel.

Material	E (GPa)	ν	f_{ck} (MPa)	f_{yk} (MPa)	f_{tk} (MPa)	τ_u (MPa)	ε_{cu} (%)	ε_u (%)
Concrete C20	24	0.2	20		1.5	3.5	0.3	0.04
Concrete C30	26	0.2	30		2.6	5.5	0.3	0.06
Steel	200	0.3	= =	440	600	= =	= =	10.0

= = Not applicable

Table C2. Mechanical properties of FRP and adhesive.

Material	Type	E (GPa)	f_t (MPa)	ε_u (%)
FRP	E1	400	2000	0.5
	E2	150	2250	1.5
	E3	50	1500	3.0
Adhesive	A1	3	60	2.0
	A2	11	33	0.3

Table C3. Effect of adhesive.

FRP type	p/a	t_p (mm)	Adhesive A1		Adhesive A2	
			Failure mode	$F_{u'}/F_u$	Failure mode	$F_{u'}/F_u$
E1	0.60	0.1	R	1.27	R	1.27
		0.5	S	1*	S	1*
		1	S	1*	S	1*
		2	S	1*	S	1*
	0.85	0.1	R	1.27	R	1.27
		0.5	S	2.00	S	2.00
		1	S	2.20	S	2.00
		2	S	1.82	S	1.82
	0.95	0.1	R	1.27	R	1.27
		0.5	R	2.73	D	2.00
		1	D	3.09	D	2.73
		2	D	2.91	D	2.91
E2	0.60	0.1	R	1.36	S	1.09
		0.5	S	1.18	S	1.09
		1	S	1*	S	1*
		2	S	1*	S	1*
	0.85	0.1	R	1.46	D	1.09
		0.5	S	2.55	D	1.64
		1	S	2.00	D	1.82
		2	S	2.00	S	2.00
	0.95	0.1	R	1.46	D	1.09
		0.5	D	2.73	D	1.64
		1	D	3.09	D	1.82
		2	D	3.27	D	2.55
E3	0.60	0.1	C	1.18	D	1*
		0.5	C	1.64	D	1.18
		1	S	1.46	S	1.27
		2	S	1.09	S	1*
	0.85	0.1	C	1.18	D	1*
		0.5	C	1.64	D	1.27
		1	C	2.18	D	1.46
		2	S	2.18	D	1.64
	0.95	0.1	C	1.18	D	1*
		0.5	C	1.64	D	1.27
		1	C	2.18	D	1.46
		2	D	2.91	D	1.64

* Shear failure or debonding are detected at load lower than the unrepaired beam, the reinforced concrete beam does not completely fail and from this point on behaves like the unrepaired.

Appendix D: Feasibility Study On Using GFRP for Tie Back Arrangements

Introduction

Abutments of bridges and dams behave as retaining walls to resist the lateral pressure from the earth backfill. Some abutments tend to move or rotate due to the vibration of the backfill, movement of traffic above the fill, or hydrostatic pressure in combination with backfill pressure. These effects on the abutment result in lateral movement of the wall or rotation of the wall with reference to the base. The conventional method of rehabilitating these walls are by using some type of tie back arrangement. This involves installing a tension member to hold the walls from further movement and some type of anchorage for the tension member into the soil in the backfill area. Traditionally, steel cables or bars are used for the tension member and a concrete dead man is used to anchor them. Since movement of the wall may continue at a lower rate, soil conditions and the distance between the wall and the dead man become very important in controlling the stresses in the tension member. Depending on the backfill soil condition, generally, twice the height of the wall is required for the length of the tension member.

There are two problems with using steel cables for the tension member to hold the walls. First, the steel is buried in soil (backfill) and, with the presence of moisture, is subject to corrosion over time. The second problem is the development of high stresses in high modulus steel (29 Msi) due to the movement of the wall. These two problems require an alternate high strength material which is noncorrosive and has a low modulus. Glass fiber reinforced polymer (GFRP) is a solution to these problems. A ½ in. diameter GFRP cable has a tensile strength of 195 ksi, a modulus of nearly 7.2 Msi and will not corrode in moist soil.

The design of the tie back arrangements with a concrete dead man and tension member is illustrated using theory and design from the *Steel Sheet Piling Design Manual* (U.S. Steel, July 1975).

Objective

This study focuses on the feasibility of using GFRP cables for a tie back arrangement instead of steel cables where corrosion and wall movement are very critical. Using the South Abutment of Leech Lake Dam in Minnesota as an application example, a design example was developed for similar sites.

Design

Design of tie back arrangements require a tension member with high tensile strength and the ability to stretch to accommodate movement of the wall in a high moisture content back fill. GFRP cables have a high tensile strength with no deterioration in soil with high moisture content. Hence GFRP cables are a good substitute for steel in a tie back arrangement. Design procedures using GFRP cables are similar to conventional methods using steel cables. The total soil pressure is calculated for a particular case to determine the number of GFRP cables required to hold the wall. The design strength of the GFRP is the only thing different from steel bars. A design example will be shown to illustrate the method of design.

Economy

Either DYWIDAG steel bars or GFRP cables can do the job. With 150 Ksi strength steel, the DYWIDAG bars require a 5/8 in. diameter while GFRP cable needs a ½ in. nominal diameter. The current cost of DYWIDAG bar is $1.50 per foot while the cost of the GFRP cable used for this study is $1.10 per foot. In addition, the steel rods will corrode and require more length for the tie back arrangement since the modulus is nearly four times that of the GFRP cables. This length difference translates into a shorter excavation requirement and associated savings in construction costs using GFRP. GFRP cables are also economical compared to the cost of Carbon or Aramid FRP cables which are much higher in cost. The GFRP material is the best choice for this application.

Codes and Specifications

No codes or specifications are available for the use of conventional materials, such as steel, for this type of application. Hence, the lack of specifications will not affect the use of the GFRP cables for tie back arrangements. The GFRP cables should be supplied from a reliable source, however, with required mechanical properties.

Laboratory Tests

Introduction

The movement of a wall produces stresses in tension members used for tie back arrangements. As a result, tie back cables and/or bars must be capable of extending with the movement of the wall. Stresses produced on these tension members depend on the modulus of elasticity and the cable/bar length. To evaluate the ability of GFRP cables and steel DYWIDAG bars to stretch with the wall movements, laboratory testing on these materials was conducted. For the design parameters, the GFRP mechanical properties were determined in the laboratory while standard published mechanical properties for steel DYWIDAG bars were used. Two GFRP cables and one steel bar were attached to a rigid steel frame. The materials were tested to evaluate their behavior under incremental stretching to simulate the movement of a wall. This section deals with those tests.

Materials

Possible material solutions to a wall movement problem are as follow:

1. Use steel cables or steel bars such as DYWIDAG threaded bars to tie back the walls to a dead man. In the Leach Lake Dam example, the moisture condition of the soil is very high and steel rods or cables will corrode with time. In addition to this a slight movement of the wall will create a very high stress in the steel due mainly to the short length of the cable and high modulus of the steel.
2. Reduce the backfill soil pressure by using a lighter material such as Styrofoam or light weight concrete. Styrofoam is not suitable in many cases if the soil has to retain moisture. Lightweight concrete is cost prohibitive.
3. A better solution is to use a tie back arrangement with a noncorrosive, low modulus, cost effective GFRP material. GFRP cables (seven E glass pultruded rods of 4 mm diameter twisted at one twist per yard) with a noncorrosive

threaded rod cable termination can be used. Table D.1* compares the mechanical properties of ½ in. diameter GFRP cable to those of 5/8 in. diameter steel DYWIDAG bars. These GFRP cables should have a stainless steel threaded rod as cable termination to stretch the cables and to adjust the tension in the cables during the life of the structure.

The length of the cable is an important factor for the excavation of the backfill. When the movement of the wall is allowed, such as in a slope stability problem, the length of the tieback system depends on the stretch of the material (cable/rod). In the case of GFRP, the modulus is one fourth that of steel and, therefore, needs only one fourth the length of cable to develop the same extension or movement of the wall. In the case of the Leech Lake Dam example where large unexpected wall movement cannot be allowed, cable length differential is not an important design factor.

Test Specimens

GFRP cables were made using seven 0.157 in. (4mm) pultruded rods and twisted at least one twist per yard (nominal diameter of the cable is ½ in.). The pultruded rods were made by NEPTCO* using E glass fibers and epoxy resin with nearly 70% fiber volume. The same type of cables were used in previous projects (Iyer 1995). A four foot cable as specified in a proposed ASTM standard test method was made for the tension test and two 18 ft long cables were made for the stretching test. Steel tube anchorages (developed by South Dakota School of Mines and Technology) were used for the GFRP cable end terminals.

A 5/8 in. diameter and 20 ft long steel bar supplied by DYWIDAG System International, USA, was used for the extension test. DYWIDAG threaded nuts were used as end terminals.

Tension Test on GFRP Cables

A four foot GFRP cable was tested for tensile strength and modulus in accordance with a proposed ASTM standard. An electrical strain gage was installed on one of the rods of the cable. A MEGADAC data acquisition system was used to monitor the strain readings during the test. A 400,000 lb capacity Tinius Olsen testing machine was used to conduct the tension test. Steel tube

* All tables are found at the end of this appendix.

anchorages were used to hold the ends of the cable. Readings were taken at every 1000 lb interval and the results are shown in Table D2. The stress versus strain diagram is shown in Figure D1*. From the diagram it can be seen that the modulus is 7.2 Msi., the ultimate stress is 195 Ksi., and the ultimate strain is 2.74%. The failed specimen is shown in Figure D2. These results agree with test results of similar GFRP cables provided by NEPTCO for previous projects.

Extension Test

A very stiff self straining frame as shown on Figure D4 was used to hold the ends of the cables/bar for the stretching test. One steel bar and two GFRP cables were used for this test. All three members were stretched so that they were snug tight as shown in Figure D4. Electrical strain gages were installed on the tension members and the MEGADAC data acquisition system was used to monitor the strain.

A turn-off-nut method was tried to extend the cable/steel bar one half inch per day. The turn-off-nut method did not work for steel bars because the threads were very coarse (high pitch). Since the threads on the GFRP cables were standard threads, (ten threads per inch) that method worked for GFRP cables. The stretching method was switched to a central hole jack for extending the rod/cables. The stretching of these members was measured and the results are shown in Table D3. Figure D5 shows the jacking end of these members.

On the fourth day of the test, the steel started yielding while the GFRP cables were still in the linear region. One of the GFRP cables was released on the 8th day of testing after it reached a load of nearly 18,000 lb. Testing continued on the other cable until it failed. The GFRP cable failed on the 11th day with nearly five inches extension on an 18 ft length (2.3% strain, close to the ultimate strain of 2.7%). The jacking load or load on the cable at the failure point was 23,800 lb. This is less than the ultimate strength of 26,000 lb. This loss in ultimate strength is mainly due to loading in stages for 11 days and leaving higher loads (above 18,000 lb) for a number of hours on the cable. The failure mode was very slow and failed by breaking fibers in each rod. Unlike steel bars, the failure occurred in the cable after a period of time had passed following the increase in load. The cable provided a warning of the impending failure with the sound of fiber breakage. The steel bar was stretched after yielding with very little

* All figures are found at the end of this appendix.

increase in load while strain increased up to 2.64%. Finally, the pulling end zone of the bar (outside the frame) failed on the 13th day with a load of 45,200 lb. It is interesting to note that the steel bar failed in the pulling section of the jack and not in between the bulk heads. This is due to stressing this section during the jacking and then releasing the load as the jack was released after tightening the nut. This created a fatigue load condition above the yield point of the steel. Failure was sudden and occurred during the loading or jacking.

Discussion of Test Results

The modulus of elasticity of GFRP is 7.2 Msi and is nearly one fourth that of steel (29 Msi). The steel bar began yielding on the fourth day or at 2-5/8 in. of elongation for the 18 ft length. The GFRP cable reached 18,000 lb on the 8th day with an elongation of 3-5/8 in. and failed on the 11th day at a load of 23,600 lb with an elongation of 5 in.

Comparing the data, the GFRP cable was able to take more extension for less load. It carried double the extension for nearly half the load carried by steel bar. This definitely proves the ability of GFRP cable to resist larger movement of a wall abutment without failure. Repeated loading of steel bars have a problem with breaking the stressing section of the bars due to fatigue and yielding.

Summary of Laboratory Testing

For an equal extension of 3.38 inches the steel bar yielded reaching a load of 39,600 lb while the load on the GFRP cable was 16,400 lb. Table D3 shows that the load in the GFRP cable was half the load of steel bar and this load difference required less cross sectional area for GFRP cables (0.123 in^2) compared to steel bar (0.301 in^2). These results confirm the basic relationship between the modulus and the cable elongation. The stretching of a material is inversely proportional to the modulus of the material. Hence the lower modulus of GFRP cable reduces the load and stresses in the cables for the same degree of elongation resulting in less possibility of failure.

In this test the turn-off-nut method did not work for the steel bar while the fine threaded rod anchorages used for the GFRP cables worked satisfactorily. Hence adjustment of tension in the GFRP cables was possible by turning the nuts without the use of jacks.

Typical Design Example

Problem Statement

The dimensions of the South Abutment wall of Leech Lake Dam near Federal Dam, Minnesota, was used as a basis for this design example. The soil properties and other backfill conditions used were also based on that site. The south abutment is a concrete structure of 5 ft wide and nearly 15 ft high. Field studies indicate that the wall is separating from the wing walls due to the effect of soil pressure behind the abutment. A stability analysis conducted by U.S. Army Engineer District Detroit (1991) on this dam corroborates this problem in the south abutment. Even with these cracks, the structure is not in imminent danger of failure and can be rehabilitated with tie back arrangements.

Design Calculations

Figure D6 shows a tie back arrangement with the dead man, the tension member, and the wall. The tension members (cables/rods) are located at a height two-thirds of the way from the top of the wall to coincide with the total soil pressure on the wall. This type of design will eliminate any differential lateral loads on the wall and reduce the bending moment in the wall. The load on the cables was calculated using the soil mechanics equations for the soil properties at the South Abutment of the Leech Lake Dam. All of the equations used in this design are extracted from the *Sheet Steel Piling Design Manual* (U.S. Steel, July 1995).

Notation Summary

γ = Soil density

ϕ = Angle of repose

δ = Friction angle between the soil and the wall

Ka = Active earth pressure coefficient

Kp = Passive earth pressure coefficient

Kr = Pressure coefficient

Ro = Anchor resistance factor

R = Resistance factor for dead man condition

q_m = Vertical effective stress on the dead man

T_{ult} = Ultimate tension in the bars/cables

T_{actual} = Actual tension in the bats/cables

Pa = Active lateral pressure on the wall

d = horizontal distance between the wall and the dead man

H1 = Wall height

H2 = Depth to bottom of dead man

h = Dead man height

l = Width of dead man

L = Deadman spacing

Δ = Horizontal Movement of the dead man

Design Assumptions

The soil is coarse sand.

The water table level is below the wall during the construction period.

The design load for 5/8 in. diameter steel DYWIDAG bar is 15000 lb.

The design load for ½ in. diameter GFRP cable is 13000 lb.

γ = 115 pcf

ϕ = 35

δ = 17.5°

H1 = 15 ft

H2 = 11 ft

h = 2 ft

l = 2 ft

Calculate Wall Loading

$$Ka = \frac{1-\sin\phi}{1+\sin\phi}$$

= (1-sin 35°) / (1 + sin 35°)

=0.27

The value of Kp is derived from the graph of Ka vs. δ/ϕ (U.S. Steel 1975, p 10)

δ/ϕ = -17.5/35

= -0.5

Kp = 6.56

$$Pa = \frac{\delta\gamma H1^2}{2}$$

= 15^2 x 115 x .27/2

= 3493 lb/ft or 3500 lb/ft

Therefore the full width of the 15 ft wall lateral pressure = 3500 x 15

= 52500 lb

Calculate the Number of Bars/Cables Needed

Number of DYWIDAG bars = 52500/15000

= 3.5 Use 5 bars

Number of GFRP bars = 52500/15000

= 4.04 Use 5 bars

NOTE: Four bars may be sufficient to carry the load. However, using four bars may require additional external framing to support the wall. Using five bars will not require added framing because tensile stresses in the wall will not be created.

The five tension members (DYWIDAG bars /GFRP cables) are spaced at 3 ft centers as shown in Figure D7. These bars/cables connect to the wall and the dead man with proper anchorages. The GFRP cables use stainless steel tube anchorages developed at South Dakota School of Mines and Technology and the DYWIDAG bars use the special threaded nuts provided by the manufacturer.

Design Of The Dead Man

Kr is determined from the graph of Kr vs. tan δ (U.S. Steel 1975, p 48)

$\tan \delta = \tan 17.5°$

$= 0.315$

and $\delta/\phi = -0.50$

$Kr = 5.8$

$Ro = Kr - Ka$

$= 5.8 - 0.27$

$= 5.53$

Force per tension member = 52500/5

= 10,500 lb

h = 2 ft (height of the dead man of 2 x2 x 2 spaced at 3 ft centers)

H2 = 11 ft (see Figures D.2 and D.3)

l/L = 2/3

= 0.67

From graph (U.S. Steel 1975, p 51)

R/Ro = 3.5

Therefore R = 3.5 R

= 3.5 x 5.53

= 19.35

q_m = 115 (H2- h/2)

= 115 (11-1)

= 1150 psf.

Ultimate Tension in the bars/cables = q_m x h x R x l/L

=1150 x 2 x 19.35 x 0.67

= 29,826 lb

Therefore the factor of safety = T_{ult}/ T_{actual}

= 29,826/10,500

= 2.84 > 2.0 and is OK.

Distance Between The Dead Man And The Wall

The abutment wall is subjected to active pressure while the dead man is subjected to passive pressure. According to Rankine's failure theory (U.S. Steel 1975, p 5), the minimum horizontal distance between the wall and the dead man is given by:

$$H1 \times \tan(45 - \phi/2) + H2 \times \tan(45 + \phi/2) = 7.8 + 21.1$$

$$= 28.9 \text{ ft}$$

A distance of 30 ft is used for this design. This is twice the height of the wall. The distance is based on the minimum required from the soil properties. The stresses on the cables/rods depend on the movement of the wall and the elongation of the tension member.

Horizontal Movement of the Dead Man

From (U.S. Steel 1975, p 113)

$$\log_{10}(\Delta/H) = 2.5 \times T_{actual}/T_{ult} - 2 \sin 35° - 2.6$$

$$= 2.5/2.47 - 1.147 - 2.6$$

$$= -2.9$$

Therefore $\Delta/H = H2/10^{2.9}$

$$= H2/794$$

$$= (11 \times 12)/794$$

$$= 0.166 \text{ in.}$$

The result is very small and no special care is needed.

Use five 2 ft by 2 ft by 2 ft concrete blocks spaced at 3 ft centers as shown in Figures D1 and D2. Place the blocks such that the centers of these blocks are 10 ft below the ground level.

Summary of Design

For a wall height of 15 ft, the soil properties of the back fill require a minimum distance or length of tie back cable to be close to 30 ft. In certain cases, such as slope stability problems, the retaining wall will move and the tie back arrangements should accommodate this movement without failure. The

modulus of elasticity of steel bar (29 Msi) is four times that of the GFRP cable (7.2 Msi) so, for the same movement of the wall, the length requirement of the steel bar must be four times that of the GFRP cable. In such a case the excavation length of the back fill will be four times that of the GFRP cable arrangement. In other words, the usage of GFRP cable reduces the overall cost of excavation for the project in addition to the savings in the cable lengths.

Findings

Advantages to using the GFRP cables instead of steel bars or cables are as follow:

1. The length of the tie back cables can be reduced to a minimum required from the soil properties and height of the wall (in this case only twice the height of the wall). This will reduce the overall cost of earth work needed for the project in addition to savings in cable lengths.
2. No corrosion of the tie back cables
3. Lower modulus of GFRP cables will reduce higher stress development in the cables due to movement of the wall and result in less likelihood of failure.
4. The cost of GFRP cable is less or equal to the cost of DYWIDAG bar.
5. Adjustment of tension in the cables, something not possible in the steel cables, are possible with GFRP cables

References

1. US Army Corps of Engineers Detroit District Report on Leech Lake Dam, 1991.

2. Steel Sheet Piling Handbook by United States Steel, 1976.

3. Steel Sheet Piling Design Manual by United States Steel, July 1975.

4. Iyer, Srinivasa "Demonstration of Advanced Composite Cables for Use as Prestressing in Concrete Waterfront Structures" Final Report to US Army Corps of Engineers Construction Engineering Research Laboratory, Illinois, November, 1995.

List of Appendix D Figures and Tables

Figures

Figure D1. Stress v. strain diagram for GFRP cable. 15
Figure D2. GFRP cable testing. 15
Figure D3. Test Setup: two GFRP cables and one DYWIDAG bar. 16
Figure D4. Closeup of tube anchorages used for GFRP cables. 16
Figure D5. Bulkhead and pulling arrangement of cables. 17
Figure D6. General view of the tie back arrangements. 17
Figure D7. Side view of the tie back arrangements. 18

Tables

Table D1. Mechanical properties of 5/8 in. diameter steel DYWIDAG bars vs. ½ in. diameter GFRP cable. 18
Table D2. Tension test on GFRP cable 19
Table D3. Extension Test on GFRP Cables and DYWIDAG Bar. 20

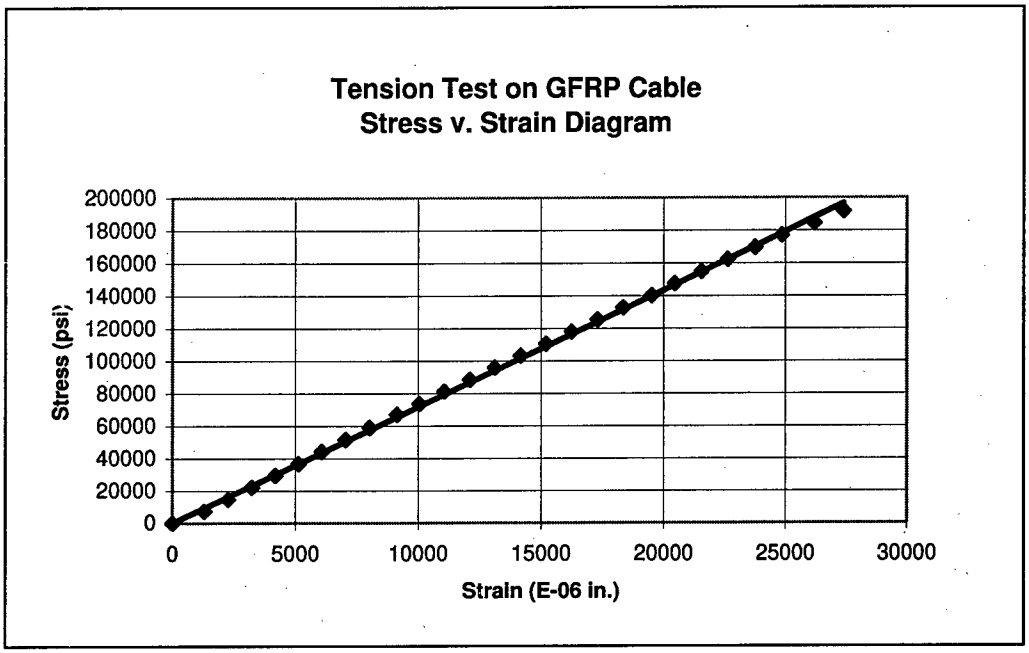


Figure D1. Stress v. strain diagram for GFRP cable.

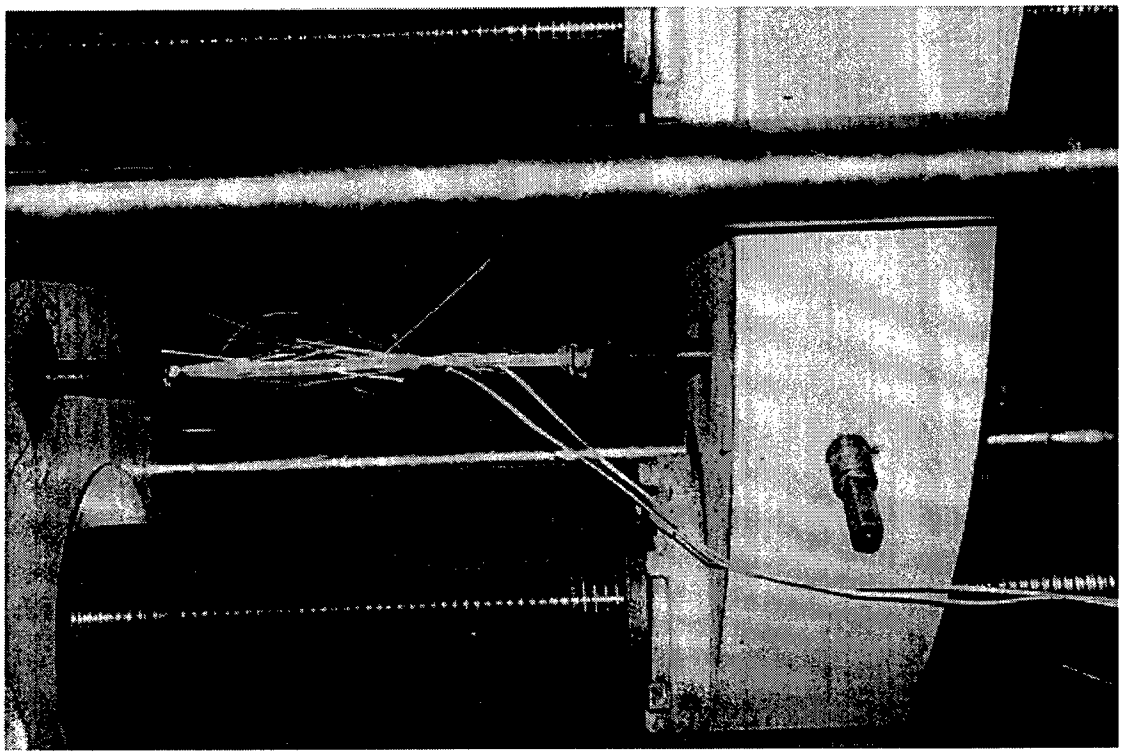


Figure D2. GFRP cable testing.

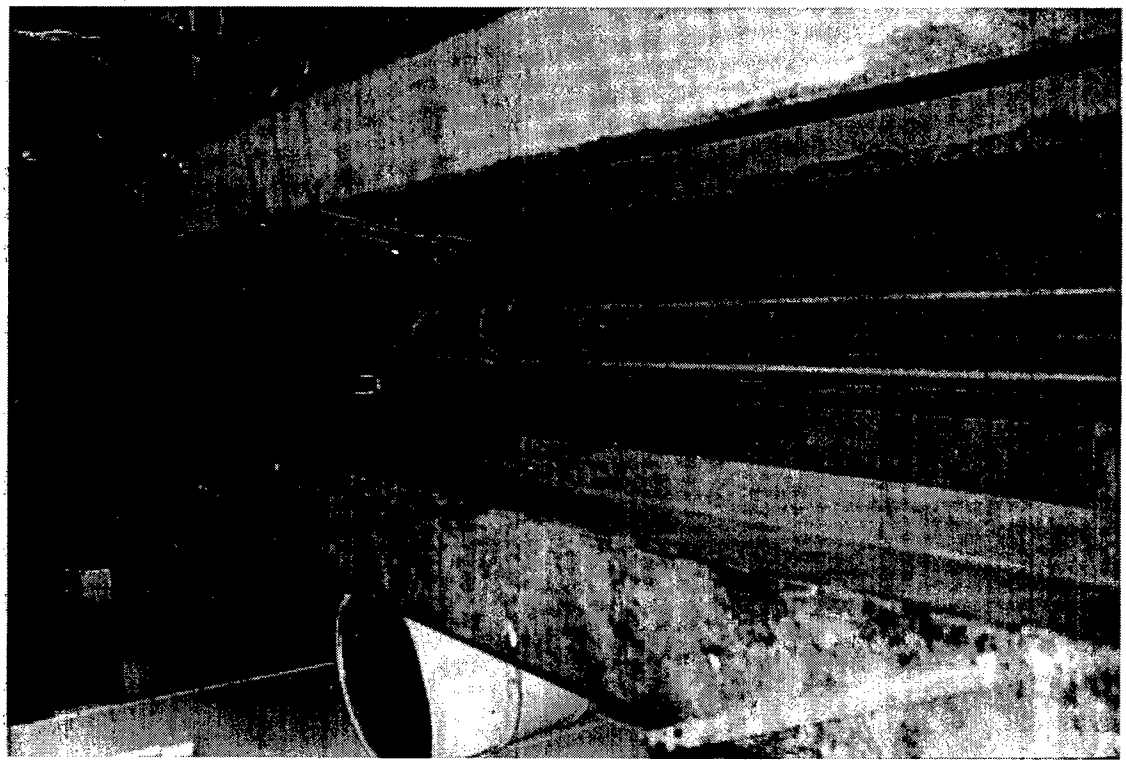


Figure D3. Test Setup: two GFRP cables and one DYWIDAG bar.

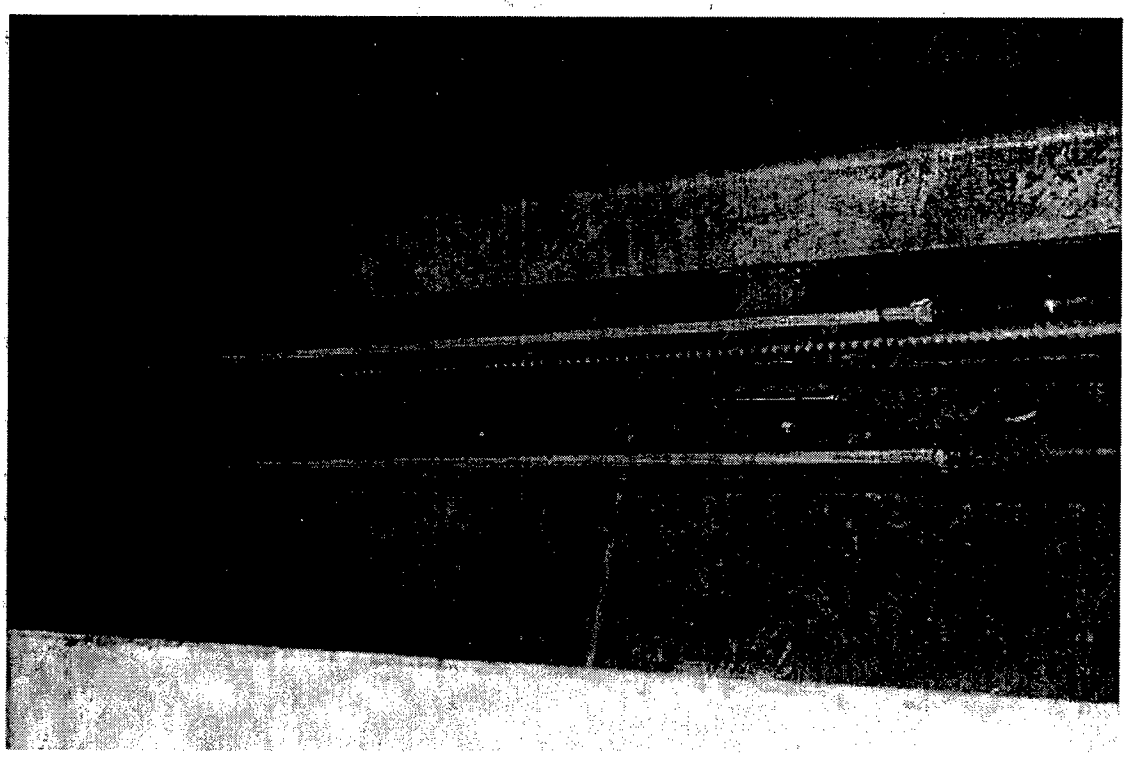


Figure D4. Closeup of tube anchorages used for GFRP cables.

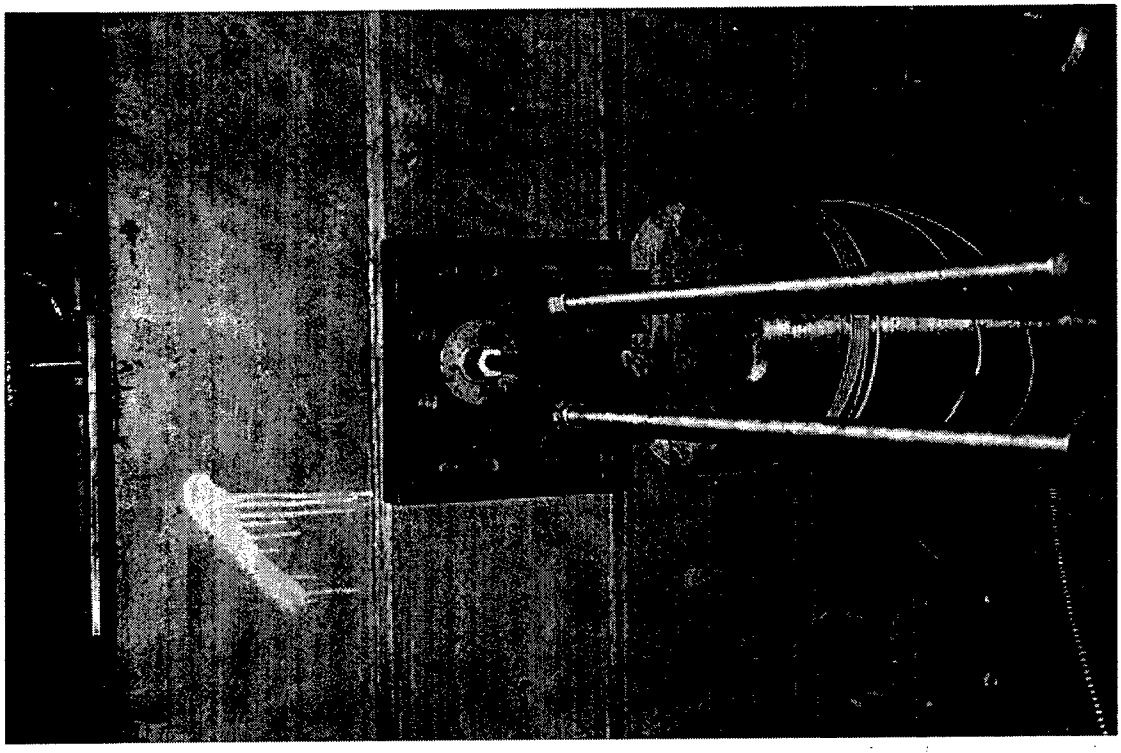


Figure D5. Bulkhead and pulling arrangement of cables.

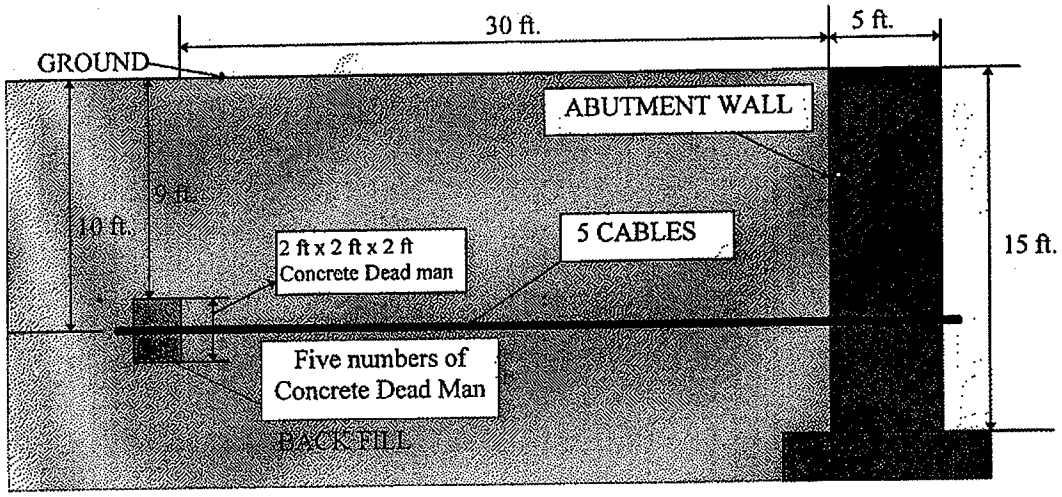


Figure D6. General view of the tie back arrangements.

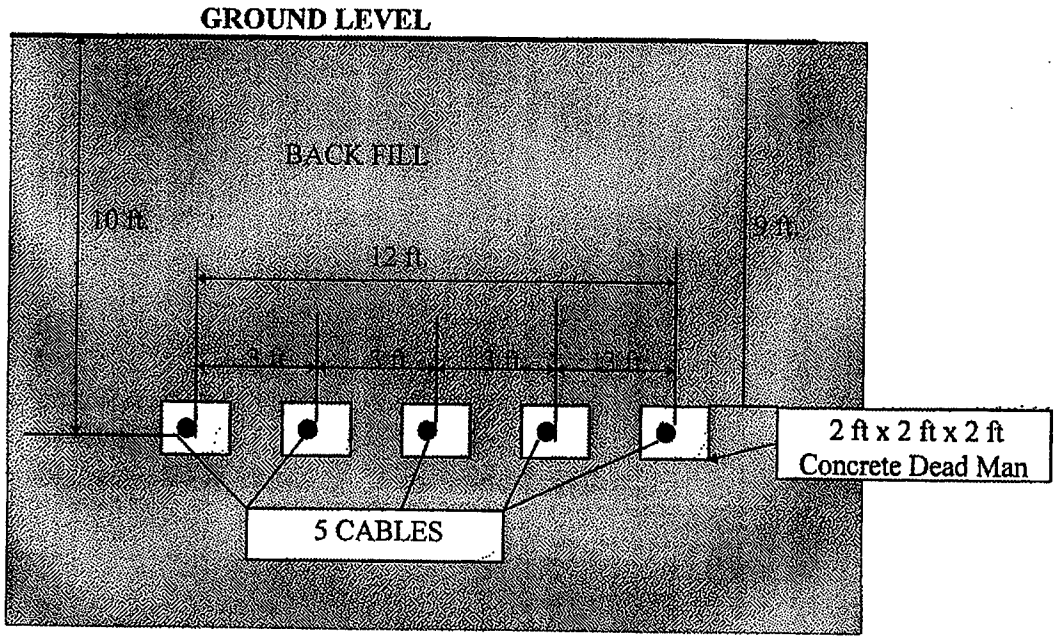


Figure D7. Side view of the tie back arrangements.

Table D1. Mechanical properties of 5/8 in. diameter steel DYWIDAG bars vs. ½ in. diameter GFRP cable.

Tie Back Material	Property	Value
DYWIDAG Bar	Tensile Strength	150 Ksi*
	Modulus	29 Msi*
GFRP	Tensile Strength	195 Ksi
	Modulus	7.2 Msi

* Standard properties for DYWIDAG bars

Table D2. Tension test on GFRP cable.

Load (lb)	Stress (psi)	Strain (Micro in.)	Remarks
0	0	0	
1000	7380	1290	
2000	14760	2260	
3000	22140	3235	
4000	29520	4186	
5000	36900	5129	
6000	44280	6075	
7000	51661	7050	
8000	59041	8025	
9100	67159	9130	
10000	73801	10056	
11000	81181	11060	
12000	88561	12100	
13000	95941	13120	
14000	103321	14165	
15000	110701	15209	
16000	118081	16245	
17000	125461	17300	
18000	132841	18345	
19000	140221	19505	
20000	147601	20445	
21000	154982	21550	
22000	162362	22630	
23000	169742	23750	
24000	177122	24850	
25000	184502	26190	
26000	191882	27400	
26421	194989		Failed

Rod dia. = 0.157 in. Test Date: 7/10/97

Cable Area = 0.135 sq. in. Anchorages: Tube anchorages at both ends

Cable Length = 48 in.

Table D3. Extension Test on GFRP Cables and DYWIDAG Bar.

Date	Day	Time	Strain gages (μ in. per in.)			Extension (in.)			Load at jack end (lb)			Remarks
			Steel	*GFRP Left*	*GFRP Right*	*Steel*	*GFRP Left*	*GFRP Right*	*Steel*	*GFRP Left*	*GFRP Right*	
11-Jul	1			0.0	0	0	0	0				
11-Jul				2501	2485		0.375	0.5				
13-Jul	3	15:40	0	2166	2485							initial reading steel
13-Jul		15:42	2241	2166	2218	0.25						
14-Jul	4		4049.5	4886	5068	0.75	1	1				
15-Jul	5		6625	7631	7609	1.5	1.5	1.685				
16-Jul	6		6630	7464	7441							
16-Jul			9109	10261	10102	2	2	2.125				
17-Jul	7		9120	10004	9843							
17-Jul			12321	12943	12507	2.75	2.5	2.685				
18-Jul	8		12300	12663	12137		-29					
18-Jul			14834	15623	15710	3.38	3.31	3.25	39600	16400	16400	steel yielding
19-Jul	9		17015.5	15370	15315							
19-Jul			16818.5	18289	17770	4	3.625	3.625	40000	18000	20400	
21-Jul	11		19197.5		20514	4.63		4.25	40000		22400	left cable released
22-Jul	12	10:30	19126.5		19977							
22-Jul		10:35	21494.5		23168	5.5		4.875	40000	23600	23600	
22-Jul		11:30										right cable failed
23-Jul	13		24187			6.13			42600			
24-Jul	14	9:40	23475			6.88			44600			rod failed @ jacking

GFRP Cable Properties:
Rod dia. = 0.157 in.
Cable Area = 0.135 sq. in.
Cable Length = 18 ft
Cable Modulus = 7.2 Msi
Anchorages: Tube anchorages at both ends

Steel DYWIDAG Bar Properties:
Bar dia. = 5/8 in.
Rod Length = 20 ft
Anchorages: Special nut anchorages

Appendix E: Low-Temperature Evaluation of FRP Composites Bonded to Concrete

Overview

For repair of concrete with composites in cold regions, compatibility is the major issue. Compatibility is the measure of the physical, chemical, electromechanical, and dimensional properties between the repair materials and the substrate. The correct choice and proper use of composites system for repair in cold-climatic conditions are critical to the achievement of long service life for repaired structure. The environment in cold regions is generally aggressive. Not only severe temperature fluctuations, but also other variables such as higher oxygen concentration, abrasion, isolated internal and external environments, and improper care can easily create conditions of failure.

CRREL's objective under this CPAR project was to study and analyze if the cold climatic conditions would impair the performance of the composite-repaired concrete structures. The most important concern in this area is the polymeric composite's inherent characteristics of inducing thermal stresses under severe temperature fluctuations. The thermal stresses can degrade the polymer composite itself, or cause damage to the concrete/composite bond interface. Although the issue is much broader, the scope of these investigations was narrowed down to the following six study areas, mainly in relation to beam loading:

1. Review of the state-of-the art composites durability under severe cold climatic conditions.
2. Influence of low temperatures on the load capacity of beams repaired with a new composite bonding technique.
3. Low-temperature fatigue-load effect on bond strength and failure load.
4. Low-temperature thermal cycling effect on composite bond to concrete.

5. Influence of low temperature on the strength development along bond length.
6. Developing a new test technique for bond strength study by tension loading.

Background

Bonding of steel plates to concrete with epoxy resin is a common practice in the rehabilitation of bridges and buildings. In cold regions, because of deicing salt and other corrosion agents, the bond at the glued steel/concrete interface deteriorates rendering the structure vulnerable to loss of strength and possible collapse. This project has attempted to use unidirectional FRP sheets of carbon (CFRP) and glass (GFRP) bonded together with a polymer matrix (epoxy, polyester, vinyl ester) to form a composite material as a substitute for steel. The advantages of this system are immunity to corrosion, a low volume to weight ratio, and elimination of joints in the reinforcing plates. Although this new construction technology has received a foothold in the construction industry (Meier 1987), no major effort has been directed to study the potential degradation of the FRP itself, and its bond to concrete, under the severe climatic conditions of the cold regions.

In the northern regions of the United States, the temperature range of exposed structures is approximately -46 to 38 °C (-51 to 100 °F) (Berwanger and Sarkar 1973). The concrete repairing techniques to be used in these regions must address the effects of such temperature extremes. There are three constituent materials that make up an FRP externally reinforced concrete beam: (a) concrete, (b) fiber-reinforced polymers (FRP), and (c) the adhesives. The low-temperature properties of these constituents are reasonably well documented. But very little is known of the overall response of such FRP-reinforced concrete beam to low-temperature exposure. This section reviews the material behavior of concrete, FRP, and some limited data on the FRP externally reinforced concrete beam at low temperatures.

Low-Temperature Behavior of Concrete

Low-temperature properties of concrete, including compressive and tensile strengths, elastic modulus, and coefficient of thermal expansion, are well documented. Rostasy et al. (1979) have performed extensive tests on the resistance of concrete in compression and tension in cold down to -30 °C (-22 °F). Yamane et al. (1978) have shown that the compressive strength of concrete increases at low temperatures with higher moisture content, producing higher strength. They also showed that the tensile strength of concrete also increases

decreasing temperatures, although far lesser in tension than in compression. Data compiled by Browne and Bamforth (1981) for flexural strength also show a similar trend of increase in flexural strength at low temperatures. They showed that the thermal expansion coefficient is sensitive to moisture, possibly because of the presence of ice in the pores. Ice in the pores is also responsible for strength increase (Neville 1981).

Low-Temperature Behavior of Composites

Composite materials are of special interest in cold climatic conditions, because they often combine at least two chemically distinct materials, which give the composites anisotropic properties in both the microscopic and macroscopic scale. Degradation of fiber reinforced plastic composites in severe cold is well known (Lord and Dutta 1988). Extreme changes in temperature of composite materials result in several important effects. Most materials expand when temperature rises. In fiber-reinforced polymer matrix composites, the coefficient of thermal expansion of the matrix is usually an order of magnitude greater than that of the fibers. When a composite is cooled contraction of the matrix is resisted by relatively stiff fibers through fiber/matrix interface bonding, setting up residual stresses within the material microstructure.

The induced stresses at the microstructure level of the matrix/fiber interfaces, within the matrix, and in the interlaminar layer has been analyzed and experimentally investigated by many investigators (Jones 1975; Lord and Dutta 1988; Dutta 1988; Dutta and Lampo 1993). Using a mechanics-of-materials approach to look at the microstructural elastic response of the unidirectional composite due to thermal expansion (or shrinking) and stresses, and assuming uniform strain in the longitudinal direction and uniform stress in the transverse direction, Tsai and Hahn (1980) computed the residual stresses in unidirectional composites in longitudinal direction as

$$\sigma_{mL} = (V_f E_f E_m)(\alpha_f - \alpha_m)(T - T_0) / (V_f E_f + V_m E_m) \qquad \text{(E1)}$$

where E is the elastic modulus, V is the volume ratio, α is the coefficient of thermal expansion, T is the temperature, σ_L is the longitudinal stress, and subscripts m and f refer to matrix and fiber, respectively. The quantity T_0 is the "stress-free" temperature, usually taken as the cure temperature of the composite.

Equation 1 shows that the magnitude of the residual stresses is proportional to the difference in curing and operating temperatures of the composite material.

Equation 1 shows that the magnitude of the residual stresses is proportional to the difference in curing and operating temperatures of the composite material. In cold regions, where large temperature differentials exist, sufficiently large stresses may induce microcracking in the material. These microcracks, in turn, can reduce the stiffness of the composite, increase permeability and water ingression through fiber/matrix interface, and thus finally contribute to the degradation processes.

Another important effect of lower temperatures is the accompanying change in matrix strength and stiffness. Most resin matrix materials become stiffer and stronger as they are cooled. These changes can influence the modes of failure. At low temperature the compressive strength increases and the material fails more violently than at warmer temperatures (Dutta 1994). The energy absorption before failure at low temperature is higher than at room temperature.

Experiments on tensile loading of unidirectional FRP at low temperatures (Dutta 1992) have shown that the longitudinal tensile strength of these composites drop at low temperatures possibly because of fiber waviness or fiber bending in hardened matrix. Experimental investigations by Madhukar and Dutta (1994) on single-fiber composites specially produced with wavy fibers of carbon have shown that indeed in the stiffer matrix the wavy fiber fractures at a lower load. Since, in externally reinforced concrete beams the FRP composite is subjected to tension, the low-temperature tensile behavior of composite is of special significance. Bader (1988), Madhukar, and Drzal (1991) have shown that the matrix and the interface properties play a significant role for tensile strength and failure modes.

In cold regions, the freeze-thaw cycling effects on composite's durability are important considerations. If a composite contains a significant percentage of interconnected voids that are filled with water, the freeze-thaw effect on the strength could be significant within the normal range of temperature (+30 to –20 °C, 86 to –4 °F). Commercially available good quality glass fiber composites usually contain about 0.4% voids, which does not allow any appreciable frozen moisture to cause any serious damage. However, stresses induced by low temperature thermal cycling can result in the formation of microcracks in the resin matrix or in the resin/fiber interface. Under prolonged thermal cycling, they can grow in density and can result in stiffness degradation and degradation of other matrix dominated properties (Dutta 1988, 1989; Dutta et al. 1988).

In thick (>6 mm, 0.25 in.) composites the problem is compounded by the induction of internal residual stresses from curing (Dutta and Hui 1996).

Manufacturing of FRP composites involves the use of strong inorganic (glass or carbon) fibers as the reinforcing phase and a thermosetting polymeric material (epoxy or polyester) as the matrix phase. The polymeric matrix, in the presence of a catalyst, heat, and pressure solidifies through an irreversible exothermic chemical reaction (cure).

Before curing, the polymer phase is a viscous fluid that flows under pressure. As it cures, the fluid becomes more viscous and the flow ceases, but reactions continue to form a tightly cross-linked structure with characteristics of a glassy solid (Rosen 1993). In thin-section composites, the heat distribution is approximately uniform from the interior of the section to the surface. But in relatively thick-section composites, as in many pultruded FRP composites, the heat distribution may not be uniform at the time of curing. Bogetti et al. (1992) have discussed the problem in a recent article on the manufacturing problem of thick composites for the U.S. Army's composite infantry fighting vehicle. The problem arises from the difficulties in controlling the reaction exotherm.

During the curing stage as the chemical reactions proceed, residual stresses are developed with progressive changes in modulus and thermal expansion coefficients, and volume shrinkage of the resin. If the processing temperature is not well-controlled in the heat curing environment, because of the exotherm the exterior regions can cure first, while the interior regions are still uncured and relatively more viscous. Thus, the continuing curing in a high heat environment can induce significant residual stresses as transverse tensile stresses in the interior, and transverse compressive stresses in the exterior. In the very low temperature environment, continuing shrinkage of the exterior past the ambient room temperature to lower temperatures would cause more severe stresses.

The large residual stresses induced at lower temperatures become potentially damaging for polymer matrix composites with curing temperature environment. The damage may begin with the formation of microscopic cracks in the matrix or at the fiber/matrix interface. When these cracks develop to a certain density and size, they will tend to coalesce to form macroscopic matrix cracks (Wang 1986). Transverse matrix cracking in composites affect stiffness, strength, dimensional stability, and fatigue resistance. Of particular interest in this study is the experiment of prolonged low temperature thermal cycling reported by Dutta and Hui (1996), showing that visible cracks grew and accumulated in a commercially available pultruded thick composite, degrading the material severely.

Low-Temperature Behavior Of FRP Composite Bonded Concrete

The amount of research data available on the low-temperature behavior of FRP externally bonded concrete beams is very small. The first significant research on the low-temperature behavior of FRP composite bonded concrete was reported by Kaiser (1989) from Switzerland, and the next was from Canada (Baumert et al. 1996a, 1996b). Hoa et al. (1996) have also reported the results of an accelerated environmental exposure in hot and cold environments. The adhesive bond damage at low temperatures for such beams was the major concern of these researchers. When one considers that the coefficient of thermal expansion for the unidirectional carbon laminate is about zero, and that for concrete is $10x10^{-6}$ /°C, significant shear stresses obviously will be induced at the concrete/CFRP interface.

The experimental research by Kaiser (1989) as presented by Baumert et al. (1996b) is of major interest for the current study and will be summarized here. Kaiser's initial test with one CFRP bonded concrete beam cooled to -60 °C did not produce any shear peeling of the composite from concrete. To study the effect of freeze/thaw cycles, he subjected three precracked and three uncracked test beams for 100 freeze/thaw cycles between 20 °C (68 °F) and -25 °C (-13 °F), and then tested them to four-point bending at room temperature. During temperature cycling, the frozen beams were thawed by flooding the freezer with water at approximately 20 °C (68 °F), so that water would enter into the cracks and with subsequent freezing expand, resulting in the debonding of the laminate. However, when the breaking loads of the frozen beams were compared with the breaking loads of the unfrozen control beams, the experiment did not show any negative effect of freeze/thaw cycling.

Hoa et al. (1996) conducted both accelerated tests and long-term environmental tests on 279.4 x 50.8 x 76.2 mm (11 x 2x 3 in.) concrete beams reinforced with CFRP sheets using two different types of adhesives. In one test they immersed the specimens for 60 days, and in another test they cycled the specimens alternatively at 40 °C for one week and refrigerated them at -23 °C for another week. The total process lasted 60 days. After testing the specimens by three-point bending, they concluded that hot and cold cycle exposure reduced the strength by about 7%. They concluded that a hot-cold cycle is an effective method for accelerated test.

In another investigation Baumert et al. (1993) conducted a study with plain and reinforced concrete beams, testing them at 21 °C and -27 °C. At both temperatures, the CFRP sheets debonded under shear. Such shear bond failure

was considered premature, as it did not allow the experimental determination of the full flexural capacities of the test beam. However, Baumert et al. observed that at low temperature the first-crack load and the yield moment increased significantly, but there was no significant increase of pre-yield or post-yield stiffness of the beams.

The investigation by Baumert et al. (1993) identified a major problem in designing suitable tests for the FRP externally bonded concrete beams. The important issue is what should be considered as the appropriate failure mode: was the laminate debonding from the beam or was the laminate yielding under the tensile stress as in steel reinforcing bars? As noted by Baumert et al. (1993) if the laminate fails under shear stress at the concrete/FRP interface, then full flexural capacities of the test beam cannot be evaluated. This issue is discussed in depth in the next section.

Repaired/Externally-Reinforced Test-Beam Design Approach

The ultimate capacity of the FRP externally bonded concrete beams without any internal reinforcement is limited by the strength of the FRP bond to the concrete, or the tensile strength of the FRP, whichever is lower. When internal steel or other reinforcement is present, the external FRP reinforcement simply shares the tensile load with this internal reinforcement. In older beams the internal reinforcement is considered weakened, and hence there is the necessity of repair using the external reinforcement. The test method must reflect this scenario of weakened interior reinforcement and stronger external reinforcement.

The basic design of the test beam was approached with the consideration that the FRP composite repairing or reinforcement will be applied in actual applications at the bottom surface of under-reinforced beams. Therefore, in the laboratory test load, deflection, and strain, where possible, will be measured. The load-deflection curve of a typical under-reinforced beam is given in Figure E1*, where region I is the pre-cracking stage, region II the post-cracking stage, and region III is the post-serviceability stage when the steel rebar yields. In the precracking stage, the load deflection curve follows a straight line exhibiting full elastic behavior. The maximum tensile stress developed in the beam is less than the modulus of rupture, f_r, of concrete. The flexural stiffness EI of the beam can

* All figures are found at the end of this appendix.

be estimated using Young's modulus (E) of concrete and the moment of inertia (I) of the uncracked reinforced concrete cross section.

At the end of the precracking region, the first flexural crack is initiated when the concrete stress reaches its modulus of rupture strength, f_r. In the post-serviceability cracking stage, extensive cracking and considerable widening of the stabilized cracks throughout the span with increased strain in steel beyond the yield strain ε_y, contribute to substantial loss in stiffness of the section.

The general loading system in the four-point bending tests would be as shown in Figure E2 with the beam depth close to $l_n/16$, where l_n is the clear span of the beam. The beam weight will be

$$w = bh\gamma_{concrete} \qquad \text{(E2)}$$

where h = total depth of beam

b = width of beam

$\gamma_{concrete}$ = unit weight of concrete.

Moment due to dead load = $M_{DL} = (w\, l_n^2)/8$ (E3)

Moment due to live load = $M_{LL} = PL/3$ (E4)

First cracking moment = $M_{CR} = (f_r I_g)/y_t$ (E5)

where

P = applied load

f_r = modulus of rupture of concrete

I_g = moment of inertia of gross concrete section about centroidal axis

y_t =distance from centroidal axis of gross section to extreme fiber in tension

The reinforced concrete cross-sectional geometry and stress/strain distribution of a singly reinforced beam is shown in Figure E3 and doubly reinforced concrete beam repaired at the bottom surface with FRP laminate is shown in Figure E4.

A typical strengthened concrete beam with a laminate in four-point flexural loading configuration is shown in Figure E5. Figure E6 shows the configuration of an actual test.

The design of the plain concrete beams is given in ASTM C78, *The Standard Test Method for Flexural Strength of Concrete*. This method requires that the test specimen must be designed according to the requirements of Methods C31 and C192. The specimens must have a test span within 2% of three times the depth. A diagram of an acceptable testing apparatus according to the ASTM standard is shown in Figure E7. During testing the load may be applied rapidly up to 50% of the ultimate load. The load application rate has to be designed so as to constantly increase the extreme fiber stress from 0.86 MPa 1.21 MPa/min (125 - 175 psi/min) until the specimen ruptures. Three measurements must be taken across each face (one at each edge and one at the center) to the nearest 1.27 mm (0.05 in.) to determine the average width, average depth, and line of fracture location of the specimen at the section of failure.

If the fracture occurs in the tension surface within the middle third of the span length, the modulus of rupture would be calculated as follows

$$R = (Pl)/(bd^2) \quad \text{(E6)}$$

where R = modulus of rupture

P = maximum applied load

l = span length

b = average width of specimen

d = average depth of specimen

Laminate and Adhesive Requirements

Careful consideration must be given in choosing the type of FRP composite laminate material for repairing structural concrete elements exposed to a cold environment. Carbon fiber reinforced polymer, CFRP, and glass fiber reinforced polymer, GFRP, are two commonly available types of composites for use in repair of concrete structures. GFRP has a very high ultimate tensile strength, but it may be subject to strength degradation in alkaline environments due to growth of surface flaws under cyclic loads. On the other hand, carbon fibers are highly

resistant to aggressive environments, and have a thermal expansion coefficient that is approximately zero. The thermal expansion coefficient mismatch with concrete may induce substantial thermal stresses at the FRP composite/concrete interface at low temperatures. Therefore, CFRP was chosen as the first test composite material for low temperature characteristics of repaired/reinforced concrete in the present study.

Different types of laminate-adhesive combinations are available in the market. For the fatigue and thermal cycling tests the relative influence of a liquid type, as opposed to a thick adhesive type, were considered. The details of these combinations are discussed in the fatigue study section later. In the load bearing and bond strength characteristics study, the ODOT-developed laminate combinations were used.

Low-Temperature Load Capacity

Low-temperature load capacity tests were conducted in collaboration with the Ohio Department of Transportation (ODOT), which has an ongoing project on the development of concrete repair and reinforcing techniques using carbon fiber composites and a proprietary adhesive system (DFI/VANAK 1997). Four large beams of 178 mm x 229 mm x 2.235 m (7 x 9 x 88 in.) were readily available for low-temperature tests from a batch of 16 beams fabricated at the ODOT facility. These beams were fabricated with two no. 4 rebars on the tension side and two no. 3 rebars on the compression side. The objective was to investigate the influence of low-temperature on the failure modes, and the load capacity. Another objective was to study the influence of the composite reinforcement thickness (ply) on load, deflection, and strain at room temperature for a low level load, and at low temperature (-30 °C [-22 °F]) for load-to-failure.

Test Beams

Beam no. 1 was bonded, as was beam no. 4, on the tension side with stitched unidirectional carbon fabric of five-ply (layer) thickness, and beam no. 2 and no. 3 were bonded with one-ply thickness using the ODOT-developed adhesive bonding process. Each beam was instrumented with multiple strain gages, including those at composite/concrete interface locations and at the midspan locations on the top and bottom sides. Before testing, the beams were subjected to six freeze-thaw cycles between room temperature and -50 °C (-58 °F) when the coldroom in which these beams were stored itself went through the temperature cycling for maintenance.

Testing Loadframe

The initial tests were run at room temperature on each beam to a low-level load of 44.5kN (10,000 lbf). These tests established the base line load deflection data and checked if the instrumentation system worked properly. The tests were performed in the CRREL High Strength Advanced Material (HISAM) testing coldroom. CRREL's HSAM load frame (Figure E8) for testing the beams is designed for 445kN (100,000 lbf). load capacity and 30% overload capacity. It is made up of 12.7 mm (0.5 in.) thick structural I-beams and joists welded to form a self standing structure, which can receive approximately 3.05 m (10 ft) long beams from the front side on its four-point loading fixture. The frame has been designed to accommodate 305 to 457 mm (12 to 18 in.) wide test beams. The load points on the test beams were located by four round bars of approximately 102 mm (4 in.) diameter, which are provided with special mounts for positioning at any location, two along the I-beams of the bottom base frame, and two along the I-beam of the load bar. At the center of the top frame is mounted a manually operated hydraulic jack. The spindle of the jack is connected through a Geokon 2,070 kN (300,0000 lbf) load cell. By the side of the load cell is mounted a LVDT with a stroke capacity of 152 mm (6 in.). A pulley arrangement, aircraft cable, and ratchet cranking system provides a convenient means of raising and lowering the load bar on the test specimen. The load point arrangement for these tests provided a 914 mm (36 in.) span between each load point in the four-point loading tests.

Datalogging System

Load, deflection, strain, and temperature are the general parameters of measurement in this test system. The outputs of the Geokon load cell, LVDT, and strain gauges mounted on specimens were recorded by a Megadac model 2200C 16-channel data acquisition system. In the current measurement program the Megadac was programmed only for four channels to receive and record readings at every one second interval from two strain gauges, the load cell, and the LVDT. The temperatures are recorded separately with a Campbell Scientific model CR-10 data logging system. The Megadac interfaces with a personal computer and all data can be imported into a Microsoft Excel file through ASCII format. Final reduction of data and analysis were done on computer using the Microsoft Excel.

HSAM Testing Coldroom

The CRREL High Strength Advanced Material (HSAM) testing coldroom has been designed to develop the ambient temperature inside the room to be down to -55 °C (-67 °F). Since, at this temperature, the currently installed hydraulic loading system cannot work properly, most loading tests are done at -30 °C (-20 °F). The room is cooled by a refrigeration system connected to a bank of four large capacity blower fans. The load frame is located in the coldroom having a floor area of about 55.74 sq. m (600 sq. ft). A large door allows large size test specimens to be conveniently brought in and taken out of the room. Instrumentation and readouts are all located in the adjacent warmer instrumentation. A forklift inside the coldroom allows the heavy test specimens to be handled conveniently.

Tests

For the test of the concrete beams, first the load points on the support were set apart at 2.086 m (82.125 in.) and on the load beam at 0.70 m (27.375 in.), so that at each end about 76.2 mm (3 in.) of overhang was left. By monitoring the air temperature and imbedded thermocouple in a concrete beam, it was ensured that the air temperature and the interior temperature of the specimens were close to each other.

To perform the room temperature tests, the coldroom was first warmed up to approximately 20 °C (68 °F), and the test beam reached the same temperature. The test beam was loaded to 44.48kN (10,000 lbf) and then unloaded. Load, deflection, and strains were measured with the Megadac datalogger sampling each parameter every second. After completion of testing at room temperature, the temperature of the room was lowered to -30 °C (-20 °F). The beam was then loaded to failure again measuring the load, deflection, and strain in the process.

Test Results

Load, deflection, and strain data from these tests are presented in Figure E9.1 through E9.5 for beam no.1, Figure E10.1 through E10.5 for beam no. 4, (both no.1 and no. 4 have five layers of composites), Figure E11.1 through E11.5 for

beam no. 3, and Figure E12.1 through E12.5 for beam no. 2. The low-temperature failure load data are summarized in Table E.1*.

Table E.1 shows that the failure load averaged at 115.95 kPa (26,068 lbf) for the one-layer composite repaired beam, and 139.28 (31,312 lbf) for the five-layer composite repaired beam, about a 20% increase in strength with five times more CFRP material.

Figure E13 shows the beam no .1 under load showing initial cracking at low temperature, and Figure E14 after complete failure. Figure E15 shows the crack extensions from the bottom surface immediately around the loading point where the concrete has also failed by crushing. Figure E16 shows that this five-layer composite simply debonded from the concrete surface when it failed. Beam no.4 which has also a five-layer composite reinforcement, debonded without any tensile fiber fracture (Figure E17). On the other hand, the one-layer composite bonded beam no. 2, when failed, fractured the fibers under tension (Figure E18) with accompanied debonding. Whether the fiber fractured or not, the debonding always appeared to be accompanied with a thin layer of concrete being sheared off, raising serious doubts about the interface of the failure, that is, whether the interface is the glue/concrete, glue/composite, or just concrete. Figure E19 is a close-up view of the five-layer composite/concrete failure surface of beam no. 1 and Figure E20 is that of one-layer beam no. 2. It can be observed that in both cases a thin layer of concrete has come off from the surface with the debonded composite laminates.

The initial data from ODOT (Morton 1998) for similarly constructed beams show that for the one-layer CFRP reinforcement the failure strength is approximately 97.86 kPa (22,000 lbf) (beam no. 13), indicating that apparently the low temperature has increased the failure load capacity by about 18%. At the time of writing of this report complete testing data are not available from ODOT.

* All tables are found at the end of this appendix.

Low-Temperature Fatigue Test

Test Beam Preparation

For the low temperature study of the fatigue behavior of the composite repaired/reinforced concrete, six concrete beams of 152.4 x 152.4 mm x 2.134 m (6 x 6 x 84 in.) were cast. The beams were longitudinally reinforced with two no. 3 steel rebars in compression and two no. 4 rebars in tension. Figure E21 shows the cross section of these reinforced beams. Shear reinforcement for all the beams consisted of no. 2 rebar stirrups. The spacing of the stirrups at both ends for the first 457 mm (18 in.) of span was 100 mm (4 in.) and over rest of the span 152 mm (6 in.). Internal strain gauges were attached to predetermined locations. The cement: sand: aggregate proportions in the concrete mix were 1:2.5:2.5 by weight with a water/cement ratio of 0.55. The maximum size of the aggregate was 12.5 mm (0.5 in.) diameter. An electrical vibrator was used to ensure good compaction of fresh concrete around the internal reinforcement.

Four 152 x 305 -mm (6 x 12 in.) concrete test cylinders were cast at the time of preparing the beams and tested to determine the mechanical properties of the concrete. The average compressive strength of this concrete as determined from cylinder test was 27.4 MPa (3975 psi).

Two types of adhesives were used for bonding the laminate to the concrete beam. The first type is Sikadur 30 and developed by the SIKA Corporation. Sikadur 30 is an epoxy-based two-component adhesive mortar. It can be bonded to concrete, stone, timber, epoxy, and steel. The mix ratio of component A to component B is 3:1 by weight. The second type of adhesive is called Hysol EA 9330, and developed by Dexter Hysol Aerospace Inc. This adhesive is also a two-component paste adhesive with a mix ratio of 3:1 by weight.

After curing for 28 days, all beams were precracked under four point flexure to 65% of their estimated ultimate load to simulate damage in the beams. Deflection and strain measurements were recorded at 0.89 kN (200 lbf) increments. The deflections as well as the first crack load were recorded during precracking. Crack propagation was traced during loading until the cracks extended to approximately 75 mm (3.0 in.) or half the thickness of the beam.

Application Of Laminate (Repairing)

The bottom tension faces of the beams were prepared for repair and strengthening before applying the adhesive and the laminate. Dry sandblasting

was performed to roughen the surface, expose the aggregate, and clean the surface from oil and grease while removing any foreign objects or loose particles. Following sandblasting the surface was thoroughly brushed and high pressure air used to force out any material left behind in the cracks. The laminates' bonding surface was thoroughly cleaned with acetone and a cloth. The laminate is considered ready for application when the cloth is no longer blackened after being passed over the surface. This procedure ensures removal of any loose fibers and oils that would contribute to reduction in the bonding of the adhesive. The second step is to mix parts A and B in a container with an electric hand mixer for a minute at low speed, the edges of the container are then scraped and the adhesive mixed for another minute. It is very important to allow for a homogeneous mixture. Each of the two adhesives have a pot life of 60 minutes. This pot life begins from the instant of combining the resin and the hardener. The pot life is shorter at higher temperatures and longer at low temperatures. Therefore, the manufacturer recommends cooling the components before mixing them to allow for a longer pot life.

Each of the two adhesive types requires different methods of application by the manufacturer. The Sikadur 30 was applied to the beam using a serrated spatula to produce a layer of thickness of 5 mm (0.1875 in.). It is very important to ensure that all voids are filled so that no cavities would be present. The adhesive is then placed on the laminate surface using a tool to control the thickness. Once the laminate is placed on the beam, a roller is used to press the laminate onto the adhesive and force out any excess adhesive. An extra coat of adhesive is applied to one side of the laminate to minimize the tendency of peeling on that end. The beams are stored in a controlled atmosphere for seven days for complete cure.

The Hysol adhesive is applied in a slightly different manner. Hysol 9330 is not as viscous as the Sikadur 30; therefore, it is difficult to control the thickness. The Hysol 9330 spreads out to a thickness of approximately 1.6 mm (0.0625 in.). Once the beam has been coated with the adhesive, the laminate is then placed on the beam and using a roller the laminate is once again pressed into the adhesive forcing out any excess material. Once the laminate has been applied to the beams, a pressure of 70–100 kPa (10–15 psi) is applied to the laminate using steel weights. The weights are left for two days and then removed, and the beams are cured for an additional five days.

Instrumentation

Embedded strain gauges were attached to the compression and tension bars at midspan prior to casting. Surface concrete strain gauges were attached after application of the laminate. Three surface gauges were attached to the side of the beam in the compression and tension zones at midspan, at distances of 25, 100, and 125 mm (1, 4, and 5 in.) from the bottom surface. A surface strain gauge was attached to the laminate on the bottom of the beam at midspan. The external strain gauges and the internal strain gauge on the tension bars were connected to an external amplifier, then were attached to the MEGADAC along with the load cell. The mechanical stud pivots were attached at locations to measure deformation using a digital micrometer. Midspan deflection was measured with a dial gauge with a magnetic base having a resolution of 0.001 inches attached to the load frame. The instrumentation of fatigue testing beams is shown in Figure E22.

Testing

The repaired control beams were subjected to fatigue at 4 Hz under four-point loading symmetric about midspan (Figure E23). Static tests were performed before the fatigue loading application at a room temperature of 24 °C (75 °F). Fatigue load was then applied and static load tests carried out after application of predetermined fatigue load cycles to evaluate the stiffness degradation. Table E2 shows the fatigue load cycles and corresponding load ranges for the two control beams with Sikadur 30 and Hysol 9330 adhesives. The fatigue loading on the Sikadur control beam 5 could not be continued due to premature failure of the beam after 150,000 cycles. The deflections, concrete strains, crack propagation, and crack widths were monitored in the control beams.

Test Results

The typical flexural strain variations across the depth of the Hysol control beam are shown in Figures E24 – E29. These strains correspond to those measured from the static tests conducted after the completion of 0, 10^5, $2.7x10^5$, $6x10^5$, $7x10^5$, and 10^6 fatigue load cycles. A significant increase in both the maximum measured compressive strain in the concrete and the tensile strain in the CFRP laminate can be observed after the completion of 10^5 load cycles, which indicates substantial degradation in stiffness. The flexural strain variations across the depth of the Sikadur beam 5 are given in Figures E30 – E34. These strains correspond to those measured from the static tests conducted after the completion of $5x10^3$, $4x10^4$, $7.5x10^4$, 10^5, and $1.5x10^5$ fatigue load cycles. The

surface strain gauges at 129.5 mm (5.1 in.) from bottom fiber failed after $7.5x10^4$ cycles.

The load deflection relationships from the static tests on the control Hysol beam 1 conducted after 0, 10^5, $2.7x10^5$, $4x10^5$, $6x10^5$, $7x10^5$, and 10^6 fatigue cycles are shown in Figure E35 from 0 to $4x10^5$ cycles and in Figure E36 from $4x10^5$ to 10^6 cycles. The stiffness degradation with an increase in deflection can be observed at $2.7x10^5$ cycles of fatigue loading in Figure E35. However, the beam does not exhibit any additional deterioration in stiffness between $2.7x10^5$ and 10^6 cycles (see Figure E36).

The typical load vs. deflection relationship for the Sikadur control beam 5 is shown in Figure E37. The degradation in stiffness is evident after the completion of $1.5x10^5$ cycles. Further data on this control beam were not available due to its failure by overloading through the hydraulic actuator after $1.5x10^5$ cycles.

Low-Temperature Effects

The concrete beams repaired with FRP were subjected to fatigue at 4 Hz under symmetric four-point loading in a controlled cold environment maintained at -20° C. Static tests were conducted prior to the fatigue loading. Tables E3 and E4 show the number of fatigue load cycles and load ranges for the beams repaired with the adhesives Sikadur 30 and Hysol 9330 respectively. Static tests were carried out at the end of intervals of the fatigue load cycles shown in the Tables E3 and E4. The observations of deflections, concrete strains, crack propagation, and crack widths were continued from 0 to 10^6 cycles.

The compressive strain variations for all beams measured at 130 mm (5.1 in.) from the bottom fiber were compared at 0, 10^5, $2.5x10^5$, $5x10^5$, $7.5x10^5$, and 10^6 cycles. The compressive strains for a cold environment beams at 0 cycles were very similar for Sikadur and Hysol adhesives. Additionally, the strains for the beams tested in the cold environment averaged approximately 25–30 microstrains less than the beams tested at room temperature. The strain gauges attached to beam 6 were recording high values of strain at 0 cycles but after fatigue the gauges seem to correlate with proper values. After 10^5 cycles, a significant increase in the compressive strain is observed in the beams cycled at room temperature, while the average increase in strain for the cold beams is much smaller. No appreciable change in the strains after $2.5x10^5$ cycles is evident in all the beams 1 through 6. As the cycles increase beyond $5x10^5$, the compressive strains for the beams tested at room temperature remain fairly

constant. The compressive strains in the beams tested in cold environment continue to increase slowly towards the values of compressive strains measured for the beams tested in room temperature as the fatigue load cycles approach 10^6. At all fatigue load cycles, the beams repaired with Sikadur show a slightly lower average compressive strains than beams repaired with Hysol, indicating an increase in stiffness.

The tensile strain variations measured on the FRP were compared at 0, 10^5, $2.5x10^5$, $5x10^5$, $7.5x10^5$, and 10^6 cycles. The FRP measured strains in the beams at room temperature increase approximately 100 microstrains at each incremental load from 0 to 10^5 cycles. After 10^5 cycles, the tensile strains in the FRP remain constant up to 10^6 cycles. The beams repaired with Sikadur adhesive have a lower tensile strain than the beams with Hysol at the same load values. The FRP strains in the beams tested in the cold environment appear to be smaller than those recorded from the test beams in room temperature. However this trend is not clear from the strains in the FRP for beam 2, which could be due to malfunctioning of the strain gauge.

The flexural strain variation across the depth of a typical Sikadur cold beam and a typical Hysol cold beam are shown in Figures E38 – E42 and E43 – E47 respectively. These strains correspond to those measured from static tests conducted after the completion of the number of cycles closest to 0, 10^5, $2.5x10^5$, $5x10^5$, $7.5x10^5$, and 10^6 cycles.

The Sikadur beams exhibit incremental strain increases at 0 cycles as the load is increased in the static test, which indicates minor cracking in the beam. As the beam is cycled to $2.5x10^5$ a large increase in tensile strain is noticed, while only a small increase in compressive strain is noticed. By $5.7x10^5$ cycles, for the maximum load of 22.2 kN (5000 lbf), the compressive strain increased to about 450 microstrain, exhibiting a softening of the beam. After $2.5x10^5$ cycles, the tensile strains are fairly constant with the maximum value at the bottom surface at about 800 microstrain. Throughout the course of cycling to 10^6 cycles there is only a small increase in compressive strain, only about 200 microstrain. The compressive strains remain very close as in beam 3. After 4.2×10^5 cycles the tensile strains increase at a small steady rate.

In the Hysol beams at 0 cycles a large increase in tensile strain is observed between 4.45 and 6.23 kN (1000 and 1400 lbf) and the compressive strain increases between 11.56 and 13.34 kN (2600 and 3000 lbf). A significant increase, almost to 800 microstrain, in the tensile strain can be observed after the completion of 10^5 cycles in the beams. The tensile strains developed in the

bottom fiber significantly with increase in load, while compressive strains increased at a lower rate. The compressive strains do not increase very rapidly; therefore they remain grouped. An increase in tensile strain can be seen only at higher load values. The tensile and compressive strain remain constant after $6x10^5$ cycles.

Stiffness Degradation

The load deflection relationships from the static tests on the Sikadur and Hysol beams tested in cold environment are shown in Figures E48 - E55. In the Sikadur beams, the slope of the precracking curve has a smaller angle than the 0 cycles repaired cold beam, indicating that the repair has supplied additional stiffness to the beam. The 0 cycles and precracking slope has the same angle up to about 6.67kN (1500 lbf) then the slope of the deflection line decreases in the precracked curve. As the beam is cycled the deflection decreases at $5x10^4$ cycles and begins to increase in deflection once again. The deflection slowly increases until $3.75x10^5$ cycles where a noticeable increase in deflection takes place. This corresponds to the increase in the tensile strain between $2.5x10^5$ and $5.7x10^5$ cycles visible in the strain profiles.

The deflection of the Hysol beams increases during cycling. The slope of the deflection line during precracking is smaller than the slope obtained at 0 cycles, exhibiting softening of the beams. As the number of cycles is increased the slope of the deflection lines tend to decrease. A large increase in deflection is noticed between 0 and $5x10^4$ cycles, while a small increase in deflection can be seen between 10^5 and $3x10^5$ cycles. The Hysol beams exhibit slightly higher deflections than the Sikadur beams. The increase in deflection is more pronounced at higher loads. The maximum deflections of the Hysol beams are greater than the maximum deflections of the Sikadur beams by as much as 1.02 mm (0.04 in.).

A comparison of load deflection relationships of the beams tested at the room temperature and cold temperature is shown in Figures E52 - E55. It can be seen that the beams subjected to the cold environment exhibit smaller deflections at the same loads than those tested at room temperature. Table E5 gives the comparison of the ultimate load behavior of all the beams.

Low-Temperature Thermal Cycling Tests

The purpose of the low temperature thermal cycling test is to investigate how temperature fluctuations affect the concrete beams repaired with CFRP laminates. Concrete, steel, adhesives, and CFRP laminates all have different coefficients of thermal expansion which causes internal stresses to develop in each layer due to mismatch in the thermal expansion coefficients. Coefficients of thermal expansion are shown in Table E6.

Casting and Thermal Cycling

Ten unreinforced concrete beams were cast and cured in lime for 14 days. After curing, the beams were instrumented and strengthened with CFRP laminate. The beams were then subjected to 200 thermal cycles from -30 °C (-22 °F) to 20 °C (68 °F), with a residence time at each temperature of approximately 1 hour. The thermal cycling was controlled by a computer program (THERMAL 9). The beams were placed in an environmental chamber (Figure E56) using evaporated liquid nitrogen as a coolant. After cycling, the beams were subjected to four point flexure tests to failure. Special attention was given to observe the damage in the concrete/adhesive and adhesive/laminate interfaces due to temperature fluctuations.

Material and Specimen Configuration

The cross section of the beams was 76 x 76 mm (3 x 3 in.) with a total length of 305 mm (12 in.). The cement: sand: aggregate proportions in the concrete mix were 1: 2.2: 3 by weight, with a maximum aggregate size of 19 mm (0.75 in.). The water/cement ratio was 0.52 and the slump was measured at 108 mm (4.25 in.). The average compressive strength of the concrete was 27.6 MPa (4000 psi). The beams were designed and tested according to ASTM C192 and ASTM C666, respectively.

Instrumentation for Thermal Cycling Beams

Prior to instrumentation and repair, the bonding surface was prepared using a hand-held grinder to expose the aggregate for proper bonding of the laminate with adhesive and concrete (Figure E57). The beams were instrumented before the laminate was applied (Figure E58). The 10 beams that were cast were divided into four groups for instrumentation. The first group consisted of two control beams, without any instrumentation. The second group of beams had thermocouples installed to monitor internal temperature variations within the

concrete and adhesive. Concrete surface strain gauges were located at midpoint on the bottom of the beam under the adhesive and the laminate in the third group of beams, whereas the fourth group of beams was not instrumented.Table E7 shows a summary of details of the concrete beams prepared for the test.

Beams 1 and 2 were instrumented with 11 thermocouples at 15 mm (0.5625 in.) spacing and 15 mm (0.5625 in.) depth on the top and sides. The bottom of the beams have one thermocouple located at midspan and one in the adhesive. The locations of the thermocouples form a grid within the beam at a depth of 15 mm. Positions 1 and 4 double as locations for horizontal and vertical temperature points. A cross section of these beams is shown below in Figure E59. Beams 3 and 4 had two strain gauges attached to the bottom surface of the beam under the adhesive and laminate to monitor the strains in the concrete during the ultimate testing of the beams. Beams 5 and 6 had no instrumentation and were tested to obtain ultimate load values after cycling. Beams 7 and 8 were not subjected to thermal cycles and tested to obtain ultimate load values for the control beams.

The beams were first instrumented and the laminate was then applied to the prepared surface, using the same techniques as the precracked reinforced concrete beams, which were subjected to fatigue load cycles in cold temperatures.

Testing

All plain concrete beams were subjected to four point flexural testing at room temperature at a rate of approximately 35.6 N/sec (8 lbf/sec). The distance between the supports was 254 mm (10 in.) and the load points were 76.2 mm (3 in.) apart (Figure E.60). Figure E61 shows a beam under test. All beams with composite bonds failed in the same manner with a diagonal shear crack originating from one of the bottom supports and propagating diagonally to the nearest loading point to the top (Figure E62.1 - E62.5). However, the control beams A and B, which were not composite bonded, failed in tension. Figures E63.1 and E63.2 show two of the failed beams with vertical cracks originating from the bottom surface by tension. These tests clearly illustrate how the failure mode changed with the composite bonding. Table E8 gives a summary of the test results. It will be seen that the failure load data are highly scattered, possibly because of the mixed-mode failures of the specimens as discussed earlier.

Low-Temperature Bond Strength Test in Flexure

The purpose of this test was to investigate at low temperature the failure modes of the bonded CFRP strips in three-point flexural loading, and the influence of using prime coat for bonding of the CFRP. Many of the techniques of ensuring a good reliable bond are still at the developmental stage; for example, the influence of applying a prime coat was not properly known at this stage. Would it enhance the bond or degrade it? Would the influence be same at low temperature as at room temperature?

Test Beams

In cooperation with the ODOT, which has been developing a carbon composite/adhesive bonding technique for concrete reinforcement and repairing, fourteen 76.2 x 101.6 x 381 mm (3 x 4 x 15 in.) concrete beams were fabricated for this series of tests. Strips of five-ply thick, 25.4 x 279 mm (1 x 11 in.) unidirectional stitched carbon laminates were bonded to the tension (76.2 mm, 3 in. wide) side of the beams. Six of the beams were bonded after prime coating (PC) the surface before applying adhesive, and in the remaining 8 beams adhesive was applied without prime coating (WPC). Figure E64 shows one such beam mounted with a series of strain gages to record strain variation along the longitudinal axis on the tension surface. Note that the composite was bonded leaving a gap of about 51 mm (2 in.) on either side for the load application in the 3-point test setup.

Testing

All tests were conducted with an MTS machine and data were collected using a Nicolet data acquisition system. Eight beam specimens, (three from PC group and five from WPC group) were tested under three-point bending (Figure E65). The results of the tests are summarized in Table E9. One specimen of WPC group was tested at room temperature. This specimen failed at 13.14kN (2955 lbf) with 1.01 mm (0.04 in.) deflection. Two specimens of PC group and five specimens of WPC group were tested at low temperature (-30 °C [-22 °F]). The average failure load of the PC group was 4.67 kN (3,225 lbf) and that of the WPC group 15.2 kN (3,418 lbf). The results show that the prime coat reduced the bond strength. At low temperature the strength increased by about 16%. Figure E66 illustrates a failed specimen in the test fixture showing the typical failure of all specimens by near vertical cracking at the mid span. Figure E67 shows that the crack did not pass through the composite bond, but in fact the bond delaminated and failure happened in the concrete and not at the composite concrete true

load, displacement, and strain records are given in Figures E68.1 through E68.15.

Split-Block Tension Testing for Bond Strength Study

In beam applications the bonded FRP on the tension side fails primarily under interfacial shear stress. It is important to know if the low temperature makes the concrete-composite glue-bond line brittle and weak. A suitable testing system, in which the mixed-mode failures are mostly eliminated, is thus desirable. It is also desirable to know to what distance from the crack edge, and at what rate the shear strength, over the bonded area, is developed. A new test method, called the *split-block test method*, is under development in cooperation with the ODOT. In this method two prismatic blocks of concrete with central holes are bonded with FRP composite strips (Figure E69). The blocks are then pulled apart by applying a tension load through two bolts, each one aligned through the central hole of each block. Initial tests of this system proved to be successful.

Specimen Preparation

Two groups of split-block concrete specimens were manufactured at the ODOT facility for this test. Group A had a 76.2 -mm (3 -in.) bond length, and group B had a 152.4 mm (6 in.) bond length (Figure E69). The Ohio DOT proprietary adhesive/CFRP composite system was applied on nine specimens of group A and four specimens of group B. Again, in applying the adhesive, four specimens in group A were prime coated (PC) and five were not (WPC). In group B, two were PC and two were WPC.

Testing

Both room-temperature and low-temperature (-35 °C [-31 °F]) tests were performed at CRREL in the MTS machine applying tension loads to the bolts (Figure E70) and measuring load and displacement simultaneously on a Megadac data acquisition system. A number of specimens were strain-gauged with multiple gages extending from the midspan point to the adhesive-bonded area (Figure E71).

Test Results

The test results are summarized in Table E10. At room temperature, a group A WPC specimen failed at 12.23 kN (2750 lbf), and a similar specimen failed at low temperature at 12.93 kN (2908 lbf), showing the effect of low temperature on increased failure load. At low temperature, group A PC specimens failed at an average load of 10.47 kN (2353 lbf), and group B PC specimens at 12.4 kN (2787 lbf), showing approximately 18% increase in failure load for the additional 76.2 mm (3 in.) bond length increase. At low temperature, group A WPC specimens failed at an average load of 13.11 kN (2949 lbf), and group B WPC specimens at 15.1 kN (3394 lbf), again, showing a 15% increase in failure load.

Conclusions and Discussion

The detailed data analysis of all tests has not yet been performed, but it has become apparent that at least on short-term basis there is no adverse influence of low temperature on the composite bond performance to concrete. Almost in all cases the load capacities increased over those at room temperature. Specific conclusions from the tests described here are summarized below.

Load Capacity Tests

For the thin one-ply bond in the four point bending load capacity tests the mode of failure was tensile accompanied by debonding, as opposed to the shear bonding of the five-ply composite.

Within about 30% load capacity there was no significant difference in the load deflection characteristics (stiffness) between the room temperature and low temperature tests (-30°C [-22°F]).

The low-temperature failure loads were in general higher than the room-temperature failure loads.

Fatigue Tests

The failure loads of the full size beams following million-cycle fatigue loading at room and low temperatures were not significantly different, but the deflection and strain at low temperatures were lower, indicating higher stiffness.

Thermal Cycling

The data from the small size specimens that were tested in 4-point bending after 200 thermal cycles were highly scattered. No significant degradation of the thermally cycled specimens was observed.

Bond Strength Test

At low temperature the bond strength improved. The influence of prime coating was negative for both room and low temperature.

Bond Strength Development Tensile Test

This special test also showed that low temperature increased the bond strength and prime coating reduced the strength. More strength is developed over a longer bond length. The length over which bond strength develops is an important parameter that can be studied by this test.

Discussion

FRP fabrics or plates are potentially a viable replacement for steel/epoxy bond material for external reinforcement and repairing of concrete. However, their reliability under the mechanical and environmental load, creep, and durability has remained open to questions.

Under this program a considerable amount of experimental data have been generated, a proper analysis of which will allow us to define the application of composite bonding to concrete with much more certainty at low temperatures. Time constraints on this project has put the analysis of these data on hold.

A more comprehensive test, encompassing extensive, and parallel room-, cold-, and high-temperature tests, needs to be performed to develop any reliable model of composite failure in the external beam reinforcement of concrete. A discussion of the model has been presented in the test program and test analysis section. This could be a starting point for a reliable model development.

Under the five areas of investigation at CRREL under this project a large amount of significant data have been generated. At the time of writing of this report, these data have not been thoroughly analyzed. When analyzed, much-needed information for establishing the reliability of this new technology in cold

regions will be available. The degradation of composites, the degradation of bond line, the cure problems in cold, the differential thermal stresses from coefficient of thermal expansion mismatch, and water ingression in voids and subsequent icing, are all pertinent cold regions problems of this technology that need to be addressed.

References

ACI-ASCE Committee 326, (1962), Shear and Diagonal Tension, Pt 2, J. ACI, vol. 59, no. 2, pp. 277-333.

Arockiasamy, M., (1997), Damage process of CFRP composites and the concrete interface under fatigue loading at low temperatures, CRREL Technical Note (Unpublished).

Bader, M.G. (1988) Tensile strength of uniaxial composites. Science and Engineering of Composite Materials, Vol.1. pp. 1-11

Baumert, M.E., Green, M.F., and Erki, M.A. (1996a), Low temperature behavior of concrete beams strengthened with FRP sheets. Proceedings of the 1996 CSCE Annual Conference, Canadian Society of Civil Engineering, Montreal, Quebec.

Baumert, M.E., Green, M.F., and Erki, M.A. (1996b) A Review of Low Temperature Response of Reinforced Concrete Beams Strengthened with FRP sheets. Advanced Composite Materials in Bridges and Structures, Proceedings of the Second International Conference on Advanced Composite Materials in Bridges and Structures, Montreal, August 11-14, M.M.El-Badry, Ed., Published by the Canadian Society for Civil Engineering, pp. 565-572.

Berwanger, C., and Sarkar, A.F. (1973) Effect of temperature and age on thermal expansion and modulus of elasticity of concrete. Behavior of Concrete under Temperature Extremes, ACI SP-39, pp.1-22.

Bogetti, T.A., Gillespie.Jr., J.W., and McCollough, R.L. (1992) Influence of processing on the development of residual stresses in thick section thermoset composites. in Thick Section Composites Technology (eds. E. S.Wright and B.M.Halpin, Jr.), Sagamore Army Materials Research Conference Proceedings, Oct. 23-26, 1989, Plymouth, MA, pp. 121-138.

Browne, R.D., and Bamforth, P.B. (1981) The use of concrete for cryogenic storage: a summary of research, past and present. First International Conference on Cryogenic Concrete, 25-27 March, New Castle, London, The Concrete Society, pp. 135-166.

DFI/VANAK, Columbus, OH; Adhesive supplier.

Dutta, P.K. (1994) Low-temperature compressive strength of glass-fiber-reinforced polymer composites". Journal of Offshore Mechanics and Arctic Engineering, vol.116, pp. 167-172.

Dutta, P.K. (1992) Tensile strength of unidirectional fiber Composites at low temperatures. Proceedings of the Sixth Japan-U.S. Conference on Composite Materials, June 22-24, Orlando, Florida, Technomic Publishing, pp. 782-792.

Dutta, P.K.(1988) Structural fiber composite materials for cold regions. ASCE Journal of Cold Regions Engineering, Vol. 2, No. 3, September, pp.124-134.

Dutta, P.K., Kalafut, J., and Farrell, D.(1988) Performance of Laminated Composites in Cold. In Proceedings of the Army Science Conference, Vol. 2, 25-27 October, Fort Monroe, Hampton, Virginia,

Office of the Assistant Secretary of the Army (RD&A), pp. 269-281.

Dutta, P.K.(1989) Fiber composite materials in an arctic environment. In Structural Materials, Proc. ASCE Specialty Conference- Seventh Annual Structures Congress, May 1-5, San Francisco, California, pp. 216-225.

Dutta, P.K., and Lampo, R.G. (1993) Behavior of fiber reinforced plastics as construction materials in extreme environments. Proc. Third Offshore and Polar Engineering Conference, Singapore, 6-11 June, 1993. pp. 339-344.

Dutta, P.K., and Hui, D. (1996) low temperature and freeze-thaw durability of thick composites, composites: Part B: Engineering, Elsevier Science Limited, Vol. 27B, No. 3/4, pp. 371-379.

Hoa, S.V., Xie, M., and Xiao, X.R., (1996), Repair of steel reinforced concrete with carbon/epoxy composites, Advanced Composite Materials in Bridges and Structures, Proceedings of the Second International Conference on Advanced Composite Materials in Bridges and Structures, Montreal, August 11-14, M.M.El-Badry, Ed., Published by the Canadian Society for Civil Engineering, pp.573-580.

Jones, R.M. (1975) Mechanics of Composite Materials. Hemisphere Publishing Corporation, New York, pp. 193-198.

Kaiser, H. (1989) Bewehren von stahlbeton mit kohlenstoffaserverstarkten epoxidharzen. (Strengthening of reinforced concrete with epoxy-bonded carbon-fiber plastics), Ph D Thesis, Diss ETH Nr. 8918, Zurich.

Lord, H.W., and Dutta, P.K. (1988), On the design of polymeric composite structures for cold regions applications. Journal of Reinforced Plastics and Composites, vol. 7, pp. 434-458.

Madhukar, M.S., and Dutta, P.K.(1994) Effect of matrix stiffness on wavy fiber behavior in single-carbon-fiber-epoxy composites. Special Report 94-10, U.S. Army Cold Regions Research and Engineering Laboratory, Hanover, NH.

Madhukar, M.S., and Drzal, L.T. (1991) Fiber-matrix adhesion and its effect on composite mechanical properties: II. Longitudinal (0°) and transverse (90°) tensile and flexural behavior of graphite/epoxy composites, Journal of Composite Materials, Vol. 25, pp. 958-991.

Meier, U. (1987) Bridge repair with high performance composite materials. Material und Technik, vol 4, pp. 125-128 (in German).

Morton, S., (1997). Personal communication, Ohio Department of Transportation.

Neville, A.M. (1981) Properties of Concrete.3rd ed. New York: John Wiley and Sons.

Nilson, A.H., and Winter, G.(1991) Design of Concrete Structures. McGraw Hill Inc., New York, p 135.

Rostasy, F.S., Schneider, U., and Weidermann, G. (1979) Behavior of mortar and concrete at very low temperatures, Cement and Concrete Research, vol.9, pp. 365-376.

Rosen, S.L.,(1993) Fundamental Principles of Polymeric Materials. John Wiley and Sons, New York, pp. 9-31.

Tsai, S.W., and Hahn, H.T. (1980) Introduction to Composite Materials. Technomic Publishing Company, Lancaster,PA. pp. 244-246.

Wang, A.S.D. (1986) On fracture mechanics of matrix cracking in composite laminates, Proc. Intn'l. Symp. on Composite Materials and Structures, Beijing, pp. 576-584.

Yamane, S., Kasami,H., and Okuno, T. (1978) Properties of concrete at very low temperatures.

List of Appendix E Figures and Tables

Figures

Figure E1. Typical load-deflection curve of an under-reinforced concrete beam under flexural load. 34

Figure E2. General loading system in a four-point flexural test. 34

Figure E3. Stress/strain distribution of a singly reinforced beam under flexure. 35

Figure E4. Stress/strain distribution of a doubly reinforced beam under flexure. 35

Figure E5. Typical flexural testing setup of a beam repaired with a composite laminate 36

Figure E6. Actual four-point flexural test setup. 36

Figure E7. Test configuration of the ASTM C78 test method. 37

Figure E8. CRREL high strength advanced materials (HISAM) flexural testing load frame. 37

Figure E9.1. Low temperature load/strain data from ODOT beam 1 (five-layer CFRP). ..38

FigureE9.2. Low temperature and room temperature load/deflection data from ODOT beam 1 (five-layer CFRP) 39

Figure E9.3. Room temperature load/deflection data from ODOT beam 1 (five-layer CFRP) 40

Figure E9.4. Low temperature load, deflection, and strain data from ODOT beam 1 (five-layer CFRP) 41

Figure E9.5. Room temperature load, deflection, and strain data from ODOT beam 1 (five-layer CFRP) 42

Figure E10.1. Room temperature load/strain data from ODOT beam 4 (five-layer CFRP). 43

Figure E10.2. Low temperature and room temperature load/deflection data from ODOT beam 4 (five-layer CFRP) 44

Figure E10.3. Room temperature load/deflection data from ODOT beam 4 (five-layer CFRP) 45

Figure E10.4. Low temperature load, deflection, and strain data from ODOT beam 4 (five-layer CFRP) 46

Figure E10.5. Room temperature load, deflection, and strain data from ODOT beam 4 (five-layer CFRP) 47

Figure E11.1. Low temperature load/strain data from ODOT beam 3 (one-layer CFRP). 48

Figure E11.2. Low temperature and room temperature load/deflection data from ODOT beam 3 (one-layer CFRP) 49

Figure E11.3. Room temperature load/deflection data from ODOT beam 3 (one-layer CFRP).....50

Figure E11.4. Low temperature load, deflection, and strain data from ODOT beam 3 (one-layer CFRP).....51

Figure E11.5. Room temperature load, deflection, and strain data from ODOT beam 3 (one-layer CFRP).....52

Figure 12.1. Low temperature load/strain data from ODOT beam 2 (one-layer CFRP)...53

Figure E12.2. Low temperature and room temperature load/deflection data from ODOT beam 2 (one-layer CFRP).....54

Figure E12.3. Room temperature load/deflection data from ODOT beam 2 (one-layer CFRP).....55

Figure E12.4. Low temperature load, deflection, and strain data from ODOT beam 2 (one-layer CFRP).....56

Figure E12.5. Room temperature load, deflection, and strain data from ODOT beam 2 (one-layer CFRP).....57

Figure E13. ODOT beam no.1 (five-layer CFRP) under four-point flexural test. 58

Figure E14. ODOT beam no.1 (five-layer CFRP) at low temperature flexure test after complete failure.....58

Figure E15. Failed beam showing crack extension from the bottom surface. 59

Figure E16. The five-layer CFRP debonded under flexural loading to failure. 59

Figure E17. The five-layer CFRP shows no sign of tensile failure.....60

Figure E18. The one-layer CFRP shows tensile fiber fracture under four-point flexural loading.....60

Figure E19. A close up view of the five-layer debonded CFRP/concrete interface.....61

Figure E20. A close up view of the one-layer debonded CFRP/concrete interface. 61

Figure E21. Cross-section of the concrete beam for fatigue testing.....62

Figure E22. Instrumentation systems for the fatigue testing beams.....63

Figure E23. Flexural loading configuration of the fatigue testing beams. 64

Figure E24. Room temp. test strain profiles of the Hysol 9330 repaired fatigue beam after 0 cycle.....64

Figure E25. Room temp. test strain profiles of the Hysol 9330 repaired fatigue beam after 10^5 cycles.....65

Figure E26. Room temp. test strain profiles of the Hysol 9330 repaired fatigue beam after $2.7x10^5$ cycles.....65

Figure E27. Room temp. test strain profiles of the Hysol 9330 repaired fatigue beam after $6x10^5$ cycles.....66

Figure E28. Room temp. test strain profiles of the Hysol 9330 repaired fatigue beam after $7x10^5$ cycles.....66

Figure E29. Room temp. test strain profiles of the Hysol 9330 repaired fatigue beam after 10^6 cycles.....67

Figure E30. Room temp. test strain profiles of the Sikadur 30 repaired fatigue beam after 0 cycle.....67

Figure E31. Room temp. test strain profiles of the Sikadur 30 repaired fatigue beam after $4x10^4$ cycles. 68

Figure E32. Room temp. test strain profiles of the Sikadur 30 repaired fatigue beam after $7.5x10^4$ cycles. 68

Figure E33. Room temp. test strain profiles of the Sikadur 30 repaired fatigue beam after 10^5 cycles. 69

Figure E34. Room temp. test strain profiles of the Sikadur 30 repaired fatigue beam after $1.5x10^5$ cycles. 69

Figure E35. Room temp. test load/deflection data of the Hysol 9330 repaired fatigued beam no.1 (0 to $4x10^5$ cycles) 70

Figure E36. Room temp. test load/deflection data of the Hysol 9330 repaired fatigued beam no.1 ($4x10^5$ to 10^6 cycles) 70

Figure E37. Room temp. test load/deflection data of the Sikadur 30 repaired fatigued beam no.5 (0 to $1.5x10^5$ cycles) 71

Figure E38. Low temp. test strain profiles of the Sikadur 30 repaired fatigue beam after 0 cycle. 71

Figure E39. Low temp. test strain profiles of the Sikadur 30 repaired fatigue beam after $2.5x10^5$ cycles. 72

Figure E40. Low temp. test strain profiles of the Sikadur 30 repaired fatigue beam after $5.7x10^5$ cycles. 72

Figure E41. Low temp. test strain profiles of the Sikadur 30 repaired fatigue beam after $6.7x10^5$ cycles. 73

Figure E42. Low temp. test strain profiles of the Sikadur 30 repaired fatigue beam after 10^6 cycles. 73

Figure E43. Low temp. test strain profiles of the Hysol 9330 repaired fatigue beam after 0 cycle. 74

Figure E44. Low temp. test strain profiles of the Hysol 9330 repaired fatigue beam after $1.5x10^5$ cycles. 74

Figure E45. Low temp. test strain profiles of the Hysol 9330 repaired fatigue beam after $2x10^5$ cycles. 75

Figure E46. Low temp. test strain profiles of the Hysol 9330 repaired fatigue beam after $5.6x10^5$ cycles. 75

Figure E47. Low temp. test strain profiles of the Hysol 9330 repaired fatigue beam after $8.5x10^5$ cycles. 76

Figure E48. Low temp. test load/deflection data of the Sikadur 30 repaired fatigued beam no.3 (0 to $5.7x10^5$ cycles) 76

Figure E49. Low temp. test load/deflection data of the Sikadur 30 repaired fatigued beam no.3 ($5.7x10^5$ to 10^6 cycles) 77

Figure E50. Low temp. test load/deflection data of the Hysol 9330 repaired fatigued beam no.2 (0 to $4.3x10^5$ cycles) 77

Figure E51. Low temp. test load/deflection data of the Hysol 9330 repaired fatigued beam no.2 ($4.3x10^5$ to $8.5x10^5$ cycles) 78

Figure E52. Comparison of low temperature effects on deflection after 0 cycle of Sikadur 30 repaired fatigued beam 78

Figure E53. Comparison of low temperature effects on deflection after 10^6 cycles of Sikadur 30 repaired fatigued beam. 79
Figure E54. Comparison of low temperature effects on deflection after 0 cycle of Hysol 9330 repaired fatigued beam. 79
Figure E55. Comparison of low temperature effects on deflection after 10^6 cycle of Hysol 9330 repaired fatigued beam. 80
Figure E56. Low temperature thermal cycling chamber loaded with the test beams. 80
Figure E57. Test specimen surface prepared by sandblasting for laminate application. 81
Figure E58. Application of the adhesive before bonding the CFRP laminate. 81
Figure E59. Thermocouple locations shown in the beam cross-section. 82
Figure E60. Loading and support points marked on the thermally cycled test beams. 82
Figure E61. Thermally cycled beam under test. 83
Figure E62.1 83
Figure E63.1 85
Figure E64. Strain gage mounted test beam for bond strength study. 86
Figure E65. Three-point flexural test configuration for bond strength study. 87
Figure E66. Typical failure in the three-point flexural tests. 87
Figure E67. Debonded CFRP laminate shows no fiber failure. 88
Figure E68.1 Load and displacement data of the prime coated specimen PC4 at room temperature. 89
Figure E68.2 Load/strain data of the prime coated specimen PC5 at low temperature. 90
Figure E68.3 Load, displacement, and strain data of the prime coated specimen PC5 at low temperature. 91
Figure E68.4. Load/strain data of the prime coated specimen PC6 at low temperature. 92
Figure E68.5 Load, displacement, and strain data of the prime coated specimen PC6 at low temperature. 93
Figure E68.6. Load/strain data of the uncoated specimen WPC4 at low temperature. 94
Figure E68.7 Load, displacement, and strain data of the uncoated specimen WPC4 at low temperature. 95
Figure E68.9 Load, displacement, and strain data of the uncoated specimen WPC5 at low temperature. 96
Figure E68.10. Load/strain data of the uncoated specimen WPC6 at low temperature. 97
Figure E.68.11 Load, displacement, and strain data of the uncoated specimen WPC6 at low temperature. 98
Figure E68.12. Load/strain data of the uncoated specimen WPC7 at low temperature. 99
Figure E68.13 Load, displacement, and strain data of the uncoated specimen WPC7 at low temperature. 100
Figure E68.14. Load/strain data of the uncoated specimen WPC8 at low temperature. 101
Figure E68.15 Load, displacement, and strain data of the uncoated specimen WPC8 at low temperature. 102
Figure E69. "Split-block" test specimens. 104

Figure E70. Tensile testing of "split block" specimens at low temperature. 104
Figure E71. Multiple strain gages mounted on each block to monitor strain development. 105

Tables

Table E1. Low temperature failure load capacities of the ODOT beams. 106
Table E2. Number of cycle and load ranges for control beams at room temperature . .. 106
Table E3. Number of cycles and load ranges for Sikadur 30 cold environment beams. 106
Table E4. Number of cycles and load ranges for Hysol 9330 cold environment beams. 107
Table E5. Ultimate loads of reinforced concrete beams. 107
Table E6. Coefficients of thermal expansion. 107
Table E7. Thermal cycling instrumentation 108
Table E8. Results from the thermally cycled beams in flexure 108
Table E9. Results of the three point bending tests of the ODOT small beams. 109
Table E10. Test results from the split block shear bond test by tension 109

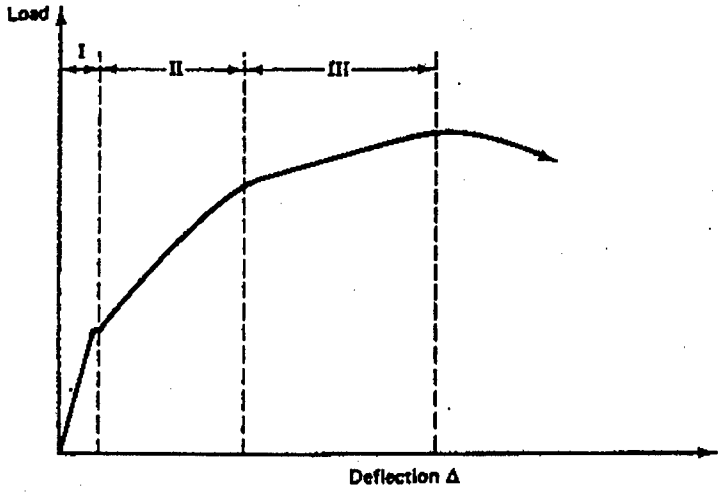


Figure E1. Typical load-deflection curve of an under-reinforced concrete beam under flexural load.

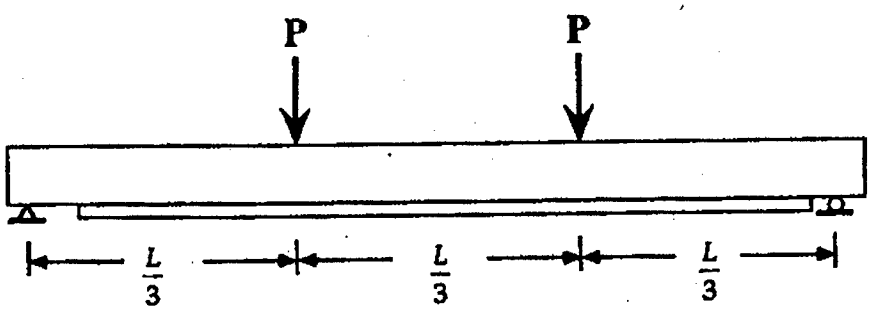


Figure E2. General loading system in a four-point flexural test.

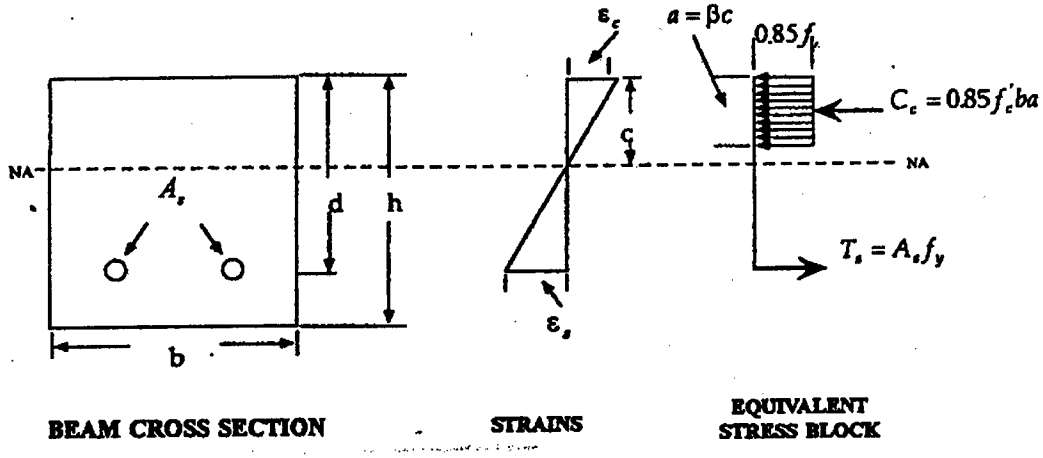


Figure E3. Stress/strain distribution of a singly reinforced beam under flexure.

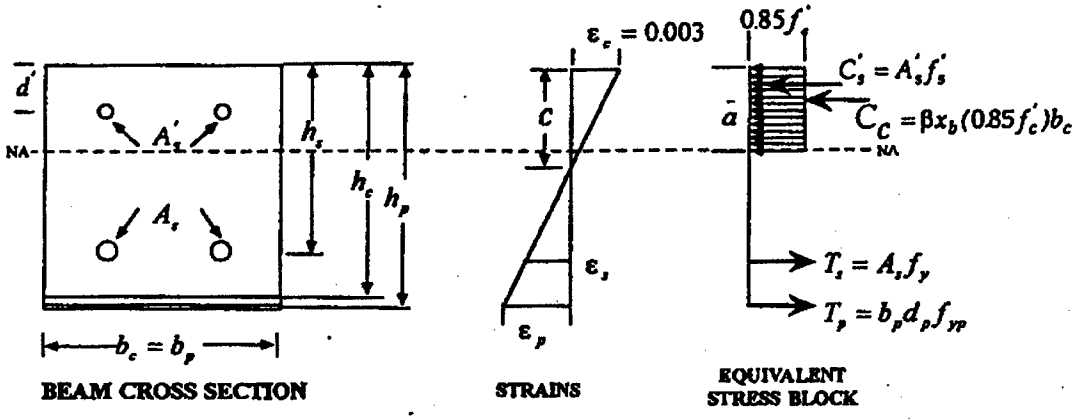


Figure E4. Stress/strain distribution of a doubly reinforced beam under flexure.

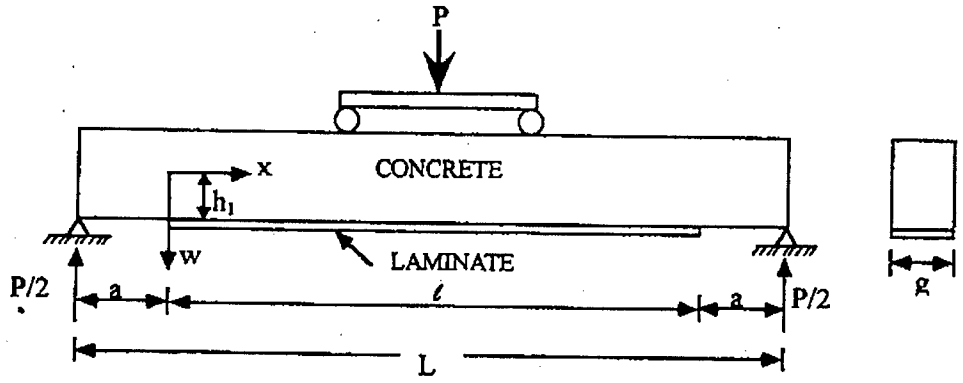


Figure E5. Typical flexural testing setup of a beam repaired with a composite laminate.

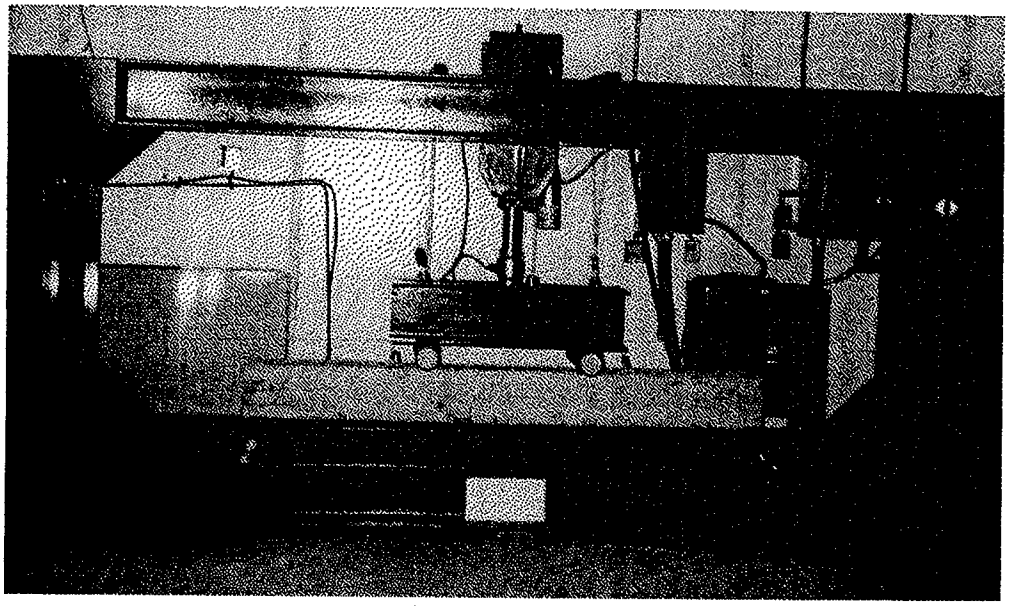


Figure E6. Actual four-point flexural test setup.

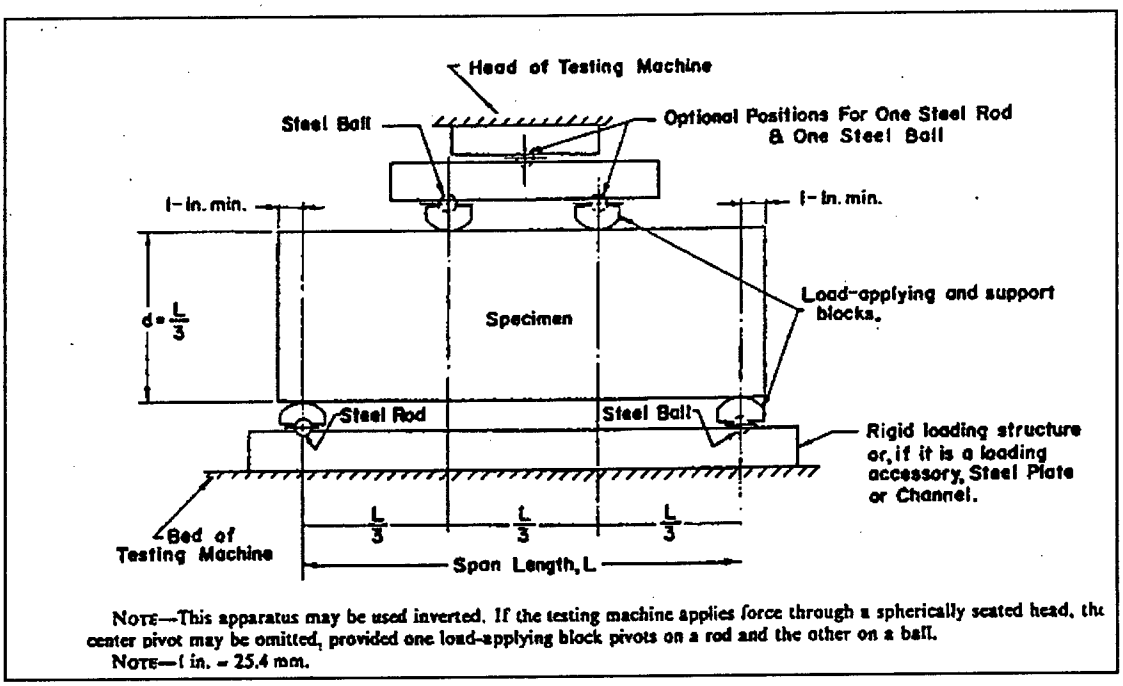


Figure E7. Test configuration of the ASTM C78 test method.

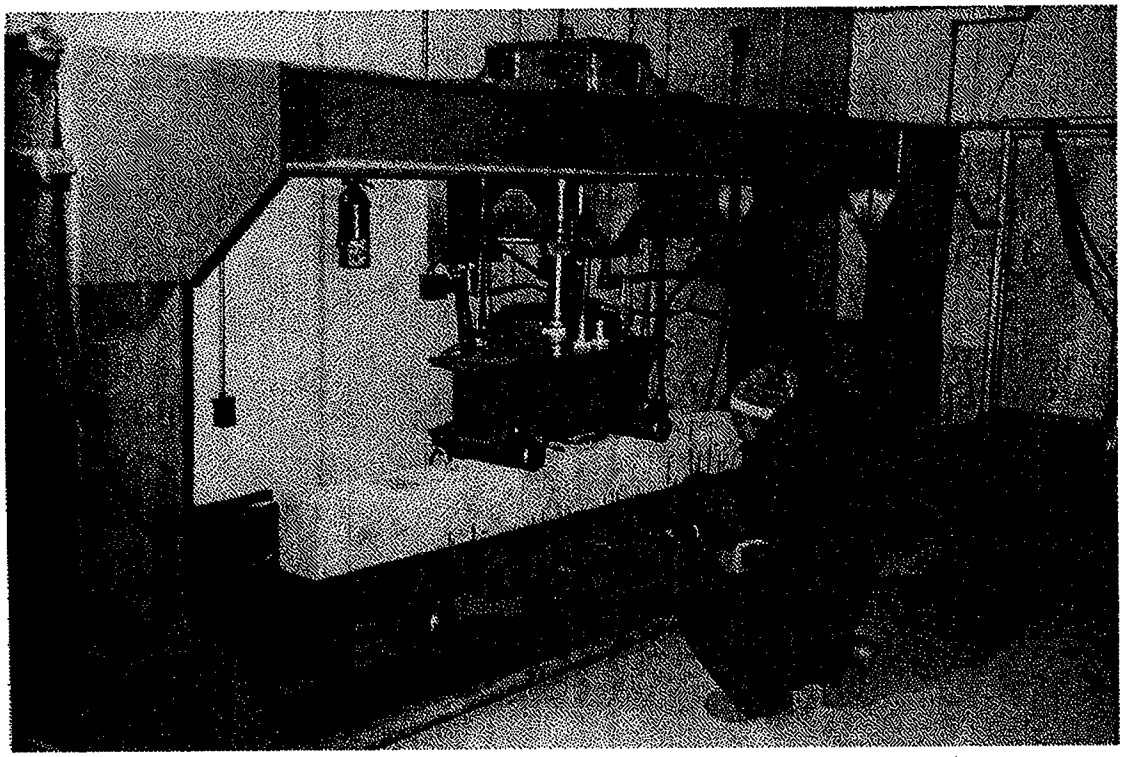


Figure E8. CRREL high strength advanced materials (HISAM) flexural testing load frame.

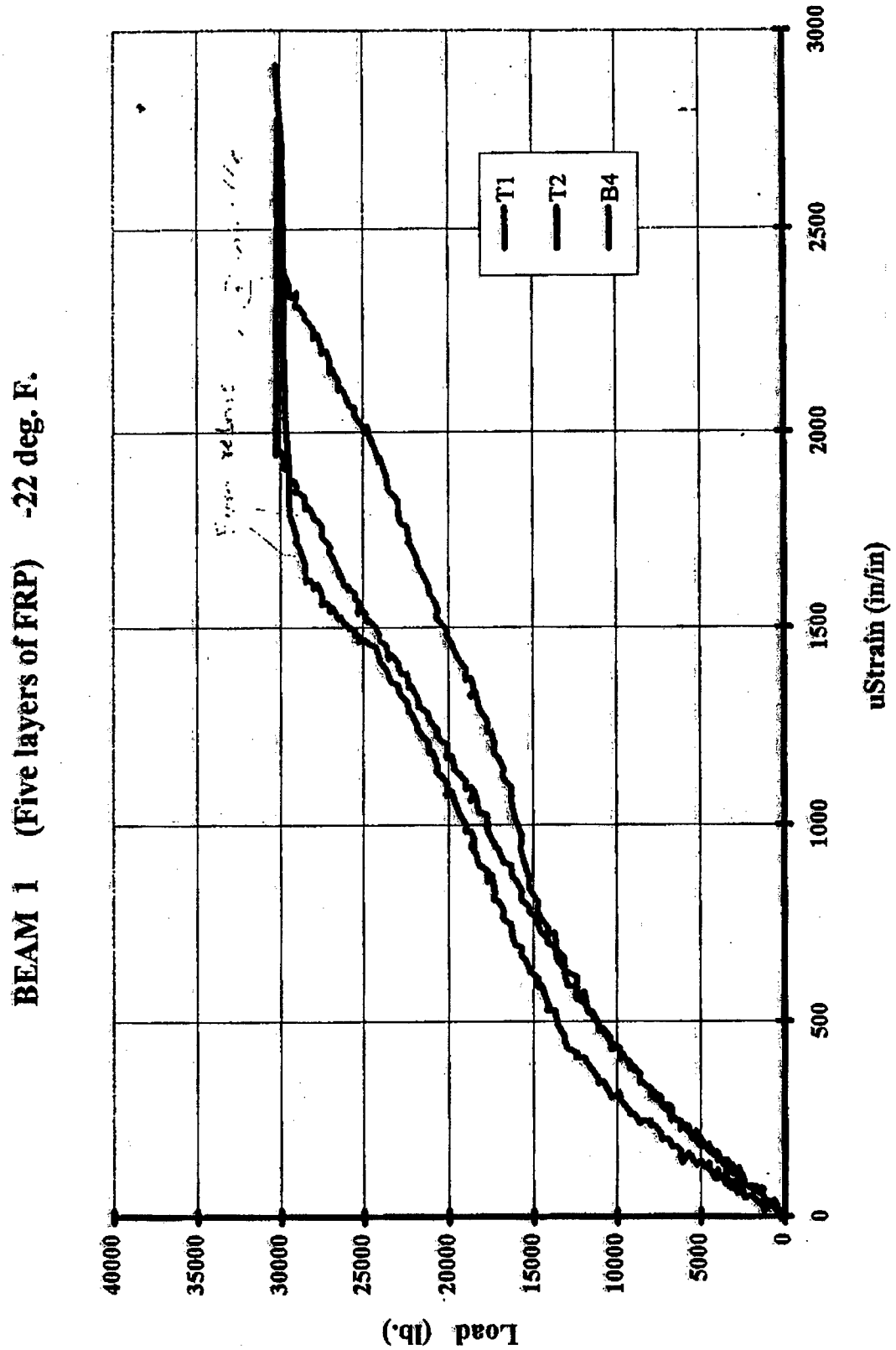
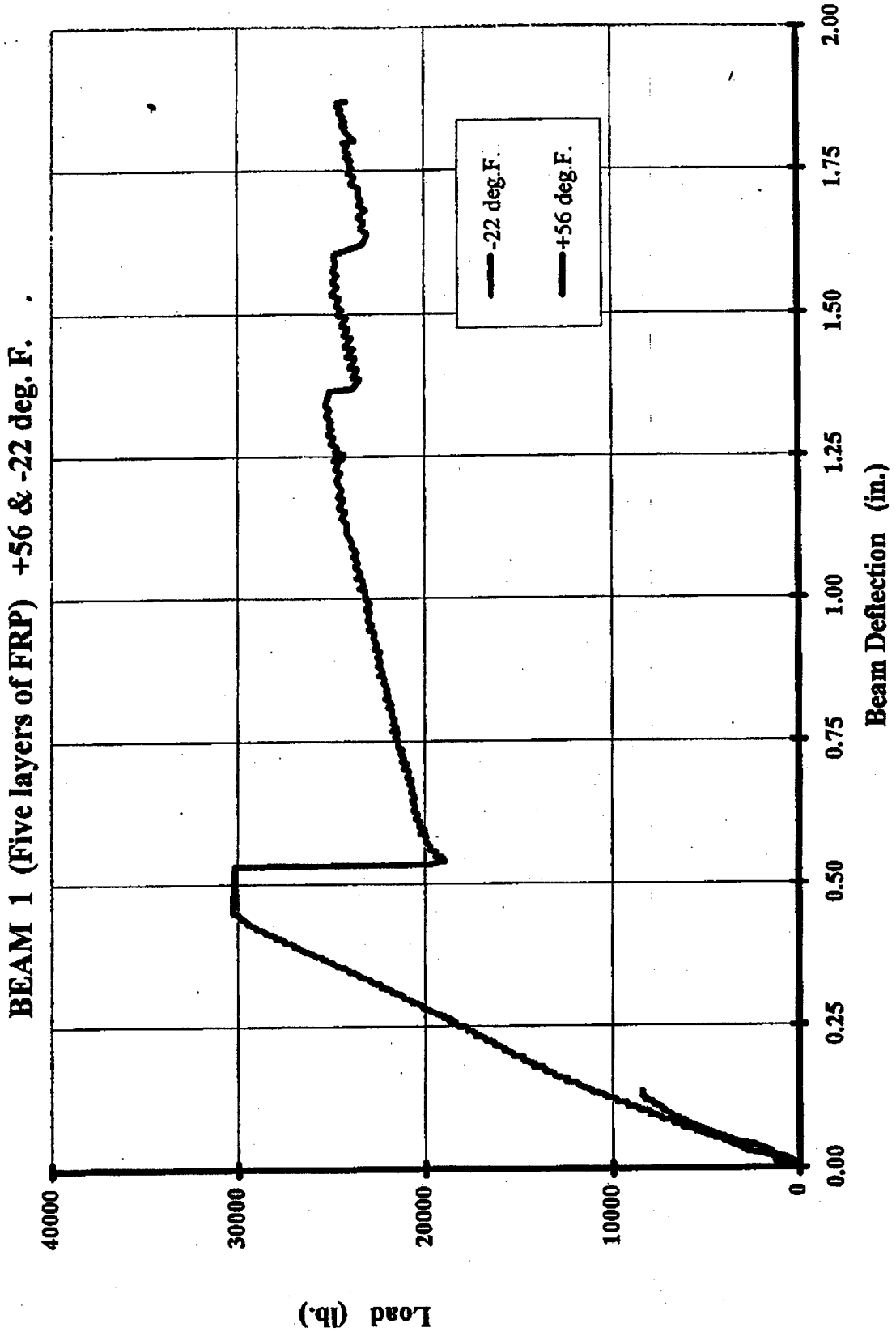


Figure E9.1. Low temperature load/strain data from ODOT beam 1 (five-layer CFRP).



FigureE9.2. Low temperature and room temperature load/deflection data from ODOT beam 1 (five-layer CFRP).

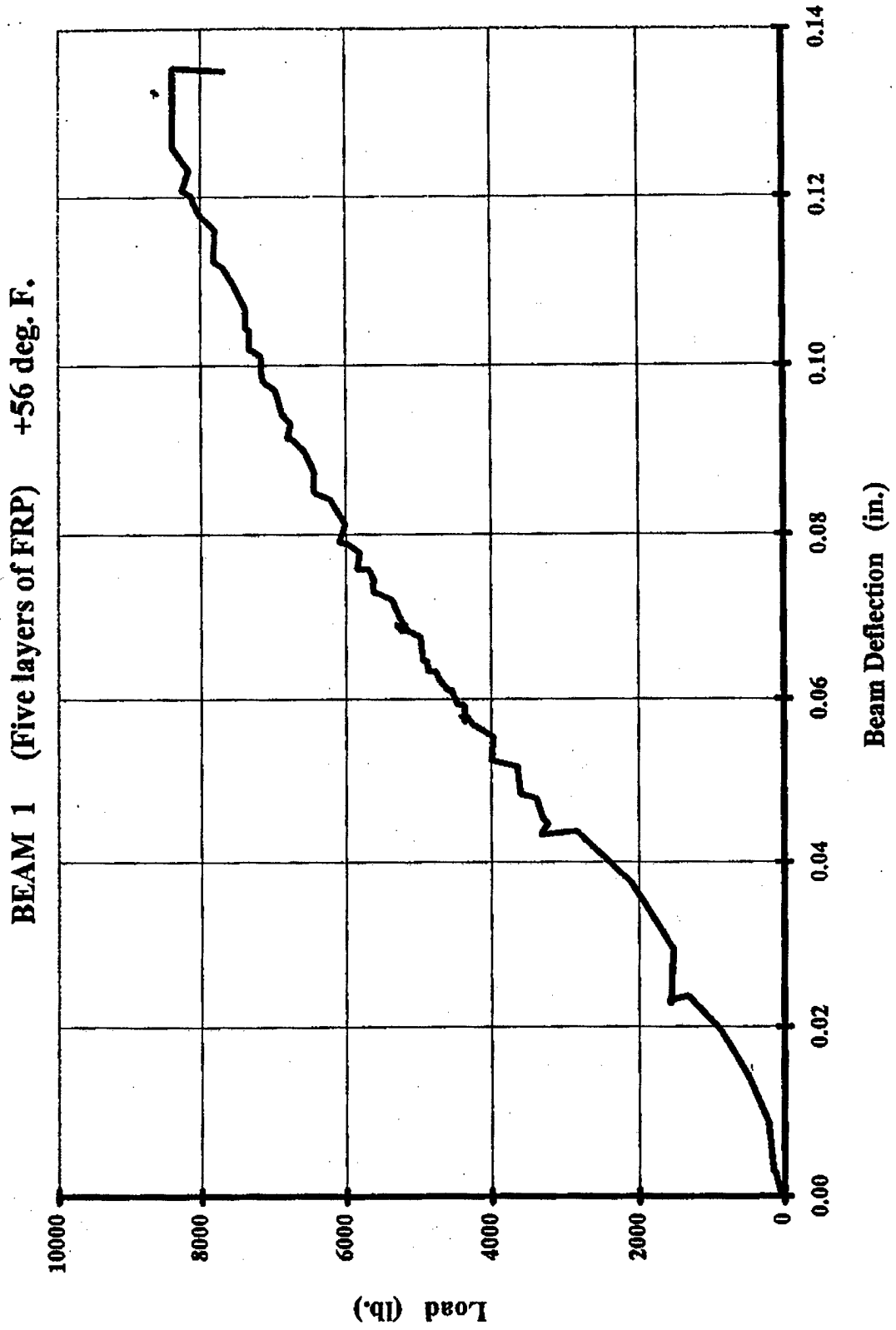


Figure E9.3. Room temperature load/deflection data from ODOT beam 1 (five-layer CFRP).

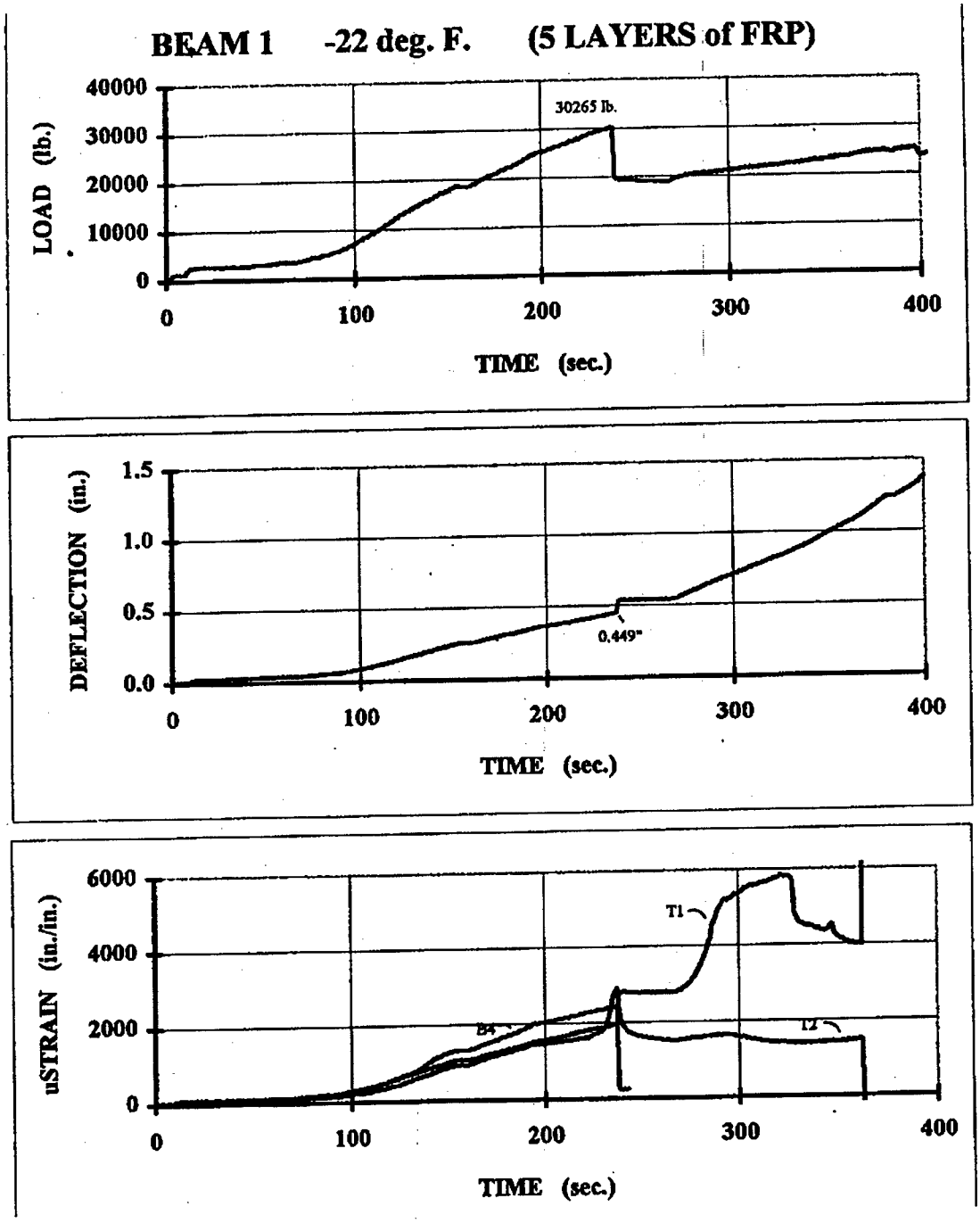


Figure E9.4. Low temperature load, deflection, and strain data from ODOT beam 1 (five-layer CFRP).

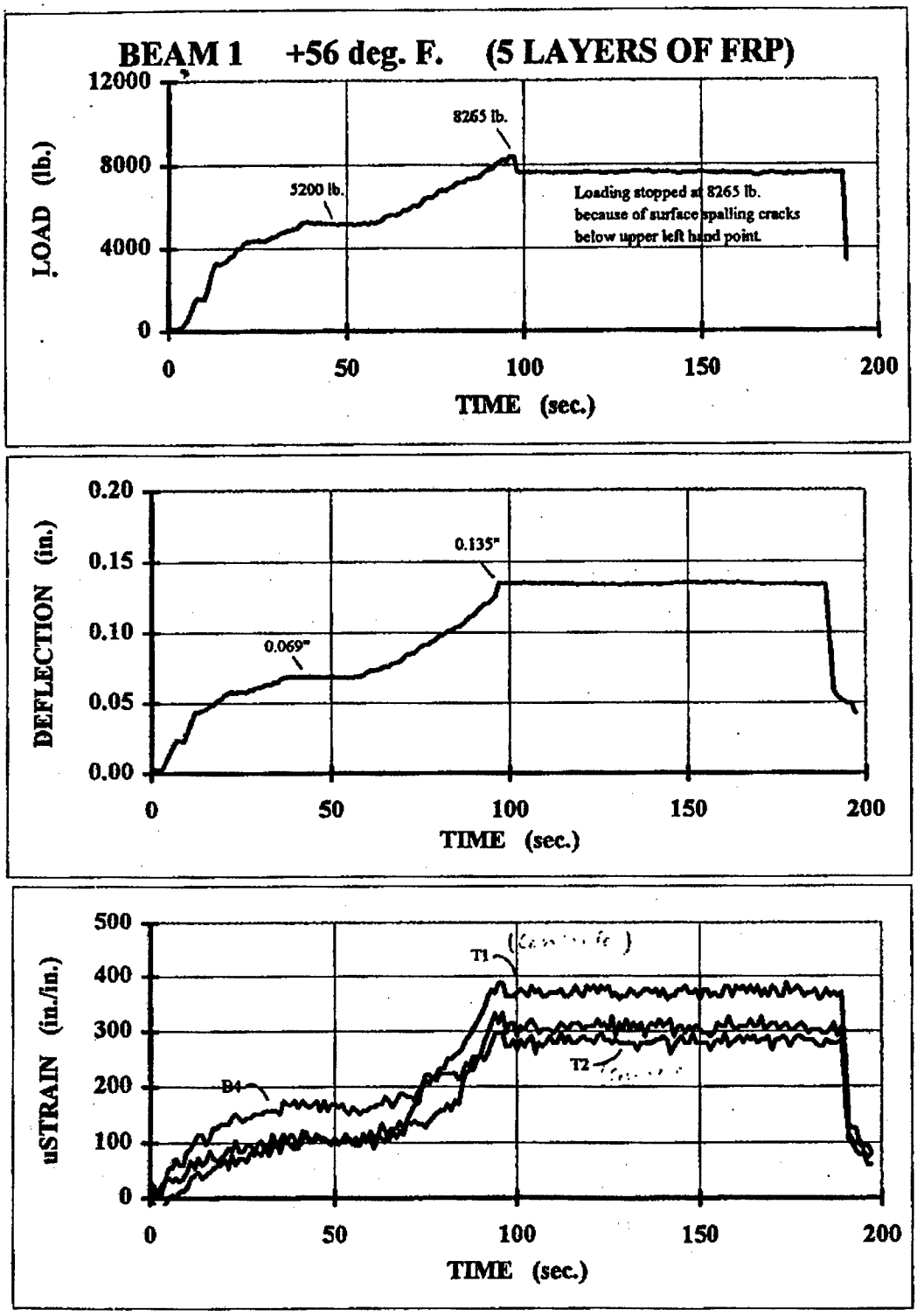


Figure E9.5. Room temperature load, deflection, and strain data from ODOT beam 1 (five-layer CFRP).

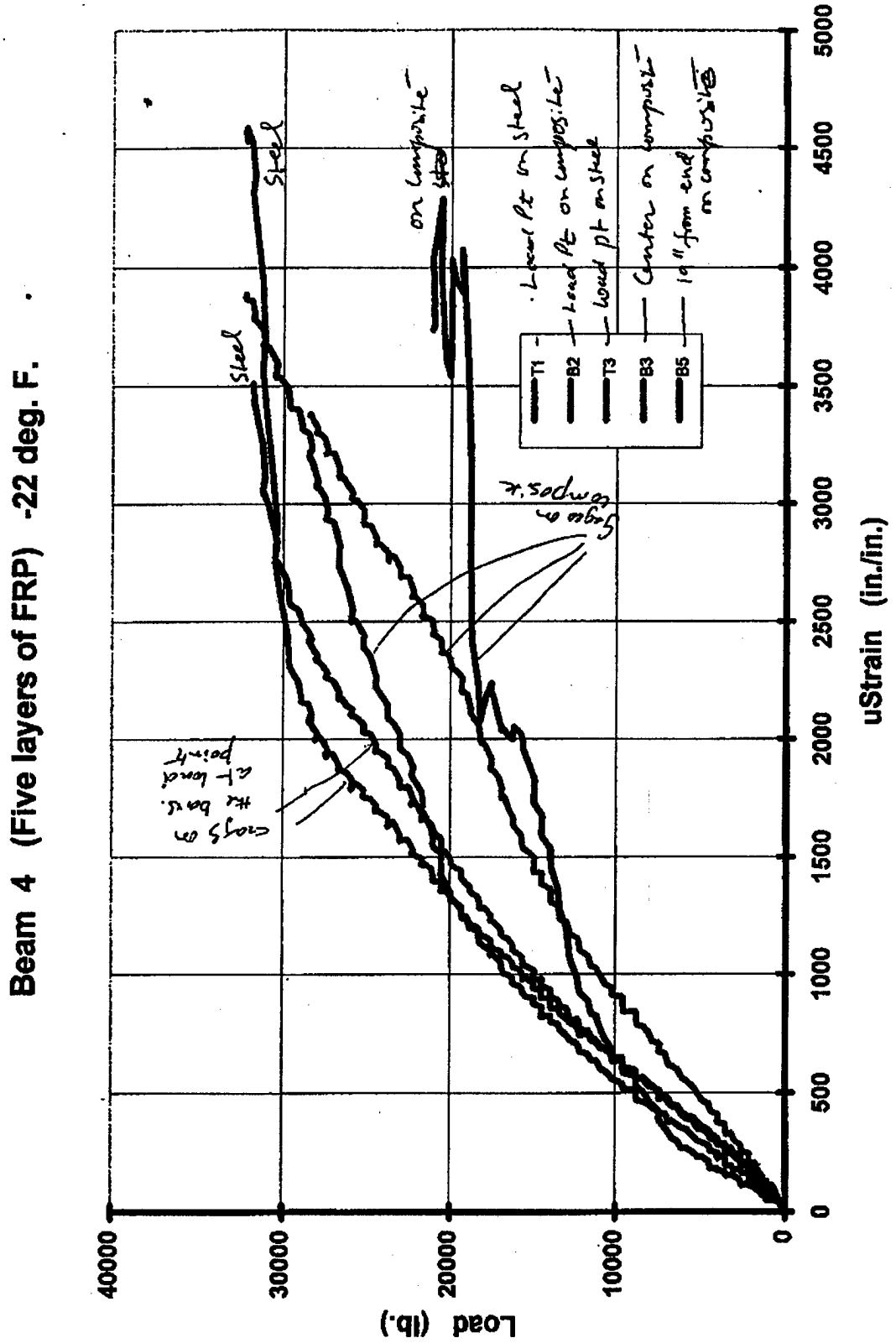


Figure E10.1. Room temperature load/strain data from ODOT beam 4 (five-layer CFRP).

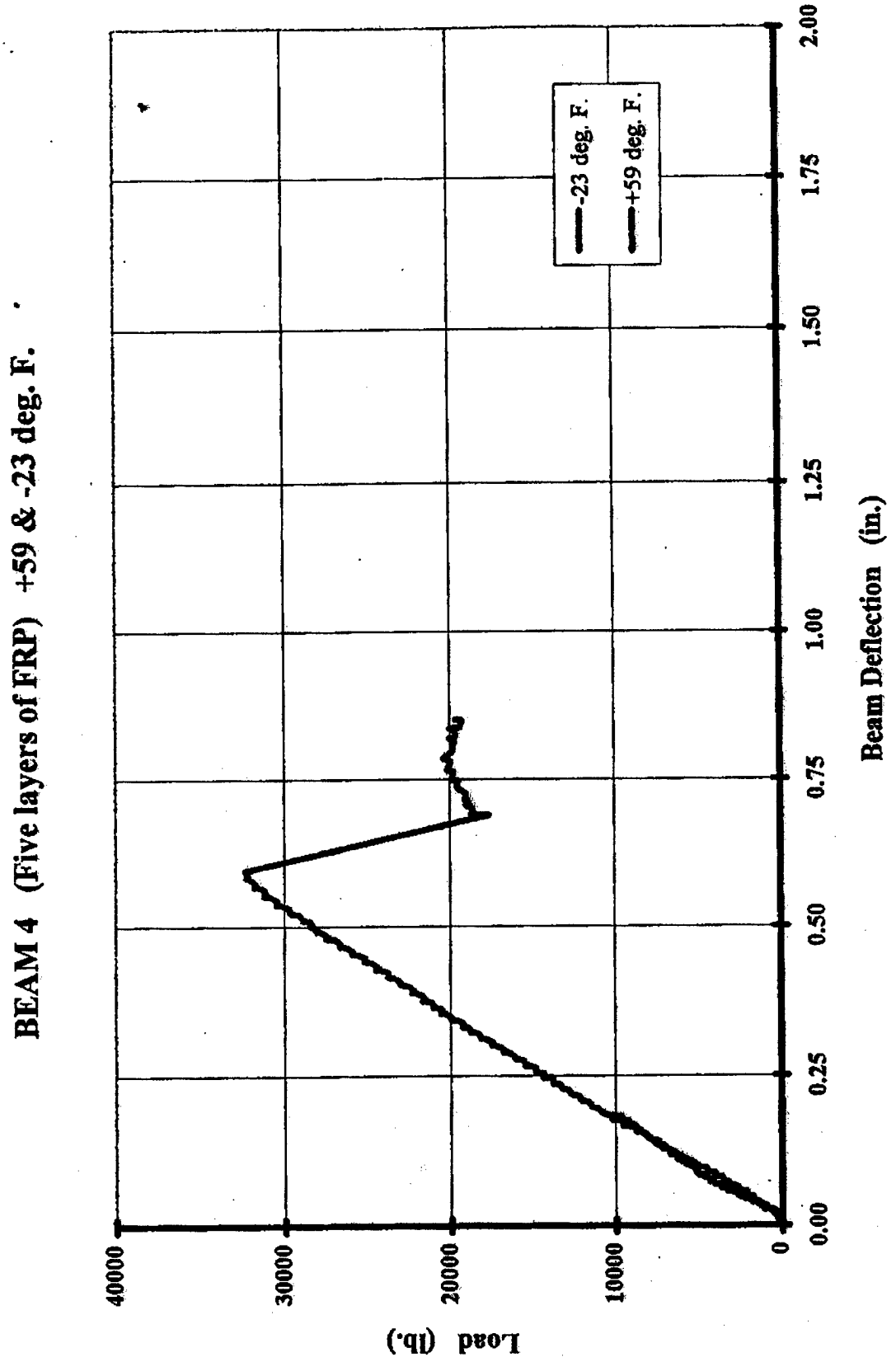


Figure E10.2. Low temperature and room temperature load/deflection data from ODOT beam 4 (five-layer CFRP).

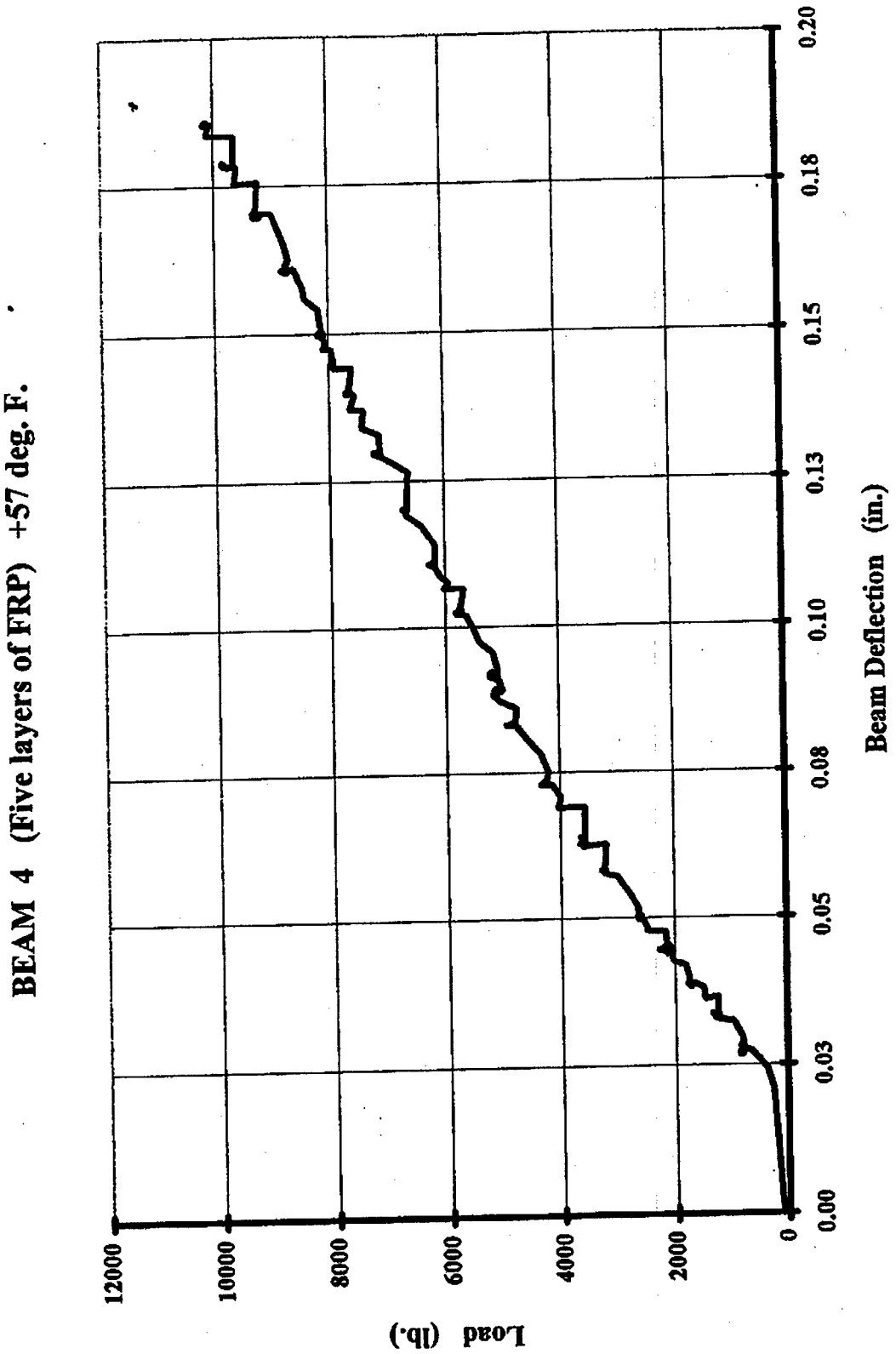


Figure E10.3. Room temperature load/deflection data from ODOT beam 4 (five-layer CFRP).

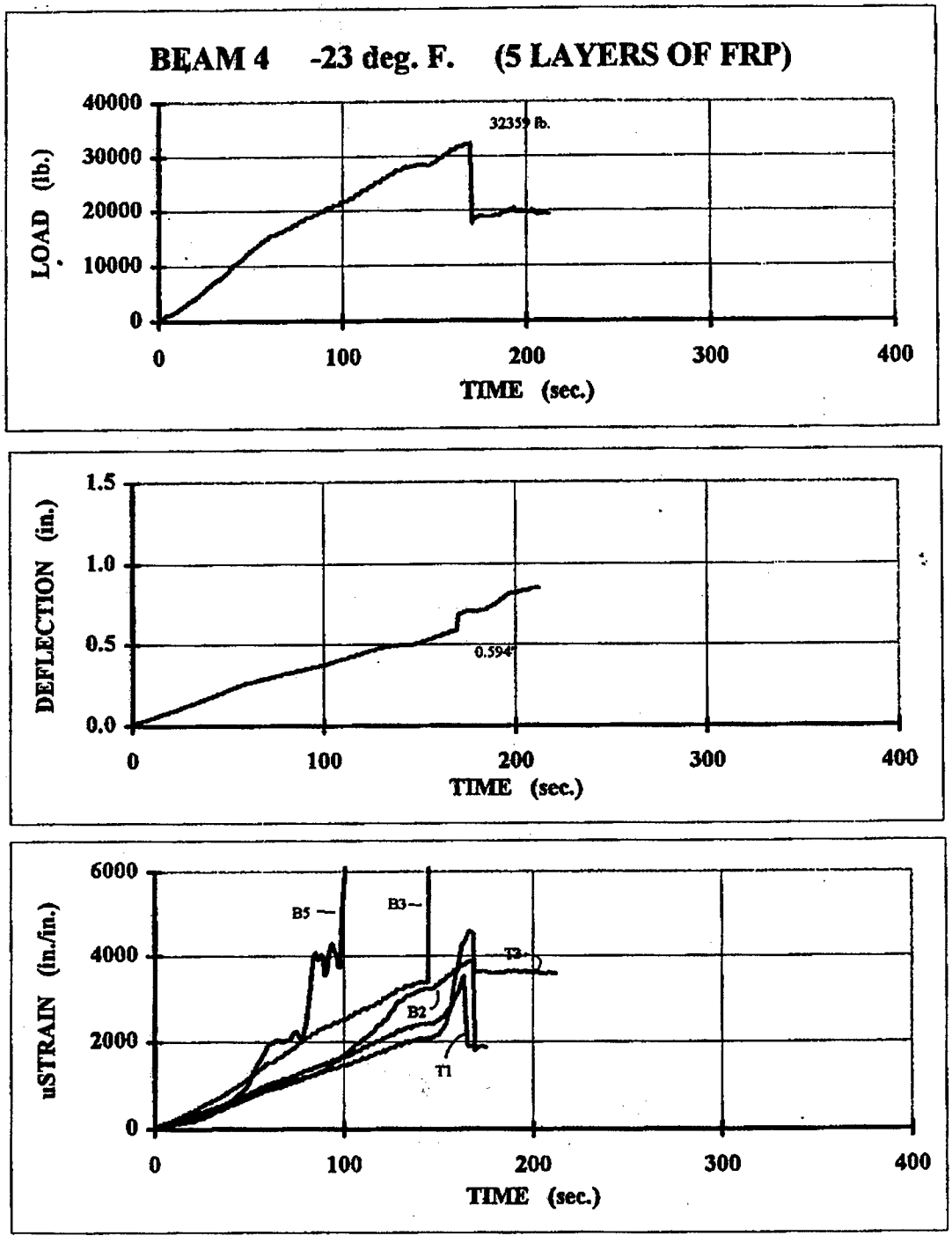


Figure E.10.4. Low temperature load, deflection, and strain data from ODOT beam 4 (five-layer CFRP).

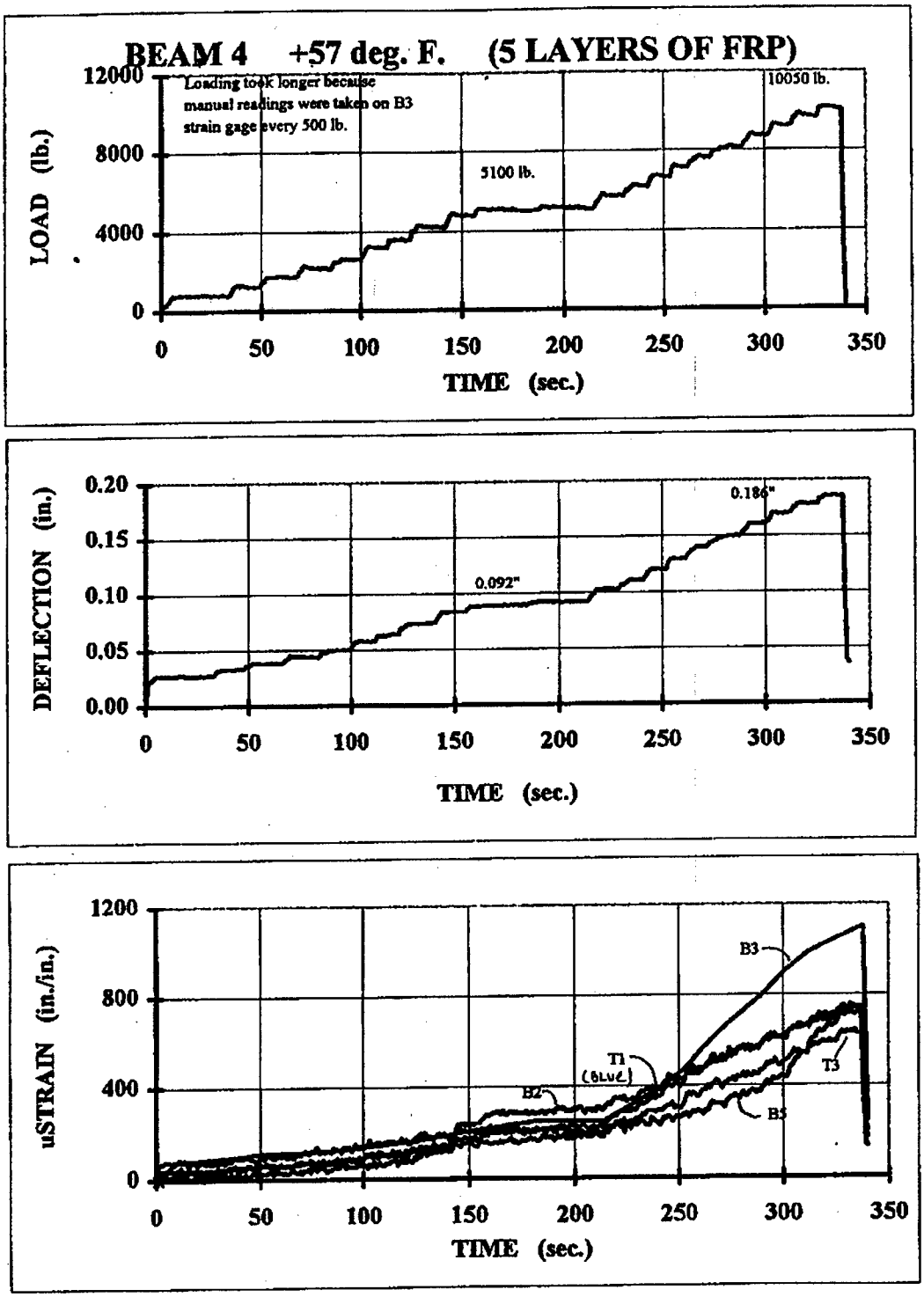


Figure E.10.5. Room temperature load, deflection, and strain data from ODOT beam 4 (five-layer CFRP).

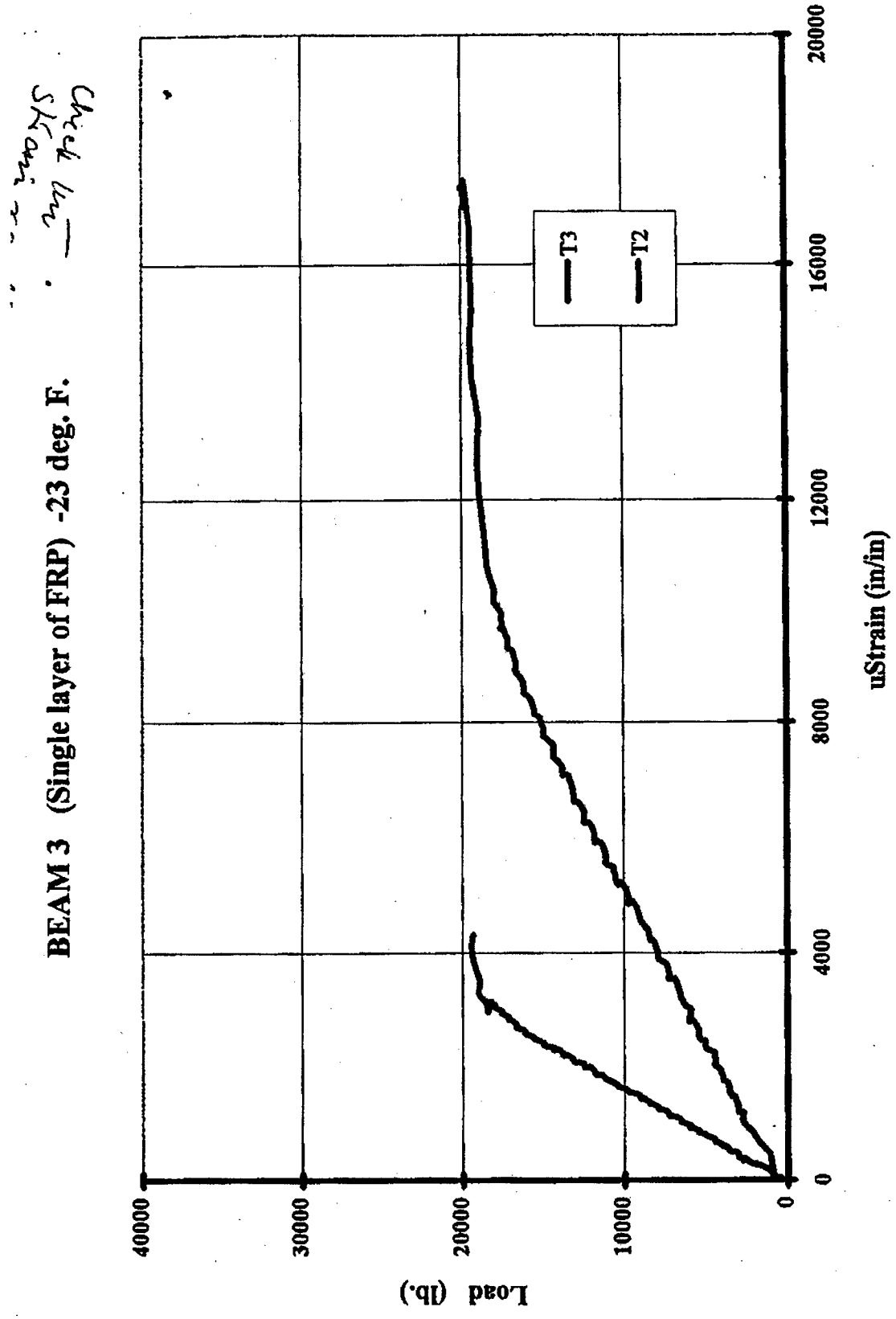


Figure E11.1. Low temperature load/strain data from ODOT beam 3 (one-layer CFRP).

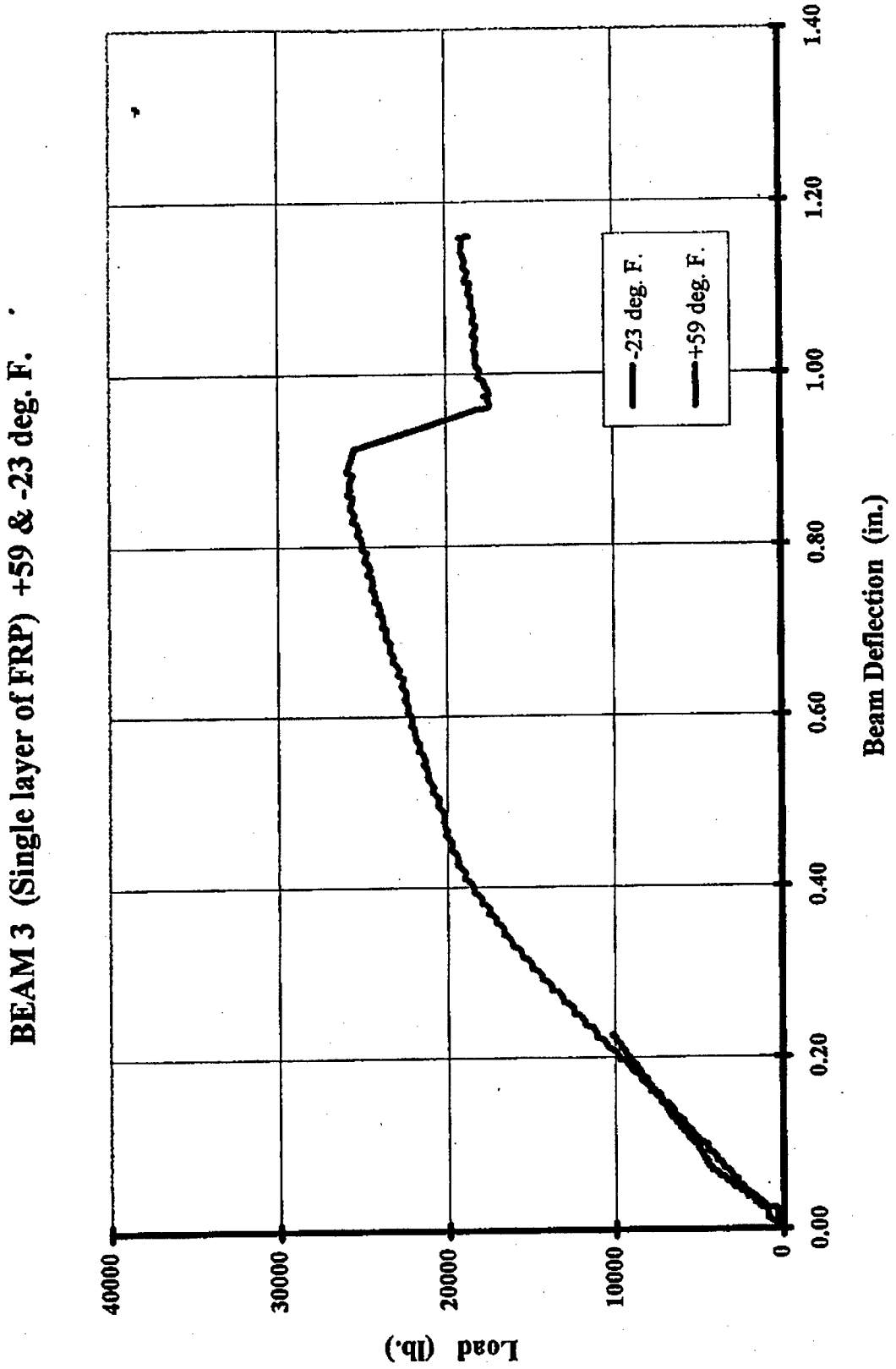


Figure E.11.2. Low temperature and room temperature load/deflection data from ODOT beam 3 (one-layer CFRP).

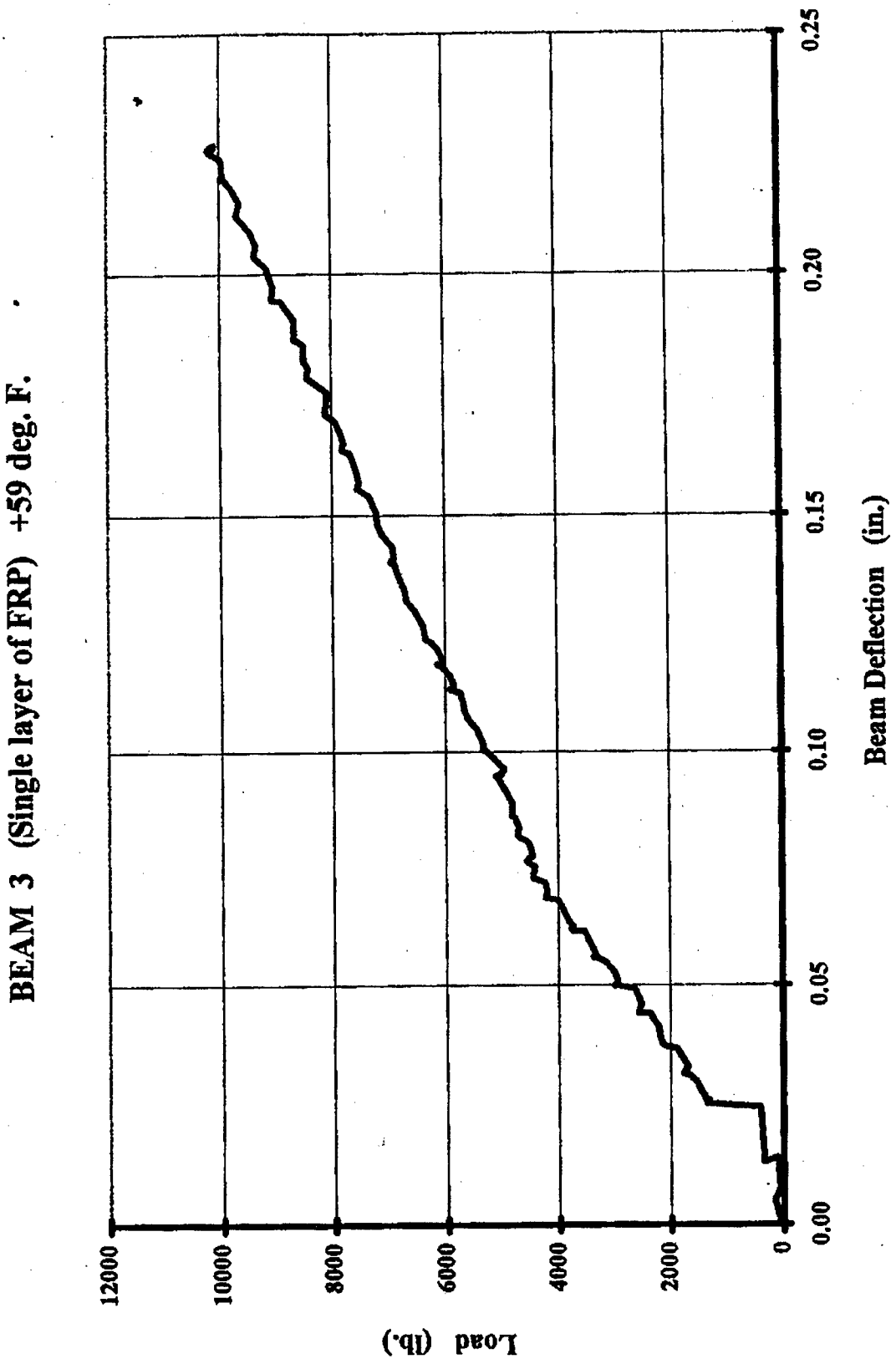


Figure E.11.3. Room temperature load/deflection data from ODOT beam 3 (one-layer CFRP).

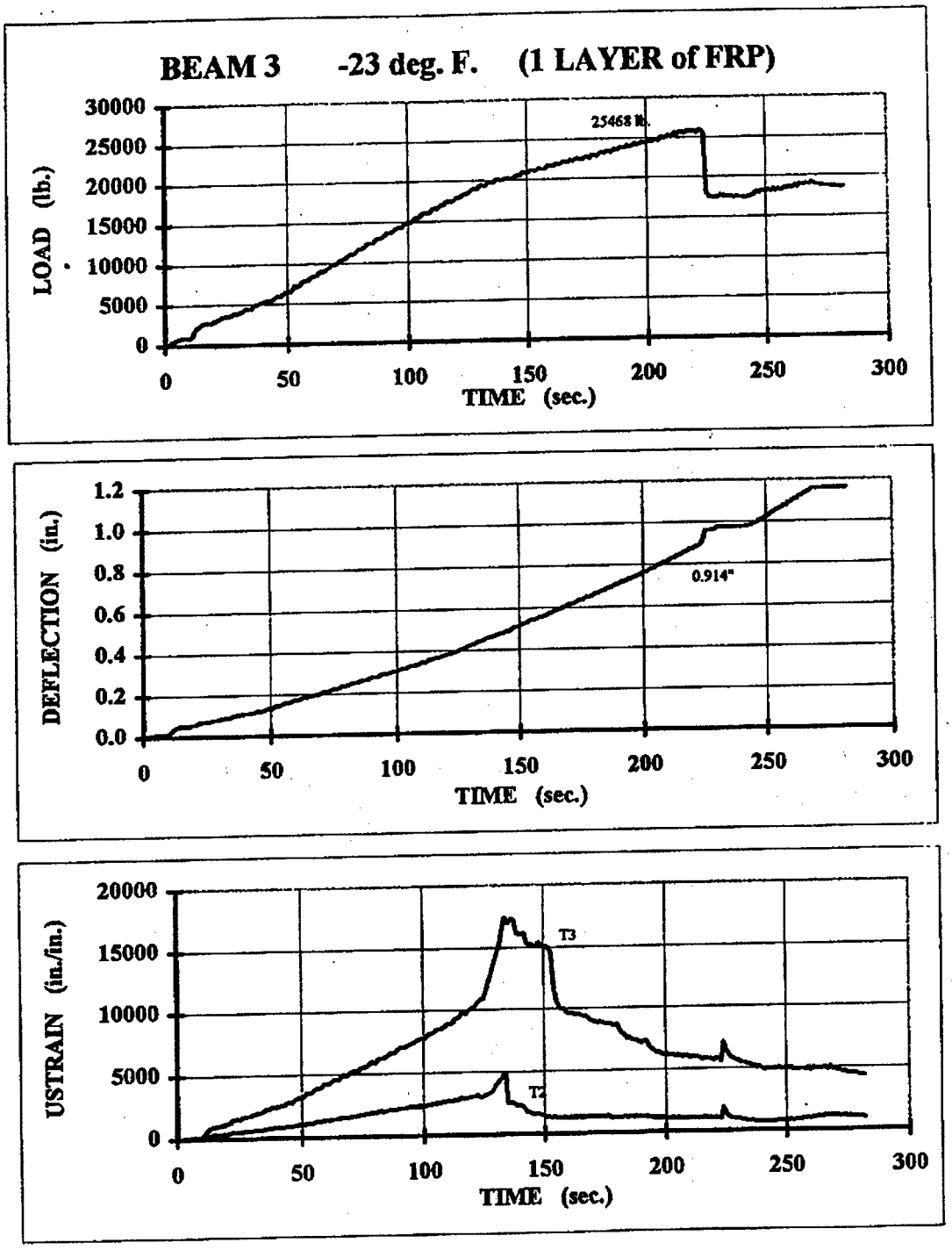


Figure E.11.4. Low temperature load, deflection, and strain data from ODOT beam 3 (one-layer CFRP).

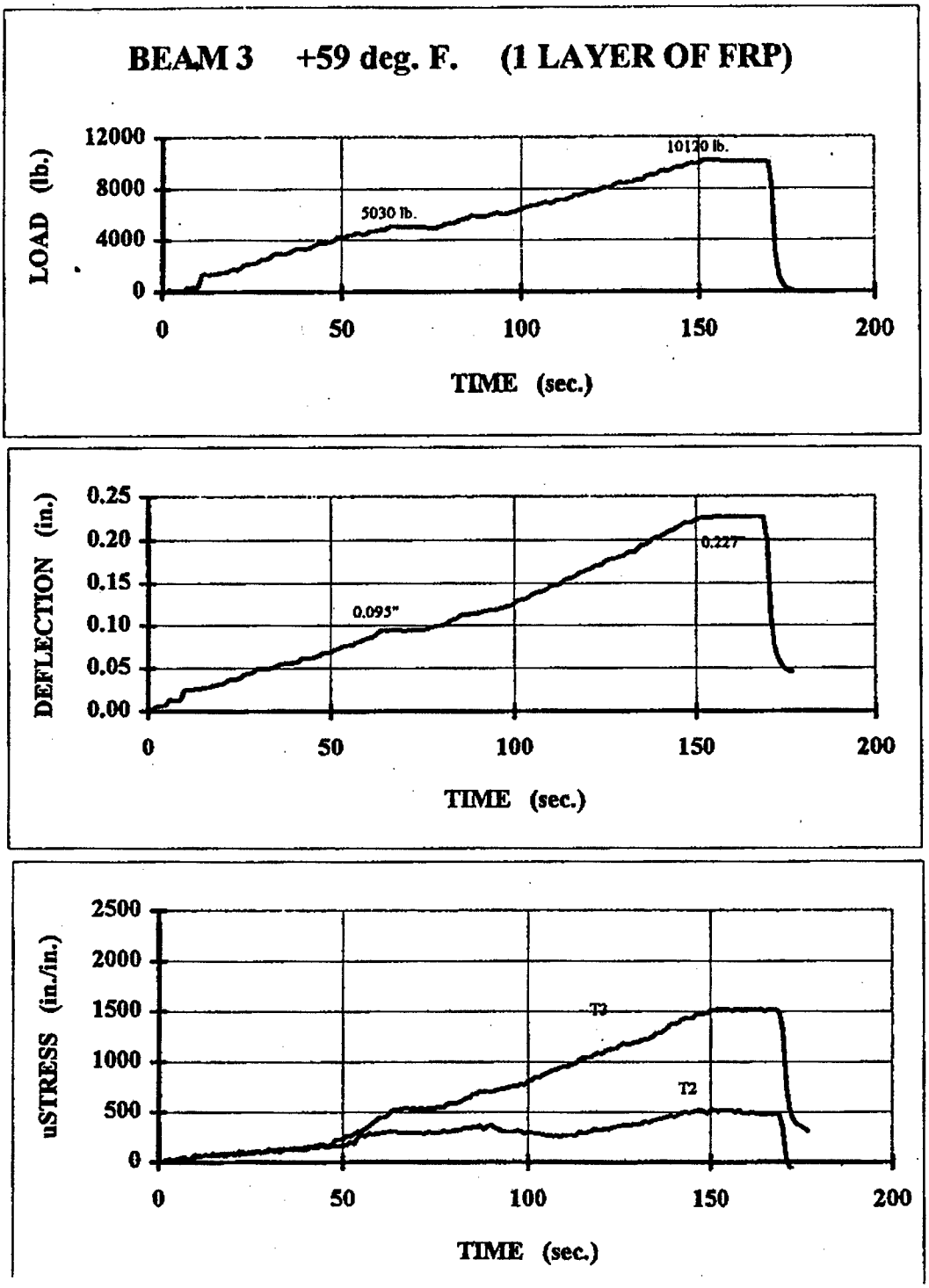


Figure E.11.5. Room temperature load, deflection, and strain data from ODOT beam 3 (one-layer CFRP).

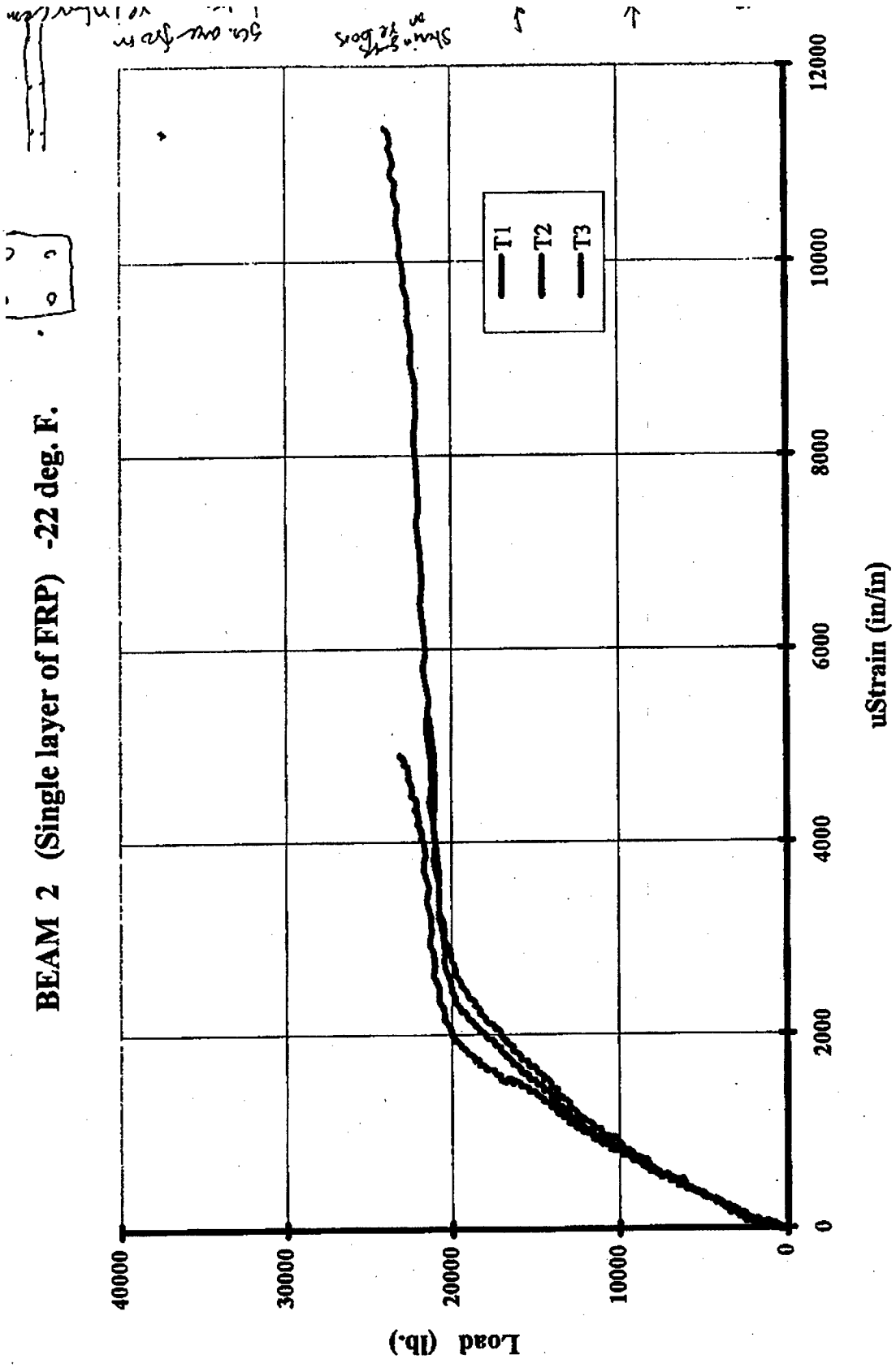


Figure 12.1. Low temperature load/strain data from ODOT beam 2 (one-layer CFRP).

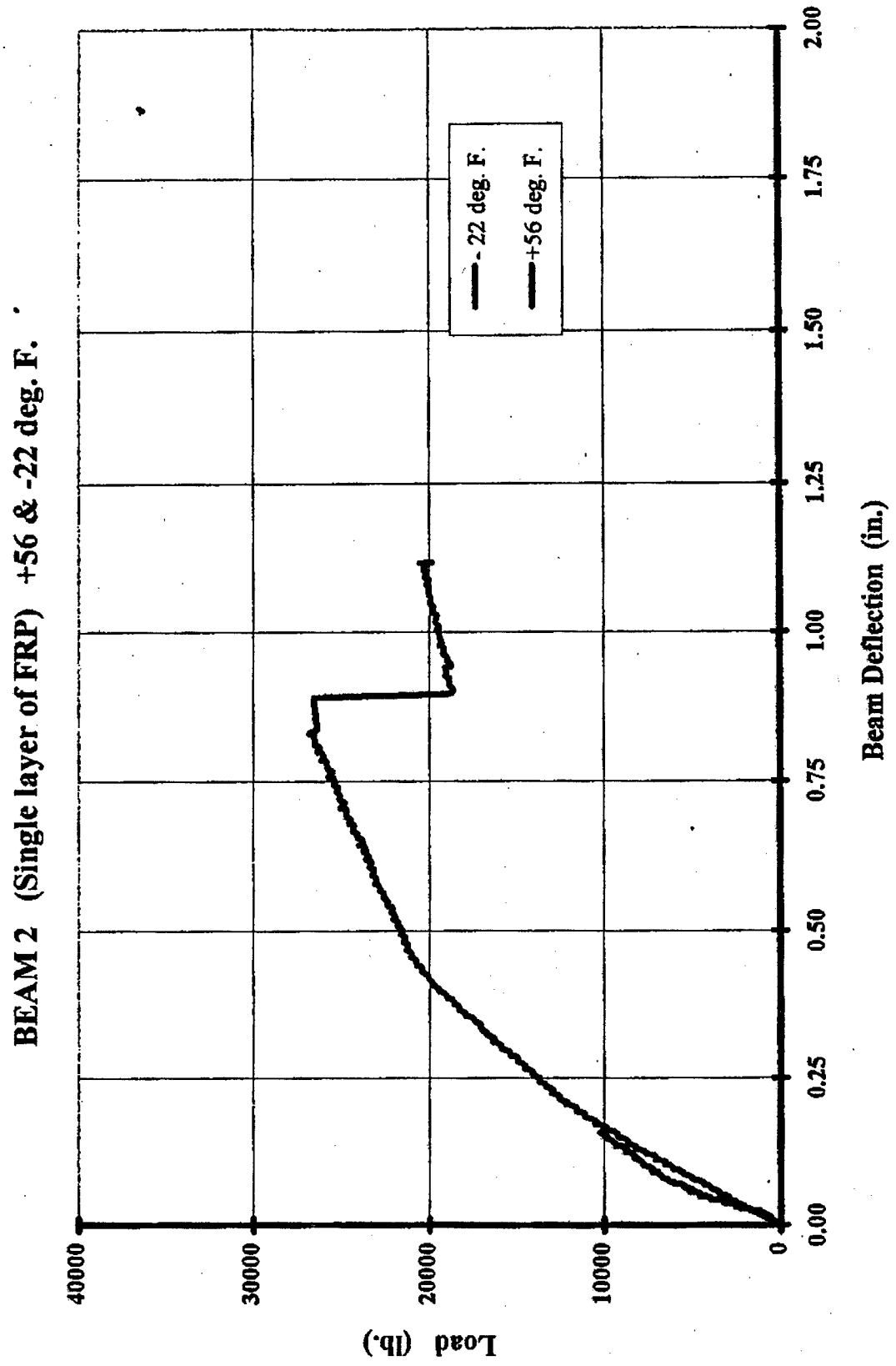


Figure E.12.2. Low temperature and room temperature load/deflection data from ODOT beam 2 (one-layer CFRP).

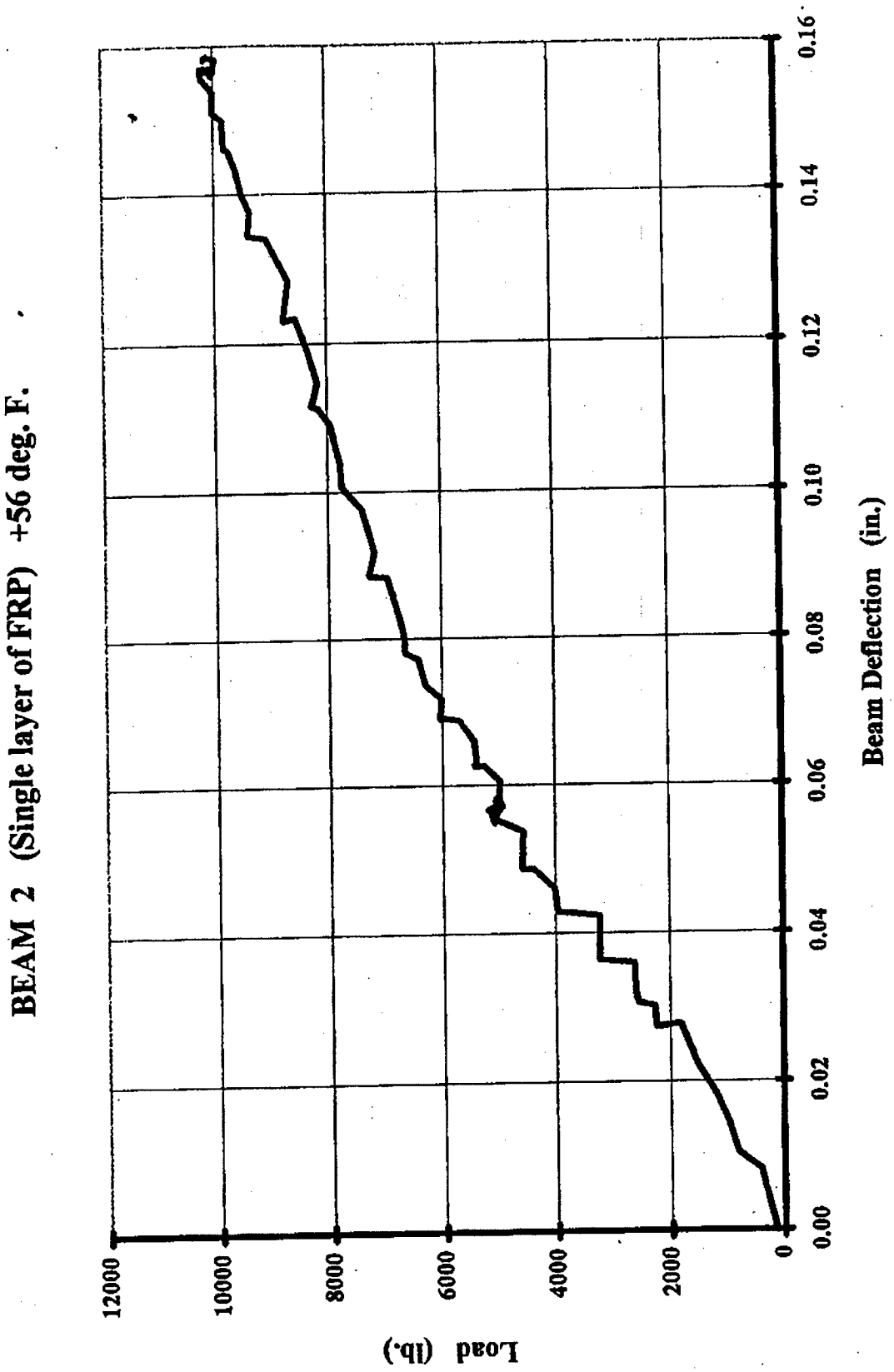


Figure E.12.3. Room temperature load/deflection data from ODOT beam 2 (one-layer CFRP).

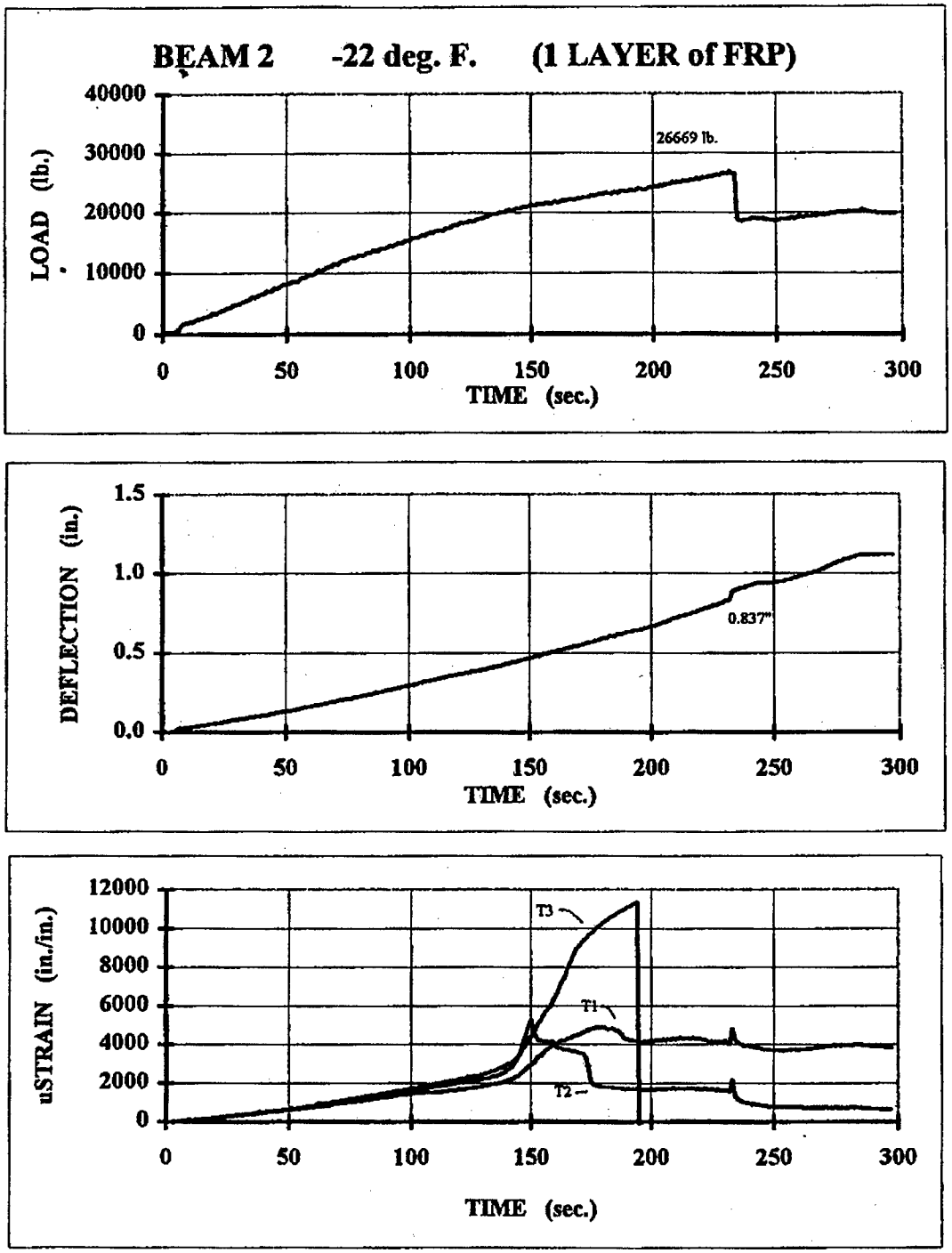


Figure E.12.4. Low temperature load, deflection, and strain data from ODOT beam 2 (one-layer CFRP).

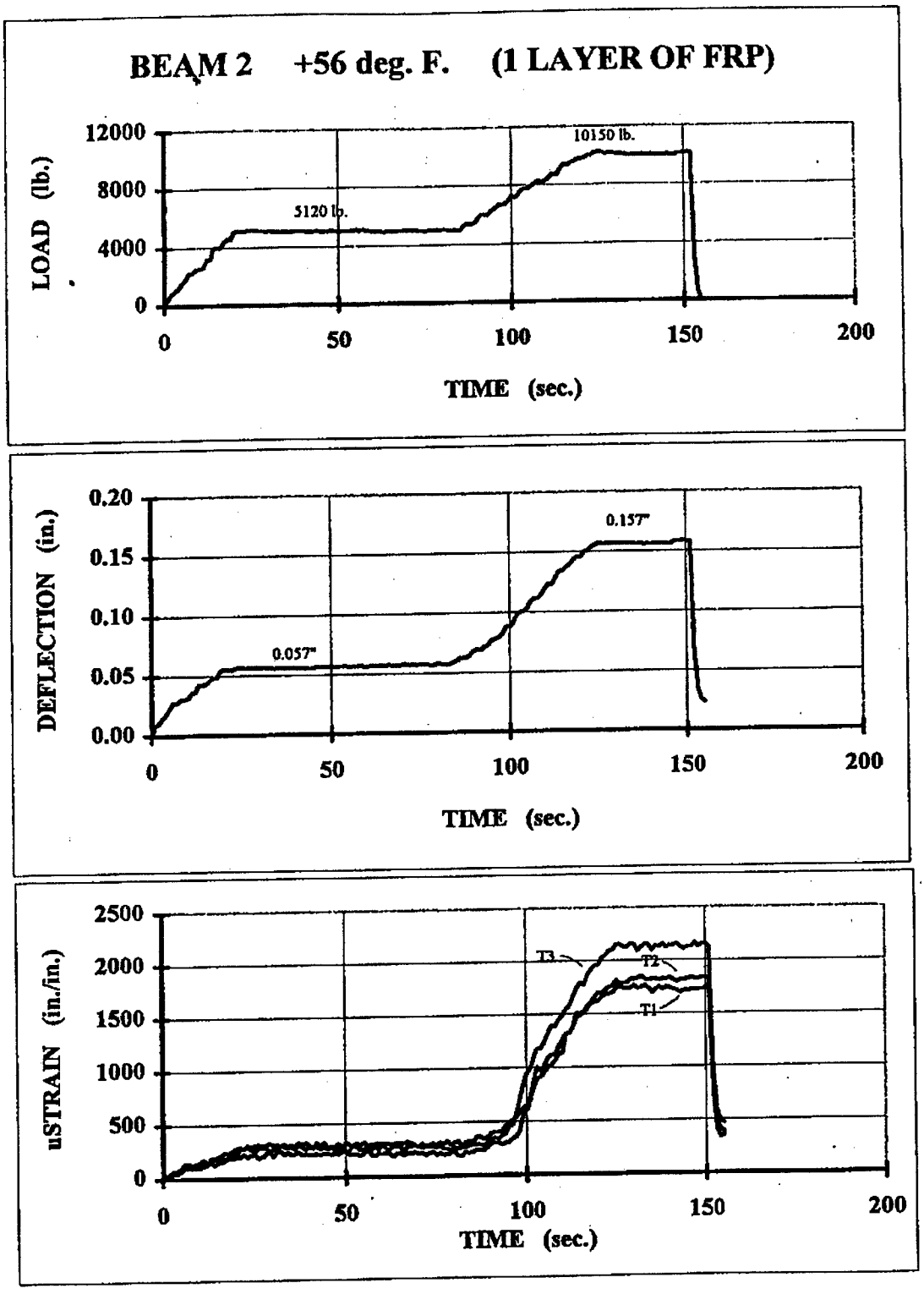


Figure E.12.5. Room temperature load, deflection, and strain data from ODOT beam 2 (one-layer CFRP).

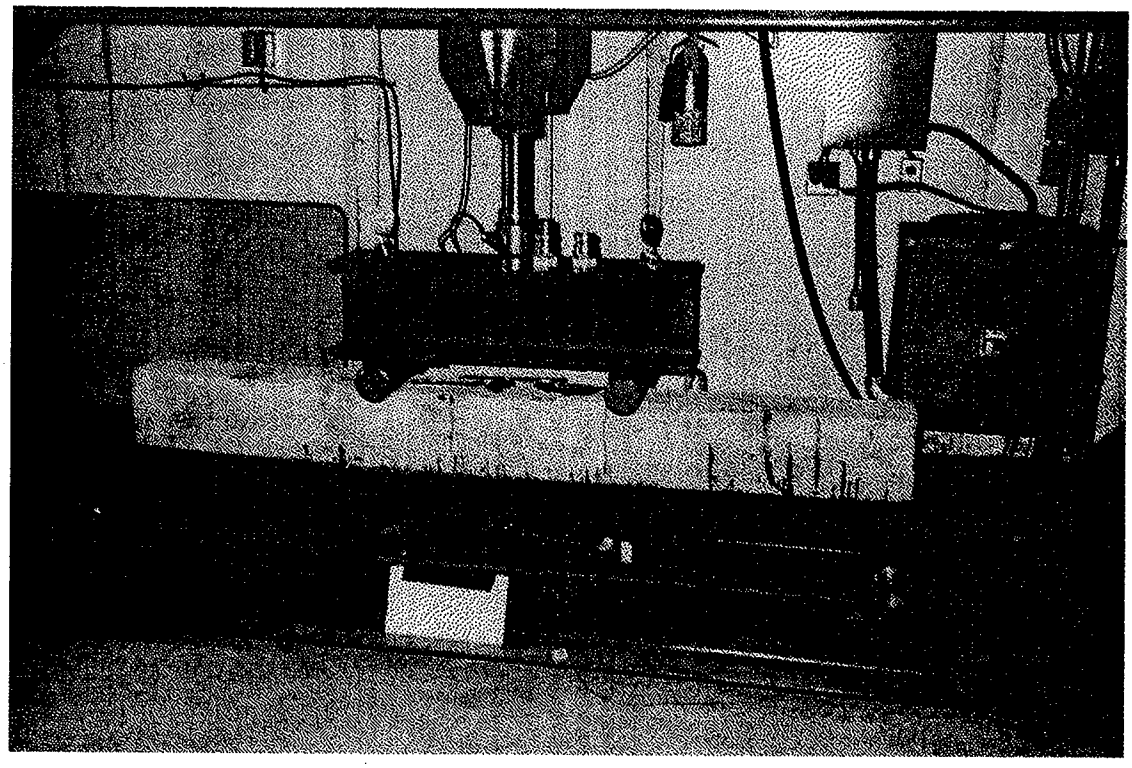


Figure E13. ODOT beam no.1 (five-layer CFRP) under four-point flexural test.

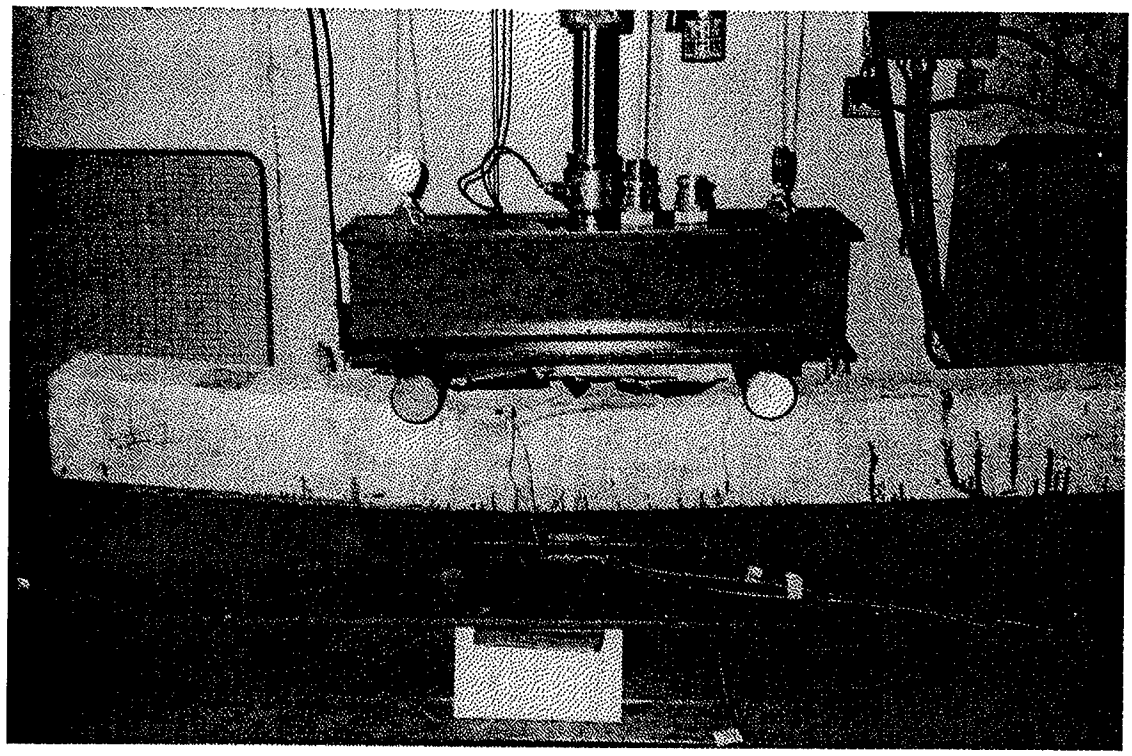


Figure E14. ODOT beam no.1 (five-layer CFRP) at low temperature flexure test after complete failure.

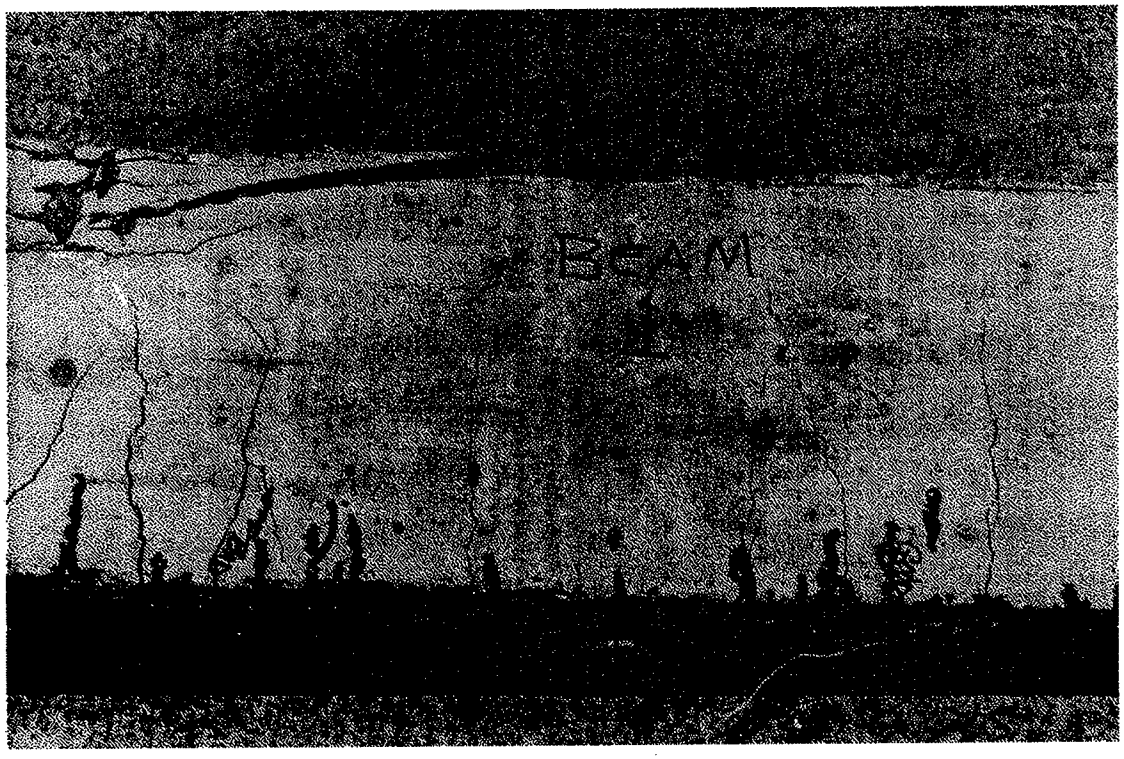


Figure E15. Failed beam showing crack extension from the bottom surface.

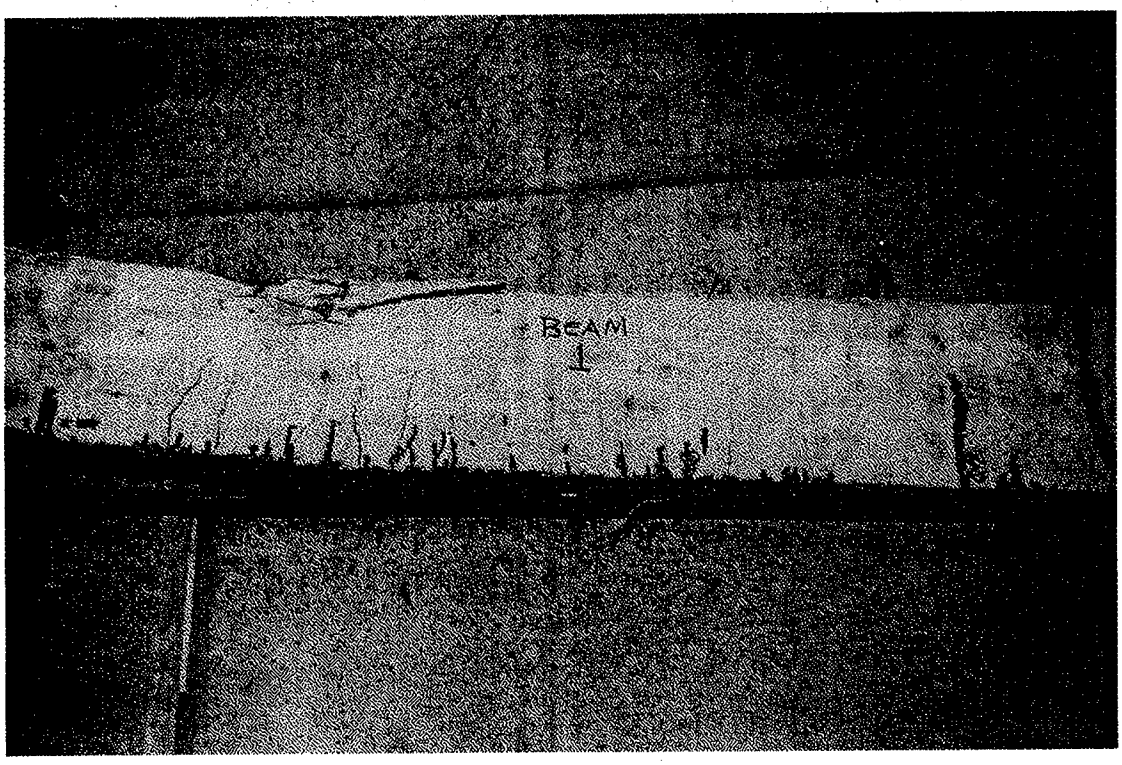


Figure E16. The five-layer CFRP debonded under flexural loading to failure.

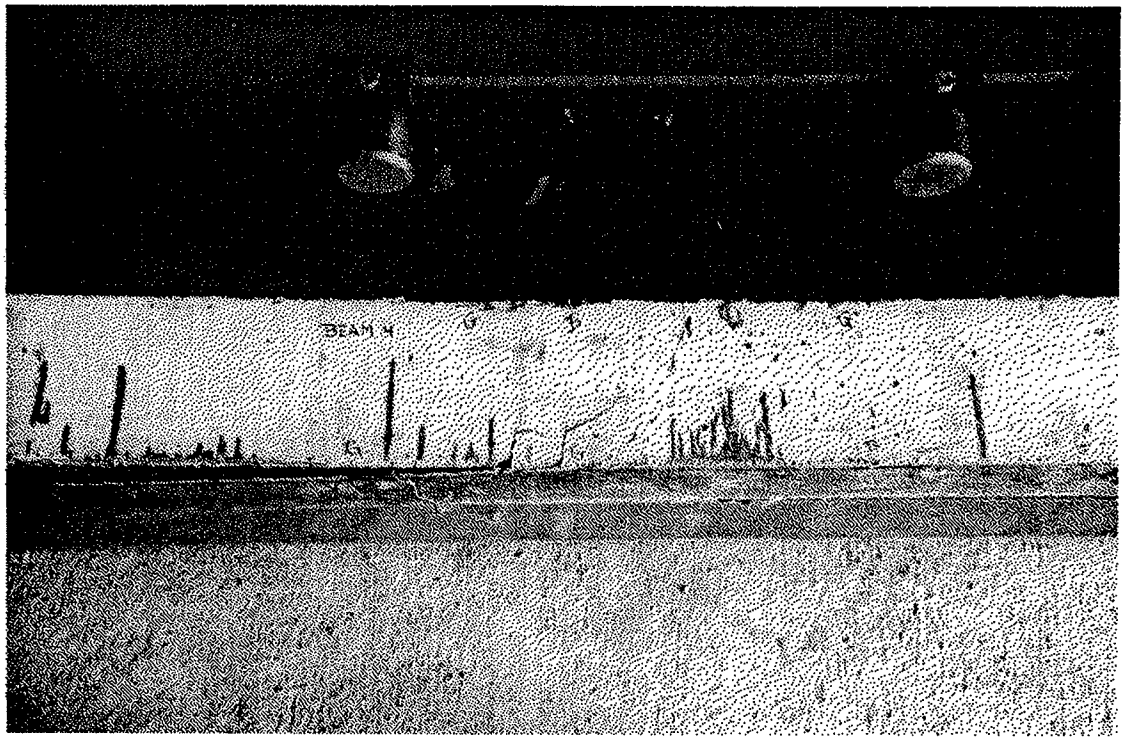


Figure E17. The five-layer CFRP shows no sign of tensile failure.

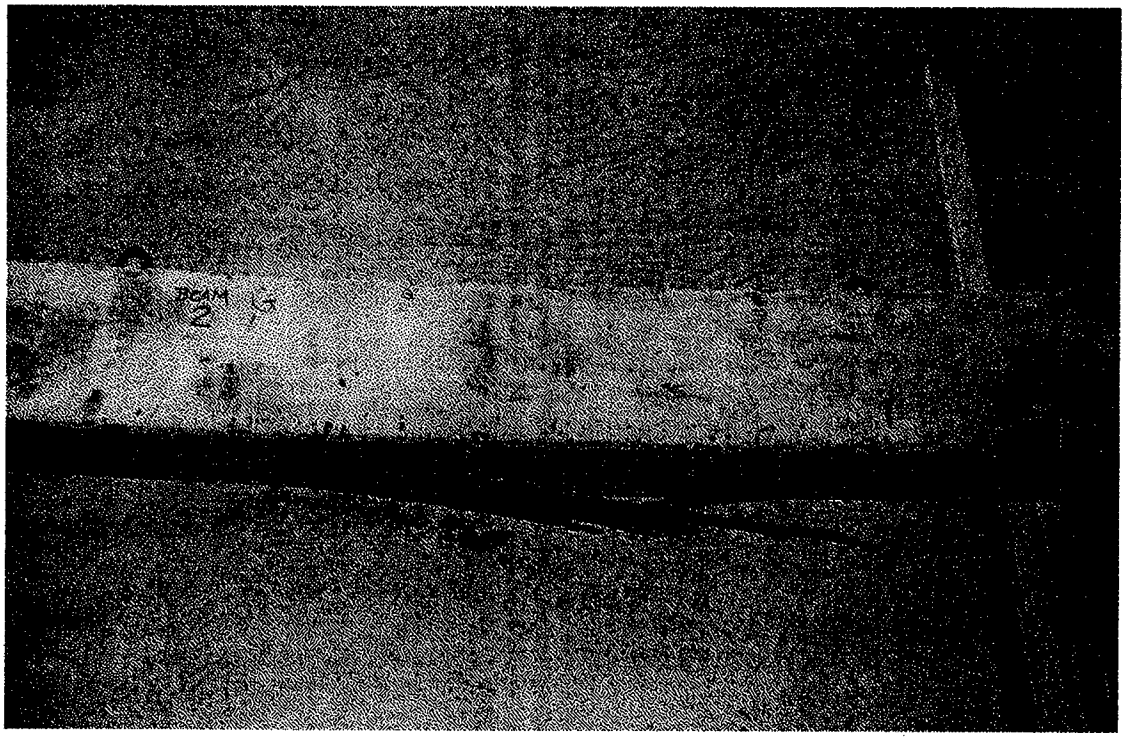


Figure E18. The one-layer CFRP shows tensile fiber fracture under four-point flexural loading.

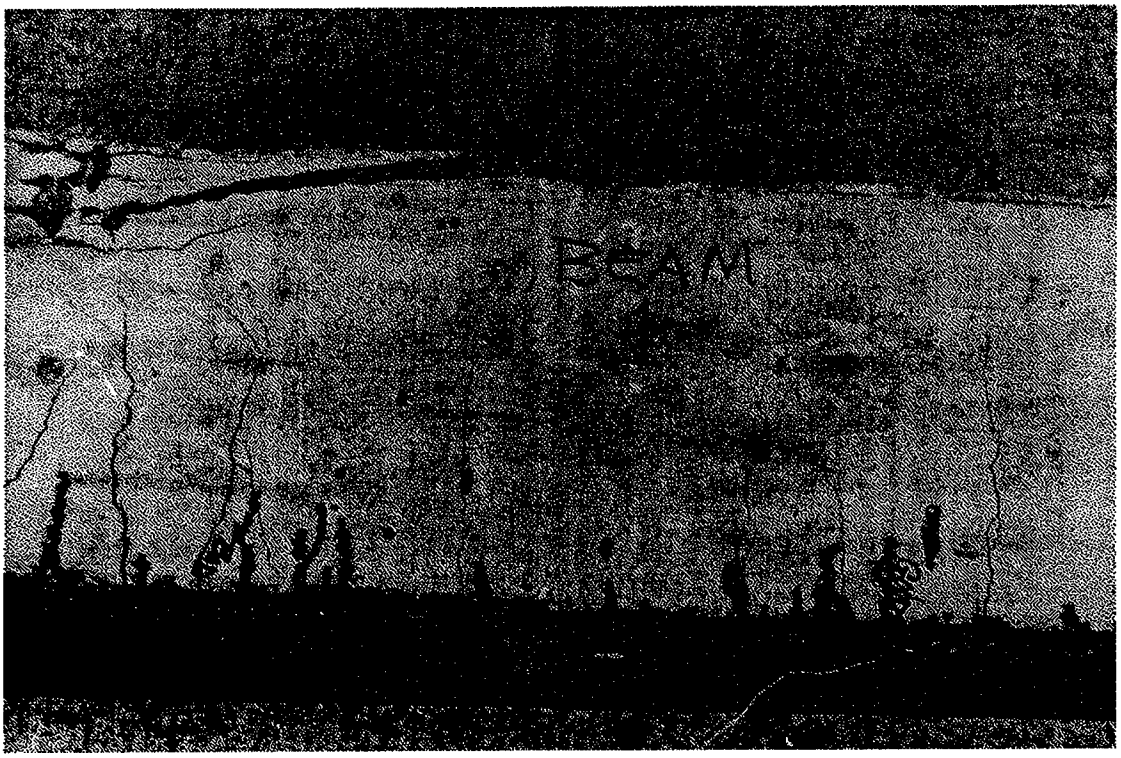


Figure E19. A close up view of the five-layer debonded CFRP/concrete interface.

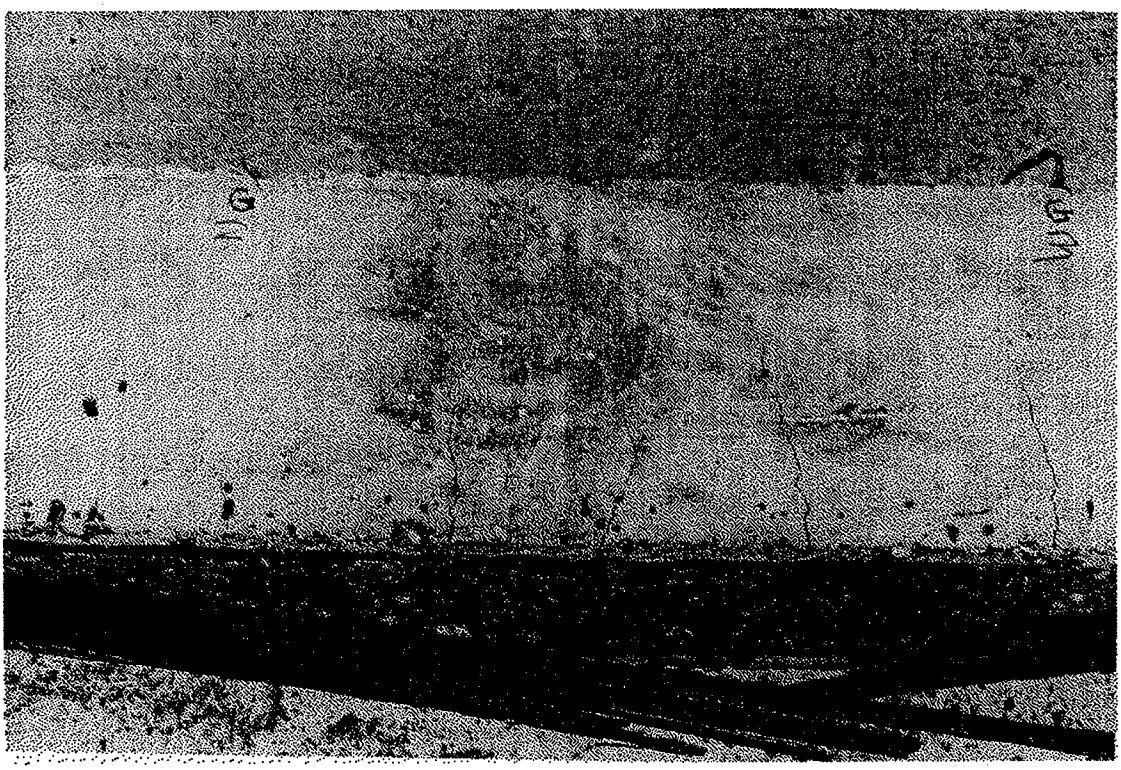


Figure E20. A close up view of the one-layer debonded CFRP/concrete interface.

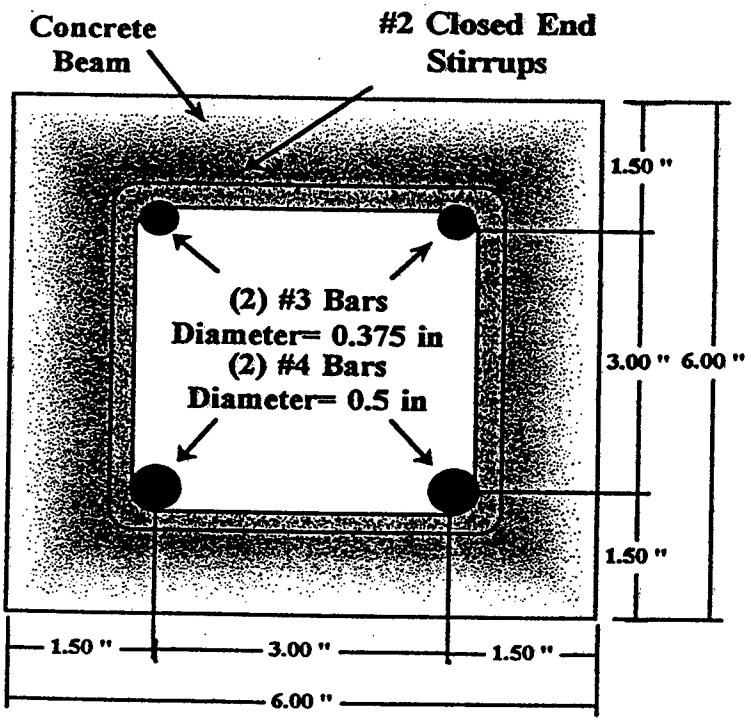


Figure E21. Cross-section of the concrete beam for fatigue testing.

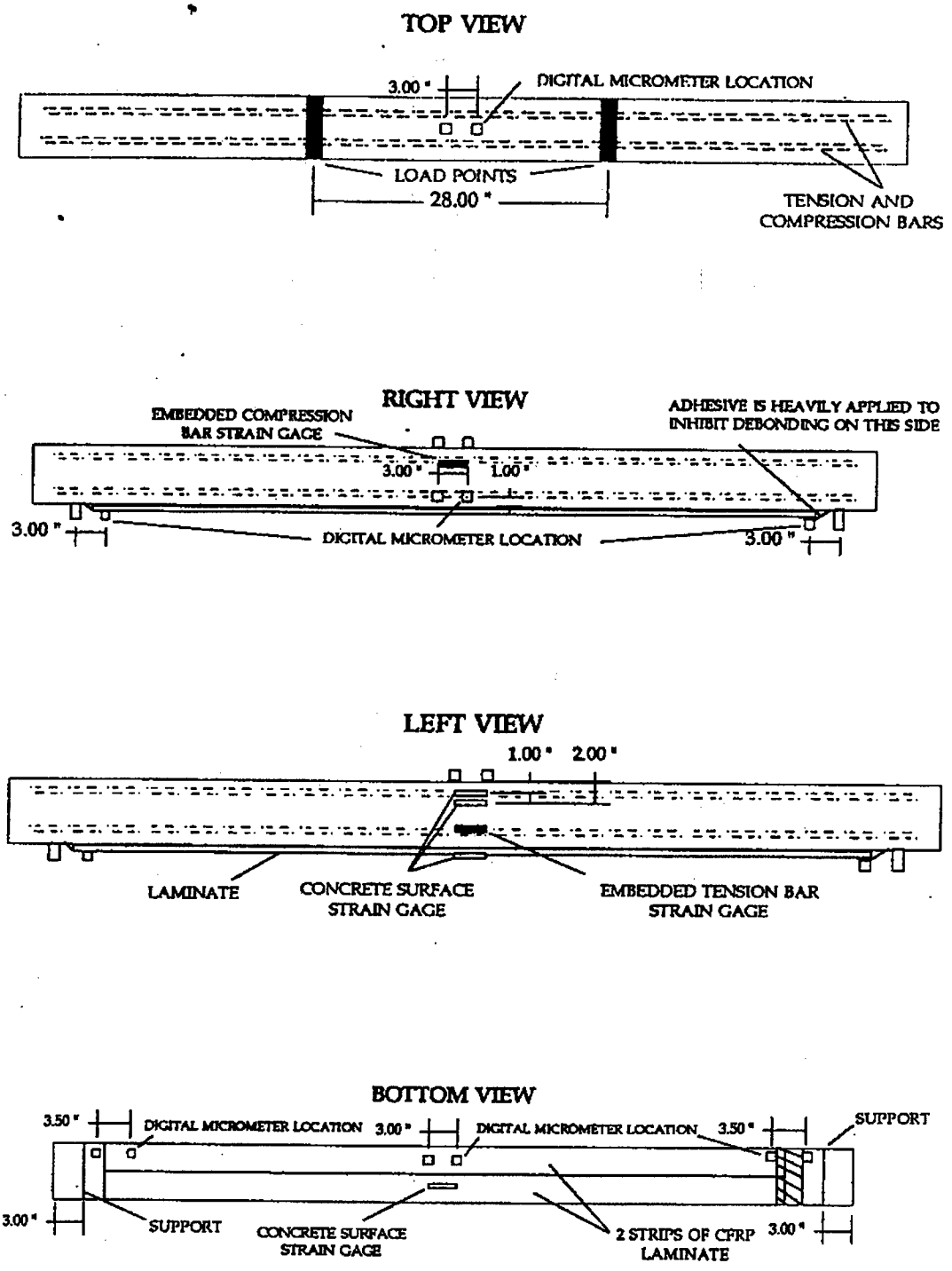


Figure E22. Instrumentation systems for the fatigue testing beams.

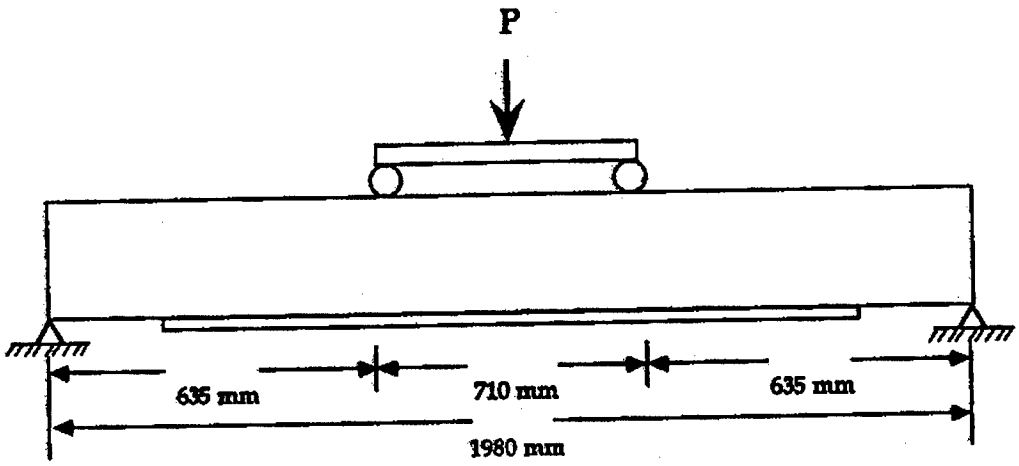


Figure E23. Flexural loading configuration of the fatigue testing beams.

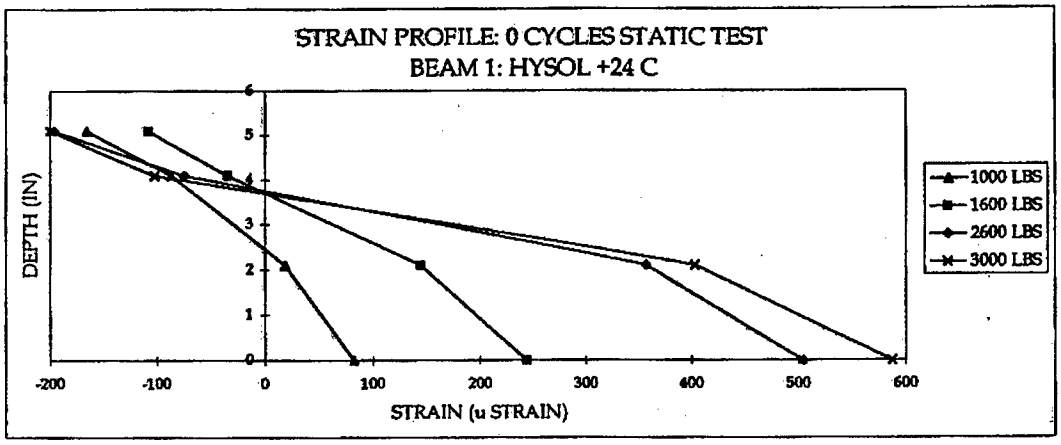


Figure E24. Room temp. test strain profiles of the Hysol 9330 repaired fatigue beam after 0 cycle.

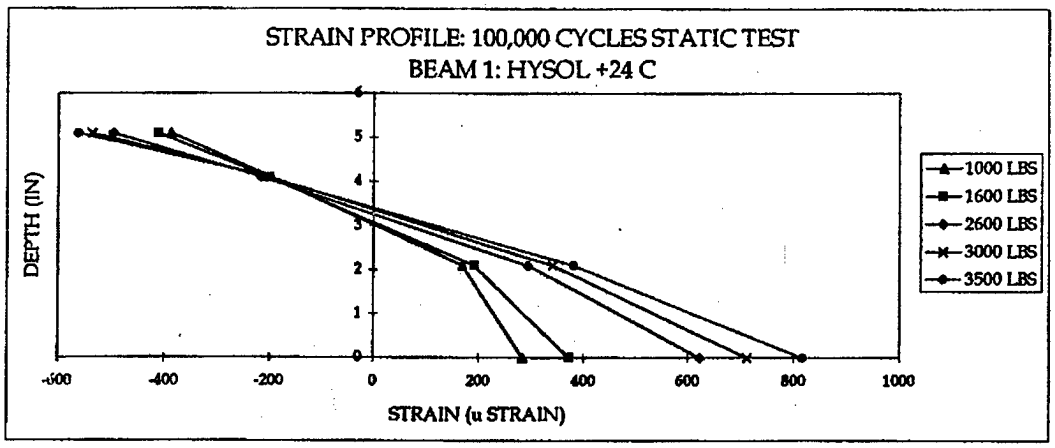


Figure E25. Room temp. test strain profiles of the Hysol 9330 repaired fatigue beam after 10^5 cycles.

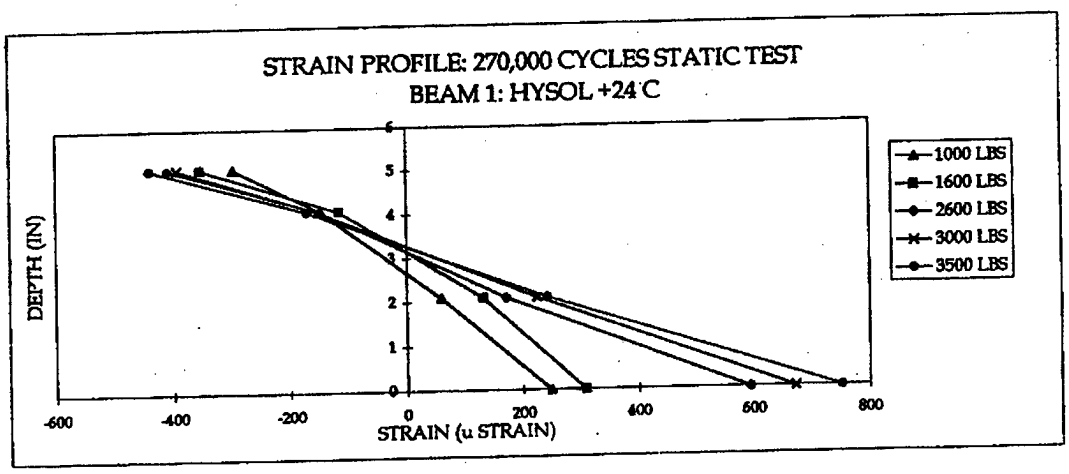


Figure E26. Room temp. test strain profiles of the Hysol 9330 repaired fatigue beam after 2.7×10^5 cycles.

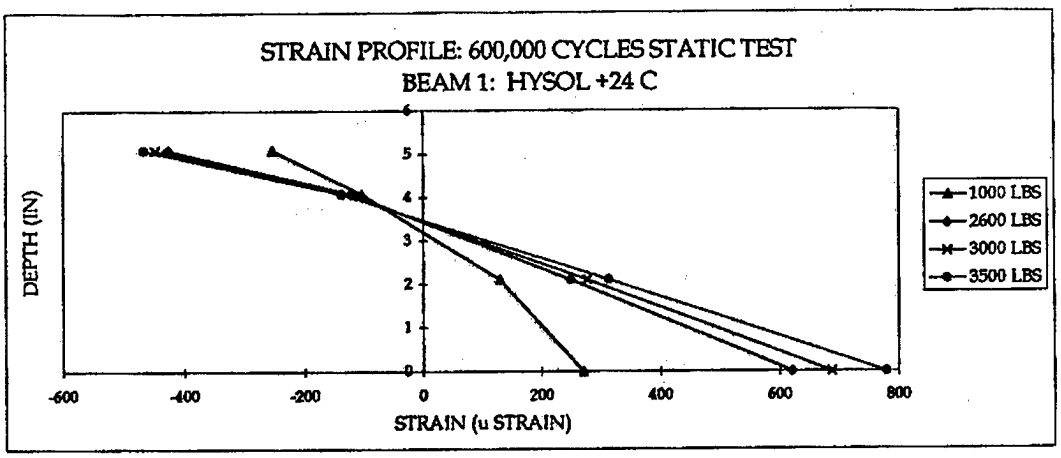


Figure E27. Room temp. test strain profiles of the Hysol 9330 repaired fatigue beam after $6x10^5$ cycles.

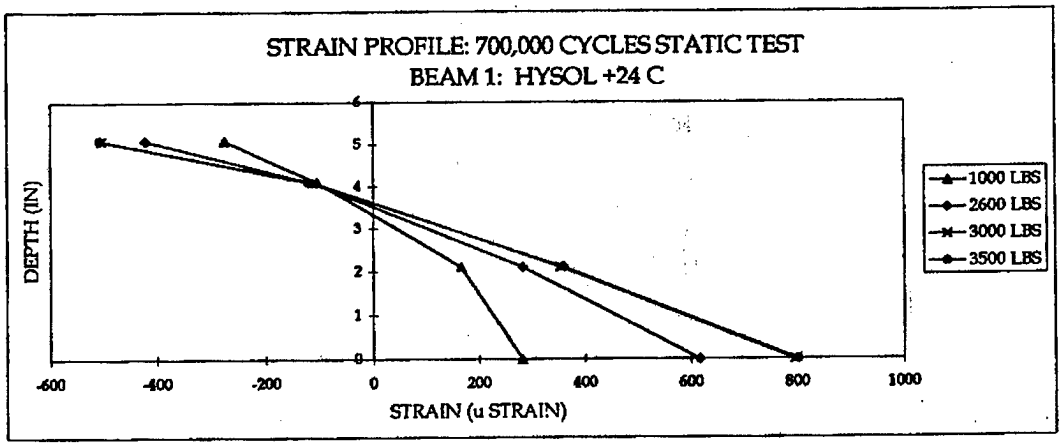


Figure E28. Room temp. test strain profiles of the Hysol 9330 repaired fatigue beam after $7x10^5$ cycles.

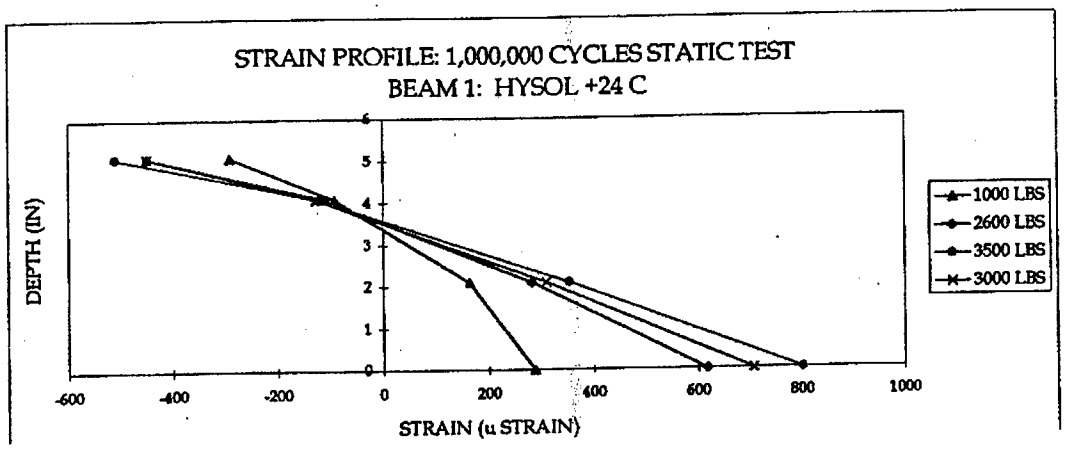


Figure E29. Room temp. test strain profiles of the Hysol 9330 repaired fatigue beam after 10^6 cycles.

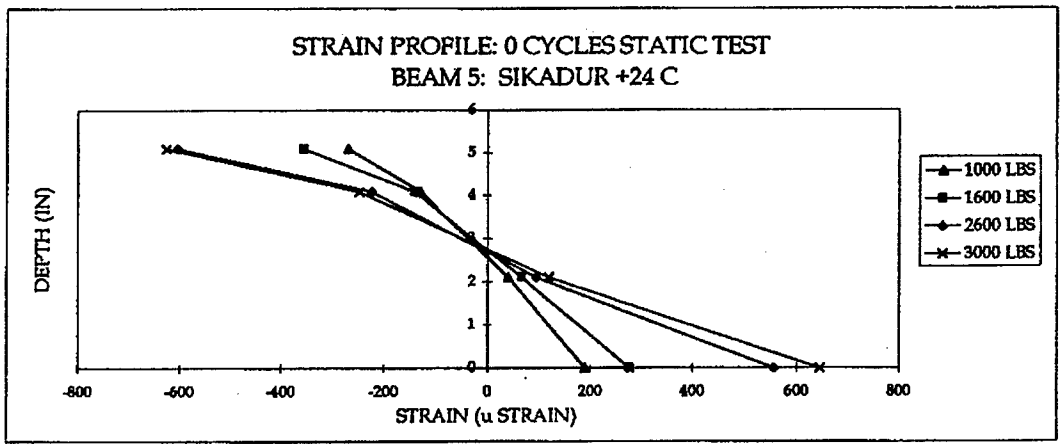


Figure E30. Room temp. test strain profiles of the Sikadur 30 repaired fatigue beam after 0 cycle.

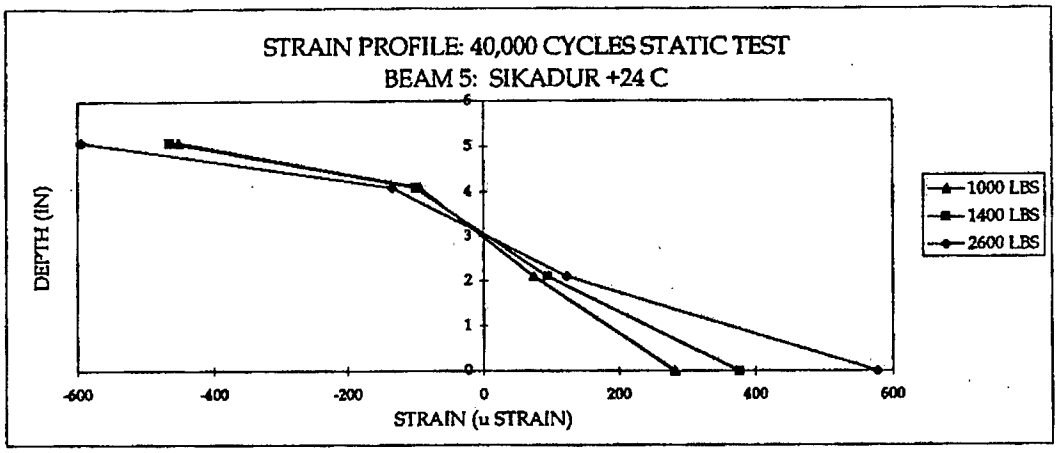


Figure E31. Room temp. test strain profiles of the Sikadur 30 repaired fatigue beam after $4x10^4$ cycles.

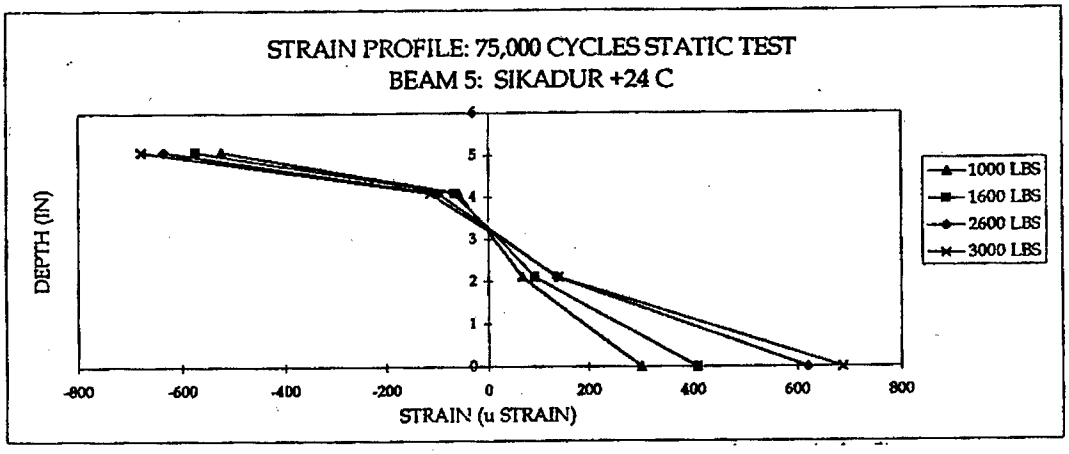


Figure E32. Room temp. test strain profiles of the Sikadur 30 repaired fatigue beam after $7.5x10^4$ cycles.

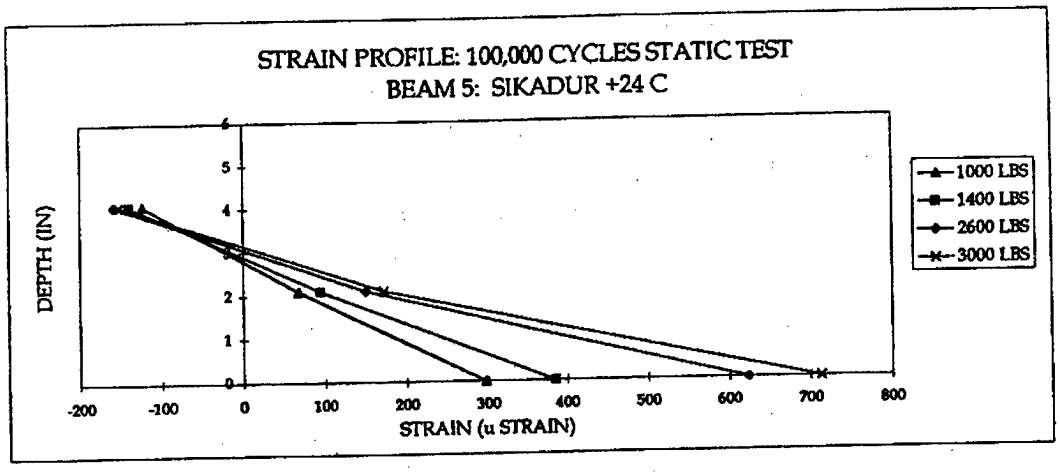


Figure E33. Room temp. test strain profiles of the Sikadur 30 repaired fatigue beam after 10^5 cycles.

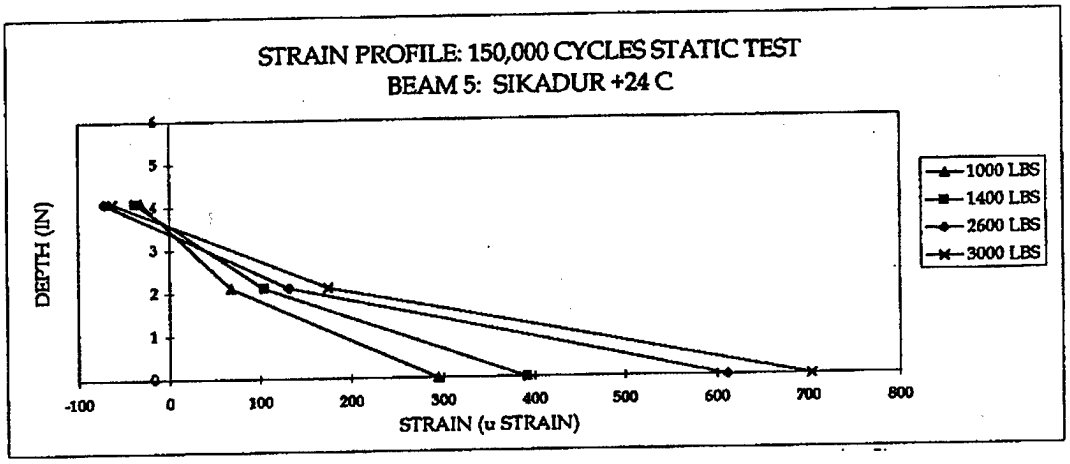


Figure E34. Room temp. test strain profiles of the Sikadur 30 repaired fatigue beam after $1.5x10^5$ cycles.

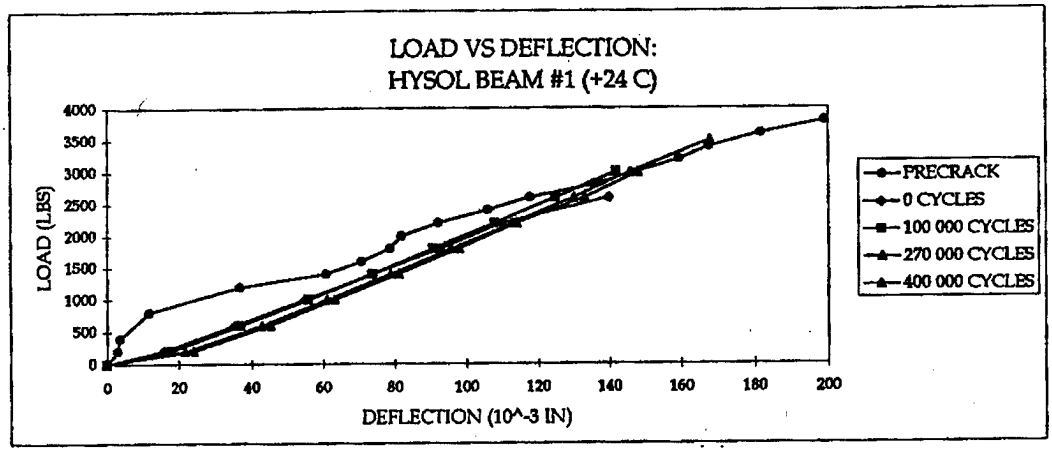


Figure E35. Room temp. test load/deflection data of the Hysol 9330 repaired fatigued beam no.1 (0 to $4x10^5$ cycles).

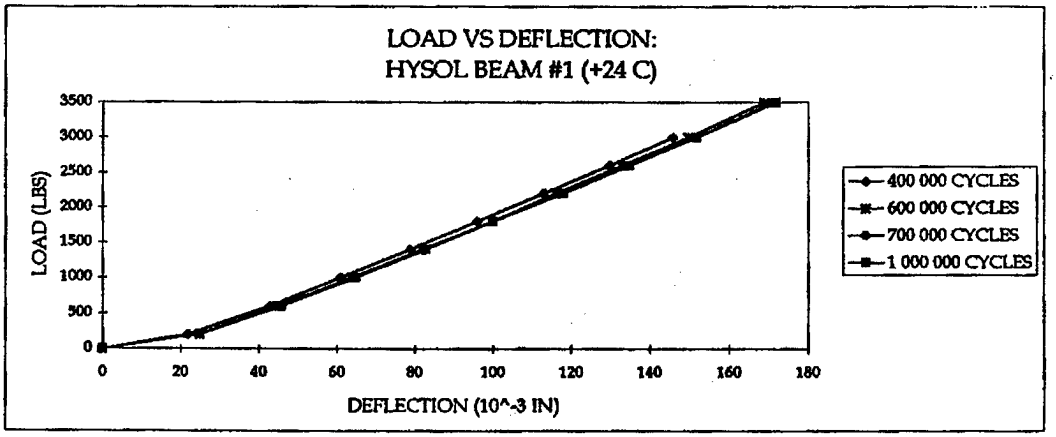


Figure E36. Room temp. test load/deflection data of the Hysol 9330 repaired fatigued beam no.1 ($4x10^5$ to 10^6 cycles).

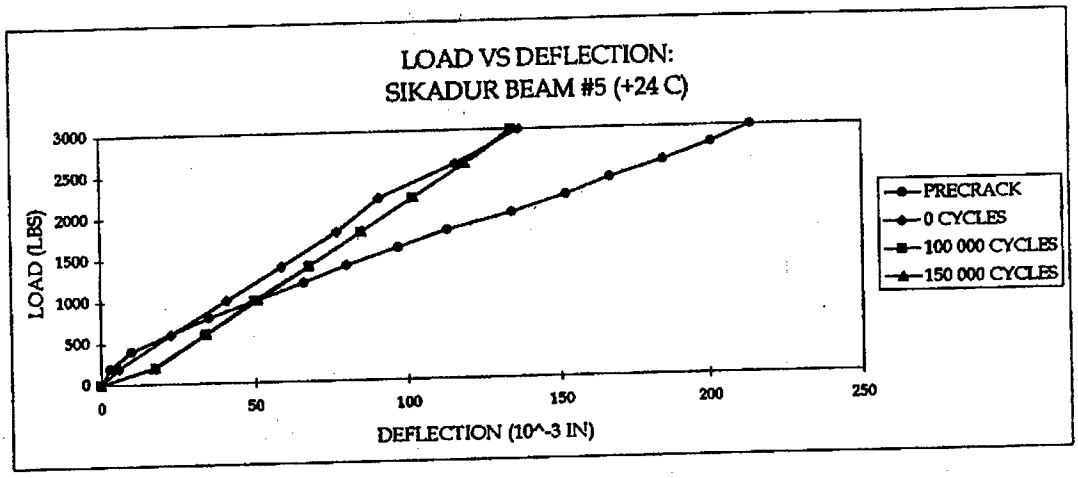


Figure E37. Room temp. test load/deflection data of the Sikadur 30 repaired fatigued beam no.5 (0 to 1.5x10^5 cycles).

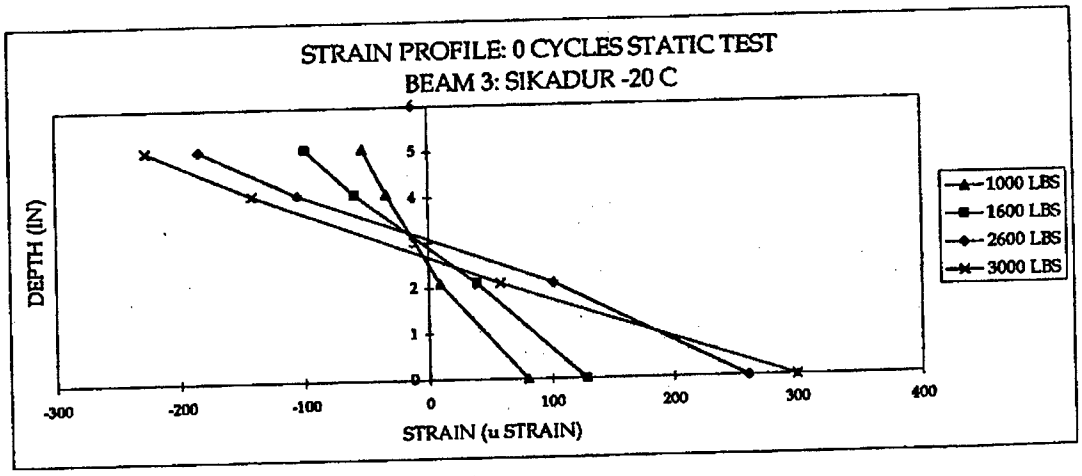


Figure E38. Low temp. test strain profiles of the Sikadur 30 repaired fatigue beam after 0 cycle.

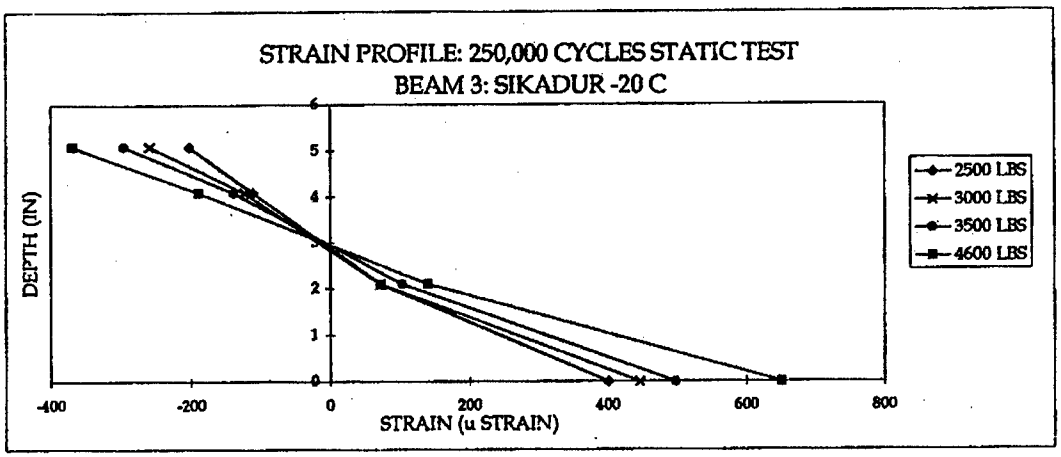


Figure E39. Low temp. test strain profiles of the Sikadur 30 repaired fatigue beam after $2.5x10^5$ cycles.

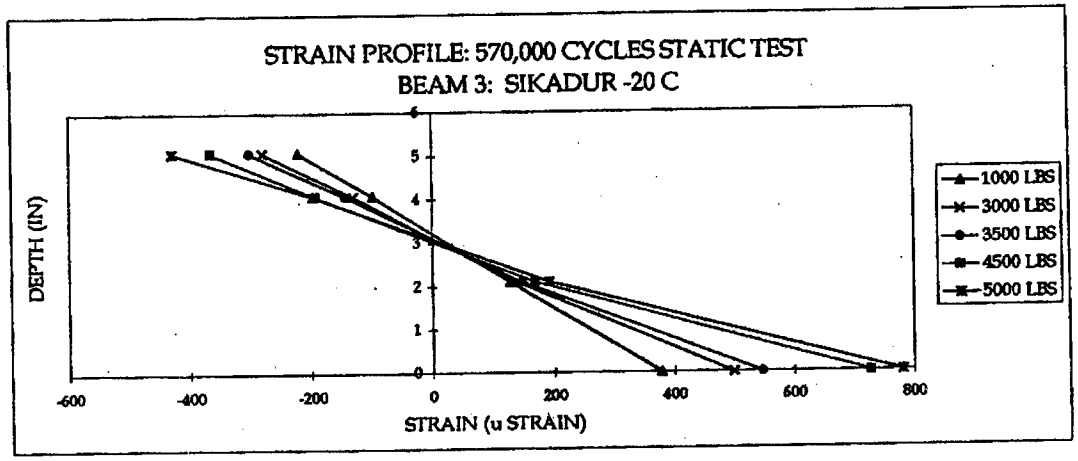


Figure E40. Low temp. test strain profiles of the Sikadur 30 repaired fatigue beam after $5.7x10^5$ cycles.

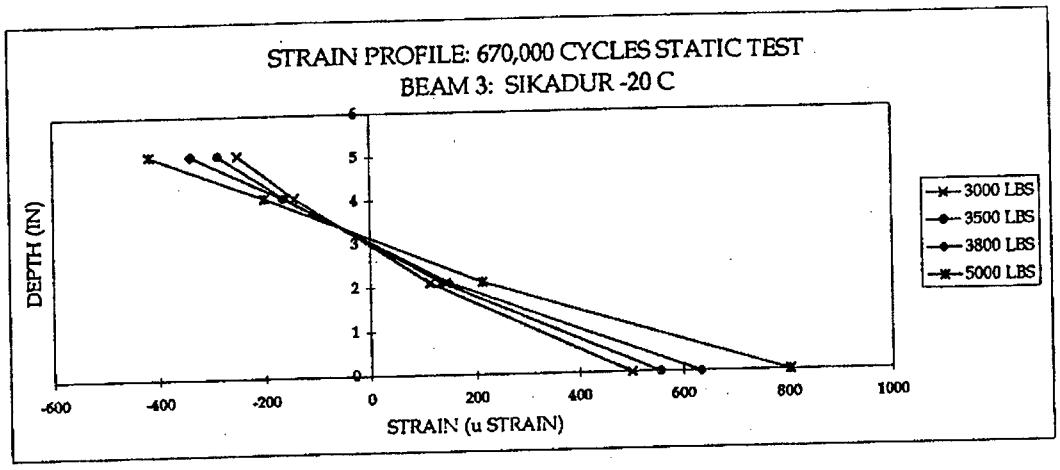


Figure E41. Low temp. test strain profiles of the Sikadur 30 repaired fatigue beam after $6.7x10^5$ cycles.

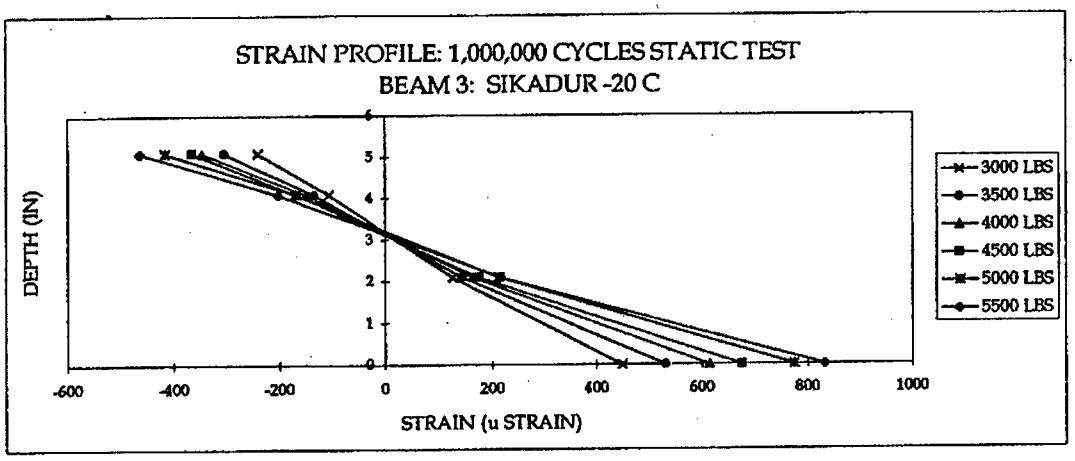


Figure E42. Low temp. test strain profiles of the Sikadur 30 repaired fatigue beam after 10^6 cycles.

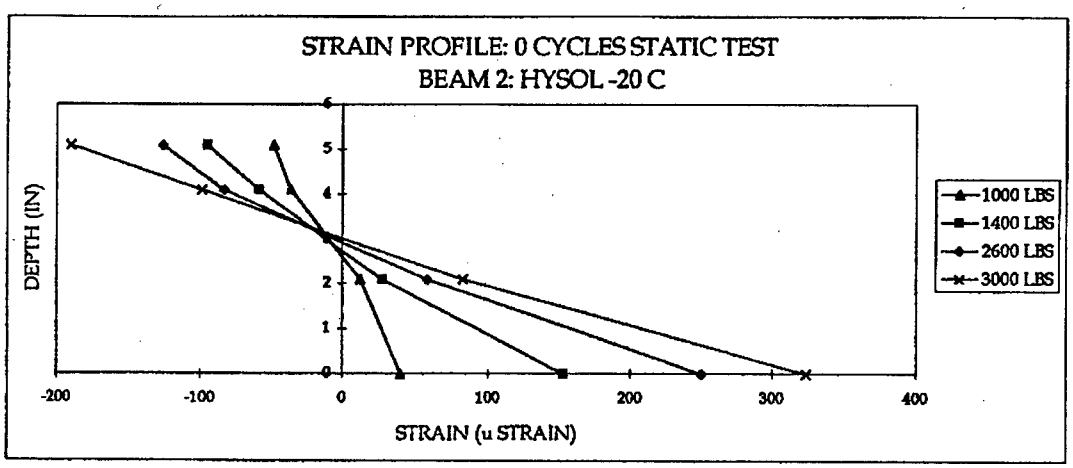


Figure E43. Low temp. test strain profiles of the Hysol 9330 repaired fatigue beam after 0 cycle.

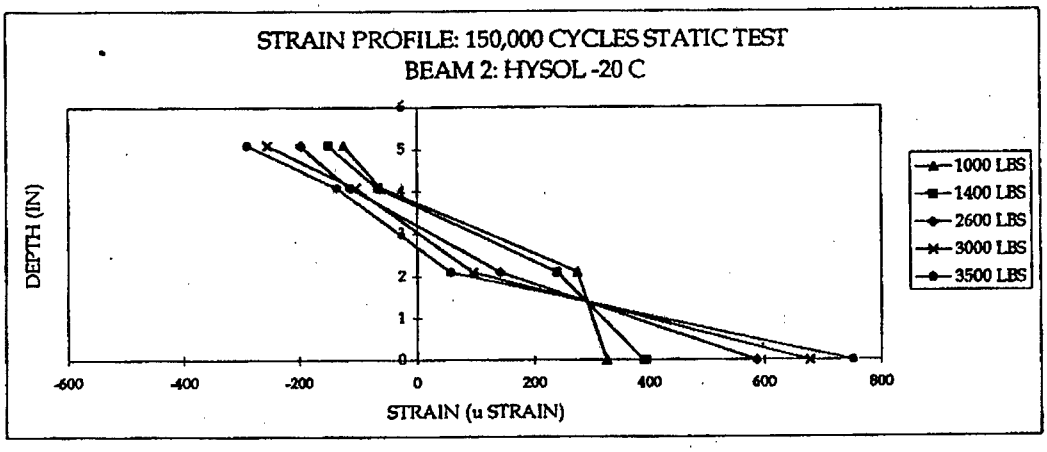


Figure E44. Low temp. test strain profiles of the Hysol 9330 repaired fatigue beam after 1.5×10^5 cycles.

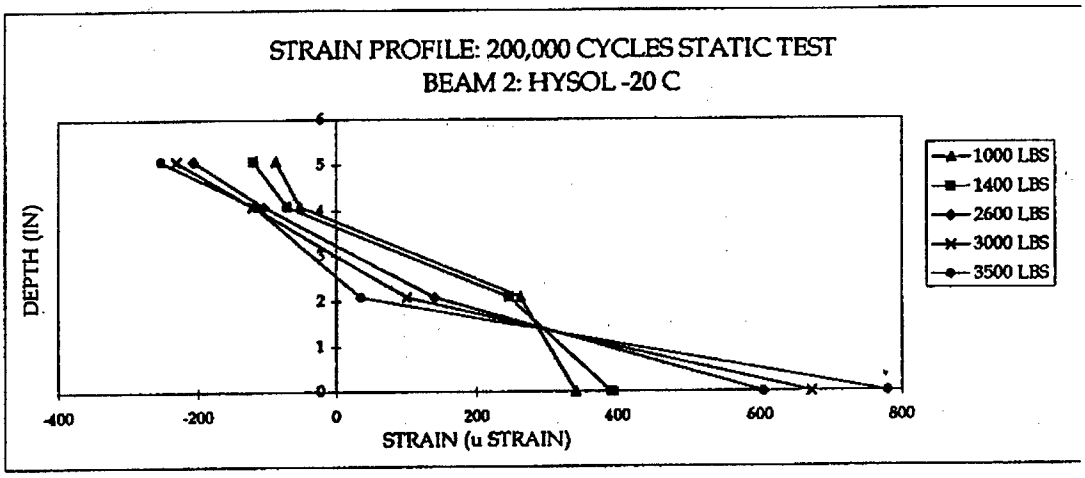


Figure E45. Low temp. test strain profiles of the Hysol 9330 repaired fatigue beam after $2x10^5$ cycles.

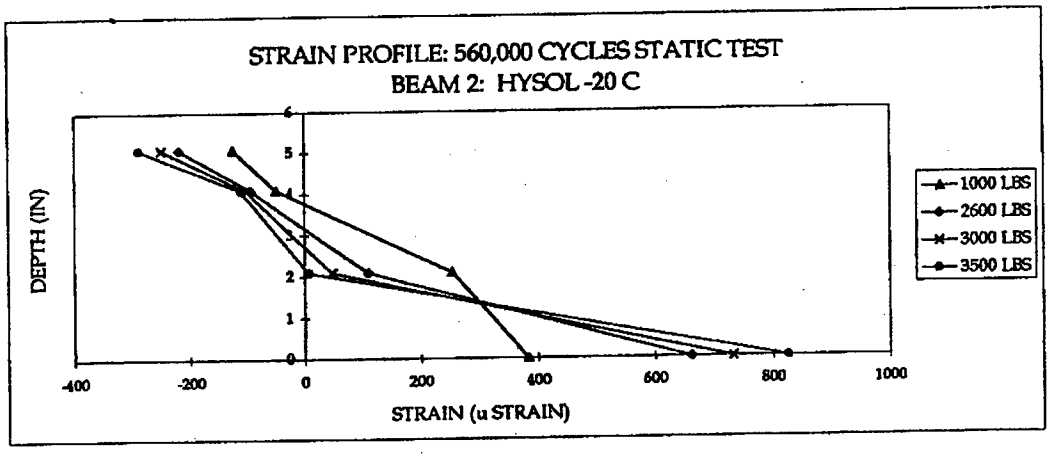


Figure E46. Low temp. test strain profiles of the Hysol 9330 repaired fatigue beam after $5.6x10^5$ cycles.

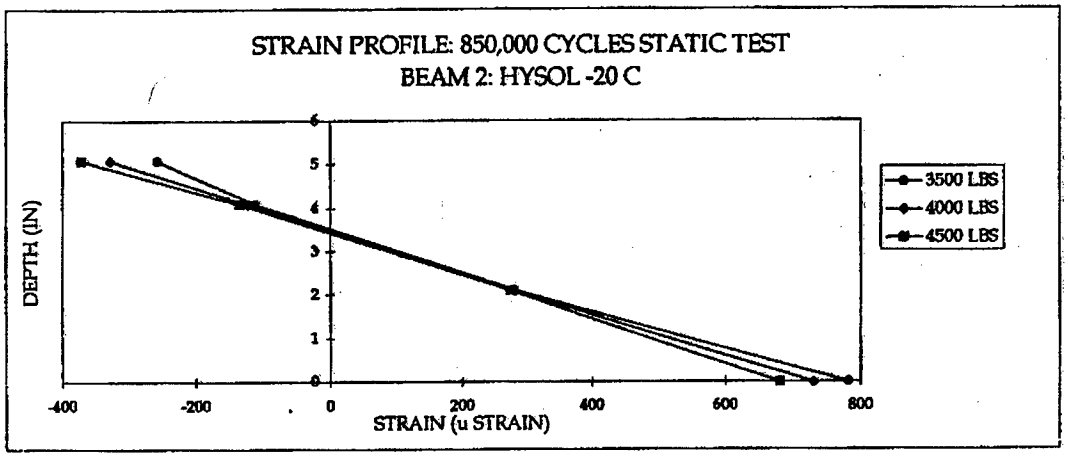


Figure E47. Low temp. test strain profiles of the Hysol 9330 repaired fatigue beam after $8.5x10^5$ cycles.

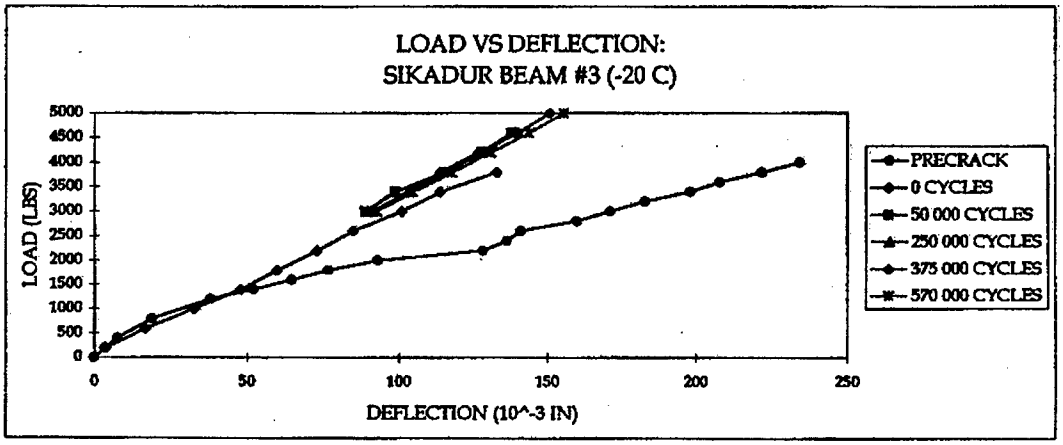


Figure E48. Low temp. test load/deflection data of the Sikadur 30 repaired fatigued beam no.3 (0 to $5.7x10^5$ cycles).

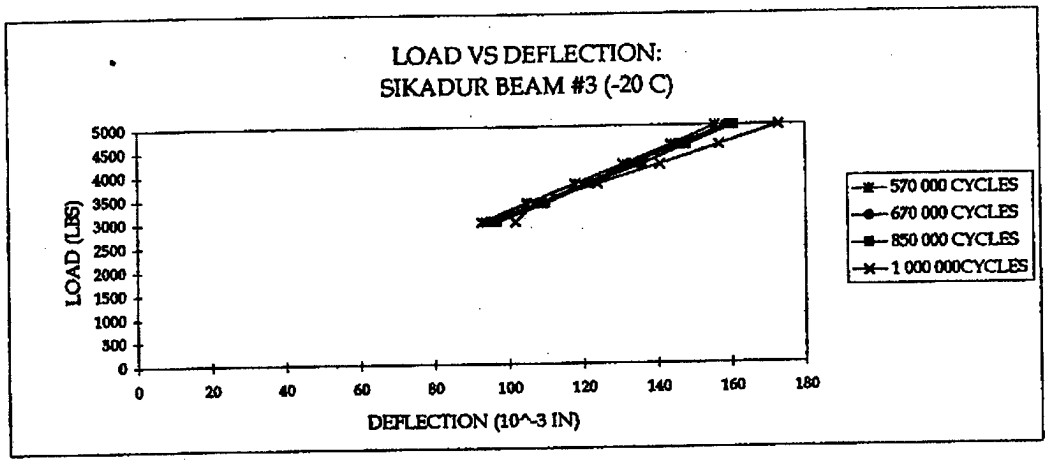


Figure E49. Low temp. test load/deflection data of the Sikadur 30 repaired fatigued beam no.3 (5.7x10^5 to 10^6 cycles).

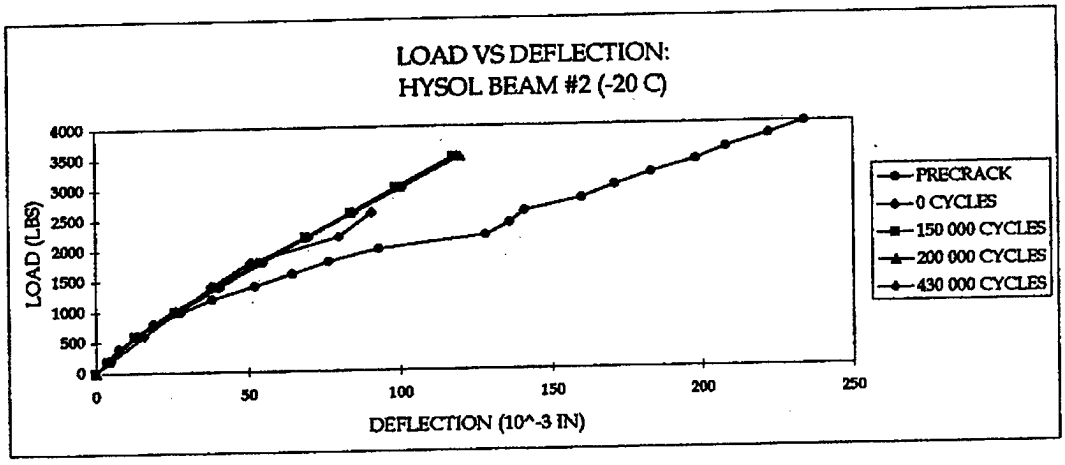


Figure E50. Low temp. test load/deflection data of the Hysol 9330 repaired fatigued beam no.2 (0 to 4.3x10^5 cycles).

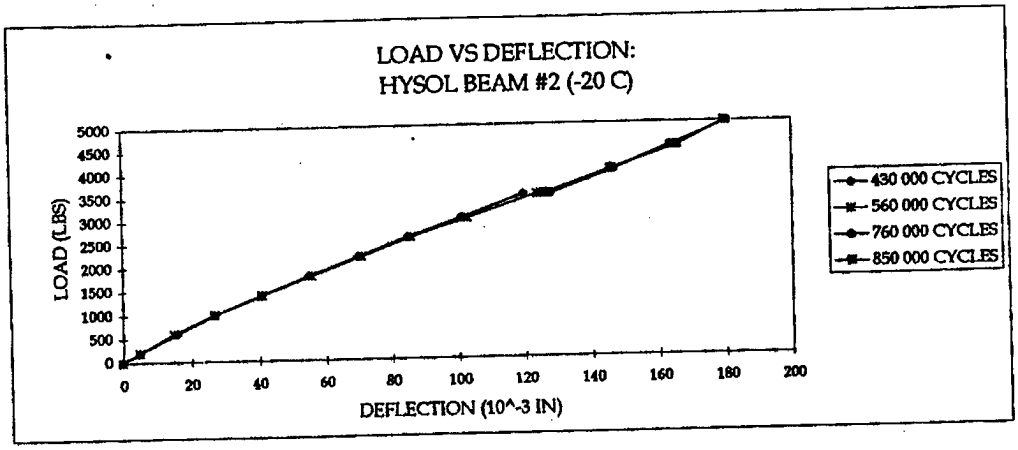


Figure E51. Low temp. test load/deflection data of the Hysol 9330 repaired fatigued beam no.2 ($4.3x10^5$ to $8.5x10^5$ cycles).

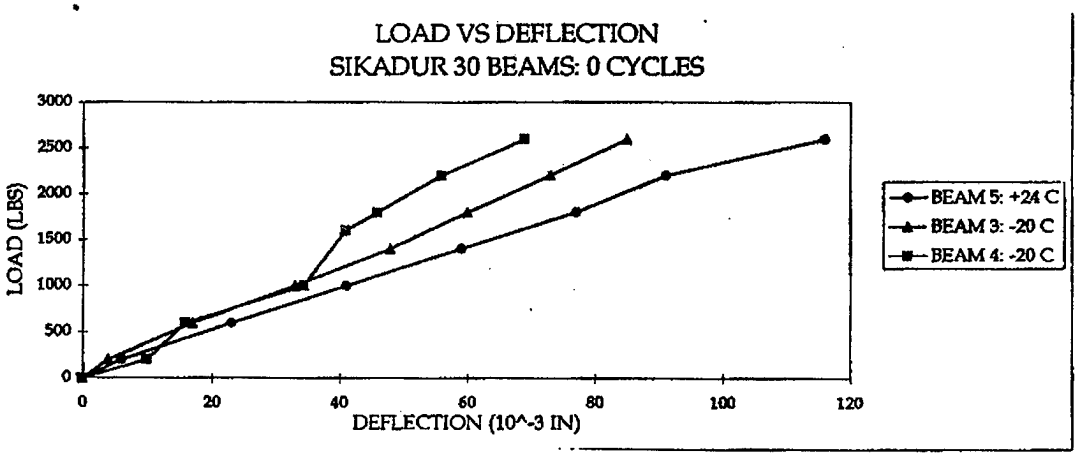


Figure E52. Comparison of low temperature effects on deflection after 0 cycle of Sikadur 30 repaired fatigued beam .

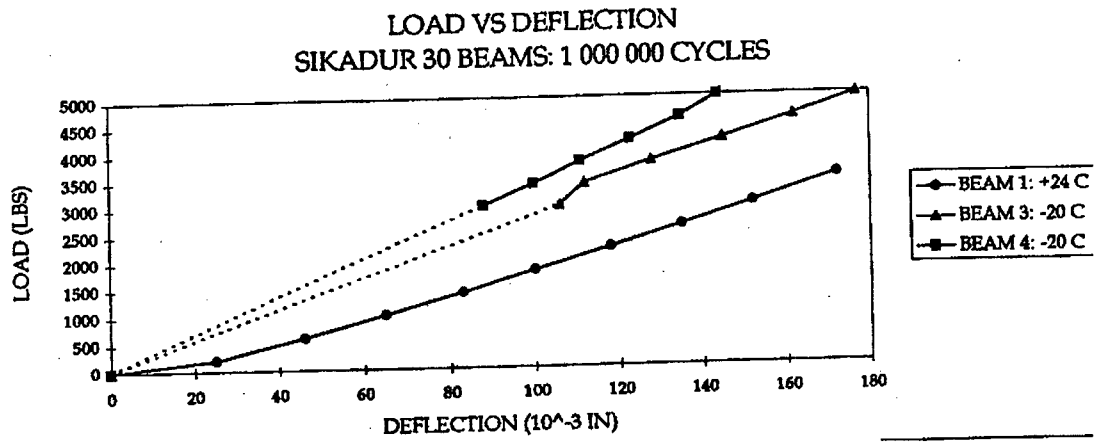


Figure E53. Comparison of low temperature effects on deflection after 10^6 cycles of Sikadur 30 repaired fatigued beam.

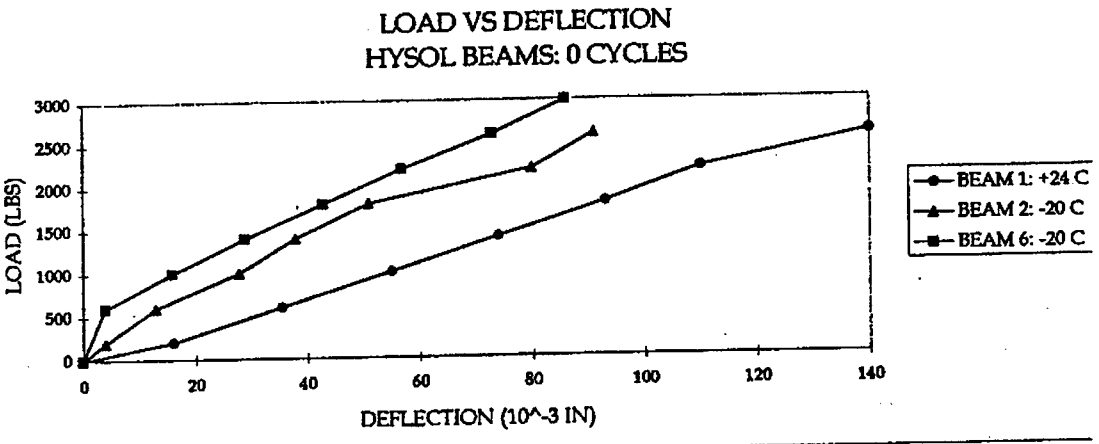


Figure E54. Comparison of low temperature effects on deflection after 0 cycle of Hysol 9330 repaired fatigued beam.

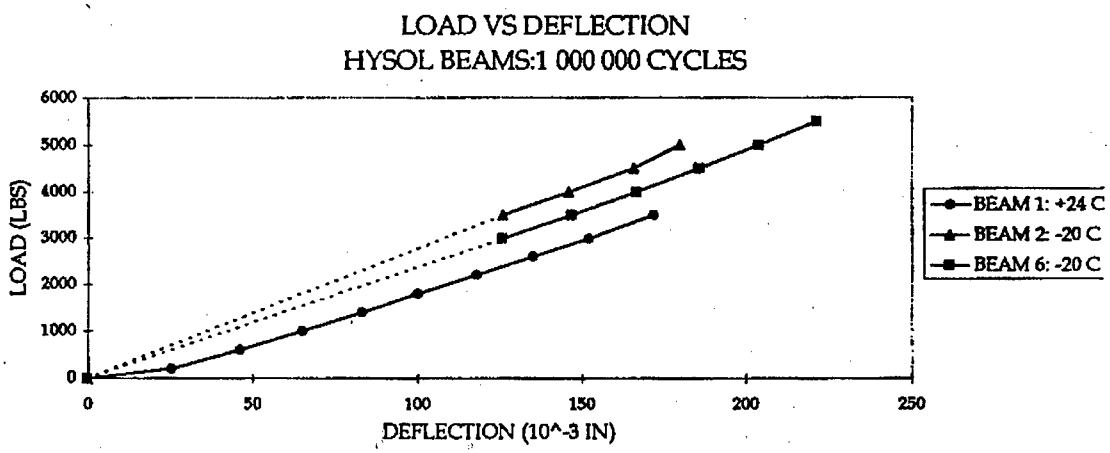


Figure E55. Comparison of low temperature effects on deflection after 10^6 cycle of Hysol 9330 repaired fatigued beam.

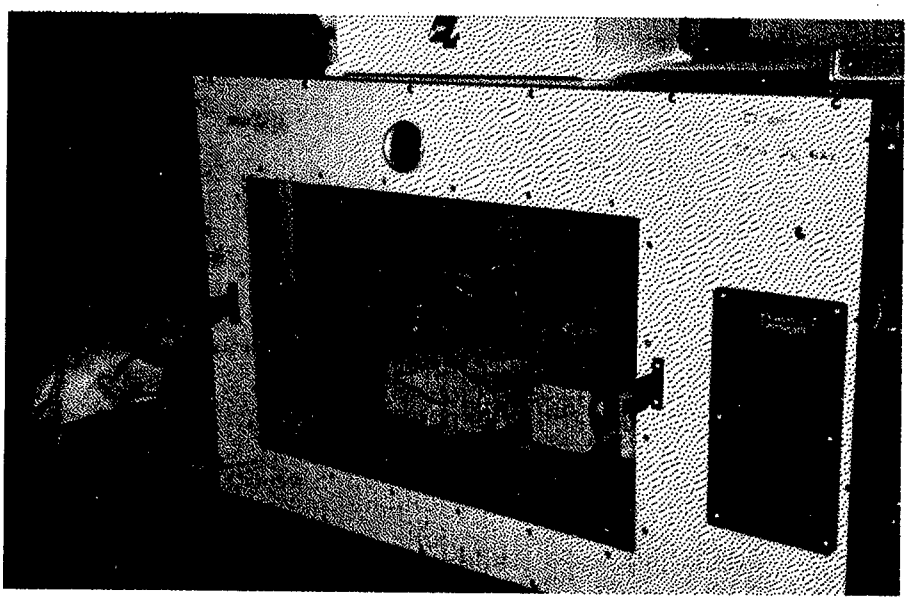


Figure E56. Low temperature thermal cycling chamber loaded with the test beams.

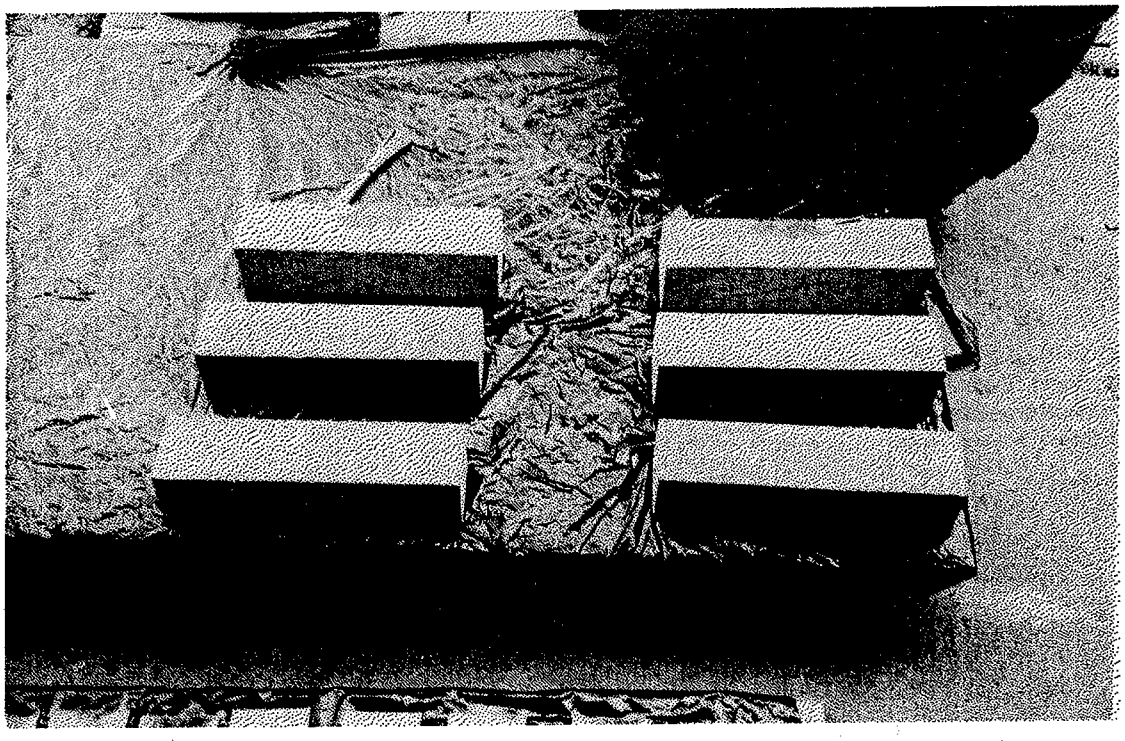


Figure E57. Test specimen surface prepared by sandblasting for laminate application.

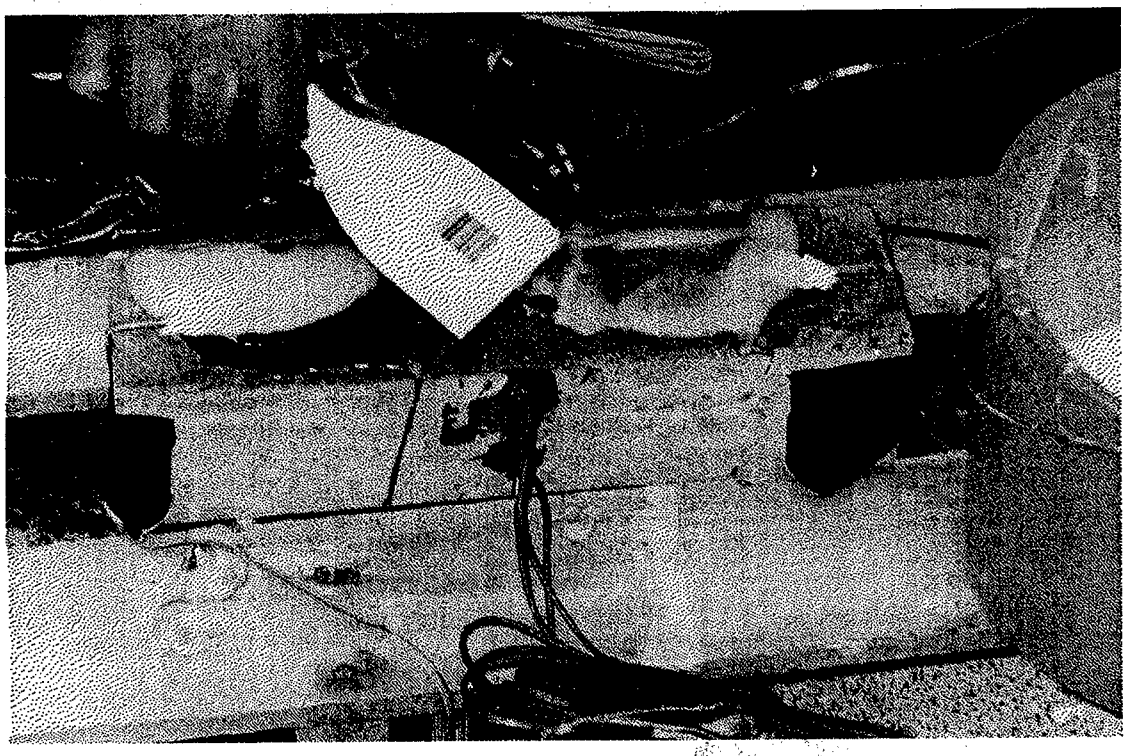


Figure E58. Application of the adhesive before bonding the CFRP laminate.

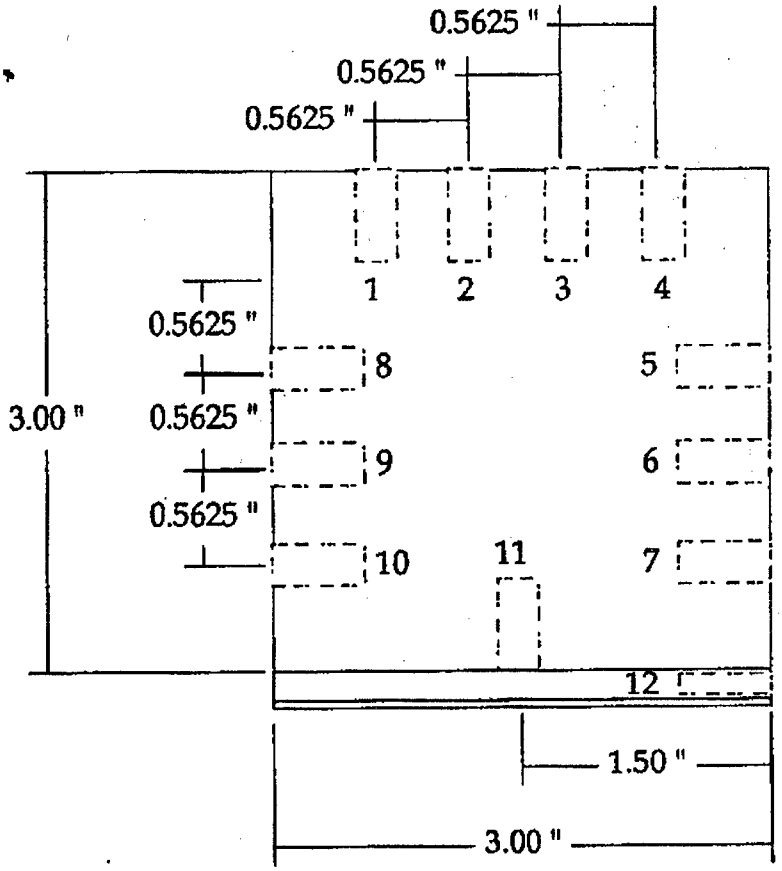


Figure E59. Thermocouple locations shown in the beam cross-section.



Figure E60. Loading and support points marked on the thermally cycled test beams.

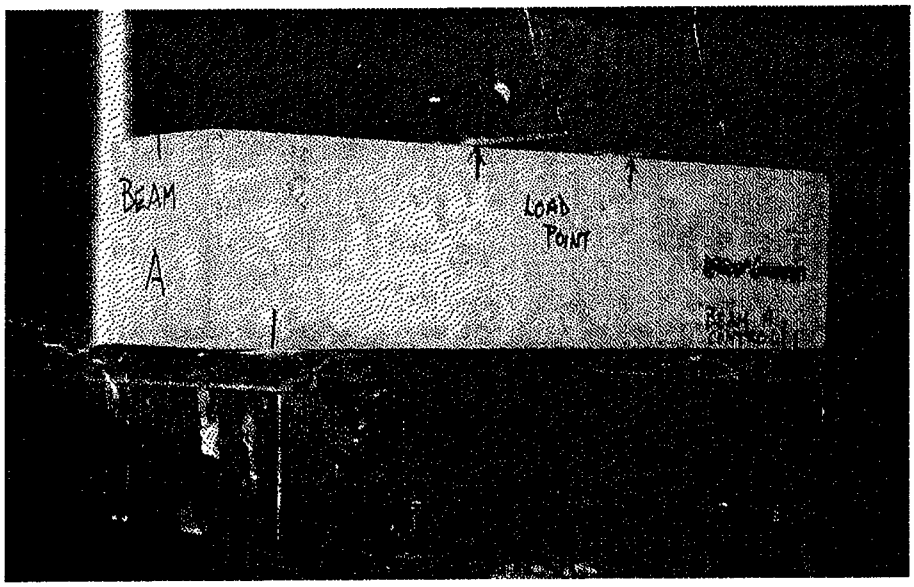


Figure E61. Thermally cycled beam under test.

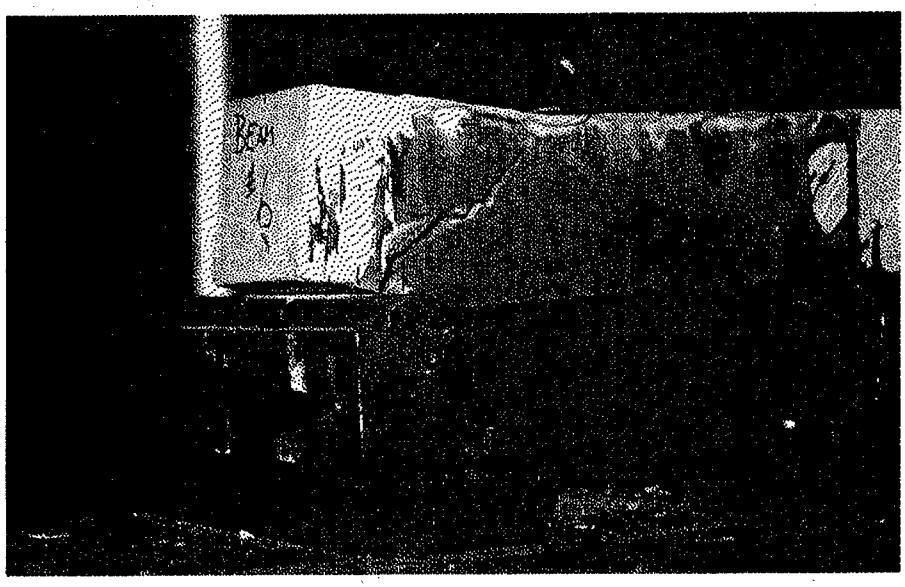
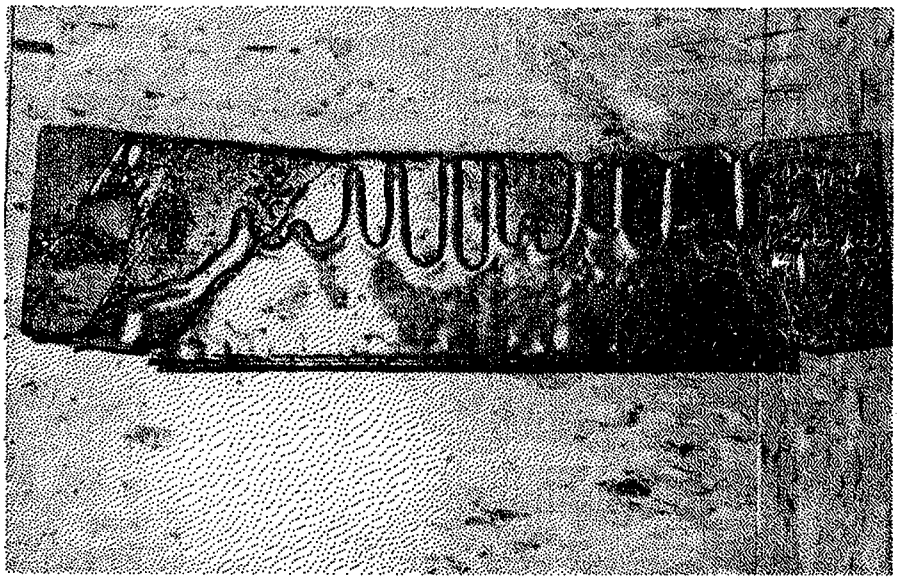
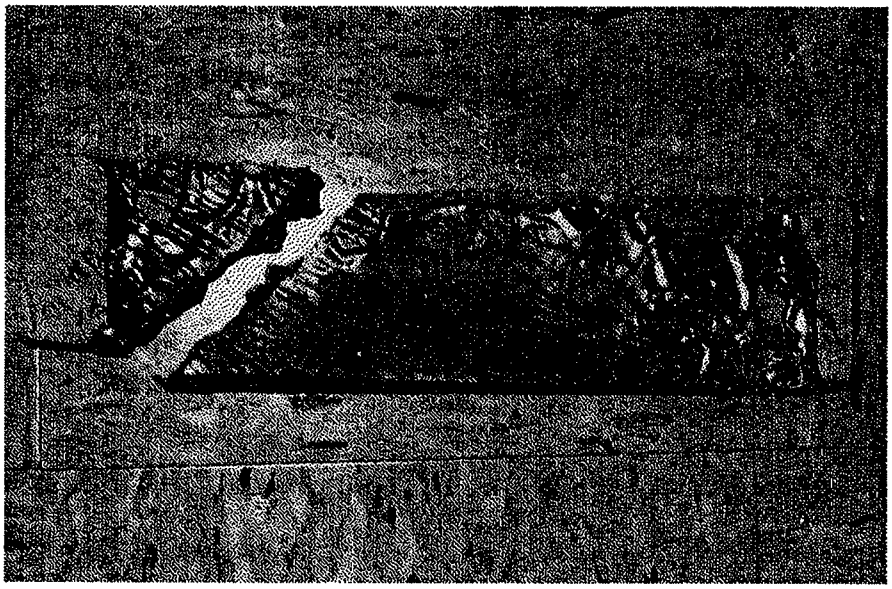


Figure E62.1






#3

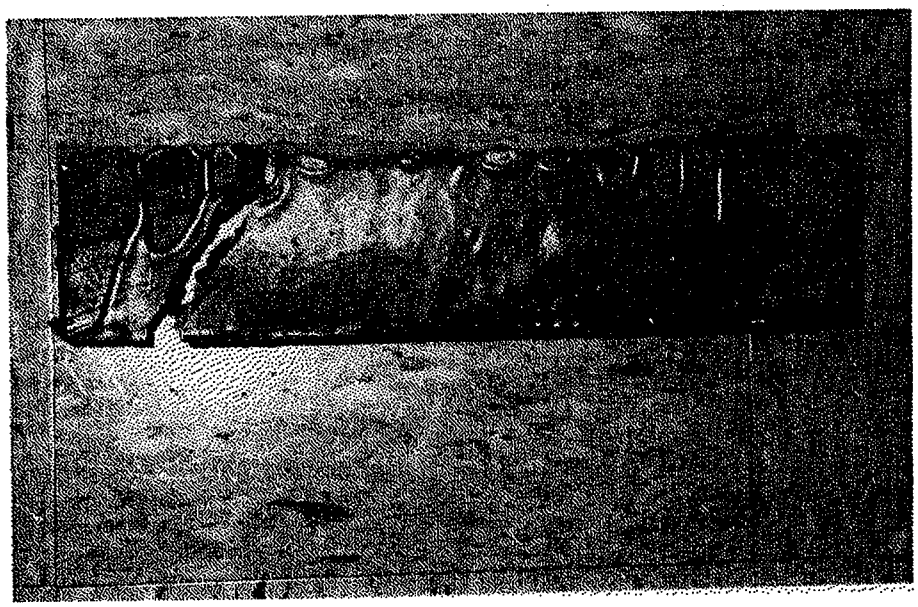


Figure E.62.1 - E.62.5 Diagonal shear crack propagation in the thermally cycled beams bonded with CFRP.

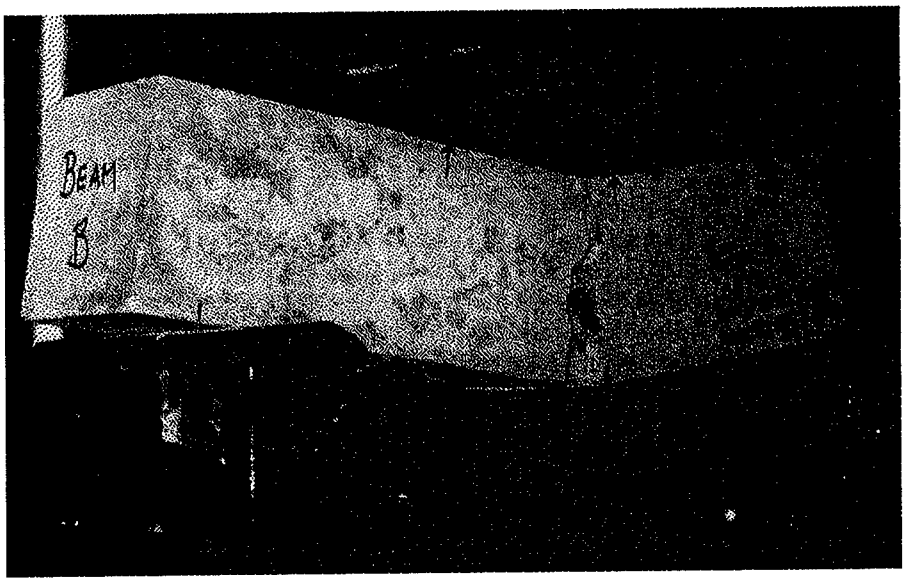


Figure E63.1



Figure E.63.1 - E.63.2. Tensile failure and vertical crack propagation in the thermally cycled beams without any laminate reinforcement.

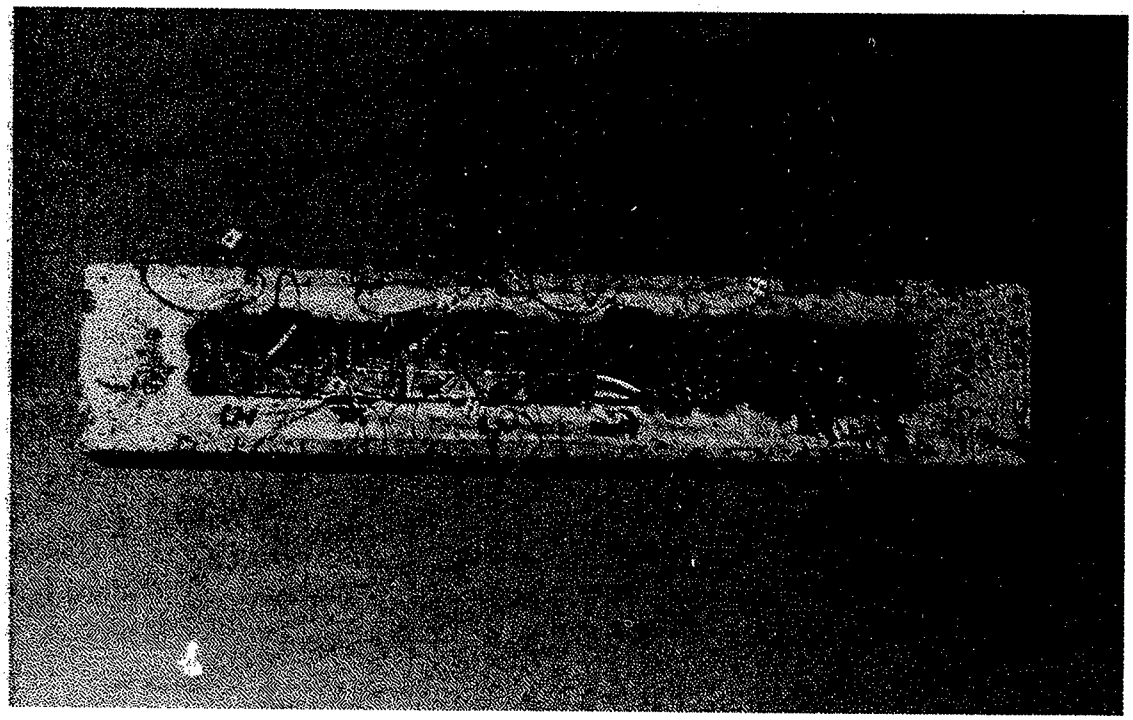


Figure E64. Strain gage mounted test beam for bond strength study.

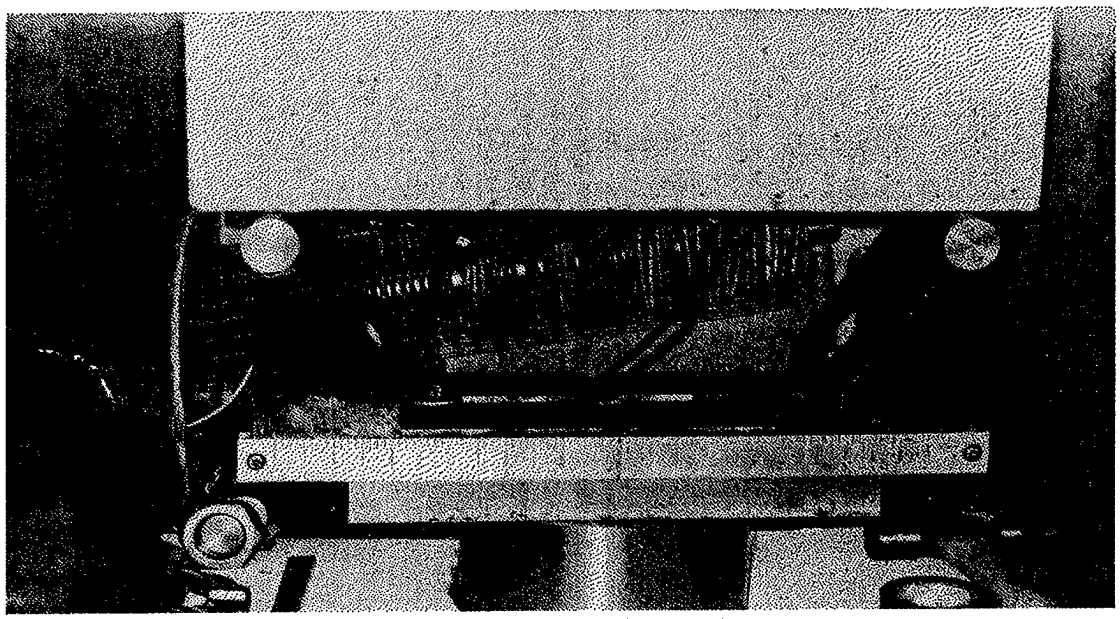


Figure E65. Three-point flexural test configuration for bond strength study.

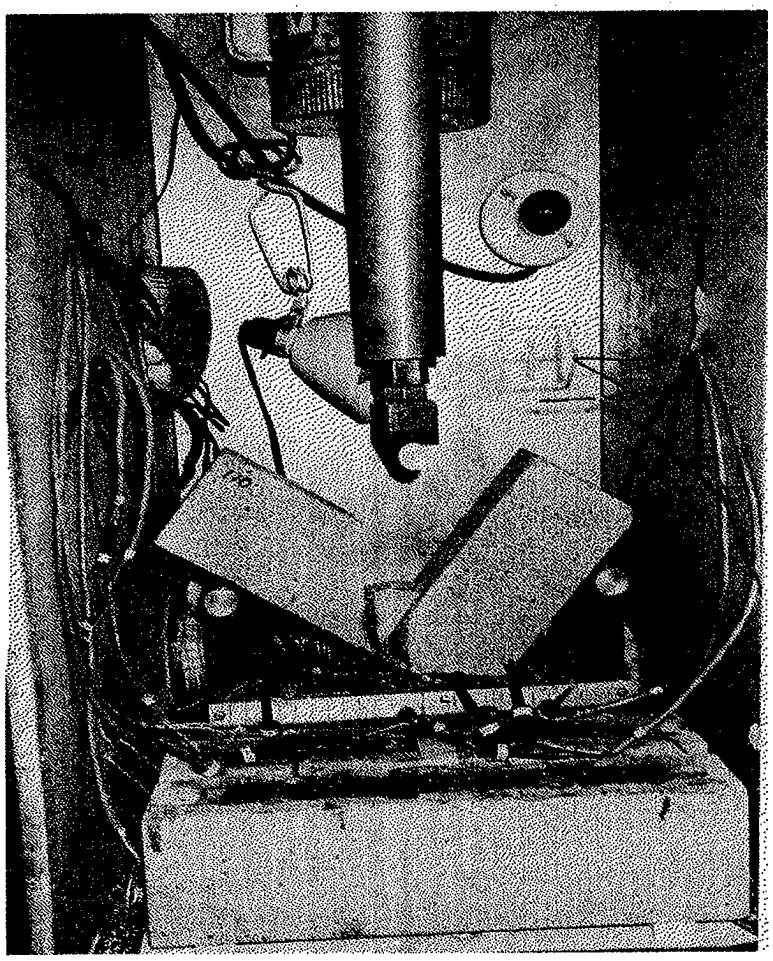


Figure E66. Typical failure in the three-point flexural tests.



Figure E67. Debonded CFRP laminate shows no fiber failure.

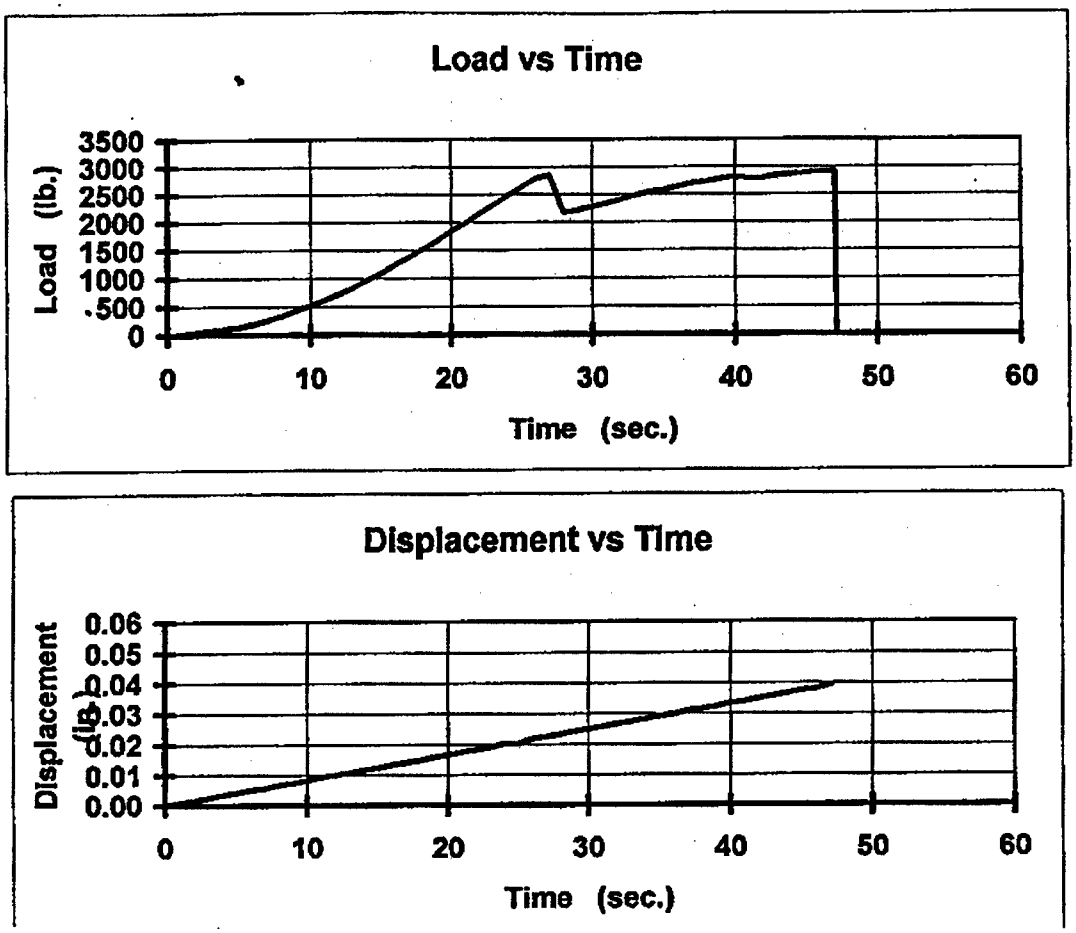


Figure E68.1 Load and displacement data of the prime coated specimen PC4 at room temperature.

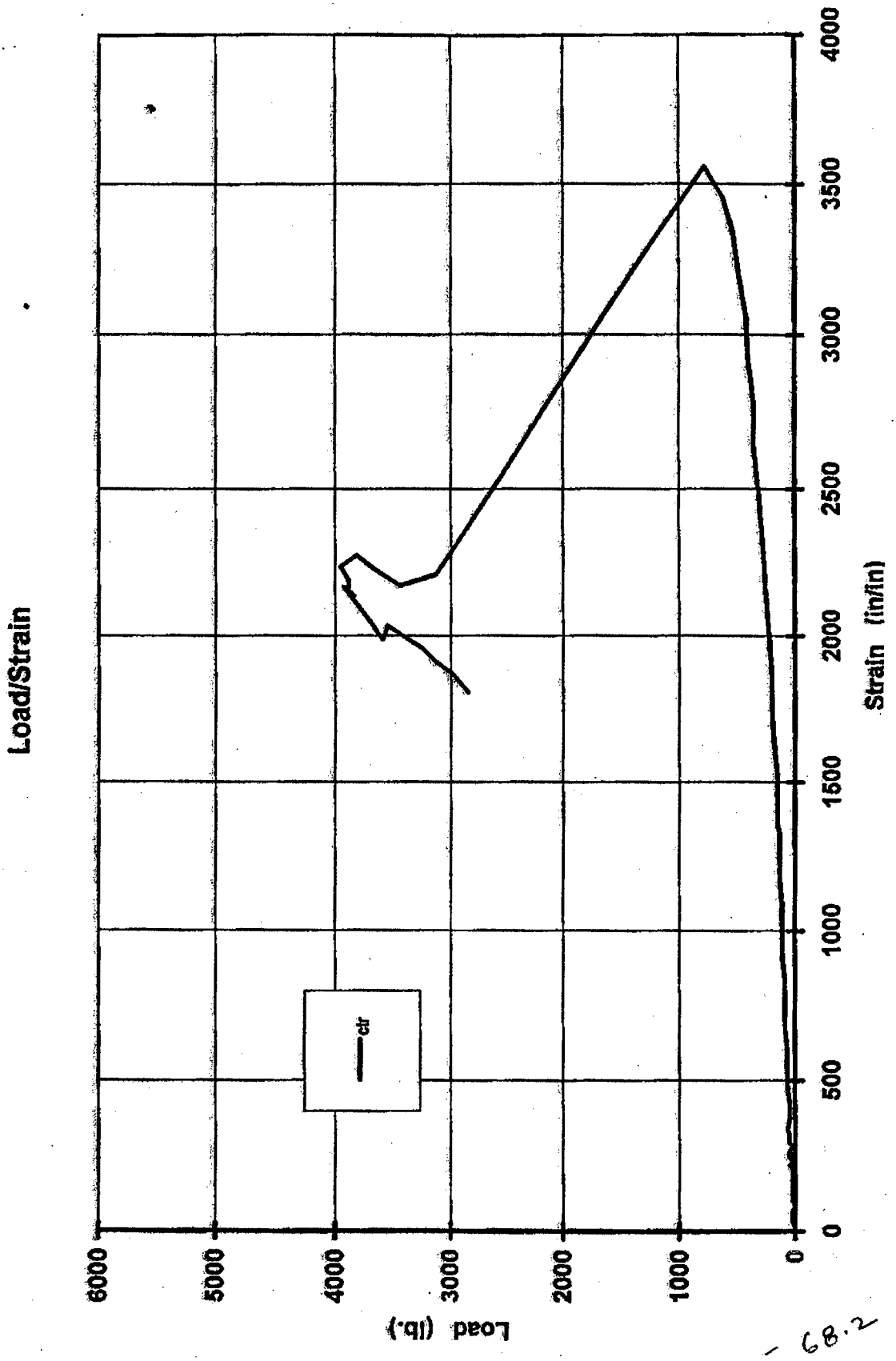


Figure E.68.2 Load/strain data of the prime coated specimen PC5 at low temperature.

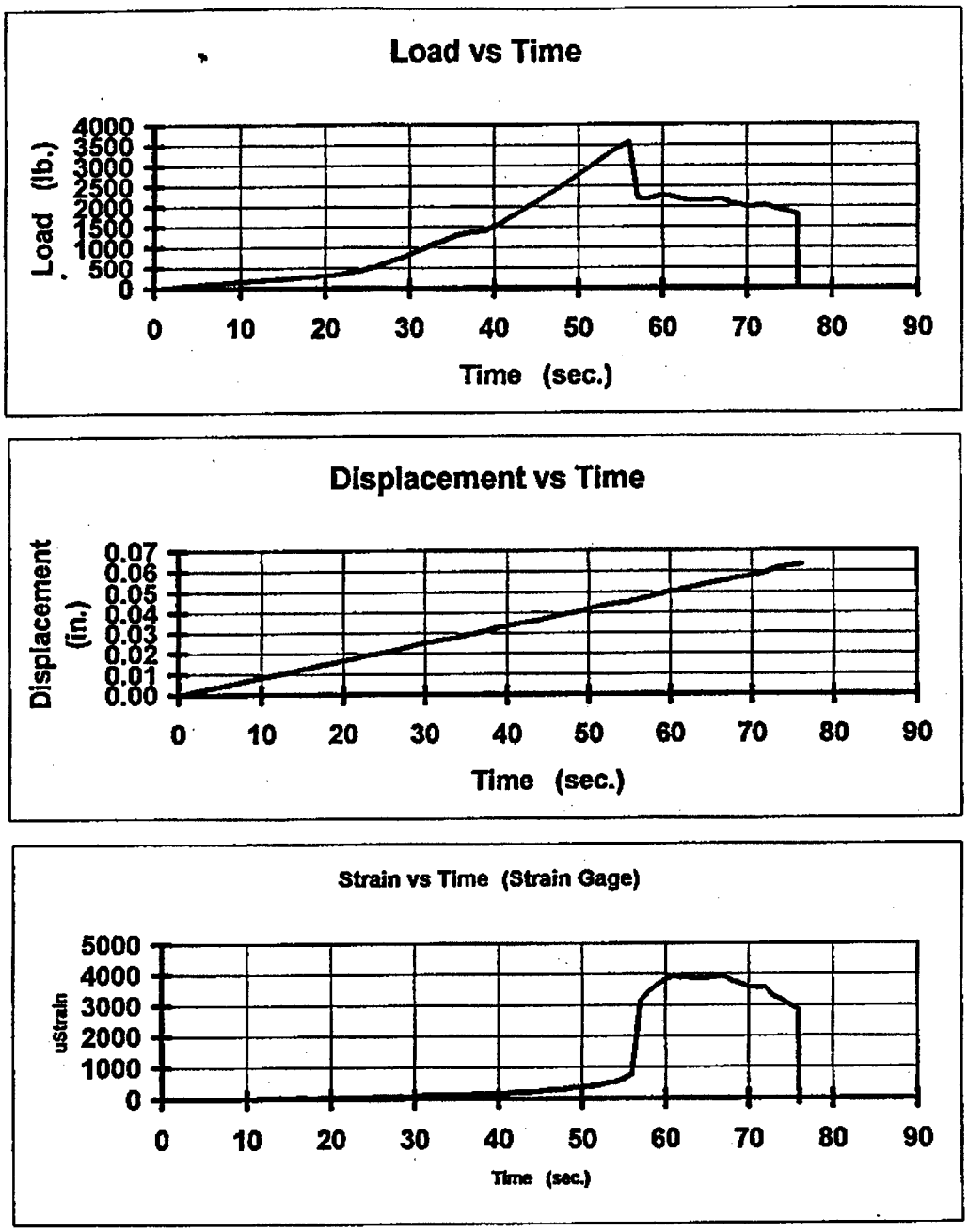


Figure E.68.3 Load, displacement, and strain data of the prime coated specimen PC5 at low temperature.

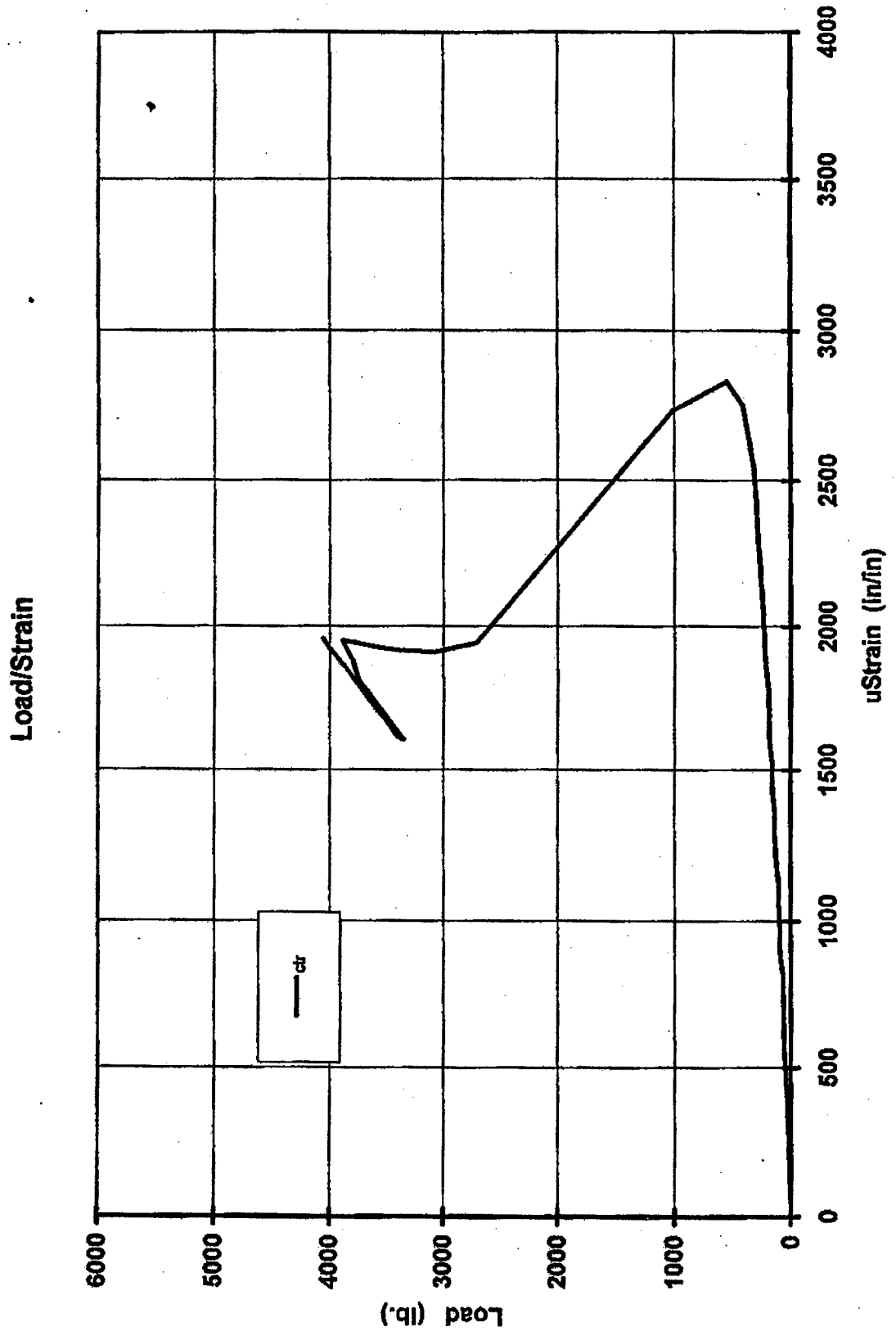


Figure E.68.4. Load/strain data of the prime coated specimen PC6 at low temperature.

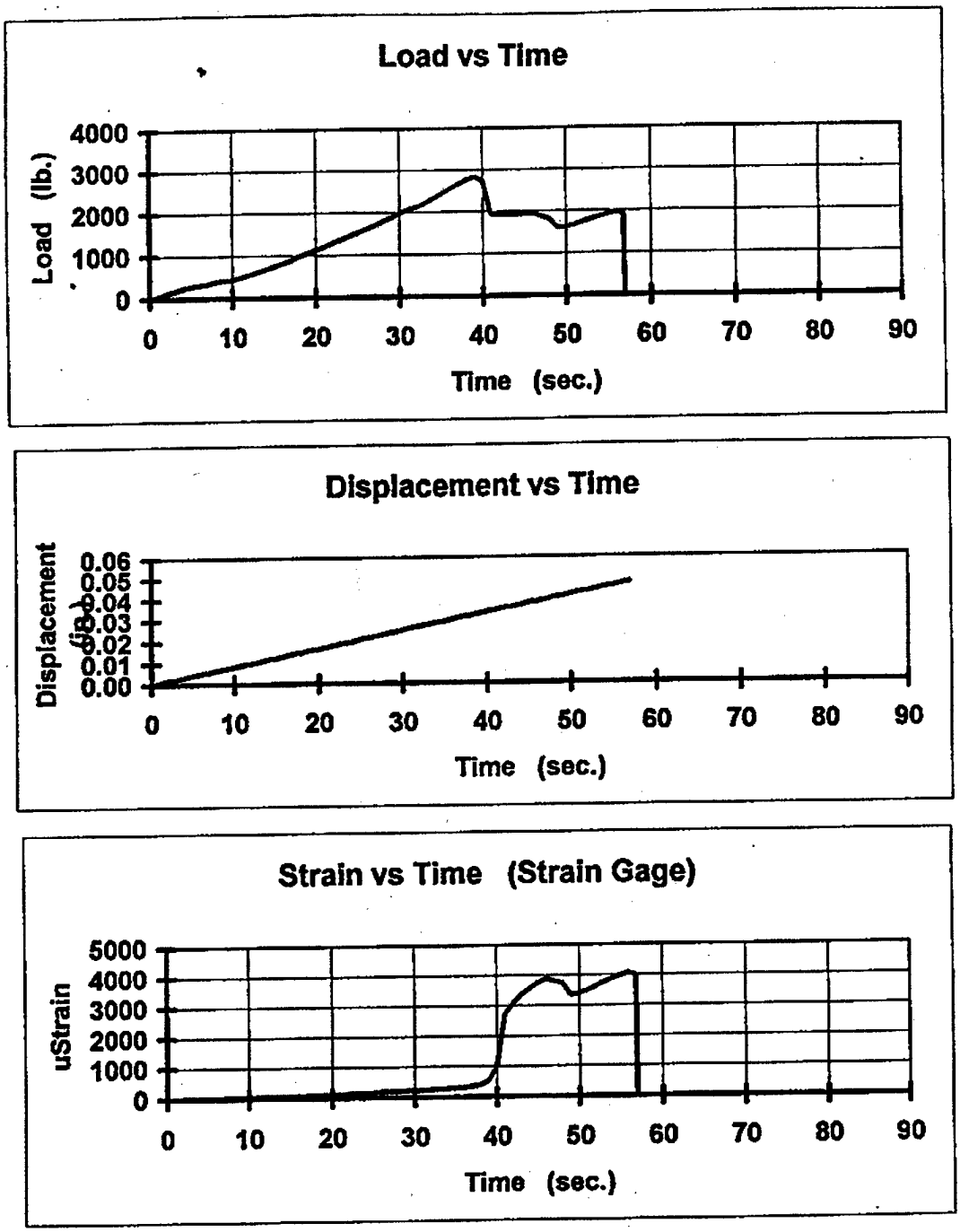


Figure E.68.5 Load, displacement, and strain data of the prime coated specimen PC6 at low temperature.

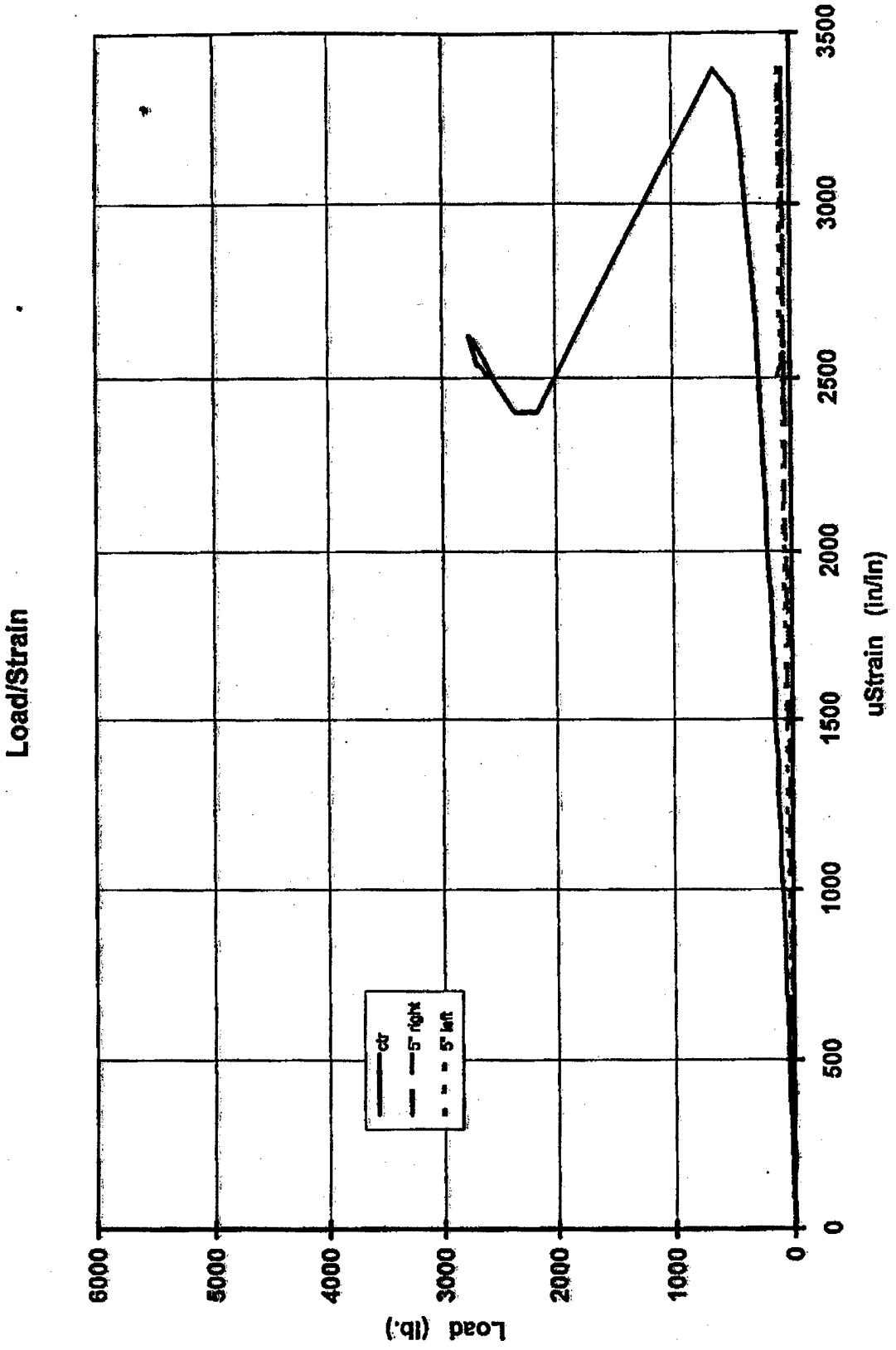


Figure E.68.6. Load/strain data of the uncoated specimen WPC4 at low temperature.

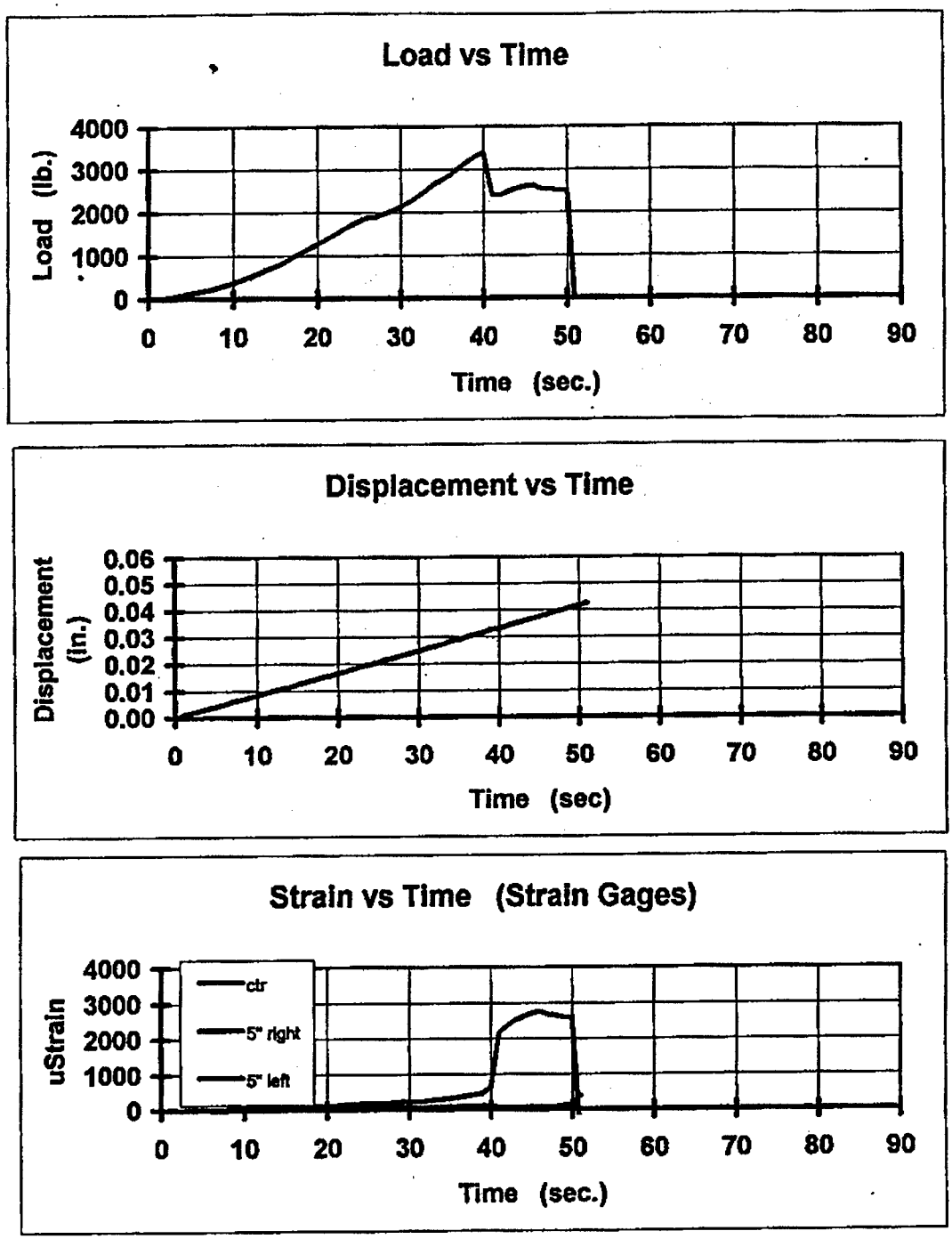


Figure E.68.7 Load, displacement, and strain data of the uncoated specimen WPC4 at low temperature.

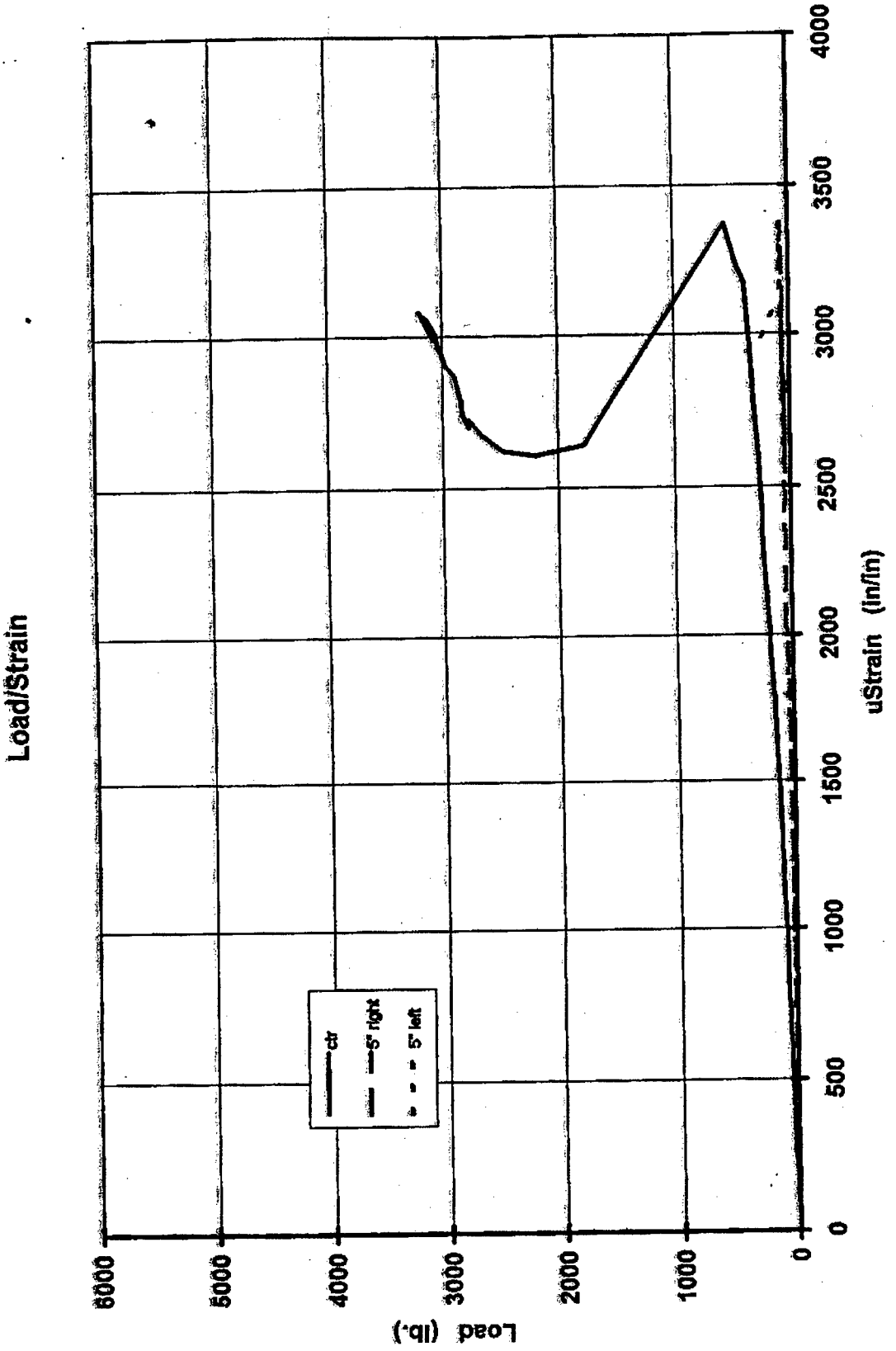


Figure E.68.8. Load/strain data of the uncoated specimen WPC5 at low temperature.

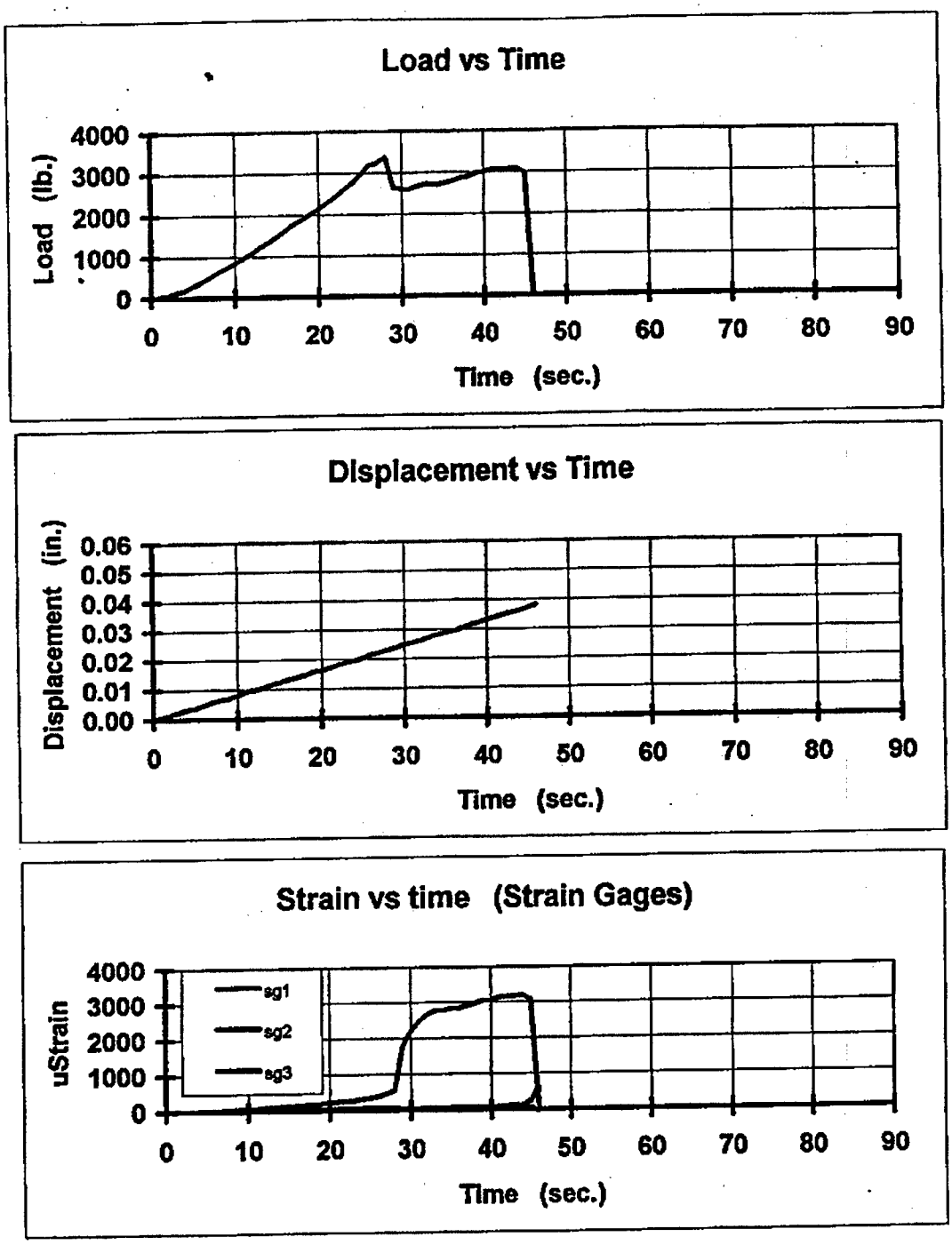


Figure E.68.9 Load, displacement, and strain data of the uncoated specimen WPC5 at low temperature.

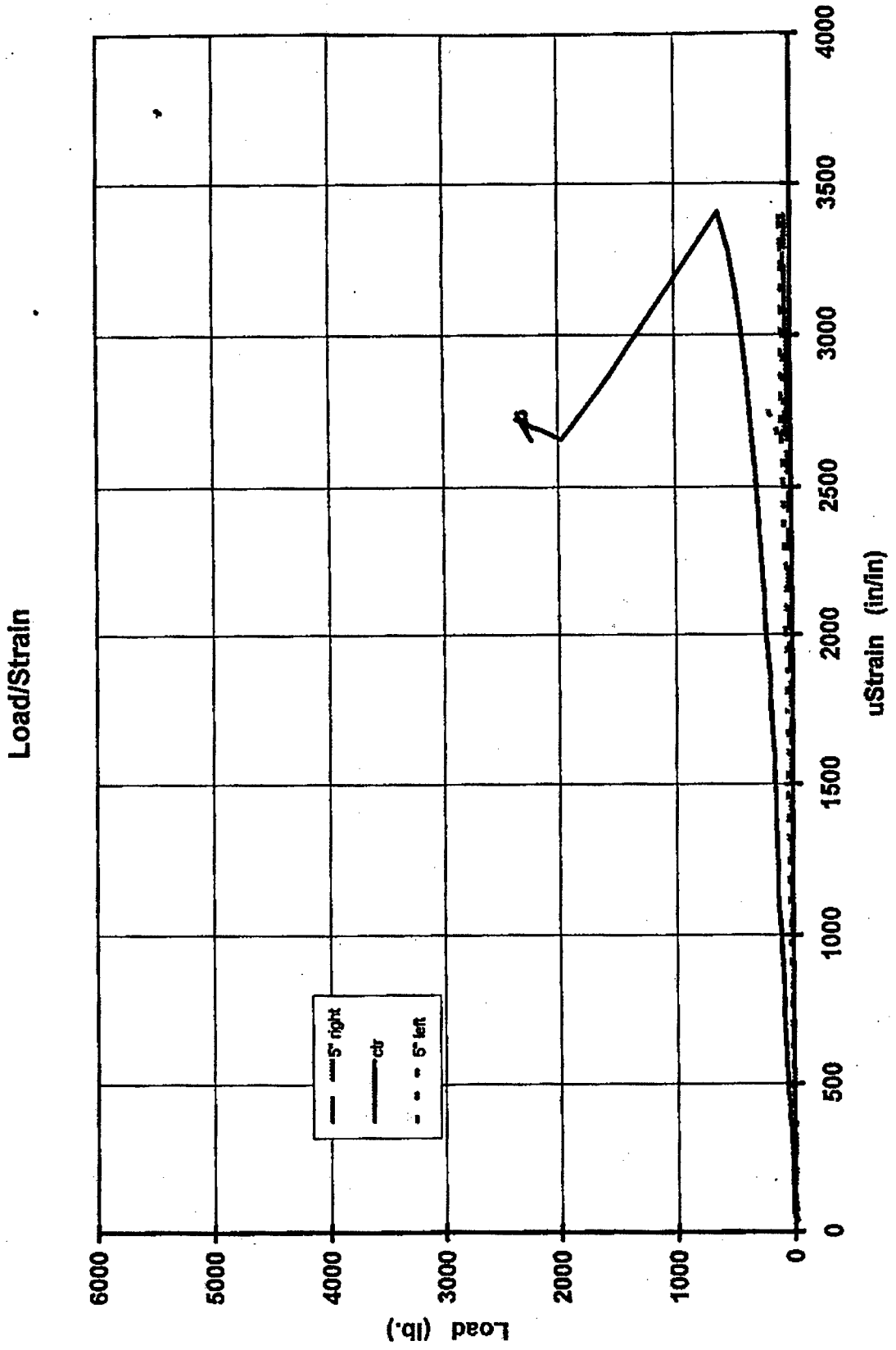


Figure E.68.10. Load/strain data of the uncoated specimen WPC6 at low temperature.

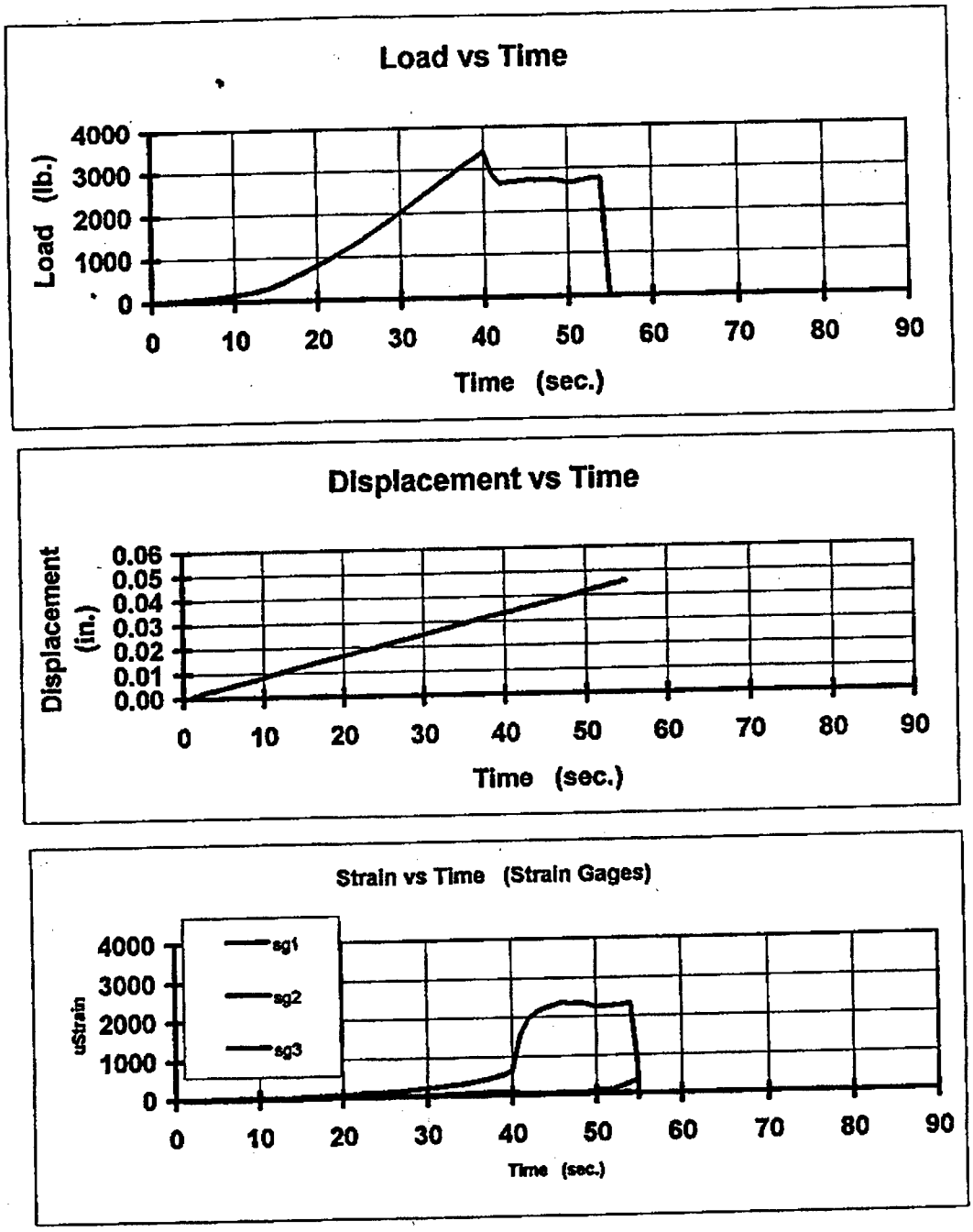


Figure E.68.11 Load, displacement, and strain data of the uncoated specimen WPC6 at low temperature.

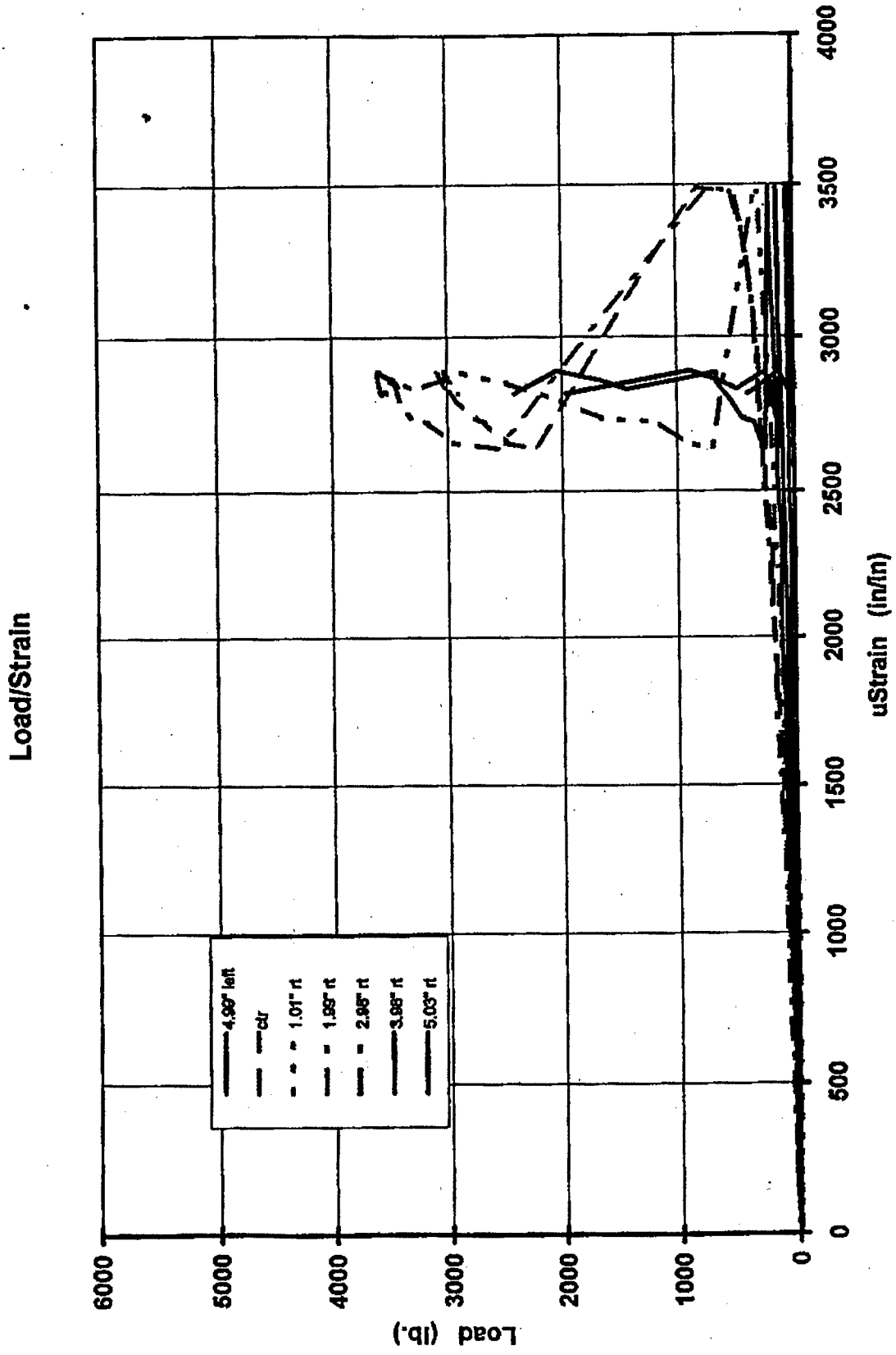


Figure E.68.12. Load/strain data of the uncoated specimen WPC7 at low temperature.

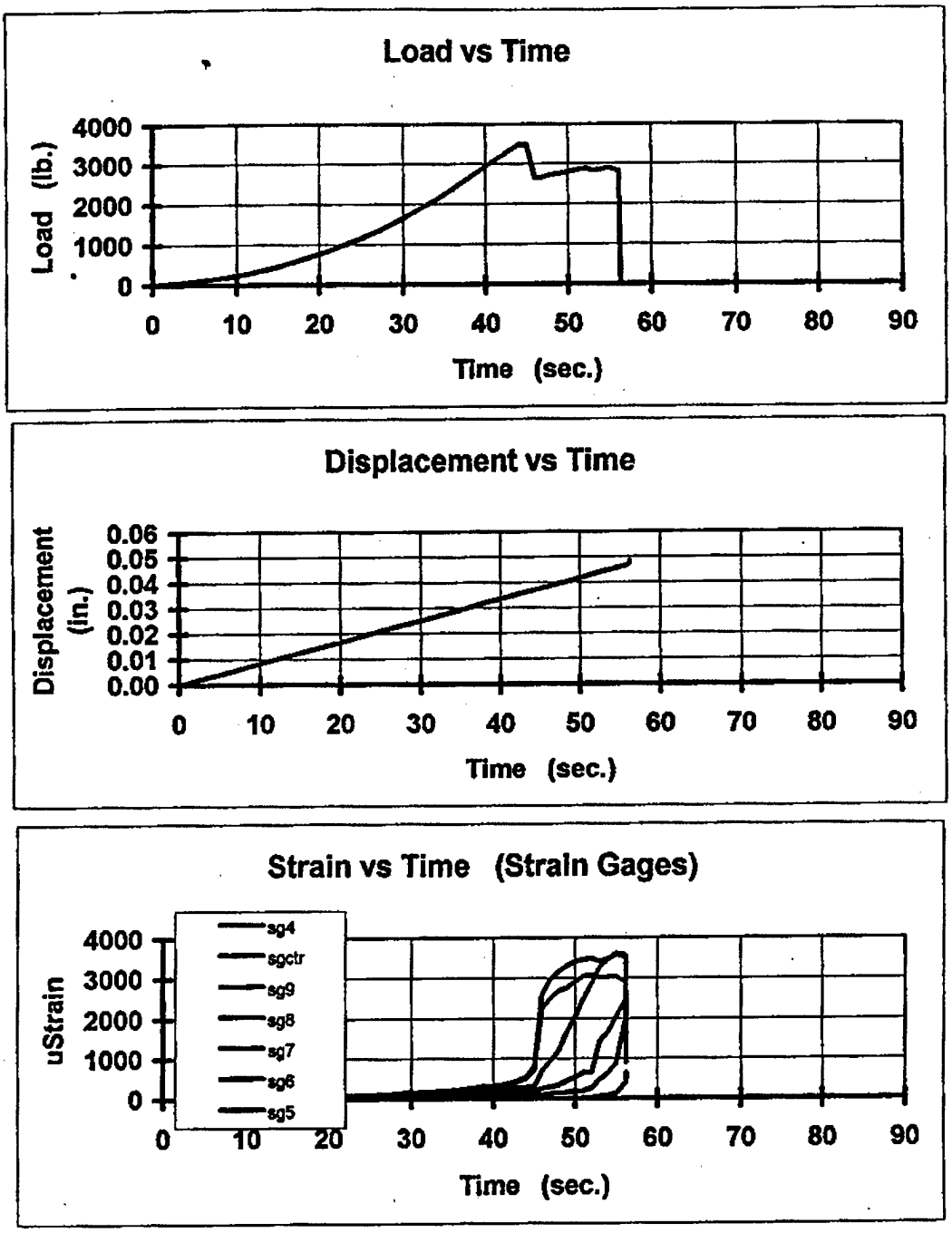


Figure E.68.13 Load, displacement, and strain data of the uncoated specimen WPC7 at low temperature.

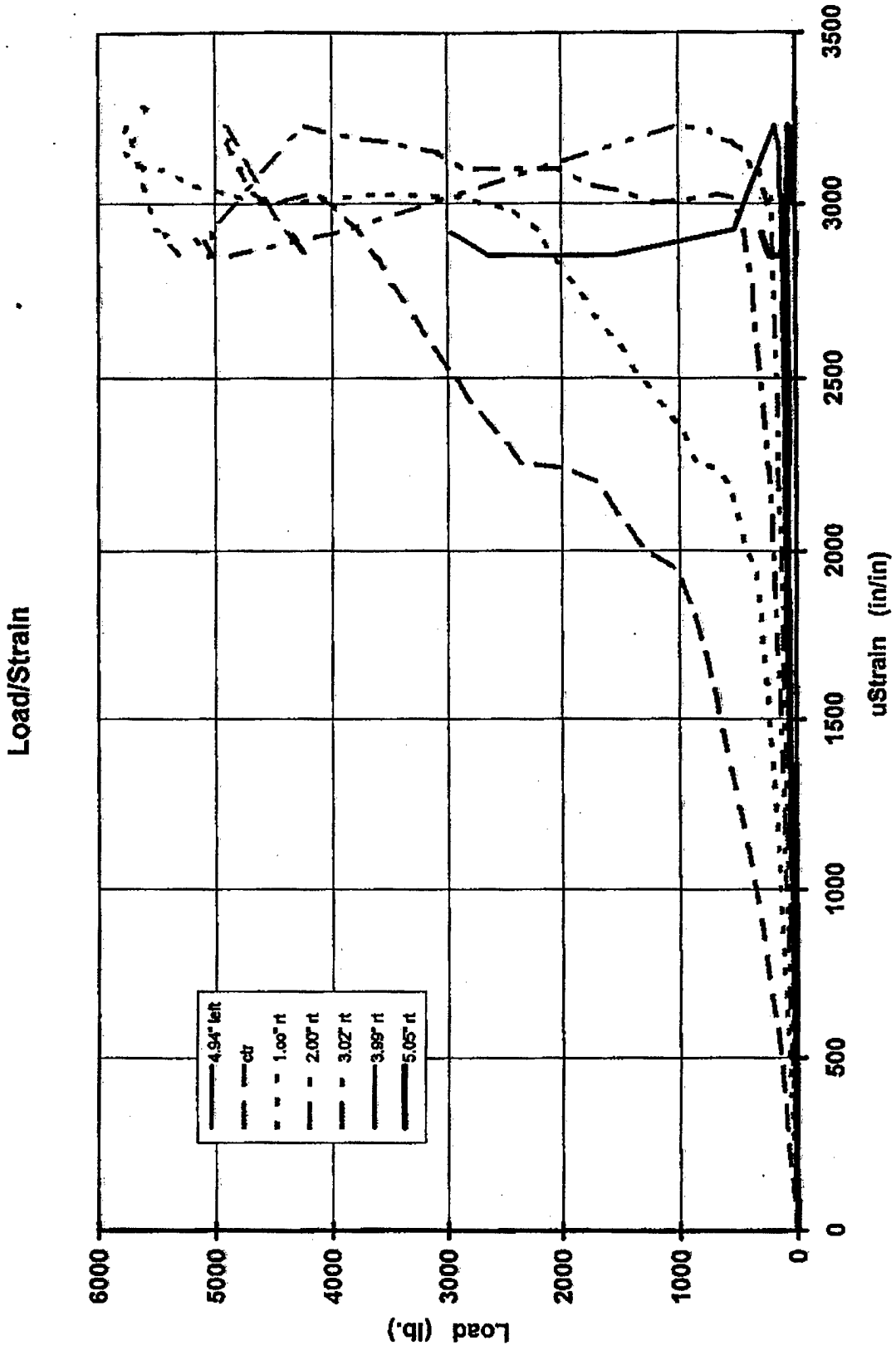


Figure E.68.14. Load/strain data of the uncoated specimen WPC8 at low temperature.

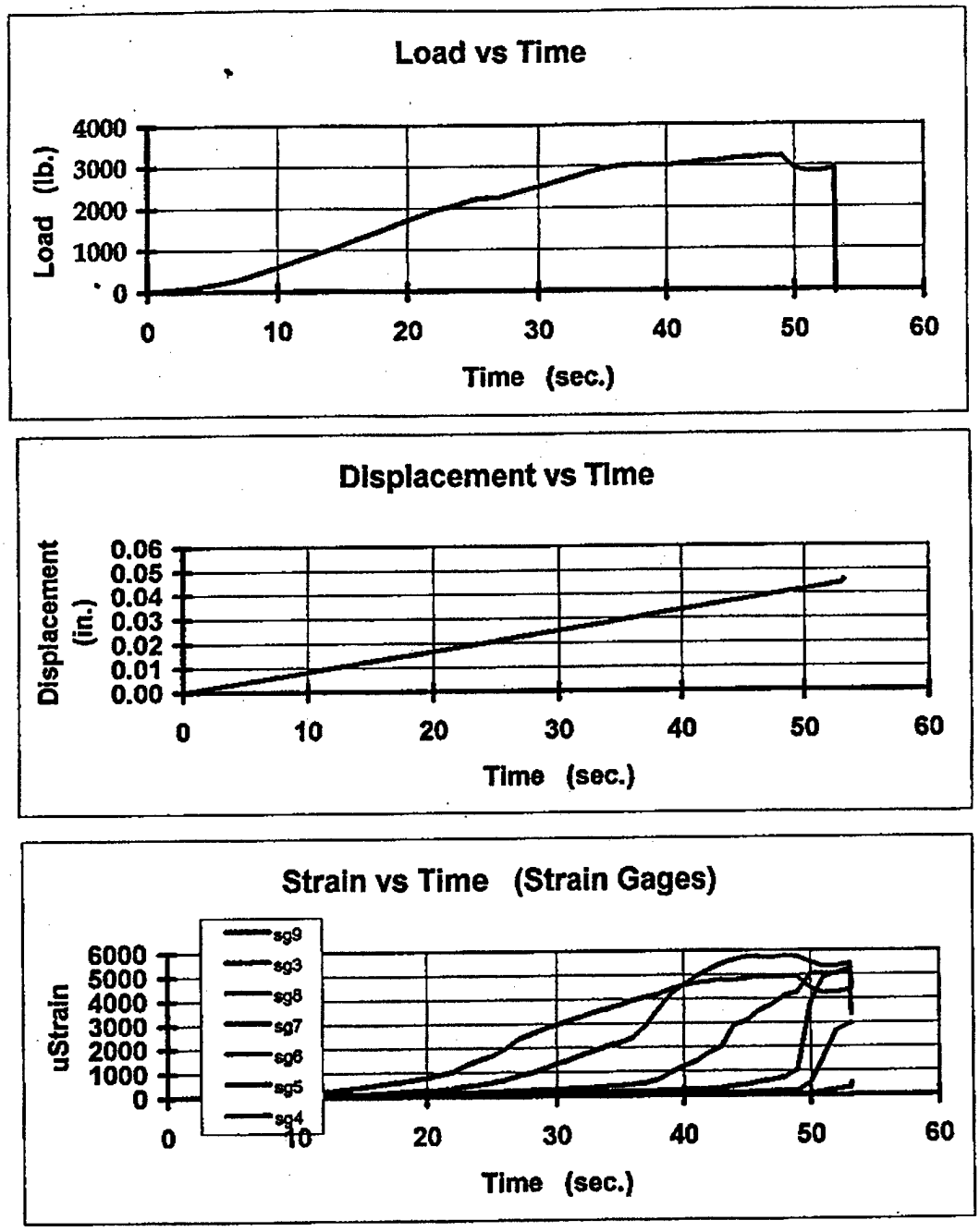


Figure E.68.15 Load, displacement, and strain data of the uncoated specimen WPC8 at low temperature.

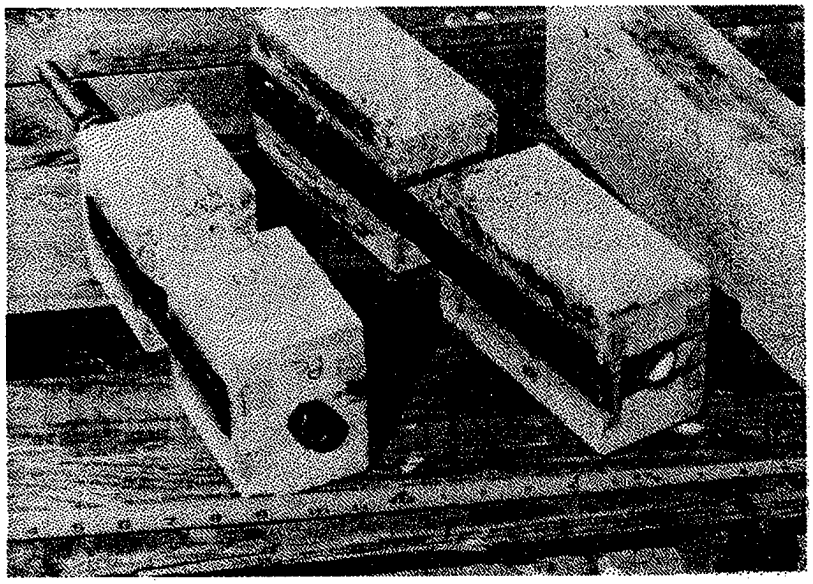


Figure E69. "Split-block" test specimens.

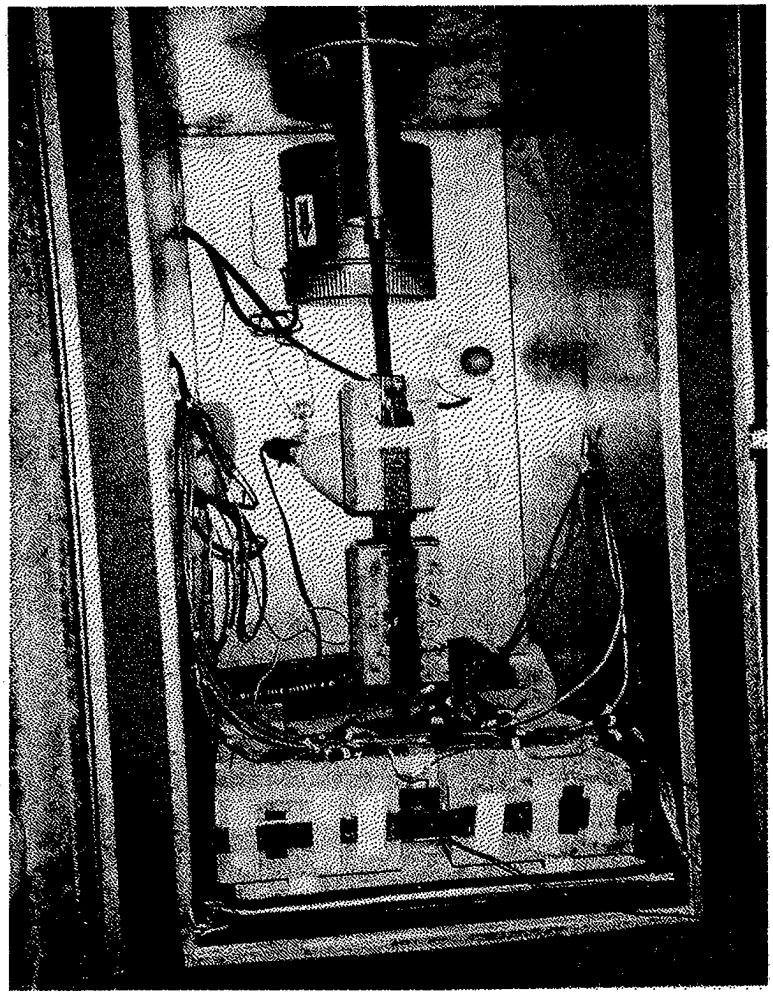


Figure E70. Tensile testing of "split block" specimens at low temperature.

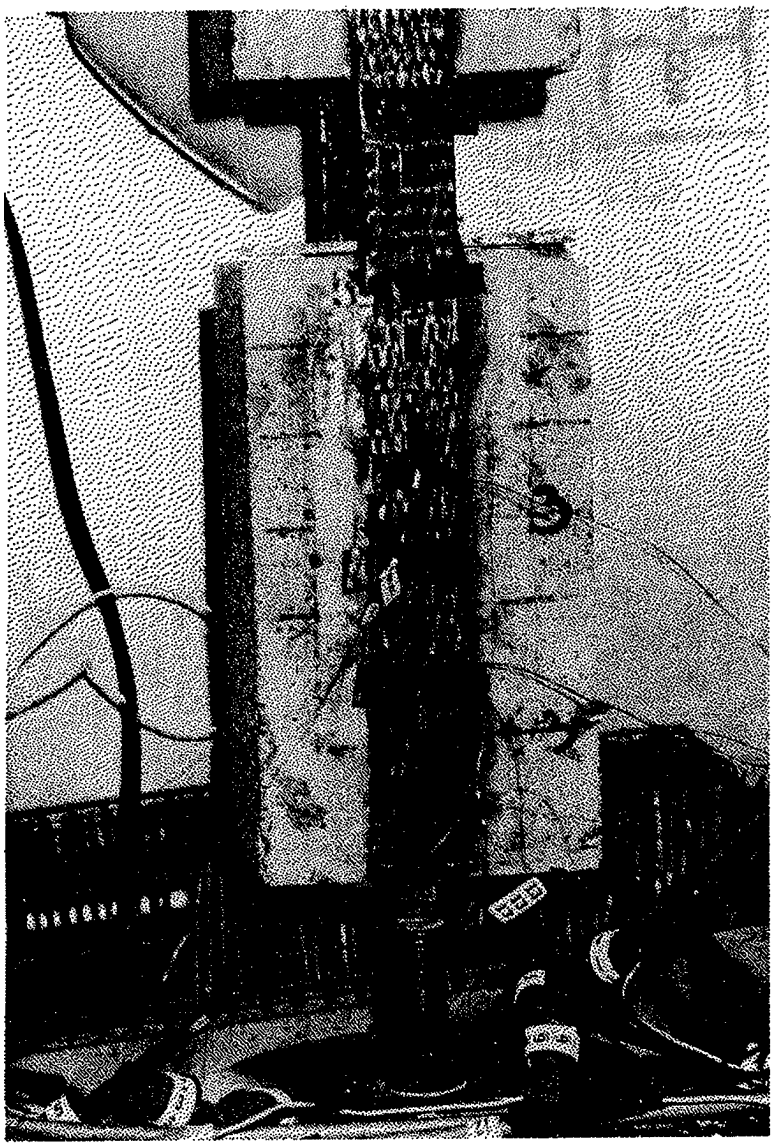


Figure E71. Multiple strain gages mounted on each block to monitor strain development.

Table E1. Low temperature failure load capacities of the ODOT beams.

Beam	No. of composite layers	Failure load kPa(lbf)	Deflection at Failure Load mm (in.)
1	5	134.62 (30,265)	11.40 (0.449)
4	5	143.93 (32,359)	15.09 (0.594)
3	1	113.28 (25,468)	23.22 (0.914)
2	1	118.62 (26,669)	21.26 (0.837)

Table E2. Number of cycle and load ranges for control beams at room temperature (24°C, 75°F).

Beam 1		Beam 5	
Hysol 9330		Sikadur 30	
No. of Cycles (x1000)	Load Range (P_{max} - P_{min}), kN (kips)	No. of Cycles (x1000)	Load Range (P_{max} - P_{min}) kN (kips)
0	5.3 – 15.6 (1.2 - 3.5)	0	5.3 – 13.3 (1.2 - 3.0)
5	5.3 – 15.6 (1.2 - 3.5)	5	5.3 – 13.3 (1.2 - 3.0)
10	5.3 – 15.6 (1.2 - 3.5)	10	5.8 – 17.8 (1.3 - 4.0)
20	5.3 – 15.6 (1.2 - 3.5)	20	5.8 – 17.8 (1.3 - 4.0)
40	5.3 – 15.6 (1.2 - 3.5)	40	5.8 – 17.8 (1.3 - 4.0)
75	5.3 – 15.6 (1.2 - 3.5)	75	5.8 – 17.8 (1.3 - 4.0)
100	5.3 – 15.6 (1.2 - 3.5)	100	5.8 – 17.8 (1.3 - 4.0)
270	5.3 – 15.6 (1.2 - 3.5)	150	5.8 – 17.8 (1.3 - 4.0)
400	5.8 – 17.8 (1.3 - 4.0)		
600	5.8 – 17.8 (1.3 - 4.0)		
700	5.8 – 17.8 (1.3 - 4.0)		
100	5.8 – 17.8 (1.3 - 4.0)		

Table E3. Number of cycles and load ranges for Sikadur 30 cold environment beams.

Beam 3		Beam 4	
Sikadur 30		Sikadur 30	
No. of Cycles (x1000)	Load Range (P_{max} - P_{min}) kN (kips)	No. of Cycles (x1000)	Load Range (P_{max} - P_{min}) kN (kips)
0	5.3 – 20 (1.2 - 4.5)	0	5.3 – 20 (1.2 - 4.5)
50	5.3 – 20 (1.2 - 4.5)	50	5.3 – 20 (1.2 - 4.5)
250	8.5-22.2 (1.9 - 5.0)	100	5.3 – 20 (1.2 - 4.5)
375	8.5-22.2 (1.9 - 5.0)	300	8.5-22.2 (1.9 - 5.0)
570	8.5-22.2 (1.9 - 5.0)	420	8.5-22.2 (1.9 - 5.0)
670	8.5-22.2 (1.9 - 5.0)	630	8.5-22.2 (1.9 - 5.0)
850	8.5-22.2 (1.9 - 5.0)	775	8.5-22.2 (1.9 - 5.0)
900	8.5-22.2 (1.9 - 5.0)	1000	8.5-22.2 (1.9 - 5.0)
1000	8.5-22.2 (1.9 - 5.0)		

Table E4. Number of cycles and load ranges for Hysol 9330 cold environment beams.

Beam 3		Beam 4	
Sikadur 30		Sikadur 30	
No. of Cycles (x1000)	Load Range (P_{max} - P_{min}) kN (kips)	No. of Cycles (x1000)	Load Range (P_{max} - P_{min}) kN (kips)
0	5.3 – 15.6 (1.2 - 3.5)	0	6.7 – 15.6 (1.5 - 3.5)
5	5.3 – 15.6 (1.2 - 3.5)	50	6.7 – 20.0 (1.5 - 4.5)
10	5.3 – 15.6 (1.2 - 3.5)	100	6.7 – 20.0 (1.5 - 4.5)
20	5.3 – 15.6 (1.2 - 3.5)	250	8.9 – 22.2 (2.0 - 5.0)
40	5.3 – 15.6 (1.2 - 3.5)	400	8.9 – 22.2 (2.0 - 5.0)
150	5.3 – 17.8 (1.2 - 4.0)	600	8.9 – 22.2 (2.0 - 5.0)
200	5.3 – 17.8 (1.2 - 4.0)	1000	8.9 – 22.2 (2.0 - 5.0)
430	5.3 – 19.1 (1.2 - 4.3)		
560	5.3 – 19.1 (1.2 - 4.3)		
760	5.3 – 19.1 (1.2 - 4.3)		
850	5.3 – 19.1 (1.2 - 4.3)		
1000	5.3 – 22.2 (1.2 – 5.0)		

Table E5. Ultimate loads of reinforced concrete beams.

Beam	Adhesive type	Fatigue Cycle Temp. °C(°F)	Maximum. fatigue cycle	Ultimate load at room temp test kN (kips)	Mode of failure
1	Hysol 9330	24 (75)	10^6	62.3 (14.0)	Plate Peeling / Shear
2	Hysol 9330	-20 (-4)	10^6	48.0 (10.8)	Plate Peeling / Shear
3	Sikadur 30	-20 (-4)	10^6	57.8 (13.0)	Diagonal Shear Failure
4	Sikadur 30	-20 (-4)	10^6	68.5 (15.4)	Diagonal Shear Failure
5	Sikadur 30	24 (75)	$1.5x10^5$	NA	Failed During Cycling
6	Hysol 9330	-20 (-4)	10^6	41.8 (9.4)	Plate Peeling / Flexural - Concrete Crushing

Table E6. Coefficients of thermal expansion.

Concrete	Steel	Sikadur 30	Hysol 9330	Sika cfrp
0.55×10^{-5} / °C	1.2×10^{-5} / °C	9.05×10^{-5} / °C	9.05×10^{-5} / °C	1.0×10^{-6} / °C

Table E7. Thermal cycling instrumentation.

Specimen number	Adhesive type	Instrumentation
A (control)	None	None
B (control)	None	None
1	Sikadur 30	12 thermocouples and 2 strain gauges
2	Hysol 9330	12 thermocouples and 2 strain gauges
3	Sikadur 30	One strain gauge at midspan
4	Hysol 9330	One strain gauge at midspan
5*	Sikadur 30	None
6*	Hysol 9330	None
7	Sikadur 30	None
8	Hysol 9330	None

* These two beams were not thermally cycled.

Table E8. Results from the thermally cycled beams in flexure.

Specimen	Adhesive	Treatment	Failure Load, kN (lbf)
A	None	Thermally cycled	29.09 (6540)
B	None	Thermally cycled	29.11 (6545)
1	Sikadur 30	Thermally cycled	No data
2	Hysol 9330	Thermally cycled	No data
3	Sikadur 30	Thermally cycled	27.13 (6100)
4	Hysol 9330	Thermally cycled	23.66 (5320)
5	Sikadur 30	Thermally cycled	40.94 (9205)
6	Hysol 9330	Thermally cycled	33.89 (7620)
7	Sikadur 30	Not thermally cycled	8.63 (1940)
8	Hysol 9330	Not thermally cycled	19.42 (4365)

Table E9. Results of the three point bending tests of the ODOT small beams.

Specimen	Test Temperature °C (°F)	Failure load KN (lbf)	Deflection at failure, mm (in.)	Remarks
PC1	–	–	–	Reserved[1]
PC2	–	–	–	Reserved
PC3	–	–	–	Reserved
PC4	24 (75.2)	13.14 (2955)	1.02 (0.040)	–
PC5	-35 (-31.0)	16.02 (3601)	1.57 (0.062)	Strain gauged
PC6	-35 (-31.0)	12.67 (2849)	1.22 (0.048)	Strain gauged
WPC1	–	–	–	Reserved
WPC2	–	–	–	Reserved
WPC3	–	–	–	Reserved
WPC4	-35 (-31.0)	15.24 (3426)	1.07 (0.042)	Strain gauged
WPC5	-35 (-31.0)	15.02 (3394)	0.99 (0.039)	Strain gauged
WPC6	-35 (-31.0)	15.41 (3465)	1.17 (0.046)	Strain gauged
WPC7	-35 (-31.0)	15.79 (3551)	1.19 (0.047)	Strain gage[2]
WPC8	-35 (-31.0)	14.49 (3258)	1.14 (0.045)	Strain gage[2]

[1] Held in reserve for future low temperature thermal cycling tests.

[2] Multiple strain gage. In other specimens strain gage was in at the mid span.

Table E10. Test results from the split block shear bond test by tension.

Specimen	Primer coat	Bond length mm (in.)	Test Temp ° C (°F)	Failure load kN (lbf)	Remarks
1	PC	76.2 (3.0)	--	--	not tested
2	PC	76.2 (3.0)	--	--	not tested
3	PC	76.2 (3.0)	-31 (-35)	10.52 (2365)	
4	PC	76.2 (3.0)	-31 (-35)	10.41 (2340)	
5	WPC	76.2 (3.0)	-31 (-35)	12.93 (2908)	
6	WPC	76.2 (3.0)	-31 (-35)	13.30 (2990)	
7	WPC	76.2 (3.0)	24 (75.2)	12.23 (2750)	
8	WPC	76.2 (3.0)			not tested
9	WPC	76.2 (3.0)			not tested
10	PC	152.4 (6.0)	-31 (-35)	12.70 (2855)	
11	PC	152.4 (6.0)	-31 (-35)	12.09 (2718)	
12	WPC	152.4 (6.0)	-31 (-35)	14.49 (3257)	
13	WPC	152.4 (6.0)	-31 (-35)	15.70 (3530)	

Appendix F: Evaluation of In-Field Test Methods to Determine Bond Strength of CFRP Repair Systems for Reinforced Concrete

Overview

Project Description

When a concrete structure or its element is strengthened with an externally bonded FRP, the most critical aspect of its behavior is that the composite action in the system must be preserved during the designed service life of the structure. This behavior is governed primarily by the ability of the bond to transfer stresses, and this in turn, depends on the bond between two phases of the system: existing concrete substrate and FRP.

Deficiencies and weaknesses in the bond when exposed to long term severe environment can be detrimental to the overall performance of the composite system.

Analysis of the published information demonstrates that there is still very limited data concerning the durability of FRP strengthening systems in severe environments. More data is necessary before confidence and reliability can be assured.

In 1994, a supplemental strengthening of reinforced concrete tank walls was performed by SPS at the Waste Water Treatment Plant (WWTP) in Hollidaysburg, PA. The overall objective of the testing program performed by SPS and Gannet Fleming that is described in this report was to perform durability testing of the CFRP strengthening system in severe environment.

Problem Statement

As was indicated earlier, a key requirement for a durable repair/strengthening composite system is the development of an adequate bond between the concrete and FRP that will remain intact throughout its service life.

Adhesives allow bond between FRP materials to concrete elements economically and without changing the outward appearance of the structure. Bonding with adhesives assures evenly distributed stress transmission over the entire contact surface. There are no stress concentrations (stress peaks) as may occur in spot-wise fixations such as anchored or bolted connections.

Despite the fact that the use of FRP for repair and strengthening of concrete structures is growing all over the world, standard bond testing procedures have still not been devised. Consequently, many projects have been carried out without any reliable monitoring of their quality. Recently some attempts have been made to overcome this problem but the results have not been completely satisfactory. Therefore, the necessity and usefulness of in-situ test methods is self-evident.

This issue impedes improvement. There is considerable pressure to develop and use reliable in-situ bond strength test methods. Unfortunately, development of such methods has not kept pace with the materials development, primarily because of the lack of appropriate field data needed for its development. The development of and an adherence to reliable QA/QC (quality assurance/quality control) test methods are avenues to wider use of composite materials for repair and strengthening of concrete structures.

Purpose, Scope, and Approach

The overall objective of the testing program was to perform durability testing of the CFRP strengthening system in severe environment. More specifically, the objective was: first, to study the bond behavior between the concrete and CFRP under different environmental exposures and second, to evaluate several bond tests methods, developed and/or modified specifically for this study.

In 1994, a supplemental strengthening of reinforced concrete tank walls at the Hollidaysburg WWTP was performed. Carbon fiber sheets were applied on two walls to control potential overstress and existing cracking of the under-reinforced concrete walls. The durability testing program, performed in 1996, after more than 2.5 years in service, included visual examination of CFRP

strengthening system and natural exposure bond testing in three (3) different environmental exposures.

Although several different bond test methods were considered and analyzed, two test methods were selected for use in the site testing: the direct pull-off tensile bond test and the torsion shear bond test. Different sizes and configurations of steel probes and composite cutting techniques were evaluated.

The results of the testing program along with the conclusions and recommendations for further studies are presented in this report.

Testing Program

Test Methods And Exposure Conditions

The testing program included natural exposure bond testing in three zones (Figures F1* and F2):

1. dry, exposed to ultraviolet (UV) rays and freezing and thawing
2. splash, exposed to freezing and thawing in water saturated condition, wetting and drying, UV, and chemical attack by waste water elements
3. submerged, exposed to chemical attack by waste water elements.

Two methods for testing the bond strength between CFRP and concrete were proposed:

- direct tension test carried out using modified ACI 503 "pull-off" method
- shear test, carried out using proposed torsion method.

In-situ tensile bond test - with this method, steel disks 2-in. diameter were glued to the CFRP on top of the 1/8-in. deep partial cores by means of epoxy resin adhesive. Then using a pull-off apparatus, a tensile force was applied to the probe and the tensile bond strength was calculated simply by dividing the failure load by the cross-sectional area of the specimen.

The partial coring was performed using a 2-in. diameter core barrel.

* All figures and tables are found at the end of this appendix.

Since the use of a core drill is not always easy in on-site QA/QC, especially where access is difficult, a pull-off test utilizing a 2-in. square steel plate was also proposed and evaluated. The CFRP laminate was cut along the perimeter of the plate using a small grinder.

The transfer of force from the concrete substrate into the carbon fiber laminate occurs by shear stress. Therefore, it is important to be able to evaluate this property of the composite system for design and quality control.

In-situ shear test - to measure the bond strength between CFRP and existing concrete, the "Torsion Method," which is a modification of the "Friction Transfer Method" proposed and developed by Naderi (1985) for concrete surface repairs and overlays.

For torsional test, the torque is applied to the special probe using the torque applying unit. Test probes 1-in. and 2-in. diameters were glued to the CFRP with epoxy adhesive. The CFRP was cut along the perimeter of the probe using a small grinder. Torsion was applied using a calibrated torque wrench with a series of hinges to eliminate any possible bonding moment due to the eccentricity (Figure F3).

Before starting the field testing, the test methods, instrumentation, and probes were evaluated in laboratory conditions using 2.5 ft x 2.5 ft sample slabs.

The purpose of the field evaluation program was to:

- establish the effect of three different environmental exposures (three zones) on the bond between CFRP and concrete
- establish applicability and reliability of the proposed bond testing methods
- assess the applicability of the testing methods in extreme site conditions.

Test Results

For photographs of the testing activities at Hollidaysburg WWTP, see figures at the end of this appendix. The results of the tensile and shear bond tests and modes of failures in different exposure zones are shown in Table F1*.

* All tables are found at the end of this appendix.

Several fracture modes (planes) were anticipated, i.e., fracture in the existing concrete or in the composite, or at the interface between the two, and finally a combination of all three, depending on their relative strengths. Another undesirable failure mode could be fracture at the interface between the steel probe and composite, which could happen due to inadequate surface preparation of FRP or steel disk, or the inadequate quality of the epoxy glue, or a combination of both.

In direct tension the predominant failure mode was a combination of partial failure in concrete and between concrete and CFRP. The average tensile stresses at failure were as follows:

Zone #1	(6 tests)	-	228 psi
Zone #2	(3 tests)	-	431 psi
Zone #3	(3 tests)	-	329 psi

The test results demonstrate more-than-adequate tensile bond between parent concrete and CFRP.

The results of the pull-off tests in Zone #1 when square probes were used, demonstrate a close numerical correlation with the test results with circular probes.

In shear tests the predominant mode of failure was in the bond between the steel probe and CFRP.

The average shear stresses at failure were as follows:

Zone #1	(3 tests)	1,730 psi
Zone #2	(3 tests)	1,423 psi
Zone #3	(3 tests)	1.322 psi

The overall averages were calculated by averaging all the readings irrespective of the mode of failures.

The results of the shear bond test demonstrate that it more than three (3) times exceeds the required value of 370 psi.

It should be indicated that obviously the occurrence of the mixed failures instead of 100% bond between CFRP and concrete makes the estimation of the true bond strength more difficult. In the case of mixed failures, the overall average tends to underestimate the real bond strength in the system.

Conclusions

The following conclusions can be drawn from this study:

- The bond between CFRP and existing concrete in all three zones of severe environment of the waste water treatment plant demonstrates good performance after 2.5 years in service.
- Test methods used demonstrate that they are practical test methods for in-situ QA/QC, but both test methods need further development.
- The variations in the results obtained with these methods are clearly in excess of reasonable limits which demonstrates the poor repeatability of these methods. To make these promising test methods and their results applicable to practice and more precise, special attempts should be made to achieve standardization in testing procedures and materials, to limit the factors which may affect the bond strength such as surface preparation of FRP and steel probes, quality of the epoxy glue, curing conditions and duration.
- No numerical correlation of tensile and shear bond strength was possible.
- The pull-off tensile bond test method using 2-in. square steel plates eliminates the necessity for core drilling. The test results reasonably correlate with the test results when 2-in. diameter disks and partial core drilling are used.
- Further extensive testing should be carried out to confirm the above correlation.

Reference

Naderi, M., "Internal Research Report," Civil Engineering Department, The Queen's University of Belfast, October 1985.

List of Appendix F Figures and Tables

Figures

Figure F1a. View of slab specimens. 9
Figure F2a. Various probes attached to CFRP for tensile and shear bond testing 9
Figure F3a. Shear bond testing. 10
Figure F4a. Shear bond testing using lab specimens 10
Figure F5a. Shear bond testing using slab specimens 11
Figure F6a. Shear test probes. 11
Figure F1b. Test area at Hollidaysburg WWTP 12
Figure F2b. Steel probe attachment 12
Figure F3b. Steel probe attachment 13
Figure F4b. Overview of three exposure zones 13
Figure F5b. Testing in dry and splash zones 14
Figure F6b. Steel disk attachment in submerged zone 14
Figure F7b. Core drilling. 15
Figure F8b. Core drilling. 15
Figure F9b. Pull-off testing of steel disk 16
Figure F10b. Pull-off testing of square steel plate. 16
Figure F11b. Pull-off testing apparatus. 17
Figure F12b. Pull-off test of steel disks 17
Figure F13b. Failure modes: composite-concrete interface, steel disk-composite interface, and within composite. 18
Figure F14b. Pull-off tests, various failure modes. 18
Figure F15b. Failure mode: between concrete and composite, and between steel disk and composite. 19
Figure F16b. Failure mode: between composite and probe. 19
Figure F17b. Shear test. 20
Figure F18b. Shear test, composite perimeter cutting 20
Figure F19b. Shear bond test. 21
Figure F20b. Shear bond test. 21

Tables

Table F1. Tensile and Shear Bond Between CFRP and Concrete 8

Table F1. Tensile and Shear Bond Between CFRP and Concrete.

Exposure zone	Test no.	Pull-off Tensile Bond, psi		Shear bond (torsional test), psi	Failure mode
		2-in. dia. disk	2-in. sq. plate		
Dry Zone # 1	1	216			Existing concrete
	2	261			Between existing concrete and composite
	3	153			Between Composite and steel disk
	4			1,830	Between probe and composite
	5			2,140	Between probe and composite
	6			1,220	Between probe and composite
	7		235		Between Composite and steel plate
	8		225		Between Composite and steel plate
	9		275		Existing concrete, composite
Splash Zone # 2	10	191			Between Composite and steel disk
	10A*	541			Composite and composite-steel disk
	11	172			Between Composite and steel disk
	11A*	242			Between Composite and steel disk
	12	153			Between Composite and steel disk
	12A*	509			Composite-concrete
	13			1,830	Between probe and composite
	14			0	No bond between composite and probe
	15			1,220	Between probe and composite
	16			1,220	Between probe and composite
Submerged Zone #3	17	407			Composite-concrete, composite
	18	274			Composite-concrete, composite
	19	306			Composite-concrete, composite
	20			915	Composite
	21			1,220	Between probe and composite
	22			1,830	Between probe and composite

* Tests were repeated with more accurate composite surface cleaning procedures

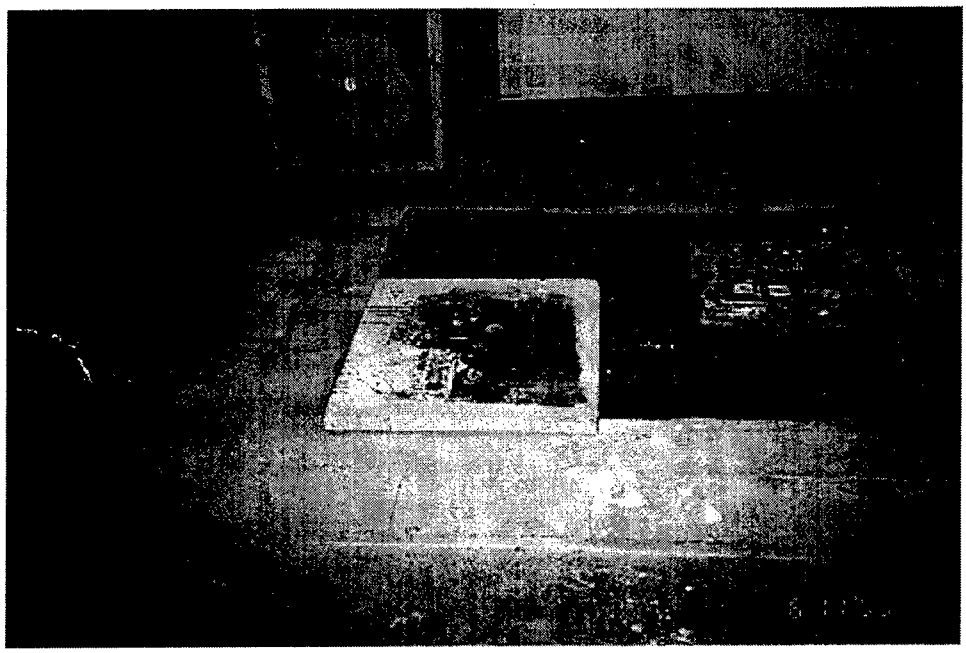


Figure F1a. View of slab specimens.

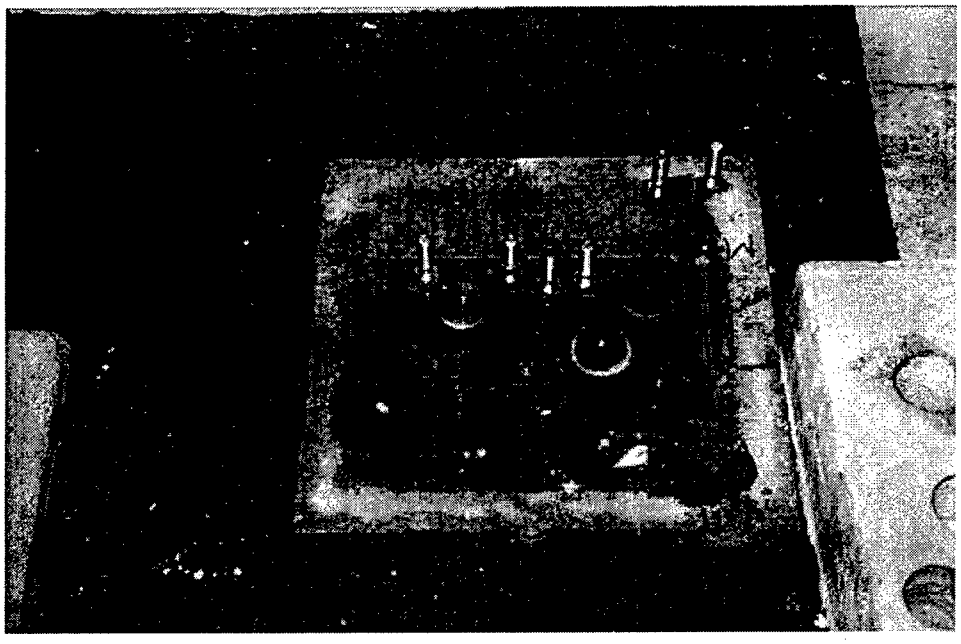


Figure F2a. Various probes attached to CFRP for tensile and shear bond testing.

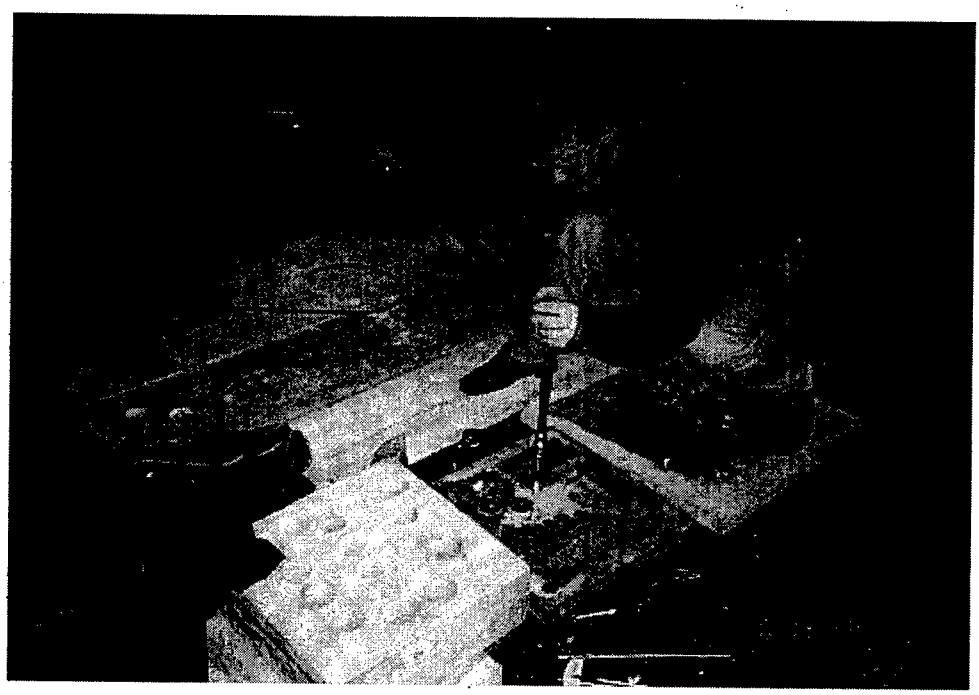


Figure F3a. Shear bond testing.

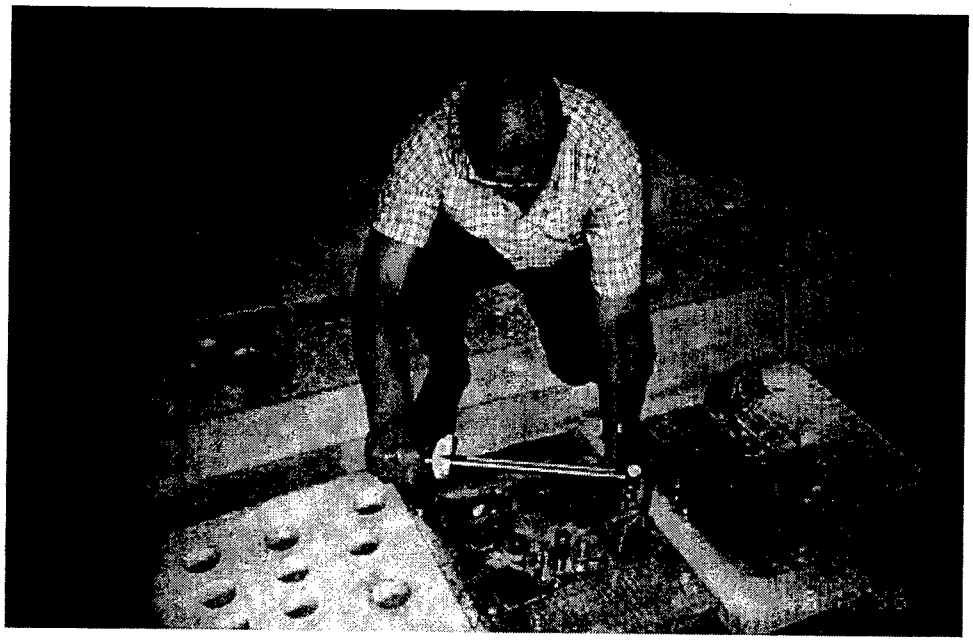


Figure F4a. Shear bond testing using lab specimens.



Figure F5a. Shear bond testing using slab specimens.

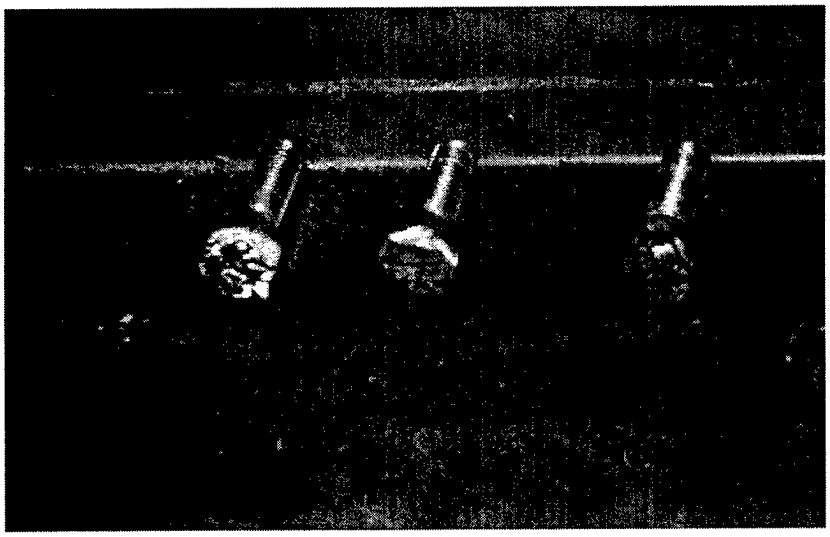


Figure F6a. Shear test probes.

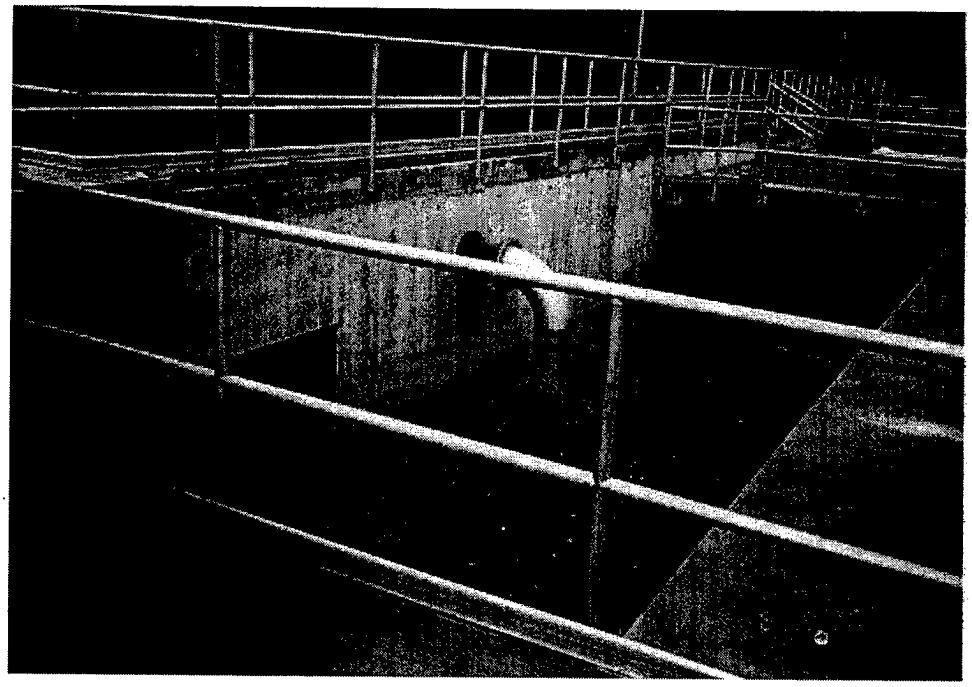


Figure F1b. Test area at Hollidaysburg WWTP.

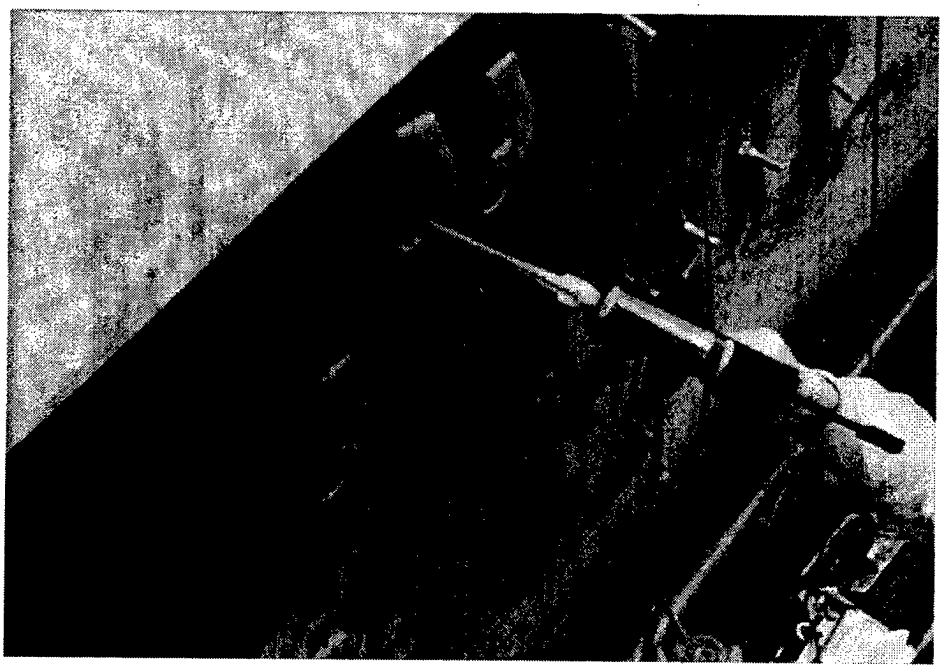


Figure F2b. Steel probe attachment.

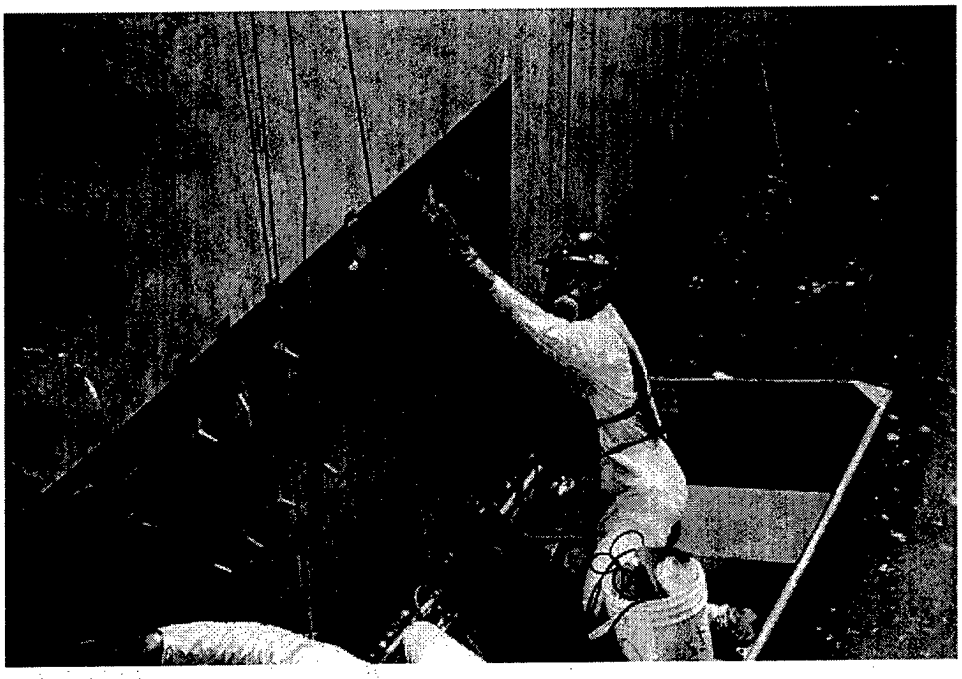


Figure F3b. Steel probe attachment.



Figure F4b. Overview of three exposure zones.

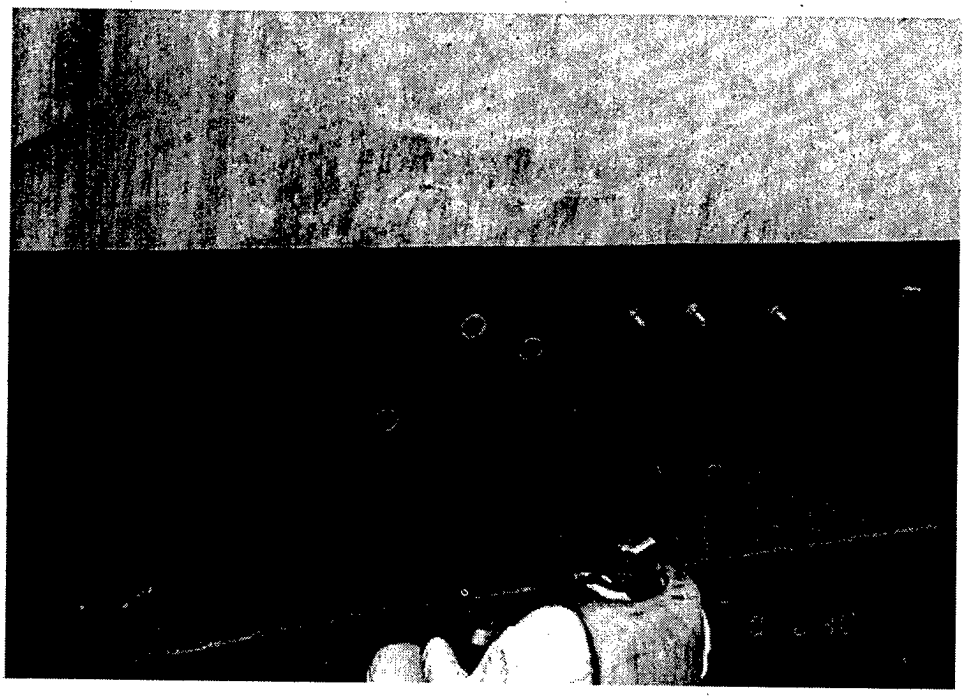


Figure F5b. Testing in dry and splash zones.



Figure F6b. Steel disk attachment in submerged zone.

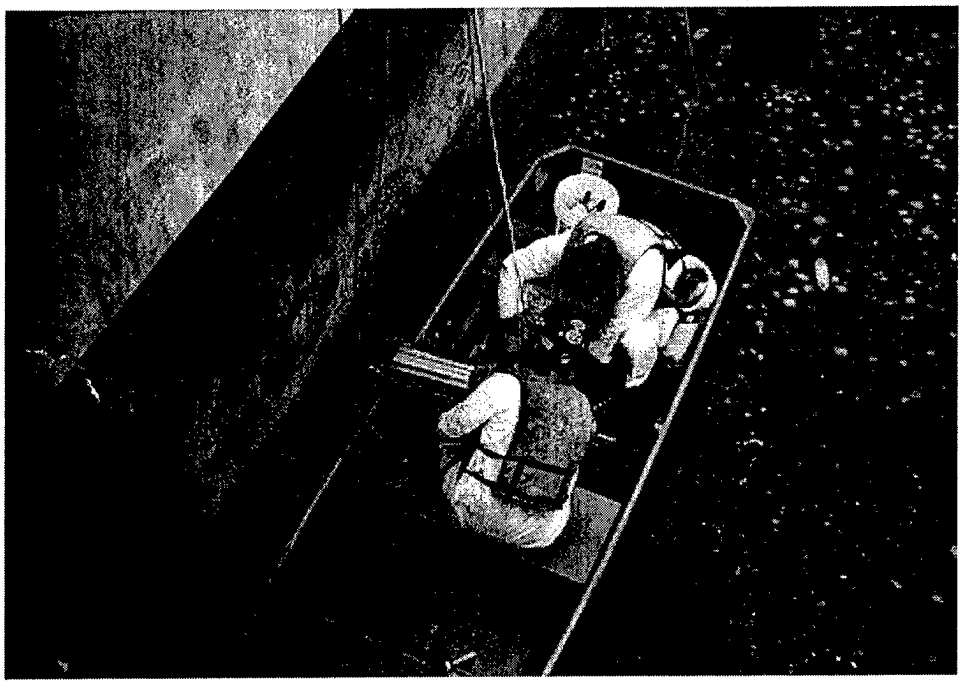


Figure F7b. Core drilling.

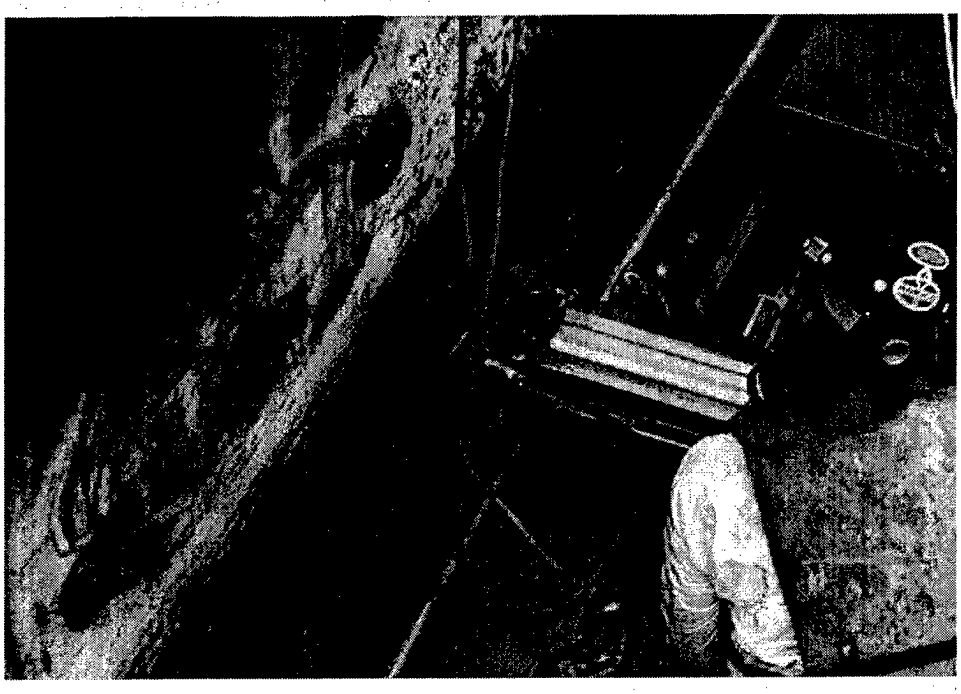


Figure F8b. Core drilling.



Figure F9b. Pull-off testing of steel disk.



Figure F10b. Pull-off testing of square steel plate.

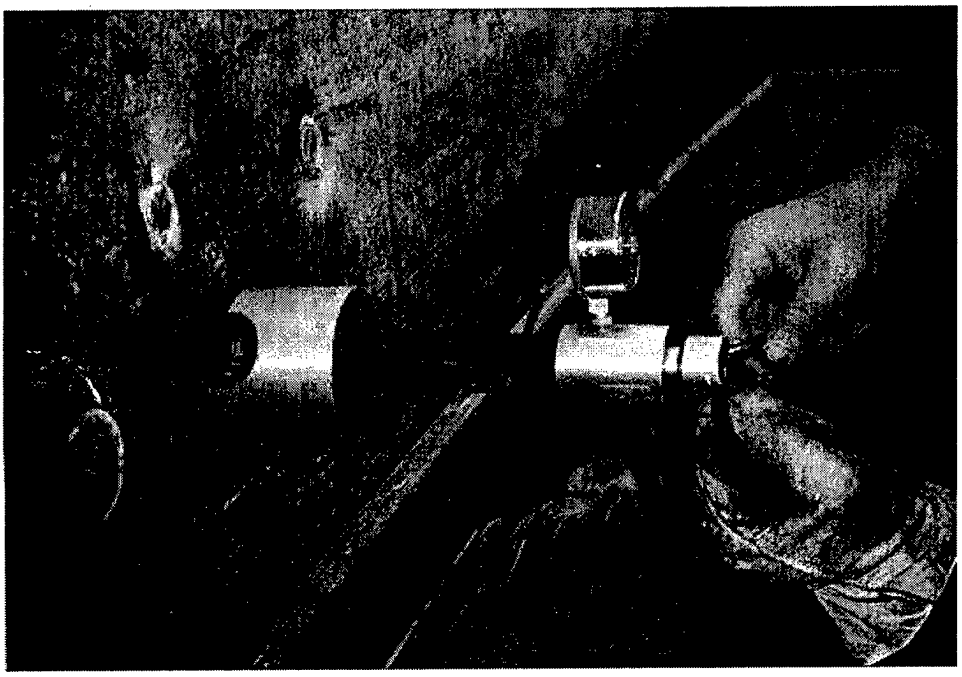


Figure F11b. Pull-off testing apparatus.

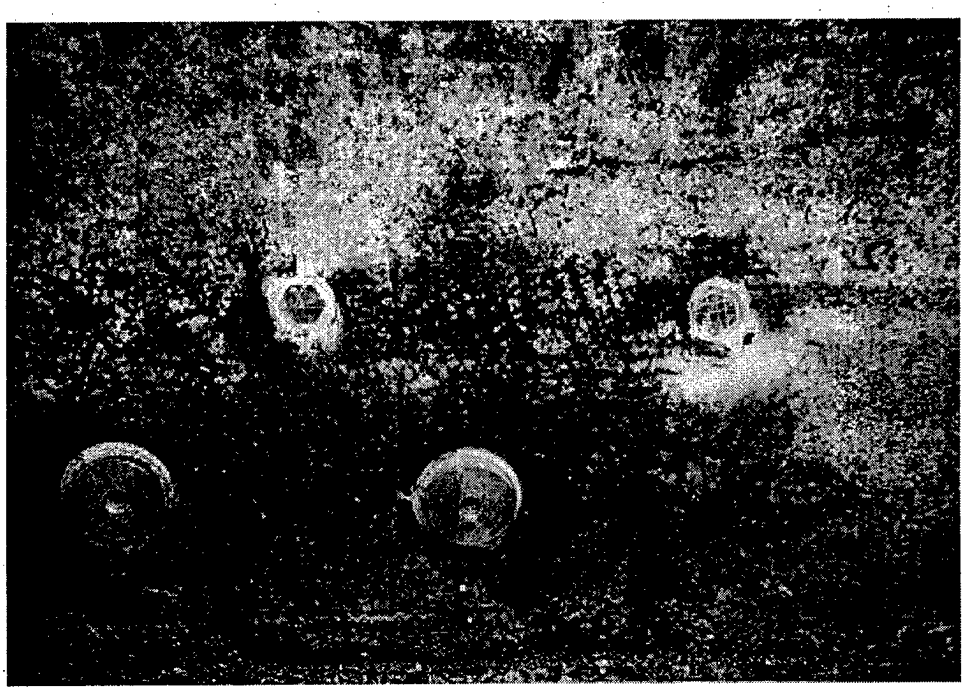


Figure F12b. Pull-off test of steel disks.

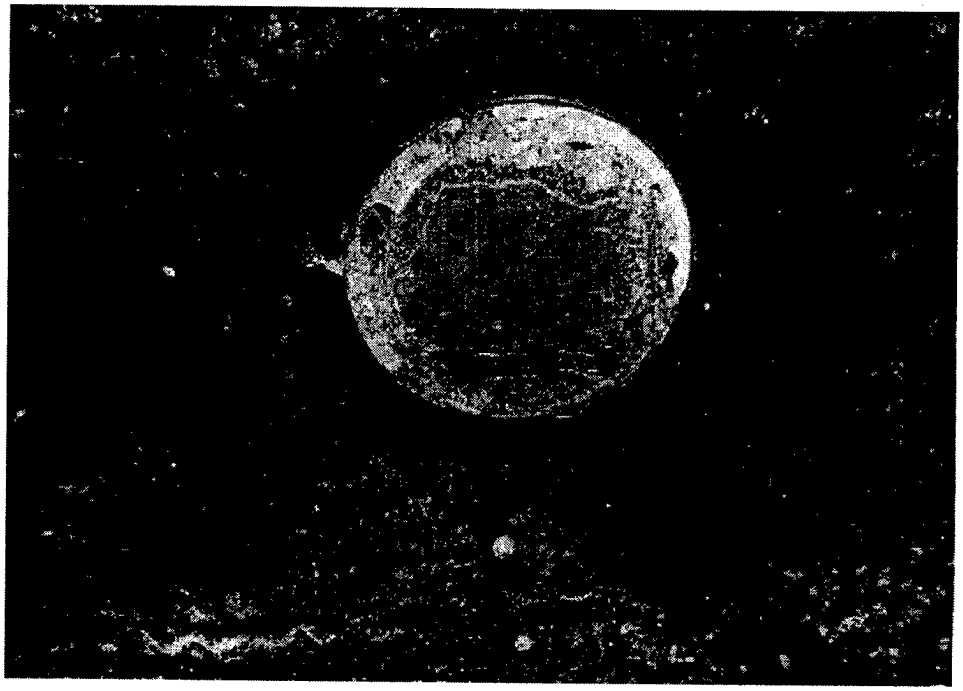


Figure F13b. Failure modes: composite-concrete interface, steel disk-composite interface, and within composite.

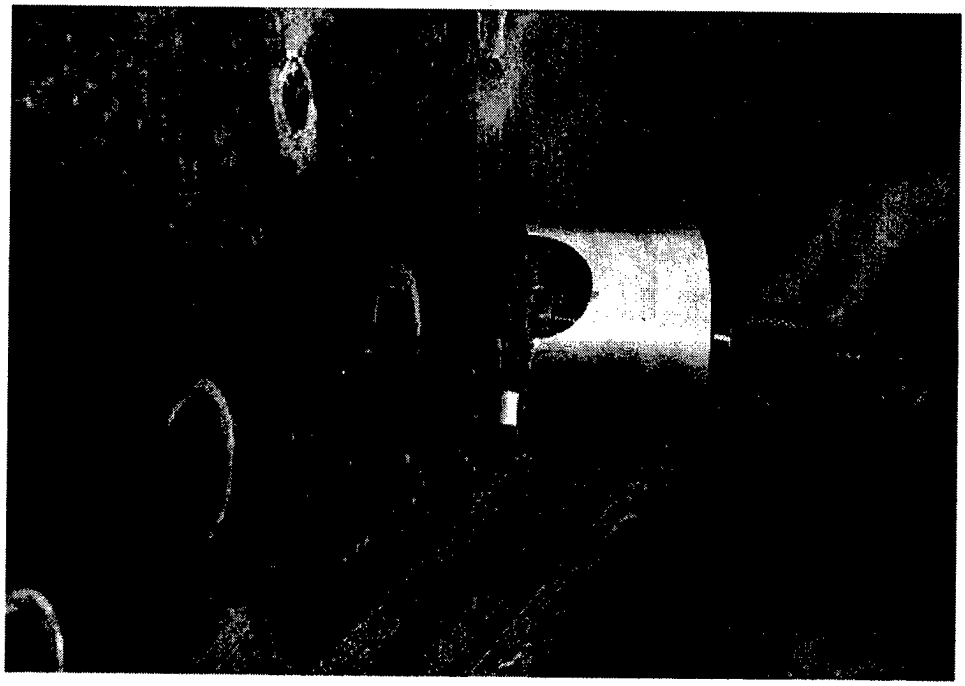


Figure F14b. Pull-off tests, various failure modes.

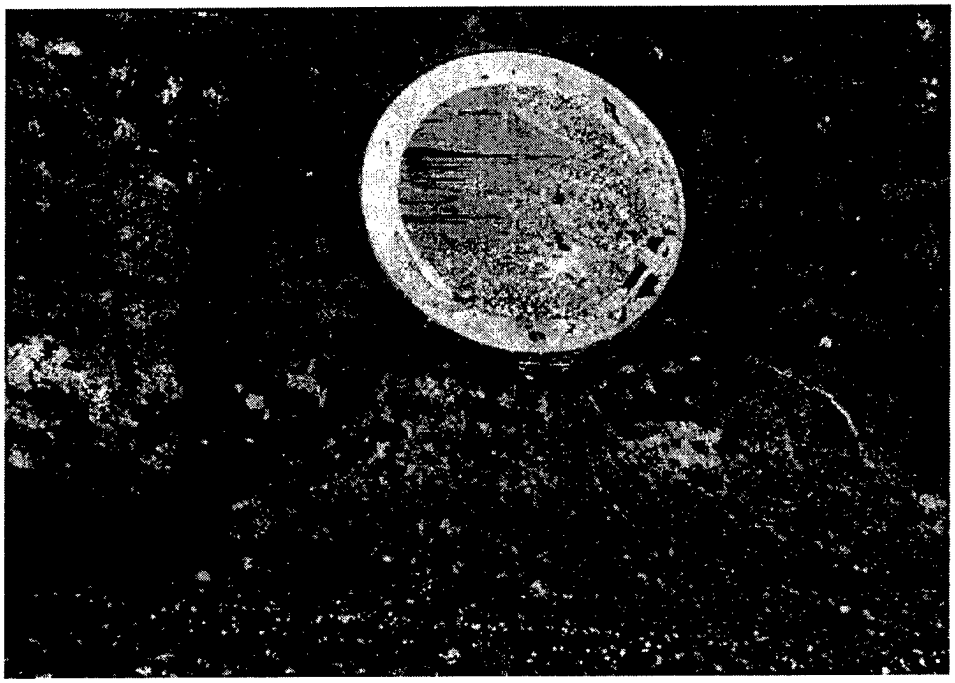


Figure F15b. Failure mode: between concrete and composite, and between steel disk and composite.

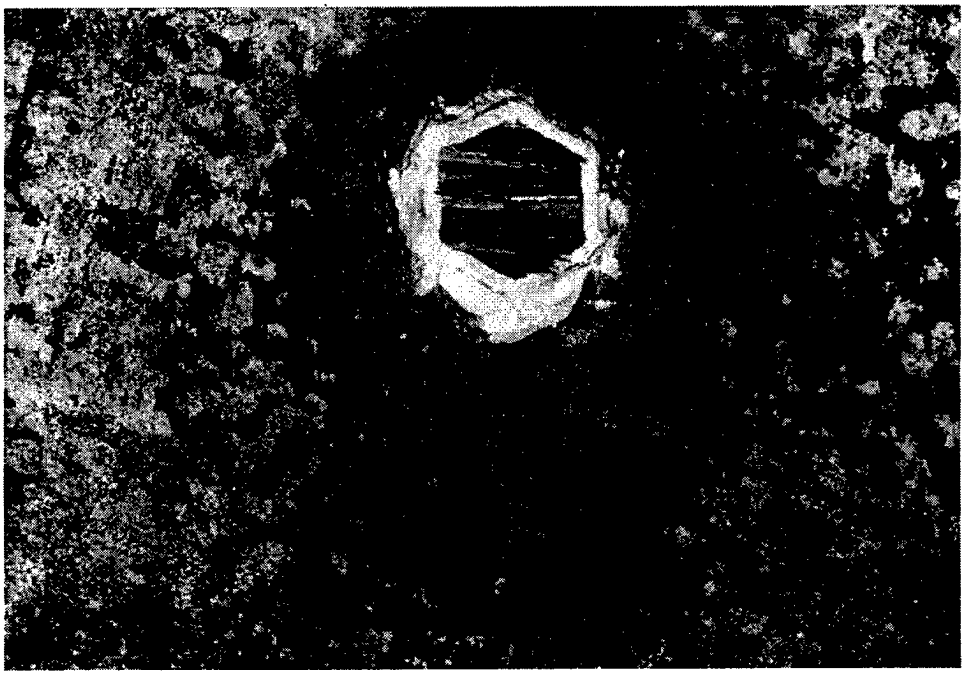


Figure F16b. Failure mode: between composite and probe.



Figure F17b. Shear test.



Figure F18b. Shear test, composite perimeter cutting.



Figure F19b. Shear bond test.

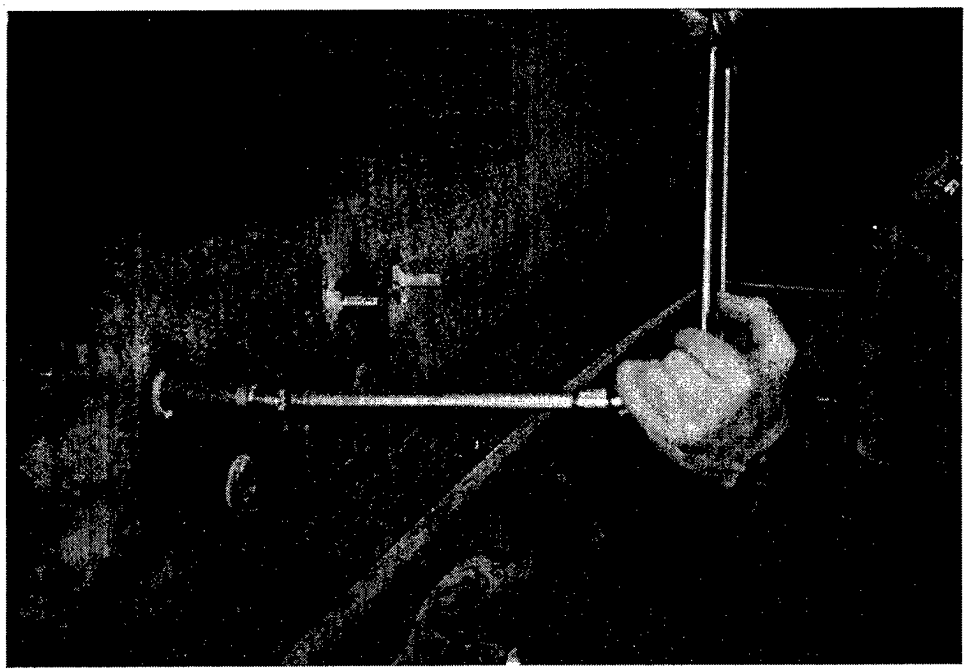


Figure F20b. Shear bond test.

Appendix G: Tendon Drape Angle Test Fixture Specification

Overview

FRP prestressing tendons must occasionally be bent around turning points. This condition occurs when prestressing I-girders, T-beams, and similar precast members and when post-tensioning beams and girders. Recently, FRP tendons and rods have been used successfully in these applications.

Structural Preservations Services (SPS) of Baltimore, MD, installed LEAD-LINE™ FRP tendons manufactured by Mitsubishi Chemicals of Japan on seven double-tee beams and a single-tee-beam in the crawl space of a condominium in Lantana, FL, in April 1996. Figure G1* is a sketch of the beam configuration. Due to extensive corrosion of the rebar in the T-beams, much of the concrete cover was spalled off and the structure was about to be condemned if repairs were not made. At the time the tendons were installed, the CPAR team installed instrumentation on the tendons added to one of the double-tee beams (see Appendix B). The beams had a single 3.5 in. outside diameter pipe suspended in the center of the beams originally for utility services. The repair design took advantage of the pipe as a king post for the post-tensioning configuration. However, due to the short span of the beams, designers were concerned about the bend angle around the pipe, between 11 degrees and 12 degrees. The tendon manufacturer had tested their tendons only to a bend angle of 7 degrees around a 2 in. diameter pin. The manufacturer guaranteed that at a 7 degree angle the ultimate tensile load was well above the design load. Since no test data existed for drape angles greater than 7 degrees, the project engineers decided to move the service pipe to the side and add a second pipe to assure that the tendon would not exceed 7 degrees during its service life.

* All figures are found at the end of this appendix.

It is a common industry practice to drape prestressing and post stressing tendons around turning points to create king- or queen-post strengthening systems. An examination of some typical beams and repair systems suggest that the total turning angle varies anywhere from 0 degrees to 15 degrees. No standard test methods exist for evaluating the performance of FRP rods or tendons for these types of applications. This research is important in order to develop a standard test fixture for use in ASTM standards to evaluate performance of FRP tendons and rods when draped around turning points up to 20 degrees.

The CPAR Team organized a meeting with experts from industry and academia to address this problem and initiate development of a test fixture. Working with Dr. Charles W. Dolan, University of Wyoming (UW), and other members of ASTM Committee D-20.18 on FRP for Concrete Reinforcement, a design for a bending or harping test fixture was developed. Plans were made for USACERL, UW, and South Dakota School of Mines and Technology to conduct individual testing of FRP tendons and share test results. An ASTM Standard will be developed based on this effort.

The CPAR team worked with ASTM Committee D-20.18 on FRP reinforcing to address the drape angle design limitation and develop a consistent test procedure for new and emerging FRP tendon and rod manufacturers to evaluate the tensile capacities of their products at drape angles up to 20 degrees.

FRP Tendon Test Fixture Design

Typical designs call for the stressing of FRP tendons to be a maximum of 50% of their ultimate strength for glass and 60% for carbon. Bending around a turning point will reduce the actual tendon strength. If a solid diameter rod is bent around a pin, the extreme fiber strain will increase by the radius of the rod around the pin. The FRP materials are strain limited due to the inability to redistribute stress through yielding. A stranded rod has much different strain response since the strands flatten over the pin and the individual strands have smaller diameters.

In order to evaluate the magnitude of strength reductions from bending, a test fixture was designed. Some of the considerations that were taken into account in the design include the ultimate strength of the straight tendons to be tested, the length needed between anchors and bending pin to assure that end or pin effects do not overlap, forces on the pin and anchorage connections, and the test

machine configuration. Using basic mechanics of materials, the maximum strain at the outer fibers is:

$$\varepsilon = \frac{r}{R}$$

where:

R= bend radius

ε = extreme fiber strain, and

r = radius of tendon

It is clear from this equation that a very important factor affecting the outer fiber strain is also the bend radius. Any evaluation of strength reduction should also take into account the bend radius.

The fixture design specified using 8 mm (0.31 in.) diameter LEADLINE™ tendons. These were the same size tendons used in the Florida demonstration described above. Therefore the design called for a maximum tensile capacity to exceed the ultimate tensile strength of the LEADLINE™ rod. Draft ASTM specifications recommend a minimum length of 50 diameters as the minimum required length between anchorages for tensile testing of tendons to eliminate end effects. A minimum length of 400 mm (15.7 in.) was therefore specified between the fixture anchor points and the bending pin. The maximum forces in the pin were assumed to be equal to the ultimate tensile forces of the tendons tested. The completed fixture was designed to be attached to a USACERL load frame for testing.

The design configuration specifies pin diameters of 2 in., 4 in., and 6 in. for the turning point pin, and bending angles of 0, 5, 10, 15, and 20 degrees. (Pins were also fabricated to simulate the 3.5 in. diameter pipes in the Lantana, FL, tests.) This resulted in a total of 12 different test configurations. The test fixture for the FRP tendon testing program was designed as an easily adjustable fixture to permit the testing of the tendons under all of the prescribed test configurations with a minimum of refixturing between tests. The tendon mounting fixture consisted of two steel mounting plates with a steel pin to serve as the turning point, and a steel anchor point for the end of the tendon. The pin and anchor points were installed between the two plates. The test assembly was then mounted in a loading frame with a hydraulic actuator suspended above it. A

cutaway view of the test fixture is shown in Figure G2 for a typical test configuration. Figures G3 and G4 are schematics for constructing the steel mounting plates, the first for bend angles of 5 degrees and 15 degrees, the second for 10 degrees and 20 degrees; Figure G5 shows the pin specifications. Figure G6 is a schematic for the steel adapter plates to attach the tendon anchor to the actuator and Figure G7 shows the overall test fixture in the loading frame.

To perform a test, standard anchors are attached to each end of a sample of the tendon and one end is attached to the tendon anchor point on the test fixture. The tendon is then placed around the turning point pin and the free end attached to the load cell adapter plate on the hydraulic actuator. The tendon is pulled in tension around the pin until failure occurs.

The tendon mounting plates were designed with a series of holes near the bottom of the fixture. These holes permitted the anchor point to be repositioned between each test to adjust the angle of bending for each of the required pin diameters. Two sets of mounting plates were fabricated to accommodate all four of the bending angles.

Conclusions

A test fixture was designed and constructed for testing the ultimate tensile strength of FRP tendons at drape angles varying from 0 degrees to 20 degrees around king- or queen-post diameters from 2 in. to 6 in. The design and specifications will be submitted to ASTM D20.18 for incorporation into draft test specifications for FRP tendons.

List of Appendix G Figures and Tables

Figures

Figure G1. Demonstration beam configuration. 6
Figure G2. Typical FRP tendon test configuration. 6
Figure G3. Schematic for mounting plate (bend angles 5 and 15 degrees). 7
Figure G4. Schematic for mounting plate (bend angles 10 and 20 degrees). 7
Figure G5. Pin specifications. 8
Figure G6. Steel adapter plates for FRP tendon test. 8
Figure G7. Test fixture in loading frame. 9

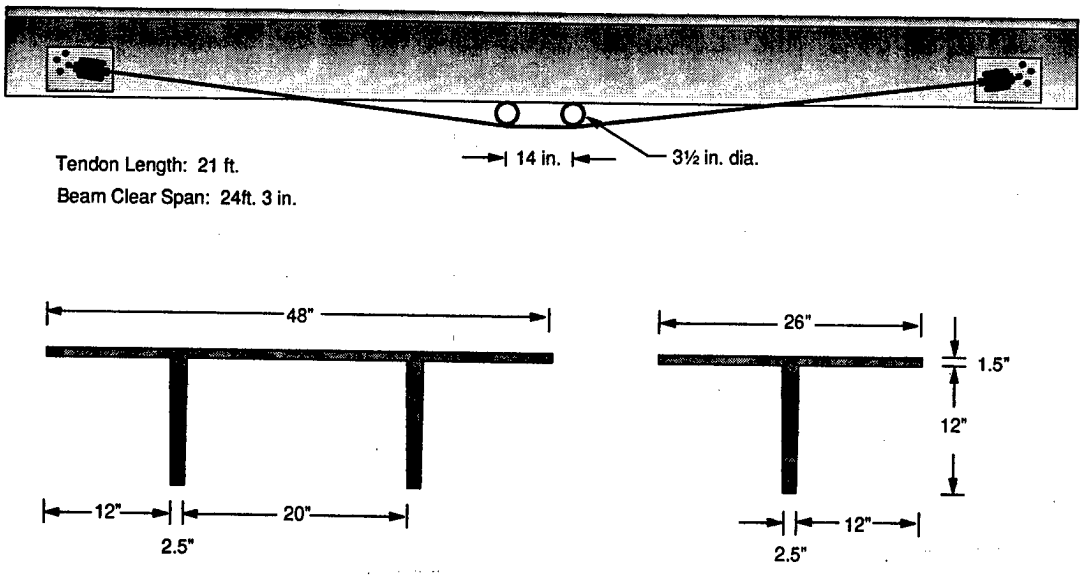


Figure G1. Demonstration beam configuration.

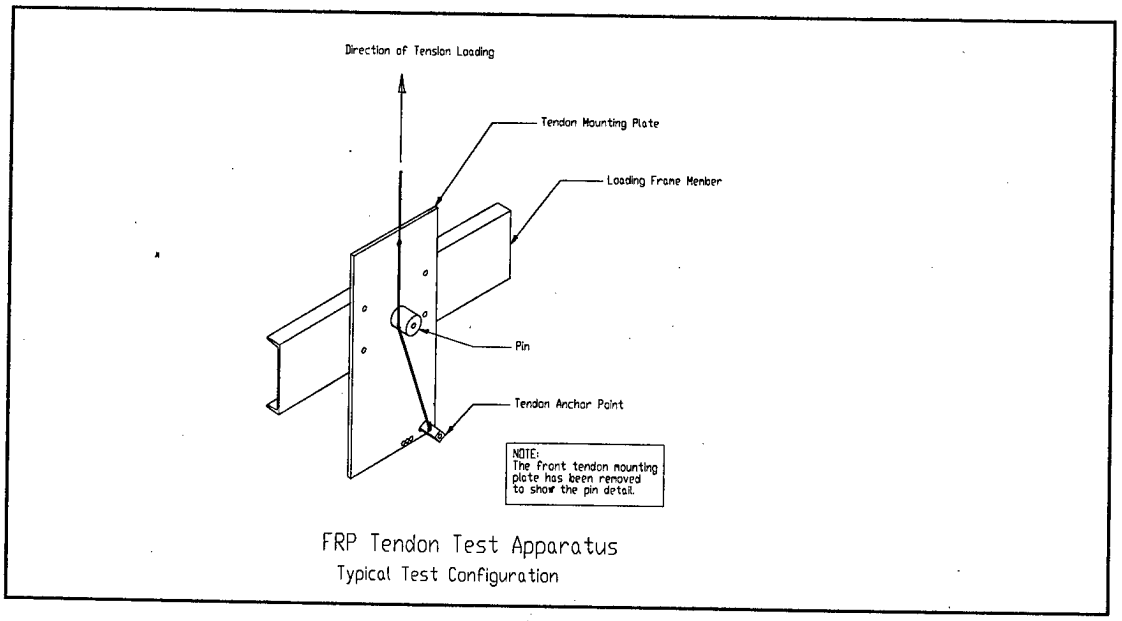


Figure G2. Typical FRP tendon test configuration.

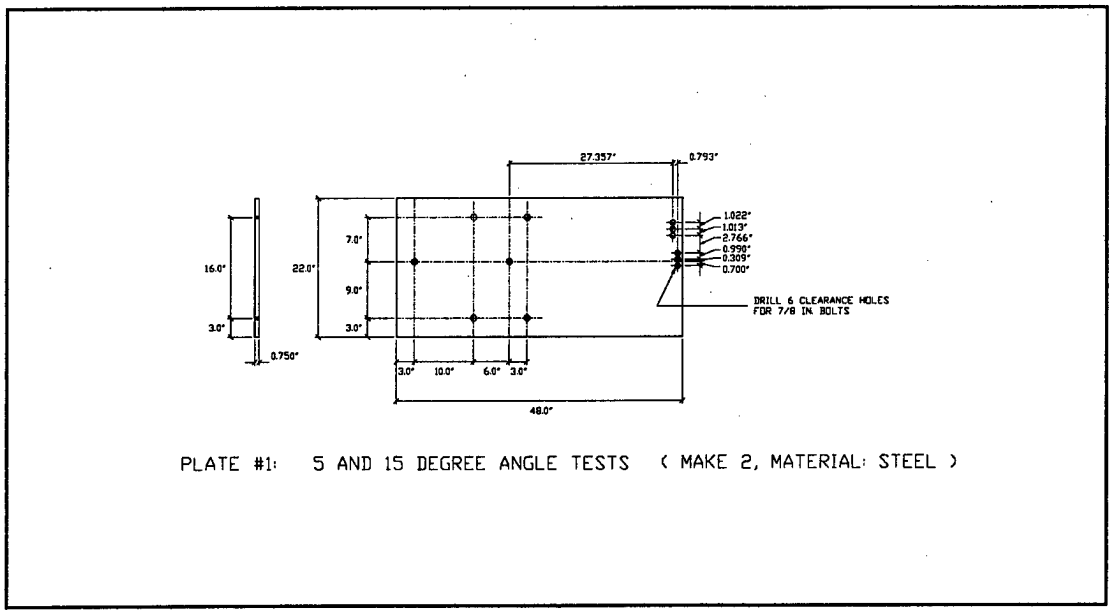


Figure G3. Schematic for mounting plate (bend angles 5 and 15 degrees).

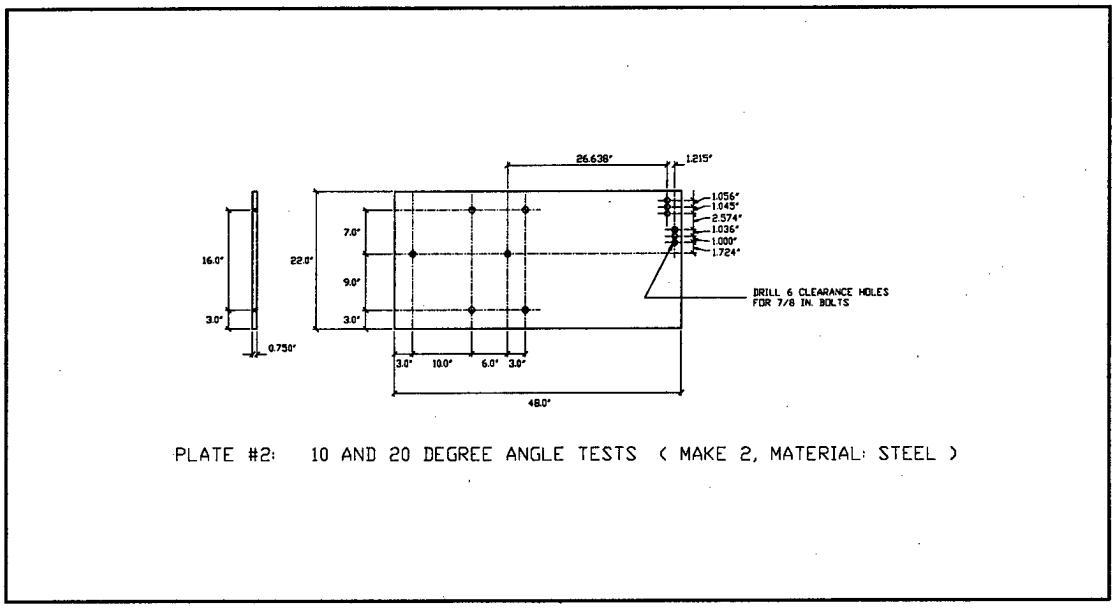


Figure G4. Schematic for mounting plate (bend angles 10 and 20 degrees).

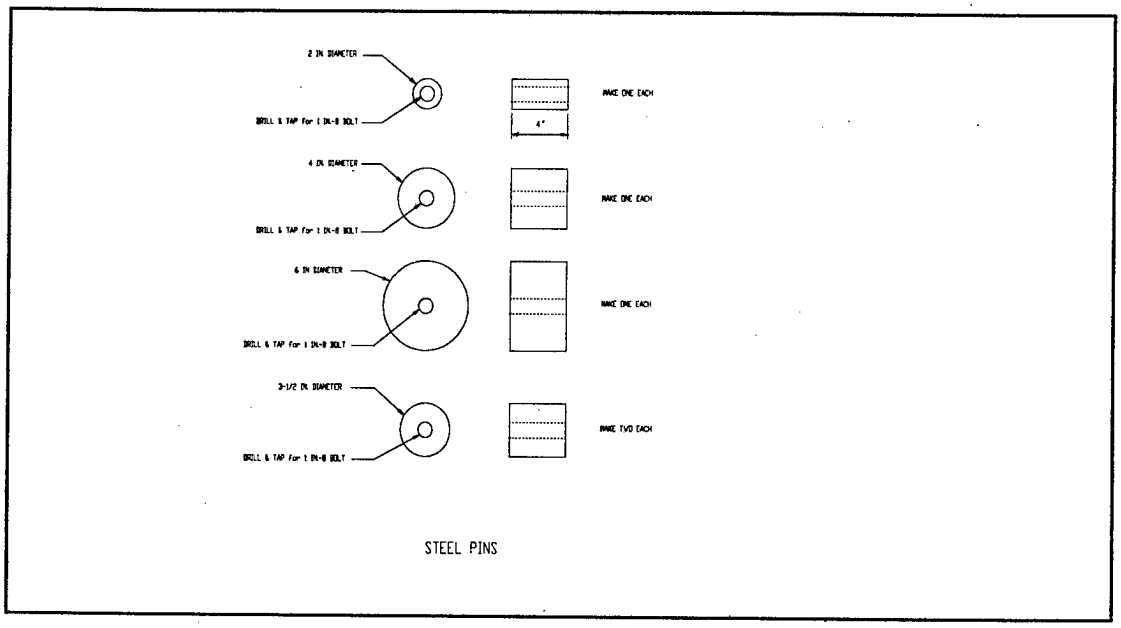


Figure G5. Pin specifications.

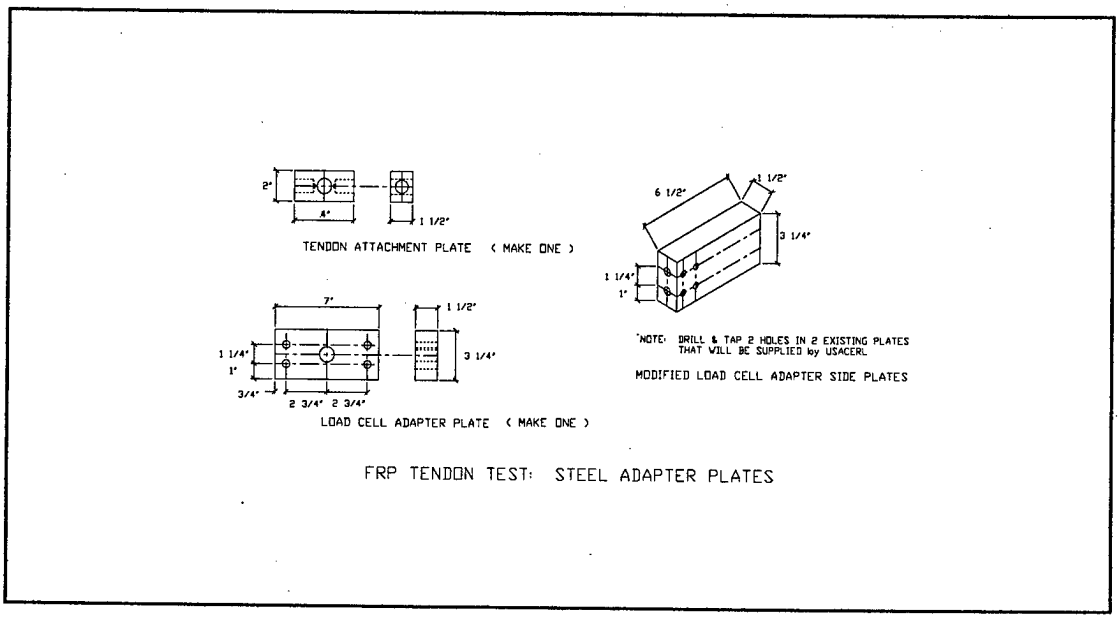


Figure G6. Steel adapter plates for FRP tendon test.

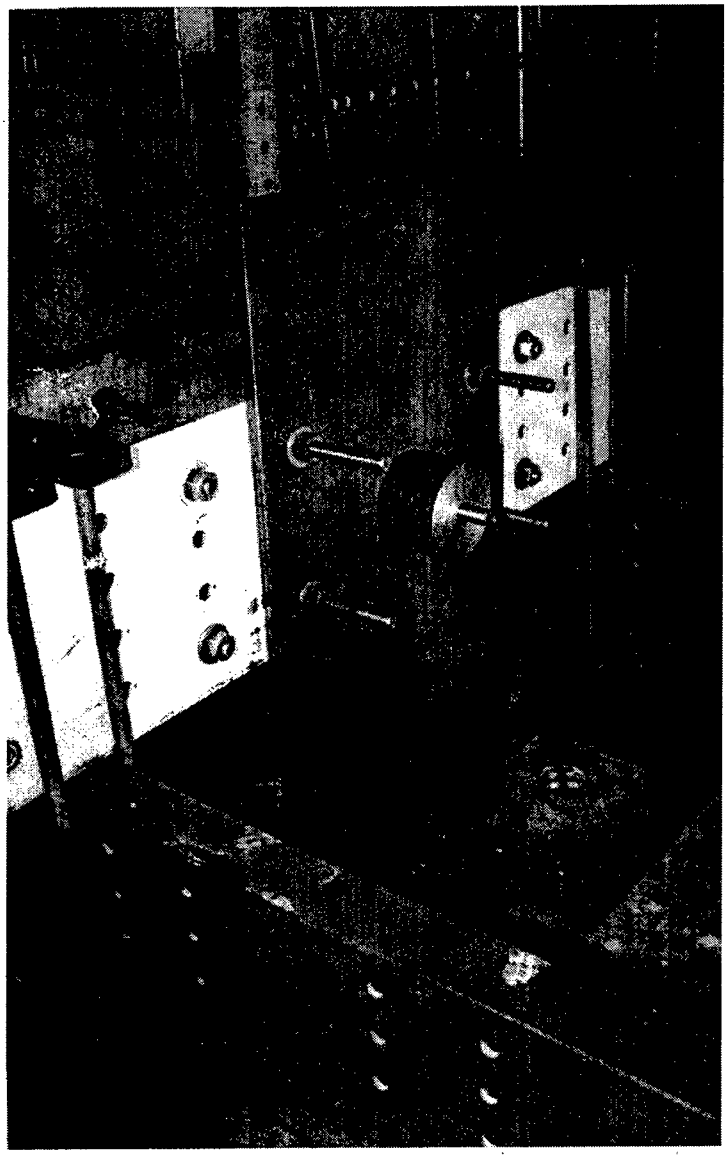


Figure G7. Test fixture in loading frame.

Appendix H: Specifications For Clark-Schwebel Tech-Fab Structural Grids*

Clark Schwebel Tech-Fab Company's thin Structural Grids (patent pending) are a glass-fiber reinforced epoxy resin non-woven composite used to reinforce a variety of traditional materials such as wood, asphalt over-lays, concrete (externally), etc.

The grids are produced in a manufacturing facility where the degree of cure (B-stage to full cure) is controlled to meet the requirements of the end-use application. Our equipment ensures the warp and weft materials are uniformly tensioned for consistent and uniform fiber loading. Production of the grids on rolls makes for ease of use. The grids are cured in a slightly curved condition but the thinness of the material ensures the grids will lay flat on a surface such as a wall or road bed.

The epoxy resin is selected to give a degree of compatibility with the various glues/adhesives used to produce the end product.

Individually designed to our customer's specifications, below are product capability guidelines to help you evaluate if Structural Grids can meet your needs:

WIDTH	Max = 96" Min = 6" (possibly less)
THICKNESS	0.002" - 0.040"
GRID OPENINGS	0.125" - 2" (possibly larger)
TENSILE STRENGTH (lb/in)	100 -2400
GLASS FIBER CONTENT	65 - 85% by weight
HOW SUPPLIED	On rolls (6" ID cardboard tube)
ROLL SIZE	Max OD = 48"
CONSTRUCTION	Balanced or tailored in warp/weft direction

* This material is reproduced from Clark-Schwebel corporate marketing literature.

Below are properties for four (4) grid configurations that have been manufactured to date.

Structural Properties for Available Grids

Property Grid Id # >	T-1009	T-1010	T-1011	T-1012
Construction (Warp/Fill Per Inch)	0.85 X 0.85	0.85 X 0.7	1.6 X 4.0	5.0 X 4.0
Weight (Osy)	4.43	5.95	12.64	12.45
Grid Description	**	**	**	**
Thickness (In) – Crossovers	0.0269	0.0276	0.0343	0.0206
Thickness (In) – Warp	0.0205	0.019	0.0283	0.0216
Thickness (In) - Fiill (Weff)	0.0275	0.0335	0.0184	0.0089
Grid Openings (In) (Warp-Warp)	1.0 - 1.1	1.0 - 1.1	0.25 - 0.40	0.06 - 0.09
Grid Openings (In) (Fill-Fill)	1.0 - 1.1	1.0 - 1.3	0.25 - 0.40	0.12 - 0.19
Warp Cross Sectional Area (In^2)(Calculated) At 30% Loi Of One (1) Warp Strand Bundle	0.00282	0.00282	0.00564	0.0176
Fill Cross Sectional Area (In^2)(Calculated) At 30% Loi Of One (1) Warp Strand Bundle	0.00141	0.00282	0.00034	0.00034
Tensile Strength - Warp (Psi)	>100,000	>100,000	>100,000	>100,000
Tensile Modulus - Warp (Psi) X 10^6	Est > 5.0	Est > 5.0	Est > 5.0	Est > 5.0
Tensile Strength - Fill (Psi)	>100,000	>100,000	>100,000	>100,000
Tensile Modulus - Fill (Psi) X 10^6	Est > 5.0	Est > 5.0	Est > 5.0	Est > 5.0

** STRUCTURAL GRIDS ARE FIBER GLASS REINFORCED EPOXY

DISCLAIMER: THESE DATA ARE BASED ON LIMITED TESTING PERFORMED BY CLARK-SCHWEBEL TECH-FAB COMPANY. THE USER OF THESE STRUCTURAL GRIDS SHOULD PERFORM ADEQUATE TESTING AND EVALUATION TO DETERMINE THE FITNESS-FOR-USE OF THESE STRUCTURAL GRID PRODUCTS.

Please give as much information as possible about your intended use of the grids and any glues or adhesives that you may use. Direct inquiries on your company's letterhead to:

Gordon Brown, Director – Commercial Development
Clark-Schwebel Tech-Fab Company
P.O. Box 807
Anderson, SC 29622
(864) 260-3268

USACERL DISTRIBUTION

Chief of Engineers
- ATTN: CEHEC-IM-LH (2)
- ATTN: CEHEC-IM-LP (2)
- ATTN: CECG
- ATTN: CECC-P
- ATTN: CECC-R
- ATTN: CECW
- ATTN: CECW-O
- ATTN: CECW-P
- ATTN: CECW-PR
- ATTN: CEMP
- ATTN: CEMP-E
- ATTN: CEMP-C
- ATTN: CEMP-M
- ATTN: CEMP-R
- ATTN: CERD-C
- ATTN: CERD-ZA
- ATTN: CERD-L
- ATTN: CERD-M (2)

ACS(IM) 22060
- ATTN: DAIM-FDP

CECPW 22310-3862
- ATTN: CECPW-E
- ATTN: CECPW-FT
- ATTN: CECPW-ZC

US Army Engr District
- ATTN: Library (42)

US Army Engr Division
- ATTN: Library (8)

American Public Works Assoc. 64104-1806

US Gov't Printing Office 20401
- ATTN: Rec Sec/Deposit Sec (2)

Defense Tech Info Center 22060-6218
- ATTN: DTIC-O (2)

83
+50
8/97

This publication was reproduced on recycled paper.

☆U.S. GOVERNMENT PRINTING OFFICE: 1998 - 646-081/80001